Clinical Connections

Peripheral Biomarker Signatures in RA-ILD

Wheeler et al, *Arthritis Rheumatol.* 2025;77:971-980.

CORRESPONDENCE
Bryant R. England, MD, PhD: bryant.england@unmc.edu

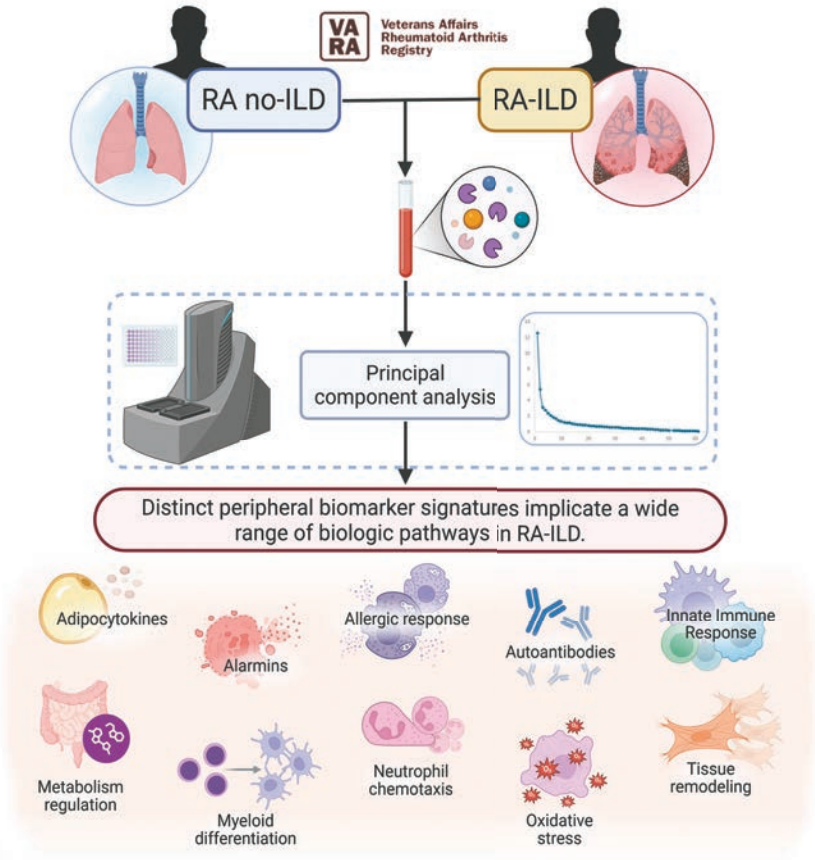

KEY POINTS

- Distinct peripheral blood biomarker signatures are associated with RA-ILD and implicate a wide range of biologic pathways in RA-ILD.
- Peripheral blood biomarker signatures improve ILD discrimination beyond clinical risk factors alone.
- The addition of the MUC5B promoter variant provides modest incremental benefit for RA-ILD risk stratification beyond broad peripheral blood biomarker analysis.
- Incorporation of peripheral blood biomarkers into predictive models could help overcome the limited predictive value of clinical risk factors for RA-ILD.

SUMMARY

Rheumatoid arthritis–associated interstitial lung disease (RA-ILD) causes substantial morbidity and mortality among people with RA, and we lack effective risk stratification methods. Investigation of peripheral biomarkers for RA-ILD has yielded a vast range of more than 100 possible candidate biomarkers. This study used an unsupervised machine-learning approach to identify unique biomarker signatures for RA-ILD and evaluate whether they improve RA-ILD prediction beyond clinical risk factors.

Wheeler et al performed a large cross-sectional study of the Veterans Affairs Rheumatoid Arthritis Registry and used principal components analysis of 60 different peripheral blood biomarkers to identify 8 distinct biomarker signatures associated with RA-ILD. The incorporation of these biomarker signatures into a risk prediction model significantly improved identification of ILD compared with clinical factors alone. Adding MUC5B promoter variant status, the strongest genetic risk factor for RA-ILD, led to incremental improvement. Together, these findings suggest a wide range of diverse pathways are involved in RA-ILD pathogenesis and that risk models, including broad biomarker profiling, may allow for improved RA-ILD risk-stratification.

A New Path Forward in SAVI: Blocking the IFN Receptor When Other Strategies Fail

Alehashemi et al, *Arthritis Rheumatol.* 2025;77:1087-1091.

CORRESPONDENCE
Sara Alehashemi, MD, MPH: sara.alehashemi@nih.gov

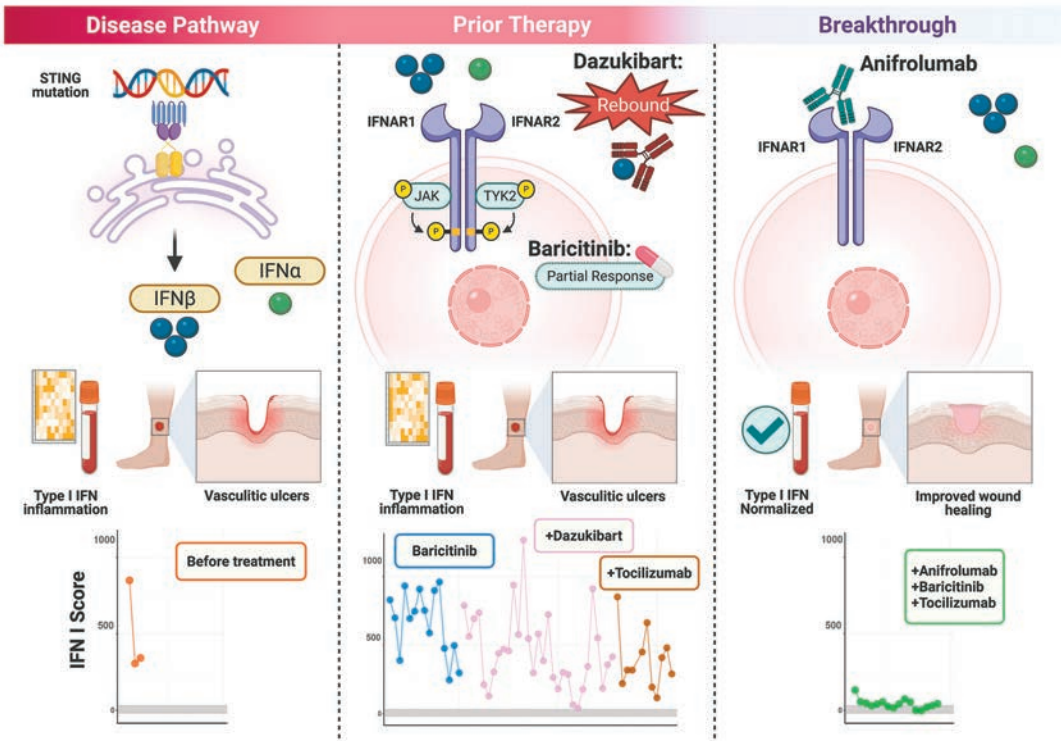

SUMMARY

STING-associated vasculopathy with onset in infancy (SAVI) is a rare and severe autoinflammatory disease driven by excessive type I interferon (IFN) signaling. Standard treatments like JAK inhibitors often provide only partial control of symptoms and can have significant side effects.

In this report, we describe a young adult with SAVI who showed limited clinical improvement with JAK inhibition and with dazukibart, a monoclonal antibody targeting IFNβ. Despite treatment, the patient's IFN signature—an indicator of ongoing disease activity—remained elevated. When therapy was switched to anifrolumab, a monoclonal antibody that blocks the interferon receptor (IFNAR1) and thereby inhibits IFNα and IFNβ signaling, the patient experienced a rapid and sustained improvement. Inflammatory markers and the IFN signature normalized, and the painful vasculitic ulcers began to heal. This patient highlights the importance of measuring the IFN signature to guide personalized treatment and demonstrates the potential of IFNAR1 blockade as a targeted and effective strategy for IFN-driven diseases like SAVI, particularly when responses to JAK inhibitors are incomplete.

KEY POINTS

- SAVI is a rare, severe autoinflammatory disease driven by dysregulated type I IFN with few effective treatment options.
- JAK inhibitors and IFNβ blockade with dazukibart were insufficient to control the disease or to sustainably promote ulcer healing in a case with severe SAVI and vasculitic ulcers.
- The IFN signature (IFN-I score) served as a dynamic biomarker to monitor disease activity and treatment response.
- Treatment with anifrolumab, an anti-IFNAR1 monoclonal antibody, led to sustained suppression of the IFN signature and improved wound healing.
- These findings support IFNAR1 blockade as a promising therapeutic strategy in refractory type I interferonopathies.

Plasma Proteomic Profiles Predict Individual Future OA Risk

Previous studies have identified plasma proteins as potential biomarkers for osteoarthritis (OA). In this issue, Kang et al (p. 981) report data that extend the current literature by building on recent methodological advances in detecting novel plasma proteins related to OA risk. Their model integrates proteomic biomarkers with clinical data, offering a potential tool for risk assessment that can optimize OA management strategies and enhance prevention efforts.

p. 981

The investigators used self-reported data and electronic health records data from the UK Biobank and applied machine learning methods to assess the interplay between multiple proteins and clinical variables. The model employed interpretable artificial intelligence methods to analyze the individual-level effects of various risk biomarkers within a comprehensive set of variables. Their analysis highlighted the significance of specific plasma proteins, particularly collagen type IX alpha 1 chain (COL9A1) and cartilage acidic protein 1 (CRTAC1), in predicting the incidence of OA. In knee OA, the most prominent predictors included CRTAC1 and COL9A1, followed by cartilage oligomeric matrix protein and chromogranin B.

The authors note that pain-related variables, such as knee pain, hip pain, pain in other parts, and painkiller usage, ranked among the top predictors in the OA risk model. They also found that the number of affected joints in OA may influence proteomic profiles. Their identification of clinical variables underscores the multifactorial nature of OA risk and highlights the importance of a comprehensive approach for risk prediction, which the authors hope can inform preventive measures.

Journal Club

A monthly feature designed to facilitate discussion on research methods in rheumatology.

Proinflammatory Dietary Pattern and the Risk of Female Gout

Rai et al, *Arthritis Rheumatol.* 2025;77:1077-1086.

Proinflammatory diets may affect gout risk by modifying the inflammatory response to hyperuricemia and monosodium urate crystal deposition. The authors evaluated whether a proinflammatory dietary pattern is associated with incident gout. They used data from three large US prospective cohorts, the Nurses' Health Study (NHS), NHS II, and the Health Professionals Follow-up Study (total N=218,931). In these cohorts, a validated food frequency questionnaire (FFQ) was used to collect dietary data on participants' habitual diet every 4 years as well as lifestyle factors, diagnoses, and medications. FFQ data were used to calculate Empirical Dietary Inflammatory Pattern (EDIP) scores, a mechanism-based pattern developed to reflect the long-term inflammatory potential of an individual's diet. EDIP was chosen as it was predictive of levels of inflammatory biomarkers in these cohorts. EDIP scores are based on consumption of 18 food groups, 9 proinflammatory (e.g., red/processed meats, refined grains) and 9 anti-inflammatory (e.g., yellow vegetables) groups.

EDIP scores were cumulatively averaged for each participant, and Cox proportional hazards models were used to evaluate the association between quintiles of EDIP and incident physician-diagnosed gout, accounting for age, smoking status, physical activity, hypertension, diuretic use, alcohol consumption, and, among women, postmenopausal status and hormone use. Given the well-established sex differences in major gout risk factors, results were presented separately for women (NHS and NHS II) and men (HPFS). Consumption of a proinflammatory diet (as measured by EDIP scores) was associated with a nearly two-fold increased risk of gout in women; this effect was attenuated with adjustment for BMI, but remained significant. A proinflammatory diet was also associated with gout risk in men, but to a lesser extent.

Questions

1. **What is the difference between a mechanism-based and guideline-based dietary pattern?**
2. **How was the EDIP developed and validated?**
3. **How did the analysis account for changes in dietary intake and covariates over time?**
4. **What is suggested by the association attenuating after further adjustment for BMI?**
5. **What are some key areas for future research into the association between proinflammatory diet and gout risk?**

In this Issue

Highlights from this issue of *A&R* | By Lara C. Pullen, PhD

Secukinumab May Prevent Enthesiophyte Progression in PsA

Mechanical stress can cause patients with psoriatic arthritis (PsA) to experience structural proliferative bony lesions at entheseal sites. Preclinical data suggest that the interleukin (IL)-17 pathway plays a vital role in this damage. To date, one prospective open-label study of the anti–IL-17A monoclonal antibody secukinumab has demonstrated that the number and volume of bone erosion remained stable after 24 weeks, with no progression in enthesiophytes. In this issue, Jin et al (p. 1015) report results of the first randomized clinical trial to investigate the effects of secukinumab on bone damage in PsA using high-resolution peripheral quantitative computed tomography (HR-pQCT). The investigators demonstrate that secukinumab may have a potential benefit in facilitating partial erosion repair and preventing enthesiophyte progression in PsA.

p. 1015

The study included 40 patients (mean age 51 years; 50% male; mean disease duration 4.7 years), who were evaluated at 24 and 48 weeks. The final analysis included 34 patients.

At week 48, the secukinumab group demonstrated a significant reduction in erosion volume compared to baseline, whereas the placebo group showed no changes. The investigators observed a similar trend for enthesiophyte volume changes in the secukinumab group, whereas no differences were noted in the placebo group.

The researchers observed that at baseline, there was only a modest association between joint swelling on physical examination and the presence of erosions or enthesiophytes on HR-pQCT. There were no statistically significant differences in clinical response between secukinumab and placebo groups at week 48.

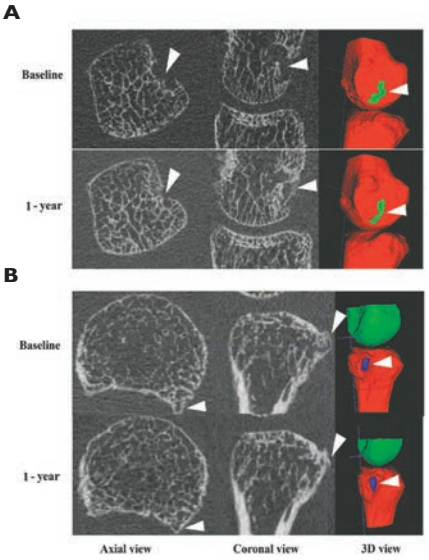

Figure 1. Representative images of changes in erosion and enthesiophyte size over one year. (A) In the secukinumab group, partial healing of erosion is depicted in green. (B) Enthesiophyte size regressed in the secukinumab group as depicted in blue.

Sex a Factor in B Cell Responses in Oligo JIA

Researchers increasingly consider disordered T peripheral helper (Tph)–B cell interactions to be central to disease pathogenesis in rheumatoid arthritis, systemic lupus erythematosus, and, more recently, oligoarticular juvenile idiopathic arthritis (oligo JIA). Previous studies have also found CD21^{lo} B cells with varying phenotypes in patients with immune dysregulation and autoimmunity. In this issue, Lam et al (p. 1092) report the results of their in-depth characterization of intra-articular B cells in the Tph–B cell axis in patients with oligo JIA. They found B cell dysregulation that implicates sex as an important biologic factor in B cell responses in the disease.

p. 1092

Using samples from the joints of patients with oligo JIA, the investigators found distinct populations of B cells with autoreactive features, as well as a broad array of autoantibodies. B cells from synovial fluid and blood of patients with oligo JIA were compared with those from the blood and tonsils of healthy controls; the researchers found an enrichment of memory B (Bmem) cells as well as a heterogeneous subset of CD21^{lo} B cells. The preferential accumulation of CD21^{lo} B cells in synovial fluid of children with oligo JIA was not found in their peripheral blood or secondary lymphoid organs.

Moreover, compared to male patients, these abnormalities were more pronounced in female patients with oligo JIA, who had a greater proportion of intra-articular Tph cells that expressed B cell help factors, as well as Bmem cells, plasmablasts, and age- and autoimmune-associated B cells. The investigators found that these sex differences in B cells found in the joints could not be explained by other disease features such as age at onset, antinuclear antibody status, or severity.

Bmem cells in synovial fluid from female patients also differed from blood Bmem cells in that they displayed characteristics of autoreactivity, including longer complementarity-determining region 3 lengths and increased usage of autoreactive B cell receptor gene segments.

Plasma Proteomic Profiles Predict Individual Future OA Risk

Previous studies have identified plasma proteins as potential biomarkers for osteoarthritis (OA). In this issue, Kang et al (p. 981) report data that extend the current literature by building on recent methodological advances in detecting novel plasma proteins related to OA risk. Their model integrates proteomic biomarkers with clinical data, offering a potential tool for risk assessment that can optimize OA management strategies and enhance prevention efforts.

p. 981

The investigators used self-reported data and electronic health records data from the UK Biobank and applied machine learning methods to assess the interplay between multiple proteins and clinical variables. The model employed interpretable artificial intelligence methods to analyze the individual-level effects of various risk biomarkers within a comprehensive set of variables. Their analysis highlighted the significance of specific plasma proteins, particularly collagen type IX alpha 1 chain (COL9A1) and cartilage acidic protein 1 (CRTAC1), in predicting the incidence of OA. In knee OA, the most prominent predictors included CRTAC1 and COL9A1, followed by cartilage oligomeric matrix protein and chromogranin B.

The authors note that pain-related variables, such as knee pain, hip pain, pain in other parts, and painkiller usage, ranked among the top predictors in the OA risk model. They also found that the number of affected joints in OA may influence proteomic profiles. Their identification of clinical variables underscores the multifactorial nature of OA risk and highlights the importance of a comprehensive approach for risk prediction, which the authors hope can inform preventive measures.

Journal Club

A monthly feature designed to facilitate discussion on research methods in rheumatology.

Proinflammatory Dietary Pattern and the Risk of Female Gout

Rai et al, *Arthritis Rheumatol.* 2025;77:1077-1086.

Proinflammatory diets may affect gout risk by modifying the inflammatory response to hyperuricemia and monosodium urate crystal deposition. The authors evaluated whether a proinflammatory dietary pattern is associated with incident gout. They used data from three large US prospective cohorts, the Nurses' Health Study (NHS), NHS II, and the Health Professionals Follow-up Study (total N=218,931). In these cohorts, a validated food frequency questionnaire (FFQ) was used to collect dietary data on participants' habitual diet every 4 years as well as lifestyle factors, diagnoses, and medications. FFQ data were used to calculate Empirical Dietary Inflammatory Pattern (EDIP) scores, a mechanism-based pattern developed to reflect the long-term inflammatory potential of an individual's diet. EDIP was chosen as it was predictive of levels of inflammatory biomarkers in these cohorts. EDIP scores are based on consumption of 18 food groups, 9 proinflammatory (e.g., red/processed meats, refined grains) and 9 anti-inflammatory (e.g., yellow vegetables) groups.

EDIP scores were cumulatively averaged for each participant, and Cox proportional hazards models were used to evaluate the association between quintiles of EDIP and incident physician-diagnosed gout, accounting for age, smoking status, physical activity, hypertension, diuretic use, alcohol consumption, and, among women, postmenopausal status and hormone use. Given the well-established sex differences in major gout risk factors, results were presented separately for women (NHS and NHS II) and men (HPFS). Consumption of a proinflammatory diet (as measured by EDIP scores) was associated with a nearly two-fold increased risk of gout in women; this effect was attenuated with adjustment for BMI, but remained significant. A proinflammatory diet was also associated with gout risk in men, but to a lesser extent.

Questions

1. **What is the difference between a mechanism-based and guideline-based dietary pattern?**
2. **How was the EDIP developed and validated?**
3. **How did the analysis account for changes in dietary intake and covariates over time?**
4. **What is suggested by the association attenuating after further adjustment for BMI?**
5. **What are some key areas for future research into the association between proinflammatory diet and gout risk?**

Arthritis & Rheumatology

An Official Journal of the American College of Rheumatology
www.arthritisrheum.org and wileyonlinelibrary.com

Cover design: Todd Machen

This journal is printed on acid-free paper.

Arthritis & Rheumatology

An Official Journal of the American College of Rheumatology
www.arthritisrheum.org and wileyonlinelibrary.com

VOLUME 77 • August 2025 • NO. 8

Cover image: The cover features multi-immunochemistry staining results of CD8 (red) and PD-1 (green) in the labial gland of a patient with Sjögren disease. This image captures a dense infiltration of CD8+ T cells, which express high levels of PD-1. These cells exhibit significant morphologic distortion and appear tightly adhered to nearby acinar and ductal cells.

Arthritis & Rheumatology
Vol. 77, No. 8, August 2025, pp 955–965
DOI 10.1002/art.43118

American College of Rheumatology
Empowering Rheumatology Professionals

REVIEW

The Gut Microbiome in Hyperuricemia and Gout

Robert Terkeltaub[1] and Dylan Dodd[2]

Humans develop hyperuricemia via decreased urate elimination and excess urate production, consequently promoting monosodium urate crystal deposition and incident gout. Normally, approximately two-thirds of urate elimination is renal. However, chronic kidney disease (CKD) and other causes of decreased renal urate elimination drive hyperuricemia in most with gout. This places more demand on elimination of urate via the gut, where diet, purine metabolism, and microbiota intersect. Heritable impairment of urate transport into the gut is common and promotes hyperuricemia, renal urate overload, and early-onset and palpable tophaceous gout phenotypes. *Lactobacilli*, by sequestering and modifying ambient purines, are being studied for the potential to suppress diet-induced urate generation and associated gout flares. Landmark preclinical studies recently revealed much higher-capacity urate-lowering effects of diverse, obligate, and facultative anaerobic human and mouse gut microbiota (predominantly of the Bacillota phylum) termed purine-degrading bacteria (PDB). A conserved gene cluster in PDB drives urate conversion to lactate or anti-inflammatory short-chain fatty acids. When mice are rendered deficient in hepatic uricase to mimic human uricase absence, microbiota depletion rapidly elevates both cecal and serum urate, which is reversible by PDB administration. In healthy human volunteers with normal renal function, antibiotic-induced gut microbiota depletion decreases the urate-lowering gene cluster unique to PDB and elevates fecal urate. Also, prior exposure to antibiotics with anaerobic coverage has been linked to heightened incident gout risk. Notably, intestinal dysbiosis that includes Bacillota depletion has been observed in gout cohorts. Therefore, the capacity of diverse gut bacterial strains to biochemically compensate for human limits in urate disposition suggests novel probiotic treatment approaches for gout with inadequate pharmacologic control of both flares and hyperuricemia. This is particularly so for severe CKD, which limits the options and maximal doses for use of conventional oral urate-lowering drugs.

Introduction

Humans are predisposed to hyperuricemia and gout in large part because of the inactivation, early in hominid evolution, of the gene for uricase, which degrades urate to allantoin. Gout is a growing public health problem globally, and hyperuricemia and gout prevalence in US adults were most recently estimated at ∼21% and 5%, respectively.[1] Because decreased urate elimination and excess urate production foster hyperuricemia, approved oral urate-lowering therapy (ULT) drugs targeting these mechanisms, and recombinant intravenous PEGylated uricase in the most severe forms of the disease, are the mainstay of disease-modifying management in gout.[2] Nevertheless, there is room for improvement of oral urate-lowering pharmacotherapy, particularly when urate elimination is compromised.[2]

The processes and translational biology of renal urate transport and disposition by the nephron are well understood.[2,3] Approximately two-thirds of urate elimination is renal in healthy individuals. Correspondingly, decreased renal urate elimination is by far the most common causative factor for hyperuricemia in gout,[4] thereby increasing the burden on intestinal urate elimination. Normally, the gut eliminates approximately one-third of urate, a proportion that can rise to nearly two-thirds in association with progressive compromise of renal function. Yet the limits on the intestinal compensatory effects for hyperuricemia mediated by renal dysfunction and excess urate production commonly predispose patients to hyperuricemia in those disorders.[5]

In this narrative review, we focus on impactful and novel discoveries on intestinal urate homeostasis and the role of gut microbiota and associated translational ULT opportunities. The gut

Supported by the National Center for Complementary and Integrative Health, NIH (grant R01-AT0-11396 to Dr Dodd) and the National Institute of General Medical Sciences, NIH (grant R35-GM1-42873 to Dr Dodd).

[1]Robert Terkeltaub, MD: University of California San Diego, La Jolla, California; [2]Dylan Dodd, MD, PhD: Stanford University, Stanford, California.

Author disclosures are available at https://onlinelibrary.wiley.com/doi/10.1002/art.43118.

Address correspondence via email to Robert Terkeltaub, MD, at rterkeltaub@health.ucsd.edu.

Submitted for publication October 22, 2024; accepted in revised form January 8, 2025.

microbiome includes bacteria, fungal mycobiota,[6] viruses,[7] and archaea,[8] all of which can metabolize purines. The discussion concentrates on intestinal bacteria, which comprise the vast majority of gut microbiota.

How intestinal urate metabolism and transport affect serum urate

Dietary purines account for approximately a third of daily urate production,[9] obliging the gut to process a considerable burden of purine nucleotides and nucleosides. The nucleotides are comprised of a nitrogenous purine base (eg, adenine, guanine, hypoxanthine, and xanthine), a sugar molecule, and a phosphate group (eg, ATP and guanosine monophosphate). Purine nucleosides are defined by a purine base attached to a sugar molecule. Processing of the dietary purine load starts mainly in the duodenum, where pancreatic nucleases and phosphodiesterases depolymerize dietary chains of nucleotides to mononucleotides and polynucleotides, which small intestinal nucleotidases and phosphatases further process to absorbable purines.[9] Concentrative nucleoside transporters, expressed on the apical (luminal) side of the intestinal epithelium (Figure 1), move the purine nucleosides.[9,10] Added to the dietary purine load are nucleotides and purines from the turnover of intestinal epithelial cells, whose half-life is limited to a few days. Selective and principally upper intestinal transporters participate in purine transit to the liver,[11] where abundant urate is produced and released into the circulation (Figure 1). In addition, enterocyte xanthine oxidase has the capacity to generate urate in the gut.[12]

How the gut eliminates urate had long remained a "black box," assumed to be driven via fecal urate excretion and the multitude of secreted microbial uricases.[13] Genetic, molecular, and clinical studies in the last 15 years advanced this field by characterizing the enterocyte-expressed, high-capacity urate

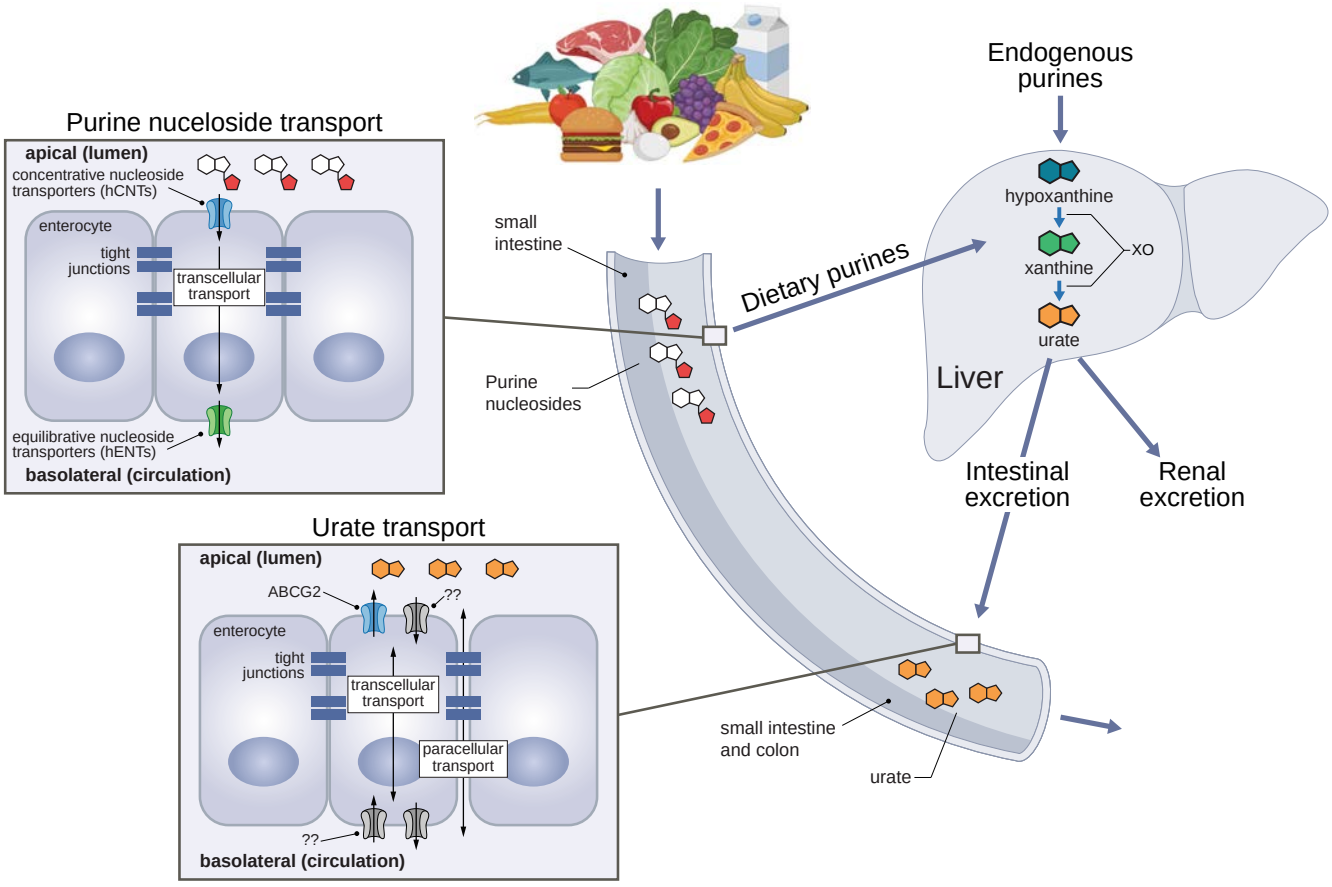

Figure 1. Role of the gastrointestinal tract in regulating serum urate. Dietary purine nucleosides are absorbed by enterocytes through human concentrative nucleoside transporters (hCNTs). Excess purine bases from the diet or from endogenous nucleic acid turnover are transported to the liver, where xanthine oxidase (XO) in hepatocytes converts them into urate. Circulating urate is then eliminated either by the kidneys or through the intestines. The transporter ATP-binding cassette superfamily G member 2 (ABCG2), located on the apical surface of enterocytes, secretes urate into the intestinal lumen. Although several other transporters are also present in enterocytes, their specific roles in urate elimination or reabsorption remain unclear. Urate in the intestines appears to be reabsorbed via active enterocyte transport and/or paracellular urate diffusion. Hence, as microbial degradation of urate increases net urate elimination, intestinal urate concentration can reflect equilibrium between secretion into the gut lumen and reabsorption from the gut into the circulation.

transporter ATP-binding cassette superfamily G member 2 (ABCG2).[14] Intestinal epithelial cell ABCG2 transports urate into the gut. ABCG2 is robustly expressed along the length of the human small intestine and colon, with the highest levels in colonic enterocytes. Diminished gut urate elimination via heritable decrease in ABCG2 nucleotide-binding domain stability promotes hyperuricemia.[5,15] *ABCG2* single-nucleotide polymorphism rs2231142, which encodes ABCG2 Q141K, is common, with allele frequency particularly high (~0.30–0.50) in many East and South Asian populations.[15] *ABCG2* rs2231142 is associated with early-onset and tophaceous clinical phenotypes of gout.[16] *ABCG2* rs2231142 promotes the renal urate overload hyperuricemia phenotype in gout, previously mistaken in many because of elevated urinary urate and urate overproduction.[17]

How gut microbiota regulate serum urate

The relationship of gut microbiota with intestinal urate is symbiotic.[18,19] Gut bacteria outnumber intestinal epithelial cells,[20] thereby buttressing the potential extent of compensation for the lack of human uricase by purine-degrading bacteria (PDB).[18,19] Humans have only ~20,000 genes, whereas the human gut microbiome harbors millions of unique genes and encodes thousands of biochemical pathways. Although the functions of most gut microbial genes remain undefined, the gut microbiome augments human biochemistry by consuming or producing many metabolites. Some major points are presented as follows:

- Human microbiota outnumber enterocytes in the gut.
- Gut microbiota genes vastly outnumber human genes.
- ~15%–20% of human gut bacteria consume urate anaerobically and, in some cases, other purines.
- Obligate anaerobic PDB grow on urate and recycle purines for carbon and nitrogen in a symbiotic host–microbiota relationship.
- Gut obligate anaerobic PDB pathways counterbalance the limits of human urate metabolism because of the absence of uricase.
- Most human gut microbiota reside in the deeply anaerobic colon environment.
- Gut obligate anaerobic PDB use a urate-inducible gene cluster encoding novel enzymatic pathways to convert urate to xanthine or to lactate and short-chain fatty acids (SCFAs).
- Microbial uricases are oxygen dependent and likely have limited activity in the anaerobic gut.
- Some *Lactobacillus* strains cleave purine nucleosides and secrete free nucleobases.
- Germ-free conditions and antibiotics with anaerobic coverage promote preclinical hyperuricemia, which is reversed by obligate anaerobic PDB.
- Gut dysbiosis is associated with gout.
- Prior exposure to antibiotics with anaerobic coverage is a risk factor for developing gout.
- Gut microbiota can increase intestinal ABCG2 expression and influence multiple common gout comorbidities that affect renal urate elimination.
- Gut obligate anaerobic PDB have antiatherogenic effects in a preclinical disease model by undefined effects suggested to include purine degradation.

There is a sharp oxygen gradient across the gut (Figure 2). The small intestinal microbiome is dominated by aerobic microbes, and aerobic microbes able to survive in anaerobic conditions (ie, facultative anaerobes) (Figure 2). Microbial uricases, from a variety of strains in proximal intestinal niches, further augment human urate homeostasis.[21]

The densities of small intestinal microbiota are relatively low. Moving distally toward the colon, obligate anaerobic bacteria become dominant, and bacteria community densities also become remarkably high (Figure 2).[22] As such, the majority of bacteria colonizing the intestine live in an anaerobic milieu.[23] Accordingly, the biochemical pathways employed by those bacteria are entirely different than human pathways. In addition, there is no uricase enzyme in the genomes of anaerobic bacteria because uricases must employ molecular oxygen.[21]

The gut microbiome impacts hyperuricemia in part by modulating several acquired, common gout comorbidities that perturb renal elimination of urate. These disorders include chronic kidney disease (CKD), hypertension, obesity, metabolic syndrome, and type 2 diabetes mellitus.[24,25] Gut microbiota also regulate intestinal enzymes that process nucleotides and purines to absorbable nucleosides and bases.[26] How gut urate disposition adapts to decreased renal urate elimination reflects incompletely characterized remote sensing and signaling,[27] modulated by ABCG2 and other renal and gut anion transporters, and is associated with regulation of gut microbiome composition.[28]

Gut PDB in urate metabolism

In 2023, landmark research from two independent laboratories first identified a gene cluster that encodes enzymes that consume urate and other purines (Figure 3A) and is widely distributed in PDB of different phyla in the mouse and human gut.[18,19] The identified PDB pathways operate at high capacity under anaerobic conditions. Studies of several hundred different human gut bacterial isolates revealed that normally, ~15% to 20% of our gut bacteria consume urate.[18,19] Most human gut PDB are members of the Bacillota phylum,[18,19] which comprises mostly gram-positive bacteria and includes microbes that survive in the presence or absence of oxygen (facultative anaerobes) such as *Lactobacilli*.[29]

Landmark preclinical studies have revealed that antibiotic treatment covering anaerobes induce rapid and marked elevation of cecal and circulating urate in uricase-deficient mice.[18]

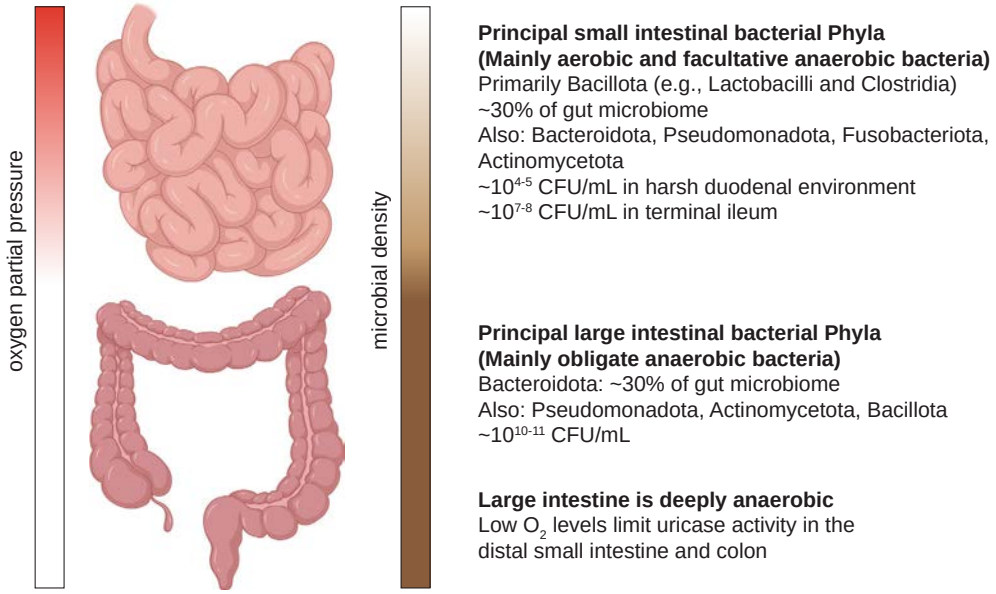

Figure 2. Distribution of the gut microbiome in healthy humans. The healthy gastrointestinal tract displays an oxygen gradient from proximal to distal with the large intestine being highly anaerobic. In the distal small intestine and colon, the low oxygen levels result in reduced activity of uricase and other oxygen-dependent enzymes. Bacterial density increases sharply along the gastrointestinal tract, with most bacteria residing within the terminal ileum and colon. The major bacterial phyla present in both the small and large intestines are listed. CFU, colony-forming units.

Marked plasma urate elevation develops in wild-type mice housed in germ-free conditions, treated with the uricase inhibitor potassium oxonate, and fed either standard or urate-enriched chow.[18,19] Also, the combination of potassium oxonate and urate-enriched chow induces acute kidney injury in wild-type germ-free mice.[18] The elevation of plasma urate concentration is lessened by colonization with urate-consuming anaerobic PDB of varied taxa.[18,19]

New human clinical research relevant to the gut microbiome and gout has included retrospective analysis in a sizable Stanford University cohort.[18] It was discovered that the risk of incident gout was elevated by ~30% (after propensity score matching) in those with prior exposure to clindamycin versus trimethoprim/sulfamethoxazole, which lacks anaerobic coverage.[18] Serum urate was not measured in that study.

The controlled feeding study Food and Resulting Microbial Metabolites (FARMM)[30] and its subsequent reanalysis[18] assessed consequences on metabolites and gut microbiota genomes (metagenomes) of short-term treatment with oral antibiotics (vancomycin and neomycin) and polyethylene glycol (Abx/PEG).[30] Thirty healthy volunteers with normal renal function were studied, with the cohort divided by three distinct diets (fiber-free synthetic diet given exclusively by enteral nutrition [EEN] compared with vegan and omnivore diets). Paired analyses revealed the association of microbiota depletion by the antibiotics with subsequent rapid and marked fecal urate elevation overall (by ~40%–50% on average).[18,30] Shortly after antibiotic administration, there was significantly decreased abundance, in the EEN feeding group, of the conserved gene cluster unique to PDB in intestinal metagenomes.[18,30]

The publicly available FARMM database (https://www.metabolomicsworkbench.org/data/DRCCMetadata.php?Mode=Project&ProjectID=PR001024) revealed a trend for marginally higher plasma urate after antibiotic administration irrespective of each diet in the small overall study population. However, extrapolating FARMM study data to hyperuricemia and gout has been limited by the small size of the cohort, compounded by subdivision of participants into three dietary groups.[30] In addition, the preserved renal function in all FARMM participants supported physiologic renal elimination of potential excesses in urate reabsorbed from the gut.[30] The FARMM study did not include more complex analysis of the intestinal abundance of the unique PDB urate-consuming gene cluster relative to serum urate.

The FARMM study demonstrated selective linkage of low dietary fiber intake with protracted recovery of microbiota involved in gut urate homeostasis after antibiotic-induced alteration of gut microbiota.[18,30] This finding is relevant to both public health and gout in the United States. There is particularly low overall consumption in the United States of dietary fiber, which nourishes healthful microbiota and whose degradation by bacteria generates SCFAs. In 2022 alone, there were over 236 million US antibiotic prescriptions dispensed from outpatient pharmacies, with close to 30% of antibiotic prescriptions judged to be medically unnecessary. Clearly, prospective studies will be needed to directly assess the effects of antibiotic prescription on the gut microbiome, hyperuricemia, and gout.

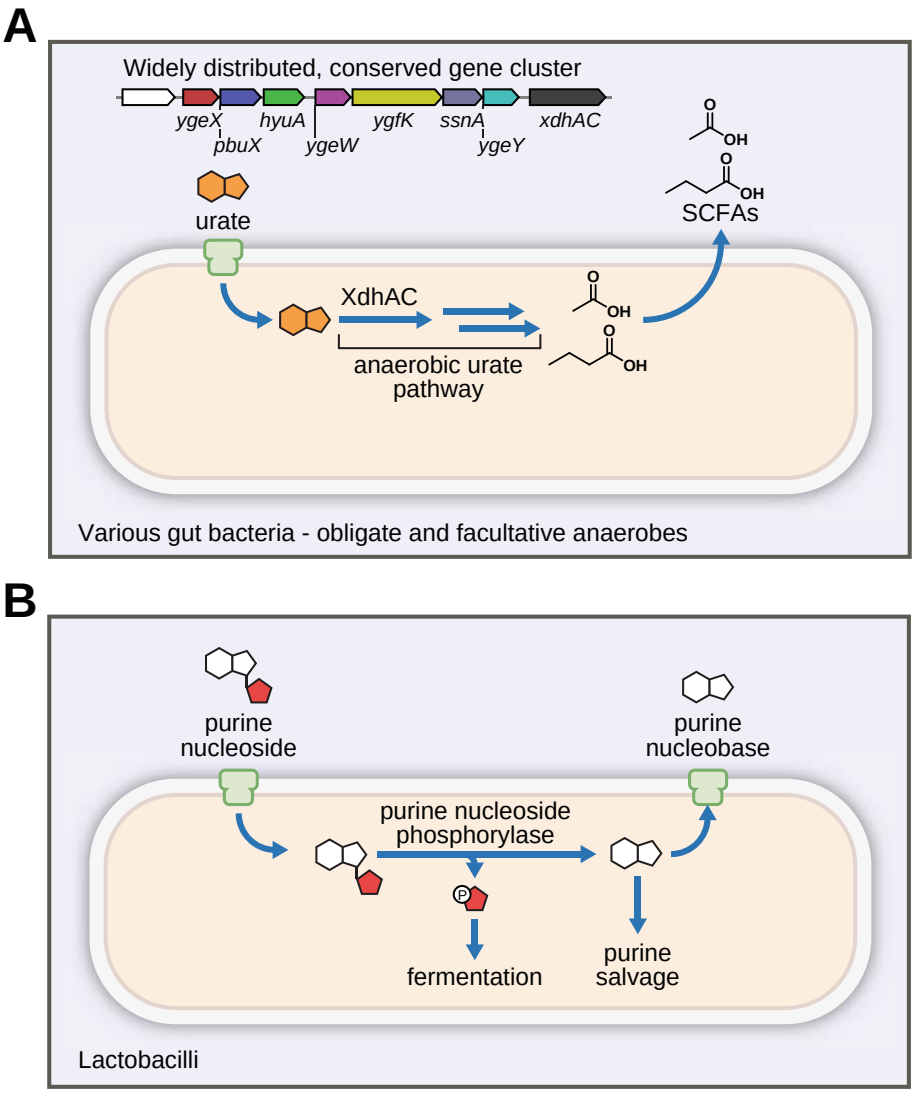

Figure 3. Distinct actions on urate and other purines by anaerobic bacteria and *Lactobacilli* in the human gut. (A) Certain strains of facultative and obligate anaerobic PDB contain a conserved gene cluster that encodes a novel pathway for urate degradation. These microbes convert urate to SCFAs through enzymes encoded by the gene cluster that include a xanthine dehydrogenase homolog (XdhAC) not expressed by humans. (B) Many *Lactobacilli* strains have lost the ability to synthesize purines de novo but use a strategy to remove purines from the environment, have purine nucleoside phosphorylase activity, and cleave purine nucleosides (such as inosine, adenosine, and guanosine), to produce ribose-1-phosphate and purine bases. The sugar phosphate can be fermented with purine bases either secreted from the cell or used as precursors for nucleic acid synthesis through purine salvage pathways. PDB, purine-degrading bacteria; SCFA, short-chain fatty acid. Color figure can be viewed in the online issue, which is available at http://onlinelibrary.wiley.com/doi/10.1002/art.43118/abstract.

Gut dysbiosis in gout

Over the last decade, multiple metagenomic human studies from countries, including China and Mexico, have characterized gut dysbiosis in gout and hyperuricemia.[31–37] The dominant microbiota in the healthy human gut are members of the Bacteroidota and Bacillota phyla, each accounting for ~30% of healthy human microbiome content (Figure 2).[26,38,39] In people with gout, distinctions in the gut microbiome compared to healthy controls dysbiosis include depletion in Bacillota, and decreased diversity and in urate-degrading microbiome functions, as well as increases in carbohydrate metabolism.[31] Conversely, there is enrichment of the Bacteroidota phylum, whose members lack PDB. Gout also has been associated with depletion of gut bacteria that produce the anti-inflammatory SCFA butyrate and decreased uricase-expressing *Enterobacter* strains. Some major features include the following:

- decrease in diversity and urate-degrading and purine metabolic microbiome functions;
- depletion of Bacillota phylum members that comprise the majority of PDB;
- enrichment in Bacteroidetes phylum members, which do not include PDB;

- depletion of uricase-expressing *Enterobacter* species;
- depletion of bacteria producing the anti-inflammatory SCFA butyrate;
- sustained urate-lowering and anti-inflammatory gout treatment partially restoring gut microbiota; and
- patient with gout intestinal metagenomes being more similar to those in ankylosing spondylitis and rheumatoid arthritis than obesity and type 2 diabetes mellitus.

Surprisingly, gout intestinal metagenomes have been reported to be more similar to those in rheumatoid arthritis and ankylosing spondylitis than to obesity and type 2 diabetes mellitus.[36] Also, sustained pharmacologic oral ULT and gout-directed anti-inflammatory therapy has been reported to partially restore healthy gut microbiota in people with gout, by unclear mechanisms.[35,36] Hence, there remains much to be learned about the factors inducing and mediating gut dysbiosis in gout.

Distinct effects of Bacillota and *Lactobacilli* on urate metabolism and the gut

Diverse strains of Bacillota and other anaerobic PDB sense urate, thereby allowing ambient urate concentration to regulate urate-consuming gene expression in PDB.[18,19] Furthering the symbiotic relationships of PDB, urate metabolism, and intestinal health, urate degradation provides carbon, nitrogen, and energy for anaerobic PDBs, and end products of urate degradation can be used as fuel by intestinal epithelial cells.[18,19] PDB also can exert beneficial effects that limit gut inflammation and mucosal permeability to toxins, such as conversion of urate to anti-inflammatory SCFAs.[18]

The conserved urate-inducible gene cluster *ygeX*, *ygeY*, *ygeW*, *ygfK*, and *ssnA*, widely distributed in varied PDB taxa, is required for SCFA generation (Figure 3A).[18,19] This gene cluster encodes a variety of currently uncharacterized enzymes with the capacity to reduce and enzymatically cleave urate (Figure 3A).[18,19] This urate-inducible gene cluster is a hallmark of gut PDB and is not present in *Lactobacilli*, which, correspondingly, do not degrade urate.[18] PDB also are enriched in *xdhAC*, which is distinct from human xanthine oxidoreductase[40,41] and likely initiates urate metabolism (Figure 3A).[18]

Many *Lactobacilli*, which predominantly reside in proximal intestinal niches,[42] lack complete pathways for de novo purine synthesis and thus are dependent on exogenous purines for survival and growth.[43] These microbes primarily take up and sequester purine nucleosides, which are then broken down by nucleoside phosphorylases into a fermentable energy source (the sugar ribose-1-phosphate) and into the free purine bases adenine, hypoxanthine, and guanine. *Lactobacilli* that process purine nucleosides demonstrate enrichment of *hprt* and a varying number of other purine salvage pathway enzymes.[44] The purine bases, via purine salvage, play a central role in satisfying *Lactobacilli* demands for nucleic acid synthesis, with excess purine bases secreted outside of the microbe (Figure 3B).[43] On the other hand, expression of purine salvage pathway genes heightens the sensitivity of *Lactobacilli* and other aerobic bacteria to antibiotics.[45]

Prospects and potential indications for novel PDB probiotics in gout

Probiotics will not displace the current mainstays of oral and parenteral urate-lowering gout pharmacotherapy. Nonetheless, there is substantial unmet need in gout for new, approved urate-lowering therapeutics with high patient acceptance. Specifically, poor adherence to urate-lowering pharmacotherapy is remarkably common and impedes success in treating people with poorly controlled gout and hyperuricemia.[46] By comparison, probiotic nutraceuticals are immensely popular, with an annual US market size of close to 20 billion dollars. Hence, patient acceptance could be substantial for effective oral ULT probiotic approaches delivered in foods, gels, or other means such as capsules (Figure 4). Such therapies could go hand in hand with productive diet modifications in gout.

In stage IV CKD, the majority of urate disposal becomes intestinal, the risk of incident gout increases up to seven-fold, conventional urate lowering with allopurinol and febuxostat cannot be dose-optimized, and uricosurics are contraindicated.[2] Hence, PDB probiotics might become particularly useful in complementing conventional oral ULT drugs in stage IV CKD. Because PDB suppress atherogenesis in susceptible mice,[19,47] testing candidate PDB strains in patients with gout and comorbid atherosclerosis would be cogent. Similarly, it would be of interest to assess potential effects of PDB in those with both gout and comorbidities mediated by purine metabolism and inflammation, with a prime example being metabolic dysfunction–associated hepatic steatohepatitis.[48]

Although the US Food and Drug Administration has approved two fecal microbiota–derived products for treating recurrent *Clostridioides difficile* infections, no probiotic therapies have received approval. Stringent challenges stand in the way of oral delivery and gut entrenchment of PDB to safely and efficiently "manufacture in house" intestinal ULT.[22,49–51] Inherent limitations of oral PDB probiotic therapy include PDB oxygen sensitivity, probiotic processing measures, and stability in handling and in intestinal transit conditions to anaerobic intestinal niches.[18,19,47] Rapidly evolving approaches for optimizing storage, distribution, and oral delivery of probiotics into the gut, including administration in extracellular vesicles and nanoparticles, could solve many of these issues.[50,51]

Urate-degrading genes also may be engineered into probiotic strains, enabling urate degradation to SCFAs in a gut-optimized nonpathogenic microbial chassis, such as *Escherichia coli* Nissle, which is used as a probiotic to treat a variety of gastrointestinal disorders.[52] Regardless, oral PDB therapeutics

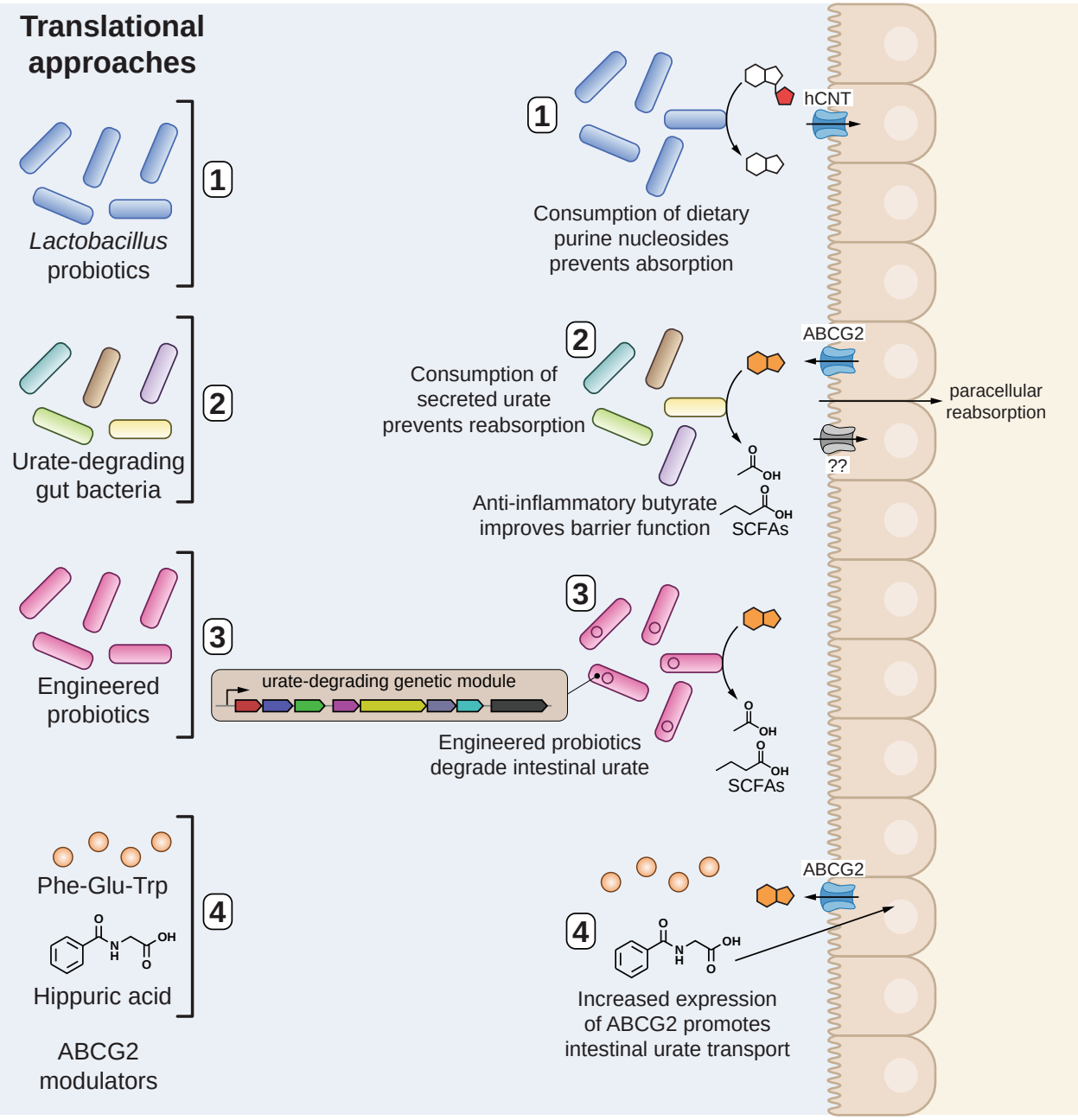

Figure 4. Potential urate-lowering approaches that employ or modulate gut microbiota and their molecules. (1) Consumption of dietary purine nucleosides by a variety of probiotic Lactobacilli prevent purine nucleoside absorption into circulation by enterocytes. (2) PDB convert urate to SCFAs. Degrading intestinal urate limits its reabsorption by paracellular transport or other as-yet undefined absorptive transporters. Production of the anti-inflammatory SCFA butyrate supports physiologic gut barrier function. (3) Urate-degrading genes may be engineered into probiotic strains, enabling urate degradation to SCFAs in a gut-optimized microbial chassis. (4) Diet-derived or microbe-derived metabolites, exemplified by hippuric acid, induce expression of ABCG2 by enterocytes, thereby promoting beneficial intestinal urate transport. ABCG2, ATP-binding cassette superfamily G member 2; hCNT, human concentrative nucleoside transporter; PDB, purine-degrading bacteria; SCFA, short-chain fatty acid. Color figure can be viewed in the online issue, which is available at http://onlinelibrary.wiley.com/doi/10.1002/art.43118/abstract.

must overcome the "colonization barrier" imposed by resident gut microbiota,[53] which limits achievement of critical mass for physiologic impact to restore dysbiosis.[54] Probiotics also can introduce gastrointestinal side effects (eg, flatulence, nausea), nosocomial infection, and antibiotic resistance genes.

Scaling of urate-lowering microbiota-associated metabolites and proteins to the human gut, an alternative to probiotic therapy, also has significant hurdles. Studies of the ULT potential of orally ingested uricases have been informative. Specifically, the robustness of preclinical results for urate lowering via ingestion

of encapsulated uricase[13] were not replicated by an exploratory clinical trial effort in healthy humans.[55] In a recent preclinical study, an oral intestinally explosive hydrogel microsphere formulated to deliver internal uricase and dopamine to the small intestinal mucosa lowered serum urate.[56] However, this would be an unwieldy approach in humans.

Microbiota transplantation into the gut is an alternative to oral ingestion of PDB probiotics. In this context, an uncontrolled, single center pilot study of 11 patients with gout in China recently tested the urate-lowering potential of colonic microbiota transplantation into healthy patients with hyperuricemia and gout.[57] The study employed freshly isolated, washed, and ultrafiltered healthy donor fecal microbiota. Results were somewhat encouraging, given significant mean serum urate reduction from ~10 mg/dL at baseline to ~8 mg/dL at 6 months, in association with decreased gout flares.[57] Nevertheless, a subsequent, large case series of participants with wide-ranging diagnoses and serum urate levels had excessive participant dropout and failure to maintain significant urate lowering at six months.[58] Essentially, the cumbersome nature of fecal microbiota transplantation is unlikely to meet with high patient acceptance in gout.

Lactobacillus-containing probiotics for gout

In reality, multiple prebiotics, probiotic nutraceutical diet supplements, and foods affecting gut urate homeostasis are already commercially dispensed. Gram-positive *Lactobacilli* and also *Bifidobacteria* (of the Actinomycetota phylum) meeting "generally recognized as safe" strain and health-promoting probiotic criteria[59,60] are employed in production and processing of yogurt, other dairy products, and many fermented foods. Such bacteria have high tolerance for the procedures involved in processing, storage and delivery. Yogurt induces increases in *Lactobacillus* and *Bifidobacterium* strains and increased alpha diversity of the gut microbiome.[61] In addition, prebiotics such as the whey protein peptide Pro-Glu-Trp may promote beneficial gut urate homeostasis changes via urate transport and how *Lactobacilli* and multiple other gut microbes tolerate stress.[62]

The association of low-fat dairy product consumption with urate lowering and reduced risk of incident gout[63] has been attributed to uricosuric effects of the milk proteins such as casein and lactalbumin.[64] However, some *Lactobacillus* strains from a variety of fermented foods, milk, or introduced in the processing of milk to other dairy items, also have lowered serum urate in preclinical models in which high microbial dosages were generally administered; urate-lowering mechanisms included modulation of purine metabolism and ABCG2 and reduction of fructose-induced hyperuricemia (Figure 3B).[65–68] Interestingly, a urate-lowering yogurt containing *Lactobacillus gasseri* PA-3 is marketed in Japan.

Limitation of high dietary purine ingestion–associated surges in serum urate that promote gout flares[69] has been supported in some preclinical investigation and ultimately could be an indication for oral *Lactobacilli* probiotic treatment. However, results reported to this date have been mixed in exploratory oral probiotic ULT clinical trials in patients with gout and hyperuricemia. Several trials assessed *Lactobacillus* "safe strains" delivered by yogurt or a small packet, with or without added *Bifidobacteria*, studying only 15 to 20 participants per treatment group.[70–72] Gout flares, recorded over the six-month study period, were significantly less frequent in one study, in which serum urate was decreased by approximately 1 mg/dL.[70] Still, maximum serum urate lowering varied from only ~0.5 to 1 mg/dL.[70–73] One trial did not include either placebo or yogurt lacking the tested *Lactobacillus* strain,[73] and results for serum urate lowering were not statistically significant in two trials using *Lactobacillus gasseri* PA-3.[71,72]

Broader questions and opportunities

Although discovery of human gut–resident PDB has raised opportunities for boosting human intestinal urate homeostasis, substantial questions remain. For example, markedly increased sugar consumption in the United States, averaging over 100 pounds annually by some estimates, has been accompanied by increasing gout prevalence.[74] In the complex, oxygen-depleted gut niches colonized by PDB, fructose provides PDB with an alternative carbon source, preferred over purines for energy generation that supports bacterial growth.[19] At the same time, fructose limits anaerobic urate degradation by PDB by suppressing transcription of the bacterial purine-degrading genes.[19] Because excess dietary fructose transits through the upper small intestine to anaerobic intestinal niches,[75] examination of dietary fructose effects specific for the urate-lowering capacity of PDB is warranted.

Gateways to improving intestinal urate homeostasis include up-regulation of the apical-localized enterocyte excretory transporter ABCG2 via prebiotics,[62] probiotics,[67,76] and a variety of diet-furnished and microbiota-derived metabolites.[77] In this light, hippuric acid derived from *Alistipes indistinctus*, a gram-negative, anaerobic bacterium of the Bacteroidota phylum, induces ABCG2 transcription and enterocyte apical membrane localization (Figure 4).[77] In a mouse model of diet-induced elevation of serum urate, *A indistinctus* supplementation by gavage increased intestinal urate excretion, and decreased the serum urate level to baseline. Notably, the risk of hyperuricemia was inversely associated with gut *A indistinctus* amounts in two independent human cohorts.[77] In addition, prolonged dietary hippuric acid significantly lowered serum urate by markedly increasing overall urate excretion.[77]

There are large gaps in understanding urate transporter physiology at the lymphatic- and the portal venous and systemic venous circulation–interfacing basolateral surface of enterocytes.[78–81] The marked hyperuricemia in germ-free, uricase-deficient mice fed urate-enriched chow[18] buttresses past, grossly observational

studies that support substantial bidirectional urate transport across the gut epithelium and back into the circulation. It is unclear whether the mechanism is via paracellular urate diffusion between enterocytes and/or by active enterocyte transporters. Regardless, intestinal urate concentration could reflect equilibrium between secretion into gut lumen and reabsorption from gut into circulation. As such, core regulation of serum urate may be via the rate of urate consumption by PDB relative to the rate of urate reabsorption from the gut into the circulation (Figure 1). We do not know whether resident gut microbiota and individual probiotics directly affect reabsorption of intestinal urate. Conversely, most PDB employ urate for growth, and we do not know how deficient urate excretory transport by ABCG2 affects the gut microbiome and whether ABCG2 deficiency affects the capacity of PDB probiotics to reverse gut dysbiosis.

It would be unrealistic to engineer, purify, and clinically develop the human gut protoplasmic PDB purinolytic enzyme XdhAC or the enzyme chain that degrades urate to SCFAs (Figure 3A). These biochemical reactions require complex anaerobic conditions and co-factors.[18,19] Still, the vast array of microbial genes may provide raw candidates to molecularly and genetically engineer[82] into novel purinolytic drugs other than uricases. Recently, such an approach corrected the severe nephrolithiasis-like and mortality-accelerating phenotype of a fruit fly uricase knockdown model in a study using anaerobic xanthine-degrading consortia of microbial enzymes from a source other than human commensal organisms.[83]

Clearly, prospective clinical trials are warranted to test for the extent of PDB biologic effects of serum urate, gout, and comorbid disorders in humans. In this context, some early human gut PDB data have been correlative, including inverse association between abundance of certain gut Clostridia with levels of serum urate and with coronary artery calcium scoring as a subclinical biomarker of atherosclerosis burden.[19] Furthermore, preclinical work demonstrating antiatherogenic effects of murine gut PDB[19,47] did not determine whether the mechanism was via lowering of circulating urate or other purines.[84–87]

Conclusions

The characterization of gut dysbiosis in gout and identification of human intestinal anaerobic PDB have opened a new translational window. It had previously been thought that oxygen-dependent microbial uricases, *Lactobacilli* purine metabolic pathways, and fecal urate elimination were the principal drivers of urate elimination in the gut. We now recognize that a widely distributed, conserved gene cluster in PDB encodes pathways for high-capacity urate degradation and generates anti-inflammatory SCFAs. Some PDB also consume multiple purines other than urate. The relationship of PDB with intestinal epithelial cells is symbiotic. In vivo, PDB have the capacity to exert major compensatory effects for the absence of uricase and other inherent limitations in human urate homeostasis. However, prospective, controlled human urate-lowering trials are awaited.

Probiotics are not likely to displace xanthine oxidase inhibitors, uricosurics, and systemic uricase therapy as the backbones of urate-lowering pharmacotherapy in gout. Also, development of effective and safe PDB oral probiotic therapeutics, and to some extent *Lactobacillus* probiotics, will demand challenging innovation. That said, successes could add beneficial probiotic classes of ULT agents to complement drug treatment, particularly so in limiting flares specifically triggered by diet, and in the approach to gout in stage IV CKD.

AUTHOR CONTRIBUTIONS

All authors contributed to at least one of the following manuscript preparation roles: conceptualization AND/OR methodology, software, investigation, formal analysis, data curation, visualization, and validation AND drafting or reviewing/editing the final draft. As corresponding author, Dr Terkeltaub confirms that all authors have provided the final approval of the version to be published, and takes responsibility for the affirmations regarding article submission (eg, not under consideration by another journal), the integrity of the data presented, and the statements regarding compliance with institutional review board/Declaration of Helsinki requirements.

REFERENCES

1. Yokose C, McCormick N, Lu N, et al. Trends in prevalence of gout among US Asian adults, 2011-2018. JAMA Netw Open 2023;6:e239501.
2. Terkeltaub R. Emerging urate-lowering drugs and pharmacologic treatment strategies for gout: a narrative review. Drugs 2023;83:1501–1521.
3. Halperin Kuhns VL, Woodward OM. Urate transport in health and disease. Best Pract Res Clin Rheumatol 2021;35:101717.
4. Dalbeth N, Choi HK, Joosten LAB, et al. Gout. Nat Rev Dis Primers 2019;5:69.
5. Ichida K, Matsuo H, Takada T, et al. Decreased extra-renal urate excretion is a common cause of hyperuricemia. Nat Commun 2012;3:764.
6. Chiaro TR, Soto R, Zac Stephens W, et al. A member of the gut mycobiota modulates host purine metabolism exacerbating colitis in mice. Sci Transl Med 2017;9:eaaf9044.
7. Chen CM, Yan QL, Guo RC, et al. Distinct characteristics of the gut virome in patients with osteoarthritis and gouty arthritis. J Transl Med 2024;22:564.
8. Brown AM, Hoopes SL, White RH, et al. Purine biosynthesis in archaea: variations on a theme. Biol Direct 2011;6:63.
9. Kaneko K, Aoyagi Y, Fukuuchi T, et al. Total purine and purine base content of common foodstuffs for facilitating nutritional therapy for gout and hyperuricemia. Biol Pharm Bull 2014;37:709–721.
10. Pastor-Anglada M, Urtasun N, Pérez-Torras S. Intestinal nucleoside transporters: function, expression, and regulation. Compr Physiol 2018;8:1003–1017.
11. Patil SD, Unadkat JD. Sodium-dependent nucleoside transport in the human intestinal brush-border membrane. Am J Physiol 1997;272:G1314–G1320.
12. Dawson RB, Rafal S, Weintraub LR. Absorption of hemoglobin iron: the role of xanthine oxidase in the intestinal heme-splitting reaction. Blood 1970;35:94–103.

13. Pierzynowska K, Deshpande A, Mosiichuk N, et al. Oral treatment with an engineered uricase, ALLN-346, reduces hyperuricemia, and uricosuria in urate oxidase-deficient mice. Front Med (Lausanne) 2020;7:569215.
14. Matsuo H, Takada T, Ichida K, et al. Common defects of ABCG2, a high-capacity urate exporter, cause gout: a function-based genetic analysis in a Japanese population. Sci Transl Med 2009;1:5ra11.
15. Cleophas MC, Joosten LA, Stamp LK, et al. ABCG2 polymorphisms in gout: insights into disease susceptibility and treatment approaches. Pharmgenomics Pers Med 2017;10:129–142.
16. He W, Phipps-Green A, Stamp LK, et al. Population-specific association between ABCG2 variants and tophaceous disease in people with gout. Arthritis Res Ther 2017;19:43.
17. Toyoda Y, Nakayama A, Nakatochi M, et al; Japan Gout Genomics Consortium (Japan Gout). Genome-wide meta-analysis between renal overload type and renal underexcretion type of clinically defined gout in Japanese populations. Mol Genet Metab 2022;136:186–189.
18. Liu Y, Jarman JB, Low YS, et al. A widely distributed gene cluster compensates for uricase loss in hominids. Cell 2023;186: 3400–3413.e20.
19. Kasahara K, Kerby RL, Zhang Q, et al. Gut bacterial metabolism contributes to host global purine homeostasis. Cell Host Microbe 2023; 31:1038–1053.e10.
20. Sender R, Fuchs S, Milo R. Are we really vastly outnumbered? Revisiting the ratio of bacterial to host cells in humans. Cell 2016;164: 337–340.
21. Zhao R, Li Z, Sun Y, et al. Engineered *Escherichia coli* Nissle 1917 with urate oxidase and an oxygen-recycling system for hyperuricemia treatment. Gut Microbes 2022;14:2070391.
22. Han S, Lu Y, Xie J, et al. Probiotic gastrointestinal transit and colonization after oral administration: a long journey. Front Cell Infect Microbiol 2021;11:609722.
23. Friedman ES, Bittinger K, Esipova TV, et al. Microbes vs. chemistry in the origin of the anaerobic gut lumen. Proc Natl Acad Sci U S A 2018; 115:4170–4175.
24. Antza C, Stabouli S, Kotsis V. Gut microbiota in kidney disease and hypertension. Pharmacol Res 2018;130:198–203.
25. Iatcu CO, Steen A, Covasa M. Gut microbiota and complications of type-2 diabetes. Nutrients 2021;14:166.
26. Ruigrok RAAA, Weersma RK, Vich Vila A. The emerging role of the small intestinal microbiota in human health and disease. Gut Microbes 2023;15:2201155.
27. Granados JC, Nigam SK. Organic anion transporters in remote sensing and organ crosstalk. Pharmacol Ther 2024;263:108723.
28. Ermakov VS, Granados JC, Nigam SK. Remote effects of kidney drug transporter OAT1 on gut microbiome composition and urate homeostasis. JCI Insight 2023;8:e172341.
29. Sun Y, Zhang S, Nie Q, et al. Gut firmicutes: relationship with dietary fiber and role in host homeostasis. Crit Rev Food Sci Nutr 2023;63: 12073–12088.
30. Tanes C, Bittinger K, Gao Y, et al. Role of dietary fiber in the recovery of the human gut microbiome and its metabolome. Cell Host Microbe 2021;29:394–407.e5.
31. Shirvani-Rad S, Khatibzade-Nasari N, Ejtahed HS, et al. Exploring the role of gut microbiota dysbiosis in gout pathogenesis: a systematic review. Front Med (Lausanne) 2023;10:1163778.
32. Guo Z, Zhang J, Wang Z, et al. Intestinal microbiota distinguish gout patients from healthy humans. Sci Rep 2016;6:20602.
33. Chen C, Zhang Y, Yao X, et al. Characterizations of the multi-kingdom gut microbiota in Chinese patients with gouty arthritis. BMC Microbiol 2023;23:363.
34. Wei J, Zhang Y, Dalbeth N, et al. Association between gut microbiota and elevated serum urate in two independent cohorts. Arthritis Rheumatol 2022;74:682–691.
35. Lin S, Zhang T, Zhu L, et al. Characteristic dysbiosis in gout and the impact of a uric acid-lowering treatment, febuxostat on the gut microbiota. J Genet Genomics 2021;48:781–791.
36. Chu Y, Sun S, Huang Y, et al. Metagenomic analysis revealed the potential role of gut microbiome in gout. NPJ Biofilms Microbiomes 2021;7:66.
37. Méndez-Salazar EO, Vázquez-Mellado J, Casimiro-Soriguer CS, et al. Taxonomic variations in the gut microbiome of gout patients with and without tophi might have a functional impact on urate metabolism. Mol Med 2021;27:50.
38. Yersin S, Vonaesch P. Small intestinal microbiota: from taxonomic composition to metabolism. Trends Microbiol 2024;32:970–983.
39. Kastl AJ Jr, Terry NA, Wu GD, et al. The structure and function of the human small intestinal microbiota: current understanding and future directions. Cell Mol Gastroenterol Hepatol 2020;9:33–45.
40. Nishino T, Okamoto K, Eger BT, et al. Mammalian xanthine oxidoreductase - mechanism of transition from xanthine dehydrogenase to xanthine oxidase. FEBS J 2008;275:3278–3289.
41. Wang CH, Zhang C, Xing XH. Xanthine dehydrogenase: an old enzyme with new knowledge and prospects. Bioengineered 2016;7: 395–405.
42. Widyastuti Y, Febrisiantosa A, Tidona F. Health-promoting properties of Lactobacilli in fermented dairy products. Front Microbiol 2021;12: 673890.
43. Kilstrup M, Hammer K, Ruhdal Jensen P, et al. Nucleotide metabolism and its control in lactic acid bacteria. FEMS Microbiol Rev 2005;29: 555–590.
44. Yamada N, Saito-Iwamoto C, Nakamura M, et al. Lactobacillus gasseri PA-3 uses the purines IMP, inosine and hypoxanthine and reduces their absorption in rats. Microorganisms 2017;5:10.
45. Liu X, Ke L, Lei K, et al. Antibiotic-induced gut microbiota dysbiosis has a functional impact on purine metabolism. BMC Microbiol 2023; 23:187.
46. Gill I, Dalbeth N, 'Ofanoa M, et al. Interventions to improve uptake of urate-lowering therapy in patients with gout: a systematic review. BJGP Open 2020;4:bjgpopen20X1010531.
47. Grelska A, Sharan D, Light SH. Purine-ifying uric acid by gut microbes. Cell Chem Biol 2023;30:706–708.
48. Jensen T, Abdelmalek MF, Sullivan S, et al. Fructose and sugar: a major mediator of non-alcoholic fatty liver disease. J Hepatol 2018; 68:1063–1075.
49. Merenstein D, Pot B, Leyer G, et al. Emerging issues in probiotic safety: 2023 perspectives. Gut Microbes 2023;15:2185034.
50. Singh TP, Natraj BH. Next-generation probiotics: a promising approach towards designing personalized medicine. Crit Rev Microbiol 2021;47:479–498.
51. Torp AM, Bahl MI, Boisen A, et al. Optimizing oral delivery of next generation probiotics. Trends Food Sci Technol 2022;119:101–109.
52. Zhao Z, Xu S, Zhang W, et al. Probiotic *Escherichia coli* NISSLE 1917 for inflammatory bowel disease applications. Food Funct 2022;13: 5914–5924.
53. Lawley TD, Walker AW. Intestinal colonization resistance. Immunology 2013;138:1–11.
54. Minelli EB, Benini A. Relationship between number of bacteria and their probiotic effects. Microb Ecol Health Dis 2008;20:180–183.
55. Terkeltaub R, Clark D, Tosone C, et al. POS1157 Safety and efficacy of ALLN-346 oral enzyme therapy in patients with hyperuricemia and chronic kidney disease (CKD): results of the phase 2A study 201. Ann Rheum Dis 2022;81:907.

56. Tang Y, Du Y, Ye J, et al. Intestine-targeted explosive hydrogel microsphere promotes uric acid excretion for gout therapy. Adv Mater 2024;36:e2310492.
57. Xie WR, Yang XY, Deng ZH, et al. Effects of washed microbiota transplantation on serum uric acid levels, symptoms, and intestinal barrier function in patients with acute and recurrent gout: a pilot study. Dig Dis 2022;40:684–690.
58. Cai JR, Chen XW, He YJ, et al. Washed microbiota transplantation reduces serum uric acid levels in patients with hyperuricaemia. World J Clin Cases 2022;10:3401–3413.
59. Gibson GR, Hutkins R, Sanders ME, et al. Expert consensus document: The International Scientific Association for Probiotics and Prebiotics (ISAPP) consensus statement on the definition and scope of prebiotics. Nat Rev Gastroenterol Hepatol 2017;14:491–502.
60. Generally recognized as safe (GRAS). US Food and Drug Administration. Accessed [Sept 30, 2024]. https://www.fda.gov/food/food-ingredients-packaging/generally-recognized-safe-gras
61. Lisko DJ, Johnston GP, Johnston CG. Effects of dietary yogurt on the healthy human gastrointestinal (GI) microbiome. Microorganisms 2017;5:6.
62. Qi X, Ma Y, Guan K, et al. Whey protein peptide Pro-Glu-Trp ameliorates hyperuricemia by enhancing intestinal uric acid excretion, modulating the gut microbiota, and protecting the intestinal barrier in rats. J Agric Food Chem 2024;72:2573–2584.
63. Choi HK, Liu S, Curhan G. Intake of purine-rich foods, protein, and dairy products and relationship to serum levels of uric acid: the Third National Health and Nutrition Examination Survey. Arthritis Rheum 2005;52:283–289.
64. Garrel DR, Verdy M, PetitClerc C, et al. Milk- and soy-protein ingestion: acute effect on serum uric acid concentration. Am J Clin Nutr 1991;53:665–669.
65. Chien CY, Chien YJ, Lin YH, et al. Supplementation of *Lactobacillus plantarum* (TCI227) prevented potassium-oxonate-induced hyperuricemia in rats. Nutrients 2022;14:4832.
66. Lee Y, Kim N, Werlinger P, et al. Probiotic characterization of *Lactobacillus brevis* MJM60390 and *in vivo* assessment of its antihyperuricemic activity. J Med Food 2022;25:367–380.
67. Li Y, Zhu J, Lin G, et al. Probiotic effects of *Lacticaseibacillus rhamnosus* 1155 and *Limosilactobacillus fermentum* 2644 on hyperuricemic rats. Front Nutr 2022;9:993951.
68. Wang H, Mei L, Deng Y, et al. *Lactobacillus brevis* DM9218 ameliorates fructose-induced hyperuricemia through inosine degradation and manipulation of intestinal dysbiosis. Nutrition 2019;62:63–73.
69. Zhang Y, Chen C, Choi H, et al. Purine-rich foods intake and recurrent gout attacks. Ann Rheum Dis 2012;71:1448–1453.
70. Rodríguez JM, Garranzo M, Segura J, et al. A randomized pilot trial assessing the reduction of gout episodes in hyperuricemic patients by oral administration of *Ligilactobacillus salivarius* CECT 30632, a strain with the ability to degrade purines. Front Microbiol 2023;14:1111652.
71. Yamanaka H, Taniguchi A, Tsuboi H, et al. Hypouricaemic effects of yoghurt containing *Lactobacillus gasseri* PA-3 in patients with hyperuricaemia and/or gout: a randomised, double-blind, placebo-controlled study. Mod Rheumatol 2019;29:146–150.
72. Kamatani N, Mochii M, Hashimoto M, et al. Placebo controlled double blind parallel randomized study to test the urate-lowering effect of yogurt containing *Lactobacillus gasseri* PA-3 in adult males with marginal hyperuricemia. Gout Nucleic Acid Metab 2016;40:21–31.
73. Hamada T, Hisatome I, Wakimizu T, et al. *Lactobacillus gasseri* PA-3 reduces serum uric acid levels in patients with marginal hyperuricemia. Nucleosides Nucleotides Nucleic Acids 2022;41:361–369.
74. Choi JW, Ford ES, Gao X, et al. Sugar-sweetened soft drinks, diet soft drinks, and serum uric acid level: the Third National Health and Nutrition Examination Survey. Arthritis Rheum 2008;59:109–116.
75. Jang C, Hui S, Lu W, et al. The small intestine converts dietary fructose into glucose and organic acids. Cell Metab 2018;27:351–361.e3.
76. Hussain A, Rui B, Ullah H, et al. *Limosilactobacillus reuteri* HCS02-001 attenuates hyperuricemia through gut microbiota-dependent regulation of uric acid biosynthesis and excretion. Microorganisms 2024;12:637.
77. Xu YX, Liu LD, Zhu JY, et al. *Alistipes indistinctus*-derived hippuric acid promotes intestinal urate excretion to alleviate hyperuricemia. Cell Host Microbe 2024;32:366–381.e9.
78. Hyndman D, Liu S, Miner JN. Urate handling in the human body. Curr Rheumatol Rep 2016;18:34.
79. Oh JH, Dossetor JB, Beck IT. Kinetics of uric acid transport and its production in rat small intestine. Can J Physiol Pharmacol 1967;45:121–127.
80. Bronk JR, Shaw MI. The transport of uric acid across mouse small intestine in vitro. J Physiol 1986;378:229–239.
81. Dukes CE, Steplock DA, Kahn AM, et al. The transport of urate in the small intestine of the rat. Proc Soc Exp Biol Med 1982;171:19–23.
82. Wang L, Hu J, Li K, et al. Advancements in gene editing technologies for probiotic-enabled disease therapy. iScience 2024;27:110791.
83. Tong Y, Wei Y, Ju Y, et al. Anaerobic purinolytic enzymes enable dietary purine clearance by engineered gut bacteria. Cell Chem Biol 2023;30:1104–1114.e7.
84. Ganji M, Nardi V, Prasad M, et al. Carotid plaques from symptomatic patients are characterized by local increase in xanthine oxidase expression. Stroke 2021;52:2792–2801.
85. Nardi V, Franchi F, Prasad M, et al. Uric acid expression in carotid atherosclerotic plaque and serum uric acid are associated with cerebrovascular events. Hypertension 2022;79:1814–1823.
86. Patetsios P, Song M, Shutze WP, et al. Identification of uric acid and xanthine oxidase in atherosclerotic plaque. Am J Cardiol 2001;88:188–191, A6.
87. Ryu HM, Kim YJ, Oh EJ, et al. Hypoxanthine induces cholesterol accumulation and incites atherosclerosis in apolipoprotein E-deficient mice and cells. J Cell Mol Med 2016;20:2160–2172.

Arthritis & Rheumatology
Vol. 77, No. 8, August 2025, pp 966–970
DOI 10.1002/art.43152

American College of Rheumatology
Empowering Rheumatology Professionals

Nociplasticity: A Proposed Concept to Understand the Symptomatology of Systemic Lupus Erythematosus

David S. Pisetsky,[1] Jennifer L. Rogers,[2] Amanda M. Eudy,[2] Katherine T. Martucci,[2] Ru-Rong Ji,[2] and Peter E. Lipsky[3]

Introduction

Systemic lupus erythematosus (SLE; lupus) is a prototypic systemic autoimmune disease characterized by antinuclear antibodies, systemic inflammation and a wide range of signs and symptoms that lead to morbidity and mortality.[1] As shown using a variety of analytic techniques, patients with SLE manifest a broad array of functional immune cell disturbances that can induce autoantibody production, aberrant cytokine production, and tissue inflammation and damage.[2]

In addition to inflammation, the course of SLE is marked by symptoms such as widespread pain, fatigue, cognitive impairment, and mood disturbance that can dramatically impair quality of life. The relationship between these symptoms and inflammation is unclear. Furthermore, whereas health care professionals generally focus on tissue inflammation (eg, nephritis, arthritis) and evidence of immunologic disturbance (eg, increased anti-DNA, decreased C3/C4) in their clinical assessments, patients may rather focus on symptoms such as pain and fatigue as their "lupus." This discordance can complicate communication, provoke patient dissatisfaction, and hinder research.[3]

To develop a new framework for evaluating and treating SLE, Pisetsky et al proposed a division of disease manifestations into two broad categories designated as type 1 and type 2 SLE.[4] Type 1 SLE corresponds to inflammatory manifestations such as nephritis, arthritis, and serositis. In contrast, type 2 SLE encompasses symptoms such as widespread pain, fatigue, and depression. Although type 2 manifestations can sometimes track with type 1 manifestations, these symptoms can be persistent and may not associate with conventional measures of disease activity nor respond to immunomodulatory therapy.[5]

The type 1 and 2 SLE model is based on the premise that at least some type 2 symptoms are intrinsic aspects of SLE as opposed to the consequences of life with a serious chronic disease or other factors. As such, this model reframes symptoms, such as widespread pain, as part of the lupus spectrum, implying that these clinical features may involve immunological mechanisms, albeit ones that may differ from those that drive the inflammation underlying arthritis or nephritis. In this discussion, we would like to build on this framework and propose a new construct that we hope will be advance both research and clinical care.

Lupus symptomatology. In many studies of SLE, approximately 20% to 30% of patients meet criteria for fibromyalgia (FM) using validated instruments.[6] This frequency is far greater than that of the general population and suggests a direct connection between FM and SLE.[7] In the current understanding, FM represents a form of nociplastic pain; nociplastic pain differs from nociceptive pain that arises from noxious stimuli and from neuropathic pain caused by nerve injury. In this construct, nociplastic pain results from central nervous system sensitization (a consequence of neuroplasticity) that leads to altered function of neural pathways related to pain processing; the result of these functional changes is pain amplification.

The effects of central nervous system sensitization are marked. Thus, amplification of signaling can lead to sensory abnormalities such as allodynia and hyperalgesia; allodynia is marked by the experience of pain with stimuli that ordinarily do not produce pain, whereas hyperalgesia involves an increase in the pain sensation from a noxious stimulus. Furthermore, central sensitization can lead to sensitivity to non-nociceptor stimuli such as light and sound. Although sensitization may also involve the peripheral nervous system, the importance of the central nervous system is highlighted by the frequent association with fatigue,

Dr Eudy's work was supported by grants from GlaxoSmithKline, Exagen, and Immunovant. Dr Lipsky's work was supported by a grant from the RILITE Foundation.

[1]David S. Pisetsky, MD, PhD: Duke University Medical Center and Durham Veterans Affairs Medical Center, Durham, North Carolina; [2]Jennifer L. Rogers, MD, Amanda M. Eudy, PhD, Katherine T. Martucci, PhD, Ru-Rong Ji, PhD: Duke University Medical Center, Durham, North Carolina; [3]Peter E. Lipsky, MD: AMPEL BioSolutions and RILITE Research Institute, Charlottesville, Virigina

Author disclosures are available at https://onlinelibrary.wiley.com/doi/10.1002/art.43152.

Address correspondence via email to David S. Pisetsky, MD, PhD, at david.pisetsky@duke.edu.

Submitted for publication November 6, 2024; accepted in revised form February 10, 2025.

cognitive impairment, and mood disturbance,[8] suggesting that central sensitization can lead to a spectrum of symptoms.

Scientific classification of signs and symptoms is always important, and any new schema is likely to elicit discussion and possible disagreement. For symptoms currently designated as part of the type 2 construct, especially those that are persistent, we propose the term "lupus-associated nociplasticity" (LAN). Implicit in this designation is the concept that nociplasticity, resulting from central nervous system sensitization and functional alteration of pain pathways, may underlie lupus symptomatology in the absence of overt peripheral inflammation.

At present, widespread pain in SLE (often diagnosed as FM) would be designated as nociplastic pain; the term nociplasticity has also been used to describe this phenomenon[9] and seems apt because it can encompass other clinical features that often accompany pain in SLE. Therefore, we propose the term nociplasticity rather than nociplastic pain to highlight the prominence of other components of this syndrome including fatigue, mood disturbance, and sleep disturbance. The various manifestations encompassed by nociplasticity, although often tracking together, can differ in intensity among patients, suggesting that a terminology that incorporates symptoms other than pain has both clinical and heuristic value.

In this construct, central nervous system sensitization can amplify pain as well as other symptoms.[10] For example, it may influence cognitive impairment, which can be one of the most distressing symptoms of patients with chronic pain. Fatigue can similarly be incorporated into this framework, because the extent of physical or mental tiredness reported by patients may be difficult to understand in terms of usual physiological systems. Indeed, central sensitization may play a role in many patients with SLE because type 1 symptoms related to inflammation, such as arthritis, may be amplified.[11]

Neuroimmune dysfunction SLE. For immune processes in the nervous system, the term neuroinflammation is frequently used to characterize changes in the properties of neurons, glia, astrocytes, and other cell types that have been perturbed by immune mediators.[12] In the context of SLE, we would suggest the term "neuroimmune dysfunction" to account for central nervous system sensitization and nociplasticity because there is little direct evidence of nervous system inflammation, recognizing that inflammation is only one manifestation of immunological activity and is defined by classic signs and symptoms (ie, pain, swelling, heat, tenderness, and functional disturbance). Because histopathological studies of brain or spinal cord may not reveal evidence of canonical inflammation (eg, cellular infiltration) in SLE, other terminology may be more illuminating.

In contrast, the term "neuroimmune dysfunction" is more general and accords well with the extensive data on the effects of cytokines and toll-like receptor agonists, whether produced centrally or peripherally, on the nervous system. Because macrophages in the peripheral blood of patients with SLE have many functional abnormalities, comparable effects on microglia, the macrophages of the nervous system, would not be unexpected. Animal models support this concept.[13]

Among immune mediators, antibodies can have profound effects on neuronal function and can induce chronic pain in conditions such as rheumatoid arthritis (RA), complex regional pain syndrome, and channelopathies.[14,15] Indeed, as shown by Goebel et al, IgG from the blood of patients with FM can induce pain behavior in mice, such as increased sensitivity to noxious stimuli.[16] Furthermore, studies have shown that IgG antibodies from patients with FM can bind to dorsal root ganglion cells and score in an in vitro binding assay using satellite glia cells.[17] Although such antibodies have not yet been demonstrated in the sera of patients with SLE, the findings with FM raise the possibility of an autoantibody-mediated etiology for symptoms related to nociplasticity, with or without evidence of systemic inflammation. In another realm, imaging modalities have indicated functional changes in the brains of patients with SLE even without clinically active disease and may signify neuroimmune dysfunction.[18]

The concept of LAN also incorporates the role of interoception, a term referring to the person's internal sense of her body. Interoception involves the awareness and accuracy of sensations as well as their experience, integrating physiological pathways in the brain for homeostasis and self-awareness.[19] As in the case of FM, the array of symptoms reported by lupus patients and their frequent concordance in the same patient suggest a common disturbance of interoception. Furthermore, studies on patients with temporomandibular disorder (TMD) indicate that an individual's experience of somatic symptoms, an aspect of interoception, is a risk factor for the development of TMD, a chronic pain condition.[20]

With central nervous system sensitization in LAN, many physiologic interactions are possible, and directionality can be difficult to elucidate (Figure 1). Other mechanisms may also be at play (eg, effects of physical or psychosocial trauma and/or emotional dysregulation). Because neuroimmune dysfunction can be associated with many etiologies and triggers, nociplasticity can be a final pathway driving diverse symptomatology. Importantly, to the provider, neuroimmune dysfunction may be invisible because the classic signs of inflammation are absent or no longer present. For the patient, however, neuroimmune dysfunction is not silent, as it can lead to distressing symptomatology.

In this construct, pain and related symptoms are essential disease manifestations of SLE that arise from neuroimmune dysfunction and the downstream effects of central nervous system sensitization (Figure 1). Furthermore, the presence of neuroimmune dysfunction may intensify and amplify the influence of other etiological factors (eg, psychological stress, trauma), making patients with autoimmune or inflammatory disease especially prone to the development of nociplasticity. In SLE, the prominence of nociplastic symptoms may reflect the confluence of

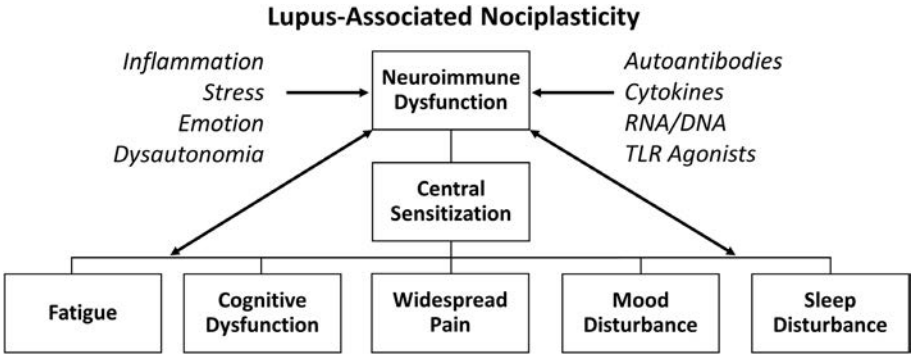

Figure 1. Lupus-associated nociplasticity. The figure illustrates a model for the relationship between neuroimmune dysfunction, central nervous system sensitization, and symptoms of SLE. As depicted in the figure, a variety of physiological factors can influence neuroimmune dysfunction which is a contributor to central nervous system sensitization; in turn, these factors may be influenced by sensitization. In this construct, central nervous system sensitization represents an overarching mechanism that can drive type 2 SLE manifestations and not just pain; central sensitization may also influence perception of type 1 SLE manifestations. Behavioral responses to these manifestations may further perpetuate neuroimmune dysfunction. Interoception represents a system by which physiological alternations (eg, inflammation) can be sensed and thereby influence the patient experience of symptoms such as pain and fatigue. In some instances, the relationships are hypothetical and require greater experimental study. SLE, systemic lupus erythematosus; TLR, toll-like receptor.

certain immune disturbances (eg, autoantibodies, aberrant cytokine production) that make these symptoms so problematic.

As indicated in the extensive literature on nociplastic pain, nociplasticity, usually designated as FM or fibromyalgianess, can occur in other autoimmune and inflammatory diseases, such as RA. The term LAN does not imply a unique or exclusive relationship to SLE and similar terminology may be applied to other diseases (eg, RA-associated neuroplasticity).[21–23] The point of the proposed terminology is to emphasize that (1) nociplasticity can be an important element of disease pathogenesis; (2) pain can arise both peripherally (tissue inflammation and peripheral sensitization) and centrally (central nervous system sensitization); and (3) nociplasticity conveys a spectrum of symptoms that are not simply binary but can change and vary.

The place of nociplasticity in patient evaluation. Although painful conditions (eg, arthritis, pleurisy) represent classification criteria, it is striking that some of the most common and disabling symptoms of SLE (ie, widespread pain, fatigue) do not.[24] This absence, however, arises from the intended use of such criteria to facilitate research and distinguish SLE from other conditions that may have related symptomatology such as widespread pain.

The instruments to assess disease activity reflect a similar perspective. The Systemic Lupus Erythematosus Disease Activity Index encompasses nervous system manifestations (eg, seizures) as well as painful conditions (eg, lupus headache) but lacks features such as widespread pain and fatigue.[25] According to the criteria, lupus headache signifies disease activity but widespread pain does not, although headache may be a manifestation of central nervous system sensitization. Furthermore, headache and widespread pain can both be part of an overlapping pain syndrome, suggesting a mechanistic link.[26]

We would suggest that, in any future development of clinical criteria, inclusion of LAN should be considered as a neuropsychiatric manifestation of SLE, especially when bolstered by serology, neuroimaging, quantitative sensory testing, or related testing. Because neuroimmune dysfunction can underlie nociplasticity, positing LAN as a manifestation of neuropsychiatric lupus is akin to that of features such as headache, anxiety, and mood disorders.

Furthermore, we would suggest consideration for the development of activity measures and patient-reported outcome measures (PROMs) that specifically address nociplastic manifestations of SLE. Nociplasticity can be captured using the validated type 2 Physician Global Assessment[27] as well as PROMs such as the polysymptomatic distress score, PROMIS-29, 36-Item Short Form Health Survey, and LupusPRO. Nociplasticity can also be part of studies to develop new biomarkers, such as transcriptomics to develop patient endotypes.[28]

Importantly, we believe that assessing nociplasticity should be included in routine clinical care to encourage clinicians to address these symptoms directly; for clinical trials, assessment of nociplasticity could determine label indications and extensions. Measures that encompass nociplasticity can also be considered to assess treatment responses and develop and refine therapies directed to LAN (eg, tricyclic antidepressants, exercise, or stress reduction).

Going forward, we believe that the terminology of LAN is more informative and instructive than secondary FM or fibromyalgianess, because it represents a spectrum of symptoms that can be tied directly to the pathogenesis of SLE; as such, it makes their amelioration an essential treatment goal, optimally determined by

a rheumatologist. We believe that referring to LAN as secondary FM does not provide mechanistic understanding and can also limit research into causation; it can also affect routine care given the uncertainty and ambiguity in the care for patients with FM. This uncertainty can lead to invalidation, the perception by patients that their condition is not adequately recognized nor supported by others, especially health care providers.[29,30]

Compared to other medical and surgical conditions, FM is rated by physicians and nurses as having low "prestige" and may therefore receive less attention in usual clinical encounters.[31,32] As a new term, nociplasticity has the advantage of bypassing the controversy around FM and validating the patient experience by assigning symptoms to lupus pathogenesis.

Because patients can consider the manifestations of nociplasticity as their "lupus," a model of care that makes these manifestations as primary (rather than as comorbidities secondary to unknown factors) has the potential to improve outcomes and increase patient satisfaction. Practically, we therefore suggest the development of a new *International Classification of Diseases, 11th Revision* code for LAN to facilitate clinical care and medication prescription.

Conclusions

Pain along with fatigue and cognitive dysfunction can be devastating in their impact and, to patients, constitute their "lupus." We propose the term LAN to highlight the role of central nervous system sensitization in the pathogenesis of SLE and to incorporate the patient experience more cogently into models of care. We hope that this terminology will stimulate discussion (even debate), novel research, and, most importantly, advances in clinical care to improve the lives of patients with SLE.

AUTHOR CONTRIBUTIONS

All authors contributed to at least one of the following manuscript preparation roles: conceptualization AND/OR methodology, software, investigation, formal analysis, data curation, visualization, and validation AND drafting or reviewing/editing the final draft As corresponding author, Dr Pisetsky confirms that all authors have provided the final approval of the version to be published, and takes responsibility for the affirmations regarding article submission (eg, not under consideration by another journal), the integrity of the data presented, and the statements regarding compliance with institutional review board/Declaration of Helsinki requirements.

REFERENCES

1. Kaul A, Gordon C, Crow MK, et al. Systemic lupus erythematosus. Nat Rev Dis Primers 2016;2(1):16039.
2. Catalina MD, Owen KA, Labonte AC, et al. The pathogenesis of systemic lupus erythematosus: harnessing big data to understand the molecular basis of lupus. J Autoimmun 2020;110:102359.
3. Rogers JL, Clowse MEB, McKenna K, et al. Patient and physician perspectives of systemic lupus erythematosus flare: a qualitative study. J Rheumatol 2024;51(5):488–494.
4. Pisetsky DS, Clowse MEB, Criscione-Schreiber LG, et al. A novel system to categorize the symptoms of systemic lupus erythematosus. Arthritis Care Res (Hoboken) 2019;71(6):735–741.
5. Eudy AM, Rogers JL, Corneli A, et al. Intermittent and persistent type 2 lupus: patient perspectives on two distinct patterns of type 2 SLE symptoms. Lupus Sci Med 2022;9(1):e000705.
6. Middleton GD, McFarlin JE, Lipsky PE. The prevalence and clinical impact of fibromyalgia in systemic lupus erythematosus. Arthritis Rheum 1994;37(8):1181–1188.
7. Wolfe F, Michaud K, Li T, Katz RS. Chronic conditions and health problems in rheumatic diseases: comparisons with rheumatoid arthritis, noninflammatory rheumatic disorders, systemic lupus erythematosus, and fibromyalgia. J Rheumatol 2010;37(2):305–315.
8. Fitzcharles MA, Cohen SP, Clauw DJ, et al. Nociplastic pain: towards an understanding of prevalent pain conditions. Lancet 2021;397(10289):2098–2110.
9. Condon LF, Yu Y, Park S, et al. Parabrachial Calca neurons drive nociplasticity. Cell Rep 2024;43(4):114057.
10. Sunzini F, Schrepf A, Clauw DJ, et al. The biology of pain: through the rheumatology lens. Arthritis Rheumatol 2023;75(5):650–660.
11. Rogers JL, Eudy AM, Pisetsky D, et al. Using clinical characteristics and patient-reported outcome measures to categorize systemic lupus erythematosus subtypes. Arthritis Care Res (Hoboken) 2021;73(3):386–393.
12. Ji RR, Nackley A, Huh Y, et al. Neuroinflammation and central sensitization in chronic and widespread pain. Anesthesiology 2018;129(2):343–366.
13. Carroll KR, Mizrachi M, Simmons S, et al. Lupus autoantibodies initiate neuroinflammation sustained by continuous HMGB1:RAGE signaling and reversed by increased LAIR-1 expression. Nat Immunol 2024;25(4):671–681.
14. Lacagnina MJ, Heijnen CJ, Watkins LR, et al. Autoimmune regulation of chronic pain. Pain Rep 2021;6(1):e905.
15. Mountford R, Adler BL, Andersson D, et al. Antibody-mediated autoimmunity in symptom-based disorders: position statement and proceedings from an international workshop. Pain Rep 2024;9(4):e1167.
16. Goebel A, Krock E, Gentry C, et al. Passive transfer of fibromyalgia symptoms from patients to mice. J Clin Invest 2021;131(13):e144201.
17. Fanton S, Menezes J, Krock E, et al. Anti-satellite glia cell IgG antibodies in fibromyalgia patients are related to symptom severity and to metabolite concentrations in thalamus and rostral anterior cingulate cortex. Brain Behav Immun 2023;114:371–382.
18. Mackay M, Tang CC, Vo A. Advanced neuroimaging in neuropsychiatric systemic lupus erythematosus. Curr Opin Neurol 2020;33(3):353–361.
19. Todd J, Plans D, Lee MC, et al. Heightened interoception in adults with fibromyalgia. Biol Psychol 2024;186:108761.
20. Fillingim RB, Ohrbach R, Greenspan JD, et al. Psychological factors associated with development of TMD: the OPPERA prospective cohort study. J Pain 2013;14(12 Suppl):T75–T90.
21. Minhas D, Murphy A, Clauw DJ. Fibromyalgia and centralized pain in the rheumatoid arthritis patient. Curr Opin Rheumatol 2023;35(3):170–174.
22. Fitzgerald GE, Maguire S, Lopez-Medina C, et al. Tender to touch-prevalence and impact of concomitant fibromyalgia and enthesitis in spondyloarthritis: an ancillary analysis of the ASAS PerSpA study. Joint Bone Spine 2022;89(6):105420.
23. Duffield SJ, Miller N, Zhao S, et al. Concomitant fibromyalgia complicating chronic inflammatory arthritis: a systematic review

and meta-analysis. Rheumatology (Oxford) 2018;57(8):1453–1460.

24. Aringer M, Costenbader K, Daikh D, et al. 2019 European League Against Rheumatism/American College of Rheumatology classification criteria for systemic lupus erythematosus. Arthritis Rheumatol 2019;71(9):1400–1412.
25. Bombardier C, Gladman DD, Urowitz MB, et al; The Committee on Prognosis Studies in SLE. Derivation of the SLEDAI. A disease activity index for lupus patients. Arthritis Rheum 1992;35(6):630–640.
26. Maixner W, Fillingim RB, Williams DA, et al. Overlapping chronic pain conditions: implications for diagnosis and classification. J Pain 2016;17(9 Suppl):T93–T107.
27. Clowse MEB, Rogers JL, Coles T, et al. Development and psychometric evaluation of a physician global assessment for type 2 systemic lupus erythematosus symptoms. Lupus Sci Med 2023;10(2):e001016.
28. Robl R, Eudy A, Bachali PS, et al. Molecular endotypes of type 1 and type 2 SLE. Lupus Sci Med 2023;10(1):e000861.
29. Kool MB, van Middendorp H, Boeije HR, et al. Understanding the lack of understanding: invalidation from the perspective of the patient with fibromyalgia. Arthritis Rheum 2009;61(12):1650–1656.
30. Santiago MG, Marques A, Kool M, et al. Invalidation in patients with rheumatic diseases: clinical and psychological framework. J Rheumatol 2017;44(4):512–518.
31. Album D, Westin S. Do diseases have a prestige hierarchy? A survey among physicians and medical students. Soc Sci Med 2008;66(1):182–188.
32. Johannessen LEF, Album D, Rasmussen EB. Do nurses rate diseases according to prestige? A survey study. J Adv Nurs 2020;76(7):1691–1697.

Arthritis & Rheumatology
Vol. 77, No. 8, August 2025, pp 971–980
DOI 10.1002/art.43149

Peripheral Biomarker Signatures in Rheumatoid Arthritis–Associated Interstitial Lung Disease

Austin M. Wheeler,[1] Joshua F. Baker,[2] Thomas R. Riley IV,[2] Tate M. Johnson,[1] Yangyuna Yang,[3] Punyasha Roul,[3] Katherine D. Wysham,[4] Grant W. Cannon,[5] Gary Kunkel,[5] Gail Kerr,[6] Dana P. Ascherman,[7] Paul Monach,[8] Andreas Reimold,[9] Scott Matson,[10] Jill A. Poole,[3] Michael J. Duryee,[1] Geoffrey M. Thiele,[1] Ted R. Mikuls,[1] and Bryant R. England[1]

Objective. Rheumatoid arthritis–associated interstitial lung disease (RA-ILD) is a significant cause of morbidity and mortality among patients with RA, yet effective risk stratification for RA-ILD is lacking. We sought to characterize unique peripheral blood biomarker signatures in RA that could improve RA-ILD discrimination beyond clinical and genetic risk factors.

Methods. We performed a cross-sectional study of participants in the Veterans Affairs Rheumatoid Arthritis Registry. ILD was validated through systematic record review. Autoantibodies (n = 14), proinflammatory cytokines/chemokines (n = 36), adipokines (n = 3), alarmins (n = 3), and matrix metalloproteinases (n = 9) were measured from banked serum or plasma. *MUC5B* rs35705950 genotyping was obtained via microarray. Principal component (PC) analysis was performed to derive unique biomarker signatures. Logistic regression was used to compare models predicting RA-ILD presence using combinations of clinical, peripheral biomarker, and genetic variables.

Results. Among 2,001 participants with RA (88.7% male, mean age 63.7 years), 121 (6.4%) had RA-ILD. A total of 15 PCs were identified, with 8 significantly associated with RA-ILD after adjusting for clinical factors. These eight included biomarker themes of innate and allergic responses, autoantibodies (anti–cyclic citrullinated peptide, rheumatoid factor, anti–malondialdehyde-acetaldehyde adduct), adipokines, alarmins, tissue remodeling, and neutrophil chemotaxis. Models with PCs (area under the receiver operating characteristic curve [AUC] 0.739) and PCs with *MUC5B* (AUC 0.751) outperformed clinical risk factors alone (AUC 0.630; $P < 0.001$).

Conclusion. Peripheral biomarker signatures are associated with RA-ILD and improve RA-ILD identification beyond clinical risk factors. In addition to demonstrating the potential for peripheral biomarkers to aid RA-ILD risk stratification, these findings suggest diverse pathways are involved in RA-ILD pathogenesis.

INTRODUCTION

Rheumatoid arthritis–associated interstitial lung disease (RA-ILD) is a significant cause of morbidity and mortality among patients with RA.[1,2] Despite the importance of this extra-articular manifestation, there are relatively few identified risk factors for RA-ILD. Clinical risk factors consistently identified include older age, male sex, cigarette smoking, and severe articular disease.[3,4]

Presented in part at 2021 and 2024 American College of Rheumatology Convergence.

The views expressed herein are those of the authors and do not reflect the official policy of the Department of Veterans Affairs or the United States government.

Dr Wheeler's work was supported by the Rheumatology Research Foundation. Dr Baker's work was supported by the Veteran Affairs (VA) Clinical Science Research and Development (CSR&D) (merit award CX001703) and the Rehabilitation Research and Development Service (merit award RX003644). Dr Riley's work was supported by the NIH Pharmacoepidemiology (grant 5T32GM075766-17). Dr Johnson's work was supported by the Rheumatology Research Foundation. Dr Wysham's work was supported by the VA CSR&D (award IK2 CX002351). Dr Poole's work was supported by the US Department of Defense (grant PR200793) and National Institute of Occupational Safety and Health (grant R01OH012045). Dr Mikuls' work was supported by the VA Biomedical Laboratory Research and Development (merit award I01 BX003635), NIH (grant 1U54-GM-115458), US Department of Defense (grant PR200793), and the Rheumatology Research Foundation. Dr England's work was supported by the VA CSR&D (award IK2 CX002203) and Rheumatology Research Foundation.

[1]Austin M. Wheeler, MD, Tate M. Johnson, MD, Michael J. Duryee, MS, Geoffrey M. Thiele, PhD, Ted R. Mikuls, MD, MSPH, Bryant R. England, MD, PhD: VA Nebraska-Western Iowa Health Care System and University of Nebraska Medical Center, Omaha; [2]Joshua F. Baker, MD, MSCE, Thomas R. Riley IV, MD: University of Pennsylvania and Corporal Michael J. Crescenz VA Medical Center, Philadelphia; [3]Yangyuna Yang, PhD, MBBS, Punyasha Roul, MS, Jill A. Poole, MD: University of Nebraska Medical Center, Omaha; [4]Katherine D. Wysham, MD: VA Puget Sound Health Care System and University of Washington, Seattle; [5]Grant W. Cannon, MD, Gary Kunkel, MD: VA Salt Lake City Healthcare System and University of Utah; [6]Gail Kerr, MD: Washington VA Medical Center, Howard University, and Georgetown University, Washington, District of Columbia; [7]Dana P. Ascherman, MD: Pittsburgh VA Medical Center-University Drive and University of Pittsburgh, Pittsburgh, Pennsylvania; [8]Paul Monach, MD, PhD: Jamaica Plain VA Medical Center, Boston, Massachusetts; [9]Andreas Reimold, MD; Dallas VA Medical Center and

There are also observed associations between prevalent RA-ILD and seropositivity with rheumatoid factor (RF), anti–cyclic citrullinated peptide (CCP) antibodies, and anti–malondialdehyde-acetaldehyde adduct (MAA) antibodies.[4,5] In addition to clinical measures and autoantibody status, genetic risk factors have been increasingly recognized for their contribution to RA-ILD development, specifically when it occurs in a usual interstitial pneumonia (UIP) pattern. The strongest genetic risk factor identified to date is the *MUC5B* rs35705950 promoter variant, a finding validated in multiple studies and independent cohorts.[6–10]

Beyond clinically available autoantibodies and these genetic risk factors, there are a number of peripheral biomarkers associated with the presence of RA-ILD. A recent systematic review by our group identified 104 unique peripheral biomarkers associated with RA-ILD among 70 different studies, including a variety of cytokines/chemokines, growth factors, extracellular matrix proteins, tumor markers, lung epithelial or surfactant proteins, and others.[11] Many of these peripheral biomarkers are also recognized to be associated with RA, regardless of ILD status.[12,13] Most studies have focused on a single or select number of peripheral biomarkers for RA-ILD. The few studies that have applied more broad peripheral biomarker analyses in RA-ILD have been performed among small, selected samples.[14,15]

Given the vast range of recognized and candidate biomarkers for RA-ILD, a multidimensional evaluation of composite biomarkers for RA-ILD risk is needed, accounting for the interrelated nature across peripheral biomarker measures. Machine learning approaches have previously been leveraged to identify unique biomarker profiles in RA and other disease states. In this study, we aimed to derive unique peripheral biomarker signatures using an unsupervised machine learning approach among a large, multicenter RA cohort and test whether these biomarker signatures would improve RA-ILD prediction beyond clinical risk factors.

PATIENTS AND METHODS

Study design, population, and demographics. This cross-sectional study was conducted within the Veterans Affairs Rheumatoid Arthritis (VARA) Registry, which is a prospective, multicenter cohort of US veterans with RA fulfilling the 1987 American College of Rheumatology classification criteria that was initiated in 2003.[16,17] This study was approved by the Veterans Affairs (VA) Nebraska-Western Iowa Health Care System Institutional Review Board (IRB; 1576193), with each site receiving IRB approval and all participants providing written informed consent. Study participants and the public were not involved in the design, reporting, or dissemination plans of this research.

Clinical and demographic data, including age, sex, race and ethnicity, body mass index (BMI; in kilograms per square meter), RA disease duration, and cigarette smoking history (categorized as ever or never smoker), were recorded at the time of registry enrollment. Race and ethnicity was self-reported from a fixed set of categories and subsequently categorized for this study as non-Hispanic White or other. The Disease Activity Score With 28-Joint Count (DAS28) and Multidimensional Health Assessment Questionnaire were documented by treating rheumatologists at enrollment. Disease-modifying antirheumatic drug (DMARD) use at enrollment was determined by linkage with administrative pharmacy dispensing data obtained through the VA Corporate Data Warehouse. Participants with missing demographic or biomarker data were excluded from the analysis (ie, complete case analysis).

ILD assessment. ILD was assessed in the cohort using screening and validation steps, as previously reported.[7,8,18] All participants were screened for possible ILD based on diagnostic codes for ILD or ILD-related terms in chest computed tomography (CT) reports.[19,20] ILD diagnoses were subsequently validated by a board-certified rheumatologist based on documentation of a diagnosis of ILD in the medical record by the treating provider with supporting findings from either imaging or lung biopsy per the radiology or pathology report (chest CT in 97% of patients with ILD).[19] Diagnostic evaluation (CT, pulmonary function testing, and lung biopsy) was performed according to clinical indication at the discretion of treating providers. Given disease latency, prevalent ILD status was defined as the presence of ILD at any time before and up to two years after registry enrollment. Participants who later developed RA-ILD or who had indeterminate ILD were excluded from analyses. When available, ILD pattern was extracted from clinical radiology reports, biopsy reports, and clinical notes. The presence of honeycombing on chest CT reports was considered additional evidence of a UIP pattern.[18] Forced vital capacity (FVC) percentage predicted was extracted from medical records at the most proximate time to enrollment.

Peripheral biomarker assessment. Biomarker assessment was performed using serum and plasma that were collected at enrollment on all participants and stored at −70°C. Biomarkers were selected based on prior associations with RA and/or RA-ILD as part of previous studies within the VARA cohort.[5,15,18,21–23] Biomarker measurement was performed via either the Mesoscale

University of Texas Southwestern, Dallas; [10]Scott Matson, MD; University of Kansas, Kansas City.

Additional supplementary information cited in this article can be found online in the Supporting Information section (https://acrjournals.onlinelibrary.wiley.com/doi/10.1002/art.43149).

Author disclosures and graphical abstract are available at https://onlinelibrary.wiley.com/doi/10.1002/art.43149.

Address correspondence via email to Bryant R. England, MD, PhD, at bryant.england@unmc.edu.

Submitted for publication October 30, 2024; accepted in revised form February 20, 2025.

Table 1. Peripheral biomarkers included in principal component analysis*

Variable	Measurement method
Adipocytokine	
Adiponectin	Mesoscale discovery
FGF-21	Mesoscale discovery
Leptin	Mesoscale discovery
Alarmin/cytokine	
IL-17e–IL-25	Mesoscale discovery
IL-33	Mesoscale discovery
TSLP	Mesoscale discovery
Antibody	
Anti-MAA-albumin IgA	ELISA
Anti-MAA-albumin IgG	ELISA
Anti-MAA-albumin IgM	ELISA
Anti-MAA-collagen IgA	ELISA
Anti-MAA-collagen IgG	ELISA
Anti-MAA-collagen IgM	ELISA
Anti-MAA-fibrinogen IgA	ELISA
Anti-MAA-fibrinogen IgG	ELISA
Anti-MAA-fibrinogen IgM	ELISA
Anti-MAA-vimentin IgA	ELISA
Anti-MAA-vimentin IgG	ELISA
Anti-MAA-vimentin IgM	ELISA
IgG-CCP	ELISA
RF	Nephelometry
Chemokine	
Eotaxin	Mesoscale discovery
MCP-1	Mesoscale discovery
MCP-4	Mesoscale discovery
MDC	Mesoscale discovery
MIP-1α	Mesoscale discovery
MIP-1β	Mesoscale discovery
MIP-3α	Mesoscale discovery
TARC	Mesoscale discovery
Collagenase	
MMP1	Mesoscale discovery
MMP3	Mesoscale discovery
MMP7	Mesoscale discovery
MMP9	Mesoscale discovery
Cytokine	
FL	Mesoscale discovery
Fractalkine	Mesoscale discovery
G-CSF	Mesoscale discovery
GM-CSF	Mesoscale discovery
IFNα2a	Mesoscale discovery
IL-1RA	Mesoscale discovery
IL-1α	Mesoscale discovery
IL-1β	Mesoscale discovery
IL-2	Mesoscale discovery
IL-3	Mesoscale discovery
IL-4	Mesoscale discovery
IL-5	Mesoscale discovery
IL-6	Mesoscale discovery
IL-7	Mesoscale discovery
IL-8	Mesoscale discovery
IL-9	Mesoscale discovery
IL-10	Mesoscale discovery
IL-12–IL-23-p40	Mesoscale discovery
IL-12-p70	Mesoscale discovery
IL-13	Mesoscale discovery
IL-15	Mesoscale discovery
IL-16	Mesoscale discovery
IL-17A	Mesoscale discovery
IL-23	Mesoscale discovery
IL-27	Mesoscale discovery
IFN	Mesoscale discovery
TNFα	Mesoscale discovery
VEGF	Mesoscale discovery

* CCP, cyclic citrullinated peptide; ELISA, enzyme-linked immunosorbent assay; FGF, fibroblast growth factor; FL, Fms-like tyrosine kinase 3 ligand; G-CSF, granulocyte colony-stimulating factor; GM-CSF, granulocyte–macrophage colony-stimulating factor; IFN, interferon; IL, interleukin; IL-1RA, IL-1 receptor antagonist; MAA, malondialdehyde-acetaldehyde adduct; MCP, monocyte chemoattractant protein; MDC, macrophage-derived chemokine; MIP, macrophage inflammatory protein; MMP, matrix metalloproteinase; RF, rheumatoid factor; TARC, thymus and activation-regulated chemokine; TNF, tumor necrosis factor; TSLP, thymic stromal lymphopoietin; VEGF, vascular endothelial growth factor.

Discovery platform, enzyme-linked immunosorbent assay (ELISA), or nephelometry (Table 1). Adipokines included adiponectin, fibroblast growth factor (FGF)-21, and leptin. Alarmins included interleukin (IL)-17e–IL-25, IL-33, and thymic stromal lymphopoietin (TSLP). RA-related antibodies included anti-MAA (IgA, IgM, and IgG against MAA-adducted albumin, collagen, fibrinogen, and vimentin; ELISA), anti-CCP (IgG; ELISA), and RF (nephelometry). Chemokines included eotaxin, monocyte chemoattractant proteins, macrophage-derived chemokine, macrophage inflammatory proteins, and thymus and activation-regulated chemokine. Collagenases included matrix metalloproteinases (MMPs). Cytokines included Fms-like tyrosine kinase 3 ligand (FL), fractalkine, granulocyte colony-stimulating factor (CSF), granulocyte–macrophage CSF, interferons (IFNs), ILs, tumor necrosis factor (TNF) α, and vascular endothelial growth factor. All biomarker concentrations were log transformed and standardized for analyses, with a mean ± SD of 0 ± 1.

Genotyping. Genotyping was performed using the Infinium Global Screening Array-24 version 2.0 microarray (Illumina Inc). *MUC5B* rs35705950 was directly measured and passed quality control measures including Hardy–Weinberg equilibrium. The *MUC5B* rs35705950 promoter variant was analyzed via an additive model according to the number of thymine copies as the variant allele.[7]

Statistical analysis. Principal component analysis (PCA) was used to identify unique peripheral biomarker signatures for RA-ILD. PCA is a statistical technique that has the powerful ability to compress large amounts of predictor variables into more accessible groups as well as illustrate patterns in the data based on these variables.[24,25] All standardized, log-transformed biomarkers (Table 1) were included in the PCA. As part of PCA, a correlation matrix was constructed for the aforementioned biomarkers, eigenvalues were calculated from this matrix, and principal components (PCs) were selected based on eigenvalue (>1,

per Kaiser–Guttman rule), scree plots, and cumulative variance.[25–27] An orthogonal varimax rotation was used to improve the interpretability of extracted PCs, forcing variables to align strongly with a single component.[24] Biomarkers with loadings >0.3 were considered to meaningfully represent the respective PC.[26] Each PC was descriptively characterized based on the function of the biomarkers with a meaningful loading. The relationship of each PC with the outcome of RA-ILD was initially evaluated as a PC score within a multivariable logistic regression model that adjusted for age, sex, race and ethnicity, and smoking status.

Clinical variables, including age, sex, race and ethnicity, and smoking history, were included in a multivariable logistic regression model, evaluating the outcome of RA-ILD among the entire cohort with RA. The 15 PCs were included together in a multivariable model assessing the predictive capacity of biomarkers alone. Subsequently, a combined clinical and biomarker logistic regression model was assessed, including the clinical factors and all 15 PCs extracted from the PCA. A final logistic regression model included the combination of clinical factors, PCs, and the *MUC5B* promoter variant. The area under the receiver operating characteristic curve (AUC) was compared among the clinical model, clinical model with PCA, and clinical model with PCA and *MUC5B*, and statistical comparisons were made via the nested likelihood ratio test to evaluate for improvement in model fit. Performance of a clinical model with *MUC5B* was assessed and compared with the clinical model with PCA and *MUC5B*. As a sensitivity analysis, this process was then repeated using an expanded clinical model that included BMI, DAS28, prednisone use, and DMARD use. Additional sensitivity analysis was performed with the inclusion of only those PCs that were individually associated with RA-ILD within the models. Internal validation was performed for all models using bootstrapping with 50 different random samples, and optimism-adjusted measures were obtained.[28]

We performed subgroup analyses of individual PC associations with RA-ILD subtypes (UIP and non-UIP) and FVC severity (FVC <80% and FVC ≥80% predicted) versus without ILD via multivariable logistic regression with adjustment for age, sex, race and ethnicity, and smoking history. Logistic regression model performance was also evaluated on the subgroup with UIP. All analyses were completed with Stata version 18.

RESULTS

Patient characteristics. Among 2,001 participants with RA, 121 (6.4%) were classified as having prevalent ILD. Participants with RA-ILD were older (average age 67.4 vs 63.5 years; $P < 0.001$) and more frequently male (94.2% vs 88.3%; $P = 0.047$) compared to patients with RA without ILD (Table 2). A cigarette smoking history (84.3% vs 77.4%; $P = 0.07$) as well as positivity for RF (86.8% vs 76.3%; $P = 0.01$) and anti-CCP (83.5% vs 76.6%; $P = 0.08$) were more frequent in those with ILD. In patients with RA-ILD, there was more frequent use of biologic or targeted synthetic DMARDs (33.9% vs 25.1%; $P = 0.03$) and prednisone (33.9% vs 17.7%; $P < 0.001$). Among those with RA-ILD, evidence of a UIP pattern was present in 62.8% of patients, and the mean FVC predicted was 77.6%. The *MUC5B* promoter variant occurred more frequently among those with RA-ILD (36.8% vs 16.8%).

PCA. A total of 15 PCs were extracted based on an eigenvalue >1 according to the Kaiser–Guttman rule.[27] These PCs explained 66% of the cumulative variance (Supplementary Table 1), with the first two PCs accounting for the largest amount of variance (PC1 15.5% and PC2 11.9%, respectively). The peripheral biomarkers that loaded onto each respective PC, a descriptive characterization of each PC, and the PC score association with RA-ILD are provided in Table 3. The first two PCs predominantly comprised proinflammatory cytokines and chemokines and were not associated with RA-ILD. Eight PCs were individually associated with RA-ILD. PC3 (adjusted odds ratio [aOR] 1.16, 95% confidence interval [CI] 1.05–1.29) was composed of cytokines involved in the innate immune response (IL-3, IFNα-2a, IL-15, and IL-5). PC4 (aOR 1.28, 95% CI 1.11–1.47), PC7 (aOR 1.18, 95% CI 1.01–1.37), and PC15 (aOR 1.26, 95% CI 1.07–1.49) were composed of distinct anti-MAA antibodies to albumin, fibrinogen, collagen, and/or vimentin. PC6 (aOR 1.17, 95% CI 1.02–1.34) was composed of anti-CCP antibodies and RF. PC8 (aOR 1.43, 95% CI 1.23–1.66) was composed of adipokines and cytokines (FL, leptin, fractalkine, and FGF-21). PC10 (aOR 1.21, 95% CI 1.03–1.41) was composed of alarmins (IL-17e–IL-25 and TSLP). PC12 (aOR 1.20, 95% CI 1.03–1.40) was composed of biomarkers related to tissue remodeling and neutrophil chemotaxis (MMP9 and IL-8). Other PCs were not significantly associated with RA-ILD.

Predictive models for RA-ILD. A logistic regression model including only clinical risk factors was able to discriminate RA-ILD with an AUC of 0.630 (95% CI 0.582–0.679). A logistic regression model composed of all 15 PCs was able to discriminate RA-ILD with an AUC of 0.713 (95% CI 0.662–0.764). When all PC scores were included with the clinical risk factors, the predictive ability of the model was significantly increased over the clinical model (AUC 0.739, 95% CI 0.693–0.786; Figure 1A). The addition of the MUC5B promoter variant to the clinical model with PC further improved performance (AUC 0.751, 95% CI 0.707–0.802; Figure 1A). This was also improved over the clinical model with *MUC5B* (AUC 0.681, 95% CI 0.637–0.726; Table 4). All model comparisons were significant via the nested likelihood ratio test ($P < 0.001$).

Sensitivity analyses with BMI, DAS28, and DMARD use included as additional clinical variables yielded slightly improved performance in clinical model (0.706, 95% CI 0.659–0.752), clinical model with PC (AUC 0.767, 95% CI 0.723–0.811), and clinical

Table 2. Characteristics of participants by RA-ILD status*

Variable	RA no-ILD (N = 1,880), n (%)	RA-ILD (N = 121), n (%)	*P* value
Age at enrollment, mean (±SD), y	63.5 (±11.2)	67.4 (±9.2)	<0.001
Male	1,660 (88.3)	114 (94.2)	0.047
Race and ethnicity			0.36
Non-Hispanic White	1,466 (78.0)	90 (74.4)	
Other	414 (22.0)	31 (25.6)	
Smoking history			0.07
Never smoker	386 (20.5)	15 (12.4)	
Ever smoker	1,456 (77.4)	102 (84.3)	
Unknown	38 (2.0)	4 (3.3)	
Body mass index, mean (±SD)	28.9 (±5.6)	28.5 (±6.1)	0.5
RA duration, mean (±SD), y	11.3 (±11.2)	12.9 (±12.7)	0.15
Anti-CCP seropositivity	1,441 (76.6)	101 (83.5)	0.08
RF seropositivity	1,435 (76.3)	105 (86.8)	0.01
DAS28-CRP, mean (±SD)	3.6 (±1.4)	3.7 (±1.3)	0.21
MD-HAQ, mean (±SD)	0.9 (±0.6)	1.0 (±0.5)	0.11
Prednisone use	332 (17.7)	41 (33.9)	<0.001
cDMARD use	1,379 (73.4)	94 (77.7)	0.29
b/tsDMARD use	471 (25.1)	41 (33.9)	0.03
MUC5B promoter variant			<0.001
0	1,471 (83.2)	74 (63.2)	
1	280 (15.8)	42 (35.9)	
2	18 (1.0)	1 (0.9)	
FVC predicted, mean (±SD), %	–	77.6 (±15.9)	–
ILD pattern			
UIP	–	76 (62.8)	–
Other ILD pattern (NSIP, etc)	–	36 (29.8)	–
Unknown/missing	–	9 (7.4)	–

* b/tsDMARD, biologic or targeted synthetic disease-modifying antirheumatic drug; CCP, cyclic citrullinated peptide; cDMARD, conventional disease-modifying antirheumatic drug; DAS28-CRP, Disease Activity Score With 28-Joint Count and C-reactive protein; FVC, forced vital capacity; MD-HAQ, Multidimensional Health Assessment Questionnaire; NSIP, nonspecific interstitial pneumonia; RA-ILD, rheumatoid arthritis–associated interstitial lung disease; RA no-ILD, rheumatoid arthritis without interstitial lung disease; RF, rheumatoid factor; UIP, usual interstitial pneumonia.

model with PC and *MUC5B* (AUC 0.776, 95% CI 0.733–0.823; Figure 1B). Again, all model comparisons were significant via the nested likelihood ratio test ($P < 0.001$). Sensitivity analysis with PCs selected based on individual associations (PC3, PC4, PC6, PC7, PC8, PC10, PC12, and PC15) did not significantly impact the results (Table 4). Internal validation was performed on all models using bootstrapping. Model performance was attenuated with optimism correction, but the overall trend in performance among the various models was preserved, as shown in Table 4.

Subgroup analyses. Subgroup analyses were performed to evaluate the association of each individual PC with RA-ILD based on ILD subtype and FVC impairment. Most PC associations with RA-ILD were consistent across subgroups (Supplementary Table 2). The exception was PC10 (IL-17e–IL-25 and TSLP), which was positively associated with UIP and negatively associated with non-UIP ILD. Additionally, PC13 (IgA/IgM antibodies to MAA-adducted collagen and adiponectin) was more closely associated with non-UIP ILD, and PC7 (IgA/IgG/IgM antibodies to MAA-adducted fibrinogen, collagen, and vimentin) was more closely associated with severe ILD (FVC < 80%), though 95% CIs for estimates were overlapping. Although a clinical model performed similarly in the subgroup with UIP (AUC 0.635 vs 0.630), there was a substantial improvement in performance of the PC model (AUC 0.768 vs 0.713) and combined models (clinical model with PC and *MUC5B* AUC 0.834 vs 0.755; Supplementary Table 3).

DISCUSSION

In this study, we identified unique peripheral biomarker signatures occurring in a large, diverse RA population and evaluated their association with the presence of RA-ILD. PCs that were positively associated with RA-ILD were characterized by biomarkers that encompassed inflammatory cytokines (IL-3, IL-5, IL-8, IL-15, INFα-2a), autoantibodies (anti-MAA, anti-CCP, RF), adipokines (FL, leptin, fractalkine, FGF-21), alarmins (IL-17e–IL-25, TSLP), and MMPs (MMP9). The variety of immune pathways and inflammatory processes associated with RA-ILD highlight the diversity of pathways that likely contribute to RA-ILD risk and pathogenesis or that are impacted by the presence of RA-ILD. Furthermore, combining these biomarker signatures with clinical risk and genetic factors improved RA-ILD risk stratification, illustrating the potential role of peripheral blood biomarkers in facilitating RA-ILD identification.

Table 3. Extracted peripheral biomarker principal components and their association with RA-ILD*

Principal component	Loading	Theme	aOR[a] for RA-ILD (95% CI)
1		Macrophage-related chemokines	0.96 (0.91–1.02)
MCP4	0.319		
MDC	0.311		
IL-16	0.310		
MCP1	0.306		
IL-27	0.304		
IL-7	0.302		
2		Proinflammatory cytokines	1.04 (0.98–1.10)
IL-1β	0.352		
IL-4	0.344		
IL-1α	0.308		
IL-6	0.304		
3		Myeloid differentiation; innate immune response; allergic response	1.16 (1.05–1.29)
IL-3	0.478		
IFNα-2a	0.407		
IL-15	0.375		
IL-5	0.309		
4		Autoantibodies; oxidative stress	1.28 (1.11–1.47)
IgA-MAA-Alb	0.565		
IgG-MAA-Alb	0.533		
IgM-MAA-Alb	0.560		
5		Adaptive immune response	0.97 (0.85–1.10)
IL-12–IL-23-p40	0.649		
IL-17A	0.532		
6		Autoantibodies	1.17 (1.02–1.34)
IgG-CCP	0.600		
RF	0.546		
7		Autoantibodies; oxidative stress	1.18 (1.01–1.37)
IgM-MAA-Fib	0.612		
IgM-MAA-Col	0.527		
IgA-MAA-Fib	0.314		
IgG-MAA-Vim	0.302		
8		Adipocytokines; metabolism regulation	1.43 (1.23–1.66)
FL	0.482		
Leptin	0.476		
Fractalkine	0.460		
FGF-21	0.391		
9		Autoantibodies; oxidative stress	1.10 (0.95–1.27)
IgG-MAA-Fib	0.588		
IgG-MAA-Col	0.468		
IgG-MAA-Vim	0.448		
10		Alarmins	1.21 (1.03–1.41)
IL-17e–IL-25	0.665		
TSLP	0.427		
11		Tissue remodeling	1.01 (0.88–1.17)
MMP3	0.652		
MMP7	0.521		
12		Tissue remodeling; neutrophil chemotaxis	1.20 (1.03–1.40)
MMP9	0.580		
IL-8	0.318		
13		Autoantibodies; oxidative stress; adipokines	1.10 (0.95–1.27)
IgA-MAA-Col	0.576		
Adiponectin	0.563		
IgG-MAA-Col	0.340		
14		Innate immune response	1.02 (0.87–1.18)
IL-33	0.641		
15		–	1.26 (1.07–1.49)
IgA-MAA-Vim	−0.439		

* Biomarkers with absolute loading value >0.3 are shown. Alb, albumin; aOR, adjusted odds ratio; CCP, cyclic citrullinated peptide; CI, confidence interval; Col, collagen; FGF, fibroblast growth factor; Fib, fibrinogen; FL, Fms-like tyrosine kinase 3 ligand; IFN, interferon; IL, interleukin; MAA, malondialdehyde-acetaldehyde adduct; MCP, monocyte chemoattractant protein; MDC, macrophage-derived chemokine; MMP, matrix metalloproteinase; RA-ILD, RA-ILD, rheumatoid arthritis–associated interstitial lung disease; RF, rheumatoid factor; TSLP, thymic stromal lymphopoietin; Vim, vimentin.

[a] Odds ratio values were adjusted for age, sex, race and ethnicity, and smoking history.

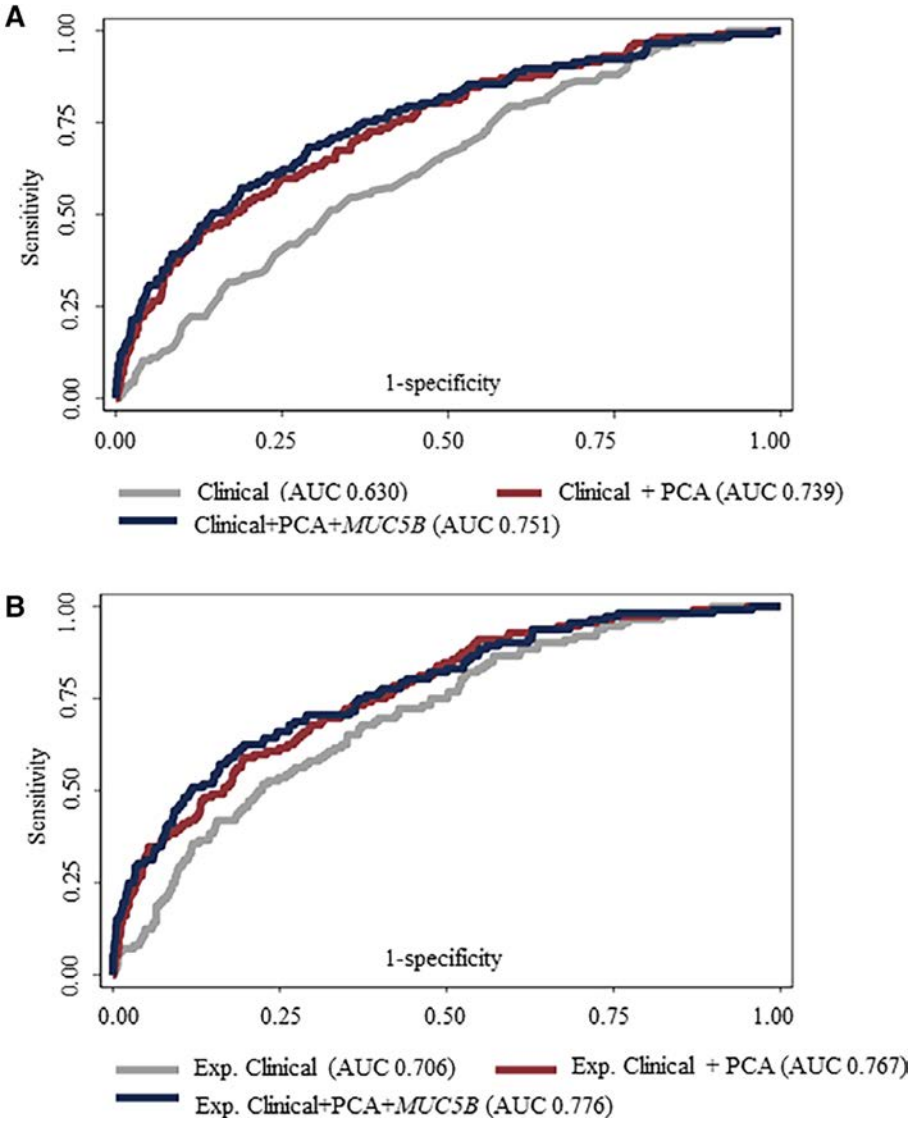

Figure 1. Receiver operating characteristic curves for logistic regression models for rheumatoid arthritis–associated interstitial lung disease including clinical risk factors, principal components, and *MUC5B* promoter variant. Receiver operating characteristic curves, along with their respective area under the receiver operating characteristic curve (AUC), are shown in each panel for clinical model alone, clinical model with principal components analysis (clinical + PCA), and clinical model with PCA and *MUC5B* promoter variant (clinical+PCA+*MUC5B*). (A) Clinical risk factors include age, sex, race and ethnicity, and smoking history. (B) Expanded (Exp.) clinical risk factors include the above plus body mass index, Disease Activity Score With 28-Joint Count, prednisone use, conventional disease-modifying antirheumatic drug (DMARD) use, and biologic or targeted synthetic DMARD use. All model comparisons were significantly different by nested likelihood ratio test ($P < 0.001$).

The current lack of RA-ILD screening strategies is due in part to a paucity of informative clinical risk factors for RA-ILD. This was evident in our study, in which models with only clinical risk factors yielded modest AUC values. Adding the biomarker PCs significantly improved the predictive performance of a model for the identification of RA-ILD over clinical risk factors alone. This improvement suggests that using peripheral blood biomarkers could help overcome the limited predictive value of clinical risk factors for RA-ILD. Although the performance of a model with clinical risk factors and peripheral biomarker signatures was statistically improved with the further addition of the *MUC5B* promoter variant, the absolute improvement in AUC was relatively modest. However, this degree of improvement was similar to the effect observed by adding the *MUC5B* promoter variant to clinical prediction models of RA-ILD,[8] suggesting that this genetic variant identifies features of susceptibility not captured through peripheral biomarkers. Additional research investigating the utility of integrating more comprehensive genetic and proteomic measurements into such models is warranted.

Biomarker themes that emerged through the PCA included myeloid differentiation, the innate immune and allergic responses, autoantibodies (specifically anti-MAA, anti-CCP, and RF),

Table 4. Performance of regression models for RA-ILD before and after internal validation*

Model	AUC (95% CI)	Optimism-adjusted AUC (95% CI)[a]
Primary analyses		
Clinical factors	0.630 (0.583–0.679)	0.609 (0.558–0.669)
PCs	0.713 (0.662–0.764)	0.677 (0.628–0.723)
Clinical with *MUC5B*	0.681 (0.637–0.726)	0.663 (0.625–0.702)
Clinical with PCs	0.739 (0.693–0.786)	0.693 (0.647–0.740)
Clinical with PCs and *MUC5B*	0.755 (0.707–0.802)	0.713 (0.667–0.758)
Sensitivity analyses		
Expanded clinical[b]	0.706 (0.659–0.752)	0.671 (0.626–0.716)
Expanded clinical with PCs	0.767 (0.723–0.811)	0.712 (0.665–0.757)
Expanded clinical with PCs and *MUC5B*	0.776 (0.731–0.821)	0.724 (0.676–0.782)
Selected PCs[c]	0.702 (0.651–0.753)	0.677 (0.621–0.732)
Clinical with selected PCs	0.731 (0.684–0.778)	0.695 (0.659–0.748)
Clinical with selected PCs and *MUC5B*	0.749 (0.701–0.797)	0.716 (0.675–0.770)

* AUC, area under the receiver operating characteristic curve; CI, confidence interval; DMARD, disease-modifying antirheumatic drug; *MUC5B*, *MUC5B* rs35705950 promoter variant; PC, principal component; RA-ILD, rheumatoid arthritis–associated interstitial lung disease.
[a] Internal validation by was achieved through bootstrapping.
[b] Expanded refers to the addition of body mass index, Disease Activity Score With 28-Joint Count, prednisone use, conventional DMARD use, and biologic or targeted synthetic DMARD use to the clinical model.
[c] Selected refers to the inclusion of only the PCs that were individually associated with RA-ILD.

adipokines/metabolism, alarmins, tissue remodeling, and neutrophil chemotaxis. These findings may hint toward the diverse pathophysiologic pathways involved in RA-ILD, many of which are supported by prior literature. It has been demonstrated that serum anti–citrullinated protein antibodies (ACPAs) correlate with local ACPA production in the lung mucosa and mucosal inflammation, leading to the "mucosal origins" hypothesis of RA.[29,30] Inflammatory cytokines such as TNF, IL-1, IL-4, IL-5, IL-13, and several chemokines are thought to likely play a role in the transition from epithelial injury to the development of lung fibrosis.[29] MAA expression in lung tissue has been shown to be higher in RA-ILD than in other forms of ILD, emphysema, or controls, and autoreactive B cells to MAA have been found in the lung and joint tissue of patients with RA.[5,31] Adipokines, specifically adiponectin and leptin, have been shown to play a regulatory role in the inflammatory response, which has been suspected to have a potential role in ILD pathogenesis.[32] MMPs (including MMP9) have been shown to be overexpressed by alveolar epithelial cells within fibroblastic foci of the lungs in idiopathic pulmonary fibrosis and drive lung fibrosis in a highly similar disease process to UIP RA-ILD.[29,33] Thus, our findings are in line with these prior studies and emphasize the need for further translational and mechanistic efforts to determine how these processes are involved in RA-ILD pathogenesis.

In the subgroup analyses, we found that the associations of PCs with UIP RA-ILD were generally consistent with those for all RA-ILD, likely reflecting the preponderance of UIP in RA-ILD. Interestingly, PC10 (IL-17e–IL-25 and TSLP) was positively associated with a UIP pattern and negatively associated with other ILD patterns. This has not been previously demonstrated, and this hypothesis-generating finding warrants further investigation into factors that differentiate specific ILD patterns and severity. Notably, because of the limited number of patients with ILD in subgroup analyses, we were unable to detect modest differences in PC associations with subgroups with RA-ILD. There was improvement in clinical/biomarker/MUC5B model performance for the outcome of UIP over all RA-ILD. This was limited by power but supports the idea that risk stratification efforts in RA-ILD may need to be pattern specific.

Strengths of this study include a large, diverse, multicenter US cohort of well-phenotyped patients with RA with comprehensive RA-ILD identification and peripheral biomarker measurements.[19] Limitations include a lack of chest CT imaging for the entirety of the cohort given that RA-ILD testing was performed as part of routine clinical care. This may result in misclassification of subclinical ILD as non-ILD. However, our results illustrate the utility of peripheral biomarker signatures for RA-ILD risk stratification in a real-world practice setting. ILD pattern (UIP, nonspecific interstitial pneumonia, etc) was unavailable for some patients (n = 9) and was based on clinical determinations rather than a separate research evaluation. Although this cohort is predominantly male, it is reflective of the national VA population, and RA-ILD preferentially affects males. Although the lack of external validation is a limitation, internal validation was performed via bootstrapping, and models underwent optimism correction, which did not impact the interpretation of findings. Given the cross-sectional nature of this study, there is potential for reverse causality between RA-ILD and peripheral biomarkers, although with the goal of identifying prevalent disease, this should not impact the interpretation of our results. We included a broad range of peripheral blood biomarkers implicated in RA and RA-ILD pathogenesis but were unable to include all previously reported biomarkers associated with ILD. This remains an evolving area of research, and future studies will need to continually reassess other novel biomarkers that would benefit from inclusion.[34–36] Last, the PCA method used allowed for the

identification of distinct biomarker profiles within a broad range of potential peripheral biomarkers and their association with RA-ILD. However, alternative approaches would be needed to identify individual biomarker cutoffs or evaluate the clinical application of predictive models, including the use of other machine learning techniques to guide efficient biomarker selection for clinical prediction models.

In conclusion, PCA identified distinct peripheral biomarker signatures that implicate a wide range of biologic pathways associated with RA-ILD. These peripheral biomarker signatures significantly improved ILD discrimination in a large cohort with RA beyond clinical risk factors alone. The addition of the *MUC5B* promoter variant resulted in a modest improvement over clinical and peripheral biomarker models. Further investigation is needed regarding the effective use of peripheral biomarkers in the identification of RA-ILD as well as applications toward ILD incidence and progression. This includes their additive contribution to other clinical and genetic risk factors and their relationship to the various pathways involved in RA-ILD pathogenesis that could impact therapeutic targeting.

AUTHOR CONTRIBUTIONS

All authors contributed to at least one of the following manuscript preparation roles: conceptualization AND/OR methodology, software, investigation, formal analysis, data curation, visualization, and validation AND drafting or reviewing/editing the final draft. As corresponding author, Dr England confirms that all authors have provided the final approval of the version to be published, and takes responsibility for the affirmations regarding article submission (eg, not under consideration by another journal), the integrity of the data presented, and the statements regarding compliance with institutional review board/Declaration of Helsinki requirements.

REFERENCES

1. Marigliano B, Soriano A, Margiotta D, et al. Lung involvement in connective tissue diseases: a comprehensive review and a focus on rheumatoid arthritis. Autoimmun Rev 2013;12(11):1076–1084.
2. Spagnolo P, Lee JS, Sverzellati N, et al. The lung in rheumatoid arthritis: focus on interstitial lung disease. Arthritis Rheumatol 2018;70(10): 1544–1554.
3. Chartrand S, Lee JS, Swigris JJ, et al. Clinical characteristics and natural history of autoimmune forms of interstitial lung disease: a single-center experience. Lung 2019;197(6):709–713.
4. Kelly CA, Saravanan V, Nisar M, et al. Rheumatoid arthritis-related interstitial lung disease: associations, prognostic factors and physiological and radiological characteristics--a large multicentre UK study. Rheumatology (Oxford) 2014;53(9):1676–1682.
5. England BR, Duryee MJ, Roul P, et al. Malondialdehyde-acetaldehyde adducts and antibody responses in rheumatoid arthritis-associated interstitial lung disease. Arthritis Rheumatol 2019;71(9):1483–1493.
6. Juge PA, Lee JS, Ebstein E, et al. MUC5B promoter variant and rheumatoid arthritis with interstitial lung disease. N Engl J Med 2018; 379(23):2209–2219.
7. Wheeler AM, Baker JF, Poole JA, et al. Genetic, social, and environmental risk factors in rheumatoid arthritis-associated interstitial lung disease. Semin Arthritis Rheum 2022;57:152098.
8. Wheeler AM, Baker JF, Riley T, et al. Development and internal validation of a clinical and genetic risk score for rheumatoid arthritis-associated interstitial lung disease. Rheumatology (Oxford) 2025;64:268–275.
9. Juge PA, Granger B, Debray MP, et al. A risk score to detect subclinical rheumatoid arthritis-associated interstitial lung disease. Arthritis Rheumatol 2022;74(11):1755–1765.
10. Matson SM, Deane KD, Peljto AL, et al. Prospective identification of subclinical interstitial lung disease in a rheumatoid arthritis cohort is associated with the MUC5B promoter variant. Am J Respir Crit Care Med 2022;205(4):473–476.
11. Van Kalsbeek D, Brooks R, Shaver D, et al. Peripheral blood biomarkers for rheumatoid arthritis-associated interstitial lung disease: a systematic review. ACR Open Rheumatol 2023;5:201–226.
12. Centola M, Cavet G, Shen Y, et al. Development of a multi-biomarker disease activity test for rheumatoid arthritis. PLoS One 2013;8(4): e60635.
13. Abdelhafiz D, Baker T, Glascow DA, et al. Biomarkers for the diagnosis and treatment of rheumatoid arthritis - a systematic review. Postgrad Med 2023;135(3):214–223.
14. Wu X, Jeong Y, Poli de Frías S, et al. Serum proteomic profiling of rheumatoid arthritis-interstitial lung disease with a comparison to idiopathic pulmonary fibrosis. Thorax 2022;77(10):1041–1044.
15. Kass DJ, Nouraie M, Glassberg MK, et al. Comparative profiling of serum protein biomarkers in rheumatoid arthritis-associated interstitial lung disease and idiopathic pulmonary fibrosis. Arthritis Rheumatol 2020;72(3):409–419.
16. Mikuls TR, Reimold A, Kerr GS, et al. Insights and implications of the VA Rheumatoid Arthritis Registry. Fed Pract 2015;32(5):24–29.
17. Arnett FC, Edworthy SM, Bloch DA, et al. The American Rheumatism Association 1987 revised criteria for the classification of rheumatoid arthritis. Arthritis Rheum 1988;31(3):315–324.
18. Luedders BA, Wheeler AM, Ascherman DP, et al. Plasma matrix metalloproteinase concentrations and risk of interstitial lung disease in a prospective rheumatoid arthritis cohort. Arthritis Rheumatol 2024;76:1013–1022.
19. England BR, Roul P, Mahajan TD, et al. Performance of administrative algorithms to identify interstitial lung disease in rheumatoid arthritis. Arthritis Care Res (Hoboken) 2020;72(10):1392–1403.
20. Luedders BA, Cope BJ, Hershberger D, et al. Enhancing the identification of rheumatoid arthritis-associated interstitial lung disease through text mining of chest computerized tomography reports. Semin Arthritis Rheum 2023;60:152204.
21. Gould PW, Zemel BS, Taratuta EG, et al. Circulating fibroblast growth factor-21 levels in rheumatoid arthritis: associations with disease characteristics, body composition, and physical functioning. J Rheumatol 2021;48(4):504–512.
22. Baker JF, England BR, George MD, et al. Elevations in adipocytokines and mortality in rheumatoid arthritis. Rheumatology (Oxford) 2022; 61(12):4924–4934.
23. Poole JA, England BR, Sayles H, et al. Serum alarmins and the risk of incident interstitial lung disease in rheumatoid arthritis. Rheumatology (Oxford) 2023;63:1998–2005.
24. Sainani KL. Introduction to principal components analysis. PM R 2014;6(3):275–278.
25. Giuliani A. The application of principal component analysis to drug discovery and biomedical data. Drug Discov Today 2017;22(7):1069–1076.
26. Field A. Discovering Statistics Using IBM SPSS Statistics. SAGE; 2013.
27. Kaiser HF. The application of electronic computers to factor analysis. Educ Psychol Meas 1960;20(1):141–151.
28. Fernandez-Felix BM, García-Esquinas E, Muriel A, et al. Bootstrap internal validation command for predictive logistic regression models. Stata J 2021;21(2):498–509.

29. Kadura S, Raghu G. Rheumatoid arthritis-interstitial lung disease: manifestations and current concepts in pathogenesis and management. Eur Respir Rev 2021;30(160):210011.
30. Holers VM, Demoruelle MK, Kuhn KA, et al. Rheumatoid arthritis and the mucosal origins hypothesis: protection turns to destruction. Nat Rev Rheumatol 2018;14(9):542–557.
31. Sahlström P, Joshua V, Valkovskaia V, et al. Autoreactive B cells against malondialdehyde-induced protein cross-links are present in the joint, lung, and bone marrow of rheumatoid arthritis patients. J Biol Chem 2023;299(11):105320.
32. Haley S, Shah D, Romero F, et al. Scleroderma-related lung disease: are adipokines involved pathogenically? Curr Rheumatol Rep 2013; 15(12):381.
33. Spagnolo P, Kropski JA, Jones MG, et al. Idiopathic pulmonary fibrosis: disease mechanisms and drug development. Pharmacol Ther 2021;222:107798.
34. Matsuo T, Hashimoto M, Ito I, et al. Interleukin-18 is associated with the presence of interstitial lung disease in rheumatoid arthritis: a cross-sectional study. Scand J Rheumatol 2019;48(2):87–94.
35. Doyle TJ, Patel AS, Hatabu H, et al. Detection of rheumatoid arthritis-interstitial lung disease is enhanced by serum biomarkers. Am J Respir Crit Care Med 2015;191(12):1403–1412.
36. Hussein MS, El-Barbary AM, Nada DW, et al. Identification of serum interleukin-13 and interleukin-13 receptor subunit expressions: rheumatoid arthritis-associated interstitial lung disease. Int J Rheum Dis 2021;24(4):591–598.

Arthritis & Rheumatology
Vol. 77, No. 8, August 2025, pp 981–995
DOI 10.1002/art.43143

American College of Rheumatology
Empowering Rheumatology Professionals

Plasma Proteomic Profiles Predict Individual Future Osteoarthritis Risk

Zijian Kang,[1] Jianzheng Zhang,[2] Wenxin Liu,[1] Chen Zhu,[3] Ying Zhu,[4] Ping Li,[5] Kai Li,[5] Qiang Tong,[6] and Sheng-Ming Dai[1]

Objective. Osteoarthritis (OA) is a widespread degenerative joint disease that causes a considerable socioeconomic burden. Despite progress in genetic and environmental insights, early diagnosis is still limited by the lack of evident symptoms during the initial phases and accurate biomarkers. This study aims to identify plasma proteins associated with future risk of OA and develop a predictive model.

Methods. We conducted a large-scale proteomic analysis of 45,307 participants from the UK Biobank, excluding those with baseline OA. Plasma samples were assayed using the Olink Explore Proximity Extension Assay targeting 1,463 unique proteins. Clinical variables and OA outcomes were extracted and linked to electronic health records. A predictive model was constructed using the LightGBM machine learning method, and SHapley Additive exPlanations (SHAP) were applied to evaluate the importance of variables.

Results. We identified a panel of proteins significantly associated with the risk of developing OA. Notably, after adjusting for multiple confounders, collagen type IX alpha 1 chain (COL9A1) and cartilage acidic protein 1 (CRTAC1) were the most significant predictors of incident OA, with hazard ratios of 1.54 (95% confidence interval [CI] 1.48–1.61) and 1.65 (95% CI 1.54–1.78), respectively. SHAP analysis allowed a profound interpretation of the contribution of each protein and clinical variable to the model, revealing the multifactorial nature of OA risk prediction. The temporal trajectories of plasma proteins indicated that the levels of COL9A1 and CRTAC1 began to deviate from normal for more than a decade before OA onset, suggesting their potential use in early detection strategies. The predictive model, developed using the LightGBM algorithm, integrated proteins with clinical covariates and demonstrated an area under the curve (AUC) of 0.729 for 5-year OA prediction, 0.721 for 10-year prediction, and 0.723 for all incident OA. The predictive accuracy of the model was further enhanced for hip and knee OA, achieving AUCs of 0.820 and 0.803 for 5-year predictions.

Conclusion. Our study identified the role of plasma proteomics in predicting future OA risk, which could contribute to preemptive measures. The innovative model, which integrates proteomic biomarkers with clinical data, offers a potential tool for risk assessment, potentially optimizing OA management strategies and enhancing prevention efforts.

INTRODUCTION

Osteoarthritis (OA) is a prevalent degenerative joint disease characterized by the progressive deterioration of the cartilage and underlying bone, leading to pain, stiffness, and reduced mobility. It is one of the highest causes of disability worldwide, with an estimated 595 million global cases in 2020, projected to increase by 74.9% for knee OA, 48.6% for hand OA, and 78.6%

Dr Kang's work was supported by the Postdoctoral Fellowship Program of China Postdoctoral Science Foundation (grant 2023M742331) and Pujiang Rheumatism Young Physicians Training Program (grant SPROG2302). Prof. C. Zhu's work was supported by the 2115 Talent Development Program of China Agricultural University.

[1]Zijian Kang, MD, Wenxin Liu, MD, PhD, Sheng-Ming Dai, MD, PhD: Shanghai Sixth People's Hospital Affiliated to Shanghai Jiao Tong University School of Medicine, Shanghai, China; [2]Jianzheng Zhang, MD, PhD: The Fourth Medical Center of Chinese People's Liberation Army (PLA) General Hospital, Beijing, China; [3]Chen Zhu, PhD: China Agricultural University, Beijing, China; [4]Ying Zhu, MD, PhD: The Eighth Medical Center of Chinese PLA General Hospital, Beijing, China; [5]Ping Li, PhD, Kai Li, PhD: Donghua University, Shanghai, China; [6]Qiang Tong, MD, PhD: Shanghai Sixth People's Hospital Affiliated to Shanghai Jiao Tong University School of Medicine, Shanghai, China, and Queen Mary Hospital, Hong Kong, China.

Drs Kang, Zhang, and Liu are co–first authors and contributed equally to this work.

Additional supplementary information cited in this article can be found online in the Supporting Information section (http://onlinelibrary.wiley.com/doi/10.1002/art.43143).

Author disclosures are available at https://onlinelibrary.wiley.com/doi/10.1002/art.43143.

Address correspondence via email to Sheng-Ming Dai, MD, PhD, at shengmingdai@163.com or Qiang Tong, MD, PhD, at jasontong1985@outlook.com.

Submitted for publication August 29, 2024; accepted in revised form January 30, 2025.

for hip OA by 2050 because of population aging.[1] This increasing prevalence imposes a considerable socioeconomic burden, highlighting the urgent need for effective diagnostic and therapeutic interventions.

Over the years, research efforts have diligently explored the mechanisms underlying OA.[2] These studies have investigated genetic, environmental, and lifestyle factors contributing to OA susceptibility.[3–5] For example, polymorphisms in multiple genes have also been identified to be responsible for increasing the risk of OA, such as aggrecan and collagen type II alpha 1 chain, which are critical players in the formation and repair of cartilage.[6] Environmental and lifestyle factors, including obesity, previous joint injury, and repetitive use of joints, have all been attributed to OA in weight-bearing joints such as knees and hips.[7] OA often manifests insidiously, and by the time symptoms become clinically evident, irreversible joint damage may have already occurred.[8,9]

Although advances in imaging techniques and biomarker discovery have enriched our understanding of early disease processes,[10] radiographic and clinical signs of OA often indicate damage only after it has occurred, making timely intervention difficult. In the preclinical stage, specific biomarkers, including plasma biomarkers, may undergo changes that indicate an increased risk of developing OA.[11] As the disease progresses to the symptomatic phase, radiographically detectable structural changes are frequently absent or minimal (Kellgren and Lawrence grade 0–1).[11] Therefore, it is crucial to predict OA before clinically detectable joint damage arises, encompassing both radiographic evidence and persistent symptoms such as frequent pain. This highlights the need for novel approaches to identify individuals at risk before overt symptoms appear. However, existing approaches are limited by small sample sizes, narrow feature sets, and the modest predictive accuracy of combining proteins.[12–14] Furthermore, the potential for prediction in individuals with OA over long periods (eg, 10 years or >10 years) has largely remained unexplored.[15] Plasma proteomics offers excellent potential as an early biomarker because of its ability to detect subtle physiologic changes associated with disease progression. This method has already proven effective in predicting disease onset and prognosis for various diseases.[16–18] Further research is necessary to fully explore this technique's potential to predict OA across various time frames.

The UK Biobank, with >500,000 participants, provides rich proteomic data that can significantly help identify molecular biomarkers associated with OA.[19,20] The availability of longitudinal data coupled with detailed clinical and lifestyle information makes the UK Biobank an invaluable tool for predictive modeling. Machine learning algorithms, especially those proficient in high-dimensional data analysis, have shown potential in developing predictive models of disease risk. LightGBM is a gradient-boosting framework ideal for large, high-dimensional datasets, efficiently managing both categorical and continuous variables.[21,22] Unlike linear models like principal component modeling or orthogonal projection to latent structures discriminant analysis, which may struggle with complex, nonlinear interactions, LightGBM captures intricate relationships and handles missing values. Its leaf-wise tree growth improves speed and accuracy, making it particularly effective for proteomic data with complex protein interactions.[18,23] This method may help synthesize various variables, ranging from genetics to environmental and lifestyle factors, and can discern intricate biologic signatures from extensive cohorts, thereby predicting an individual's OA risk.

In this study, we focused on identifying plasma proteins significantly associated with OA risk using the UK Biobank dataset. In addition, we developed a predictive model based on plasma proteins and clinical variables using the LightGBM machine learning method. SHapley Additive exPlanations (SHAP) were also used to evaluate the variables within the machine learning model. Our model not only identifies risk factors and proteins associated with incident OA but also identifies patients at higher risk of developing OA, offering insights for early intervention and improved disease management.

PATIENTS AND METHODS

Study population. The UK Biobank is an ongoing, large-scale, population-based prospective cohort study with extensive proteomic and phenotypic data collected from >500,000 individuals aged 39 to 70 years from 2006 to 2010. They were registered under the UK NHS and drawn from 22 assessment centers across the UK. We excluded participants with baseline OA, those lost to follow-up, and those with missing proteomic data for analytical purposes.

Blood proteomics. Baseline blood samples were collected from 22 regional assessment centers in the UK. Blood samples were randomly drawn from the participants' first visit at baseline. For each participant, blood was drawn into EDTA tubes and immediately centrifuged at 2,500*g* at 4°C for 10 min to separate the plasma. The supernatant was aliquoted and stored at −80°C for further processing. The samples were then sent on dry ice to the Olink Analysis Service Center in Sweden for uniform quantification using the antibody-based Olink Explore Proximity Extension Assay.[24]

Proteomic analysis was conducted on plasma samples from 54,306 participants. The experimentalists were blinded to the sample characteristics and clinical data. Processing and storage procedures have been described in previous publications.[25] A total of 1,463 unique proteins were measured after stringent quality control measures, representing cardiometabolic, inflammatory, neurologic, and oncologic proteins. Protein levels are reported as normalized protein expression (NPX) values. NPX values were estimated by taking the counts for each sample and each assay, dividing them by the counts of the extension controls, and then

log2 transforming the results. Sources of variation were adjusted using the median normalized counts of the extension controls, batch-specific median NPX values, and assay-specific median NPX values for each batch. Proteomic variables are defined in detail in Supplementary Table 1.

Clinical variables. A wide variety of clinical variables from the UK Biobank database was chosen to study their association with the risk of OA. The selection was guided by the potential influence of these variables on the risk of OA. The following were included: baseline characteristics, such as age, sex, ethnicity, and socioeconomic factors, including occupation, household income, and Townsend index. Anthropometric measures, including body mass index (BMI), weight, height, basal metabolic rate, and trunk fat mass, were used to assess body composition, metabolism, and fat distribution. Lifestyle factors considered included data on participants' smoking status, alcohol intake, physical activity, diet history, and sleep behavior. We also recorded comorbid conditions in the disease, such as hypertension, type 2 diabetes, cardiovascular diseases, and chronic kidney disease, to estimate other health issues that an OA-diagnosed individual might have. Medication use was also reviewed to identify potential interactions or effects associated with OA management or treatment. The detailed clinical variables are presented in Supplementary Table 1.

OA outcomes. Diagnostic data were linked with UK electronic health records, wherein OA symptoms were reported by professional clinicians in hospitals, family doctors in the primary care system, or staff in the UK death registration system. OA was defined using the three-digit *International Classification of Diseases, Tenth Revision* codes for knee, hip, or other OA.[26,27] The main outcome measures were incident cases of OA identified by the earliest date reported in primary care, hospital episode statistics, mortality records, and self-reports. Definitions of the exclusion criteria and diseases are provided in Supplementary Table 2. The date of OA diagnosis was defined as the earliest recorded date in the data described above. Follow-up visits started from the date of entry into the study from the assessment center and ended at the earliest date of diagnosis or death or the last date provided by the hospital or general practitioner, whichever came first. The last recorded and available date is August 2023.

Statistics and analysis. We applied the chi-square test to compare differences among categorical variables. For differences in continuous variables, we used Student's *t*-test for descriptive analysis of the variables of interest. The Cox proportional hazards regression model was used to estimate the association of the NPX values of each plasma protein with the incidence of OA. The reported results are presented as hazard ratios (HRs), 95% confidence intervals (CIs), and *P* values. Model 1 was adjusted for age, sex, BMI, Townsend index, and ethnicity. Model 2 was further adjusted for smoking, drinking, physical activity, hypertension, and diabetes.

To account for the multiplicity of tests, Bonferroni correction was applied to assess significant associations, considering the number of proteins tested (n = 1,463). This correction was used to control the family-wise error rate, ensuring that the significance threshold was set at $P < 0.05$.[28] Following this correction, we performed enrichment analysis on the significant proteins from models 1 and 2 using the ClusterProfiler R package.[29] Benchmarking against the whole background provided by the complete Olink protein set enabled a better understanding of biologic implications. Statistical significance in the analysis was determined using the Fisher exact test, with *P* values further adjusted for multiple comparisons using the Benjamini-Hochberg method to control the false discovery rate.

Significant proteins, identified after Bonferroni correction in both model 1 and model 2 of the Cox proportional hazards regression, were initially subjected to feature selection using Lasso regression (L1 regularization). Lasso was chosen for its ability to manage multicollinearity and impose sparsity, effectively refining the feature set by penalizing less relevant or redundant features. Subsequently, a LightGBM classifier was used to evaluate and refine the selected features.[30] Two feature selection methods, sequential forward selection (SFS) and recursive feature elimination (RFE), were employed to compare model performance under varying numbers of selected features. In the SFS approach, proteins were incrementally added to the LightGBM model based on their ranked importance as assessed by SHAP values. Selection concluded when the optimal area under the curve (AUC) performance was reached, defined as no incremental improvement detected in two consecutive DeLong tests, indicating no significant enhancement in the model performance with additional proteins. The selected proteins were visualized using SHAP plots to elucidate their importance.[31]

The combined effect of these proteins was derived from the LightGBM model and the significant proteins identified during the protein ranking process. Model establishment and assessment were conducted via internal leave-one-area-out cross-validation. The dataset was divided into 10 subgroups. For each iteration, nine subgroups were used as the training set, and the remaining subgroup served as the test set. This process was repeated 10 times, ensuring that each subgroup was tested once. An optimal model for LightGBM was developed by combining the optimal learning rate, maximum tree depth, and number of leaves with hyperparameters adjusted using Bayesian hyperparameter optimization. The receiver operating characteristic curve analysis was used to assess the accuracy of the selected significant proteins and clinical indicators. We implemented a 10-fold cross-validation approach to evaluate the model's performance iteratively across different subsets of the data. The accuracy of the models was compared using AUC values, sensitivity, specificity, and accuracy, with 95% CIs for these metrics calculated based on cross-validation results.

To evaluate the generalizability and robustness of the predictive accuracy of the selected proteins, we replicated the analyses

in the following target populations: OA with onset within 5 years, 10 years, and >10 years, all incident cases, and for knee and hip OA with the same timeframes. In these analyses, individuals who developed OA after the time of interest were considered healthy (eg, in the 10-year prediction analysis, those who developed OA after 10 years were regarded as OA-free because incident cases beyond the 10-year observation period were unknown). For the >10-year analysis, individuals who developed OA within 10 years were also excluded. This design posits a longer follow-up period to determine the predictive value of proteins for developing OA >10 years from the baseline visit.

We illustrated the clinical progression of OA events by high and low baseline protein levels using Kaplan-Meier survival curves. The optimal cutoff point for protein levels was established based on the maximum Youden index, which incorporates sensitivity and specificity in choosing the best threshold to differentiate among groups. The time until the occurrence of OA events in the two groups was plotted using Kaplan-Meier curves. Participants were also stratified by baseline protein levels into tertiles, and the incidence rates of OA were subsequently analyzed.

Using a nested case-control design, we monitored plasma protein dynamics for about 14 years, leading to the diagnosis of OA. Cases were defined as individuals who developed OA during follow-up, and incidence density sampling was applied to select controls from the OA-free cohort members. To reduce potential confounding and ensure comparability between cases and controls, we employed a propensity score matching method. Specifically, we conducted a 1:5 matching of cases and controls based on age, sex, and BMI using a caliper width of 0.1 SDs (0.1 σ). Mean plasma protein concentrations were presented over time up to the index date using a locally weighted scatterplot smoothing curve for both cases and controls. Temporal changes in plasma proteins between those with and without OA were tested using the Mann-Kendall trend test, a robust nonparametric approach to longitudinal data.

Ethical approval. The UK Biobank has obtained ethical approval from the North West Multi-centre Research Ethics Committee (reference number: 11/NW/0382, https://www.ukbiobank.ac.uk/learn-more-about-uk-biobank/about-us/ethics). Informed consent was collected from all study participants via electronic signature.

Data availability. The data supporting this study's findings are available on UK Biobank at http://www.ukbiobank.ac.uk/. Code generated or used during the study is available by reasonable request.

RESULTS

Participant selection and baseline characteristics. The UK Biobank database encompasses a total of 502,357 participants. After excluding 449,655 participants owing to missing proteomics data, 7,190 participants with OA at baseline, and 132 participants without follow-up data, our study included 45,307 participants (Figure 1A). Most participants were White (92.8%), with an average age of 56.15 years. Among them, 52.9% (n = 23,978) were female and 47.1% (n = 21,329) were male (Supplementary Table 3). Over a mean follow-up period of 14.68 years, 7,281 patients were diagnosed with OA during the study period with 2,906 cases occurring within 5 years and 5,376 cases within 10 years (Figure 1A and B). Among the incident OA cases, 1,688 were diagnosed with hip OA, 2,560 with knee OA, 803 with polyarticular OA, and 151 with carpometacarpal (CMC) OA, with hip arthritis and knee arthritis being the predominant types of OA. The median ages at first diagnosis were 67.13 years for OA, 68.95 years for hip OA, and 67.04 years for knee OA (Figure 1B; Supplementary Figure 1A–C).

Incident patients with OA had a higher mean age at recruitment, a greater proportion were female, a higher prevalence were overweight, and higher prevalence had hypertension compared with the control group ($P < 0.001$). Similar results were observed for both hip and knee OA. The key baseline characteristics stratified by incident OA status are presented in Supplementary Table 3.

Identifying proteins associated with incident OA. To identify the proteins that are truly associated with the OA outcome, we used Cox analysis and adjusted for known clinical factors to control for potential confounding effects. Our comprehensive analysis of 1,463 proteomic biomarkers revealed a significant association among a subset of proteins, incident OA, and its subtypes (Figure 2A–C; Supplementary Figure 2A and B). After adjusting for age, sex, BMI, Townsend index, and ethnicity in model 1,387 proteins were found to be significantly correlated with new-onset OA after Bonferroni correction. As a sensitivity analysis, we re-ran all analyses using model 2, which was additionally adjusted for smoking status, drinking status, daily activity, hypertension, and diabetes. A total of 301 proteins remained significantly associated with the development of new-onset OA (Figure 2D). For example, collagen type IX alpha 1 chain (COL9A1) and cartilage acidic protein 1 (CRTAC1) were the most significant predictors of incident OA, with HRs of 1.54 (95% CI1.48–1.61) and 1.65 (95% CI 1.54–1.78), respectively. These biomarkers were also associated with an increased risk of both hip and knee OA. In contrast, BOC cell adhesion associated oncogene regulated and carbonic anhydrase 14 (CA14) exhibited HRs of 0.76 (95% CI 0.71–0.85) and 0.83 (95% CI 0.79–0.88), respectively, suggesting a negative correlation with OA risk (Supplementary Table 4).

We also compared HRs of these protein biomarkers across different OA subtypes, including single-joint OA (hip OA, knee OA, and CMC OA) and polyarticular OA. Our analysis revealed some proteins were associated with all types of OA, such as α-1-microglobulin/bikunin precursor (AMBP), CRTAC1,

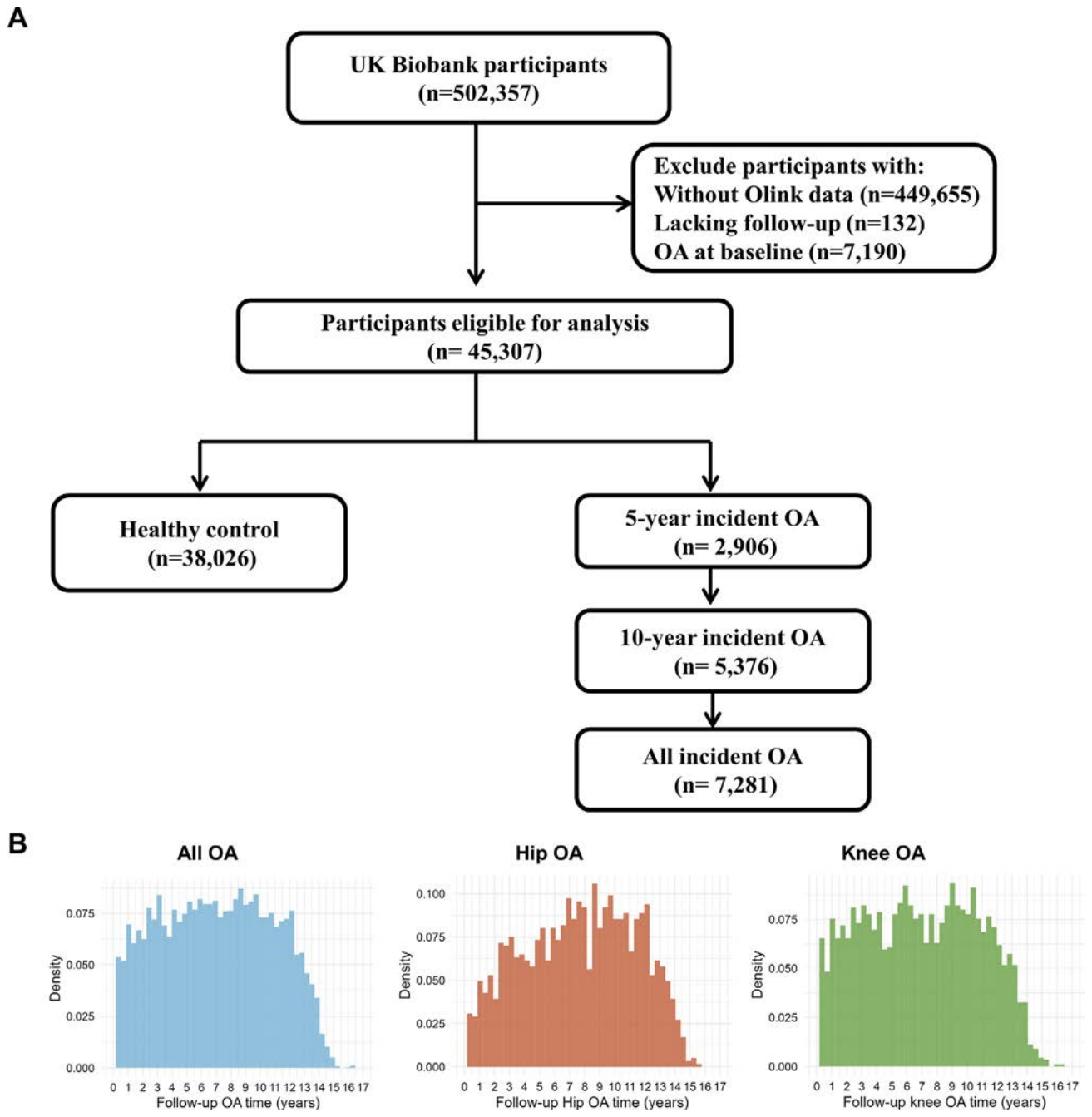

Figure 1. Flowchart of participant selection. (A) In the UK Biobank cohort, individuals who reported OA at baseline or those lacking follow-up time and Olink proteomic data were excluded from the analysis. The remaining participants were categorized based on the year of the first reported OA following baseline. (B) Distribution of the observation period for the first reported OA (left), hip OA (middle), and knee OA (right) since baseline. OA, osteoarthritis.

adrenomedullin, asialoglycoprotein receptor 1, and neurocan. There are also variations in HRs for specific proteins in the risk of OA subtypes. For example, AMBP and basigin (BSG) demonstrated stronger associations for polyarticular OA, CRTAC1 for knee OA, COL9A1 and matrilin 3 (MATN3) for hip OA, and galectin 3 for CMC OA (Supplementary Figure 3). These findings highlight both common and subtype-specific protein biomarkers associated with OA, underscoring the heterogeneity of the disease.

Enrichment analysis revealed several biologic pathways associated with the significantly correlated proteins, such as metabolism proteins, cytokines, cytokine receptor interactions, integral components of the membrane, and the AMP-activated protein kinase pathway, which may provide insights into the

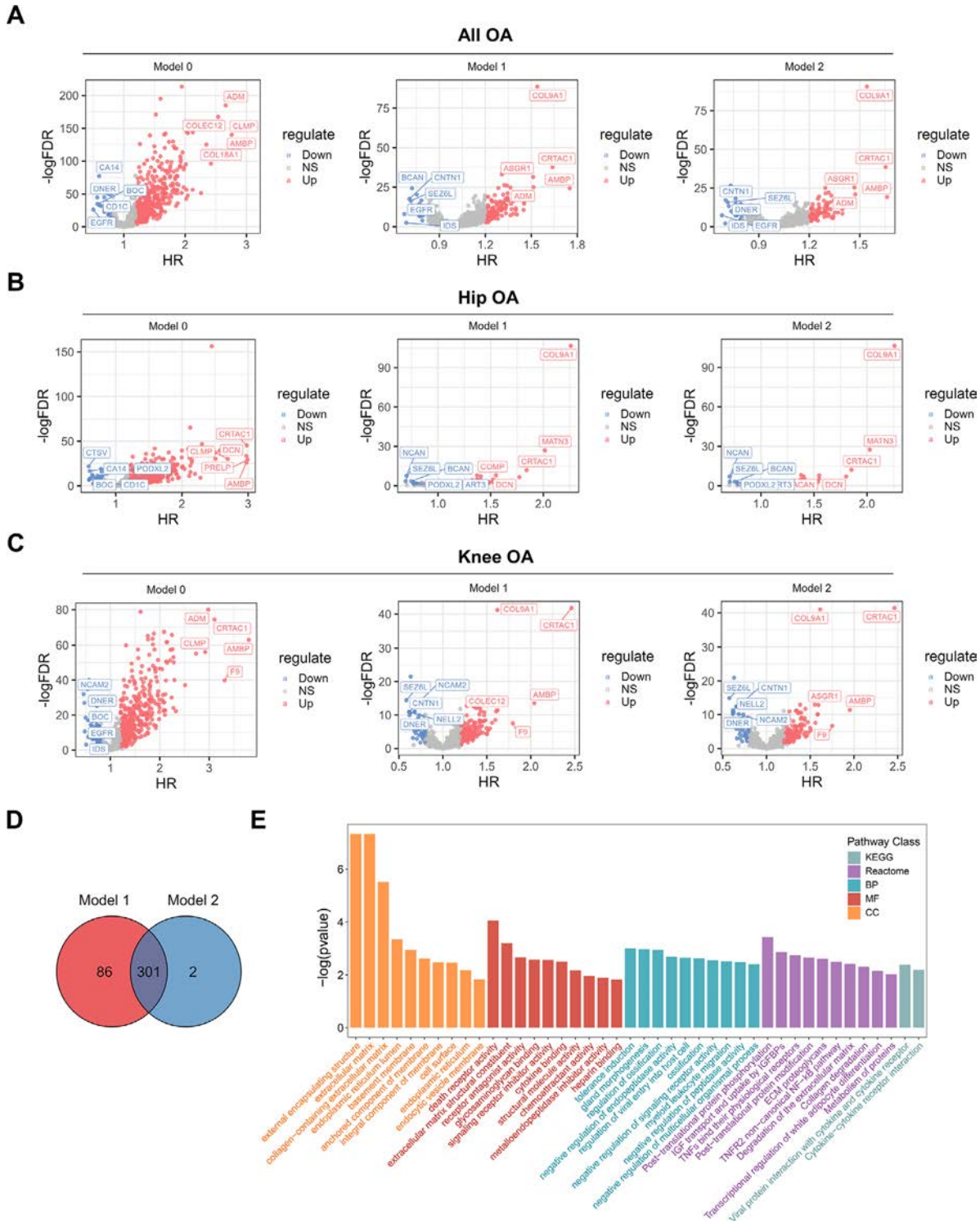

Figure 2. Association of plasma proteins with incident OA. (A–C) Volcano plot depicting the association of 1,463 plasma proteins with (A) incident OA, (B) hip OA, and (C) knee OA in terms of HRs on the x-axis and –log (FDR) on the y-axis. Cox proportional hazards regression in model 0 (left), model 1(middle), and model 2 (right) results are presented here. Model 0 is the crude model. Model 1 is adjusted for age, sex, body mass index, ethnicity, and Townsend index. Model 2 included additional adjustments for daily activities, smoking, alcohol consumption, hypertension, and diabetes. (D) Venn diagram showing the proteins shared between model 1 and model 2. (E) Enrichment of GO, KEGG, and Reactome pathways. Significant proteins identified in either model 1 or model 2 after Bonferroni correction were subjected to enrichment analysis using the Olink protein panel as the background gene set. BP, biologic process; CC, cellular component; ECM, extracellular matrix; FDR, false discovery rate; GO, gene ontology; HR, hazard ratio; IGF, insulin-like growth factor; IGFBP, insulin-like growth factor binding protein; KEGG, Kyoto Encyclopedia of Genes and Genomes; MF, molecular function; NF-κB, nuclear factor κB; NS, not significant; OA, osteoarthritis; TNF, tumor necrosis factor.

molecular mechanisms underlying the development of OA (Figure 2E; Supplementary Table 5).

Protein importance ranking via SHAP analysis. Given that hip and knee OA represent the predominant types of OA, we further constructed predictive models for OA and these two subtypes based on proteomic data. We initially employed the Lasso method to perform a preliminary screening of OA risk proteins (Supplementary Figure 4A and B). Subsequently, we found that the model constructed using SFS outperformed those built with RFE, as illustrated in Supplementary Figure 4C.

The predictive power of the SFS-selected proteins was highlighted by their consistent ranking in the AUC analysis, as shown in a line graph in which the model's AUC rises significantly upon the addition of more predictors then marginally improves. COL9A1 and CRTAC1 emerged as the most significant predictors for OA and its subtypes (Figure 3A; Supplementary Figures 5–7). Specifically, for all OA, COL9A1 was the strongest predictor, followed by CRTAC1, ectodysplasin A2 receptor (EDA2R), and leptin (LEP) (Figure 3A; Supplementary Figure 5A–C). COL9A1 was the strongest predictor of hip OA, followed by CRTAC1, MATN3, and adenosine diphosphate ribosyltransferase 3 (ART3) (Supplementary Figure 6A and B). CRTAC1 was the top predictor for knee OA, followed by COL9A1, cartilage oligomeric matrix protein (COMP), and chromogranin B (CHGB) (Supplementary Figure 7A and B).

The predictive power for OA increased when the first few proteins were included and gradually leveled off as more proteins were added (Figure 3A; Supplementary Figures 6A and 7A). Using this system based on order of importance, we ultimately selected the top six proteins (COL9A1, CRTAC1, EDA2R, LEP, ART3, and growth differentiation factor 15 [GDF15]) for OA prediction, eight proteins (COL9A1, CRTAC1, ART3, EDA2R, MATN3, actin alpha 2 smooth muscle, BOC and follistatin) for hip OA prediction, and eight proteins (CRTAC1, COL9A1, COMP, CHGB, LEP, AMBP, kallikrein-related peptidase 14, and CD200 molecule) for knee OA prediction for subsequent protein model construction.

SHAP plots were used to visually interpret the impact of each selected protein through the magnitude of its values (encoded by a color gradient) and the direction of its tendency on the horizontal axis (the likelihood of developing OA), as shown in Figure 3B, Supplementary Figure 6B, and Supplementary Figure 7B. For instance, COL9A1 has the broadest range among new-onset OA and hip OA, indicating its most significant predictive power. Moreover, participants with higher CRTAC1 levels were more likely to develop knee OA. Patients with high ART3 and CA14 levels remained healthy, suggesting a negative correlation with disease risk. Similar interpretations have been provided for the remaining proteins.

Prognostic value and temporal dynamics of plasma proteins in OA progression. We further investigated the predictive ability of baseline plasma protein levels for the development of OA. Baseline protein data were divided into high and low groups with cutoff values optimized to maximize the Youden index for delineating between those who had and had not developed OA in the follow-up period. Participants with higher baseline levels of COL9A1, CRTAC1, EDA2R, LEP, and GDF15 exhibited an increased risk of developing OA. ART3 expression was associated with a lower risk of OA (Figure 4A). This finding was also evident in hip OA and knee OA (Supplementary Figures 8A and 9A).

Next, we explored how proteins stratified the risk of incident OA. Participants with higher baseline protein percentiles had a higher rate of events than those with lower protein percentiles (Figure 4B). This was consistent across the OA subgroups (Supplementary Figures 8B and 9B). Finally, we determined the temporal trajectories of plasma proteins from the time to OA diagnosis. A 14-year retrospective time scale was used to track these changes. Protein trajectories in individuals who developed OA were then compared with those in individuals who remained OA-free during the same period. Smoothed splines demonstrated that plasma levels of COL9A1 and CRTAC1 deviated from normal values >10 years before the onset of OA, whereas their expression levels remained stable in the control cohort (Supplementary Figure 10A). Consistent patterns were observed in both hip and knee OA. EDA2R and GDF15 also gradually increased as the onset of OA approached, and their levels are elevated compared with those of the control cohort. Other proteins in hip and knee OA did not show significant differences during the time approaching disease onset (Supplementary Figure 11A and B). The above findings indicate that changes in plasma COL9A1 and CRTAC1 could be evident years before the onset of OA.

We also evaluated the diagnostic performance of each protein for OA, and the results indicated that the predictive power of individual proteins for OA is approximately between 0.55 and 0.6, suggesting a moderate ability to predict OA outcomes (Supplementary Figures 12 and 13A and B). These results highlight the importance of combining them with other variables to enhance predictive power.

Clinical data selection and importance ranking via SHAP analysis. We introduced approximately 150 clinical variables in the prediction of OA by adding demographic characteristics, lifestyle habits, income, occupation, activity status, biochemical indicators, and pain questionnaires. Through the initial screening process using Lasso, a subset of candidate factors was identified, most of which have been previously reported to correlate with OA risk (Supplementary Figure 14A and B). The AUC value for variable selection using SFS was also higher than that achieved with RFE (Supplementary Figure 14C). The top 50 predictive factors were developed and ordered based on their values to predict the results. (Figure 5A). Several predictive factors

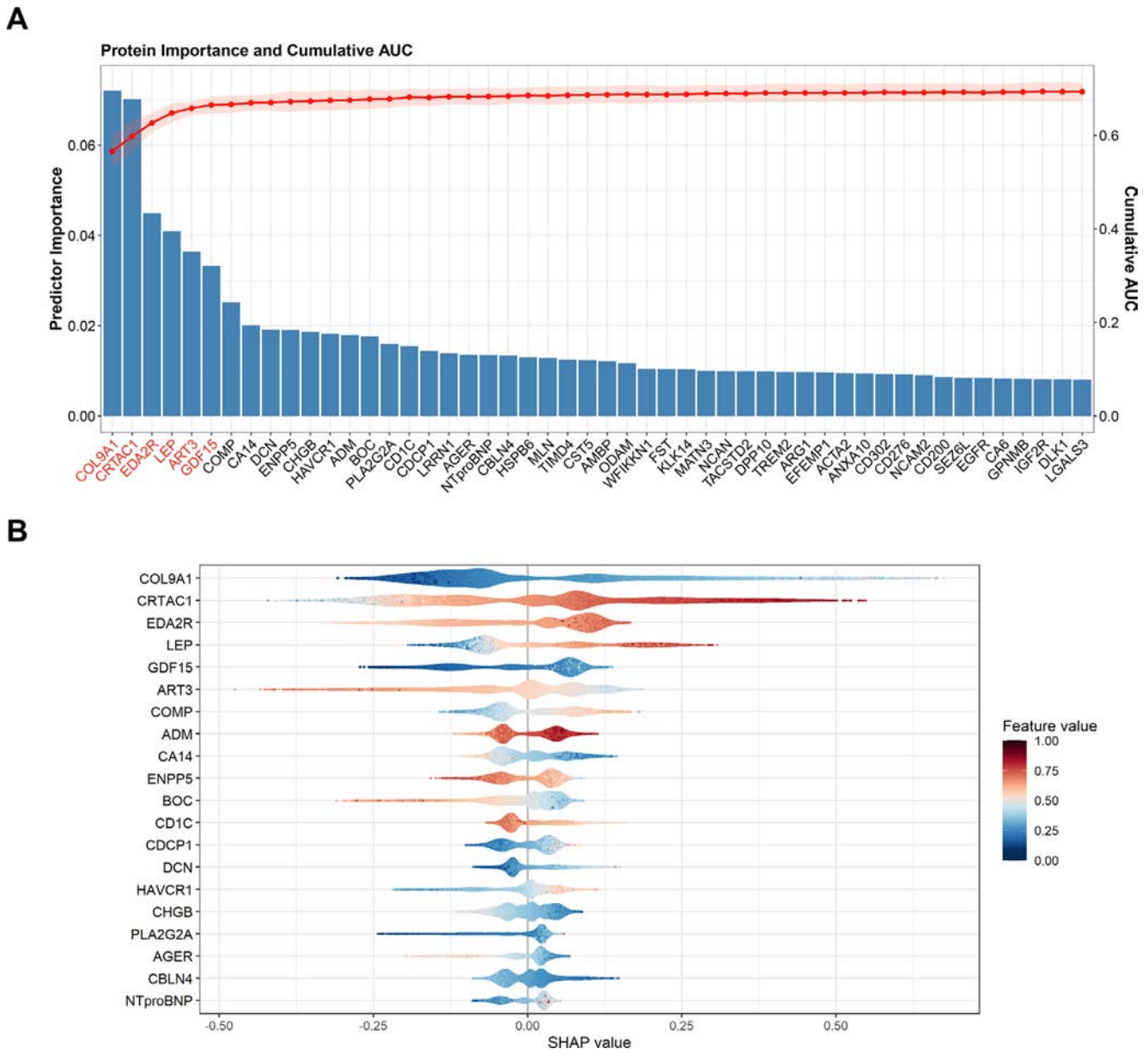

Figure 3. Protein importance ranking and SHAP visualization for all incident OA populations. (A) Sequential forward selection from a pool of candidate proteins. The bar chart illustrates the importance of the ranked proteins based on their contribution to predicting future OA, as judged by the SHAP values. The line graph shows each iteration's cumulative AUC values (right y-axis) as proteins are included individually. The top selected proteins are highlighted in red. The shaded area represents the SE. (B) SHAP visualization of the top proteins. The width of the horizontal bars can be interpreted as the degree of contribution to the prediction of OA: the wider the range, the more significant the contribution. The color of the horizontal bars indicates the magnitude of the plasma proteins encoded in a gradient from dark blue (low) to red (high), as shown in the color bar on the right. The x-axis represents the likelihood of developing OA (right side) or remaining healthy (left side). ART3, ADP-ribosyltransferase 3; AUC, area under the curve; COL9A1, collagen type IX alpha 1 chain; CRTAC1, cartilage acidic protein 1; EDA2R, ectodysplasin A2 receptor; GDF15, growth differentiation factor 15; LEP, leptin; OA, osteoarthritis; SHAP, SHapley Additive exPlanations.

exhibited strong correlations, including age, sex, BMI, and recent pain in specific body regions (Supplementary Figure 15A–C). Finally, the 13 highest-ranking clinical features, including pain questionnaires, were selected for use as predictors in the model.

The SHAP plots visualized the impact of individual clinical features, with color gradients representing value magnitude and the horizontal axis indicating their influence on OA development probability. They demonstrated the broadest variation in age among all patients with new-onset OA, followed by BMI, knee pain, sex, other parts pain, and painkiller medication (Figure 5B). In addition to these general clinical hazards, testosterone, total proteins, and alkaline phosphatase also contribute to the inception of hip OA (Supplementary Figure 16A and B). Knee pain, vitamin D, and cystatin C were identified to have a higher impact on the risk of knee OA (Supplementary Figure 17A and B). This finding suggests that the pathogenesis

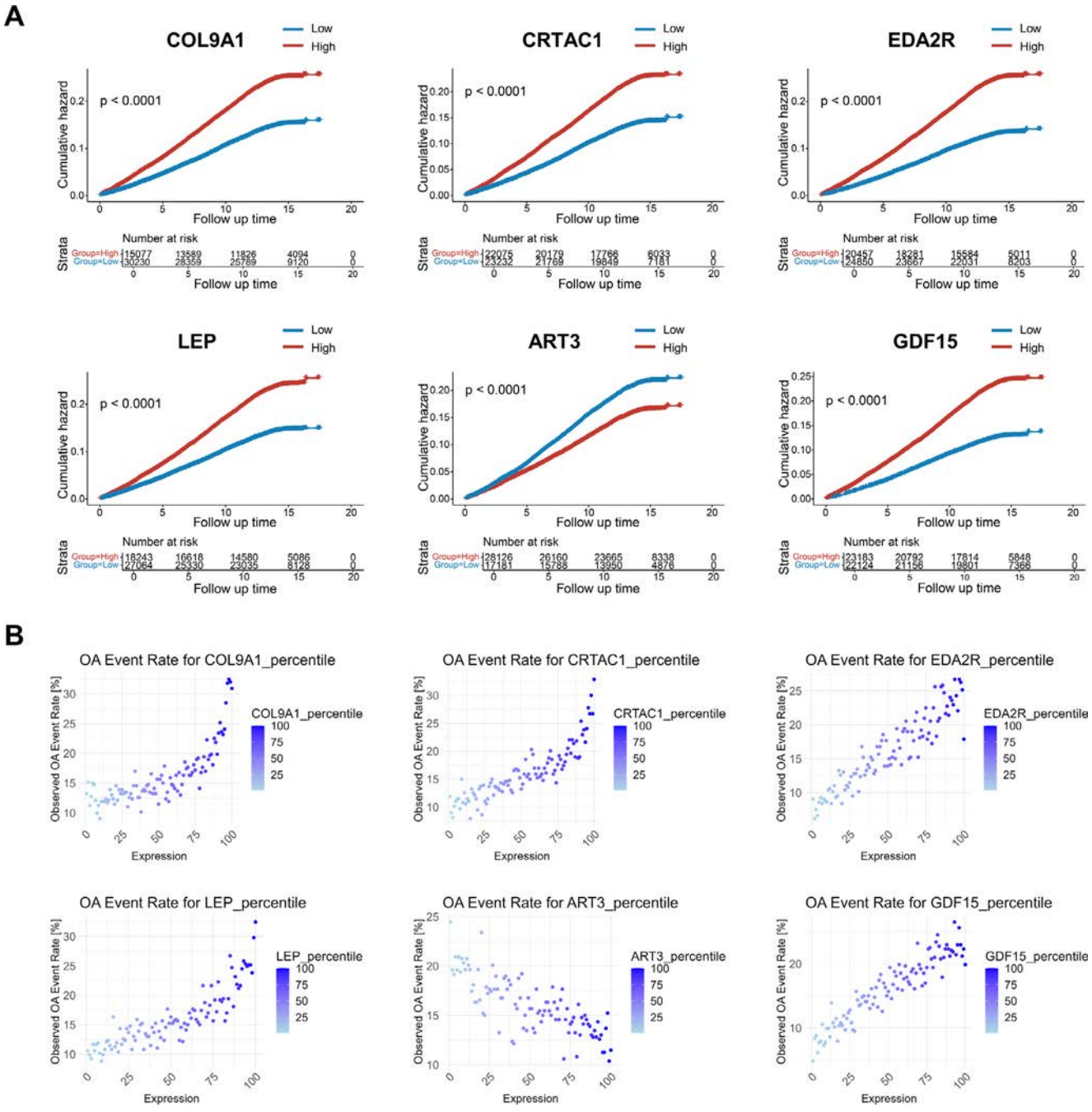

Figure 4. Predictive performance of baseline protein levels on the risk of clinical progression of OA. (A) The Kaplan-Meier curves demonstrate clinical progression over time for all incident OA, visualizing individuals with low (blue lines) and high (red lines) baseline plasma levels of COL9A1, CRTAC1, EDA2R, LEP, ART3, and GDF15. The cutoff points for stratifying the high- and low-protein level groups were calculated by obtaining the maximum Youden index. (B) The relationship between the observed event rate of incident OA and baseline protein levels by percentile in the entire study population. The scatter plot illustrates the correlation between the observed event rate of new-onset OA and baseline levels of specific proteins stratified by their percentile ranks within the entire study cohort. ART3, adenosine diphosphate ribosyltransferase 3; COL9A1, collagen type IX alpha 1 chain; CRTAC1, cartilage acidic protein 1; EDA2R, ectodysplasin A2 receptor; GDF15, growth differentiation factor 15; LEP, leptin; OA, osteoarthritis.

of OA may be multifactorial and may result from complex interactions among hormonal, enzymatic, genetic, and biochemical components that differentially affect the development of OA at different joint sites.

Predictive accuracy of plasma proteins. To construct a high-performing OA risk model, we incorporated proteins, clinical variables, and pain questionnaires to enhance the model's overall predictive accuracy for future OA risk. Proteins alone

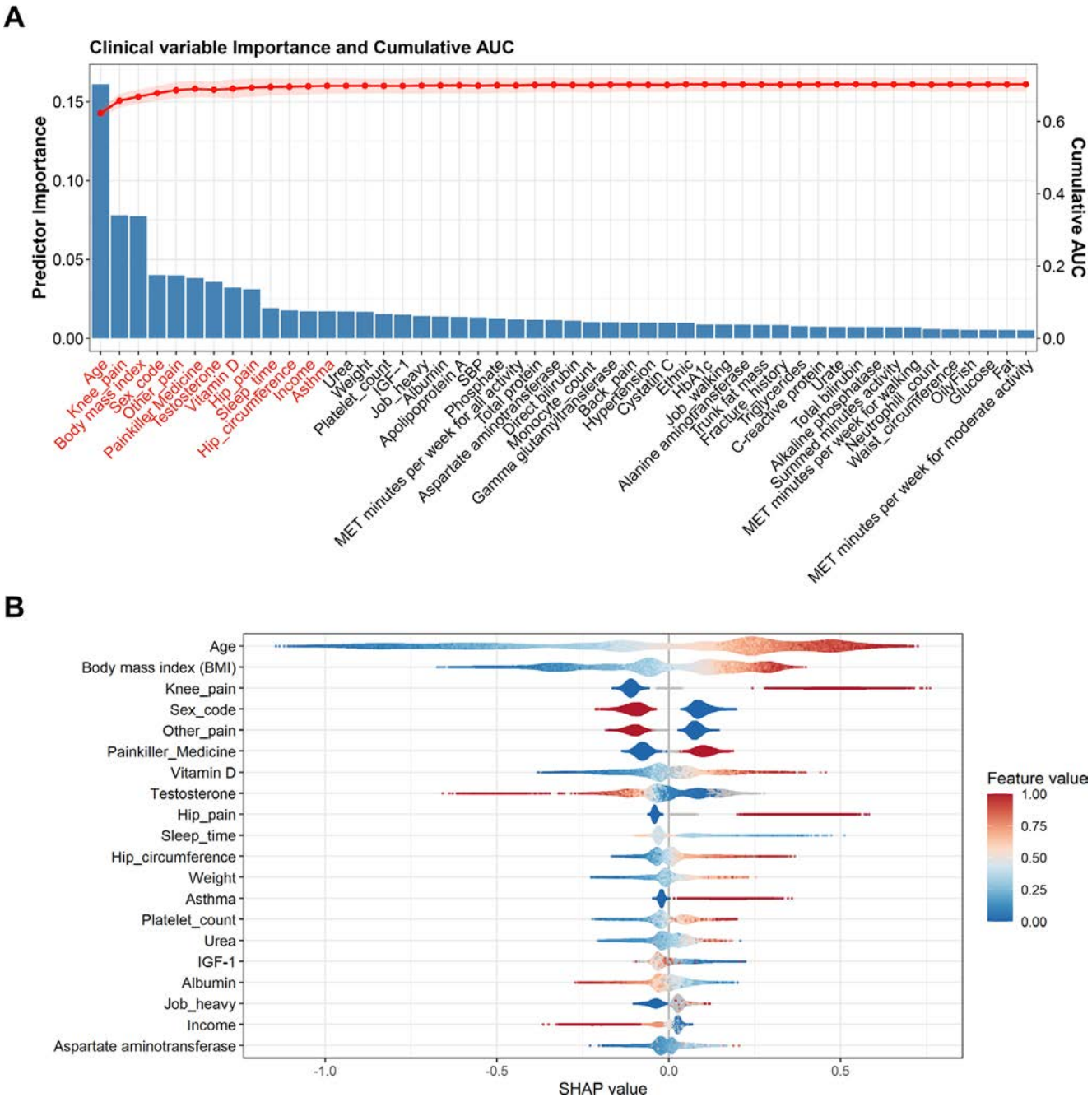

Figure 5. Clinical variable importance ranking and SHAP visualization for incident OA. (A) Sequential forward selection from a pool of candidate clinical variables. The bar chart illustrates the importance of the ranked clinical variables based on their contribution to predicting future OA, as judged by the SHAP values. The line graph shows each iteration's cumulative AUC values (right y-axis) as proteins are included individually. The top selected clinical variables are highlighted in red. The shaded area represents the SE. (B) SHAP visualization of the top clinical variables. The width of the horizontal bars can be interpreted as the degree of contribution to the prediction of OA: the wider the range, the greater the contribution. The color of the horizontal bars indicates the magnitude of the plasma proteins encoded in a gradient from dark blue (low) to red (high), as shown in the color bar on the right. The gray color indicates the missing values. The x-axis represents the likelihood of developing OA (right) or remaining healthy (left). Sex code: 0 represents female and 1 represents male. Pain questionnaire: 1 represents pain and 0 represents no pain. Other pain refers to any pain other than hip pain, knee pain, back pain, neck pain, abdominal pain, and generalized pain. AUC, area under the curve; HbA1c, glycosylated hemoglobin; IGF-1, insulin-like growth factor 1; MET, metabolic equivalent of task; OA, osteoarthritis; SBP, systolic blood pressure; SHAP, SHapley Additive exPlanations.

yielded AUCs of 0.676, 0.673, and 0.665 for 5-year OA, 10-year OA, and all incident OA, respectively. The corresponding AUCs for the clinical variables were 0.698, 0.688, and 0.667, respectively, for the same timeframe. After combining proteins with clinical factors, the model showed improvement in the AUC, which increased to 0.713, 0.701, and 0.711, respectively

(Figure 6A). When pain questionnaires were added to the model, the AUC values further increased to 0.729, 0.721, and 0.723, respectively. Additionally, the sensitivity, specificity, and accuracy improved in the combined model (Supplementary Table 7). The model's performance was equally stable for both hip and knee OA. The full model, combining proteins, clinical variables, and pain questionnaires, showed a relatively high predictive performance: 0.820, 0.802, and 0.757 for hip OA at 5 years, 10 years, and all

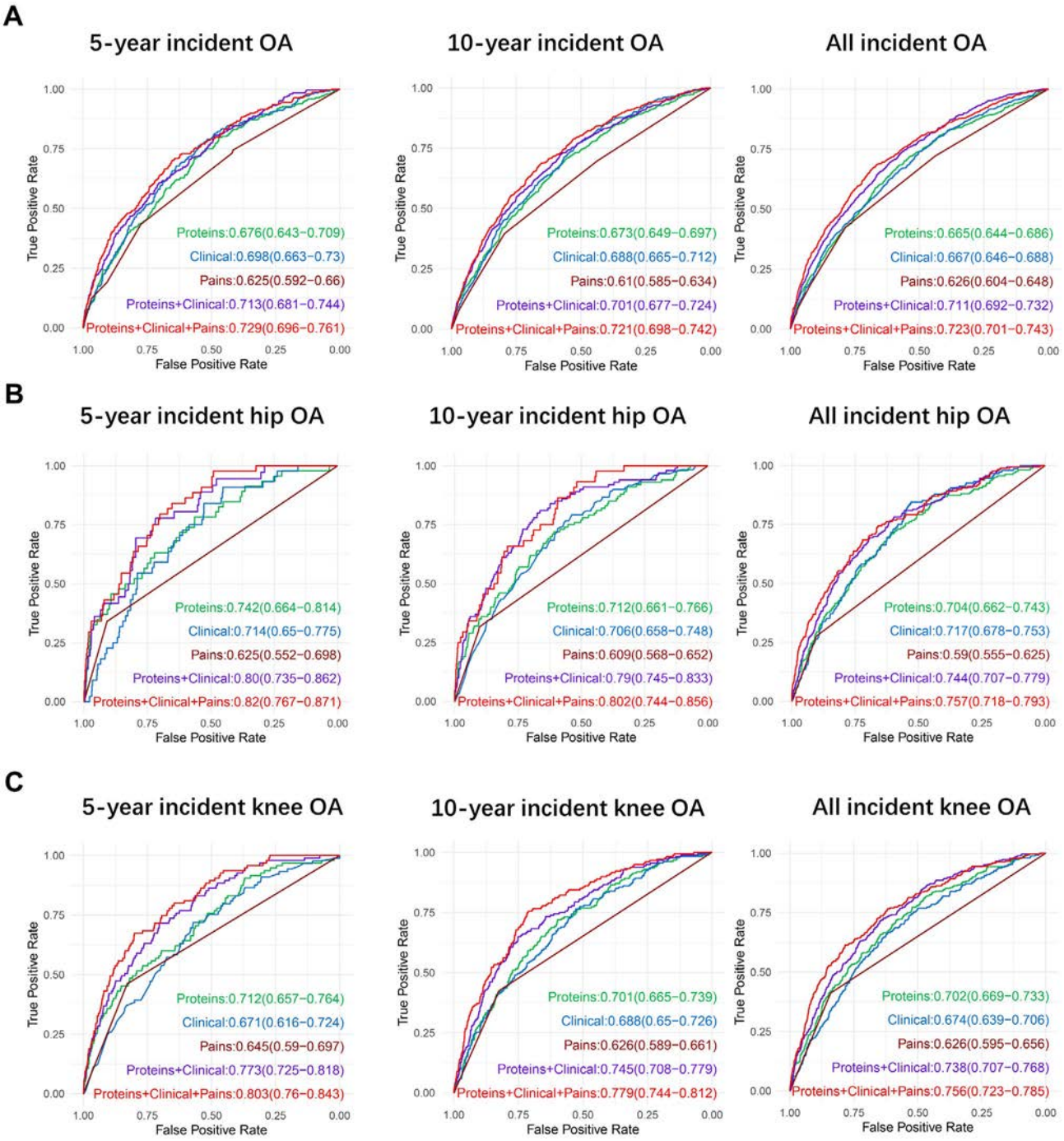

Figure 6. Predictive accuracy of the proteins alone or in combination with clinical variables and pain questionnaires for incident OA, hip OA, and knee OA. (A) The ROC curves illustrating the predictive performance of the proteins, clinical variables, pains, and the combination of these factors in identifying 5-year incident OA (left), 10-year incident OA (middle), and all incident OA (right). (B) The ROC curves illustrating the predictive performance of proteins, clinical variables, pains, and the combination of these factors in identifying 5-year incident hip OA (left), 10-year incident hip OA (middle), and all incident hip OA (right). (C) The ROC curves illustrating the predictive performance of the proteins, clinical variables, pains, and the combination of these factors in identifying 5-year incident knee OA (left), 10-year incident knee OA (middle), and all incident knee OA (right). OA, osteoarthritis; ROC, receiver operating characteristic.

incident hip OA, respectively (Figure 6B; Supplementary Table 8). The AUCs were 0.803, 0.779, and 0.756 for knee OA at the same time points (Figure 6C; Supplementary Table 9). We also evaluated the predictive value of proteins in patients who developed OA in >10 years. Proteins combined with clinical variables and pain questionnaire still yielded relatively high AUCs: 0.712, 0.704, and 0.725 for all OA, hip OA, and knee OA, respectively (Supplementary Figure 18A–C). These results indicate that our model shows relatively good performance across a broad range of timeframes, supporting its generalizability and credibility.

To further understand the contribution of individual proteins to clinical outcomes, we assessed the association of each protein in the signatures with clinical outcomes using LightGBM SHAP values. Most proteins demonstrated strong associations with clinical outcomes in the combined model (Supplementary Figure 19A–C). Notably, COL9A1 and CRTAC1 demonstrated high relevance, with high SHAP values in the model. This underscores their robust contribution to outcome prediction. Overall, combining proteins, clinical data, and pain questionnaires improved OA prediction accuracy, demonstrating the consistent reliability and robustness of the model for all different types and time frames of OA, especially in predicting hip and knee OA.

DISCUSSION

Our study leveraged the extensive dataset of the UK Biobank to provide novel proteomic insights into the prediction of OA risk. Our findings highlight the significance of specific plasma proteins, notably COL9A1 and CRTAC1, in predicting OA incidence, including its subtypes, such as hip and knee OA. The predictive model developed by integrating these proteins with clinical variables using the LightGBM machine learning method demonstrated improved accuracy in identifying individuals at risk of developing OA.

Our results align with those of previous studies that identified plasma proteins as potential biomarkers for OA.[32,33] By analyzing a more diverse cohort, we unveiled a broader array of associated proteins, enhancing the generalizability of our results. COL9A1 and CRTAC1 are strong predictors of OA, irrespective of subtype, which may reflect their possible involvement in the common pathophysiologic mechanisms of the disease. COL9A1 is a structural protein associated with the extracellular matrix and may thus signify early changes within the cartilage matrix before OA of clinical relevance.[34] CRTAC1 has been associated with cartilage-related processes and could indicate a role in the early stages of OA development.[35] More recent research has also identified an association between CRTAC1 and the severity of OA.[36] However, various proteins exhibit differential expression because of some unique pathologic mechanisms, particularly knee or hip joint degeneration. This could be related to different biomechanical stressors and tissue composition within the hip joint, which could influence the expression and importance of these proteins in the disease process. For instance, ART3, EDA2R, and MATN3 have been identified as secondary predictors following COL9A1 and CRTAC1 in hip OA. This could be attributed to the unique biomechanical stressors and tissue composition of the hip joint, which may influence the expression and significance of these proteins in the disease process.[37,38]

In knee OA, the most prominent predictors included CRTAC1 and COL9A1, followed by COMP and CHGB. The significant prominence of CRTAC1 in knee OA might be related to the overexpressed proinflammatory cytokines interleukin-1β and tumor necrosis factor α, which play a role in cartilage inflammation.[39] The identification of COMP and CHGB as significant predictors further emphasizes the importance of cartilage integrity in knee OA pathogenesis.[40] However, because of the limited number of CMC joint OA cases, the sample size was insufficient to develop a reliable predictive model for this subtype, so we did not create a separate model in the present study.

The number of affected joints in OA may also influence proteomic profiles. Previous studies have suggested that systemic inflammation and disease burden may affect biomarker expression in conditions involving multiple joints, such as polyarticular OA.[41] We compared protein HRs between single-joint and polyarticular OA, revealing that polyarticular OA, reflecting greater systemic involvement, is associated with stronger expression of proteins such as AMBP and BSG. These findings suggest that disease burden may play a role in shaping systemic protein marker profiles. However, as the UK Biobank does not provide detailed information on the number of joints affected or the degree of joint involvement, our results are preliminary. Future research is needed to explore how the burden of disease within an individual, including the number and type of affected joints, influences biomarker expression and OA progression.

The identification of clinical variables in our study underscores the multifactorial nature of OA risk, highlighting the importance of a comprehensive approach for risk prediction. The selection of top clinical variables, including age, sex, and BMI, aligns with established risk factors for OA subtypes, emphasizing the need for early intervention strategies targeting these modifiable factors.[14] Aging and other hormonal or anatomic factors lead to a higher incidence of OA in women. Furthermore, increased BMI results in higher mechanical loading on the joints, causing cartilage damage and inflammation.[42]

However, as OA is a heterogeneous disease with different subtypes, the potential for clinical variables will differ in some respects. For instance, we found a pronounced sex effect on hip OA, contrasting with a milder impact on knee OA. A possible explanation may be the postmenopausal decrease in estrogen, which has a protective effect on the bone and is considered more crucial in different biomechanics.[43] The greater female pelvis may also affect hip OA, and knee configuration may neutralize this propensity. Furthermore, testosterone and alkaline phosphatase have been reported to play roles in hip OA. Testosterone is

generally lower in women and may influence bone metabolism and joint tissues.[44] In contrast, alkaline phosphatase, an enzyme involved in bone remodeling, could reflect active bone turnover and the risk of joint degeneration in hip OA.[45] Elevated BMI and knee pain are more significant predictors of knee OA, with increased BMI intensifying mechanical stress and hastening cartilage degradation. Knee pain, indicative of symptomatic expression and potential local inflammation, significantly influences disease initiation and progression. An association between systemic pain and cystatin C, a cysteine protease inhibitor involved in regulating inflammation and linked to kidney function and systemic inflammatory responses, may suggest that systemic inflammatory processes and metabolic factors play a role in disease pathogenesis.[46]

Pain-related variables, such as knee pain, hip pain, other parts pain, and painkiller usage, ranked among the top predictors in our OA risk model, highlighting their strong association with disease development. Knee pain was closely tied to knee-specific OA risk, reflecting its role as an early indicator of joint pathology. Although these variables improved model accuracy, their overlap with symptomatic OA features emphasizes the need to balance clinical and subclinical predictors.[47] These findings reinforce the multifactorial nature of OA and suggest that future models should prioritize subclinical biomarkers to enhance early detection and intervention strategies.

Our study is innovative, as we applied machine learning methods to evaluate the interplay of multiple proteins and clinical variables. In contrast with previous studies applying classical statistical methods, this approach will provide detailed insights into the multifactorial nature of OA risk prediction.[14] Although Nielsen et al[15] leveraged machine learning techniques for the prediction of OA, that study was limited to a 5-year outcome, potentially missing the long-term progression of the disease. Our research employs LightGBM, outperforming XGBoost used by Nielsen et al in predictive accuracy owing to its efficiency with large datasets and categorical features.[48] We also provided a more extensive analysis with a broader timeframe, offering a deeper insight into the trajectory of OA and its influencing factors. The enhanced predictive power of our model could serve as a more reliable tool for risk assessment and intervention planning for clinicians and patients.

Our model employs interpretable artificial intelligence methods for SHAP estimation to analyze the individual-level effects of various risk biomarkers within many comprehensive variables. This detailed analysis helps prioritize preventive strategies by identifying the most influential modifiable factors contributing to OA risk.[15] However, the effectiveness of these strategies needs validation through clinical trials, as our research did not definitively establish whether intervening with these biomarkers would reduce the risk of OA, to what extent, or the causal relationship between these biomarkers and the disease.

Although our study presented a significant advancement in OA risk prediction, several limitations should be mentioned. First, the study depended on self-reported data and electronic health records, which may have information biases. Second, despite the stringent quality control measures adopted, residual confounding cannot be entirely ruled out. Third, the cross-sectional nature of proteomic data precluded drawing firm conclusions regarding causality. Fourth, the model conducted in our study relies on internal validation. The use of an external test set from independent cohorts is necessary to validate the generalizability and robustness of the model on truly unseen data. Future studies, therefore, should include longitudinal data for proteomics and consider temporal dynamics in protein expression with OA development. Furthermore, these results may be further strengthened by objective clinical measurements and biofluid analyses. This research may also be conducted as a collaborative effort using data from multiple cohorts to increase statistical power and generalizability.

In summary, our study extends the current literature by building on the recent methodologic advances in detecting novel plasma proteins related to OA risk. These findings, integrated with a contemporary understanding of the molecular mechanisms of OA, indicate that this field has advanced in discovering biomarkers and predicting the risk of OA.

ACKNOWLEDGMENTS

The authors express their sincere gratitude to all participants and professionals who have contributed to the UK Biobank. This research was conducted using the UK Biobank Resource under Application Number 106397. The authors extend their sincere gratitude to Professor Xiangtian Yu and Professor Suna Wang for their guidance and support in the statistical analysis of this study.

AUTHOR CONTRIBUTIONS

All authors contributed to at least one of the following manuscript preparation roles: conceptualization AND/OR methodology, software, investigation, formal analysis, data curation, visualization, and validation AND drafting or reviewing/editing the final draft. As corresponding author, Prof. Dai confirms that all authors have provided the final approval of the version to be published, and takes responsibility for the affirmations regarding article submission (eg, not under consideration by another journal), the integrity of the data presented, and the statements regarding compliance with institutional review board/Declaration of Helsinki requirements.

REFERENCES

1. Steinmetz JD, Culbreth GT, Haile LM, et al; GBD 2021 Osteoarthritis Collaborators. Global, regional, and national burden of osteoarthritis, 1990-2020 and projections to 2050: a systematic analysis for the Global Burden of Disease Study 2021. Lancet Rheumatol 2023;5(9):e508–e522.
2. Miao MZ, Lee JS, Yamada KM, et al. Integrin signalling in joint development, homeostasis and osteoarthritis. Nat Rev Rheumatol 2024;20(8):492–509.
3. Waheed A, Rai MF. Osteoarthritis year in review 2023: genetics, genomics, and epigenetics. Osteoarthritis Cartilage 2024;32(2):128–137.

4. Smith N, Shirazi S, Cakouros D, et al. Impact of environmental and epigenetic changes on mesenchymal stem cells during aging. Int J Mol Sci 2023;24(7):24.
5. Magnusson K, Turkiewicz A, Rydén M, et al. Genetic influence on osteoarthritis versus other rheumatic diseases. Arthritis Rheumatol 2024;76(2):206–215.
6. Zhai G, Huang J. Genetics of osteoarthritis. Best Pract Res Clin Rheumatol 2024;38(4):101972.
7. Tong L, Yu H, Huang X, et al. Current understanding of osteoarthritis pathogenesis and relevant new approaches. Bone Res 2022; 10(1):60.
8. Abhishek A, Doherty M. Diagnosis and clinical presentation of osteoarthritis. Rheum Dis Clin North Am 2013;39(1):45–66.
9. Motta F, Barone E, Sica A, et al. Inflammaging and osteoarthritis. Clin Rev Allergy Immunol 2023;64(2):222–238.
10. Roemer FW, Guermazi A, Demehri S, et al. Imaging in osteoarthritis. Osteoarthritis Cartilage 2022;30(7):913–934.
11. Mahmoudian A, Lohmander LS, Mobasheri A, et al. Early-stage symptomatic osteoarthritis of the knee - time for action. Nat Rev Rheumatol 2021;17(10):621–632.
12. Jamshidi A, Pelletier J-P, Martel-Pelletier J. Machine-learning-based patient-specific prediction models for knee osteoarthritis. Nat Rev Rheumatol 2019;15(1):49–60.
13. Binvignat M, Pedoia V, Butte AJ, et al. Use of machine learning in osteoarthritis research: a systematic literature review. RMD Open 2022;8(1):8.
14. Appleyard T, Thomas MJ, Antcliff D, et al. Prediction models to estimate the future risk of osteoarthritis in the general population: a systematic review. Arthritis Care Res (Hoboken) 2023;75(7): 1481–1493.
15. Nielsen RL, Monfeuga T, Kitchen RR, et al. Data-driven identification of predictive risk biomarkers for subgroups of osteoarthritis using interpretable machine learning. Nat Commun 2024;15(1): 2817.
16. Gadd DA, Hillary RF, Kuncheva Z, et al; Biogen Biobank Team. Blood protein assessment of leading incident diseases and mortality in the UK Biobank. Nat Aging 2024;4(7):939–948.
17. You J, Guo Y, Zhang Y, et al. Plasma proteomic profiles predict individual future health risk. Nat Commun 2023;14(1):7817.
18. Guo Y, You J, Zhang Y, et al. Plasma proteomic profiles predict future dementia in healthy adults. Nat Aging 2024;4(2):247–260.
19. Sun BB, Chiou J, Traylor M, et al; Alnylam Human Genetics; AstraZeneca Genomics Initiative; Biogen Biobank Team; Bristol Myers Squibb; Genentech Human Genetics; GlaxoSmithKline Genomic Sciences; Pfizer Integrative Biology; Population Analytics of Janssen Data Sciences; Regeneron Genetics Center. Plasma proteomic associations with genetics and health in the UK Biobank. Nature 2023; 622(7982):329–338.
20. Dhindsa RS, Burren OS, Sun BB, et al; AstraZeneca Genomics Initiative. Rare variant associations with plasma protein levels in the UK Biobank. Nature 2023;622(7982):339–347.
21. You J, Zhang YR, Wang HF, et al. Development of a novel dementia risk prediction model in the general population: a large, longitudinal, population-based machine-learning study. EClinicalMedicine 2022; 53:101665.
22. Qiang YX, You J, He XY, et al. Plasma metabolic profiles predict future dementia and dementia subtypes: a prospective analysis of 274,160 participants. Alzheimers Res Ther 2024;16(1):16.
23. Argentieri MA, Xiao S, Bennett D, et al. Proteomic aging clock predicts mortality and risk of common age-related diseases in diverse populations. Nat Med 2024;30(9):2450–2460.
24. Wik L, Nordberg N, Broberg J, et al. Proximity extension assay in combination with next-generation sequencing for high-throughput proteome-wide analysis. Mol Cell Proteomics 2021; 20:100168.
25. Elliott P, Peakman TC; UK Biobank. The UK Biobank sample handling and storage protocol for the collection, processing and archiving of human blood and urine. Int J Epidemiol 2008;37(2): 234–244.
26. Zhang S, Wang D, Zhao J, et al. Metabolic syndrome increases osteoarthritis risk: findings from the UK Biobank prospective cohort study. BMC Public Health 2024;24(1):233.
27. Karlsson T, Hadizadeh F, Rask-Andersen M, et al. Body mass index and the risk of rheumatic disease: linear and nonlinear mendelian randomization analyses. Arthritis Rheumatol 2023;75(11): 2027–2035.
28. Korthauer K, Kimes PK, Duvallet C, et al. A practical guide to methods controlling false discoveries in computational biology. Genome Biol 2019;20(1):118.
29. Wu T, Hu E, Xu S, et al. clusterProfiler 4.0: a universal enrichment tool for interpreting omics data. Innovation (Camb) 2021;2(3): 100141.
30. Machado MR, Karray S, De Sousa IT. LightGBM: an effective decision tree gradient boosting method to predict customer loyalty in the finance industry. *14th Int Conf Comput Sci Educ (ICCSE)* 2019; 1111–1116.
31. Van den Broeck G, Lykov A, Schleich M, et al. On the tractability of SHAP explanations. J Artif Intell Res 2022;74:851–886.
32. Szilagyi IA, Vallerga CL, Boer CG, et al. Plasma proteomics identifies CRTAC1 as a biomarker for osteoarthritis severity and progression. Rheumatology (Oxford) 2023;62(3):1286–1295.
33. Ritter SY, Collins J, Krastins B, et al. Mass spectrometry assays of plasma biomarkers to predict radiographic progression of knee osteoarthritis. Arthritis Res Ther 2014;16(5):456.
34. Imagawa K, de Andrés MC, Hashimoto K, et al. Association of reduced type IX collagen gene expression in human osteoarthritic chondrocytes with epigenetic silencing by DNA hypermethylation. Arthritis Rheumatol 2014;66(11):3040–3051.
35. Styrkarsdottir U, Lund SH, Saevarsdottir S, et al. The CRTAC1 protein in plasma is associated with osteoarthritis and predicts progression to joint replacement: a large-scale proteomics scan in Iceland. Arthritis Rheumatol 2021;73(11):2025–2034.
36. Ouyang Z, Dong L, Yao F, et al. Cartilage-related collagens in osteoarthritis and rheumatoid arthritis: from pathogenesis to therapeutics. Int J Mol Sci 2023;24(12):24.
37. Long L, Zou G, Cheng Y, et al. MATN3 delivered by exosome from synovial mesenchymal stem cells relieves knee osteoarthritis: evidence from in vitro and in vivo studies. J Orthop Translat 2023;41: 20–32.
38. Asmar A, Barrett-Jolley R, Werner A, et al. Membrane channel gene expression in human costal and articular chondrocytes. Organogenesis 2016;12(2):94–107.
39. Ge X, Ritter SY, Tsang K, et al. Sex-specific protection of osteoarthritis by deleting cartilage acid protein 1. PLoS One 2016;11(7): e0159157.
40. Maly K, Andres Sastre E, Farrell E, et al. COMP and TSP-4: functional roles in articular cartilage and relevance in osteoarthritis. Int J Mol Sci 2021;22(5):22.
41. Mobasheri A, Thudium CS, Bay-Jensen AC, et al. Biomarkers for osteoarthritis: current status and future prospects. Best Pract Res Clin Rheumatol 2023;37(2):101852.
42. O'Neill TW, McCabe PS, McBeth J. Update on the epidemiology, risk factors and disease outcomes of osteoarthritis. Best Pract Res Clin Rheumatol 2018;32(2):312–326.

43. Gulati M, Dursun E, Vincent K, et al. The influence of sex hormones on musculoskeletal pain and osteoarthritis. Lancet Rheumatol 2023;5(4): e225–e238.
44. Szulc P. Role of sex steroids hormones in the regulation of bone metabolism in men: evidence from clinical studies. Best Pract Res Clin Endocrinol Metab 2022;36(2):101624.
45. Vimalraj S. Alkaline phosphatase: structure, expression and its function in bone mineralization. Gene 2020;754:144855.
46. Henrotin Y. Osteoarthritis in year 2021: biochemical markers. Osteoarthritis Cartilage 2022;30(2):237–248.
47. Perrot S, Anne-Priscille T. Pain in osteoarthritis from a symptom to a disease. Best Pract Res Clin Rheumatol 2023; 37(2):101825.
48. Zhang D, Gong Y. The comparison of LightGBM and XGBoost coupling factor analysis and prediagnosis of acute liver failure. IEEE Access 2020;8:220990–221003.

American College of Rheumatology
Empowering Rheumatology Professionals

Arthritis & Rheumatology
Vol. 77, No. 8, August 2025, pp 996–1005
DOI 10.1002/art.43139

Associations and Diagnostic Accuracy of Ultrasound Features in Knee Osteoarthritis: Cross-Sectional Results From a Large Community-Based Cohort

Katherine A. Yates,[1] Carolina Alvarez,[2] Todd A. Schwartz,[2] Serena Savage-Guin,[2] Jordan B. Renner,[2] Catherine J. Bakewell,[3] Minna J. Kohler,[4] Janice Lin,[5] Jonathan Samuels,[6] Tessa Walker,[2] Yvonne M. Golightly,[7] and Amanda E. Nelson[2]

Objective. Our study objectives were (1) to determine associations among ultrasound (US) features of knee osteoarthritis (KOA), radiographic KOA (rKOA), and patient-reported symptoms and (2) to determine diagnostic accuracy of US definitions for rKOA, in a community-based cohort.

Methods. Participants enrolled in the Johnston County Health Study (JoCoHS; 2019–2024, n = 902) provided demographics, comorbidities, clinical features, and symptoms, along with imaging with standardized acquisition and scoring protocols. Logistic regression models provided odds ratios adjusted for age, sex, race, ethnicity, body mass index (BMI), education level, comorbidities, and knee injury for associations among US features and KOA outcomes. Diagnostic accuracy was assessed using standard metrics with rKOA as the gold standard.

Results. Complete imaging data were available for 861 participants (1,711 knees): 34% men, 25% Black, 10% Hispanic, mean age 55 years, and mean BMI 33. Half of knees were symptomatic, one-third had rKOA, and one in five had symptomatic rKOA. US-identified osteophytes, effusion, meniscal extrusion, cartilage damage, calcium crystals, and popliteal cysts were associated with KOA outcomes. A US definition including both mild osteophytes and mild cartilage damage gave an area under the receiver operating characteristic curve of 0.76 for diagnosing rKOA (validated in an external cohort).

Conclusion. We identified common US features in participants with and without KOA, along with significant associations between US features and rKOA, symptomatic rKOA, and symptoms. US-based diagnosis of rKOA shows promise for general use. US is a valuable and accessible modality for assessment of knee OA features in clinical and research settings, including those with limited resources.

INTRODUCTION

Osteoarthritis (OA) is the most common form of arthritis, with prevalence rates continuing to increase along with other common chronic conditions.[1] More than 300 million adults worldwide suffer from knee OA (KOA), with increasing rates of disability.[2] KOA is most often categorized using radiography and symptoms. Radiographic KOA (rKOA) is most often defined using the Kellgren-Lawrence grade (KLG), which was developed more than 60 years ago.[3] Over the decades, many limitations of the KLG have been recognized, including its lack of soft tissue imaging, poor sensitivity to change, issues with positioning for longitudinal study, varying interpretation in different cohorts, and imperfect reproducibility.[4–6]

Alternative imaging modalities such as computed tomography, magnetic resonance imaging (MRI), and ultrasound

Supported in part by an Innovative Research Award from the Rheumatology Research Foundation and by the National Institute of Arthritis and Musculoskeletal and Skin Diseases, NIH (grants R01-AR-077060, P30-AR-072580, and K24-AR-081368). The funders had no role in the work or decision to publish.

[1]Katherine A. Yates, MD: Thurston Arthritis Research Center, University of North Carolina at Chapel Hill, and Ohio State University, Columbus; [2]Carolina Alvarez, MS, Todd A. Schwartz, DrPH, Serena Savage-Guin, RT(R), Jordan B. Renner, MD, Tessa Walker, MPH, Amanda E. Nelson, MD, MSCR, RhMSUS: Thurston Arthritis Research Center, University of North Carolina at Chapel Hill; [3]Catherine J. Bakewell, MD, RhMSUS: Intermountain Health Care, Salt Lake City, Utah; [4]Minna J. Kohler, MD, RhMSUS: Massachusetts General Hospital and Harvard Medical School, Boston; [5]Janice Lin, MD: Stanford University School of Medicine, Palo Alto, California; [6]Jonathan Samuels, MD, RhMSUS: New York University Langone Health, New York; [7]Yvonne M. Golightly, PT, MS, PhD: Thurston Arthritis Research Center, University of North Carolina at Chapel Hill, and College of Allied Health Professions, University of Nebraska Medical Center, Omaha.

Additional supplementary information cited in this article can be found online in the Supporting Information section (https://acrjournals.onlinelibrary.wiley.com/doi/10.1002/art.43139).

Author disclosures and graphical abstract are available at https://onlinelibrary.wiley.com/doi/10.1002/art.43139.

Address correspondence via email to Amanda E. Nelson, MD, MSCR, RhMSUS, at amanda_nelson@med.unc.edu.

Submitted for publication November 26, 2024; accepted in revised form February 10, 2025.

(US) and various additions (contrast, weight-bearing, etc) have been studied in KOA as they allow improved soft tissue imaging and sensitivity, although issues around reproducibility, access, and scoring persist. US in particular is a promising modality for use in a wide range of research and clinical settings as it is portable, less expensive, and useful at the point of care and allows dynamic and multiple joint imaging without limitations related to implants, body size, or radiation. Therefore, establishment of US as a valid, reproducible modality could enhance research and clinical imaging of OA.[7]

Although a majority of OA imaging research is focused on MRI, there is a body of work supporting the use of US for KOA. A systematic review of 89 studies on US in OA found that the majority of studies focused on the knee joint, and features including effusion, medial meniscal extrusion, and popliteal cyst were associated with progression of KOA (radiographic development, worsening, or need for total joint replacement).[8] This review also supported overall good diagnostic performance of US, strong correlations with similar features assessed on MRI, and greater sensitivity of US compared with radiography, particularly for osteophytes.[8] The Xiangya Osteoarthritis (XO) study recently published results from a large population-based cohort in China (57% women, mean age 64 years, mean body mass index [BMI] 24) in which about one-third of participants had chronic knee pain and 37% had rKOA, finding that synovial hypertrophy was present in 18%, effusion in nearly half, and power Doppler in 5% of knees, in line with prior reports[9,10] that these features are common in the general population. We have published similar findings in the Johnston County Osteoarthritis Project (JoCoOA), in which knees with and without rKOA had US pathologies that were correlated with KLG and individual radiographic grades (eg, for osteophytes and joint space narrowing).[10]

Despite this evidence for US, radiographs (and the KLG) remain the gold standard for diagnosis and classification of KOA, and MRI remains the research modality of choice. A search of PubMed from 1994 to 2024 showed that although all KOA citations were increasing, radiography was the most frequently used, followed by MRI, and then US (eg, 70, 26, and 9 per 100,000 citations in 2023, respectively; Supplemental Figure A).[11] Given the prominence of radiography in knee US, its wide availability in both modern and historical cohorts, and its common use for both clinical and research applications, radiography is the most important comparator for understanding the potential utility of US, particularly where MRI is not available. Therefore, this analysis had two primary goals: to (1) determine the association of features of KOA on US with patient-reported symptoms and rKOA and (2) determine the diagnostic accuracy of US definitions for rKOA in a large community-based cohort study.

PARTICIPANTS AND METHODS

The Johnston County Health Study. The Johnston County Health Study (JoCoHS) is a prospective community-based study that enrolled 902 residents from Johnston County, North Carolina, in the Southeastern United States from 2019 to 2024. Recruitment was conducted without regard for OA status, joint pain, or other medical symptoms or conditions. Listings of all households in Johnston County were supplied by a vendor (Marketing Systems Group, Inc), and a random sample from the list was used for recruitment. Qualifying households were mailed recruitment materials and were contacted approximately seven days after mailing to determine whether individual residents in the household met eligibility criteria (ie, aged 35–70 years, spoke fluent English or Spanish, and identifying as Black/African American, White, or Hispanic). Once this determination was made, eligible individuals who agreed to participate were consented and scheduled for a single (~3 hour) research clinic visit. Baseline assessments included questionnaires, physical function, musculoskeletal examination, blood and urine collection, knee US, and radiographs of knees, hips, hands, ankles, and feet. All participants provided informed consent; the study was approved and monitored by the University of North Carolina at Chapel Hill Institutional Review Board (no. 18-0438). Further information on this study is available in a recent review.[12]

Patient and public involvement. Johnston County community members have been involved as staff and participants since the inception of the original JoCoOA and throughout the JoCoHS. An advisory board formed in 2018 of prior JoCoOA participants and individuals who met eligibility criteria for the planned JoCoHS participated in selection of measures, development of questionnaires, assessment of participant burden, and recruitment efforts. Participants receive updates via newsletter, and the advisory board is invited to attend an annual research day in which findings are presented.

Images and scoring. Posteroanterior semiflexed knee radiographs (using the Synaflexer device) were read for KLG by an expert musculoskeletal radiologist (JBR) with high reliability as previously described.[13,14] Standardized knee US images (7 images per knee) were obtained by a trained sonographer (SSG) using a Sonosite Edge II-MSK with HFL50x/6- to 15-mHz linear transducer (mid-range "Gen" setting, FUJIFILM SonoSite Inc), following a published protocol.[10] Each participant's set of US images was read according to a published scoring atlas for all features[10] (ie, effusion/synovitis, osteophytes, cartilage damage, meniscal extrusion, popliteal cysts, and calcium deposition) by two randomly selected expert readers (CJB, MJK, JL, AEN, JS) using an online system (Qualtrics) customized for this purpose. A third randomly selected reader adjudicated any images with scoring disagreements and entered the final score for that image. Reliability by Kendall concordance coefficient, as previously reported using the same protocol and atlas, ranged from 0.6 to 0.9; repeat analysis in 2020 and 2023 showed similar agreement (data not shown). In the present analysis, we required

100% agreement between two readers, or a third adjudicator (anonymized to the other reader's scores) was assigned who gave a final score, rendering reliability metrics inapplicable (this was done primarily to avoid 0.5 gradations due to use of means). Signs of crystal deposition were almost always agreed upon (only 3%–13% adjudicated), whereas other features ranged from 23% (medial meniscal extrusion) to 66% (gray scale synovitis) adjudicated. Among adjudicated scores, <20% were outside the range of the first two readers' scores for effusion/synovitis, synovitis, and cartilage damage, whereas <10% were outside the range for power Doppler signal, osteophytes, or popliteal cyst; these scores were on average only one unit higher or lower than the original range.

All US features are defined and illustrated in our published atlas[10]; these were based on prior publications and adapted to our images, and they are briefly summarized here. Given challenges with static identification of effusion versus synovitis, we used three scores, one for effusion alone (yes/no), one for synovitis alone (none, minimal, moderate or severe distention), and one for the combination based on size of the hypoechoic area visualized on orthogonal suprapatellar views, with or without power Doppler signal. Osteophytes were graded from 0 to 3 as none, small (but distinct), larger, and very large/bulky in both the medial and lateral longitudinal views, where meniscal extrusion (ie, the meniscus was partially or completely extruded beyond the bony joint line) was graded as present or absent. Cartilage damage was defined on the suprapatellar transverse view in full flexion as none (0), hyperechogenicity or loss of sharpness but maintained width (1), local thinning (2), or complete loss of cartilage (3) separately for the medial and lateral aspect. Popliteal cysts were defined as absent (0), small/possible (1), or definite (2). Calcium crystal deposition was identified if present (yes/no) in any of the suprapatellar longitudinal, medial and lateral longitudinal, or posterior transverse views as recommended by the OMERACT Calcium Pyrophosphate Deposition Disease Ultrasound Subtask Force.[15]

For the analysis of diagnostic accuracy, six US definitions were compared to a radiographic definition of KOA (ie, rKOA), which required grade 1 or higher for both osteophytes and joint space narrowing and was in 99% agreement with defining rKOA as KLG ≥2. The six definitions were (1) small but distinct medial or lateral osteophytes and minimal medial or lateral cartilage thinning (ie, grade 1 or greater), (2) larger medial or lateral osteophytes and mild or local medial or lateral cartilage thinning (ie, grade 2 or greater), (3) small but distinct medial or lateral osteophytes and minimal medial or lateral cartilage thinning and joint capsule distention parallel to bone gray scale effusion or synovitis, (4) small but distinct medial or lateral osteophytes and minimal medial or lateral cartilage thinning and medial or lateral meniscal extrusion, (5) small but distinct medial osteophytes and minimal medial cartilage thinning and medial meniscal extrusion, and (6) small but distinct lateral osteophytes and minimal lateral cartilage thinning and lateral meniscal extrusion.

Outcomes. Self-reported pain, aching, or stiffness (PAS; 0–3, none to severe) was scored based on its presence on "most days of any one month in the past 12 months" in each knee. Knee outcome definitions included any knee PAS (ie, score ≥1), at least moderate severity PAS (ie, score ≥2), and severe knee PAS (ie, score = 3). RKOA was defined in a knee with KLG ≥2, whereas severe rKOA required KLG ≥3, and symptomatic KOA (sxKOA) was the combination of both PAS ≥1 and rKOA in a given knee. A sensitivity analysis considered US features in knees with KLG = 1 versus those with KLG = 0 to reflect features of the initial stages of rKOA. The Knee Injury and Osteoarthritis Outcome Score (KOOS) was obtained for the knee with greater PAS score (if both knees were equal, the knee with greater PAS in the past 30 days was used; if still equal, a random knee was selected so there was only one KOOS score per person). The KOOS includes five subscales (pain, other symptoms, function in daily living, function in sport and recreation, and knee-related quality of life) that are separately scored from 0 to 100, reflecting extreme to no problems.

Covariates. Participants self-reported their date of birth (used to calculate age), sex (male or female), race (Black or White), ethnicity (Hispanic or non-Hispanic), and highest level of education achieved (dichotomized to less than a college degree vs a college degree or higher). Body weight (to the nearest pound) and height (to the nearest half centimeter) were measured at the research clinic visit, which were used to calculate BMI. Participants completed the Charlson Comorbidity Index, which was weighted and scored for each participant (range 0–9).[16] The presence of knee injury was based on an affirmative response to the question: "Have you ever injured a [right/left knee] badly enough that it limited your ability to walk for at least two days?"

Statistical analysis. Descriptive statistics for all relevant person-level or knee-level variables were produced using either mean ± SD or median (interquartile range; IQR) for continuous variables, and frequencies and percentages for categorical variables. We fitted logistic regression models to test and quantify the associations (through adjusted odds ratios and 95% confidence intervals [CIs]) between each US feature and dichotomous KOA outcomes. Models were adjusted for age, sex, race, ethnicity, BMI, education, Charlson Comorbidity Index, and history of knee injury. Models were defined at the knee level so that generalized estimating equations (GEEs) were used to account for within-person correlation between knees. In an exploratory manner, effect modification between all covariables and US features was assessed using each US feature and covariable pairwise interaction terms at a conservative 0.01 α level using backward elimination (to account for multiple comparisons) and reported in stratified models in the supplemental material. For continuous KOOS outcomes, person-level, zero-inflated negative binomial models modeling KOOS outcome (reversed to 100 – KOOS subscore)

were used to test and estimate the association between US features and KOOS subscore and produce adjusted mean ratios and 95% CIs.

Measures of accuracy for the US definitions compared with rKOA diagnosis included sensitivity, specificity, area under the receiver operating characteristic curve (AUC), and positive and negative predictive values (PPV and NPV). Population-averaged logistic models using GEEs, with an exchangeable working correlation between knees, were used to estimate unadjusted measures of accuracy and corresponding 95% CIs for each US definition versus the reference standard definition (rKOA). Sensitivity and specificity were produced from intercept-only models with the index test as the dependent variable, stratified by reference. PPV and NPV were produced from intercept-only models with the reference as the dependent variable, stratified by index test. For AUC, predicted probabilities from the population-averaged model were used to then produce the estimates for AUC using an intercept-only model of the predicted probabilities with the reference as the dependent variable. Analyses were externally validated in the independent JoCoOA cohort, consisting of completely different participants than those in JoCoHS. All analyses were conducted using SAS software version 9.4.

Data availability. All data are available upon reasonable request and appropriate agreements; please request from author AEN (amanda_nelson@med.unc.edu). All US images and limited metadata are currently available through the Harvard Dataverse at https://doi.org/10.7910/DVN/SKP9IB.

RESULTS

Overall. Of 902 participants enrolled in the baseline visit of the JoCoHS, 39 had bilateral total knee replacement (TKR), 9 had unilateral TKR, and 2 did not undergo US, leaving 861 participants with 1,711 knees for this analysis (Figure 1). Of these 861 individuals, 34% were men, 25% were Black, 10% were Hispanic, 51% had less than a college degree, and there was a mean ± SD age of 55 ± 10 (range 35–70) years and a mean BMI ± SD of 33 ± 8 (range 17–71). Comorbidities per the Charlson Index were infrequent, with an IQR of 0 to 1. Seventeen percent of knees were reported to have prior injury (Table 1). Of the 1,711 included knees, 868 (51%) had any knee PAS in the past 12 months, whereas 517 (30%) had rKOA and 360 (21%) had sxKOA (Table 2).

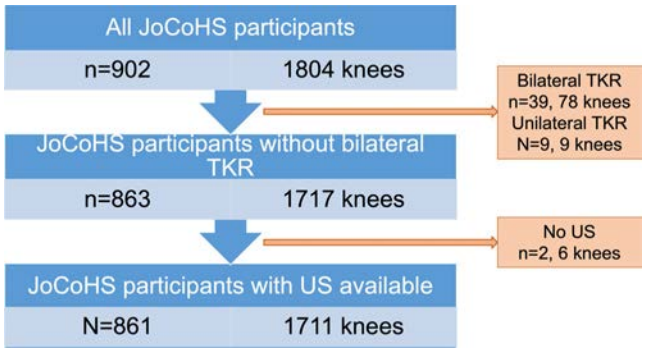

Figure 1. Diagram of patient selection. JoCoHS, Johnston County Health Study; TKR, total knee replacement; US, ultrasound.

Frequency of US findings. The frequencies of US features in all knees are described in Table 2. More than half of knees had evidence of effusion and or gray scale synovitis, with approximately one in five having moderate or severe findings (grade 2 or 3). Positive power Doppler was infrequent and usually minimal. Approximately 40% of knees had at least mild osteophytes, similar in medial and lateral aspects of the joint. Lateral meniscal extrusion was slightly more frequent than medial (19% and 14%, respectively). About half of knees had at least mild cartilage damage, with around a quarter having moderate/severe thinning. Definite popliteal cysts were infrequent (<5%), although small/possible cysts were seen in 37%. Calcium crystals were identified in 13% in any view, most frequently in the lateral longitudinal view. Figure 2 provides an example of radiographic and sonographic images of the same knee in a 59-year-old White woman with a BMI of 35. Distributions of select cognate features on US and radiography are available in Supplemental Table A.

Associations of US features with knee outcomes: PAS. Effusion, and moderate to large medial or lateral osteophytes were consistently associated with significantly increased odds of any and moderate/severe PAS (Table 3). Inconsistent associations were seen for synovitis. Medial meniscal extrusion, medial cartilage damage, and calcium crystal deposition conferred approximately 50% higher odds of moderate/severe PAS, whereas definite popliteal cyst more than doubled these odds.

Associations of US features with knee outcomes: radiographic and sxKOA. All US features other than power Doppler were statistically significantly associated with rKOA. Medial and lateral osteophytes were strongly associated with

Table 1. Descriptive statistics for JoCoHS with available US (n = 861)*

Characteristics	Value
Male, n %	290 (33.7)
Age, mean ± SD (range 35–70), y	54.7 ± 9.6
Black, n %	215 (25.0)
Hispanic, n %	88 (10.2)
Education below college degree, n % (missing = 5)	438 (50.9)
Body mass index, mean ± SD (range = 17–71), kg/m^2	33.2 ± 8.3
Charlson Comorbidity Index, median (IQR) (range = 0–9)	0 (0–1)
Knee injury (at knee level, total n = 1,711), n %	284 (16.6)

* IQR, interquartile range; JoCoHS, Johnston County Health Study; US, ultrasound.

Table 2. Descriptive statistics at the knee level (n = 1,711 knees)*

Knee-level features	n (%)
US features	
GS effusion/synovitis (missing = 2)	
0: no joint capsular distention	751 (43.9)
1: a small hypo/anechoic line beneath the capsule	572 (33.4)
2: elevated joint capsule parallel to joint area	333 (19.5)
3: convex distension of the joint capsule	55 (3.2)
GS synovitis	
0: none	829 (48.5)
1: minimal distention of recess by hypo/anechoic material	496 (29.0)
2: moderate distention with flat or concave limit	334 (19.5)
3: severe or bulging distention of joint recess	52 (3.0)
GS effusion: abnormal hypo/anechoic intra-articular material (present/absent)	612 (35.8)
Suprapatellar PD	
0: no intra-articular signal	1,273 (74.4)
1: trace to 10% intra-articular color signal	382 (22.3)
2: 10%-50% intra-articular color signal	54 (3.2)
3: >50% intra-articular color signal	2 (0.1)
Osteophytes, medial tibiofemoral (missing = 1)	
0: none	1,009 (59.0)
1: small but distinct	403 (23.6)
2: medium/larger	217 (12.7)
3: large, bulky, prominent	81 (4.7)
Osteophytes, lateral tibiofemoral	
0: none	1,056 (61.7)
1: small but distinct	417 (24.4)
2: medium/larger	205 (12.0)
3: large, bulky, prominent	33 (1.9)
Meniscal extrusion,[a] medial tibiofemoral (missing = 1)	235 (13.7)
Meniscal extrusion,[a] lateral tibiofemoral	329 (19.2)
Cartilage damage, medial femur/trochlea (missing = 2)	
0: normal	392 (22.9)
1: hyperechoic, loss of sharpness	802 (46.9)
2: localized thinning	442 (25.8)
3: complete cartilage loss	73 (4.3)
Cartilage damage, lateral femur/trochlea (missing = 2)	
0: normal	521 (30.5)
1: hyperechoic, loss of sharpness	760 (44.4)
2: localized thinning	355 (20.7)
3: complete cartilage loss	73 (4.3)
Popliteal cyst (missing = 65)	
0: absent	936 (54.7)
1: small/possible	634 (37.1)
2: definite	76 (4.4)
Calcium crystal deposition, any view	216 (12.6)
Calcium crystal deposition, suprapatellar transverse (missing = 2)	74 (4.3)
Calcium crystal deposition, medial tibiofemoral (missing = 1)	34 (2.0)
Calcium crystal deposition, lateral tibiofemoral	134 (7.8)
Calcium crystal deposition, posterior transverse (missing = 65)	6 (0.4)
Double contour sign, suprapatellar transverse (missing = 2)	15 (0.9)
Knee outcomes	
Any knee PAS (missing = 4)	868 (50.7)
At least moderate PAS (missing = 4)	512 (29.9)
Severe PAS (missing = 4)	177 (10.3)
rKOA (KLG ≥2) (missing = 5)	517 (30.2)
Severe rKOA (KLG ≥3) (missing = 5)	282 (16.5)
sxKOA (rKOA + PAS) (missing = 9)	360 (21.0)

* GS, gray scale; KLG, Kellgren-Lawrence grade; PAS, pain, aching, and stiffness; PD, power Doppler; rKOA, radiographic knee osteoarthritis; sxKOA, symptomatic knee osteoarthritis; US, ultrasound.
[a] Meniscal extrusion was graded as present if the meniscus was partially or completely extruded beyond the bony joint line, and absent if normal or uncertain.

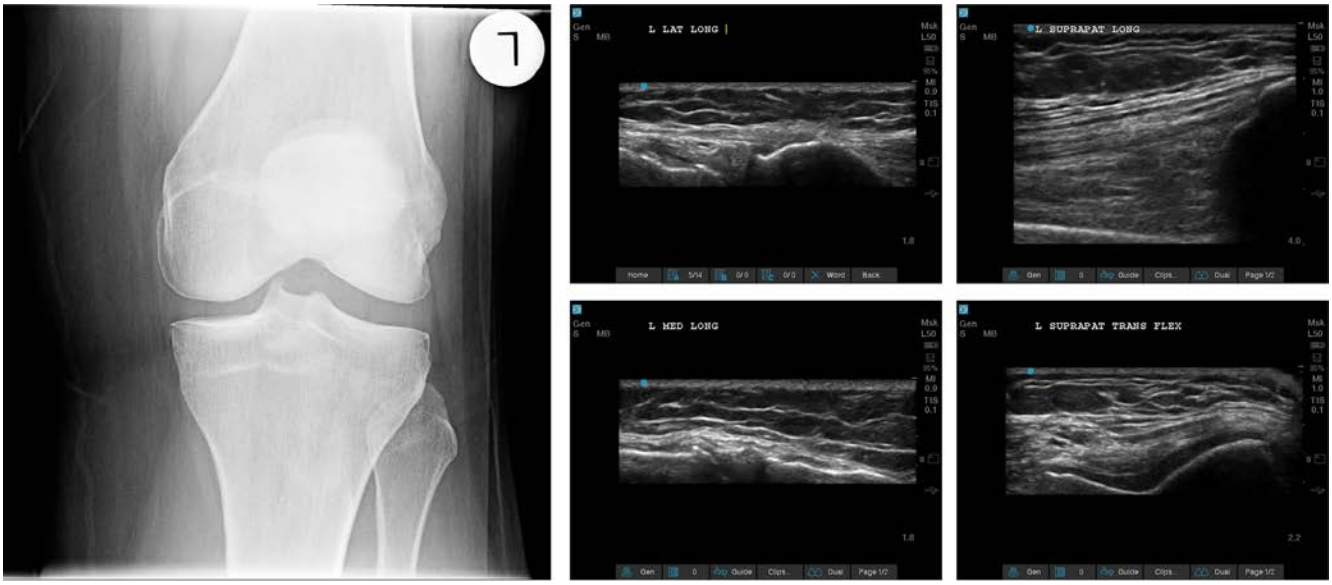

Figure 2. Radiograph and representative US images of a left knee. Clockwise from left: weight-bearing PA knee radiograph, US: lateral longitudinal, anterior suprapatellar longitudinal, anterior suprapatellar in maximal flexion, medial longitudinal. Left knee KLG = 1, White woman aged 59 years, BMI 35. US feature scores: effusion/synovitis, power Doppler, meniscal damage, popliteal cyst and calcium crystal deposition were all absent (score = 0), whereas both medial and lateral osteophytes, and medial and lateral cartilage damage were all mild (score = 1). BMI, body mass index; KLG, Kellgren-Lawrence grade; PA, posteroanterior; US, ultrasound.

three times or higher odds of rKOA, increasing with US severity. Moderate/severe effusion/synovitis or cartilage damage was associated with at least double the odds of rKOA. Medial meniscal extrusion or definite popliteal cysts tripled the odds of rKOA, whereas calcium crystals conferred 60% higher odds of rKOA (Table 3). All US features were significantly associated with sxKOA presence, most strongly for severe effusion/synovitis, osteophytes, cartilage damage, and definite popliteal cyst. Of note, moderate or severe power Doppler (grade 2–3) was associated with 79% higher odds of sxKOA (Table 3).

We also explored relationships among those knees with KLG ≤1 (n = 1,194) as a reflection of no, or initial, rKOA. In these knees, the more severe US features were less common, but higher scores for synovitis and osteophytes were still significantly associated with KLG = 1 (versus KLG = 0). The odds of cartilage damage were 14% to 76% higher but not statistically significant in knees with KLG = 1 versus 0 (Supplemental Table B). Exploratory effect modification analyses are in Supplemental Methods; Supplemental Table C; and Supplemental Figures B and C.

Associations of US features with knee outcomes: KOOS. Effusion and synovitis, alone or in combination, were consistently significantly associated with the KOOS activities of daily living and quality of life subscales but not with KOOS pain or symptoms subscales. Medial and lateral osteophytes were associated with worse scores on all KOOS subscales, as were medial (but not lateral) meniscal extrusion, popliteal cysts, and calcium crystal deposition (Supplemental Table D).

Diagnostic accuracy of US features for radiographically defined KOA. Knees with complete data (n = 1,703) were used for the diagnostic analysis. The comparison of six US definitions to rKOA is shown in Table 4. The US definition including small, but distinct, medial or lateral osteophytes, and minimal medial or lateral cartilage thinning resulted in the highest sensitivity and AUC in comparison to rKOA (0.81 and 0.76, respectively; Definition 1 in Table 4). Including meniscal extrusion in the US definition (Definition 4) resulted in a higher specificity but lower sensitivity (0.90 and 0.39, respectively). Findings were validated in an external independent cohort (Supplemental Methods; Supplemental Table E).

DISCUSSION

We report findings from a large, diverse, community-based cross-sectional study (JoCoHS) using our previously published standardized US acquisition protocol and atlas-based expert scoring. About half of individuals reported any knee PAS in the year before enrollment, one-third had rKOA, and one in five had sxKOA; thus about half were without signs or symptoms of KOA. US-identified osteophytes, effusion, meniscal extrusion, cartilage damage, calcium crystals, and popliteal cyst were all associated with knee symptoms (PAS), rKOA, and sxKOA. Power Doppler signal was infrequent but, when present, was associated with sxKOA. Osteophytes, medial meniscal extrusion, popliteal cysts, and calcium crystals on US were associated with poorer

Table 3. Adjusted associations between US features and knee PAS and rKOA outcomes, OR (95% CI)*

Ultrasound features	Outcomes					
	Any knee PAS, OR (95% CI)	At least moderate knee PAS, OR (95% CI)	Severe knee PAS, OR (95% CI)	rKOA (KLG ≥2), OR (95% CI)	Severe rKOA (KLG ≥3) OR (95% CI)	sxKOA (rKOA + PAS), OR (95% CI)
GS effusion/synovitis						
1 (vs 0)	0.95 (0.77–1.16)	1.11 (0.88–1.40)	1.19 (0.84–1.69)	**1.77 (1.33–2.35)**	1.35 (0.99–1.85)	**1.79 (1.32–2.42)**
2 (vs 0)	**1.28 (1.00–1.62)**	**1.39 (1.04–1.85)**	**2.08 (1.39–3.11)**	**2.46 (1.77–3.41)**	**2.15 (1.46–3.19)**	**2.64 (1.87–3.75)**
3 (vs 0)	0.97 (0.58–1.62)	1.35 (0.75–2.45)	2.01 (0.96–4.24)	**4.92 (3.03–7.99)**	**2.11 (1.16–3.82)**	**4.36 (2.54–7.50)**
GS synovitis						
1 (vs 0)	1.02 (0.83–1.25)	1.19 (0.94–1.50)	1.22 (0.84–1.77)	**1.87 (1.40–2.49)**	1.39 (0.97–2.01)	**1.86 (1.37–2.52)**
2 (vs 0)	**1.28 (1.02–1.60)**	1.31 (1.00–1.72)	**2.02 (1.36–2.98)**	**2.14 (1.58–2.89)**	**2.01 (1.40–2.89)**	**2.24 (1.61–3.11)**
3 (vs 0)	0.94 (0.54–1.66)	1.02 (0.52–1.98)	1.37 (0.52–3.64)	**3.99 (2.32–6.85)**	1.79 (0.96–3.34)	**3.46 (1.90–6.31)**
GS effusion	1.19 (0.99–1.43)	**1.53 (1.24–1.90)**	**1.86 (1.34–2.58)**	**1.97 (1.55–2.50)**	**1.81 (1.37–2.39)**	**2.10 (1.65–2.68)**
Suprapatellar PD						
1 (vs 0)	1.11 (0.90–1.36)	1.05 (0.82–1.35)	1.05 (0.70–1.58)	1.10 (0.85–1.44)	1.02 (0.74–1.41)	1.21 (0.91–1.62)
2 or 3 (vs 0)	**1.50 (1.04–2.18)**	1.11 (0.74–1.67)	ne	1.11 (0.62–1.97)	1.40 (0.81–2.43)	**1.79 (1.08–2.98)**
Osteophytes, medial						
1 (vs 0)	1.24 (1.00–1.55)	**1.33 (1.03–1.71)**	**1.73 (1.13–2.66)**	**3.20 (2.34–4.38)**	**3.89 (2.49–6.10)**	**3.01 (2.13–4.27)**
2 (vs 0)	**1.97 (1.39–2.78)**	**2.81 (1.94–4.07)**	**3.10 (1.85–5.20)**	**13.9 (9.13–21.2)**	**20.9 (13.0–33.5)**	**8.86 (5.77–13.6)**
3 (vs 0)	**3.08 (1.72–5.53)**	**3.71 (2.20–6.24)**	**3.82 (2.01–7.26)**	ne	**41.3 (21.4–79.8)**	**24.5 (13.0–46.0)**
Osteophytes, lateral						
1 (vs 0)	**1.48 (1.18–1.86)**	**1.62 (1.25–2.11)**	**1.89 (1.31–2.70)**	**3.78 (2.90–4.94)**	**5.68 (3.66–8.83)**	**4.07 (2.96–5.60)**
2 (vs 0)	**1.89 (1.34–2.65)**	**2.13 (1.49–3.04)**	**3.16 (1.89–5.30)**	**12.2 (7.92–18.9)**	**21.2 (12.9–35.0)**	**8.45 (5.51–13.0)**
3 (vs 0)	ne	**8.66 (4.55–16.5)**	**6.30 (2.30–17.3)**	**13.7 (6.00–31.4)**	**47.6 (18.8–120)**	**18.9 (8.34–43.0)**
Meniscal extrusion, medial	1.24 (0.93–1.66)	**1.64 (1.22–2.21)**	1.42 (0.92–2.18)	**3.17 (2.33–4.31)**	**3.21 (2.24–4.60)**	**2.31 (1.65–3.22)**
Meniscal extrusion, lateral	1.22 (0.96–1.55)	1.19 (0.92–1.53)	1.06 (0.72–1.55)	**1.33 (1.00–1.77)**	**1.71 (1.21–2.41)**	**1.48 (1.08–2.01)**
Cartilage damage, medial						
1 (vs 0)	1.15 (0.91–1.44)	**1.34 (1.02–1.76)**	1.11 (0.77–1.61)	**1.78 (1.26–2.53)**	1.36 (0.89–2.08)	**1.61 (1.07–2.42)**
2 (vs 0)	**1.39 (1.06–1.82)**	**1.56 (1.15–2.12)**	**1.55 (1.02–2.37)**	**2.25 (1.53–3.31)**	**1.85 (1.17–2.91)**	**2.26 (1.49–3.45)**
3 (vs 0)	**2.22 (1.34–3.68)**	**2.00 (1.19–3.35)**	1.39 (0.70–2.76)	**3.68 (2.13–6.38)**	**2.08 (1.10–3.94)**	**3.43 (1.87–6.31)**
Cartilage damage, lateral						
1 (vs 0)	1.09 (0.89–1.34)	1.25 (0.98–1.60)	1.40 (0.95–2.08)	**1.48 (1.09–2.01)**	**1.63 (1.13–2.34)**	1.40 (0.98–2.00)
2 (vs 0)	**1.47 (1.13–1.91)**	**1.47 (1.09–1.98)**	**1.60 (1.02–2.51)**	**2.40 (1.69–3.40)**	**2.01 (1.35–3.00)**	**2.46 (1.69–3.59)**
3 (vs 0)	1.41 (0.81–2.43)	1.70 (0.93–3.09)	1.06 (0.44–2.55)	**2.85 (1.54–5.26)**	1.81 (0.95–3.48)	**2.60 (1.38–4.90)**
Popliteal cyst						
1 (vs 0)	1.12 (0.93–1.36)	1.23 (1.00–1.51)	1.23 (0.90–1.68)	1.29 (0.99–1.68)	1.12 (0.82–1.55)	1.28 (0.96–1.71)
2 (vs 0)	**1.77 (1.11–2.84)**	**2.16 (1.31–3.57)**	1.45 (0.71–2.93)	**3.17 (2.02–4.96)**	**3.24 (1.83–5.75)**	**3.43 (2.08–5.67)**
Calcium crystal deposition	1.27 (0.98–1.65)	**1.38 (1.06–1.81)**	**1.74 (1.23–2.46)**	**1.62 (1.17–2.24)**	**1.62 (1.09–2.38)**	**1.50 (1.06–2.11)**

* Logistic regression modeling log odds of each knee outcome and its association with each US feature, separately, using generalized estimating equation for correlation between knees. Each model adjusts for age, sex, race, ethnicity, body mass index, education, Charlson Comorbidity Index, and knee injury. Values are bold when significant at 0.05 level. CI, confidence interval; GS, gray scale; KLG, Kellgren-Lawrence grade; ne, not estimable for cells with <5 counts; OR, odds ratio; PAS, Self-reported pain, aching or stiffness; PD, power Doppler; rKOA, radiographic knee osteoarthritis; sxKOA, symptomatic knee osteoarthritis; US, ultrasound.

KOOS outcomes. As a diagnostic study, a US definition of at least small osteophytes and minimal cartilage damage (mirroring the commonly used KLG) provided 81% sensitivity and an AUC of 0.76 for diagnosing rKOA (validated in an independent population with sensitivity = 0.79 and AUC = 0.76).

Although US is commonly criticized for reproducibility, these issues are not specific to US—reliability is less than perfect for radiographic and MRI grading, or even clinical examination.[6,17,18] A standardized protocol such as that used here, along with appropriate training and oversight, is essential for acquiring adequate images on a large scale. Oo et al reported on a small study of 89 individuals with KOA who underwent US and MRI on the same day, with excellent interrater reliability and very strong correlations between US- and MRI-defined pathologies including synovitis, medial meniscal extrusion, and osteophytes.[19] Grayscale and power Doppler US are also strongly correlated with synovitis detected by contrast-enhanced MRI.[20] In addition, the use of a scoring atlas, again with appropriate training and recalibration sessions, enhances reproducibility within and across studies and is similar to what is done with other imaging modalities. There are many benefits to the use of US in a community setting for OA, including the lack of exclusions based on implants or body size (many radiography and MRI tables are limited to 300 lb; the latter often use coils that limit knee size), ease of access, lack of radiation, relatively lower cost, and dynamic and multiple joint scanning. In addition to these advantages, US shares many of the benefits of MRI, including the ability to image soft tissue features, physiologic imaging (eg, power Doppler), and increased sensitivity to initial changes over radiography. These features make US much more attractive for clinical translation than is MRI.

Table 4. Diagnostic accuracy for six US definitions of knee OA compared to radiographic knee OA defined by both osteophytes and joint space narrowing in the Johnston County Health Study (n = 1,703 knees)*

Def	Index US definition	Level	Total	No rKOA (n = 1,206)	Mild rKOA (n = 497)	Sensitivity (95% CI)	Specificity (95% CI)	Area under curve (95% CI)	Positive predictive value (95% CI)	Negative predictive value (95% CI)
1	Small but distinct med/lat osteophytes AND minimal med/lat cartilage thinning	no yes	929 774	838 368	91 406	0.81 (0.78–0.85)	0.69 (0.66–0.72)	0.76 (0.73–0.78)	0.50 (0.46–0.54)	0.89 (0.87–0.92)
2	Larger med/lat osteophytes AND mild/local med/lat cartilage thinning	no yes	1,467 236	1,157 49	310 187	0.36 (0.31–0.41)	0.96 (0.94–0.97)	0.67 (0.65–0.69)	0.78 (0.72–0.84)	0.78 (0.75–0.80)
3	Small but distinct med/lat osteophytes AND minimal med/lat cartilage thinning AND JCD parallel to bone GS effusion/synovitis	no yes	1,233 470	1,000 206	233 264	0.53 (0.48–0.58)	0.83 (0.80–0.85)	0.68 (0.66–0.70)	0.55 (0.50–0.60)	0.80 (0.77–0.83)
4	Small but distinct med/lat osteophytes AND minimal med/lat cartilage thinning AND med/lat meniscal extrusion	no yes	1,391 312	1,091 115	300 197	0.39 (0.34–0.43)	0.90 (0.88–0.92)	0.65 (0.63–0.67)	0.61 (0.55–0.67)	0.77 (0.74–0.80)
5	Small but distinct med osteophytes AND minimal med cartilage thinning AND med meniscal extrusion	no yes	1,540 163	1,170 36	370 127	0.25 (0.21–0.29)	0.97 (0.96–0.98)	0.61 (0.59–0.63)	0.77 (0.71–0.84)	0.75 (0.72–0.77)
6	Small but distinct lat osteophytes AND minimal lat cartilage thinning AND lat meniscal extrusion	no yes	1,555 149	1,158 49	397 100	0.20 (0.16–0.24)	0.96 (0.95–0.97)	0.58 (0.56–0.60)	0.66 (0.57–0.74)	0.73 (0.71–0.76)

* Correlation between an individual's knees were accounted for using generalized estimating equation through an exchangeable working correlation structure; therefore, the estimates are model based. CI, confidence interval; Def, definition; GS, gray scale; JCD, joint capsule distention; lat, lateral med, medial; OA, osteoarthritis; KOA, radiographic knee osteoarthritis; US, ultrasound.

This work confirms associations between US features and rKOA as recently reviewed.[8] The association between meniscal extrusion and rKOA has been well documented. One longitudinal study found that 7.5% of participants with meniscal extrusion on US without evidence of rKOA at baseline went on to develop rKOA, and >10% of patients with medial extrusion and rKOA were found to have progression of rKOA over five years.[21] In a Chinese community-based cohort, synovial hypertrophy was present in 18% and conferred four times higher odds of rKOA.[22] Oo et al also found strong correlations among US features and KLG in participants with sxKOA.[23] As might be expected from the increased sensitivity and expanded tissue imaging, US features are often more strongly associated with pain and symptoms than are radiographic features. In the XO study, synovial hypertrophy conferred about double the odds of knee pain.[22] Oo et al found that power Doppler positivity and meniscal extrusion were associated with worse KOOS pain.[23] Interestingly, a Canadian group specifically identified associations between US synovitis and the constant pain scale of the intermittent and constant OA pain scale, particularly in knees with early rKOA.[24] This group has also begun to explore the difference between synovial damage and synovial inflammation on US and histology.[25] Our work contributes to the field by including comprehensive US assessment, expert radiographic grading, and extensive self-reported and clinical data in a unique, diverse, community-based cohort.

As noted above, KOA is often defined on imaging using radiography, generally based on a KLG of 2 or more. MRI definitions have been in development for many years.[26] Recent work by Liew et al on MRI-based KOA diagnosis highlighted the importance of osteophytes.[27] This work also found that including cartilage damage into the definition of KOA on MRI increased the AUC of the proposed definitions (0.7–0.8). This is comparable to the most accurate US diagnosis we identified, which included both osteophytes and cartilage damage, with 81% sensitivity and AUC = 0.76 for diagnosing rKOA. A smaller hospital-based study from Argentina also identified osteophytes and cartilage damage as key features, with a sensitivity of 75% and specificity of 94% for rKOA as the referent.[28] Although binary definitions are useful in identifying cases and are frequently used as inclusion/exclusion criteria, additional systems could be developed to define probabilities of KOA using quantitative or semiquantitative feature scoring from US. A group from Japan recently reported on a novel weight-bearing US-based index for medial rKOA incorporating quantitative measures of osteophytes and interbone distance.[29] Such quantitative assessments, as well as composites across multiple US features,[30] may improve utility and accuracy of US in future work.

Limitations include the cross-sectional nature of the cohort, although we hope to do follow-up in the future. We used a published protocol and scoring atlas to enhance rigor and reproducibility, although generalizability to other populations using other systems is limited. The US machine used in this study was selected for simplicity and utility but may not be the most sensitive, particularly for power Doppler. Additionally, there is disagreement in the field around what portion(s) of the femoral articular cartilage and therefore of the tibiofemoral versus patellofemoral articulations) are visualized in these US views.[31,32] The radiography comparator is most practical and available but does not allow comparison to more similar modalities such as MRI. Strengths of this study include the detailed data from two large, diverse and independent cohorts resulting in the collection of nearly 1,400 standardized knee US images. These cohorts were recruited to be representative of Johnston County, North Carolina, and thereby possibly to the general US population, with a focus on groups often underrepresented in research studies. This generalizability is evident in the participant characteristics, including the frequency of obesity which mirrors the population in the Southeastern United States.[33] Participants were recruited without regard for KOA status or symptoms resulting in a range of disease severity, including the initial stages of KOA.

There are several potential future directions in US. Teleultrasonography holds promise for remote monitoring of disease incidence and progression in OA.[34] Technological advancements including developments in quantitative, three-dimensional, contrast-enhanced, and high-resolution US are ongoing.[35] Finally, US holds promise for clinical and research use in low and middle income countries[36] as well as other resource-limited settings, including multisite studies.

In conclusion, we report associations among US features, radiographic scores, and symptoms in a large, diverse, community-based study in the Southeastern United States. By using a published, standardized protocol and scoring atlas in this highly phenotyped group, we identified common US features in the population as well as significant associations between US features and radiographic and symptomatic radiographic features and symptoms in participants with and without KOA. We propose a US-based rKOA definition, with support in the literature, for further validation. US is a valuable and accessible modality for assessment of KOA features in clinical and research settings, including those with limited resources.

ACKNOWLEDGMENTS

We would like to thank the current and former staff, collaborators, and all participants in the Johnston County studies, without whom this work would not be possible.

AUTHOR CONTRIBUTIONS

All authors contributed to at least one of the following manuscript preparation roles: conceptualization AND/OR methodology, software, investigation, formal analysis, data curation, visualization, and validation AND drafting or reviewing/editing the final draft. As corresponding author, Dr Nelson confirms that all authors have provided the final approval of the version to be published and takes responsibility for the affirmations regarding article submission (eg, not under consideration by another journal), the integrity of the data presented, and the statements regarding compliance with institutional review board/Declaration of Helsinki requirements.

REFERENCES

1. Allen KD, Thoma LM, Golightly YM. Epidemiology of osteoarthritis. Osteoarthritis Cartilage 2022;30(2):184–195.
2. Yang G, Wang J, Liu Y, et al. Burden of knee osteoarthritis in 204 countries and territories, 1990-2019: results from the Global Burden of Disease Study 2019. Arthritis Care Res (Hoboken) 2023; 75(12):2489–2500.
3. Kellgren JH, Lawrence JS. Radiological assessment of osteo-arthrosis. Ann Rheum Dis 1957;16(4):494–502.
4. Macri EM, Runhaar J, Damen J, et al. Kellgren/Lawrence grading in cohort studies: methodological update and implications illustrated using data from a Dutch hip and knee cohort. Arthritis Care Res (Hoboken) 2022;74(7):1179–1187.
5. Schiphof D, Boers M, Bierma-Zeinstra SM. Differences in descriptions of Kellgren and Lawrence grades of knee osteoarthritis. Ann Rheum Dis 2008;67(7):1034–1036.
6. Schiphof D, de Klerk BM, Kerkhof HJ, et al. Impact of different descriptions of the Kellgren and Lawrence classification criteria on the diagnosis of knee osteoarthritis. Ann Rheum Dis 2011;70(8): 1422–1427.
7. Nelson AE. Turning the page in osteoarthritis assessment with the use of ultrasound. Curr Rheumatol Rep 2020;22(10):66.
8. Nevalainen MT, Uusimaa AP, Saarakkala S. The ultrasound assessment of osteoarthritis: the current status. Skeletal Radiol 2023; 52(11):2271–2282.
9. Abraham AM, Pearce MS, Mann KD, et al. Population prevalence of ultrasound features of osteoarthritis in the hand, knee and hip at age 63 years: the Newcastle thousand families birth cohort. BMC Musculoskelet Disord 2014;15(1):162.
10. Yerich NV, Alvarez C, Schwartz TA, et al. A standardized, pragmatic approach to knee ultrasound for clinical research in osteoarthritis: the Johnston County Osteoarthritis Project. ACR Open Rheumatol 2020;2(7):438–448.
11. Sperr E. PubMed by Year. Github. https://esperr.github.io/pubmed-by-year/.
12. Golightly YM, Renner JB, Helmick CG, et al. Looking back on 30+ years of the Johnston County Osteoarthritis Project while looking forward with the Johnston County Health Study: a narrative review. Osteoarthritis Cartilage 2024;32(4):430–438.
13. Jordan JM, Linder GF, Renner JB, et al. The impact of arthritis in rural populations. Arthritis Care Res 1995;8(4):242–250.
14. Jordan JM, Helmick CG, Renner JB, et al. Prevalence of knee symptoms and radiographic and symptomatic knee osteoarthritis in African Americans and Caucasians: the Johnston County Osteoarthritis Project. J Rheumatol 2007;34(1):172–180.
15. Filippou G, Scirè CA, Damjanov N, et al. Definition and reliability assessment of elementary ultrasonographic findings in calcium pyrophosphate deposition disease: a study by the OMERACT Calcium Pyrophosphate Deposition Disease Ultrasound Subtask Force. J Rheumatol 2017;44(11):1744–1749.
16. Charlson ME, Pompei P, Ales KL, et al. A new method of classifying prognostic comorbidity in longitudinal studies: development and validation. J Chronic Dis 1987;40(5):373–383.
17. Maricar N, Callaghan MJ, Parkes MJ, et al. Clinical assessment of effusion in knee osteoarthritis-a systematic review. Semin Arthritis Rheum 2016;45(5):556–563.
18. Roemer FW, Jarraya M, Hayashi D, et al. A perspective on the evolution of semi-quantitative MRI assessment of osteoarthritis: past, present and future. Osteoarthritis Cartilage 2024;32(4):460–472.
19. Oo WM, Linklater JM, Bennell KL, et al. Reliability and convergent construct validity of quantitative ultrasound for synovitis, meniscal extrusion, and osteophyte in knee osteoarthritis with MRI. J Ultrasound Med 2022;41(6):1559–1573.
20. de Vries BA, Breda SJ, Meuffels DE, et al. Diagnostic accuracy of grayscale, power Doppler and contrast-enhanced ultrasound compared with contrast-enhanced MRI in the visualization of synovitis in knee osteoarthritis. Eur J Radiol 2020;133:109392.
21. Chiba D, Sasaki E, Ota S, et al. US detection of medial meniscus extrusion can predict the risk of developing radiographic knee osteoarthritis: a 5-year cohort study. Eur Radiol 2020;30(7):3996–4004.
22. Jiang T, Yang T, Zhang W, et al. Prevalence of ultrasound-detected knee synovial abnormalities in a middle-aged and older general population-the Xiangya Osteoarthritis Study. Arthritis Res Ther 2021;23(1):156.
23. Oo WM, Linklater JM, Bennell KL, et al. Are OMERACT knee osteoarthritis ultrasound scores associated with pain severity, other symptoms, and radiographic and magnetic resonance imaging findings? J Rheumatol 2021;48(2):270–278.
24. Philpott HT, Birmingham TB, Pinto R, et al; WOREO Knee Study Group. Synovitis is associated with constant pain in knee osteoarthritis: a cross-sectional study of OMERACT knee ultrasound scores. J Rheumatol 2022;49(1):89–97.
25. Philpott HT, Birmingham TB, Carter MM, et al; WOREO Knee Study Group. Association between synovial tissue damage and pain in late-stage knee osteoarthritis: a cross-sectional study. Osteoarthritis Cartilage 2024;32(11):1503–1512.
26. Hunter DJ, Arden N, Conaghan PG, et al; OARSI OA Imaging Working Group. Definition of osteoarthritis on MRI: results of a Delphi exercise. Osteoarthritis Cartilage 2011;19(8):963–969.
27. Liew JW, Rabasa G, LaValley M, et al. Development of a magnetic resonance imaging-based definition of knee osteoarthritis: data from the multicenter osteoarthritis study. Arthritis Rheumatol 2023;75(7):1132–1138.
28. Brom M, Gandino IJ, Zacariaz Hereter JB, et al. Performance of ultrasonography compared to conventional radiography for the diagnosis of osteoarthritis in patients with knee pain. Front Med (Lausanne) 2020;7:319.
29. Kiso T, Okada Y, Kawata S, et al. Diagnostic accuracy of a novel ultrasound imaging index for knee osteoarthritis: evaluation of sensitivity, specificity, and predictive values. J Clin Ultrasound 2024;52(6):687–699.
30. Sawani S, Arbeeva L, Yates K, et al. Patterns of shared variation in knee ultrasound for osteoarthritis: a machine learning approach. Arthritis Rheumatol 2024;76:1207.
31. Kauppinen K, Casula V, Zbýň Š, et al. Ultrasonographic assessment of the normal femoral articular cartilage of the knee joint: comparison with 3D MRI. ScientificWorldJournal 2021;2021:9978819.
32. Schmitz RJ, Wang HM, Polprasert DR, et al. Evaluation of knee cartilage thickness: a comparison between ultrasound and magnetic resonance imaging methods. Knee 2017;24(2):217–223.
33. Emmerich SD, Fryar CD, Stierman B, et al. Obesity and severe obesity prevalence in adults: United States, August 2021–August 2023. NCHS Data Brief 2024;(508).
34. D'Agostino V, Sorriento A, Cafarelli A, et al. Ultrasound imaging in knee osteoarthritis: current role, recent advancements, and future perspectives. J Clin Med 2024;13(16):4930.
35. Vendries V, Ungi T, Harry J, et al. Three-dimensional ultrasound for knee osteophyte depiction: a comparative study to computed tomography. Int J Comput Assist Radiol Surg 2021;16(10):1749–1759.
36. Stewart KA, Navarro SM, Kambala S, et al. Trends in ultrasound use in low and middle income countries: a systematic review. Int J MCH AIDS 2020;9(1):103–120.

American College of Rheumatology
Empowering Rheumatology Professionals

Arthritis & Rheumatology
Vol. 77, No. 8, August 2025, pp 1006–1014
DOI 10.1002/art.43155

Association of Physical Therapy Care With Use of Intra-Articular Injections in People With Knee Osteoarthritis: A Real-World Cohort Study

Tuhina Neogi, Maureen Dubreuil, Christine Peloquin, Lee Marinko, James Camarinos, David T. Felson, and Deepak Kumar

Objective. The objective of this study was to assess the relation of physical therapy (PT) timing, dose, and type with risk of future intra-articular therapy use in people with knee osteoarthritis (OA) who receive PT.

Methods. We used data from a deidentified claims database (Optum Labs Data Warehouse) from American adults with incident knee OA referred for PT within the first year of their knee OA diagnosis. We categorized people as having previously had intra-articular therapies or not. We examined the association of timing of PT initiation, number of PT sessions, and type of PT (predominantly active or passive) with intra-articular therapy use over a period of one year following the first year of diagnosis.

Results. Of the 67,245 individuals with knee OA (age 61.5 ± 11 years, 61% female, 10% Black, 6% Hispanic), 34,804 and 32,441 did and did not have prior intra-articular therapies, respectively. Among those who had prior intra-articular therapies, initiating PT at 9 to 12 months post diagnosis was associated with an adjusted risk ratio of 1.44 for future intra-articular therapy (95% confidence interval 1.35–1.55) compared with those who initiated within a month. For both groups, ≥13 PT sessions was associated with a 10% and 12% lower risk, respectively, compared with 1 to 5 sessions. Active PT was not related to lower risk compared to passive PT interventions.

Conclusion. Initiating PT earlier and more than 12 PT sessions were significantly associated with lower risk of future intra-articular therapy use in people with newly diagnosed knee OA.

INTRODUCTION

Knee osteoarthritis (OA) is a leading cause of chronic pain and disability worldwide.[1] Intra-articular therapies, including intra-articular corticosteroids (IACS) and intra-articular hyaluronic acid (IAHA), remain highly used for knee OA. Among patients scheduled for knee replacement, up to half have received IACS and one in six have received IAHA.[2,3] The most recent guidelines from five professional medical and/or research societies have recommended use of IACS for management of knee OA based on their short-term efficacy.[4] However, recent reports raise concerns about a potential increased risk of cartilage loss and knee replacement with repeated IACS injections, although findings are inconsistent.[5–8] Given publication bias, high risk of bias in published studies, and risk of flare-ups and other adverse events,[9] the 2019 American College of Rheumatology and 2021 American Academy of Orthopaedic Surgeons guidelines conditionally recommended against IAHA for people with knee OA,[10,11] whereas others conditionally recommend its use.[4] Despite the lack of strong support by specialty societies for IAHA use, IAHA was the most commonly selected intervention not recommended by their own society's clinical practice guidelines in a survey of orthopedic surgeons.[12] Use of either IACS or IAHA has also been associated with greater odds of opioid use, suggesting poor pain management.[2,13] There is a need to promote the use of other safer and more effective therapies and reduce the use of these minimally effective or potentially harmful intra-articular therapies.

Supported by the National Institute of Arthritis and Musculoskeletal and Skin Diseases, NIH (grant K24-AR-070892 to Dr Neogi, grant K23-AR-069127 to Dr Dubreuil, grant P30-AR-0702571 to Dr Felson, and grant K01-AR-069720 to Dr Kumar). The sponsors had no role in the design and conduct of the study; collection, management, analysis, and interpretation of the data; preparation, review, or approval of the manuscript; and decision to submit the manuscript for publication.

Tuhina Neogi, MD, PhD, Maureen Dubreuil, MD, Christine Peloquin, MPH, Lee Marinko, PT, ScD, James Camarinos, PT, David T. Felson, MD, Deepak Kumar, PT, PhD: Boston University, Boston, Massachusetts.

Additional supplementary information cited in this article can be found online in the Supporting Information section (https://acrjournals.onlinelibrary.wiley.com/doi/10.1002/art.43155).

Author disclosures and graphical abstract are available at https://onlinelibrary.wiley.com/doi/10.1002/art.43155.

Address correspondence via email to Deepak Kumar, PT, PhD, at kumard@bu.edu.

Submitted for publication July 17, 2024; accepted in revised form February 25, 2025.

Exercise and education, typically delivered as part of physical therapy (PT), lead to meaningful improvements in pain and function and are recommended as first-line interventions for knee OA in all guidelines,[14–17] though implementation of these recommendations remains poor.[18] When compared to IACS, an exercise-based PT intervention provided greater and longer-term reduction in pain and improvement in function in people with knee OA.[19] Given that PT interventions can reduce pain in people with knee OA, it is possible that they may also reduce the risk of future use of intra-articular therapies, assuming use of intra-articular therapies reflects failure of pain management. Specifically, in people diagnosed with knee OA and referred to PT, whether early versus late initiation of PT, number of PT visits, or nature of PT care (ie, active vs passive) influence the risk of future use of intra-articular therapies merits evaluation. Timing, dose, and type of PT interventions for people with incident knee OA can be highly variable, and this knowledge can help with standardization or practice and also guide payers and providers toward delivering optimal PT interventions for this population.[20]

The objective of our study was to assess the association of timing, dose, and type of PT interventions with risk of future use of intra-articular therapies in people with incident knee OA referred to PT. We hypothesized that shorter time to first PT visit, greater PT dose, and active PT treatment will all be associated with reduced use of intra-articular therapies in people with incident knee OA referred to PT.

PATIENTS AND METHODS

Data source. We used data from the Optum Labs Data Warehouse (OLDW), which includes deidentified medical and pharmacy claims, PT claims, laboratory results, and enrollment records for more than 200 million commercial and Medicare Advantage enrollees. Members in the database had full insurance coverage for physician, hospital, and prescription drug services.[21] The database contains longitudinal health information on patients representing a diverse mix of ages, races, and US geographic regions. Since this study involved analysis of preexisting, deidentified data, it was exempt from institutional review board review.

Study sample. We included persons aged 40 or older who had had incident knee OA (index event) between 2001 and 2016 and received PT treatment within 12 months after their incident knee OA diagnosis. Incident knee OA was defined as a claim for knee OA in an individual with no prior knee OA claim during the prior 24-month period. Knee OA was identified using *International Classification of Disease* (ICD) codes 715.x6 (9th revision) and M17.x (10th revision). To minimize confounding by indication, we only included persons who received PT treatment after the knee OA diagnosis. We only included persons with continuous coverage over the study period. We excluded persons with any of the following in the 24 months preceding the incident knee OA diagnosis: knee replacement, knee surgeries, high-risk cancer, or rheumatoid arthritis. We also excluded persons who received PT within 12 months before the incident knee OA diagnosis and persons who did not have any PT treatment codes that were categorized as active or passive or who had missing data for age, sex, insurance type, and geographic region.

We further stratified our study cohort into those who had prior intra-articular injections in any body region versus those who did not based on presence of codes for IACS or IAHA (Supplementary Table 1) in the 2 years before the index date up to the start of the first PT episode of care (EOC). This was to address the potential that any prior experience with intra-articular injections, regardless of body site, could influence future use of such injections. Intra-articular therapy use during the PT EOC was included as a covariate. Intra-articular therapy use after the PT EOC but within the first 12 months after the index date was not included in the outcome because we were interested in the longer-term impact of PT attributes on intra-articular therapy use.

Exposures. The exposures included PT timing, PT dose, and PT type. PT timing was defined as the time between the index date (ie, incident knee OA diagnosis) and the start of the first PT EOC (Figure 1). The first PT EOC was defined as occurring between the date of the first outpatient PT claim with a PT evaluation Current Procedural Terminology (CPT) code after the index date and the date of the PT claim preceding the ≥12-week period of no PT claims (Figure 1).[22] Outpatient PT was identified using CPT codes (Supplementary Table 2). One PT researcher reviewed all ICD codes from the first PT claim and excluded all ICD codes that were not related to knee OA. Hence, only PT care that was related to knee OA was included. Timing was modeled as a categorical exposure with the following categories: <1 month, 1 to <3 months, 3 to <6 months, 6 to <9 months, and 9 to <12 months after the index date.[22] PT dose was defined as the number of PT claims on unique dates during the first PT EOC. PT dose was modeled as a categorical exposure with the following categories: 1 to 5 sessions, 6 to 12 sessions, and >13 sessions.[22] PT type was categorized into active or passive PT using CPT codes (Supplementary Table 1) from PT claims during the PT EOC. The PT care was categorized as active PT (eg, exercise, gait training) if ≥50% were active PT codes; examples considered passive PT include ultrasound, thermal therapies, etc.[22,23]

Outcomes. The outcome was use of IACS and/or IAHA based on Healthcare Common Procedure Coding System codes (Supplementary Table 2) modeled as a dichotomous variable. Only IACS and IAHA claims with concurrent knee pain or OA codes were included. We assessed the occurrence of the outcome starting 12 months after the index date for a one-year follow-up period (Figure 1).

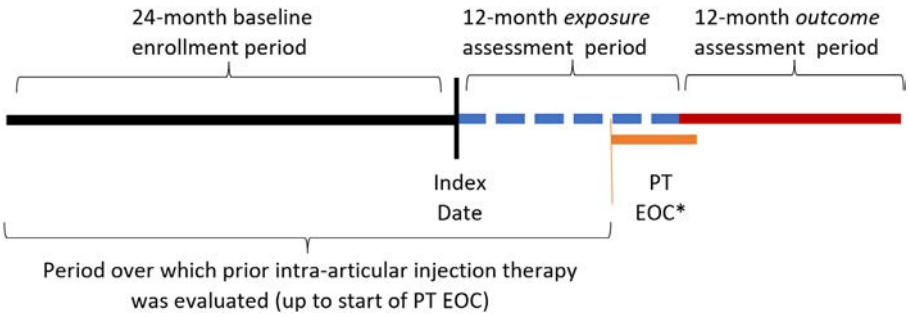

Figure 1. Study design depicting baseline enrollment period, exposure assessment period, outcome assessment period, a hypothetical PT EOC starting within the first 12 months post index date, and the time over which prior intra-articular therapy was evaluated. *The PT EOC can start anytime within the 12-month period following the index date. In cases in which the PT EOC is initiated close to the end of the 12-month period, it may extend into the outcome assessment period. EOC, episode of care; PT, physical therapy.

Covariates. All analyses were adjusted for age, sex, race, insurance (commercial or Medicare Advantage), geographic location, comorbidities, obesity, health care use, calendar year, and receipt of intra-articular injections during the PT EOC. Comorbidities were identified throughout the 24 months before the index date using the Elixhauser Index and modeled as a continuous count, excluding obesity.[24,25] Obesity, identified using the Elixhauser Index, was entered into the model as a separate variable given its association with knee OA and opioid use.[26] Health care use was calculated as the number of outpatient claims seven or more days apart within the two years before the index date.[22] Calendar year was added as a covariate for all models to account for secular trends. Use of intra-articular therapies for knee pain or OA concurrently with PT was modeled as a dichotomous variable.

Statistical analyses. In each stratum (of prior injection vs no prior injection), we evaluated the relation of PT timing, dose, and type to any use of IACS or IAHA using Poisson regression with a robust variance to obtain risk ratios adjusted for confounders.[27] To examine the robustness of the findings to unmeasured residual confounding, we calculated E-values, which reflect the minimum strength of association needed between an unmeasured confounder and both the exposure and the outcome to nullify the observed effect estimate.[28] We also report the results stratified by sex and race and ethnicity, acknowledging that race and ethnicity serve as a proxy for numerous differential structural systemic societal impacts. Analyses were conducted using SAS version 9.4 (SAS Institute, Inc).

RESULTS

We identified 2,194,144 individuals with any knee OA claim between 2001 and 2016. After applying the various inclusion and exclusion criteria, we identified 67,245 individuals who met all criteria for incident knee OA; 32,441 had not received any intra-articular therapies in the assessment period, and 34,804 did (Figure 2). Characteristics of the study sample and the distribution of exposures are shown in Table 1. A majority of the cohort was White and had commercial insurance. Nonsteroidal anti-inflammatory drug (NSAID) use was fairly common. Approximately three-fifths (45,391 of 67,245) received outpatient PT care within three months of knee OA diagnosis; the median time to PT was 42 days after incident knee OA diagnosis. About one in five (15,301 of 67,245) received more than 12 sessions of outpatient PT. More than 75% (52,168 of 67,245) received active PT treatment. Of those who had a prior intra-articular therapy for any body region, the mean number of injections was 2.8 (SD 3.4).

Overall, 14.1% (9,497 of 67,245) of the study sample had at least one intra-articular injection during the follow-up period (ie, in the 12-month period following the first year of diagnosis), with 19.1% (6,650 of 34,804) occurring among those who had previously received such an injection and 8.8% (2,847 of 32,441) among those who were intra-articular injection naive. In terms of types of intra-articular injection, 11.4% (7,648 of 67,245) received IACS and 5.2% (3,517 of 67,245) received IAHA during the follow-up period (the total is greater than 14.1% because some received both agents). A total of 20,463 injections were delivered during the outcome assessment period; 66.1% (13,534 of 20,463) were claims from orthopedic surgeons, 11.6% (2,375 of 20,463) were claims from family medicine or primary care, 7.2% (1,472 of 20,463) were claims from physiatrists, 3.8% (779 of 20,463) were claims from rheumatologists, and the rest were claims from other specialties.

For PT timing (ie, time to starting PT after the incident knee OA diagnosis claim), among those who had received prior intra-articular therapies, their risk for receiving an intra-articular injection in the year after the first year of diagnosis increased with greater time to starting PT, with those waiting at least 9 to 12 months before the start of PT having a 44% higher risk of intra-articular injection therapy than those who started PT within a month of their knee OA diagnosis. In contrast, those who had not received intra-articular therapies previously did not experience a statistically significantly higher risk of receiving an intra-articular injection

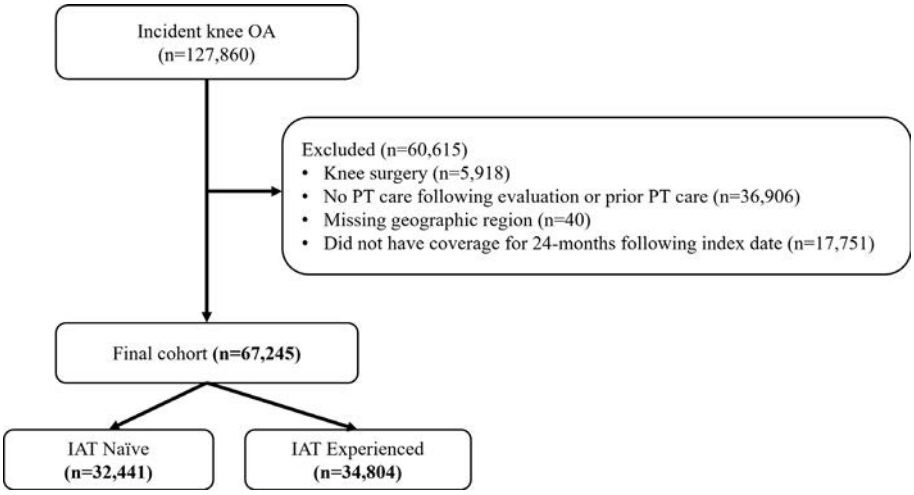

Figure 2. Cohort selection. OA, osteoarthritis, IAT, intra-articular therapy; PT, physical therapy.

with longer the time to starting PT post diagnosis, though there was a numerically higher risk of approximately 10% to 15% among those whose PT started at least 6 months post diagnosis versus those who started within the first month (Figure 3). In general, findings were similar for both men and women and all available races and ethnicities, except for the small group of participants with self-reported Asian background, for whom no relation was seen for PT timing and future injections (Supplementary Table 3).

For PT dose, 13 or more PT sessions in an EOC was significantly associated with a lower risk of receiving intra-articular injections in the year following the first year after diagnosis in both groups compared to 1 to 5 PT sessions, albeit with small associations (Figure 4). For example, for those who had not received

Table 1. Study cohort characteristics*

	IAT naive (n = 32,441)	IAT experienced (n = 34,804)	Whole sample (N = 67,245)
Age, mean (SD), y	60.8 (11.1)	62.3 (10.9)	61.5 (11.0)
Female, % (n)	58.3 (18,903)	63.2 (22,005)	60.8 (40,908)
Obesity, % (n)	13.9 (4,517)	17.2 (5,976)	15.6 (10,493)
Race and ethnicity, % (n)			
Asian	2.8 (899)	1.6 (572)	2.2 (1,471)
Black	10.0 (3,240)	10.7 (3,718)	10.3 (6,958)
Hispanic	6.4 (2,092)	6.2 (2,171)	6.3 (4,263)
White	77.8 (25,244)	78.9 (27,444)	78.4 (52,688)
Missing	3.0 (966)	2.6 (899)	2.8 (1,865)
US region, % (n)			
Midwest	34.2 (11,106)	32.3 (11,257)	33.3(22,363)
Northeast	15.9 (5,170)	10.3 (3,594)	13.0 (8,764)
South	34.1 (11,054)	45.1 (15,694)	39.8 (26,748)
West	15.8 (5,111)	12.2 (4,259)	13.9 (9,370)
Insurance type, % (n)			
Commercial	76.1 (24,688)	70.4 (24,508)	73.2 (49,196)
Medicare advantage	23.9 (7,753)	29.6 (10,296)	26.8 (18,049)
Elixhauser minus obesity (counts), mean (SD)	2.0 (2.1)	2.4 (2.2)	2.2 (2.1)
NSAID use, % (n)	36.5 (11,850)	47.0 (16,366)	42.0 (28,216)
Health care use, % (n)			
0–3	24.0 (7,784)	15.3 (5,321)	19.5 (13,105)
4–6	28.8 (9,346)	24.4 (8,484)	26.5 (17,830)
7–10	26.9 (8,713)	30.0 (10,447)	28.5 (19,160)
11+	20.3 (6,598)	30.3 (10,552)	25.5 (17,150)
IAT for knee pain or OA used during PT episode of care, % (n)	4.7 (15,123)	8.1 (2,809)	6.4 (4,322)

* NSAIDs include celecoxib, diclofenac, diflunisal, fenoprofen, flurbiprofen, ibuprofen, indomethacin, ketoprofen, ketorolac, meloxicam, naproxen, nabumetone, oxaprozin, phenylbutazone, rofecoxib, salsalate, sulindac, tolmetin, and valdecoxib. IAT, intra-articular therapy; NSAID, nonsteroidal anti-inflammatory drug; OA, osteoarthritis; PT, physical therapy.

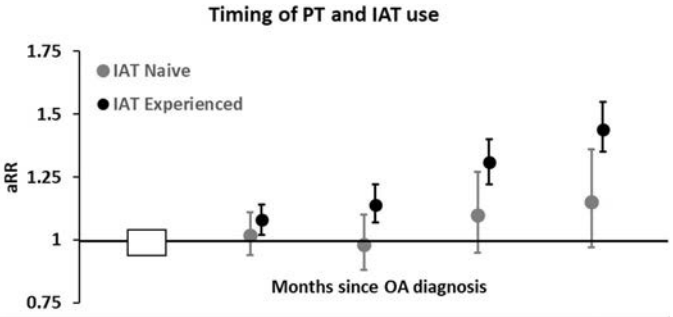

	Timing	<1	1-<3	3-<6	6-<9	9-12
IAT Naïve	Subjects, % (n/N)	52.8 (17127/32441)	25.2 (8162/32441)	11.9 (3864/32441)	6.0 (1954/32441)	4.1 (1334/32441)
	IAT Use, % (n/N)	8.8 (1511/17127)	8.6 (700/8162)	8.4 (324/3864)	9.3 (181/1954)	9.8 (131/1334)
	Adjusted RR	REF	1.02 (0.94, 1.11)	0.98 (0.88, 1.10)	1.10 (0.95, 1.27)	1.15 (0.97, 1.36)
IAT Experienced	**Subjects, % (n/N)**	**33.1 (11507/34804)**	**24.7 (8595/34804)**	**19.3 (6723/34804)**	**12.9 (4480/34804)**	**10.1 (3499/34804)**
	IAT Use, % (n/N)	**17.2 (1981/11507)**	**18.2 (1564/8595)**	**19.1 (1287/6723)**	**21.8 (975/4480)**	**24.1 (843/3499)**
	Adjusted RR	**REF**	**1.08 (1.02, 1.14)**	**1.14 (1.07, 1.22)**	**1.31 (1.22, 1.40)**	**1.44 (1.35, 1.55)**

Figure 3. Relation of timing of PT initiation with IAT use in individuals without previous IAT use (gray) and with previous IAT use (black). The aRR represents the risk of experiencing the outcome in each category relative to the refence category after adjusting for the confounders. For instance, an aRR of 1.44 reflects a 44% greater risk of receiving IAT in people who initiated PT 9 to 12 months after diagnosis compared to those who initiated PT within one month of diagnosis in the IAT-experienced group. aRR, adjusted risk ratio; IAT, intra-articular therapy; PT, physical therapy.

prior intra-articular therapies, having 13 or more sessions was associated with a 12% significantly lower risk than having 1 to 5 sessions, whereas for those who had received prior intra-articular therapies, there was a 10% lower risk (Figure 4). Among those with prior intra-articular therapies, similar results were seen for both sexes and for those with Asian or White race but not for

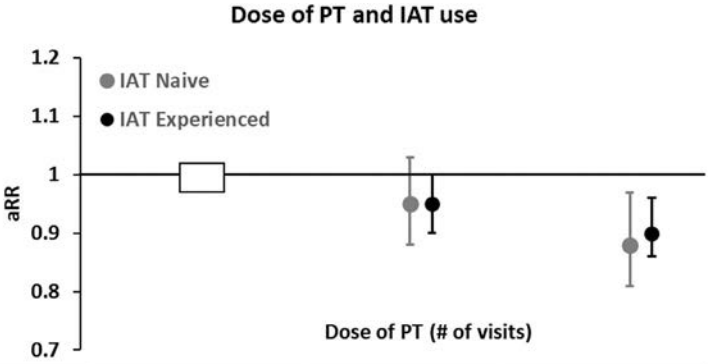

	Dose	1-5	6-12	13+
IAT Naïve	Subjects, % (n/N)	45.6 (14809/32441)	31.8 (10327/32441)	22.5 (7305/32441)
	IAT Use, % (n/N)	8.9 (1314/14809)	8.7 (903/10327)	8.6 (630/7305)
	Adjusted RR	REF	0.95 (0.88, 1.03)	0.88 (0.81, 0.97)
IAT Experienced	**Subjects, % (n/N)**	**45.3 (15759/34804)**	**31.7 (11049/34804)**	**23.0 (7996/34804)**
	IAT Use, % (n/N)	**19.3 (3037/15759)**	**18.9 (2084/11049)**	**19.1 (1529/7996)**
	Adjusted RR	**REF**	**0.95 (0.90, 1.00)**	**0.90 (0.86, 0.96)**

Figure 4. Relation of dose of PT with IAT use in individuals without previous IAT use (gray) and with previous IAT use (black). The aRR represents the risk of experiencing the outcome in each category relative to the refence category after adjusting for the confounders. For instance, an aRR of 0.90 reflects a 10% lower risk of receiving IAT in people who received ≥13 sessions of PT compared to those who received 1 to 5 sessions in the IAT-experienced group. aRR, adjusted risk ratio; IAT, intra-articular therapy; PT, physical therapy.

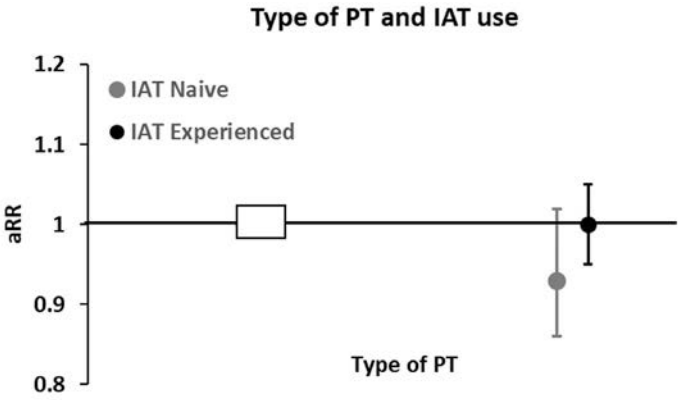

	Type	Passive	Active
IAT Naïve	Subjects, % (n/N)	22.6 (7318/32441)	77.4 (25123/32441)
	IAT Use, % (n/N)	9.3 (682/7318)	8.6 (2165/25123)
	Adjusted RR	REF	0.93 (0.86, 1.02)
IAT Experienced	**Subjects, % (n/N)**	**22.3 (7759/34804)**	**77.7 (27045/34804)**
	IAT Use, % (n/N)	**19.2 (1491/7759)**	**19.1 (5159/27045)**
	Adjusted RR	**REF**	**1.00 (0.95, 1.05)**

Figure 5. Relation of type of PT with IAT use in individuals without previous IAT use (gray) and with previous IAT use (black). The aRR represents the risk of experiencing the outcome in each category relative to the refence category after adjusting for the confounders. For instance, an aRR of 0.93 reflects a 7% lower risk of receiving IAT in people who received active PT compared to those who received passive PT in the IAT-naive group. aRR, adjusted risk ratio; IAT, intra-articular therapy; PT, physical therapy.

those with Black or Hispanic race and ethnicity (Supplementary Table 4). Among those without prior intra-articular therapies, similar associations were seen in men and those with White or Hispanic race and ethnicity but not in women or those with Asian or Black race (Supplementary Table 4).

For PT type, there was no statistically significant association of active PT care with risk of future intra-articular injections compared to passive PT care (Figure 5), although there was a numerically smaller risk of approximately 7% in those who did not have prior intra-articular injections. Similar results were seen when stratified by sex or race and ethnicity, except a protective effect with active PT was seen in men without prior experience with intra-articular therapies (Supplementary Table 5).

We considered the possibility of unmeasured residual confounding by computing E-values. The E-values ranged from 1.29 to 2.24, indicating large residual confounding would need to be present to nullify our results.

DISCUSSION

In this large real-world cohort of people with incident knee OA referred to PT, among those who had prior intra-articular therapies, a group more likely to have future intra-articular therapies, the greater the time to starting PT after their knee OA diagnosis, the greater the risk of receiving an intra-articular injection in the year following the first year post diagnosis. Starting PT by 9 to 12 months was associated with a 44% higher risk of receiving an intra-articular injection in the follow-up period compared to starting PT within 1 month. For those who had not received intra-articular injections previously, time to first PT after diagnosis was not significantly associated with a greater risk of intra-articular injections in the follow-up period, though the effect estimate suggested a numerically greater 10% to 15% risk. Similarly, receiving more than 12 PT sessions was associated with a modest lower risk of receiving intra-articular injections in both groups compared to receiving 1 to 5 sessions, though the clinical significance of this magnitude of effect is unclear. We did not observe an association between active PT care and future risk of intra-articular injections when compared to passive PT care. These findings provide evidence to support earlier initiation of PT and >12 PT visits in people who are diagnosed with knee OA and referred to PT.

We observed a reduced risk of future intra-articular therapy use with early initiation of PT care but only in those with previous use of intra-articular injections. We are not aware of any trials that have specifically tested earlier versus later initiation of PT for knee

OA outcomes. In our study design, in which outcomes were assessed over a one-year period starting 12 months after the index date, it is possible that with earlier initiation of PT care, the time period for the person to develop healthier behaviors was greater and there was greater opportunity for implementation of self-management strategies that reduced the need for future intra-articular therapies. This may also explain the almost dose–response relationship seen between timing of PT initiation and risk of future use of intra-articular therapies. Our findings support and extend previous work in which earlier initiation of PT after knee OA diagnosis was related to reduced future risk of opioid use.[22] Our results are also aligned with research in populations with low back pain in which early initiation of PT has been reported to be related to reduces downstream health care use, cost, and opioid use.[29] It is unclear why the relationship between timing of PT initiation and risk of intra-articular therapies was only seen in people with prior intra-articular therapy use and not in individuals who had not used intra-articular therapies previously. This may reflect a lower incidence of intra-articular therapy use in this latter cohort and a greater proportion of patients initiating PT in the first month overall. It may also be related to disease severity, something that we are not able to directly assess in this study using insurance claims. The evidence from our study and prior real-world studies supports early initiation of PT in patients with incident knee OA who are referred for PT. A majority of the patients initiated PT more than one month after diagnosis, which may be due to referral patterns, challenges with access, or patient preferences.[30] Strategies such as reimbursement for telehealth PT, self-referral, and broader implementation of practice guidelines are some approaches to encourage early initiation of PT care.

We further observed a reduced risk of future intra-articular therapies with more than 12 sessions of PT compared to fewer than 5 sessions in people who did and did not have prior intra-articular injections. However, the crude prevalence of intra-articular injection use was similar across the exposure categories, and the clinical significance of the adjusted findings indicating a modest risk reduction is unclear given the relatively small magnitude of effect. Further examination of duration (number of sessions) of PT on OA outcomes is merited. Although there is no consensus on the appropriate number of exercise sessions for people with knee OA, meta-analyses suggest a greater benefit with a greater number of sessions.[31] In our cohort, almost half of the patients attended five or fewer PT sessions. In people with incident knee OA who are referred to PT, our findings suggest that more visits may be beneficial, information that may be useful for payers and providers.

We did not observe a reduced risk with active (ie, exercise-based) PT interventions when compared to passive interventions, a finding that was consistent across the two cohorts. Our results differ from a prior report of active PT being related to a small but statistically significant reduction in risk of future opioid use in people with incident knee OA.[22] Exercise and education are recommended as first-line interventions for people with knee OA in all guidelines.[4] However, recent studies have questioned whether the effects of exercise on knee pain in people with OA may be mostly due to contextual factors.[32–34] Although limited by lack of detailed information about the interventions, our findings suggest further work is needed to understand the relation of active PT interventions with clinically relevant knee OA outcomes.

Although the effect estimates noted were small, the absolute risk reduction would still be meaningful given the high prevalence of OA in the general population. For example, a crude 1% to 2% risk difference (as seen for some of the PT exposures) would mean that 50 to 100 people would need to be treated with appropriate PT interventions to avoid an intra-articular injection. Given the millions of people with knee OA worldwide, millions of people would be able to avoid intra-articular injections, including repeated injections, that have questionable long-term benefit and concerns about potential harms. Indeed, a nontrivial proportion of individuals in our study received an intra-articular injection in the year following the first year of diagnosis; given that OA is a chronic disease, this would typically indicate an intention of repeated injections over time. Again, given the safety and broader benefits of exercise and PT, a strategy of earlier active PT with an adequate number of sessions would provide the benefit of reduced need to use intra-articular injection. These compelling real-world observational data support the utility of early PT initiation that involves a minimum number of sessions for knee OA management to avoid use of less recommended or nonrecommended therapies. However, referral to PT, access to PT, and insurance coverage of PT remain limiting factors for many patients.

Our study's results must be interpreted in light of some limitations. First, to minimize confounding by indication, we limited our study design to those with a new diagnosis of knee OA who undergo PT at some point during the first year after their diagnosis. This is because individuals who do not undergo PT at all are systematically different from those who do, and such differences cannot be readily accounted for in an observational study. Thus, our study results are only applicable to those who undergo PT in the first year after their knee OA diagnosis. We recognize that this is a small subgroup of people diagnosed with knee OA. Further, because we used claims data, we were unable to verify knee OA diagnoses. However, misclassification is unlikely to meaningfully alter the results, particularly because we limited the PT treatments to knee OA pain-related reasons. Misclassification is also possible in people who received IACS or IAHA before the index date because these individuals may have had knee pain that was really knee OA but undiagnosed. Stratifying by prior use, as we have done, mitigates this issue in the interpretation of the results among those without prior injection use. Additionally, secular trends were addressed by accounting for calendar year. We also did not have information on knee pain severity; we did adjust for prescription NSAID use, which could be considered a proxy

for symptom severity, stratified by prior intra-articular injection use, which may reflect more severe symptoms, and adjusted for health care use. As with any observational study, residual confounding remains a possibility despite accounting for pertinent potential confounders. However, our E-value analysis indicates that a very large unmeasured confounder would need to be present to nullify our results. It is also possible that patient and/or provider preferences or unmeasured socioeconomic factors may have influenced the results. For instance, the intra-articular injection–experienced group may reflect patient and/or provider preference for injections before initiating PT.

In summary, longer time to initiation of PT after the diagnosis of knee OA was associated with greater risk of intra-articular therapy, and this was more so in those who had prior such therapy. Further, a greater number of PT sessions, but not active PT interventions, was associated with modestly lower risk of intra-articular therapy in the year following the first year of a knee OA diagnosis. These real-world data provide support for optimizing treatment recommendations and practical guidance for implementation regarding PT timing and dose to optimize knee OA outcomes while minimizing the need for more invasive therapies that themselves may have minimal (if any) long-term benefit along with concerns about long-term safety.

AUTHOR CONTRIBUTIONS

All authors contributed to at least one of the following manuscript preparation roles: conceptualization AND/OR methodology, software, investigation, formal analysis, data curation, visualization, and validation AND drafting or reviewing/editing the final draft. As corresponding author, Dr Kumar confirms that all authors have provided the final approval of the version to be published and takes responsibility for the affirmations regarding article submission (eg, not under consideration by another journal), the integrity of the data presented, and the statements regarding compliance with institutional review board/Declaration of Helsinki requirements.

REFERENCES

1. Long H, Liu Q, Yin H, et al. Prevalence trends of site-specific osteoarthritis from 1990 to 2019: findings from the Global Burden of Disease Study 2019. Arthritis Rheumatol 2022;74(7):1172–1183.
2. Berger A, Bozic K, Stacey B, et al. Patterns of pharmacotherapy and health care utilization and costs prior to total hip or total knee replacement in patients with osteoarthritis. Arthritis Rheum 2011; 63(8):2268–2275.
3. Dhawan A, Mather RC III, Karas V, et al. An epidemiologic analysis of clinical practice guidelines for non-arthroplasty treatment of osteoarthritis of the knee. Arthroscopy 2014;30(1):65–71.
4. Overton C, Nelson AE, Neogi T. Osteoarthritis treatment guidelines from six professional societies: similarities and differences. Rheum Dis Clin North Am 2022;48(3):637–657.
5. McAlindon TE, LaValley MP, Harvey WF, et al. Effect of intra-articular triamcinolone vs saline on knee cartilage volume and pain in patients with knee osteoarthritis: a randomized clinical trial. JAMA 2017; 317(19):1967–1975.
6. Wijn SRW, Rovers MM, van Tienen TG, et al. Intra-articular corticosteroid injections increase the risk of requiring knee arthroplasty. Bone Joint J 2020;102-B(5):586–592.
7. Zeng C, Lane NE, Hunter DJ, et al. Intra-articular corticosteroids and the risk of knee osteoarthritis progression: results from the Osteoarthritis Initiative. Osteoarthritis Cartilage 2019;27(6):855–862.
8. Latourte A, Rat AC, Omorou A, et al. Do Glucocorticoid injections increase the risk of knee osteoarthritis progression over 5 years? Arthritis Rheumatol 2022;74(8):1343–1351.
9. Rutjes AW, Jüni P, da Costa BR, et al. Viscosupplementation for osteoarthritis of the knee: a systematic review and meta-analysis. Ann Intern Med 2012;157(3):180–191.
10. Kolasinski SL, Neogi T, Hochberg MC, et al. 2019 American College of Rheumatology/Arthritis Foundation guideline for the management of osteoarthritis of the hand, hip, and knee. Arthritis Rheumatol 2020;72(2):220–233.
11. American Academy of Orthopaedic Surgeons. Management of Osteoarthritis of the Knee (Non-Arthroplasty): Evidence-Based Clinical Practice Guideline. American Academy of Orthopaedic Surgeons; 2021.
12. Carlson VR, Ong AC, Orozco FR, et al. Compliance with the AAOS guidelines for treatment of osteoarthritis of the knee: a survey of the American Association of Hip and Knee Surgeons. J Am Acad Orthop Surg 2018;26(3):103–107.
13. Wilson LA, Liu J, Fiasconaro M, et al. Increased use of intra-articular steroid injection to treat osteoarthritis is associated with chronic opioid dependence after later total knee arthroplasty but not total hip arthroplasty. J Arthroplasty 2020;35(8):1979–1982.
14. Bannuru RR, Osani MC, Vaysbrot EE, et al. OARSI guidelines for the non-surgical management of knee, hip, and polyarticular osteoarthritis. Osteoarthritis Cartilage 2019;27(11):1578–1589.
15. National Collaborating Centre for Chronic Conditions. Osteoarthritis: National Clinical Guideline for Care and Management in Adults. Royal College of Physicians; 2008.
16. Pelegrinelli ARM, Guenka LC, Dias JM, et al. Isokinetic muscle performance after anterior cruciate ligament reconstruction: a case-control study. Int J Sports Phys Ther 2018;13(5):882–889.
17. Hochberg MC, Altman RD, April KT, et al; American College of Rheumatology. American College of Rheumatology 2012 recommendations for the use of nonpharmacologic and pharmacologic therapies in osteoarthritis of the hand, hip, and knee. Arthritis Care Res (Hoboken) 2012;64(4):465–474.
18. Khoja SS, Almeida GJ, Freburger JK. Recommendation rates for physical therapy, lifestyle counseling, and pain medications for managing knee osteoarthritis in ambulatory care settings: a cross-sectional analysis of the National Ambulatory Care Survey (2007-2015). Arthritis Care Res (Hoboken) 2020;72(2):184–192.
19. Deyle GD, Allen CS, Allison SC, et al. Physical therapy versus glucocorticoid injection for osteoarthritis of the knee. N Engl J Med 2020; 382(15):1420–1429.
20. MacKay C, Hawker GA, Jaglal SB. How Do physical therapists approach management of people with early knee osteoarthritis? A qualitative study. Phys Ther 2020;100(2):295–306.
21. OptumLabs. OptumLabs and OptumLabs Data Warehouse (OLDW) Descriptions and Citation. Eden Prairie, MN:n.p., March 2022. PDF. Reproduced with permission from Optum Labs.
22. Kumar D, Neogi T, Peloquin C, et al. Delayed timing of physical therapy initiation increases the risk of future opioid use in individuals with knee osteoarthritis: a real-world cohort study. Br J Sports Med 2023;57(15):958–964.
23. Fritz JM, Cleland JA, Brennan GP. Does adherence to the guideline recommendation for active treatments improve the quality of care for

patients with acute low back pain delivered by physical therapists? Med Care 2007;45(10):973–980.

24. Centers for Medicare and Medicaid Services. Chronic Condition Data Warehouse (CCW) algorithm. 2020. Accessed August 2020. https://www.cms.gov/data-research/research/statistical-resources-dually-eligible-beneficiaries/data-tools-researchers.
25. Elixhauser A, Steiner C, Harris DR, et al. Comorbidity measures for use with administrative data. Med Care 1998;36(1):8–27.
26. Stokes A, Lundberg DJ, Sheridan B, et al. Association of obesity with prescription opioids for painful conditions in patients seeking primary care in the US. JAMA Netw Open 2020;3(4):e202012.
27. Spiegelman D, Hertzmark E. Easy SAS calculations for risk or prevalence ratios and differences. Am J Epidemiol 2005;162(3):199–200.
28. VanderWeele TJ, Ding P. Sensitivity analysis in observational research: introducing the E-value. Ann Intern Med 2017;167(4):268–274.
29. Arnold E, La Barrie J, DaSilva L, et al. The effect of timing of physical therapy for acute low back pain on health services utilization: a systematic review. Arch Phys Med Rehabil 2019;100(7):1324–1338.
30. Christiansen MB, Dix C, Master H, et al. "I've been to physical therapy before, but not for the knees." A qualitative study exploring barriers and facilitators to physical therapy utilization for knee osteoarthritis. Musculoskeletal Care 2020;18(4):477–486.
31. Fransen M, McConnell S, Harmer AR, et al. Exercise for osteoarthritis of the knee: a Cochrane systematic review. Br J Sports Med 2015;49(24):1554–1557.
32. Bandak E, Christensen R, Overgaard A, et al. Exercise and education versus saline injections for knee osteoarthritis: a randomised controlled equivalence trial. Ann Rheum Dis 2022;81(4):537–543.
33. Englund M, Turkiewicz A. The emperor's new clothes? Osteoarthritis Cartilage 2023;31(5):549–551.
34. Messier SP, Beavers DP, Queen K, et al. Effect of diet and exercise on knee pain in patients with osteoarthritis and overweight or obesity: a randomized clinical trial. JAMA 2022;328(22):2242–2251.

Arthritis & Rheumatology
Vol. 77, No. 8, August 2025, pp 1015–1025
DOI 10.1002/art.43154

American College of Rheumatology
Empowering Rheumatology Professionals

Effects of Secukinumab on Enthesiophyte and Erosion Progression in Psoriatic Arthritis: A One-Year Double-Blind, Randomized, Placebo-Controlled Trial Using High-Resolution Peripheral Quantitative Computed Tomography

Yingzhao Jin,[1] Isaac T. Cheng,[1] Ho So,[1] Billy T. Lai,[2] Shirley K. Ying,[3] Kitty Y. Kwok,[4] James Griffith,[1] Vivian Hung,[1] Cheuk-Chun Szeto,[1] Jack J. Lee,[1] Ling Qin,[1] and Lai-Shan Tam[1]

Objective. This study aimed to ascertain the effect of secukinumab on erosion and enthesiophyte progression in psoriatic arthritis (PsA) by using high-resolution peripheral quantitative computed tomography (HR-pQCT).

Methods. This was a phase 4, double-blind, randomized, placebo-controlled trial. Patients with active PsA and ≥1 erosion in metacarpophalangeal joints (MCPJs) 2 to 4 were randomly assigned in a 1:1 ratio to subcutaneous secukinumab or placebo. HR-pQCT of MCPJs 2 to 4 were performed at baseline, week 24, and week 48. The primary outcome was the changes in the volume of erosions on MCPJs 2 to 4 measured by HR-pQCT at 24 and 48 weeks.

Results. Forty patients (mean ± SD age 51.9 ± 13.4 years, 20 [50%] male, mean ± SD disease duration 4.7 ± 6.7 years) were recruited. Thirty-four patients who completed study treatment were included in the per-protocol analysis. At baseline, week 24, and week 48, the secukinumab group showed a significant reduction in erosion volume, whereas no changes were observed in the placebo group (median change in the secukinumab group −0.1 [interquartile range −0.5 to 0.0] vs 0.0 [interquartile range −0.2 to 0.4] in the placebo group, $P = 0.004$). A similar trend was observed for enthesiophyte volume changes in the secukinumab group, whereas no differences were noted in the placebo group (median change in the secukinumab group −0.1 [interquartile range −0.8 to 0.0] vs 0.0 [interquartile range −0.4 to 1.3] in the placebo group, $P = 0.067$). Generalized estimating equations results showed that the odds ratio (OR) for enthesiophyte progression in the secukinumab group was 0.264 (95% confidence interval [CI] 0.080–0.878, $P = 0.030$), whereas the OR for partial erosion healing in the secukinumab group was 2.882 (95% CI 1.130–7.349, $P = 0.027$).

Conclusion. Secukinumab demonstrates a potential benefit in facilitating partial erosion repair and preventing enthesiophyte progression in PsA.

INTRODUCTION

Psoriatic arthritis (PsA) is a destructive disease that leads to change in the joint and entheseal architecture.[1] Enthesitis is an early and characteristic musculoskeletal manifestation of PsA that is associated with greater disease activity and reduced quality of life.[1] New bone formation at the entheseal regions of the joints in PsA (enthesiophyte) is the earliest structural change in PsA associated with functional decline.[2,3] Bone erosion is the second important structural lesion in PsA.[1] High-resolution peripheral quantitative computer tomography (HR-pQCT) enables detailed bone microstructure analysis with good reproducibility in assessing bony erosion.[4] With its high spatial isotropic resolution, HR-pQCT has a higher sensitivity in detecting erosion compared with radiography and magnetic resonance imaging.[5] Importantly, quantitative

ClinicalTrials.gov identifier: NCT03623867.
Supported by Novartis Pharmaceuticals (HK) Ltd.
[1]Yingzhao Jin, PhD, Isaac T. Cheng, PhD, Ho So, MD, James Griffith, MD, Vivian Hung, MPhil, Cheuk-Chun Szeto, MD, Jack J. Lee, PhD, Ling Qin, PhD, Lai-Shan Tam, MD: The Chinese University of Hong Kong, Hong Kong; [2]Billy T. Lai, FRCP: Tseung Kwan O Hospital, Hong Kong; [3]Shirley K. Ying, FRCP: Princess Margaret Hospital, Hong Kong; [4]Kitty Y. Kwok, FRCP: Queen Elizabeth Hospital, Hong Kong.
Drs Jin and Cheng contributed equally to this work.

Additional supplementary information cited in this article can be found online in the Supporting Information section (https://acrjournals.onlinelibrary.wiley.com/doi/10.1002/art.43154).

Author disclosures and graphical abstract are available at https://onlinelibrary.wiley.com/doi/10.1002/art.43154.

Address correspondence via email to Lai-Shan Tam, MD, at lstam@cuhk.edu.hk.

Submitted for publication May 1, 2024; accepted in revised form February 25, 2025.

measurement of erosion and enthesiophyte volume can also be achieved.[6–8] Whether erosion repair occurs after tumor necrosis factor (TNF) inhibition as reflected by reduction in erosion size on HR-pQCT has been a subject of controversy in patients with PsA. However, it has been observed that enthesiophyte progression continues despite TNF inhibition.[9,10]

Interleukin 17 (IL-17) is a proinflammatory cytokine produced by the type Th17 cells. It is the key cytokine in the pathogenesis of PsA[11] responsible for the development of bone erosion.[12] Levels of IL-17^{+}CD8^{+} T cells show a correlation with measures of disease activity and the extent of radiographic erosion in patients with PsA.[12] IL-17 participates in the pathway that amplifies entheseal inflammation and is strongly associated with new bone formation by promoting both catabolic and anabolic changes in bone.[13] In an IL-23 overexpressed animal model, inhibition of IL-17 led to significant reduction of new bone formation.[14] Similarly, in a spondyloarthritis rat model, preventive and therapeutic inhibition of IL-17A reduced inflammation and new bone formation.[15] Secukinumab, an anti–interleukin-17A monoclonal antibody, is efficacious in reducing disease activity and the rate of radiographic joint damage compared with a placebo.[16] One prospective open-label study demonstrated that 24 weeks of secukinumab treatment may prevent the progression of bone erosions and enthesiophytes evaluated by HR-pQCT.[17] Nonetheless, these results need to be confirmed by longer term, placebo-controlled, randomized trials.

Therefore, the aim of this study was to evaluate the effects of secukinumab compared to placebo on the progression of bone erosion and enthesiophyte in patients with PsA using HR-pQCT over a one-year period.

PATIENTS AND METHODS

Study design and study participants. This was an investigator-initiated, one-year, randomized, placebo-controlled, double-blind study. Forty patients with PsA who fulfilled the Classification Criteria for Psoriatic Arthritis were recruited from four regional hospitals in Hong Kong (Prince of Wales Hospital, Tai Po Hospital, Queen Elizabeth Hospital, and Tseung Kwan O Hospital) during May 2020 to August 2021. The inclusion criteria were (1) age ≥18 years old; (2) without destruction in the metacarpophalangeal joints (MCPJs), with joint destruction being defined as the presence of bone erosions or osteophytes that disrupt the normal joint structure[18]; (3) with active disease, which was defined as ≥3 tender joints and ≥3 swollen joints, despite previous treatment with nonsteroidal anti-inflammatory drugs (NSAIDs) or conventional synthetic disease-modifying antirheumatic drugs (csDMARDs); and (4) presence of at least one erosion at MCPJs 2 to 4 on HR-pQCT. Exclusion criteria were (1) limited in ability to perform usual self-care, vocational, and avocational activities; (2) pregnancy; (3) previous therapy with biologic or targeted synthetic DMARDs (b/tsDMARDs); (4) the presence of active inflammatory disease other than PsA; (5) active infection in two weeks before randomization or a history of ongoing, chronic, or recurrent infections including tuberculosis; (6) history of hepatitis B or C; (7) history of malignant disease within the past five years (excluding basal cell carcinoma or actinic keratosis, in situ cervical cancer, or noninvasive malignant colon polyps); and (8) contraindications to secukinumab.

The study was approved by the Ethics Committee of the Chinese University of Hong Kong. Written informed consents were obtained from all participants according to the Declaration of Helsinki and International Council for Harmonisation and good clinical practice guidelines. The study was registered in clinicaltrial.gov (identifier: NCT03623867).

Randomization and treatment. Randomization was performed using a computer-generated randomization list, using a permuted blocks design with block sizes of 4 and 6. Allocation concealment was ensured using sequentially numbered, opaque, sealed envelopes. Patients were randomly assigned in a 1:1 ratio to secukinumab (n = 20) or placebo (n = 20) group. To maintain masking, secukinumab and placebo were identical in appearance, packaging, and administration method. Both the participants and the physicians were unaware of which treatment each participant was receiving. They received subcutaneous placebo (saline) or secukinumab (Novartis Pharmaceuticals [HK] Ltd) at 150 mg once a week from baseline for four weeks, and then once every four weeks until week 48. Patients attended follow-up visits at weeks 2, 4, and 12 and then every 12 weeks until week 48 and also attended a safety visit at week 52. Patients were treated throughout the study period following a standard protocol with the goal of achieving minimal disease activity (MDA) (Supplementary Figure 1).

Changes in the baseline treatment, including dosage of NSAIDs or csDMARDs or the addition of a new csDMARD (individually or in combination), steroids, or NSAIDs, were allowed after week 12 if the patient could not achieve MDA. For patients who (1) did not achieve MDA after week 12 and (2) fulfilled the criteria for and expressed willingness to initiate b/tsDMARDs, the codes were broken, and they were excluded from the final analysis. When three csDMARDs failed to achieve the treatment goal, patients became eligible for b/tsDMARDs in accordance with the local guideline, provided they passed the financial assessment (phase 3b in Supplementary Figure 1). However, because b/tsDMARDs were not reimbursed in Hong Kong, some patients were unable to start b/tsDMARDs despite not meeting the treatment goal due to financial constraints. Therefore, the codes were not broken for patients who were not willing to initiate b/tsDMARDs, and they were included in the final analysis. Because the objective of this study was to compare the actual effects of bone damage prevention between secukinumab and

placebo, only patients who initiated a biologic in the placebo group were excluded. All adverse effects were recorded.

Assessment. *Evaluation of disease activity and severity.* At baseline and at each visit, the following domains were assessed: pain, physician global assessment of disease severity (PhGA) and patient global assessment of disease severity (PtGA), number of tender and swollen joints (using the 68 tender and 66 swollen joint count), number of joints irreversibly damaged (baseline and end of study only), enthesitis (Spondyloarthritis Research Consortium of Canada Enthesitis Index), number of digits with dactylitis, levels of acute-phase reactant including erythrocyte sedimentation rate (ESR) and C-reactive protein (CRP), and the Health Assessment Questionnaire (HAQ) Disability Index. For the skin domain, Psoriasis Area and Severity Index (PASI) was assessed at baseline and each visit.

Image acquisition by HR-pQCT. Metacarpal bone erosion and enthesiophyte were assessed at MCPJs 2 to 4 of the more severely affected or the dominant hand if both hands were equally affected using a HR-pQCT system (XtremeCT II; Scanco Medical AG). This system enables the simultaneous acquisition of CT slices with an isotropic resolution (voxel size) of 61 μm. HR-pQCT scanning was performed by a single investigator (V.H.) who was masked to all the clinical information of the patients. A single examination was performed for measurements of MCPJs 2 to 4. An anteroposterior scout view was used to define the region of interest (ROI). The scan region was 80 slices distal and 242 slices proximal of the upper margin of the head[19] of MCPJ 3. HR-pQCT examinations were performed at baseline, 24 weeks, and 48 weeks. The ROI of each MCPJ was cropped using an automatic cropping algorithm.[20] Images were evaluated by two independent readers (I.T.C and Y.J.) with five and two years of experience, respectively, in evaluating erosions and enthesiophytes and measuring the volume of these pathologies, masked to the clinical data. The intraobserver reproducibility was 0.962 and 0.986 for erosion and enthesiophyte volume, respectively.

Erosion assessment. Erosions were defined as sharply marginated bone lesions with juxta-articular localization with a cortical break seen in at least two adjacent slices, which were often accompanied by loss of the adjacent trabecular bone. Erosions were differentiated from physiologic breaks due to nutrient blood vessels by the linear shape of the latter and occurrence at predilection sites. Pseudoerosions, structures similar to cortical breaks presented by osteophytes, were excluded.[21] Erosion volume was automatically calculated by the Bone Analysis Modules of an open-source image analysis tool (3D slicer).[22]

Enthesiophytes assessment, volumetric bone mineral density, and microstructural analysis. Enthesiophytes were defined as new bone formation arising from the periosteal bone cortex at the insertion sites of the capsule, ligament, or tendons or at the location of functional enthesis.[2] A semiautomated method based on ITK-SNAP was used to calculate enthesiophyte volume on colocalized baseline and follow-up ROIs, as described before.[10,23] The Supplementary Video 1 demonstrates that slides were aligned through image registration, confirming that the observed enthesiophyte progression is not due to any shift in the image stack. In addition, a 3D reconstructed video was also provided (Supplementary Video 2). Intraarticular (second MCP head; cortical, trabecular, and total) volumetric bone mineral density (vBMD) was obtained based on manufacturer's standard analysis software[24] after exclusion of the region with bone erosion and enthesiophyte, as previously described.[6,25]

Smallest detectable changes and definition of healing of erosion and progression of enthesiophytes. Twenty entheisophytes and 20 erosions were randomly chosen and scored twice to determine the smallest detectable change (SDC), which refers to the minimum difference in a measurement that can be differentiated from measurement error or inherent variability.[26] SDC was then calculated for enthesiophyte and erosion volume using the formula $SDC = \pm 1.96 \times SD\Delta_{(CHANGE\text{-}SCORES)} / (\sqrt{2} \times \sqrt{k})$, in which "$\Delta_{(CHANGE\text{-}SCORES)}$" was the SD of change in scores and "k" was the number of readings.[26] Partial erosion healing was defined as decrease in erosion volume exceeding SDC (0.1 mm^3). Enthesiophyte progression was defined as either an increase in enthesiophyte volume exceeding SDC (0.12 mm^3) or development of a new enthesiophyte.

Study outcomes. The primary outcome of the study was the difference in change of erosion volume over MCPJs 2 to 4 between the secukinumab and placebo group, as measured by HR-pQCT from baseline to 24 and 48 weeks. Secondary outcomes include the proportion of erosions showing partial healing, changes in the volume of enthesiophytes, the proportion of enthesiophytes exhibiting progression, and changes in vBMD and microstructural parameters.

Data processing and analysis. Statistical analyses were conducted using the Statistics Package for Social Sciences (version 25.0). Per-protocol analysis was employed to ascertain the actual effect of IL-17 inhibition on preventing bone damage compared to placebo. Descriptive statistics were used to analyze demographic and clinical variables, including frequencies, means and SDs, and medians and interquartile ranges (IQRs). The *t*-test, Mann-Whitney U-test, and chi-square test were used to evaluate differences in baseline characteristics between the secukinumab group and placebo group. Differences in the outcome measurements between groups were assessed using the *t*-test, Mann-Whitney U-test, repeated measures analysis of variance, Friedman test, or chi-square test, when appropriate. When analyzing proportions (eg, proportion of patients with erosion healing

or enthesiophyte progression) across multiple time points in two treatment arms, the generalized estimating equation (GEE) provides several key advantages. First, it can handle binary (proportion) outcomes. Second, GEE accounts for within-subject correlation, which violates the independence assumption in standard regression. GEE incorporates this correlation, improving the validity of SEs and *P* values. Third, it provides population-averaged (or "marginal") estimates, which are often more clinically interpretable when comparing typical responses between treatment groups over time. Fourth, the "sandwich" variance estimator used in GEE remains reliable (ie, SEs remain valid) even if the assumed within-subject correlation structure is not perfectly specified. In this study, GEE regression analysis was employed to investigate the factors associated with erosion healing or enthesiophyte progression. A two-tailed probability value of $P < 0.05$ was considered statistically significant.

RESULTS

Forty patients (mean ± SD age 51.9 ± 13.4 years, 20 of 40 [50%] female, mean ± SD disease duration 4.7 ± 6.7 years) were recruited (Table 1). Patients in both groups had moderate to high disease activity (mean ± SD Disease Activity in Psoriatic Arthritis [DAPSA] score 28.3 ± 8.8 vs 31.5 ± 6.8 in the placebo group and secukinumab group, respectively). There were no significant differences in baseline age, sex, body mass index, disease duration, disease activity markers (ESR, CRP, PASI, and DAPSA), and HAQ between the two groups (Table 1).

Table 1. Patient characteristics at baseline*

Characteristic	Placebo (n = 20)	Secukinumab (n = 20)
Age, median (IQR), y	55.0 (35.9–60.8)	56.3 (42.9–64.9)
Female, n (%)	11 (55.0)	9 (45.0)
BMI, mean ± SD	24.8 ± 3.0	24.1 ± 3.6
PsO duration, median (IQR), y	10.6 (3.0–23.3)	12.6 (7.4–20.1)
PsA duration, median (IQR), y	0.5 (0.2–9.4)	1.0 (0.2–6.4)
ESR, median (IQR), mm/hr	29.0 (18.0–51.3)	49.5 (22.3–74.3)
CRP, median (IQR), mg/L	5.0 (1.9–13.0)	15.5 (3.7–22.4)
PASI, median (IQR)	4.1 (1.7–7.3)	4.3 (1.4–7.3)
HAQ, median (IQR)	0.5 (0.2–1.1)	1.1 (0.4–1.4)
Tender joint count, median (IQR)	10.0 (7.3–15.3)	10.0 (8.0–14.8)
Swollen joint count, median (IQR)	4.5 (3.3–6.8)	4.0 (3.0–6.0)
Damage joint count, median (IQR)	2.0 (1.3–6.0)	2.5 (1.0–6.0)
Presence of dactylitis, n (%)	11 (55.0)	9 (45.0)
Number of dactylitis, median (IQR), digit	1.0 (0.0–2.0)	0.0 (0.0–1.0)
Presence of enthesitis, n (%)	9 (45.0)	8 (40.0)
Enthesitis, median (IQR)	0.0 (0.0–1.8)	0.0 (0.0–1.8)
NRS pain, mean ± SD, 0–10cm	5.3 ± 1.8	6.5 ± 1.9
NRS PtGA, median (IQR), 0–10 cm	5.0 (5.0–7.8)	7.0 (6.0–8.0)
NRS PhGA, median (IQR), 0–10 cm	6.5 (5.3–8.0)	6.0 (5.0–7.8)
DAPSA, mean ± SD	28.3 ± 8.8	31.5 ± 6.8
MDA achievement, n (%)	0 (0.0)	0 (0.0)
csDMARDs, n (%)	12 (60.0)	12 (60.0)
Methotrexate	10 (50.0)	12 (60.0)
Sulfasalazine	1 (5.0)	1 (5.0)
Cyclosporine	2 (10.0)	0 (0.0)
Glucocorticoids	0 (0.0)	1 (5.0)
NSAIDs, n (%)	15 (75.0)	15 (75.0)

* BMI, body mass index; CRP, C-reactive protein; csDMARDs, conventional synthetic disease-modifying antirheumatic drugs; DAPSA, Disease Activity in Psoriatic Arthritis; ESR, erythrocyte sedimentation rate; HAQ, Health Assessment Questionnaire score; IQR, interquartile range; MDA, minimal disease activity; NRS, Numeric Pain Rating Scale; NSAIDs, nonsteroidal anti-inflammatory drugs; PASI, Psoriasis Area and Severity Index; PhGA, Physician Global Assessment; PsA, psoriatic arthritis; PsO, psoriasis; PtGA, Patient Global Assessment.

Clinical response. After one year, 18 of 20 patients (90%) versus 16 of 20 patients (80%) completed study treatment in the secukinumab group and placebo group, respectively. In the placebo group, four patients (20%) were excluded from the final analysis because they required escape therapy with b/tsDMARDs before study completion due to treatment inefficacy (Figure 1). Over the one-year period, patients in the secukinumab group had a greater reduction in ESR, CRP, PASI, HAQ, pain, PtGA, PhGA, and DAPSA scores compared to the placebo group (Supplementary Table 1). For the per-protocol analysis, 7.8% and 18.6% of the MCPJs were swollen and tender at baseline, respectively. At year 1, 7.8% of the MCPJs remained swollen, whereas 17.6% were tender. There was no significant difference between the two groups regarding the csDMARD and NSAID treatments (Supplementary Figure 2). Only one patient in the secukinumab group received oral glucocorticoids at baseline, and none received them at year 1. In the placebo group, no patients were taking oral glucocorticoids at either baseline or year 1. In the secukinumab group, a rapid reduction in DAPSA to below 14 (indicating low disease activity [LDA]) was observed from week 12 onward (Supplementary Figure 3A). Conversely, the reduction in DAPSA was more gradual in the placebo group, with achievement of LDA from week 36 onward. Regarding the MDA attainment rate, the secukinumab group achieved 27.8% at week 12 and 55.6% at week 48, whereas the placebo group achieved 18.8% at week 12 and 31.3% at week 48 (Supplementary Figure 3B).

Changes in HR-pQCT parameters. A total of 36 and 34 patients were analyzed at week 24 and week 48, respectively. At baseline, 61 and 44 erosions were identified in the secukinumab and placebo groups, respectively. There were no statistically significant differences in baseline erosion volume (placebo group, median 1.2 [IQR 0.3–3.2] mm^3 vs secukinumab group, median 0.9 [IQR 0.3–3.3] mm^3; $P = 0.785$) and baseline enthesiophyte volume (placebo group, median 4.2 [IQR 1.2–9.2] mm^3 vs secukinumab group, median 2.1 [IQR 1.2–5.7] mm^3; $P = 0.154$)

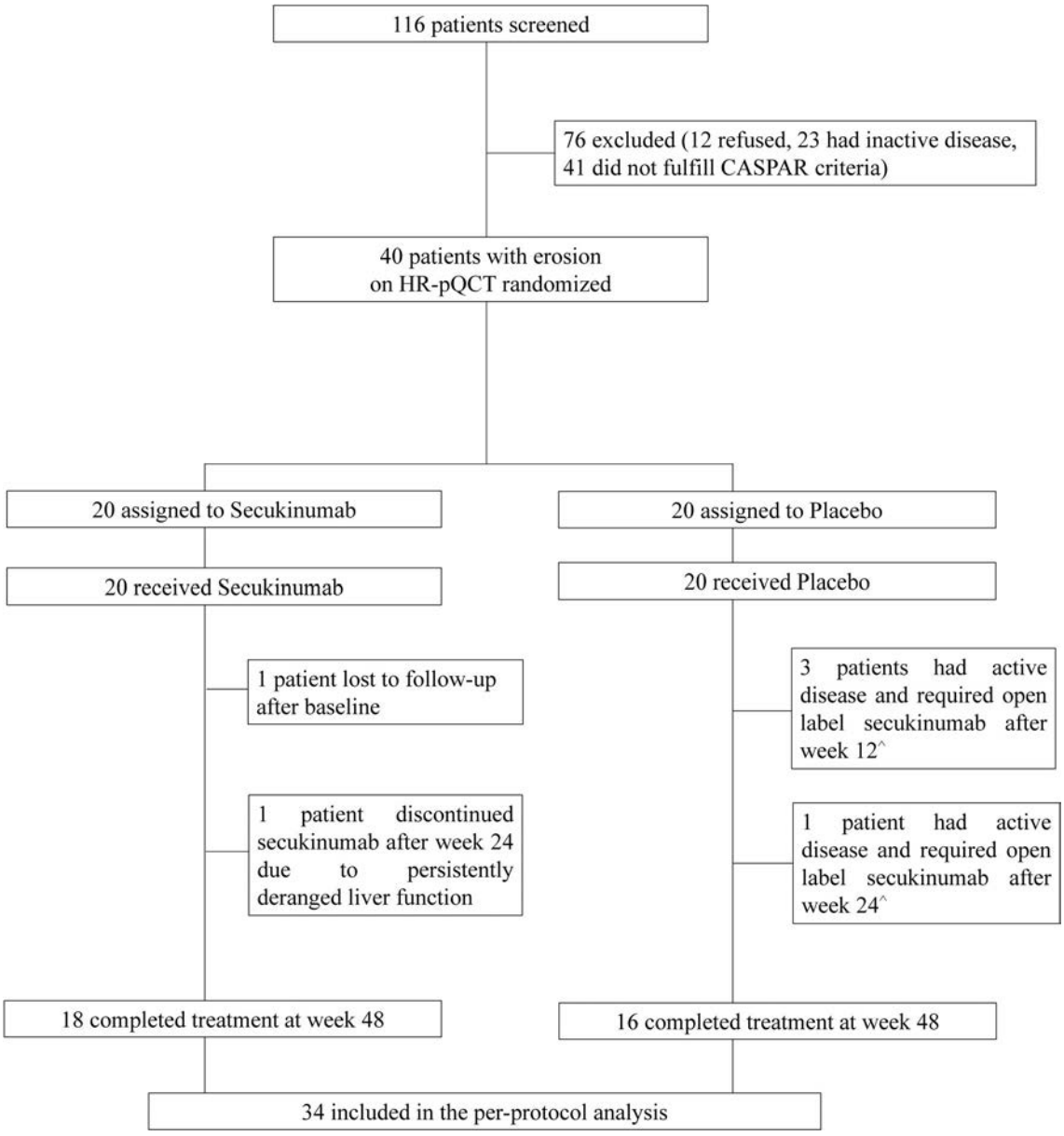

Figure 1. Participant flow diagram. ^Changes in baseline treatment, such as adjusting the dosage of conventional synthetic disease-modifying antirheumatic drugs (csDMARDs) or adding a new csDMARD or nonsteroidal anti-inflammatory drug, were permitted after week 12 if the patient failed to achieve minimal disease activity. Patients requiring open-label secukinumab were excluded from the per-protocol analysis. HR-pQCT assessment of metacarpophalangeal joints 2 to 4 was performed at weeks 24 and 48. CASPAR, Classification Criteria for Psoriatic Arthritis; HR-pQCT, high-resolution peripheral quantitative computed tomography.

between the two groups (Supplementary Table 2). Figure 2 illustrates typical changes in erosion and enthesiophyte over a one-year period. After one year, a significant difference in the change in the volume of pre-existing erosion between the two groups (secukinumab group, median change –0.1 [IQR –0.5 to 0.0] mm^3 vs placebo group, median change 0.0 [IQR –0.2 to 0.4] mm^3, $P = 0.004$) was found (Supplementary Table 2). The erosion volume at baseline (median 0.9 [IQR 0.3–3.3]), week 24 (median 0.9 [IQR 0.3–3.1]), and week 48 (median 0.9 [IQR 0.2–2.5]) revealed significant reduction in the secukinumab group, whereas no differences were observed in the placebo group (baseline, median 1.2 [IQR 0.3–3.2]; week 24, median 1.1 [IQR 0.3–4.3]; week 48, median 1.3 [IQR 0.3–3.7]) (Figure 3A). One new erosion developed in one patient in the secukinumab group, whereas six erosions developed in five patients in the placebo group ($P = 0.078$) (Figure 3B). A significantly higher proportion of erosions with partial healing was observed in the secukinumab group compared with the placebo group (51% vs 30%, $P = 0.029$) (Figure 3C). In this study, at baseline, the mean erosion volume at MCPJ 3 was positively correlated with the number of tender MCPJs (r =

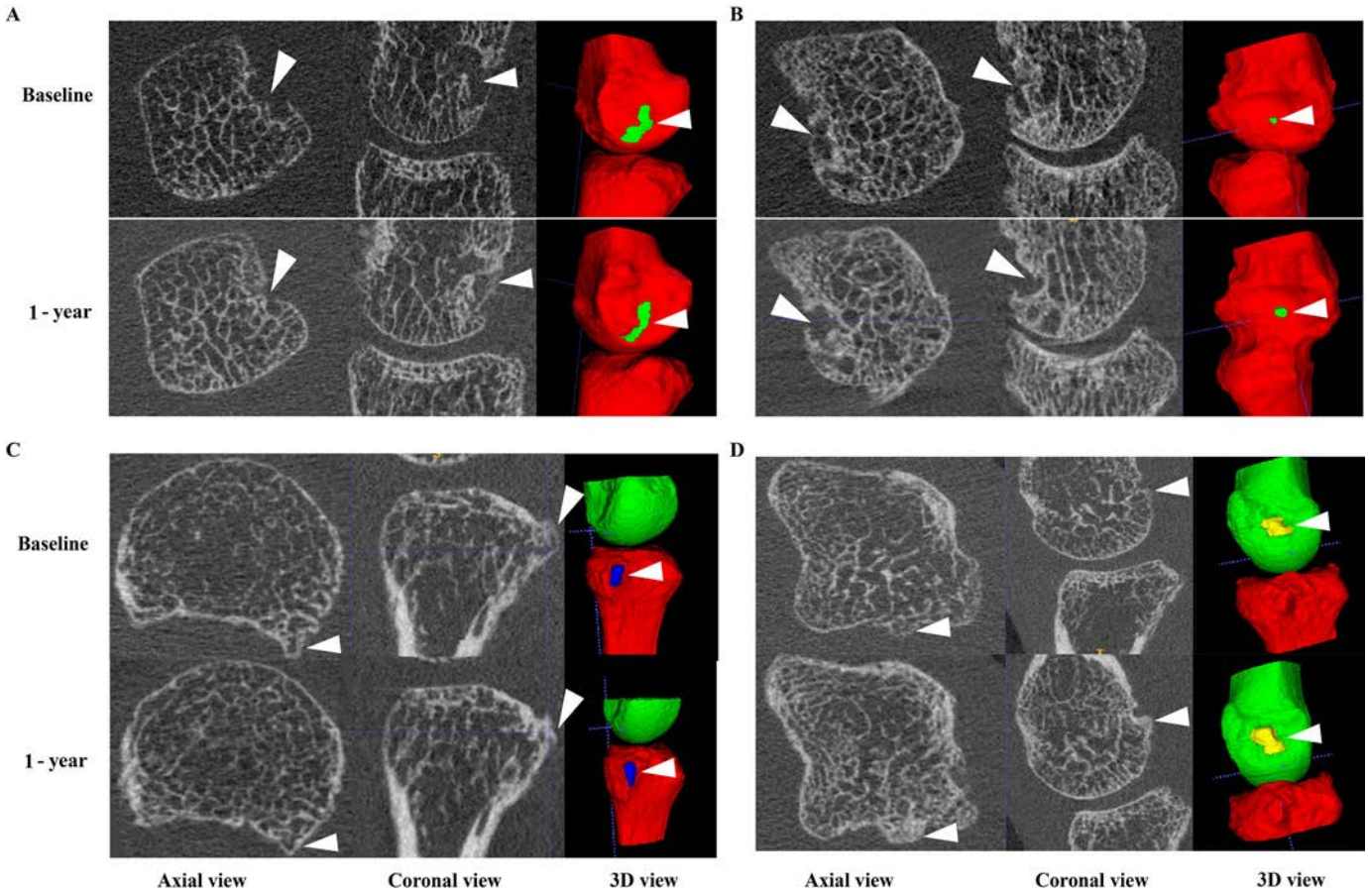

Figure 2. Representative images depicting changes in erosion and enthesiophyte size over a period of one year. (A) In the secukinumab group, there was partial healing of erosion as depicted in green. (B) Erosion progressed in the placebo group as depicted in green. (C) Enthesiophyte size regressed in the secukinumab group as depicted in blue. (D) Enthesiophyte progressed in the placebo group as depicted in yellow. Arrows indicate the presence of erosion in parts A and B and enthesiophyte in parts C and D.

0.435, P = 0.010). However, the number of tender or swollen joints did not correlate with the mean erosion volume of other MCPJs.

A total of 25 enthesiophytes were identified in both the secukinumab and placebo groups at baseline. At one year, the change in pre-existing enthesiophyte volume was not statistically significant between the two groups (secukinumab group, median change −0.1 [IQR −0.8 to 0.0] mm^3; placebo group, median change 0.0 [IQR −0.4 to 1.3] mm^3; P = 0.067), although a trend was seen (Supplementary Table 2). The enthesiophyte volume at baseline (median 2.1 [IQR 1.1–5.7] mm^3), week 24 (median 1.8 [IQR 0.8–5.6] mm^3), and week 48 (median 1.9 [IQR 0.8–4.1] mm^3) revealed significant differences in the secukinumab group and no differences in the placebo group (baseline, median 4.2 [IQR 1.2–9.2] mm^3; week 24, median 4.5 [IQR 1.1–10.4] mm^3; week 48, median 5.5 [IQR 1.5–10.1] mm^3) were observed (Figure 3D). At week 48, one enthesiophyte (in one patient) and four enthesiophytes (in three patients) were newly identified in the secukinumab group and placebo group, respectively (Figure 3E). Altogether, 16% and 40% of enthesiophytes progressed in the secukinumab group and placebo group, respectively (Figure 3F). Tenderness or swelling in the MCPJs showed no correlation with the mean enthesiophyte volume.

Regarding intraarticular vBMD and microstructural analysis, the results showed stabilization of vBMD and microstructure in both groups. A significant difference in the change in trabecular number (increase in trabecular number in the secukinumab group, median 0.006 [IQR −0.011 to 0.067] and decrease in trabecular number in the placebo group, median −0.015 [IQR −0.034 to −0.002]; P = 0.032) was noted (Supplementary Table 3).

Cumulative probability plot for changes in the erosion and enthesiophyte volume over a one-year period is shown in Figure 4. Univariate GEE showed that no clinical parameters were associated with partial erosion healing and enthesiophyte progression (Supplementary Tables 4 and 5). The results showed that the odds ratio (OR) for enthesiophyte progression in the secukinumab group was 0.264 (95% confidence interval [CI] 0.080–0.878, P = 0.030), whereas the OR for partial erosion healing in the secukinumab group was 2.882 (95% CI 1.130–7.349, P = 0.027) (Table 2).

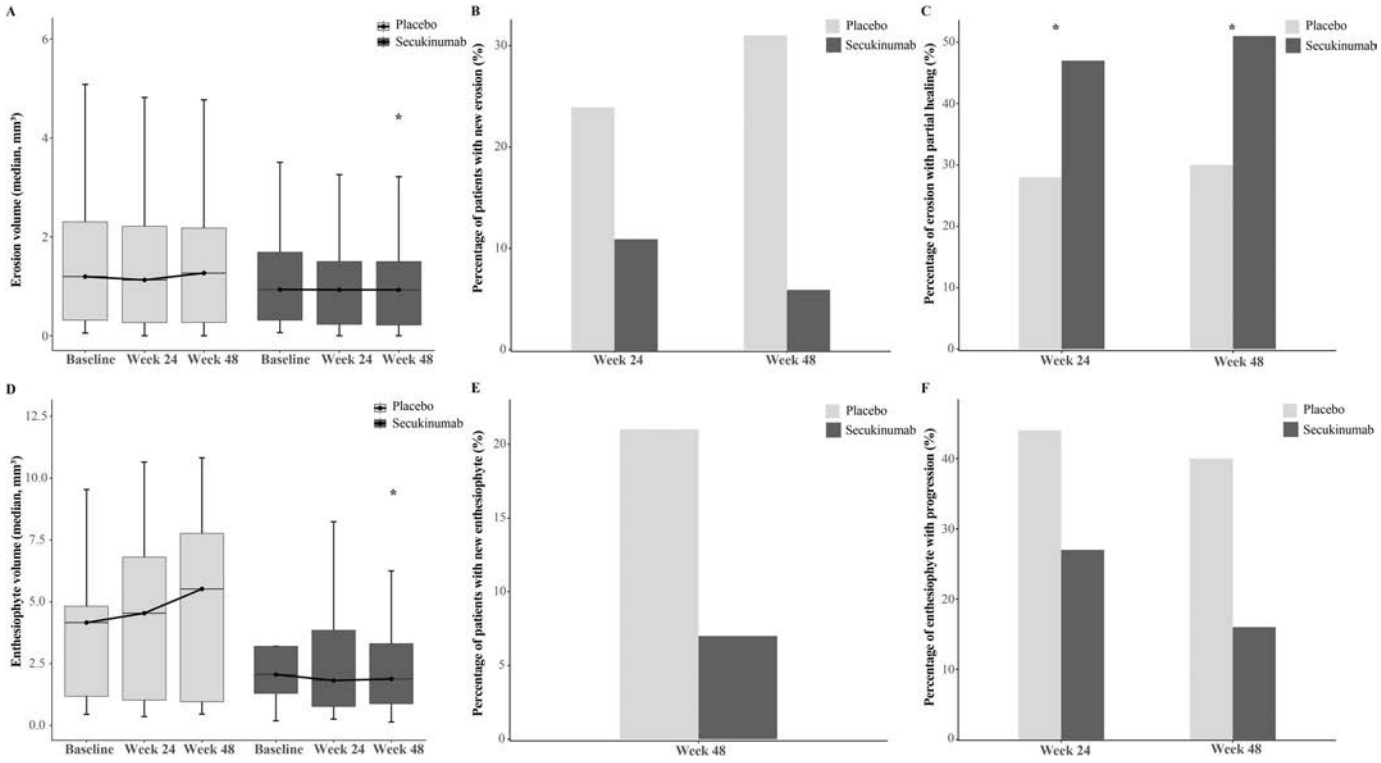

Figure 3. Erosion and enthesiophyte parameters and their changes over time by HR-pQCT. (A) Pre-existing erosion volume at baseline, week 24, and week 48; (B) percentage of patients with new erosion identified at week 24 and week 48; (C) percentage of pre-existing erosion with partial healing at week 24 and week 48; (D) pre-existing enthesiophyte volume at baseline, week 24, and week 48; (E) percentage of patients with new enthesiophyte identified at week 48; (F) percentage of pre-existing enthesiophyte with progression at week 24 and week 48. The Friedman test was used to assess within-group changes across a period of one year (A and D), and the chi-square test was employed to analyze differences between groups (C). *$P < 0.05$. HR-pQCT, high-resolution peripheral quantitative computed tomography.

Adverse and severe adverse events. There was a total of 25 adverse events (AEs) documented in the secukinumab group and 15 AEs documented in the placebo group (Supplementary Table 6). No severe AEs were reported.

DISCUSSION

This is the first randomized clinical trial to investigate the effects of secukinumab for preventing bone damage in PsA using HR-pQCT. Previous study demonstrated that secukinumab effectively reduced radiographic progression, as measured by the change from baseline on the modified Total Sharp Score (mTSS), compared to placebo over a period of 24 weeks.[27] Furthermore, 84.3% of patients in the secukinumab–150 mg group showed no radiographic disease progression at two years.[28] However, mTSS evaluates only erosions and joint space narrowing but not new bone formation, a hallmark of structural damage in PsA. Only one prospective open-label study demonstrated that no significant change in bone erosion volume and enthesiophyte height by HR-pQCT after 24 weeks of secukinumab treatment.[17] HR-pQCT allows for precise analysis of bone microstructure with high reproducibility, enabling the definition and quantification of structural bone alterations (erosion and enthesiophyte) in patients with inflammatory arthritis.[29,30] The main finding of this study was that it confirmed significant differences between the secukinumab and placebo groups in terms of reduction in erosion volume, as measured by HR-pQCT, after one year. More importantly, secukinumab was more effective in achieving partial erosion healing (OR 2.9) and preventing enthesiophyte progression (OR 0.26) compared with placebo in this treat-to-target study, highlighting the possibility of pathway-specific bone remodeling in PsA. The change in trabecular number provides an important piece of information suggesting that anti–IL-17 therapy may abrogate inflammation-induced trabecular bone loss in the intra-articular metacarpal bone in patients with PsA, as we have previously reported.[6]

There were no statistically significant differences in clinical response—including the proportion of patients achieving MDA and changes in tender and swollen joint counts, enthesitis, and dactylitis—between the secukinumab and placebo groups at week 48 in our study. This finding confirms adherence to the study's protocol, which aimed for both groups to achieve MDA. If patients did not reach the treatment target, they were permitted to receive single or combination csDMARDs; indeed, a numerically higher proportion of patients in the placebo group ultimately received csDMARDs (Supplementary Figure 2). Regarding clinical

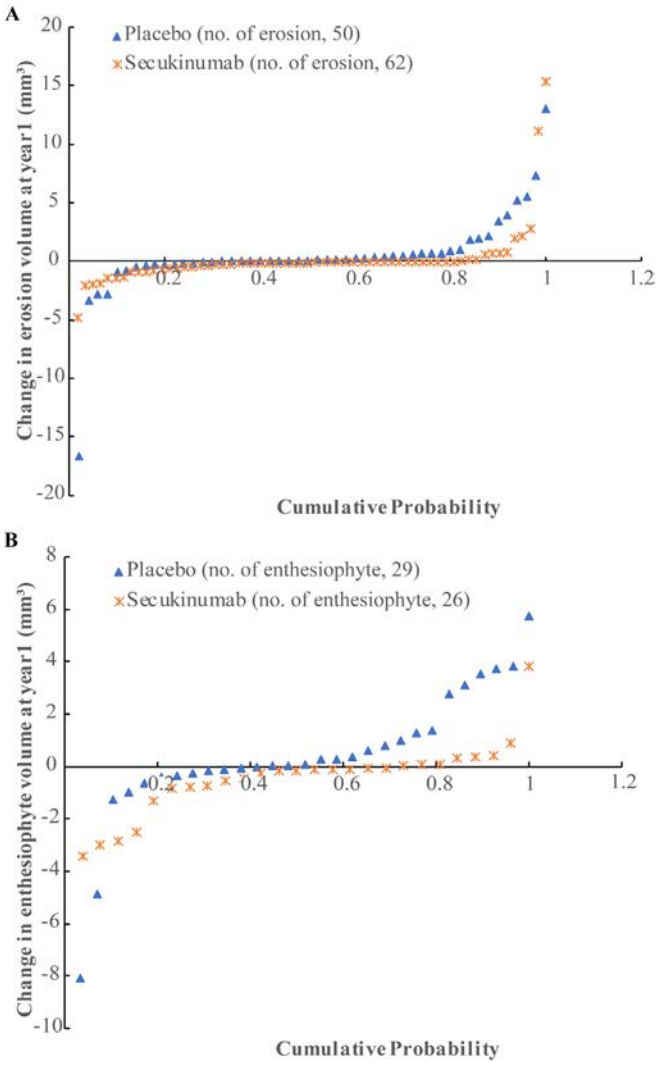

Figure 4. Cumulative probability plot of change in erosion and enthesiophyte volume by high-resolution peripheral quantitative computed tomography (HR-pQCT). (A) Cumulative probability plot of change in erosion volume by HR-pQCT; (B) cumulative probability plot of change in enthesiophyte volume by HR-pQCT. Each dot represents one erosion. The x-axis indicates the proportion of patients; the y-axis indicates the change of erosion or enthesiophyte volume for individual lesion from baseline to week 48.

responses, the MDA rate of 27.8% at week 12 in our secukinumab group was comparable to the 32% at week 16 reported in a previous study.[31] By week 48, the MDA rate in our secukinumab group increased to 55.6%, surpassing the 39% reported in the same study, likely due to the treat-to-target approach. Similarly, the MDA response in the placebo group was 18.8% at week 12, higher than the 12% reported in the same study. By week 48, the MDA response rate in the placebo group had increased to 31.3%. This rate was slightly lower than that reported in a previous treat-to-target study (40.7%), in which those patients also received csDMARD monotherapy or combination therapy. This could probably be because the latter tight

Table 2. Effects of secukinumab on partial erosion healing and enthesiophyte progression compared with placebo using generalized estimating equations*

Outcomes	OR (95% CI)	*P* value
Partial erosion healing	2.882 (1.130–7.349)	**0.027**
Enthesiophyte progression	0.264 (0.080–0.878)	**0.030**

* Bold values indicate statistically significant differences ($P < 0.05$).
CI, confidence interval; OR, odds ratio.

control group was reviewed every 4 weeks compared to every 12 weeks in our study.[32] Nevertheless, there were no statistically significant differences in MDA rate between secukinumab group and placebo group at week 48 in our study. It might be attributed to the fact that patients in the placebo group were also taking other csDMARD active treatment through a treat-to-target approach. However, despite the similar clinical response, a differential effect on bone damage was observed. This suggests that bone damage may be driven by pathway-specific mechanisms rather than solely by controlling inflammation.

Preclinical data implicate the IL-17 pathway in the irreversible structural damage observed in PsA.[33] Our data provide further evidence that IL-17A may be a mediator of this process. The differentiation of IL-17-producing cells, known as type 17 cells, is governed by the master transcription factor retinoic acid receptor-related orphan receptor gamma-t (RORγt).[34] Inhibiting RORγt influences various downstream mediators, including IL-17A, IL-17F, and IL-22. Following treatment with the RORγt antagonist PF-06747711, improvements were observed in bone density and cortical and trabecular thickness, and the presence of surface erosions as analyzed by μCT in a rat model of PsA-like disease.[33] Targeting cytokines such as IL-23, IL-17, and TNF can effectively slow down erosive damage progression in PsA by interrupting osteoclast formation mediated by synovitis-induced macrophage colony-stimulating factor and RANKL.[1] The current study represents the first confirmation of the role of secukinumab in enhancing partial erosion healing in patients with PsA. Although only one new erosion developed in the secukinumab group (in one patient), six new erosions occurred in five patients in the placebo group ($P = 0.078$; Figure 3B), suggesting a potential role of secukinumab in preventing new bone damage.

PsA is distinguished by the formation of structural osteoproliferative lesions at entheseal sites in reaction to mechanical stresses, such as enthesiophytes or structural entheseal lesions.[35] It is presumed that the initial structural changes in PsA manifest as entheseal lesions, which are localized areas of new bone formation occurring near the joints.[36] Exposure to IL-17 up-regulates the expression of the RANK on osteoclast lineage cells, which enhances the potential of RANKL to induce osteoclastogenic potential in these cells.[13] On the other hand, IL-17A accelerates bone formation by stimulating the proliferation and differentiation of osteoblasts from mesenchymal progenitor cells after injury.[14]

Blocking IL-17A could be pivotal in halting new bone formation in PsA by inhibiting the inflammatory cascade that stimulates mesenchymal cell differentiation into osteoblasts at entheseal sites.[1] In this study, we demonstrated the feasibility of antiproliferative effect of IL-17A inhibition in patients with PsA through HR-pQCT. Preventing structural joint damage is a primary objective of treatment.[37] Therefore, secukinumab can reduce bone erosion and prevent the progression of new bone formation, emphasizing its advantageous impact in managing bone diseases in patients with PsA. On the other hand, TNF inhibition and csDMARD patient groups had similar changes in the size of erosions and enthesiophytes, with a comparable proportion of progression observed in both groups.[10]

Although joint swelling on physical examination is an important clinical indicator of inflammation, there appears to be only a modest association between joint swelling and the presence of erosions or enthesiophytes on HR-pQCT at baseline. Specifically, although physical examination detected swelling in eight MCPJs, six of these (75%) showed erosions or enthesiophytes. However, among all MCPJs that showed erosions or enthesiophytes, fewer than 15% were swollen. Nonetheless, we believe that a single time point assessment may not fully capture the historical inflammatory burden of a joint. Persistent, subclinical, low-grade chronic inflammation can cause localized structural damage even in the absence of visible swelling at the time of examination. Previous inflammatory events may have driven erosive or proliferative changes that persist after clinical swelling has subsided, as evidence by a multimodality imaging study that had demonstrated stable erosive or proliferative changes in MCPJs among patients with PsA after synovitis had resolved.[17] Although HR-pQCT may not be as sensitive as ultrasound for detecting peripheral joint inflammation, it is highly sensitive for visualizing and quantifying structural and microstructural bone damage.[38] Moreover, enthesiophytes detected on HR-pQCT have been associated with functional loss, underscoring their clinical relevance.[3] Future studies should seek to address this important question by performing ultrasound-guided synovial biopsies to document subclinical inflammation.

The strength of our study lies in its ability to build on previous research. To date, only one prospective open-label study has demonstrated that bone erosion number and volume remained stable after 24 weeks, with no progression in enthesiophyte semi-quantitative grading based on enthesiophyte height. Our study extends this observation period to one year, allowing for a more comprehensive assessment of the long-term effects of secukinumab compared to a treat-to-target group using csDMARDs. Moreover, we enhance the analysis by assessing enthesiophyte progression through volume measurements. This extended duration and detailed quantification provide further insight into the protective effects observed in our study regarding both erosion and enthesiophyte progression. In addition, we provide detailed intra-articular vBMD and microstructural analysis, demonstrating potential beneficial effects of secukinumab by stabilizing vBMD and increasing trabecular number. These findings underscore the critical role of IL-17 in bone remodeling in PsA.

This study has several limitations. First, the small size of patients with PsA and short study duration restrict the interpretation of the effects. Second, the relatively uniform study population might limit the generalizability to diverse global populations. The results still require external validation. In our previous study, tenderness or swelling in the joints showed no correlation with any of the joint space parameters assessed by HR-pQCT.[39] In future studies, the correlation between imaging findings (erosion or enthesiophyte volume) and clinical features (joint tenderness or swelling), as well as imaging modalities (ultrasound or magnetic resonance imaging) and histologic activity (biopsy), should be further investigated. Moreover, the study was planned in 2017 and commenced early in 2018, predating the publication of the previous study on secukinumab in patients with PsA using HR-pQCT.[17] The absence of relevant data prompted our pilot study, with 20 patients per arm similar to the previous HR-pQCT studies in PsA.[9,17] In this study, 61 erosions were identified in the secukinumab group and 44 erosions were identified in the placebo group at baseline. The median change in individual erosion volume was –0.1 (IQR –0.5 to 0.0) for the secukinumab group and 0.0 (IQR –0.2 to 0.4) for the placebo group, resulting in an effect size of 0.52. The actual power achieved was 78% given a two-tail α level of 0.05 (calculated using G*Power version 3.1.9.6). Finally, we did not include imaging of the distal radius, and therefore data on biomechanical analysis were unavailable.

In conclusion, secukinumab may facilitate partial erosion repair and prevent enthesiophyte progression in patients with PsA. Further research with a larger sample size and longer follow-up period would be helpful to validate these findings.

ACKNOWLEDGMENTS

We are immensely grateful to patients, physicians, and the study personnel for their contribution to this study.

AUTHOR CONTRIBUTIONS

All authors contributed to at least one of the following manuscript preparation roles: conceptualization AND/OR methodology, software, investigation, formal analysis, data curation, visualization, and validation AND drafting or reviewing/editing the final draft. As corresponding author, Dr Tam confirms that all authors have provided the final approval of the version to be published and takes responsibility for the affirmations regarding article submission (eg, not under consideration by another journal), the integrity of the data presented, and the statements regarding compliance with institutional review board/Declaration of Helsinki requirements.

ROLE OF THE STUDY SPONSOR

Novartis Pharmaceuticals (HK) Ltd had no role in the study design or in the collection, analysis, or interpretation of the data, the writing of the manuscript, or the decision to submit the manuscript for publication.

Publication of this article was not contingent upon approval by Novartis Pharmaceuticals (HK) Ltd. Novartis Pharmaceuticals (HK) Ltd provided the study drugs and an unrestricted grant to support this study.

REFERENCES

1. Schett G, Rahman P, Ritchlin C, et al. Psoriatic arthritis from a mechanistic perspective. Nat Rev Rheumatol 2022;18(6):311–325.
2. Simon D, Faustini F, Kleyer A, et al. Analysis of periarticular bone changes in patients with cutaneous psoriasis without associated psoriatic arthritis. Ann Rheum Dis 2016;75(4):660–666.
3. Simon D, Kleyer A, Faustini F, et al. Simultaneous quantification of bone erosions and enthesiophytes in the joints of patients with psoriasis or psoriatic arthritis - effects of age and disease duration. Arthritis Res Ther 2018;20(1):203.
4. Fouque-Aubert A, Boutroy S, Marotte H, et al. Assessment of hand bone loss in rheumatoid arthritis by high-resolution peripheral quantitative CT. Ann Rheum Dis 2010;69(9):1671–1676.
5. Lee CH, Srikhum W, Burghardt AJ, et al. Correlation of structural abnormalities of the wrist and metacarpophalangeal joints evaluated by high-resolution peripheral quantitative computed tomography, 3 Tesla magnetic resonance imaging and conventional radiographs in rheumatoid arthritis. Int J Rheum Dis 2015;18(6):628–639.
6. Wu D, Griffith JF, Lam SHM, et al. Comparison of bone structure and microstructure in the metacarpal heads between patients with psoriatic arthritis and healthy controls: an HR-pQCT study. Osteoporos Int 2020;31(5):941–950.
7. Fedorov A, Beichel R, Kalpathy-Cramer J, et al. 3D Slicer as an image computing platform for the Quantitative Imaging Network. Magn Reson Imaging 2012;30(9):1323–1341.
8. Al-Khoury Y, Finzel S, Figueiredo C, et al. Erosion Identification in metacarpophalangeal joints in rheumatoid arthritis using high-resolution peripheral quantitative computed tomography. J Vis Exp 2023;(200):e65802.
9. Finzel S, Kraus S, Schmidt S, et al. Bone anabolic changes progress in psoriatic arthritis patients despite treatment with methotrexate or tumour necrosis factor inhibitors. Ann Rheum Dis 2013;72(7):1176–1181.
10. Wu D, Griffith JF, Lam SHM, et al. Progressive structural bone changes and their relationship with treatment in patients with psoriatic arthritis: a longitudinal HR-pQCT study. Arthritis Res Ther 2019;21(1):265.
11. Miossec P, Korn T, Kuchroo VK. Interleukin-17 and type 17 helper T cells. N Engl J Med 2009;361(9):888–898.
12. Menon B, Gullick NJ, Walter GJ, et al. Interleukin-17+CD8+ T cells are enriched in the joints of patients with psoriatic arthritis and correlate with disease activity and joint damage progression. Arthritis Rheumatol 2014;66(5):1272–1281.
13. Gravallese EM, Schett G. Effects of the IL-23-IL-17 pathway on bone in spondyloarthritis. Nat Rev Rheumatol 2018;14(11):631–640.
14. Sherlock JP, Joyce-Shaikh B, Turner SP, et al. IL-23 induces spondyloarthropathy by acting on ROR-gammat+ CD3+CD4-CD8- entheseal resident T cells. Nat Med 2012;18(7):1069–1076.
15. van Tok MN, van Duivenvoorde LM, Kramer I, et al. Interleukin-17A inhibition diminishes inflammation and new bone formation in experimental spondyloarthritis. Arthritis Rheumatol 2019;71(4):612–625.
16. Mease PJ, McInnes IB, Kirkham B, et al; FUTURE 1 Study Group. Secukinumab inhibition of interleukin-17A in patients with psoriatic arthritis. New Engl J Med 2015;373(14):1329–1339.
17. Kampylafka E, d'Oliveira I, Linz C, et al. Resolution of synovitis and arrest of catabolic and anabolic bone changes in patients with psoriatic arthritis by IL-17A blockade with secukinumab: results from the prospective PSARTROS study. Arthritis Res Ther 2018;20(1):153.
18. Stach CM, Bäuerle M, Englbrecht M, et al. Periarticular bone structure in rheumatoid arthritis patients and healthy individuals assessed by high-resolution computed tomography. Arthritis Rheum 2010;62(2):330–339.
19. Finzel S, Rech J, Schmidt S, et al. Interleukin-6 receptor blockade induces limited repair of bone erosions in rheumatoid arthritis: a micro CT study. Ann Rheum Dis 2013;72(3):396–400.
20. Zhang X, Cheng I, Liu S, et al. Automatic 3D joint erosion detection for the diagnosis and monitoring of rheumatoid arthritis using hand HR-pQCT images. Comput Med Imaging Graph 2023;106:102200.
21. Finzel S, Ohrndorf S, Englbrecht M, et al. A detailed comparative study of high-resolution ultrasound and micro-computed tomography for detection of arthritic bone erosions. Arthritis Rheum 2011;63(5):1231–1236.
22. Zhao M, Tse JJ, Kuczynski MT, et al. Open-source image analysis tool for the identification and quantification of cortical interruptions and bone erosions in high-resolution peripheral quantitative computed tomography images of patients with rheumatoid arthritis. Bone 2022;165:116571.
23. Yushkevich PA, Yang G, Gerig G. ITK-SNAP: an interactive tool for semi-automatic segmentation of multi-modality biomedical images. Annu Int Conf IEEE Eng Med Biol Soc 2016;2016:3342–3345.
24. Boutroy S, Bouxsein ML, Munoz F, et al. In vivo assessment of trabecular bone microarchitecture by high-resolution peripheral quantitative computed tomography. J Clin Endocrinol Metab 2005;90(12):6508–6515.
25. Yang H, Yu A, Burghardt AJ, et al. Quantitative characterization of metacarpal and radial bone in rheumatoid arthritis using high resolution- peripheral quantitative computed tomography. Int J Rheum Dis 2017;20(3):353–362.
26. Bruynesteyn K, Boers M, Kostense P, et al. Deciding on progression of joint damage in paired films of individual patients: smallest detectable difference or change. Ann Rheum Dis 2005;64(2):179–182.
27. Mease PJ, McInnes IB, Kirkham B, et al; FUTURE 1 Study Group. Secukinumab inhibition of interleukin-17A in patients with psoriatic arthritis. N Engl J Med 2015;373(14):1329–1339.
28. Kavanaugh A, Mease PJ, Reimold AM, et al; FUTURE 1 Study Group. Secukinumab for long-term treatment of psoriatic arthritis: a two-year followup from a phase III, randomized, double-blind placebo-controlled study. Arthritis Care Res (Hoboken) 2017;69(3):347–355.
29. Geusens P, Chapurlat R, Schett G, et al. High-resolution in vivo imaging of bone and joints: a window to microarchitecture. Nat Rev Rheumatol 2014;10(5):304–313.
30. Srikhum W, Virayavanich W, Burghardt AJ, et al. Quantitative and semiquantitative bone erosion assessment on high-resolution peripheral quantitative computed tomography in rheumatoid arthritis. J Rheumatol 2013;40(4):408–416.
31. Coates LC, Mease PJ, Gossec L, et al. Minimal disease activity among active psoriatic arthritis patients treated with secukinumab: 2-year results from a multicenter, randomized, double-blind, parallel-group, placebo-controlled phase III study. Arthritis Care Res (Hoboken) 2018;70(10):1529–1535.
32. Coates LC, Moverley AR, McParland L, et al. Effect of tight control of inflammation in early psoriatic arthritis (TICOPA): a UK multicentre, open-label, randomised controlled trial. Lancet 2015;386(10012):2489–2498.
33. Mortier C, Gracey E, Coudenys J, et al: RORgammat inhibition ameliorates IL-23 driven experimental psoriatic arthritis by predominantly modulating gammadelta-T cells. Rheumatology (Oxford) 2023;62(9):3169–3178.
34. Venken K, Jacques P, Mortier C, et al: RORgammat inhibition selectively targets IL-17 producing iNKT and gammadelta-T cells enriched in Spondyloarthritis patients. Nat Commun 2019;10(1):9.

35. Minopoulou I, Kleyer A, Yalcin-Mutlu M, et al. Imaging in inflammatory arthritis: progress towards precision medicine. Nat Rev Rheumatol 2023;19(10):650–665.
36. Liphardt AM, Manger E, Liehr S, et al. Similar impact of psoriatic arthritis and rheumatoid arthritis on objective and subjective parameters of hand function. ACR Open Rheumatol 2020;2(12):734–740.
37. Coates LC, Soriano ER, Corp N, et al; GRAPPA Treatment Recommendations domain subcommittees. Group for research and assessment of psoriasis and psoriatic arthritis (GRAPPA): updated treatment recommendations for psoriatic arthritis 2021. Nat Rev Rheumatol 2022;18(8):465–479.
38. Jin Y, Cheng IT, Wu D, et al. Imaging in psoriatic arthritis: established methods and emerging techniques. Ther Adv Musculoskelet Dis 2024;16. doi: 1759720X241288060.
39. Jin Y, Cheng IT, So H, et al. Role of inflammatory burden and treatment on joint space width in psoriatic arthritis-a high-resolution peripheral quantitative computed tomography study. Arthritis Res Ther 2023;25(1):138.

American College of Rheumatology
Empowering Rheumatology Professionals

Arthritis & Rheumatology
Vol. 77, No. 8, August 2025, pp 1026–1040
DOI 10.1002/art.43144

Identification of Pathogenic PD-1$^+$CD8$^+$ T Cells for Effective Chimeric Antigen Receptor Therapy in a Murine Model of Sjögren Disease

Jin-Fen Ma,[1] Ting Xu,[2] Hao-Xian Zhu,[1] Xiao-Min Chen,[1] Liang Li,[2] Zhi-Bin Zhao,[2] Liwei Lu,[3] Yang Li,[2] Zhe-Xiong Lian,[4] and Cai-Yue Gao[2]

Objective. Activated T cells play a pivotal pathogenic role in the progression of Sjögren disease (SjD); however, there are currently no targeted therapies specifically designed to address them. This study aims to identify pathogenic CD8$^+$ T cells in SjD and develop targeted therapeutic strategies.

Methods. *Il12b-/-Il2ra-/-* mice, a murine model for overlapping primary biliary cholangitis and SjD, were employed in this study. Pathogenic CD8$^+$ T cells were identified through single-cell RNA sequencing and flow cytometry analyses of samples from both patients with SjD and relevant murine models. Shared T cell receptor analysis was conducted to trace the potential precursors of pathogenic CD8$^+$ T cells. The efficacy of PD-1-targeted chimeric antigen receptor (CAR)–T cell therapy was evaluated through the assessment of salivary gland secretory function, immunologic profiles, and histopathological changes in the murine model.

Results. We identified PD-1 as a comprehensive marker of clonally expanded and activated pathogenic CD8$^+$ T cells in the salivary glands and peripheral tissues. Flow cytometry further confirmed the activation phenotype and cytotoxicity of PD-1$^+$CD8$^+$ T cells in the salivary glands of patients with SjD. Notably, the number of PD-1$^+$CD8$^+$ T cells in the labial glands positively correlated with disease activity in patients with SjD. These findings highlight the therapeutic potential of depleting PD-1$^+$CD8$^+$ T cells in SjD. Furthermore, PD-1-targeted CAR-T cell therapy significantly alleviated SjD symptoms in a murine model.

Conclusion. We identified the pathogenic role of PD-1$^+$CD8$^+$ T cells in both patients with SjD and a murine model and demonstrated the efficacy of PD-1-targeted CAR-T cell therapy in SjD model mice. Our findings suggest a promising avenue for developing clinical therapeutic strategies for patients with SjD.

INTRODUCTION

Sjögren disease (SjD) is a systemic autoimmune disorder characterized by lymphoplasmacytic infiltration of exocrine glands, resulting in xerostomia and xerophthalmia. As the disease progresses, it may affect multiple organ systems, including the lungs, liver, and kidneys, and elevate the risk of non-Hodgkin lymphoma.[1,2] Current treatment modalities for SjD are predominantly symptomatic and empirical, with systemic manifestation and major organ damage generally managed using steroids and immunosuppressant drugs, although the evidence supporting these interventions is limited. There is currently no effective therapeutic agent specifically targeting SjD.[3]

Inflammatory damage to the salivary glands (SGs) because of immune cell infiltration serves as a key diagnostic criterion for SjD. Patients may exhibit focal lymphocytic infiltration, ductal

Supported by the National Natural Science Foundation of China (grants 82120108013, 81901653, and 82302016).

[1]Jin-Fen Ma, BS, Hao-Xian Zhu, BS, Xiao-Min Chen, BS: South China University of Technology, Guangzhou, Guangdong, China; [2]Ting Xu, MD, PhD, Liang Li, PhD, Zhi-Bin Zhao, PhD, Yang Li, MD, PhD, Cai-Yue Gao, PhD: Guangdong Provincial People's Hospital (Guangdong Academy of Medical Sciences), Southern Medical University, Guangzhou, Guangdong, China; [3]Liwei Lu, PhD: The University of Hong Kong, Hong Kong, China; [4]Zhe-Xiong Lian, MD, PhD: South China University of Technology and Guangdong Provincial People's Hospital (Guangdong Academy of Medical Sciences), Southern Medical University, Guangzhou, Guangdong, China.

Drs Ma, Xu, and Zhu are co-first authors and contributed equally to this work.

Additional supplementary information cited in this article can be found online in the Supporting Information section (http://onlinelibrary.wiley.com/doi/10.1002/art.43144).

Author disclosures are available at https://onlinelibrary.wiley.com/doi/10.1002/art.43144.

Address correspondence via email to Cai-Yue Gao, PhD, at carolgoh@mail.ustc.edu.cn; Zhe-Xiong Lian, MD, PhD, at zxlian@gdph.org.cn; or Yang Li, MD, PhD, at liyang@gdph.org.cn.

Submitted for publication July 15, 2024; accepted in revised form January 22, 2025.

dilation, acinar atrophy, and even interstitial fibrosis in the SGs.[1,4–6] The hyperactivation of T cells is a crucial factor in the pathogenesis of SjD.[7,8] Several studies, including our recent research, have demonstrated a significant presence of activated $CD8^+$ T cells in the labial glands (LGs; minor SGs commonly used for biopsy) and peripheral blood of patients with SjD.[9–11] In *IL12B*$^{-/-}$*IL2RA*$^{-/-}$ mice, a model of overlapping SjD and primary biliary cholangitis, as well as in nonobese diabetic (NOD) mice, $CD8^+$ T cells significantly contributed to SjD symptoms, thereby reinforcing their pathogenic role in SjD.[12,13] Our prior investigations, along with those conducted by Pranzatelli et al, have identified a population of clonally expanded pathogenic HLA-DR$^+$*GZMK*$^+$ $CD8^+$ T cells in the LGs of patients with SjD.[10,11] Notably, these cells did not exhibit obvious proliferation but shared clones with *GZMK*$^+$$CD8^+$ T cells that were specifically enriched in the peripheral blood,[10] suggesting that their precursors may reside in the peripheral circulation and subsequently infiltrating the glands thereby contributing to disease progression. Consequently, targeted therapies directed at these pathogenic $CD8^+$ T cells and their precursors may provide a more precise treatment strategy.

Activated T cells up-regulate the expression of the inhibitory costimulatory molecule PD-1 to maintain tolerance.[14] PD-1 binds to its ligands, PD-L1 or PD-L2, to inhibit T cell activation, particularly in the context of antitumor immunity.[15–17] However, in autoimmune diseases such as autoimmune diabetes, juvenile idiopathic arthritis, and psoriasis, PD-1 appears to be ineffective in suppressing T cell activation and is instead highly expressed on tissue-infiltrating Teff cells.[18–20] Consistently, PD-1/PD-L1 blockade in patients with cancer enhances PD-1^+ T cell function, leading to immune-related adverse events such as skin toxicities and SjD,[21–23] whereas depleting PD-1^+ cells in autoimmune diseases alleviates symptoms, underscoring their key role in disease development.[24] Specifically, PD-$1^+$$CD8^+$ T cells have been shown to respond to self-antigens in the skin,[25] collectively suggesting that targeting PD-1 could be a strategy to modulate T cells associated with autoimmune inflammation. PD-$1^+$$CD8^+$ T cells were also found to be enriched in the LGs of patients with SjD, but the characteristics of these cells and their role in SjD remain unclear.

Chimeric antigen receptor (CAR) T cell therapy has revolutionized treatment for hematologic malignancies and shows promising potential in autoimmune diseases, such as refractory systemic lupus erythematosus, systemic sclerosis, and antisynthetase syndrome.[26–29] Here, we report that PD-1 expression is highly enriched on $CD8^+$ T cells from patients with SjD, particularly on *GZMK*$^+$$CD8^+$ T cells, which have been identified by our group and others as pathogenic T cells in SjD.[10,11] These PD-$1^+$$CD8^+$ T cells are clonally expanded and exhibit greater cytotoxicity than PD-$1^-$$CD8^+$ T cells in both patients with SjD and murine models. Consequently, we developed PD-1-targeted CAR-T cells, which significantly alleviated SjD symptoms in a murine model. These findings hold promise for more precise, cell-targeted therapies for SjD.

MATERIALS AND METHODS

Mice. The wild-type mice were purchased from Hunan Slack Laboratory (China). The *IL12B*$^{-/-}$ (B6.129S1-Il12btm1Jm/J), *IL2RA*$^{-/-}$ (B6.129S4-Il2ratm1Dw/J), NOD/ShiLtJ (NOD), and *PDCD1*$^{-/-}$ (B6. Cg-Pdcd1tm1.1Shr/J) mice were initially obtained from The Jackson Laboratories (USA). The generation of *IL12B*$^{-/-}$*IL2RA*$^{-/-}$ mice as a murine model of SjD, with *IL12B*$^{-/-}$*IL2RA*$^{+/-}$ mice used as controls, has been previously reported.[12] For CD4 depletion or CAR-T cell therapy, the mice were treated from 8 to 10 weeks of age. NOD mice aged 24 to 26 weeks were used. Mice were housed in individually ventilated cages under specific pathogen-free conditions at South China University of Technology. All animal experiments were approved by the Institutional Animal Care and Use Committee.

Patients. Fifty-eight patients diagnosed with primary SjD were recruited from the Rheumatology and Immunology Department of Guangdong Provincial People's Hospital between April 2021 and September 2023. All participants fulfilled the classification criteria established by the American-European Consensus Group in 2002[30] or the American College of Rheumatology/EULAR in 2016[31] and had not been treated with glucocorticoids or immunosuppressants prior to enrollment. Patients with malignancies, infections, or other autoimmune disorders were excluded from the study. The non-SjD control group included 22 patients who were admitted for SjD screening because of symptoms such as xerostomia or xerophthalmia. These patients tested negative for autoantibodies, specifically anti-Ro/SSA or anti-La/SSB, and exhibited no focal lymphocytic infiltration, thereby not meeting the criteria for any autoimmune diagnosis. Detailed demographic and clinical information regarding the participants can be found in Supplemental Table 1. We also submitted an additional supplemental file containing the clinical metadata for each recruited individual.

Cell isolation. For mouse SG cells, the collagenase digestion method was used. Specifically, mouse submandibular glands were cut into small pieces and digested with RPMI 1640 (Gibco) supplemented with 1 mg/mL collagenase Type II (Sigma) in a shaking incubator at 180 revolutions per minute and 37°C for 20 minutes. The digested cells were filtered through a 70μm nylon mesh, and cold phosphate-buffered saline (PBS) containing 2% bovine serum albumin (BSA) was added to terminate the digestion. Mouse lymph nodes were ground on glass slides, and PBS containing 0.2% BSA was added. The tissues were filtered through 70 μm nylon mesh.

Human peripheral blood was separated by Ficoll centrifugation, and human LGs were digested in the same manner as

mouse SGs. Trypan blue staining was used to determine cell viability and count the cells.

Flow cytometry. The cell suspension was blocked with CD16/32 (BioLegend) at 4°C for 15 minutes and then labeled with a flow cytometry antibody cocktail at 4°C for 20 minutes. For cytoplasmic antigens, a Cytofix/Cytoperm Fixation/Permeabilization Kit was used following the manufacturer's instructions. For intranuclear antigens, the Transcription Factor Staining Buffer Set (eBioscience) was used following the manufacturer's instructions. Surface CD107a expression was measured following ex vivo restimulation with eBioscience Cell Stimulation Cocktail at 37°C for 4 hours, with the antibody added to the culture medium during stimulation. Data were acquired using Cytek Aurora and analyzed with FlowJo Version 10.8.1. Antibodies used for flow cytometry are listed in Supplemental Table 2. Gating strategies for human and mouse cells not explicitly referenced are provided in Supplemental Figure.

RNA sequencing. Total RNA was extracted from mouse SG tissues and draining lymph nodes (dLNs) $CD8^+$ T cells using the TRIzol (Takara) method. VAHTS messenger RNA (mRNA) Capture Beads (Vazyme, China) were used to isolate the mRNA, and the VAHTS Universal V8 RNA-seq Library Prep Kit for Illumina (Vazyme) was used to construct sequencing libraries. The NovaSeq 6000 sequencing system (Illumina) platform was used for sequencing 150 bp paired-end reads.

Single-cell RNA-seq library preparation and sequencing. For the single-cell RNA-seq (scRNA-seq) experiment, four *IL12B*$^{-/-}$ *IL2RA*$^{-/-}$ (SjD) mice and four *IL12B*$^{-/-}$ *IL2RA*$^{+/-}$ (Control) mice were used. Cells from SG and dLN were isolated, and $CD45^+$ leukocytes sorted (BD FACSAria) into four samples: Ctrl_SG, SjD _SG, Ctrl_dLN, and SjD _dLN for scRNA-seq.

ScRNA-seq libraries were prepared using the Chromium Single Cell 5' Reagent Kits User Guide (v2 – Dual Index), and the full-length V(D)J fragment of complementary DNA (cDNA) was enriched and amplified using the Chromium Single-cell V(D)J enrichment kit (10× Genomics). The experimental steps included single-cell GEM (gel beads in-emulsion) formation and inversion into cDNA, oil breaking, cDNA amplification, T cell receptor (TCR) sequence enrichment, TCR library construction, and gene expression library construction. The NovaSeq 6000 sequencing system platform was used for sequencing 150 bp paired-end reads.

Single-cell transcriptome and TCR sequencing data processing. The raw scRNA-seq data were processed by Cell Ranger (version 6.1.2). Cell Ranger was run with default parameters using STAR (version 2.7.10a) for alignment against the mouse genome (mm10) reference. Seurat (version 4.1.0) was used for analysis. The preprocessed data matrix was read in by Read10X and converted to a Seurat object for each sample using the CreateSeuratObject function. We calculated the normalization data for log normalization and determined the top 2000 most variable genes via the "vst" method in FindVariableFeatures. In addition, we used ScaleData, RunPCA, FindNeighbors, FindClusters, RunTSNE, and RunUMAP for downstream analysis. DoubletFinder (version 2.0) removes duplicate information. Cells with more than 6,000 or less than 200 unique genes, more than 50% mitochondrial genes, or high levels of mitochondrial genes but low unique molecular identifier counts were removed. Principal component analysis was used to reduce the dimensionality of highly variable genes. Using the first 30 principal components as inputs, Uniform Manifold Approximation and Projection (UMAP) was used to visualize the data in two dimensions. Subsequently, we used the Dimplot, Featureplot, and VlnPlot functions to perform gene dimensionality reduction and distribution visualization.

Gene set enrichment analysis. Gene set enrichment analysis (GSEA) was performed using the ClusterProfiler package (version 3.16.1). The preranked genes according to the GSEA function were used to calculate *P* values and enrichment scores.

Volcano plot and Cell trajectory analysis. Volcano plot analysis was performed with the FindMarkers function in the Seurat package to identify the differentially expressed genes (DEGs) of the defined cell groups. The criteria for the significantly DEGs were $|\log2FC|>0.3$ and P value <0.01. We used the ggplot function with log2FC as the horizontal axis and -Log10P as the vertical axis. Cell trajectory analysis was performed using the Monocle3 (version 1.3.4) software, which integrates the information from UMAP cell clustering and coordinate axes.

TCR analysis. The scRepertoire (version 1.6.0) was used for TCR analysis, and the input data were annotated using filtered contigs obtained from Cell Ranger. The combined TCR function filters cells with at least one not available and retains T-cell receptor alpha and beta for further analysis. The CompareClonotype function was used to display shared clones between samples or different cell clusters and was visualized with the ggalluvial package. The clonalOverlap and clonalProportion functions were used to analyze the TCR information of different samples and cell subsets. The combineExpression was used to integrate TCR and genomic information, the filterNA parameter was TRUE, and the cloneCall parameter was aa (amino acid). In addition, we used the exportTable parameter with TRUE to obtain tables for further analysis and visualized them in R using the ggplot package.

Construction of anti-PD1 CAR and CAR-T cell viral packaging systems. PD-1-targeted CAR-T cells, in which the CAR was designed to contain the PD-L1 extracellular region sequence, were fused with the CD28 hinge and transmembrane domains, CD28 costimulatory domains, and CD3ζ signaling domains. The pMSGV-CAR-IRES-Thy1.1 plasmid was

constructed by inserting the above CAR sequences into the pMSCV retrovirus vector containing Thy1.1 as a selective marker (pMSCV-IRES-Thy1.1), and the constructed plasmid sequence was determined by genome sequencing. The plasmid was subsequently transformed into *E coli*, which were subsequently amplified and extracted. Retroviral vectors encoding anti-PD-1 CAR or empty vectors were transduced into HEK293T cells together with pCL-Eco retroviral packaging vectors. Lipo8000 (Beyotime, C0533) was used as the transfection reagent. After 48 hours, the cell culture supernatants containing the viruses were filtered through a 0.45 μm filter.

Generation of anti-PD1 CAR-T cells. $CD8^+$ T cells were isolated from the spleens of PD-1-deficient mice using magnetic beads (Miltenyi Biotec, 130-049-401). A total of 12-well plates were coated with 4 μg/mL anti-CD3 (BioLegend, 100238) overnight at 4°C. The T cell culture medium (RPMI-1640 medium containing fetal bovine serum [10%], sodium pyruvate [1 mM], penicillin–streptomycin [100 U/mL], anti-CD28 [2 μg/mL, BioLegend, 102116], and interleukin (IL)-2 [100 U/mL, PeproTech, PHC0027]) was used to activate the $CD8^+$ T cells for two days.

Activated $CD8^+$ T cells were resuspended in 1 mL of medium containing virus, and IL2 (100 U/mL) and polybrene (10 μg/mL; Biosharp, BL628A) were added. After centrifugation at 2000 rpm for 90 minutes, 1 mL of T cell culture medium containing IL2 was added, after which the cells were cultured for 12 to 24 hours with fresh T cell culture medium containing IL2. After 24 hours, magnetic beads were used to isolate Thy1.1-positive CAR-T cells. Finally, the cytokines IL7 (20 ng/mL; PeproTech, 200-07-1MG) and IL15 (20 ng/mL; PeproTech, 200-15-100UG) were used to expand CAR-T cells for five days. Ctrl-T cells were transfected with an empty plasmid containing Thy1-1, and the other procedures were the same as those used for CAR-T cells.

Saliva collection. After the mice were anesthetized with pentobarbital sodium, 1 mg/kg pilocarpine hydrochloride (Aladdin, China) was intraperitoneally injected, and the saliva was collected with a 10 μl pipet for 15 minutes. The saliva volume was determined after 10 minutes of centrifugation at 12,000×g at room temperature.

Autoantibodies against SSA/Ro52 and SSA/Ro60 detection. Autoantibodies in mouse serum were measured using enzyme-linked immunosorbent assay kits following the manufacturer's instructions (Alpha Diagnostic International), including anti-SSA/Ro52 (#5730) and anti-SSA/Ro60 (#5710). Briefly, serum samples (diluted 1:50) were added to microtiter plates coated with purified SSA/Ro52 or SSA/Ro60, followed by incubation with hydrogen peroxidase–conjugated antimouse Ig antibodies. The reaction solution and stop solution were subsequently added, and absorbance was measured at 450 nm using a Cytation 5 microplate reader (BioTek).

Histology. Mouse submandibular glands were fixed in 10% formalin, embedded in paraffin, sectioned at 4 μm thickness, and stained with hematoxylin and eosin or Masson's trichrome. A focus was defined as a lesion containing at least 50 lymphocytes per 4 mm^2. Duct damage and acinar atrophy were graded as none (0), minimal (0.5), mild (1), moderate (2), or severe (4). Pathologic assessments were performed by a pathologist in a blinded manner. Masson's trichrome staining was quantified by ImageJ software (version 1.53g).

Multiplex immunohistochemistry. Formalin-fixed labial gland (human) and submandibular gland (mouse) tissues were cut into 4 μm pieces, and multiplex immunohistochemistry was performed using an Opal Polaris 7-Color Manual IHC Kit (Akoya Bioscience, NEL861001KT). Primary antibodies used for staining human LGs were CD8 (CST, Cat# 70306, 1:400) and PD-1 (CST, Cat# EH33, 1:50); primary antibodies used for staining mouse SGs included E-cad (CST, Cat# 3195, 1:400), AQP5 (abcam, Cat# ab78486, 1:500), Ki67 (abcam, Cat# ab16667, 1:500), CD45 (CST, Cat# 70257,1:200), and Thy-1.1 (Invitrogen, Cat# 14-0900-81,1:100). Secondary antibodies and fluorescent dyes were obtained from Akoya kits. Nuclear staining was performed with 4',6-diamidino-2'-phenylindole (Beyotime, C1005). The staining results were scanned by Vectra Polaris (Akoya Bioscience). Statistical analysis was performed using Halo software.

CAR-T cell therapy in vivo experiments. CAR-T cells or Ctrl-T cells (1×10^6) were injected into mice through the tail vein. Treatment began at 8 weeks of age, at which time CAR-T cells were injected on days 1 and 14. Mice were sacrificed either one week or four weeks after the first injection. Unless specified as "one week," all CAR-T cell therapy data refer to the four-week time point.

Anti-CD4 in vivo experiments. Mice aged 8 to 12 weeks were injected intraperitoneally with 200 μg of an anti-CD4 antibody (BioXCell, Clone: GK1.5) three times a week for a total of 4 weeks. The mice were sacrificed 3 days after the last injection.

Statistical analysis. All values were presented as the mean ± SD, as indicated in the figure legends. In the figures, asterisks denote statistical significance: $^*P < 0.05$, $^{**}P < 0.01$, and $^{***}P < 0.001$. Paired or unpaired comparisons were calculated using the Wilcoxon signed-rank test or Mann–Whitney U test. For comparisons across multiple groups, two-way analysis of variance was used. The data represent two or three independent experiments with two-sided *P* values.

The scRNA-seq and RNA-seq data have been deposited in the GEO database under the ID codes GSE253042, GSE284327 and GSE253818. The research followed the Declaration of Helsinki, and the study protocols were approved by Guangdong Provincial People's Hospital (KY2020-334-01).

Participants gave informed consent to participate in the study before taking part in the study.

RESULTS

PD-1$^+$CD8$^+$ T cells display pathogenic roles in the LGs of patients with SjD. Consistent with previous observations,[11,32] CD8$^+$ T cells from peripheral blood and LGs of patients with SjD could be divided into four subsets based on GZMK and GZMB expression levels. In terms of the proportion of granzyme-secreting CD8$^+$ T cells, GZMK$^+$CD8$^+$ T cells were more prevalent in the LGs compared with peripheral blood in patients with SjD (Supplemental Figure 1A). Compared with non-SjD, GZMK$^+$CD8$^+$ T cells are significantly increased in the LGs and highly express HLA-DR in patients with SjD (Figure 1A). This finding corroborates earlier reports highlighting a specific increase in disease-associated HLA-DR$^+$CD8$^+$ T cells in SjD LGs.[9] And compared with other CD8$^+$ T cells, HLA-DR$^+$GZMK$^+$CD8$^+$ T cells exhibit a cytotoxic phenotype, characterized by a higher proportion of cells expressing GZMB and Perforin, as well as increased proportions of PD-1$^+$ cells and mean fluorescence intensity of PD-1 (Figure 1B–D, Supplemental Figure 1B and C). The expression level of PD-1 on CD8$^+$ T cells increased with the rise in HLA-DR expression (Supplemental Figure 1D). Moreover, the proportion of PD-1$^+$CD8$^+$ T cells was noticeably higher in the LGs than in the peripheral blood mononuclear cells in patients with SjD (73.8 ± 15.2% vs 23.4 ± 8.8%; $P < 0.001$) (Figure 1E).

Because the coexpression of PD-1 and HLA-DR on CD8$^+$ T cells was associated with antigen stimulation,[33,34] our data indicate that these cells in the patients with SjD may have undergone prolonged antigen stimulation. Further analysis using our recently published scRNA-seq data (Supplemental Figure 1E)[11] revealed that clonal expanded CD8$^+$ T cells, especially those that are hyperexpanded, exhibited a higher level of *PDCD1* (encoding PD-1) transcript than nonclonal CD8$^+$ T cell within the LGs (Figure 1F and G). In addition, the CD8 cytotoxicity pathway was enriched alongside increased *PDCD1* transcript levels in CD8$^+$ T cells (Figure 1H). Consistent with observations on tissue infiltrated GZMK$^+$CD8$^+$ T cells,[10,11] PD-1$^+$CD8$^+$ T cells in the LGs also exhibited morphologic distortion and closely adhered to the surrounding acinar and ductal cells (Figure 1I). The infiltration of PD-1$^+$CD8$^+$ T cells was found to positively correlate with several clinical parameters, including focus score (Figure 1J), IgA (Figure 1K), rheumatoid factor (RF) (Figure 1L), and erythrocyte sedimentation rate (ESR) (Figure 1M). In contrast, the number of PD-1$^-$CD8$^+$ T cells showed no association with these SjD clinical parameters in Supplemental Figure 1F–I. Therefore, PD-1$^+$CD8$^+$ T cells could represent the pathogenic GZMK$^+$CD8$^+$ T cells identified in our earlier studies.[11] For the convenience of in vivo functional studies, we simplified GZMK$^+$CD8$^+$ T cells to PD-1$^+$CD8$^+$ T cells in subsequent experiments.

Furthermore, *PDCD1* mRNA expression level was found to be elevated in patients with SjD compared with non-SjD controls (Supplemental Figure 2A), and there was a moderate to strong correlation with transcript levels of the SjD risk gene *HLA-DRB1*[35] and *GZMK*, based on a public LGs transcriptome data[36] (Supplemental Figure 2B and C). And in parallel with the former results (Figure 1B and C), *PDCD1* expression showed a positive correlation with the cytotoxic markers *GZMB* and *PRF1* (encoding Perforin) in patients with SjD (Supplemental Figure 2D and E). Disease-related indicators such as the focus score and leukocyte infiltration areas were consistently linked to increased *PDCD1* expression in both labial and parotid glands (Supplemental Figure 2F–H). These results underscore that *PDCD1* transcriptional level significantly correlates with the intensity of immune responses in the LGs of patients with SjD. Collectively, these data demonstrate that PD-1$^+$CD8$^+$ T cells with pathogenic functions were associated with disease activity in patients with SjD.

PD-1$^+$CD8$^+$ T cells in the SGs of SjD model mice undergo clonal expansion and exhibit cytotoxic effects. Acknowledging the pathogenic roles of PD-1$^+$CD8$^+$ T cells in patients with SjD, we investigated whether these cells are present in a mouse model. We previously reported that *Il12b-/-Il2ra-/-* mice display clinical features analogous to those of patients with SjD. Administration of anti-CD8a antibodies resulted in a reduction of T cell infiltration in the SGs and a restoration of salivary secretion, underscoring the pathogenic role of CD8$^+$ T cells in this model.[12] To precisely classify the pathogenic CD8$^+$ T cells, we performed scRNA-seq to identify the relevant cell subsets within the SGs. All T cell subsets and their proportions in SGs and dLNs are detailed in Supplemental Figure 3A–C, with key gene expressions illustrated in Supplemental Figure 3D. Notably, the proportion of cytotoxic CD8$^+$ T cells was higher than that of cytotoxic CD4$^+$ T cells in the SGs of SjD mice (Supplemental Figure 3C).

We deconvolved CD8$^+$ T cells into four subsets based on their expression profiles: T1_Itgae (characterized by high expression of tissue-resident genes *Itgae and Itga1*), T2_Stem-like (selectively expressing stemness markers *TCF7* and *IL7R*, and circulating markers *GPR183*), T3_Cytotoxic (marked by cytotoxic genes *NKG7*, *GZMB*, and *PRF1*, chemokines *CCL3*, *CCL4*, and *CCL5*, coinhibitory receptors *PDCD1* and *LAG3*, and tissue-resident genes *CXCR6*), and T4_Proliferative (expressing genes associated with proliferation, such as *STMN1* and *MKI67*) subset (Figure 2A and B; Supplemental Figure 4A; refer to Supplemental Table 3 for gene profile). Notably, the T1_Itgae subset was the predominant CD8$^+$ T cell subset in the SGs of control mice, whereas the T3_ Cytotoxic subset formed the largest cluster in SjD mice (Figure 2A). DEGs of CD8$^+$ T cells in the SGs of control and SjD model mice were analyzed (Figure 2C). *PDCD1* (encoding PD-1) was markedly enriched among the DEGs and predominantly concentrated in the T3_Cytotoxic and T4_Proliferative subsets (Figure 2C and D), which were the most clonally

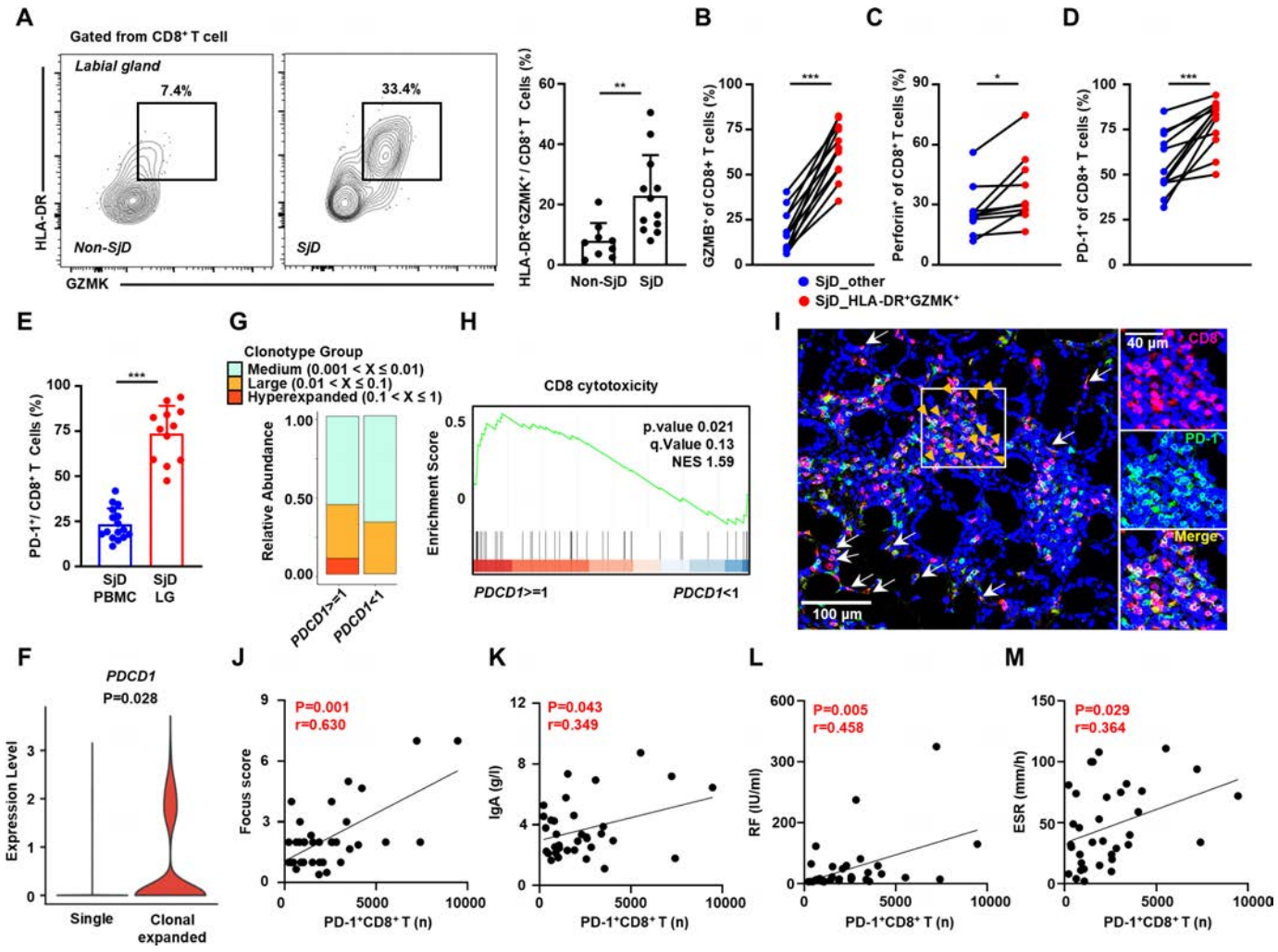

Figure 1. PD-1$^+$CD8$^+$ Trm cells display pathogenic roles in the LGs of patients with SjD. (A) Expression of HLA-DR and *GZMK* in CD8$^+$ T cells from LGs of non-SjD (n = 9) and patients with SjD (n = 12). The graph shows the proportion of *GZMK*$^+$HLA-DR$^+$CD8$^+$ T cells among total CD8$^+$ T cells. (B–D) Expression of GZMB (n = 12), Perforin (n = 10, 2 samples missing), and PD-1 (n = 12) is measured in *GZMK*$^+$HLA-DR$^+$CD8$^+$ T cells and other CD8$^+$ T cells from LGs of patients with SjD. (E) Proportion of PD-1$^+$ cells in CD8$^+$ T cells from PBMCs (n = 16) and LGs (n = 12) of patients with SjD. (F) Violin plot showing *PDCD1* gene expression in single CD8$^+$ T cells and clonally expanded CD8$^+$ T cells. (G) Clonotype size distribution based on the relative *PDCD1* expression levels, with values greater than or equal to one and less than one. (H) GSEA plot showing the enrichment score of the CD8 cytotoxic pathway between clusters from (G). (I) mIHC staining images of LGs from patients with SjD. Scale bars represent 40 μm and 100 μm, as indicated. Triangles (orange) point to PD-1$^+$CD8$^+$ T cells, and arrows (white) point to PD-1$^+$CD8$^+$ T cells surrounding tissue cells. (J–M) Correlation between the number of infiltrated PD-1$^+$CD8$^+$ T cells in LGs and (J) focus score, (K) IgA, (L) RF, and (M) ESR (n = 36) in patients with SjD. *$P < 0.05$, **$P < 0.01$, ***$P < 0.001$. (A) Mann–Whitney U test, (B–D) paired two-tailed Student's *t*-test, (E and F) unpaired two-tailed Student's *t*-test, and (J–M) Pearson correlation coefficient. Data are presented as mean ± SD. ESR, erythrocyte sedimentation rate; GSEA, gene set enrichment analysis; LG, labial gland; mIHC, multiplex immunohistochemistry; NES, normalized enrichment scores; PBMC, peripheral blood mononuclear cell; RF, rheumatoid factor; SjD, Sjögren disease; Trm, tissue-resident memory.

expanded T cell populations in SjD mice, with the top 10 most expanded clonotypes primarily localized within these two subsets (Figure 2E; refer to Supplemental Table 4 for the top 10 clonotypes). Additionally, TCR repertoire diversity was observed to be higher than that in the T3_Cytotoxic and T4_Proliferative subsets, where the clonotypes were predominantly larger (clonotypes > 30) (Figure 2F). Consistently, TCR activation and cytotoxicity scores were higher in the T3_Cytotoxic and T4_Proliferative subsets (Figure 2G and H; see Supplemental Table 5 for the associated gene sets). For example, genes associated with TCR activation (such as *ZAP70*, *LCK*, *CD27*, and *ENTPD1*) and T cell cytotoxicity (including *Prf1, Gzma, Gzmb, Nkg7, and Ifng*) cell populations (Figure 2I and J). These results were validated by flow cytometry, showing an increased population of CD8$^+$ T cells expressing high levels of PD-1 in the SGs of SjD model mice (Figure 2K). These cells exhibited significant potential expression of cytotoxic molecules, including Perforin, granzymes (GZMA and GZMB), FASL, and surface CD107a upon stimulation with

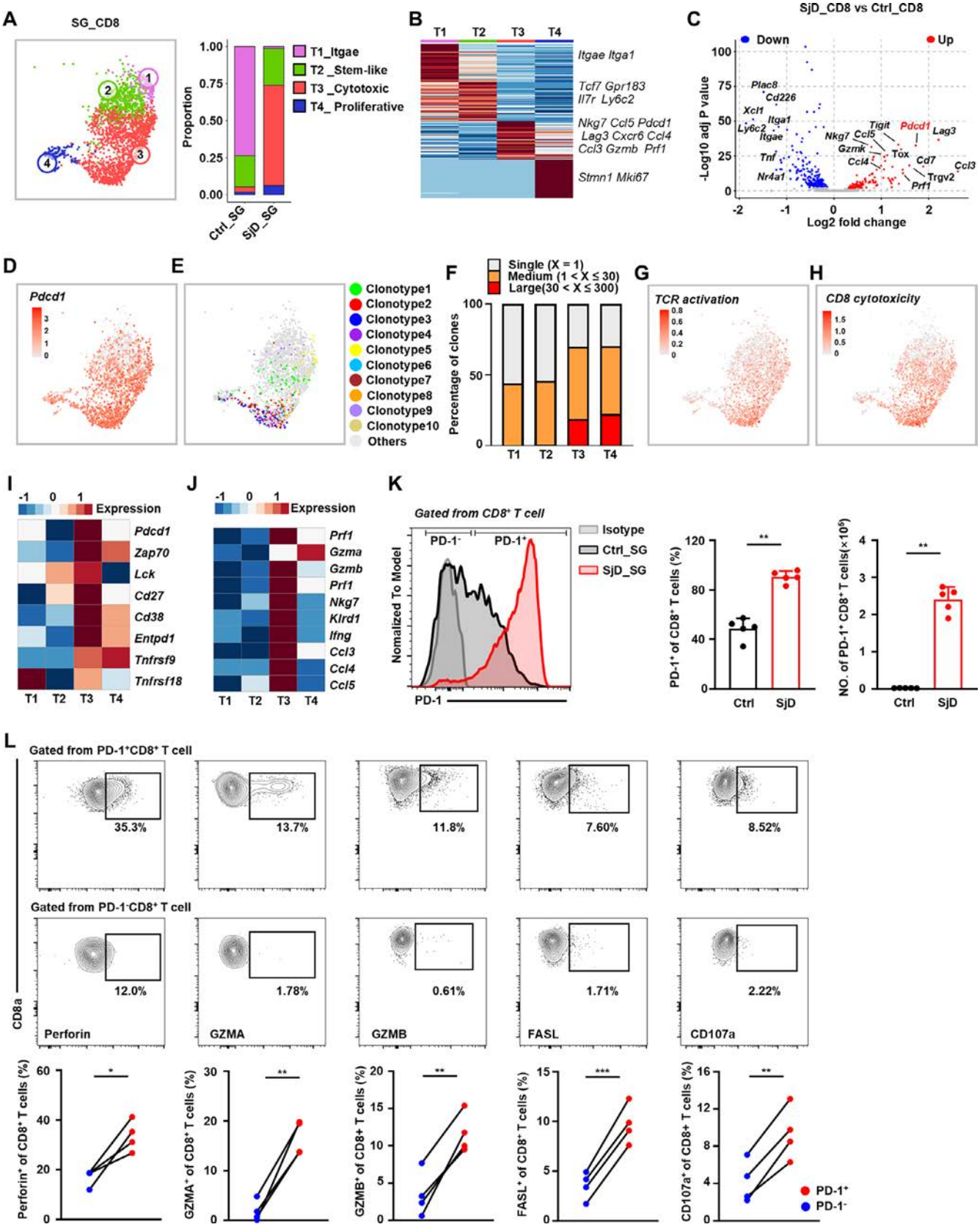

(Figure legend continues on next page.)

PMA/ionomycin (Figure 2L). Furthermore, PD-1$^+$CD8$^+$ T cells down-regulated the expression of precursor-related markers (TCF1, CD127, CD73, and LY6C) while expressing high residency-related molecules (CXCR6, CD49D, CD69, and part of CD103) (Supplemental Figure 4B), indicating a tissue-resident memory (Trm) profile.

These characteristics were also validated in an alternative SjD model, the NOD mice.[37] Specifically, the proportion of infiltrating PD-1$^+$CD8$^+$ T cells displayed a positive correlation with their cytotoxicity score, implying that a higher number of infiltrating PD-1$^+$CD8$^+$ T cells is associated with increased tissue toxicity (Supplemental Figure 5A and B). Consistent with the findings in *Il12b-/-Il2ra-/-* mice, PD-1$^+$CD8$^+$ T cells in NOD mice exhibited a Trm phenotype as well (Supplemental Figure 5C). These findings suggested that the characteristics and functions of infiltrating PD-1$^+$CD8$^+$ T cells in the SGs are not specific to one particular SjD murine model, but consistent across various SjD murine models. Notably, the transcriptomic profiles of these PD-1$^+$CD8$^+$ T cells from both dLNs and SGs closely mirrored those of their human counterparts in patients with SjD (Supplemental Figure 4C), indicating that the SjD murine model is an appropriate platform for more in-depth studies of this cell population.

GZMK$^+$PD-1$^+$CD8$^+$ T cells represent the precursors of potential pathogenic CD8$^+$ Trm cells in SjD model mice. During the process of immune response in tissues, dLNs serve as important training grounds and supply centers for immune cells within the tissue. Antigen-activated T cells leave the lymph nodes and enter the bloodstream, circulating to specific tissue sites.[38,39] Our previous findings indicated that GZMK$^+$CD8$^+$T cell (hereafter referred to as PD-1$^+$CD8$^+$ T cell) in the LGs of patients with SjD are rarely expanded in situ but rather supplied by CXCR6$^+$GZMK$^+$CD8$^+$ T cell from periphery.[11] This study aims to investigate the precursors of cytotoxic PD-1$^+$CD8$^+$ T cells in the SG dLNs and to characterize their properties. To mitigate biases arising from differences in cell numbers, we normalized CD8$^+$ T cell counts between healthy control and SjD mice. We analyzed shared cell clones within the SGs and dLNs of SjD model mice and found that these shared clones were predominantly localized in the dLN_*Gzmk* subset (Figure 3A and B; Supplemental Figure 6A). In addition, compareClonotypes and clonalOverlap analyses indicated that CD8$^+$ T cells in the SGs and dLNs of SjD mice exhibited greater clonal overlap than CD4$^+$ T cells (Supplemental Figure 6B–D; refer to Supplemental Tables 6 and 7 for shared TCRs). To illustrate the distribution of CD8 TCR clonotypes in specific dLNs and SGs clusters, we presented the top 50 clonotypes for dLNs and SGs, respectively. Among them, 22 clonotypes with high ranking in the dLN were primarily found in the dLN_*GZMK* cluster, whereas 14 were concentrated in the dLN_Memory cluster (Supplemental Figure 6E). In the SGs, the top clonotypes were primarily located in the cytotoxic cluster (Supplemental Figure 6E). Notably, approximately 20% of the top 50 clonotypes in the SGs were shared with those in the dLNs, suggesting that the dLNs served as an important clonotypic reservoir for the SGs in SjD (Supplemental Figure 6E). These shared clonotypes represent various stages of CD8$^+$ T cell differentiation in the SGs, reflecting a dynamic process of T cell differentiation in response to antigen stimulation following their infiltration into the SGs (Supplemental Figure 6E and F).

Pseudotime analysis identified the dLN_*GZMK* subset as a transitional population from peripheral CD8$^+$ T cells to SG CD8$^+$ Trm cells (Figure 3C), accompanied by the upregulation of Trm-related genes[40] (Figure 3D). The dLN_*GZMK* subset exhibited characteristics analogous to SG PD-1$^+$CD8$^+$ T cells, including elevated expression of coinhibitory (TIGIT and *PDCD1*) and cytotoxicity-related molecules (NKG7, *GZMB*, CCL4, and CCL5), suggesting a differentiation relationship between them (Figure 3E, Supplemental Figure 6A). We identified a unique subset of CD8$^+$ T cells coexpressing PD-1 and TIGIT in the dLNs of SjD model mice (Figure 3F). Considering the lack of flow cytometry antibodies with good specificity for murine *GZMK*, we sorted PD-1$^+$CD8$^+$ T cells from dLNs and conducted transcriptome sequencing to validate their association with the dLN_*GZMK* subset identified in single-cell sequencing. Compared with PD-1$^-$CD8$^+$ T cells, PD-1$^+$CD8$^+$ T cells exhibited higher transcription levels of *GZMK* and up-regulated the transcription of genes that positively regulate Trm differentiation (eg, IL15RA, RUNX2, RUNX3[41,42]), while downregulating the transcription of genes that negatively regulate Trm differentiation (Figure 3G). GSEA further revealed that the

(Figure legend continued from previous page.)

Figure 2. PD-1$^+$CD8$^+$ Trm cells in the SGs of SjD model mice are clonally expanded and exhibit cytotoxic effects. (A) UMAP plot showing RNA-defined Seurat clusters of CD8$^+$ T cells in SGs colored by cluster. The proportion of cells in each cluster is displayed for control and SjD mice. (B) Heatmap of the top 50 differentially expressed genes for each cluster; selected genes are shown on the right, with the complete list of top genes available in Supplemental Table 3. (C) Volcano plot showing differentially expressed genes in CD8$^+$ T cells between SjD and control mice. (D) UMAP plot visualizing *PDCD1* expression in SjD CD8$^+$ T cells. (E) The top 10 CD8$^+$ T cell clonotypes displayed in the merged UMAP plot. (F) Histogram showing clone size of each CD8$^+$ T cell cluster. (G and H) UMAP plots showing (G) TCR activation and (H) CD8 cytotoxicity gene set expression. (I and J) Heatmaps of genes associated with (I) TCR activation and (J) CD8 cytotoxicity. (K) Histogram overlays of PD-1 expression in salivary gland CD8$^+$ T cells from control (n = 5) and SjD (n = 5) mice. Graphs show the proportion and number of PD-1$^+$CD8$^+$ T cells. (L) Representative flow cytometry plots and cumulative data on expression levels of Perforin, GZMA, GZMB, FASL, and CD107a in PD-1$^+$ and PD-1$^-$CD8$^+$ T cells (n = 4 mice). (K and L) are representative of more than two independent experiments. $^*P < 0.05$, $^{**}P < 0.01$, $^{***}P < 0.001$. (K) Mann–Whitney U test, (L) paired two-tailed Student's *t*-test. Data are presented as mean ± SD. Ctrl-T, control T cell; SG, salivary gland; SjD, Sjögren disease; TCR, T cell receptor; Trm, tissue-resident memory; UMAP, Uniform Manifold Approximation and Projection.

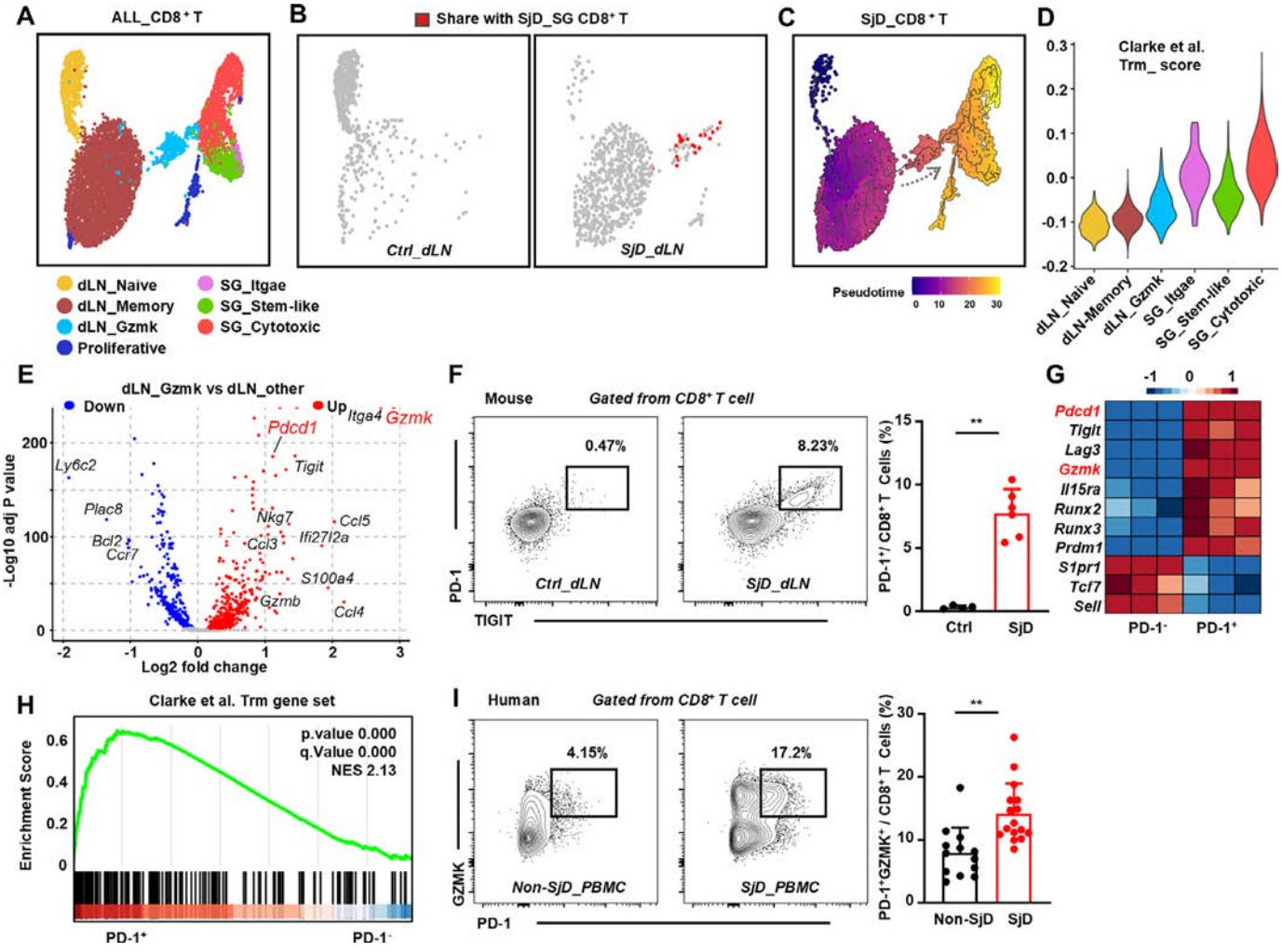

Figure 3. GZMK⁺PD-1⁺CD8⁺ T cells represent the precursors of pathogenic CD8⁺ Trm cells in SjD model mice. (A) UMAP plot of RNA-defined Seurat clusters of CD8⁺ T cell in dLNs and SGs. (B) Clonal distribution of CD8⁺ T cells shared with the SGs of SjD mice in dLNs. (C) Monocle3 pseudotime analysis reveals CD8⁺ T cell differentiation trajectories for total CD8⁺ T cells from dLNs and SGs. (D; Clarke et al[40]) Violin plot showing the Trm scores of CD8⁺ T cell clusters. (E) Volcano plot showing differentially expressed genes between the Gzmk_CD8⁺ T cells and other CD8⁺ T cells in dLNs. (F) PD-1 and TIGIT expression in CD8⁺ T cells from dLNs of control (n = 4) and SjD (n = 6) mice. The graph shows the proportion of PD-1⁺CD8⁺ T cells among total CD8⁺ T cells. Representative of more than two independent experiments. (G) Heatmap of scaled normalized expression of selected genes comparing PD-1⁺CD8⁺ T cells with PD-1⁻CD8⁺ T cells from dLNs in SjD mice. (H; Clarke et al[40]) GSEA for the Trm gene set in PD-1⁺CD8⁺ T cells and PD-1⁻CD8⁺ T cells from dLNs in SjD mice. (I) *GZMK* and PD-1 expression in peripheral blood of non-SjD controls (n = 13) and patients with SjD (n = 16). Graph shows the proportion of *GZMK*⁺PD-1⁺CD8⁺ T cells among CD8⁺ T cells. Representative of more than two independent experiments. $^{**}P < 0.01$. (F) Mann–Whitney U test, (I) unpaired two-tailed Student's *t*-test. Data are presented as mean ± SD. Ctrl-T, control T cell; dLN, draining lymph node; GSEA, gene set enrichment analysis; NES, normalized enrichment scores; PBMC, peripheral blood mononuclear cell; SG, salivary gland; SjD, Sjögren disease; Trm, tissue-resident memory; UMAP, Uniform Manifold Approximation and Projection.

transcriptional profile of PD-1⁺CD8⁺ T cells aligns more closely with the Trm phenotype[40] than that of PD-1⁻CD8⁺ T cells (Figure 3H, see Supplemental Table 5 for the pathway gene sets). Furthermore, peripheral *GZMK*⁺CD8⁺ T cells, previously identified as potential precursors to pathogenic CD8⁺ T cells in the LGs of patients with SjD,[11] also demonstrated increased PD-1 expression compared with non-SjD controls (Figure 3I). Collectively, our data suggest that *GZMK*⁺PD-1⁺CD8⁺ T cells in the dLNs may serve as potential precursors to pathogenic CD8⁺ Trm cells in the SGs.

PD-1-targeted CAR-T cells effectively alleviate inflammatory infiltration in SG of SjD model mice. Considering the pathogenic potential of PD-1⁺CD8⁺ T cells in SjD, we engineered CAR-T cells incorporating the extracellular domain of PD-L1 alongside the intracellular domains of CD28 and CD3ζ, enabling selective and sustained targeting of PD-1⁺ cells in SjD murine models (Figure 4A). In vitro assessments revealed that PD-1-targeted CAR-T cells exhibited strong cytotoxicity against PD-1⁺CD8⁺ T cells sourced from both SGs and

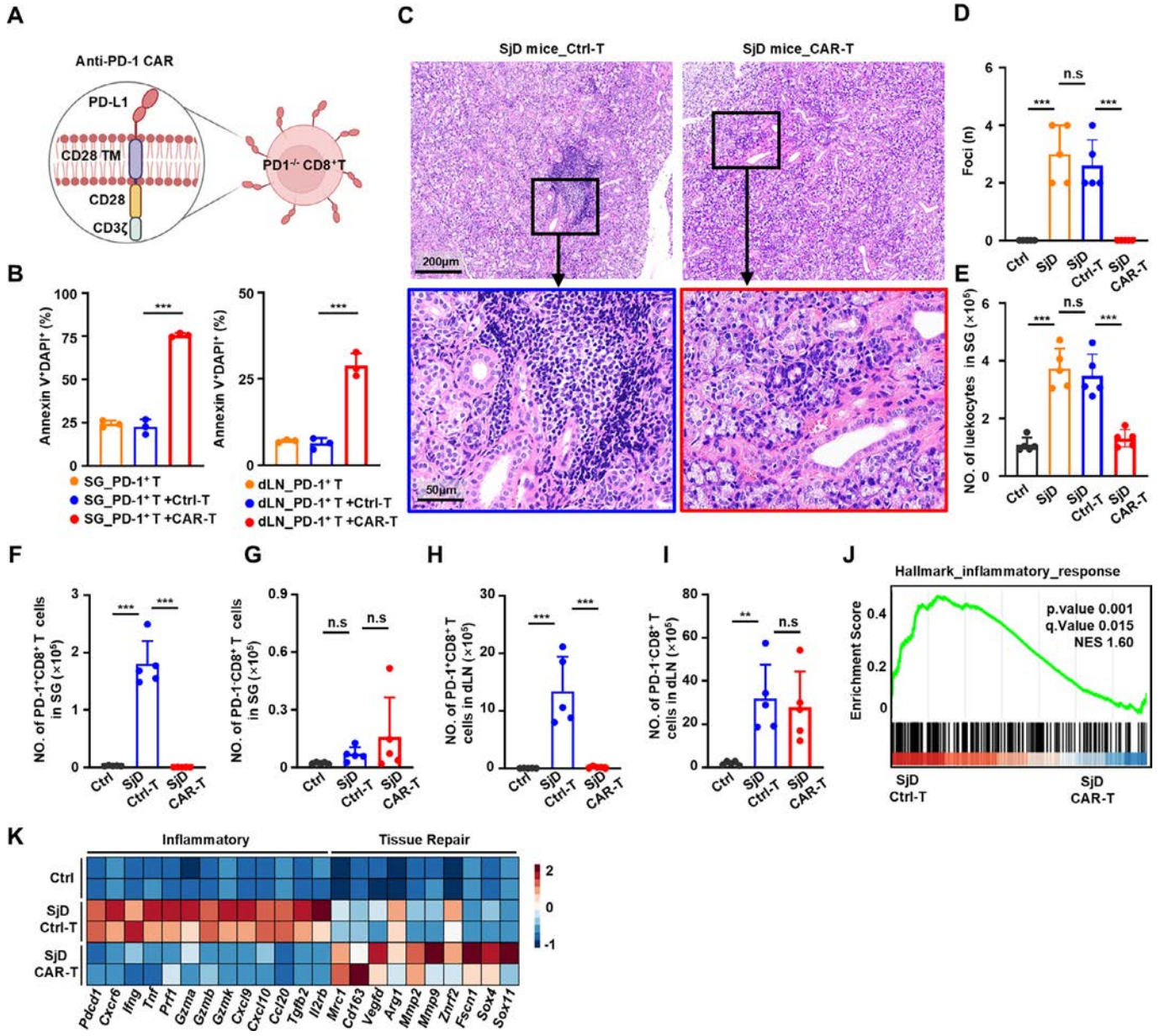

Figure 4. PD-1-targeted CAR-T cells effectively alleviate inflammatory infiltration in salivary gland of SjD model mice. (A) Structural diagram of CAR-T cells. (B) Death ratio of PD-1$^+$CD8$^+$ T cells from SGs or dLNs cocultured with Ctrl-T (n = 3) or CAR-T cells (n = 3) for 12 hours. (C) Representative H&E staining images following treatment with either Ctrl-T or CAR-T. Scale bars represent 50 μm and 200 μm, as indicated. (D) Number of lymphocyte foci in control mice, SjD mice, SjD mice treated with Ctrl-T cells, and SjD mice treated with CAR-T cells (n = 5 mice per group). (E) Number of CD45$^+$ leukocytes in SGs (n = 5 mice per group). (F and G) Number of PD-1$^+$CD8$^+$ T cells and PD-1$^-$CD8$^+$ T cells in SGs (n = 5 mice per group). (H and I) Number of PD-1$^+$CD8$^+$ T cells and PD-1$^-$CD8$^+$ T cells in dLNs (n = 5 mice per group). (J) GSEA plot showing the enrichment score of the Hallmark_inflammatory_response pathway in SGs. (K) Heatmap of scaled normalized expression of selected genes in SGs. All experiments were repeated at least twice. *P < 0.05, **P < 0.01, ***P < 0.001, n.s, not significant, one-way ANOVA with Tukey's multiple comparisons test (B, D–I). Data are presented as mean ± SD. ANOVA, analysis of variance; CAR, chimeric antigen receptor; Ctrl-T, control T cell; dLN, draining lymph node; GSEA, gene set enrichment analysis; H&E, hematoxylin and eosin; NES, normalized enrichment scores; n.s., not significant; SG, salivary gland; SjD, Sjögren disease.

dLNs, with a stronger effect on SG-derived PD-1$^+$CD8$^+$ T cells (Figure 4B). In vivo applications of CAR-T therapy resulted in a significant reduction of both lymphocytic infiltration foci score and leukocyte count in the SGs (Figure 4C–E, Supplemental Figure 7A–C), effectively depleting PD-1$^+$CD8$^+$ T cells in the SGs and potential pathogenic precursor PD-1$^+$CD8$^+$ T cells in the dLNs while preserving PD-1$^-$CD8$^+$ T cells (Figure 4F–I). The CAR-T cells preferentially localized to the lymphocytic infiltration foci, possibly attributable to the high antigen load, and sustained their cell count and therapeutic effect in the SGs

throughout the treatment duration (Supplemental Figure 7D–F). Following treatment, the composition and proportions of immune cell subsets in the SGs, including macrophages, natural killer cells, $CD8^+$ T cells, $CD4^+$ T cells, and B cells, were similar to those in the control mice (Supplemental Figure 8A–G). Transcriptomic analysis revealed a marked reduction in inflammatory responses within the SGs and restored SG weight (Figure 4J, Supplemental Figure 7G). Inflammatory gene transcripts (eg, *Il2rb*, *Cxcl9*, Cxcl10, *GZMB*, *GZMK*, and *IFNG*) were significantly down-regulated, whereas tissue remodeling and repair-associated genes (eg, *Sox11*, *Sox4*, *Fscn1*, *Mmp9*, *Mmp2*, *Arg1*, and *Cd163*) were up-regulated (Figure 4K). Crucially, PD-1-targeted CAR-T cells did not impair SG function, as determined by SG weight, saliva flow rate, leukocyte count, and histopathology, nor induce damage to other organs in healthy control mice, underscoring their safety profile[43] (Supplemental Figure 7H–K). Additionally, in conjunction with the SGs inflammation reduction, CAR-T therapy facilitated an improvement in systemic inflammatory responses, as evidenced by the restoration of body weight in treated mice, without incurring mortality (Supplemental Figure 7L–N).

Given that SG $CD4^+$ T cells also expressed PD-1 and were significantly depleted by CAR-T cells (Supplemental Figure 7D and 8F), we investigated their contribution to the overall therapeutic efficacy of PD-1-targeted CAR-T cell using CD4-depleting antibodies (Supplemental Figure 9A and B). The findings indicated that CD4-depleting antibodies nearly eliminated all $CD4^+$ T cells in the SGs of SjD model mice but had minimal impact on overall SG inflammation (Supplemental Figure 9C–J, L, M) and tissue repair (Supplemental Figures 5E–K and 9K, N, O). However, CD4 depletion did partially restore saliva secretion rates and significantly reduced serum anti-SSA/Ro60 autoantibody levels (Supplemental Figure 9P–R). Collectively, our results substantiate that PD-1-targeted CAR-T cells effectively alleviate inflammation in SG of SjD model mice, primarily via the efficient elimination of pathogenic PD-1^+CD8^+ T cells.

Treatment with PD-1-targeted CAR-T cells restore the SG function in SjD model mice. Following CAR-T therapy, we noted an upregulation of tissue repair-associated genes in SjD model mice (Figure 4K) and conducted a comprehensive assessment of the morphologic structure and physiologic function of the SGs. Pathologic analysis revealed significant interlobular connective tissue proliferation, ductal damage, and acinar atrophy in the SG of SjD model mice (Figure 5A–C). These pathologic changes showed marked improvement post-PD-1-targeted CAR-T therapy (Figure 5A–C). We observed a significant increase in mRNA levels of ductal markers (*Epcam*, *Cdh1*, *Tjp1*, *Dcpp1* and *Klk1*) in the SGs of SjD model mice, suggesting abnormal ductal architecture regeneration that normalized following therapy (Figure 5D). Staining for E-cad (ductal cell marker), AQP5 (acinar cell marker), and Ki-67 consistently demonstrated improvements in ductal lumen dilation and atrophic acini (Figure 5E–I, Supplemental Figure 9K). However, no significant alterations were observed in acini cell proliferative capacity (Figure 5I), likely because of the timing of assessment occurring four weeks post-treatment, a period when it was already not the most vigorous stage of acinar cell proliferation. Additionally, the progression of interlobular and intralobular fibrosis, indicative of dysregulated connective tissue hyperplasia, was alleviated by CAR-T therapy, as evidenced by Masson staining (Figure 5J and K). Notably, the saliva flow rate, a key indicator of SG function, returned to baseline level following CAR-T cell treatment (Figure 5L). Collectively, our findings indicated that PD-1-targeted CAR-T cell therapy significantly improved SG function while maintaining a favorable safety profile in SjD model mice.

DISCUSSION

Current therapeutic approaches for SjD primarily focus on alleviating glandular symptoms and systemic manifestations; however, these strategies are predominantly empirical and frequently ineffective, often accompanied by significant adverse effects. There is a notable deficiency in effective therapeutic strategies that specifically target pathogenic cells, likely attributable to an insufficient understanding of the immune pathogenesis of SjD. Previous studies have identified potential pathogenic $CD8^+$ T cells in patients with SjD, characterized by the expression of *GZMK* and HLA-DR.[10,11] Our findings indicate that *GZMK*$^+$$CD8^+$ T cells in patients with SjD, along with high expression of HLA-DR, also significantly up-regulated PD-1 expression. The number of labial gland PD-1^+CD8^+ T cells in patients with SjD shows a positive correlation with clinical parameters, including focus score, IgA, RF, and ESR, but not with European League Against Rheumatism Sjögren's Syndrome Disease Activity Index (probably ascribable to the small proportion of our patients with clinically relevant systemic manifestations), suggesting that these cells represent a more specifically pathogenic subset in SjD. This hypothesis has also been validated in *IL12B*$^{-/-}$*IL2RA*$^{-/-}$ and NOD murine models, as identified by using scRNA-seq and flow cytometry, and further supported by PD-1-targeted CAR-T cell therapy depleting PD-1^+ $CD8^+$ T cells effectively alleviating SjD symptoms in *IL12B*$^{-/-}$*IL2RA*$^{-/-}$ murine model.

Although PD-1 is frequently regarded as a marker of $CD8^+$ T cell exhaustion in the context of tumors and chronic infections,[15–17] it is also an important marker of TCR activation, indicating full T cell activation and the acquisition of effector functions. Recent studies have demonstrated that in certain infections and chronic inflammatory diseases like autoimmune diseases,[18–20,43,44] T cells expressing high levels of PD-1 exhibited an effector phenotype rather than exhaustion. Moreover, PD-1 blockade has resulted in severe autoimmune complications in experimental allergic encephalomyelitis (EAE) and NOD mice,[18,44] whereas the depletion of PD-1^+ cells has been

shown to alleviate both EAE and type 1 diabetes.[24] In our SjD model, PD-1^{+}CD8^{+} T cells displayed enhanced cytotoxicity, as evidenced by increased expression of GZMB, Perforin, CD107a, and other cytotoxic molecules, along with elevated gene transcription of *GZMK*. In patients with SjD, these cells also exhibited high levels of HLA-DR expression and predominantly coexpressed *GZMK* with either *GZMB* or *GZMK* alone, indicating an activated and cytotoxic effector phenotype.

Autoantigen-specific T cells frequently develop an exhausted-like phenotype, for example, characterized by PD-1

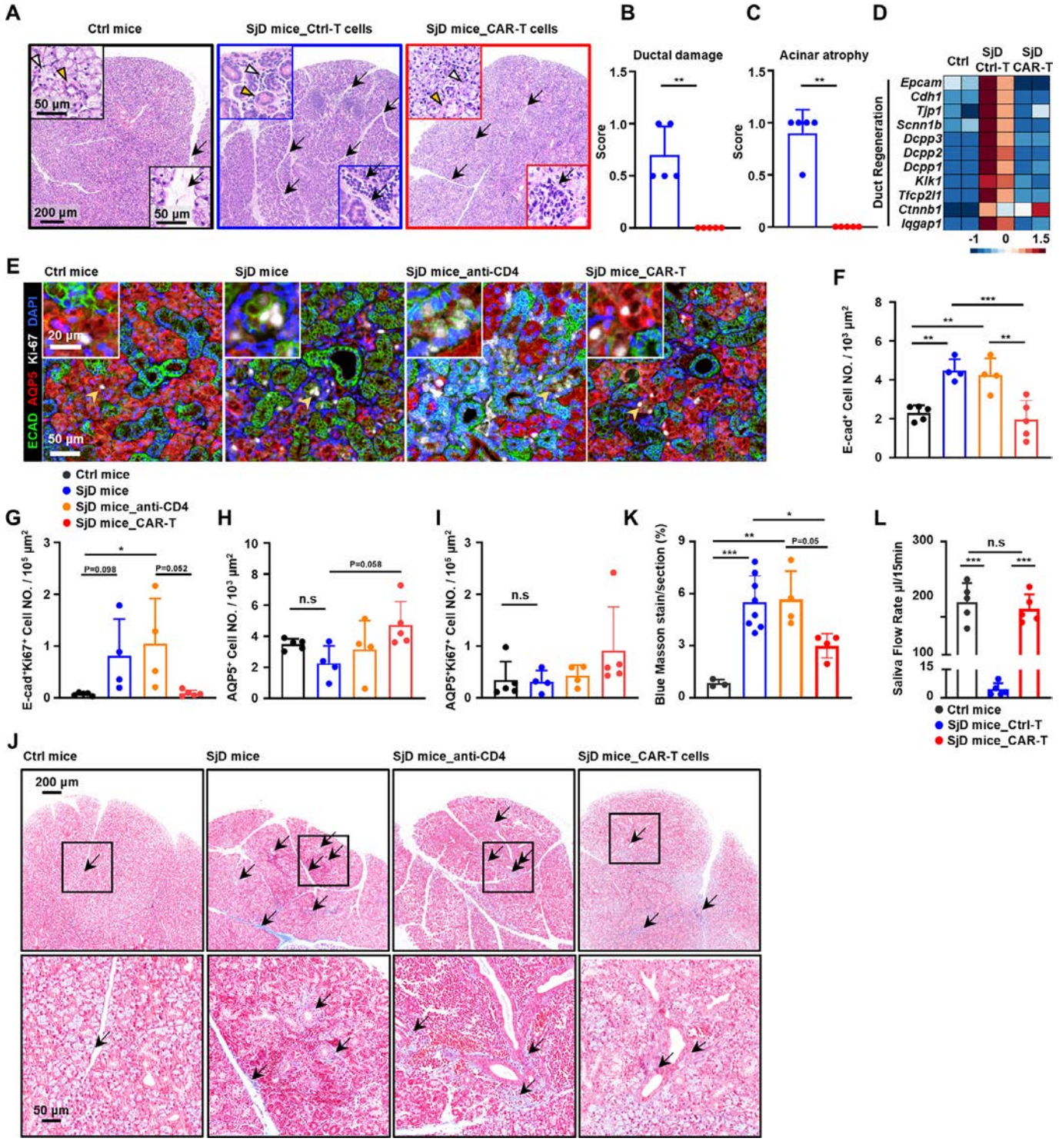

(Figure legend continues on next page.)

expression, to persist in autoimmune diseases.[45] PD-1 plays a critical role in the development and function of $CD8^+$ T cell memory.[46,47] We observed that PD-1^+CD8^+ T cells expressed a higher frequency of resident memory markers, such as CXCR6, CD69, CD49d, and CD103 in SGs from SjD model mice. These findings suggest that increased PD-1 expression on T cells in autoimmune diseases, in combination with Trm markers, may facilitate the localization and adaptation of T cells to the inflammatory environment under the chronic antigen stimulation, thereby prolonging their function and survival rather than leading to exhaustion. Nonetheless, the precise role of the PD-1 in SjD needs further investigation. Additionally, we identified $CD8^+$ T cells in dLNs that shared clones with SG $CD8^+$ Trm cells, exhibiting characteristics indicative of Trm precursors while expressing elevated levels of *GZMK* and PD-1, which is consistent with a hypothesis that Trm-precursor form in the lymph node lumen.[42] This finding reinforces our earlier conclusion that *GZMK*$^+CD8^+$ T cells in the periphery of patients with SjD served as precursors to glandular pathogenic $CD8^+$ Trm cells.[11] These potential precursor cells may contribute to the replenishment of SG PD-1^+CD8^+ Trm cells from the periphery. Consequently, effective treatment strategies should also target these precursor cells to prevent the replenishment of SG $CD8^+$ Trm from periphery.

In our previous study, we established that the depletion of $CD8^+$ T cells alleviated SjD-like symptoms in SjD model mice[12]; however, this strategy is not clinically feasible because of their critical role in antitumor and antiinfection immunity. In contrast, CAR-T therapy has shown promise in the treatment of autoimmune diseases by effectively depleting pathogenic cells in circulation and tissues while facilitating drug-free remission.[28,29,48] Unlike antibody-based therapies, which effeteness rely on antibody concentrations and availability of effector cells, CAR-T cells possess the capability to actively migrate and infiltrate solid organs, directly depleting the target cells, rendering them particularly suitable for autoimmune diseases that affect these organs.[49] Moreover, CAR-T cell therapy has demonstrated efficacy with minimal side effects in the treatment of other autoimmune and infectious diseases.[48] Therefore, with appropriate management of potential side effects, CAR-T therapy may provide a viable strategy for the management of SjD.

Based on a refined understanding of pathogenic $CD8^+$ T cell phenotypes, our study demonstrates that targeting PD-1^+CD8^+ T cells with CAR-T cells can specifically deplete PD-1^+CD8^+ T cells in the SGs, as well as their precursors in the periphery, thereby achieving therapeutic effects comparable with the total clearance of $CD8^+$ T cells.[12] Furthermore, PD-1-targeted CAR-T cell therapy promotes the restoration of compromised SG tissue, effectively addressing conditions such as acinar atrophy, ductal dilation, and interstitial fibrosis. This is consistent with prior research suggesting that *GZMK*$^+CD8^+$ T cells (or PD-1^+CD8^+ T cells) may play a role in acinar cell pathogenesis.[10] Tissue rejuvenation is likely facilitated by the presence of stem cells in the adult SG and the rapid proliferation of tissue cells.[50,51] Importantly, we opted to exclude lymphodepletion as a preconditioning step to eliminate potential bias in therapy assessment and to mitigate the risk of infection in SjD model mice. In fact, whether lymphocyte depletion is necessary for CAR-T therapy of patients with autoimmune disease is less clear; therefore, using animal models to determine the appropriate regimen is essential. Our findings confirm that CAR-T therapy can be both effective and safe in the absence of preconditioning, corroborating results observed in asthma models.[52] Additionally, the removal of $CD4^+$ T cells led to a partial increase in saliva secretion along with a decrease in anti-SSA autoantibodies, indicating that, compared with the direct cytotoxic effect of $CD8^+$ T cells, $CD4^+$ T cells may have a supportive role in the progression of SjD, whereas their targeting could provide limited therapeutic benefits. However, the depletion of PD-1^+ T cells may increase vulnerability to infections and malignancies, warranting caution. Future investigations should prioritize long-term treatment trials across diverse SjD mouse models to refine therapeutic approaches and broaden patient cohorts to further investigate the $CD8^+$ T cell phenotype in SjD. Taken together, our study offers insights for the development of therapeutic interventions for SjD and other chronic inflammatory conditions characterized by similar pathogenic $CD8^+$ T cell profiles.[20,32]

(Figure legend continued from previous page.)

Figure 5. Treatment with PD-1-targeted CAR-T cells restore the salivary gland function in SjD model mice. (A) Representative H&E staining images of control mice, SjD mice treated with Ctrl-T, and SjD mice treated with CAR-T cells. Scale bars represent 50 μm and 200 μm, as indicated. Black arrows point to interlobular connective tissue. Magnification highlights acinar (white triangles), ductal (orange triangles), and interlobular connective tissue (black arrows). (B and C) Scores for ductal damage (B) and acinar atrophy (C) in SjD mice treated with either Ctrl-T or CAR-T cells. (D) Heatmap of scaled normalized expression of selected genes in SGs. (E) Immunohistochemical images showing the expression of E-cad (green), AQP5 (red), and Ki-67 (white) in control mice, SjD mice, and SjD mice treated with anti-CD4, or CAR-T cells. Scale bars represent 20 μm and 50 μm, as indicated. (F–I) Quantification of the density of (F) E-cad$^+$ cells, (G) E-cad$^+$Ki67$^+$ cells, (H) AQP5$^+$ cells, and (I) AQP5$^+$Ki67$^+$ cells in SGs at four weeks post-CAR-T cell treatment. (J) Representative Masson's trichrome-stained images of SGs from control mice, SjD mice, and SjD mice treated with anti-CD4 or CAR-T cells. Scale bars represent 50 μm and 200 μm, as indicated. Black arrows indicate regions of interlobular and intralobular fibrosis. (K) Quantification of blue Masson stain area using ImageJ. (L) Quantification of saliva flow rate in control mice, SjD mice treated with Ctrl-T, and SjD mice treated with CAR-T cells (n = 5 mice per group). *$P < 0.05$, **$P < 0.01$, ***$P < 0.001$, Mann–Whitney U test (B and C), one-way ANOVA with Tukey's multiple comparisons test (F–I, K–L). Data are presented as mean ± SD. ANOVA, analysis of variance; CAR, chimeric antigen receptor; Ctrl-T, control T cell; H&E, hematoxylin and eosin; n.s., not significant; SG, salivary gland; SjD, Sjögren disease.

ACKNOWLEDGMENT

We thank Xin Li from Guangdong Provincial People's Hospital, Medical Research Institute, for providing valuable suggestions for the study.

AUTHOR CONTRIBUTIONS

All authors contributed to at least one of the following manuscript preparation roles: conceptualization AND/OR methodology, software, investigation, formal analysis, data curation, visualization, and validation AND drafting or reviewing/editing the final draft. As corresponding author, Dr Lian confirms that all authors have provided the final approval of the version to be published, and takes responsibility for the affirmations regarding article submission (eg, not under consideration by another journal), the integrity of the data presented, and the statements regarding compliance with institutional review board/Declaration of Helsinki requirements.

REFERENCES

1. Brito-Zerón P, Baldini C, Bootsma H, et al. Sjögren syndrome. Nat Rev Dis Primers 2016;2:16047.
2. Verstappen, GM, Pringle S, Bootsma H, Kroese FGM. Epithelial-immune cell interplay in primary Sjögren syndrome salivary gland pathogenesis. Nat Rev Rheumatol 2021;17(6):333–348.
3. Seror R, Nocturne G, Mariette X. Current and future therapies for primary Sjögren syndrome. Nat Rev Rheumatol 2021;17(8):475–486.
4. Chisholm DM, Mason DK. Labial salivary gland biopsy in Sjögren's disease. J Clin Pathol 1968;21(5):656–660.
5. Nocturne G, Mariette X. B cells in the pathogenesis of primary Sjögren syndrome. Nat Rev Rheumatol 2018;14(3):133–145.
6. Verstappen GM, Kroese FGM, Bootsma H. T cells in primary Sjögren's syndrome: targets for early intervention. Rheumatology (Oxford) 2021;60(7):3088–3098.
7. Lu C, Pi X, Xu W, et al. Clinical significance of T cell receptor repertoire in primary Sjogren's syndrome. EBioMedicine 2022;84:104252.
8. Yao Y, Ma J-F, Chang C, et al. Immunobiology of T cells in Sjögren's syndrome. Clin Rev Allergy Immunol 2021;60(1):111–131.
9. Mingueneau M, Boudaoud S, Haskett S, et al. Cytometry by time-of-flight immunophenotyping identifies a blood Sjögren's signature correlating with disease activity and glandular inflammation. J Allergy Clin Immunol 2016;137(6):1809–1821.e12.
10. Pranzatelli TJF, Perez P, Ku A, et al. GZMK+CD8+ T cells Target A specific acinar cell type in Sjögren's disease. Res Sq 2024:rs-3601404. doi: https://doi.org/10.21203/rs.3.rs-3601404/v1
11. Xu T, Zhu H-X, You X, et al. Single-cell profiling reveals pathogenic role and differentiation trajectory of granzyme K+CD8+ T cells in primary Sjögren's syndrome. JCI Insight 2023;8(8):e167490.
12. Gao CY, Yao Y, Li L, et al. Tissue-resident memory CD8+ T cells acting as mediators of salivary gland damage in a murine model of Sjögren's syndrome. Arthritis Rheumatol 2019;71(1):121–132.
13. Barr JY, Wang X, Meyerholz DK, et al. CD8 T cells contribute to lacrimal gland pathology in the nonobese diabetic mouse model of Sjögren syndrome. Immunol Cell Biol 2017;95(8):684–694.
14. Patsoukis N, Wang Q, Strauss L, et al. Revisiting the PD-1 pathway. Sci Adv 2020;6(38):eabd2712.
15. Iwai Y, Ishida M, Tanaka Y, et al. Involvement of PD-L1 on tumor cells in the escape from host immune system and tumor immunotherapy by PD-L1 blockade. Proc Natl Acad Sci U S A 2002;99(19):12293–12297.
16. Barber DL, Wherry EJ, Masopust, et al. Restoring function in exhausted CD8 T cells during chronic viral infection. Nature 2006;439(7077):682–687.
17. Sharpe AH, Pauken KE. The diverse functions of the PD1 inhibitory pathway. Nat Rev Immunol 2018;18(3):153–167.
18. Ansari MJ, Salama AD, Chitnis T, et al. The programmed death-1 (PD-1) pathway regulates autoimmune diabetes in nonobese diabetic (NOD) mice. J Exp Med 2003;198(1):63–69.
19. Petrelli A, Mijnheer G, van Konijnebburg DPH, et al. PD-1+CD8+ T cells are clonally expanding effectors in human chronic inflammation. J Clin Invest 2018;128(10):4669–4681.
20. Phadungsaksawasdi P, Fujuyama T, Kurihara K, et al. PD-1 expression defines epidermal CD8(+)CD103(+) T cells preferentially producing IL-17A and using skewed TCR repertoire in psoriasis. J Invest Dermatol 2021;141(10):2426–2435.e5.
21. Sibaud V. Dermatologic reactions to immune checkpoint inhibitors: skin toxicities and immunotherapy. Am J Clin Dermatol 2018;19(3):345–361.
22. Kuchroo JR, Hafler DA, Sharpe AH, et al. The double-edged sword: Harnessing PD-1 blockade in tumor and autoimmunity. Sci Immunol 2021;6(65):eabf4034.
23. Ramos-Casals M, Maria A, Suárez-Almazor ME, et al. Sicca/Sjögren's syndrome triggered by PD-1/PD-L1 checkpoint inhibitors. Data from the International ImmunoCancer Registry (ICIR). Clin Exp Rheumatol 2019;37 Suppl 118(3):114–122.
24. Zhao P, Wang P, Dong S, et al. Depletion of PD-1-positive cells ameliorates autoimmune disease. Nat Biomed Eng 2019;3(4):292–305.
25. Damo M, Hornick NI, Venkat A, et al. PD-1 maintains CD8 T cell tolerance towards cutaneous neoantigens. Nature 2023;619(7968):151–159.
26. Müller F, Boeltz S, Knitza J, et al. CD19-targeted CAR T cells in refractory antisynthetase syndrome. Lancet 2023;401(10379):815–818.
27. Kansal R, Richardson N, Neeli I, et al. Sustained B cell depletion by CD19-targeted CAR T cells is a highly effective treatment for murine lupus. Sci Transl Med 2019;11(482):eaav1648.
28. Mackensen A, Müller F, Mougiakakos D, et al. Anti-CD19 CAR T cell therapy for refractory systemic lupus erythematosus. Nat Med 2022;28(10):2124–2132.
29. Müller F, Taubmann J, Bucci L, et al. CD19 CAR T-cell therapy in autoimmune disease - a case series with follow-up. N Engl J Med 2024;390(8):687–700.
30. Vitali C, Bombardieri S, Jonsson R, et al. Classification criteria for Sjögren's syndrome: a revised version of the European criteria proposed by the American-European Consensus Group. Ann Rheum Dis 2002;61(6):554–558.
31. Shiboski CH, Shiboski SC, Seror R, et al. 2016 American College of Rheumatology/European League Against Rheumatism classification criteria for primary Sjögren's syndrome: a consensus and data-driven methodology involving three international patient cohorts. Arthritis Rheumatol 2017;69(1):35–45.
32. Jonsson AH, Zhang F, Dunlap G, et al. Granzyme K(+) CD8 T cells form a core population in inflamed human tissue. Sci Transl Med 2022;14(649):eabo0686.
33. Ahmadzadeh M, Johnson LA, Heemskerk B, et al. Tumor antigen-specific CD8 T cells infiltrating the tumor express high levels of PD-1 and are functionally impaired. Blood 2009;114(8):1537–1544.
34. Kumagai S, Togashi Y, Kamada T, et al. The PD-1 expression balance between effector and regulatory T cells predicts the clinical efficacy of PD-1 blockade therapies. Nat Immunol 2020;21(11):1346–1358.
35. Cruz-Tapias P, Rojas-Villarraga A, Maier-Moore S, et al. HLA and Sjögren's syndrome susceptibility. A meta-analysis of worldwide studies. Autoimmun Rev 2012;11(4):281–287.

36. Verstappen GM, Gao L, Pringle S, et al. The transcriptome of paired major and minor salivary gland tissue in patients with primary Sjögren's syndrome. Front Immunol 2021;12:681941.

37. Park Y-S, Gauna AE, Cha S. Mouse models of primary Sjogren's syndrome. Curr Pharm Des 2015;21(18):2350–2364.

38. Gearty SV, Dündar F, Zumbo P, et al. An autoimmune stem-like CD8 T cell population drives type 1 diabetes. Nature 2022;602(7895): 156–161.

39. Mellman I, Chen DS, Powles T, et al. The cancer-immunity cycle: indication, genotype, and immunotype. Immunity 2023;56(10):2188–2205.

40. Clarke J, Panwar B, Madrigal A, et al. Single-cell transcriptomic analysis of tissue-resident memory T cells in human lung cancer. J Exp Med 2019;216(9):2128–2149.

41. Zitti B, Hoffer E, Zheng W, et al. Human skin-resident CD8(+) T cells require RUNX2 and RUNX3 for induction of cytotoxicity and expression of the integrin CD49a. Immunity 2023;56(6):1285–1302.e7.

42. Kok L, Masopust D, Schumacher TN. The precursors of CD8(+) tissue resident memory T cells: from lymphoid organs to infected tissues. Nat Rev Immunol 2022;22(5):283–293.

43. Zhu H-X, Yang S-H, Gao C-Y, et al. Targeting pathogenic CD8(+) tissue-resident T cells with chimeric antigen receptor therapy in murine autoimmune cholangitis. Nat Commun 2024;15(1):2936.

44. Salama AD, Chitnis T, Imitola J, et al. Critical role of the programmed death-1 (PD-1) pathway in regulation of experimental autoimmune encephalomyelitis. J Exp Med 2003;198(1):71–78.

45. Saggau C, Bacher P, Esser D, et al. Autoantigen-specific CD4(+) T cells acquire an exhausted phenotype and persist in human antigen-specific autoimmune diseases. Immunity 2024;57(10):2416–2432.e8.

46. Pauken KE, Godec J, Odorizzi PM, et al. The PD-1 pathway regulates development and function of memory CD8(+) T cells following respiratory viral infection. Cell Rep 2020;31(13):107827.

47. Kalia V, Yuzefpolskiy Y, Vegaraju A, et al. Metabolic regulation by PD-1 signaling promotes long-lived quiescent CD8 T cell memory in mice. Sci Transl Med 2021;13(615):eaba6006.

48. Baker DJ, Arany Z, Bauer JA, et al. CAR T therapy beyond cancer: the evolution of a living drug. Nature 2023;619(7971):707–715.

49. Schett G, June CH. CAR T cells in autoimmune disease: on the road to remission. Immunity 2024;57(12):2705–2709.

50. Rocchi C, Barazzuol L, Coppes RP. The evolving definition of salivary gland stem cells. NPJ Regen Med 2021;6(1):4.

51. Pringle S, Van Os R, Coppes RP. Concise review: adult salivary gland stem cells and a potential therapy for xerostomia. Stem Cells 2013; 31(4):613–619.

52. Jin G, Liu Y, Wang L, et al. A single infusion of engineered long-lived and multifunctional T cells confers durable remission of asthma in mice. Nat Immunol 2024;25(6):1059–1072.

Arthritis & Rheumatology
Vol. 77, No. 8, August 2025, pp 1041–1051
DOI 10.1002/art.43129

American College of Rheumatology
Empowering Rheumatology Professionals

Efficacy, Safety, Pharmacokinetics, and Immunogenicity of ABBV-154 in Adults With Glucocorticoid-Dependent Polymyalgia Rheumatica: A Phase 2, Randomized, Double-Blind, Placebo-Controlled Trial

Robert F. Spiera,[1] Valerie Devauchelle-Pensec,[2] Claire E. Owen,[3] Federico Díaz-González,[4] Tsutomu Takeuchi,[5] Edit Drescher,[6] Jaclyn Anderson,[7] Dilek Arikan,[7] Ronilda D'Cunha,[7] Julie Parmentier,[7] Denise T. Kruzikas,[7] Weihan Zhao,[7] Yang Yang,[7] Karen Stellpflug,[7] and Frank Buttgereit[8]

Objective. An unmet need exists for glucocorticoid-sparing treatments for patients with polymyalgia rheumatica (PMR). The antibody-drug conjugate ABBV-154 comprises adalimumab conjugated to a glucocorticoid receptor modulator. We evaluated ABBV-154 versus placebo in patients with glucocorticoid-dependent PMR.

Methods. In this phase 2, randomized, double-blind, placebo-controlled, dose-ranging study, eligible patients had confirmed PMR, glucocorticoid response and two or more unequivocal PMR flares while tapering glucocorticoids and still on ≥5 mg daily prednisone equivalent. Randomized patients received subcutaneous placebo or ABBV-154 40, 150, or 340 mg once every other week. The primary efficacy endpoint was time to flare. The sponsor voluntarily terminated the study early.

Results. Overall, 181 patients were randomized (placebo, n = 50; ABBV-154: 40 mg, n = 42; 150 mg, n = 45; 340 mg, n = 44), and 67.4% completed study drug at week 24. Time to flare was longer for patients receiving ABBV-154 than those receiving placebo, with Kaplan-Meier estimate of 24-week flare-free rate being lower for placebo. The hazard ratios of ABBV-154 versus placebo were 0.49 (95% confidence interval [CI], 0.27–0.88), $P = 0.017$ for 40 mg; 0.44 (95% CI, 0.25–0.79), $P = 0.006$ for 150 mg; 0.20 (95% CI, 0.09–0.42), $P < 0.001$ for 340 mg. Incidences of treatment-emergent adverse events were similar between groups, and the most common across ABBV-154 cohorts was COVID-19 (16.0%).

Conclusion. Treatment effects were observed for ABBV-154 cohorts compared with placebo for time to flare. ABBV-154 was generally well tolerated. Due to early study termination, results should be interpreted with caution.

INTRODUCTION

Polymyalgia rheumatica (PMR) is an inflammatory rheumatic disease characterized by shoulder, neck, and hip pain and morning stiffness.[1] EULAR and American College of Rheumatology (ACR) treatment guidelines for PMR recommend oral glucocorticoids (prednisone or equivalent) for the shortest effective duration with individualized dose-tapering after achieving remission.[2]

ClinicalTrials.gov identifier: NCT04972968.
Supported by AbbVie Inc.
[1]Robert F. Spiera, MD: Hospital for Special Surgery and Weill Medical College of Cornell University, New York, New York; [2]Valerie Devauchelle-Pensec, MD, PhD: INSERM U 1227, Brest University Hospital, Brest, France; [3]Claire E. Owen, PhD: Austin Clinical School, University of Melbourne, Melbourne, Victoria, Australia; [4]Federico Díaz-González, MD, PhD: Hospital Universitario de Canarias and Universidad de La Laguna, La Laguna, Spain; [5]Tsutomu Takeuchi, MD, PhD: Keio University School of Medicine, Shinjuku-ku, Tokyo, and Saitama Medical University, Saitama, Japan; [6]Edit Drescher, MD: Csolnoky Ferenc Hospital, Veszprém, Hungary; [7]Jaclyn Anderson, DO, MS, Dilek Arikan, MD, Ronilda D'Cunha, PhD, Julie Parmentier, MS, Denise T. Kruzikas, PhD, MPH, Weihan Zhao, PhD, Yang Yang, PhD, Karen Stellpflug, MD: AbbVie Inc., North Chicago, Illinois; [8]Frank Buttgereit, MD: Charité – Universitätsmedizin Berlin, corporate member of Freie Universität Berlin and Humboldt-Universität zu Berlin, Berlin, Germany.

AbbVie is committed to responsible data sharing regarding the clinical trials we sponsor. This includes access to anonymized individual and trial-level data (analysis data sets), as well as other information (eg, protocols, clinical study reports, or analysis plans), as long as the trials are not part of an ongoing or planned regulatory submission. This includes requests for clinical trial data for unlicensed products and indications. These clinical trial data can be requested by any qualified researchers who engage in rigorous, independent, scientific research and will be provided following review and approval of a research proposal and Statistical Analysis Plan (SAP) and execution of a Data Sharing Agreement (DSA). Data requests can be submitted at any time after approval in the United States and Europe and after acceptance of this manuscript for publication. These data will be accessible for 12 months, with possible extensions considered. For more information on the process or to submit a request, visit the following link: https://vivli.org/ourmember/abbvie/ then select "Home."

Additional supplementary information cited in this article can be found online in the Supporting Information section (https://acrjournals.onlinelibrary.wiley.com/doi/10.1002/art.43129).

Author disclosures are available at https://onlinelibrary.wiley.com/doi/10.1002/art.43129.

Address correspondence via email to Robert F. Spiera, MD, at spierar@hss.edu.

Submitted for publication August 30, 2024; accepted in revised form January 17, 2025.

Unfortunately, glucocorticoid reduction can lead to PMR flares, resulting in continued long-term glucocorticoid use and potential glucocorticoid-associated morbidity.[3–5] In one meta-analysis (>2,000 patients), glucocorticoid usage was 77%, 51%, and 25% at one, two, and five years, respectively.[6] In a registry study of 16,703 patients with PMR in the United States, 64% were still receiving glucocorticoids beyond one year.[7] Higher mean cumulative glucocorticoid doses are associated with adverse events (AEs) such as osteoporosis ($P < 0.0001$), fragility fractures ($P < 0.0001$), and arterial hypertension ($P = 0.01$), especially in patients receiving glucocorticoids for more than two years.[8] Long-term glucocorticoid use has been associated with development of hyperglycemia, insulin resistance, and other metabolic effects.[9]

Although interleukin-6 receptor antagonists (sarilumab or tocilizumab) or methotrexate are used to treat patients with PMR, glucocorticoids remain the primary treatment option.[2,7,10,11] Thus, an unmet need exists for glucocorticoid-sparing treatments for PMR, but PMR pathophysiology remains poorly defined, making identifying potential therapeutic targets a challenge.

ABBV-154 is a novel antibody-drug conjugate (ADC) comprising adalimumab (a human monoclonal anti–tumor necrosis factor [TNF]) antibody) conjugated to a proprietary glucocorticoid receptor modulator (GRM payload; an agonist of the glucocorticoid receptor that stimulates anti-inflammatory glucocorticoid-like effects).[12] By delivering the GRM payload to cells expressing transmembrane TNF, including activated immune cells, ABBV-154 was designed to reduce systemic glucocorticoid exposure and risks of related side effects.[13] ABBV-154 has been evaluated for PMR, rheumatoid arthritis, and Crohn disease in phase 2 clinical trials.[12] Although elevated levels of TNF were reported in symptomatic patients with PMR,[14,15] studies of anti-TNF treatments have yielded mixed results, leaving the role of TNF in the disease pathology unclear.[16–21] Therefore, the primary mechanism of action of ABBV-154 is expected via the anti-inflammatory effects of the intracellular GRM payload.

We report the results of a placebo-controlled study (AIM-PMR) evaluating efficacy and safety of ABBV-154 in patients with glucocorticoid-dependent PMR receiving doses of ≥5 mg/day prednisone or equivalent.

PATIENTS AND METHODS

Study design and treatment. AIM-PMR (study M20-370; NCT04972968) was a phase 2, randomized, double-blind, placebo-controlled, dose-ranging study conducted September 9, 2021, to July 24, 2023, across 70 centers in Australia, Austria, Canada, France, Germany, Hungary, Italy, Japan, Netherlands, New Zealand, Poland, Spain, United Kingdom, and the United States. The sponsor voluntarily terminated the study on April 27, 2023, after review of interim data and determining that ABBV-154 did not demonstrate an adequately differentiated benefit-risk profile compared with available therapies. Development of ABBV-154 was discontinued based on the totality of data reviewed from studies on PMR, rheumatoid arthritis, and Crohn disease. The study was terminated before the planned primary analysis, which would have occurred after all patients had completed the week 24 visit or withdrawn from the study.

Per the study protocol, patients were randomized to treatment arms in a 2:1:1:1 ratio of placebo administered subcutaneously (SC) or ABBV-154 SC once every other week in 40-mg, 150-mg, or 340-mg doses. All patients received study drug in combination with an identical glucocorticoid taper (see Supplementary Table 1). The protocol was amended (February 2022) to a randomization ratio of 1:1:1:1 for each treatment arm, thereby decreasing the number of patients randomized to placebo. At baseline, patients received the same dose of oral prednisone/prednisolone (5–15 mg/day, rounded to the nearest milligram [provided by the sponsor]) as they had received immediately before the baseline visit. Beginning at week 3, all patients tapered glucocorticoid per identical schedules (Supplementary Table 1), based on the baseline glucocorticoid dose, to reach 0 mg/day by week 24. Patients remained off glucocorticoids unless a confirmed PMR flare occurred. Study visits occurred at baseline, week 1, week 2, and every other week for 52 weeks (per protocol), with a safety follow-up visit performed approximately 70 days after the last study drug dose.

The independent ethics committee or institutional review board at each study site reviewed and approved the study protocol, informed consent forms, and recruitment materials before patient enrollment. The study was conducted in accordance with the International Conference for Harmonisation guidelines, applicable regulations, and the Declaration of Helsinki. All patients provided written informed consent before screening or undergoing any study-specific procedures.

Patients and eligibility criteria. Enrolled patients (aged ≥50 years) met the 2012 EULAR/ACR provisional classification criteria for PMR[22] and had a confirmed PMR diagnosis. Eligible patients must have experienced a clinical response to glucocorticoids following PMR diagnosis and must have had two or more episodes of unequivocal PMR flare while attempting to taper glucocorticoids (prednisone dose ≥5 mg/day or equivalent at the time of flare and the most recent flare within 24 weeks of baseline). Unequivocal PMR flare was defined as clinical signs and symptoms of PMR (shoulder and/or hip girdle pain with inflammatory stiffness, neck pain with inflammatory stiffness, or new or worsened limited range of motion in the hips and/or shoulders) resulting in increased glucocorticoid dose. Inflammatory stiffness associated with flares was determined by the expert clinical judgments of the investigators based on patient-reported symptoms and findings on physical examination; however, the study protocol did not specify any assessment of specific markers of inflammation. Patients must not have exhibited any clinical signs or symptoms of PMR within two weeks of baseline. They must have

received a stable glucocorticoid dose (prednisone 5–15 mg/day or equivalent) for two or more weeks before baseline and must not have been treated with a prior TNF antagonist. Patients with giant cell arteritis, rheumatoid arthritis, inflammatory arthritis not due to PMR, or a positive test for anticitrullinated protein were ineligible.

Assessments. The primary efficacy endpoint was time to flare (defined as the presence of clinical signs and symptoms of PMR and requirement to increase the glucocorticoid dose per investigators). A subgroup analysis of time to flare by time since most recent flare before baseline (≤12 weeks vs >12 weeks) was conducted. Secondary efficacy endpoints were achievement of flare-free state up to week 24, mean cumulative glucocorticoid dose by week 24, and change from baseline in glucocorticoid dose at week 24. Additional efficacy endpoints at week 24 were achievement of erythrocyte sedimentation rate (ESR) ≤30 mm/h, achievement of high-sensitivity C-reactive protein (hsCRP) less than or equal to the upper limit of normal (ULN), and time to flare based on Polymyalgia Rheumatica Activity Score (PMR-AS) increase from baseline by ≥6.6 and also by ≥9.35. The PMR-AS is a composite score that combines hsCRP, patient-reported pain on a numerical rating scale (NRS; 0–10, higher scores indicating worse pain), Physician Global Assessment of Disease Activity (NRS 0–10; higher scores noting more activity), morning stiffness duration in minutes × 0.1, and elevation of upper limbs (scale of 3–0, with higher scores specifying less elevation).

Patient-reported outcome endpoints included pain severity measured by NRS, stiffness severity measured by NRS (0–10, with higher scores indicating more stiffness), duration of morning stiffness, and the Health Assessment Questionnaire Disability Index (HAQ-DI; scale of 0–3, with higher scores noting more disability). Pain and stiffness severity were based on patient-recorded daily diaries. Analyses of stiffness duration and HAQ-DI were based on data collected at site visits every four weeks. All patient-reported outcome endpoints were evaluated for change from baseline to week 24.

Concentrations of ABBV-154 (ie, serum ADC), serum total antibody, and plasma unconjugated GRM payload were measured at multiple postbaseline timepoints, including week 24 in patients who received ABBV-154. Development of antidrug antibodies (ADAs) to ABBV-154 was also evaluated from blood samples taken at baseline and every four weeks afterwards through the end of the study; if confirmed positive, titers were measured. Samples with confirmed ADA positivity were further evaluated using a validated neutralizing antibody (nAb) assay.

Safety assessments included monitoring treatment-emergent AEs (TEAEs), defined as AEs that begin or worsen either on or after the first dose of study drug and within 70 days after the last dose of study drug. Any AEs of special interest (AESIs) were also monitored, including serious infections, opportunistic infections, active tuberculosis, serious allergic reactions, hypersensitivity reactions, malignancies, systemic glucocorticoid side effects, adrenal insufficiency, and iatrogenic Cushing syndrome. Investigators monitored signs and symptoms of adrenal insufficiency (eg, nausea, vomiting, lightheadedness, paleness, weight loss, hypotension, electrolyte abnormalities); if suspected, further assessment and management followed local standard of care. All TEAEs were coded using the Medical Dictionary of Regulatory Activities version 26.0. Safety assessments included laboratory analyses (hematology, clinical chemistry, and urinalysis parameters), vital signs, body weight monitoring, and 12-lead electrocardiogram evaluations.

Statistical analyses. Because the goal of this study was to obtain initial data on efficacy and dose-response relationships, a sample size of 40 patients in each treatment group was planned to ensure appropriate accrual of flares, based on an assumption of a total of 37 flares in the ABBV-154 340-mg group and the placebo group, and provided >90% power to detect a hazard ratio (HR) of 0.296 at a two-sided significance level of 0.1. The primary analysis was planned to occur when the last patient reached their week 24 visit, and at that point in time, many other patients could have completed subsequent visits or the entire study. Thus, the HR of 0.296 was determined on the assumption that flares would occur during glucocorticoid tapering and up to 12 weeks afterward (up to week 36) and that 70% and 30% of patients would still be flare free by week 36 in the ABBV-154 340-mg and placebo groups, respectively. However, due to the voluntary early study termination, data were limited due to sample size and duration of study drug exposure.

Efficacy was evaluated in the intent-to-treat population (randomized patients who received one or more doses of study drug). Safety was evaluated in the safety population (randomized patients who received one or more doses of study drug).

For time-to-event endpoints, the number of events was compared between each ABBV-154 dose and placebo based on log-rank test with stratification factors. Median time to event and flare-free rate (point and 95% confidence interval [CI]) for each group were reported based on Kaplan-Meier curves. HRs and corresponding CIs for each ABBV-154 group compared with placebo were estimated using Cox regression analysis adjusting for stratification factors. *P* values were provided by log-rank test with stratification factors. For all analyses of time-to-event endpoints, patients without an event at the time of the analysis were administratively censored at the time of the last available assessment.

Categorical variables were assessed by comparison between each ABBV-154 dose and placebo using the Cochran-Mantel-Haenszel test, adjusting for stratification factors, with nonresponder imputation incorporating multiple imputation to handle missing data due to COVID-19. To handle missing values, continuous variables, other than glucocorticoid dose, were compared between each ABBV-154 dose and placebo based on the

mixed-effect model repeated measures adjusting for visit, interaction between treatment and visit, actual values of stratification factors as fixed factors, and baseline value as a covariate. Glucocorticoid dose was analyzed by comparing each ABBV-154 dose and placebo based on analysis of covariance, adjusting for stratification factors as fixed factors and baseline glucocorticoid dose as a covariate.

RESULTS

Patients. Overall, 235 patients were screened; 181 patients were randomized and dosed (placebo, n = 50; ABBV-154: 40 mg, n = 42; 150 mg, n = 45; 340 mg, n = 44) (Figure 1). Furthermore, 67.4% of patients completed study drug to week 24; the most common reason for study drug discontinuation was termination of the study by the sponsor (n = 40 [22.1%]). In total, 19.3% of patients completed study drug to week 52, with termination of the study by the sponsor remaining the most common reason for discontinuation from study drug for 112 (61.9%) patients.

The mean overall age (69.4 years) of patients was relatively balanced between treatment groups (Table 1). Most patients were female (64.6%) and White (87.8%). The median overall duration of PMR was 1.6 years; 59.6% of patients reported their most recent flare within ≤12 weeks of baseline. Most patients (61.3%) had received glucocorticoid treatment for PMR more than one year before baseline, and the median glucocorticoid dose was 10 mg/day at baseline.

The mean ± SD duration of study drug exposure in the placebo group was 235.2 ± 109.0 days and in the ABBV-154 cohorts was 239.9 ± 95.7 days with 40 mg, 234.6 ± 106.3 days with 150 mg, and 230.3 ± 89.8 days with 340 mg.

Efficacy. The primary endpoint, time to flare, was longer for patients in the ABBV-154 cohorts than in the placebo cohort (Figure 2A), with 24-week flare-free rate based on Kaplan-Meier estimate being lower for placebo. The HRs of ABBV-154 vs placebo were 0.49 (95% CI, 0.27–0.88), $P = 0.017$ for the 40 mg ABBV-154 dose; 0.44 (95% CI, 0.25–0.79), $P = 0.006$ for 150 mg; and 0.20 (95% CI, 0.09–0.42), $P < 0.001$ for 340 mg. In a subgroup analysis of time to flare by time since most recent flare before baseline, a numerically higher proportion of patients with flares ≤12 weeks before baseline had flares regardless of treatment group than patients with flares >12 weeks before baseline (placebo, 74.1% vs 59.1%; ABBV-154 40 mg, 60.9% vs 23.5%; ABBV-154 150 mg, 44.0% vs 35.0%; ABBV-154 340 mg, 22.6% vs 15.4%, respectively). Based on Kaplan-Meier estimate among patients with flares ≤12 weeks before baseline, the estimated 24-week flare-free rates were lower with placebo than any ABBV-154 dose group. The HRs of ABBV-154 versus placebo were 0.59 (95% CI, 0.29–1.19), $P = 0.140$ for the 40-mg dose; 0.37 (95% CI, 0.17–0.78), $P = 0.009$ for the 150-mg

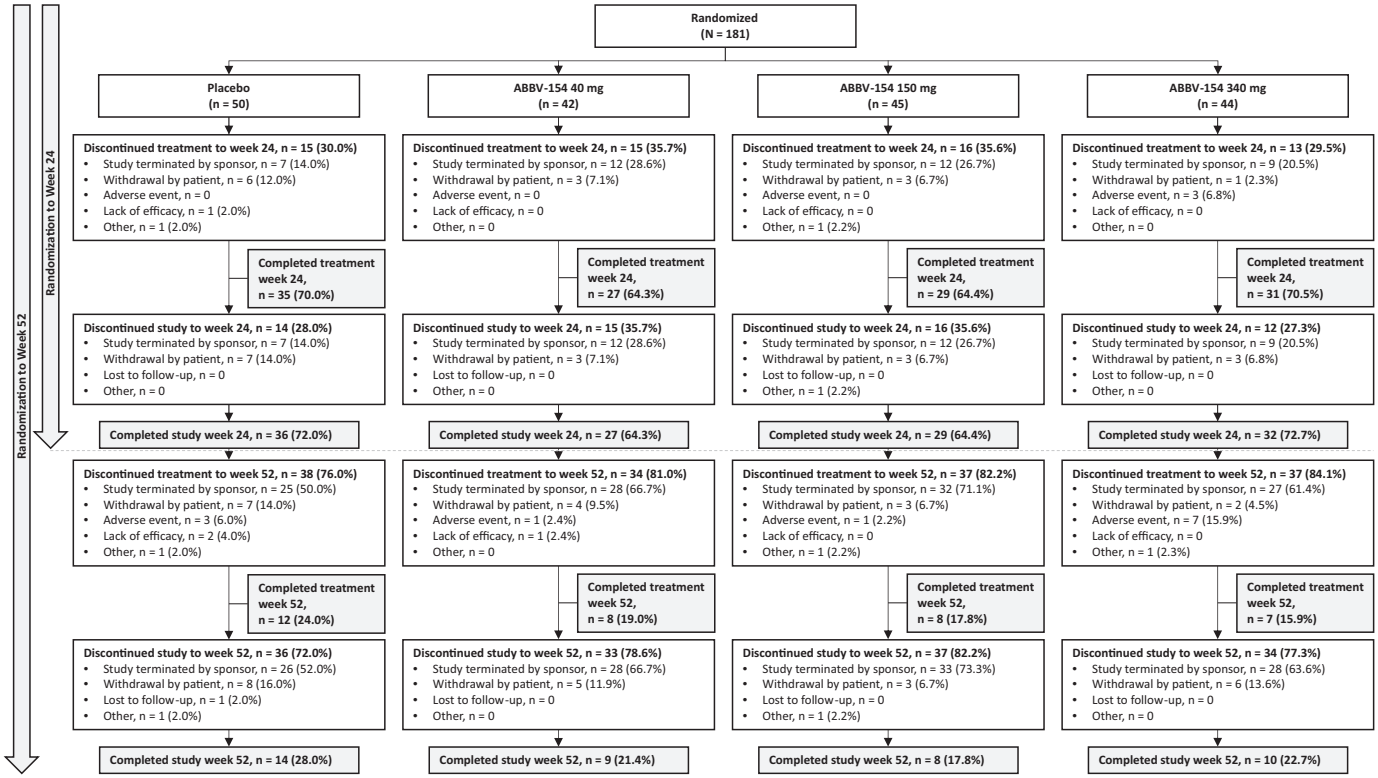

Figure 1. Patient disposition during the double-blind treatment period (full analysis set).

Table 1. Baseline demographics and disease characteristics (full analysis set)*

Characteristic	Placebo (n = 50)	ABBV-154 40 mg (n = 42)	ABBV-154 150 mg (n = 45)	ABBV-154 340 mg (n = 44)
Female, n (%)	33 (66.0)	30 (71.4)	25 (55.6)	29 (65.9)
Age, y, mean ± SD	71.0 ± 7.2	67.5 ± 8.0	69.8 ± 8.3	69.1 ± 6.2
Race, n (%)				
White	42 (84.0)	37 (88.1)	41 (91.1)	39 (88.6)
Asian	8 (16.0)	5 (11.9)	4 (8.9)	5 (11.4)
Hispanic or Latino, n (%)	1 (2.0)	0	2 (4.4)	2 (4.5)
BMI, mean ± SD	28.2 ± 5.5	28.4 ± 5.5	27.9 ± 4.5	29.1 ± 5.1
Duration of PMR, y, median (range)	2.0 (0.2–22.1)	1.2 (0.3–10.5)	1.3 (0.3–11.3)	1.8 (0.3–12.0)
Time since last PMR flare,[a] n (%)	49	40	45	44
≤12 wk	27 (55.1)	23 (57.5)	25 (55.6)	31 (70.5)
>12 wk	22 (44.9)	17 (42.5)	20 (44.4)	13 (29.5)
hsCRP ± mg/L, mean ± SD	8.6 ± 14.4	5.0 ± 8.5	4.4 ± 6.9	5.2 ± 13.0
ESR ± mm/h, mean ± SD	25.1 ± 17.2	22.7 ± 17.6	17.6 ± 14.1	18.9 ± 15.2
Glucocorticoid dose (mg/day),[b] mean ± SD	9.2 (3.8)	9.5 (3.4)	9.1 (3.5)	9.5 (3.3)
Duration of prior glucocorticoid treatment for PMR, n (%)				
≤1 y	16 (32.0)	17 (40.5)	18 (40.0)	19 (43.2)
>1 y	34 (68.0)	25 (59.5)	27 (60.0)	25 (56.8)
Prior bDMARDs and/or csDMARDs, n (%)				
bDMARD[c]	0	1 (2.4)	0	2 (4.5)
csDMARD[d]	16 (32.0)	15 (35.7)	10 (22.2)	17 (38.6)
Pain NRS, mean ± SD; n	3.4 ± 2.6; 49	3.0 ± 2.8	2.9 ± 2.4; 44	3.2 ± 2.7; 43
Stiffness NRS, mean ± SD; n	2.0 ± 1.9; 26	2.3 ± 2.5; 24	3.1 ± 2.0; 29	2.6 ± 2.6; 22
HAQ-DI, mean ± SD; n	0.7 ± 0.6; 49	0.7 ± 0.6; 40	0.6 ± 0.6; 41	0.7 ± 0.6; 41

* BMI, body mass index; bDMARD, biologic disease-modifying antirheumatic drug; csDMARD, conventional synthetic disease-modifying antirheumatic drug; ESR, erythrocyte sedimentation rate; HAQ-DI, Health Assessment Questionnaire Disability Index; hsCRP, high-sensitivity C-reactive protein; NRS, numerical rating scale; PMR, polymyalgia rheumatica.
[a] Percentages calculated on nonmissing values.
[b] Glucocorticoid dose is calculated based on the prednisone equivalent dose.
[c] Sarilumab or tocilizumab.
[d] Azathioprine, bucillamine, iguratimod, leflunomide, methotrexate/methotrexate sodium, sulfasalazine, or tacrolimus monohydrate.

dose; and 0.15 (95% CI, 0.06–0.38), $P < 0.001$ for the 340-mg dose (Figure 2B). The 24-week flare-free rate was lower with placebo than with ABBV-154 in those who experienced their last flare >12 weeks before baseline. The HRs of ABBV-154 versus placebo were 0.27 (95% CI, 0.08–0.88), $P = 0.030$ for the 40-mg dose; 0.44 (95% CI, 0.17–1.15), $P = 0.093$ for the 150-mg dose; and 0.22 (95% CI, 0.05–1.03), $P = 0.054$ for the 340-mg dose (Figure 2C).

Secondary endpoints included achievement of flare-free state up to week 24, cumulative glucocorticoid dose by week 24, and change from baseline in glucocorticoid dose at week 24. Compared with patients receiving placebo (28.2%; 95% CI, 14.1–42.3), a higher proportion of patients receiving ABBV-154 achieved a flare-free state up to week 24 (40 mg: 46.4% [95% CI, 28.0–64.9]; $P = 0.107$; 150 mg: 46.9% [95% CI, 29.6–64.2]; $P = 0.092$; 340 mg: 70.6% [95% CI, 55.3–85.9]; $P < 0.001$) (Figure 3).

The mean (95% CI) treatment difference (ABBV-154 – placebo) showed that cumulative glucocorticoid dose by week 24 was higher for patients receiving placebo than ABBV-154 (ABBV-154 40 mg, –88.7 mg [95% CI, –208.0 to 30.7]; $P = 0.144$; ABBV-154 150 mg, –164.8 mg [95% CI, –283.6 to –45.9]; $P = 0.007$; ABBV-154 340 mg, –182.6 mg [95% CI, –300.5 to –64.6]; $P = 0.003$) (Figure 4A). Also, the mean (95% CI) treatment difference for change from baseline in daily glucocorticoid dose at week 24 supported that patients receiving placebo experienced smaller reductions in glucocorticoid use than those receiving ABBV-154 (ABBV-154 40 mg, –1.6 [95% CI, –3.1 to –0.1]; $P = 0.039$; ABBV-154 150 mg, –2.7 [95% CI, –4.2 to –1.2]; $P < 0.001$; ABBV-154 340 mg, –3.0 [95% CI, –4.5 to –1.5]; $P < 0.001$) (Figure 4B).

Compared with placebo, more patients receiving ABBV-154 achieved ESR ≤30 mm/h (difference in response rate ABBV-154 vs placebo: 40 mg, 15.6% [95% CI, –0.1–31.3]; $P = 0.051$; 150 mg, 23.9% [95% CI, 7.4–40.4]; $P = 0.005$; 340 mg, 33.5% [95% CI, 17.0–49.9]; $P < 0.001$) (Supplementary Figure 1A). Similarly, compared with placebo, a higher proportion of patients receiving ABBV-154 achieved hsCRP less than or equal to the ULN (difference in response rate ABBV-154 vs placebo: 40 mg, 9.2% [95% CI, –6.1 to 24.4]; $P = 0.239$; 150 mg, 16.7% [95%

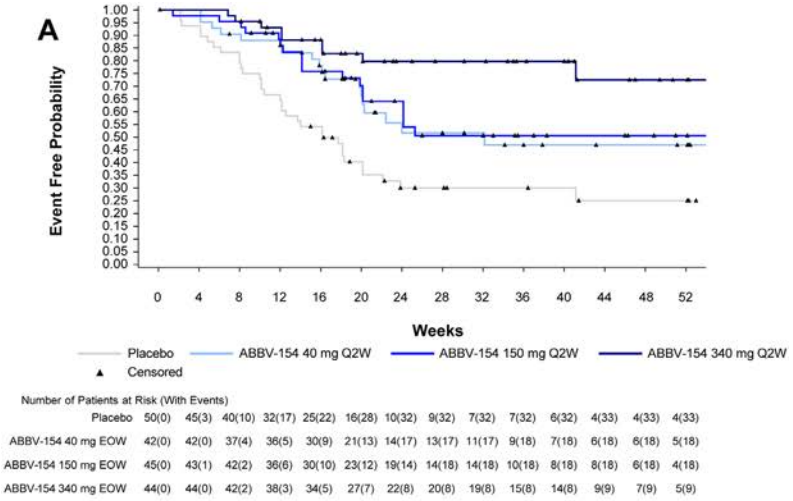

Number of Patients at Risk (With Events)

Placebo	50(0)	45(3)	40(10)	32(17)	25(22)	16(28)	10(32)	9(32)	7(32)	7(32)	6(32)	4(33)	4(33)	4(33)
ABBV-154 40 mg EOW	42(0)	42(0)	37(4)	36(5)	30(9)	21(13)	14(17)	13(17)	11(17)	9(18)	7(18)	6(18)	6(18)	5(18)
ABBV-154 150 mg EOW	45(0)	43(1)	42(2)	36(6)	30(10)	23(12)	19(14)	14(18)	14(18)	10(18)	8(18)	8(18)	6(18)	4(18)
ABBV-154 340 mg EOW	44(0)	44(0)	42(2)	38(3)	34(5)	27(7)	22(8)	20(8)	19(8)	15(8)	14(8)	9(9)	7(9)	5(9)

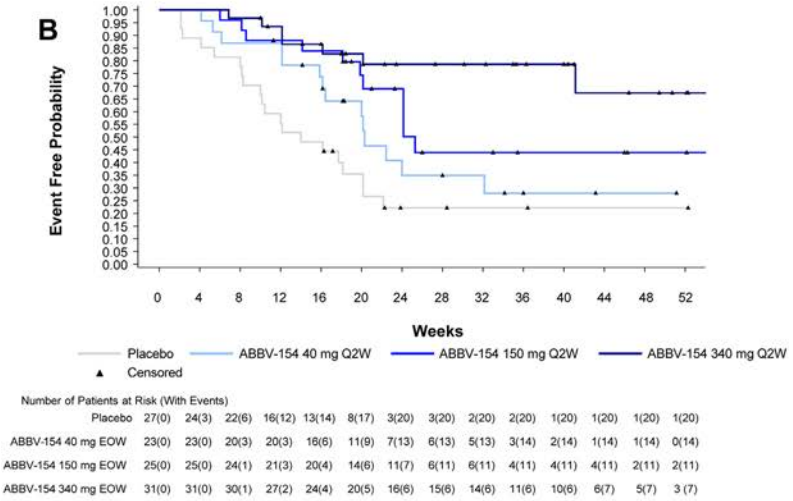

Number of Patients at Risk (With Events)

Placebo	27(0)	24(3)	22(6)	16(12)	13(14)	8(17)	3(20)	3(20)	2(20)	2(20)	1(20)	1(20)	1(20)	1(20)
ABBV-154 40 mg EOW	23(0)	23(0)	20(3)	20(3)	16(6)	11(9)	7(13)	6(13)	5(13)	3(14)	2(14)	1(14)	1(14)	0(14)
ABBV-154 150 mg EOW	25(0)	25(0)	24(1)	21(3)	20(4)	14(6)	11(7)	6(11)	6(11)	4(11)	4(11)	4(11)	2(11)	2(11)
ABBV-154 340 mg EOW	31(0)	31(0)	30(1)	27(2)	24(4)	20(5)	16(6)	15(6)	14(6)	11(6)	10(6)	6(7)	5(7)	3 (7)

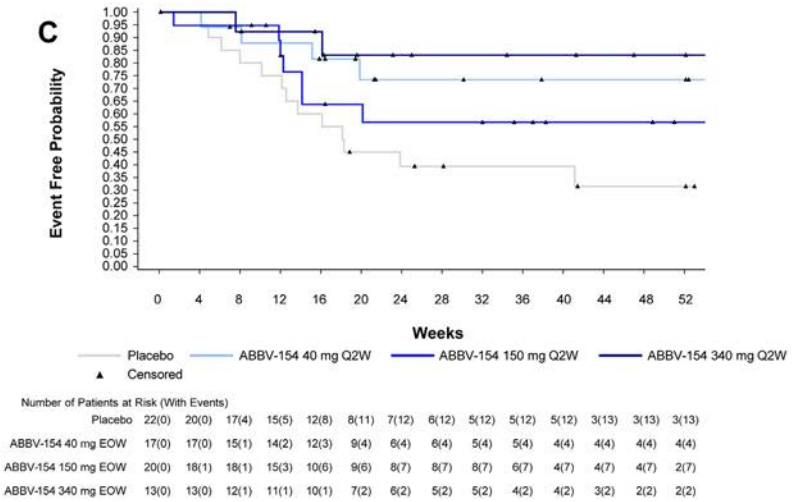

Number of Patients at Risk (With Events)

Placebo	22(0)	20(0)	17(4)	15(5)	12(8)	8(11)	7(12)	6(12)	5(12)	5(12)	5(12)	3(13)	3(13)	3(13)
ABBV-154 40 mg EOW	17(0)	17(0)	15(1)	14(2)	12(3)	9(4)	6(4)	6(4)	5(4)	5(4)	4(4)	4(4)	4(4)	4(4)
ABBV-154 150 mg EOW	20(0)	18(1)	18(1)	15(3)	10(6)	9(6)	8(7)	8(7)	8(7)	6(7)	4(7)	4(7)	4(7)	2(7)
ABBV-154 340 mg EOW	13(0)	13(0)	12(1)	11(1)	10(1)	7(2)	6(2)	5(2)	5(2)	4(2)	4(2)	3(2)	2(2)	2(2)

Figure 2. Kaplan-Meier curves for time to flare (ITT population). (A) Time to flare overall, (B) time to flare in patients whose most recent flare occurred ≤12 weeks before baseline, and (C) time to flare in patients whose most recent flare occurred >12 weeks before baseline. EOW, every other week; ITT, intent-to-treat; Q2W, every two weeks.

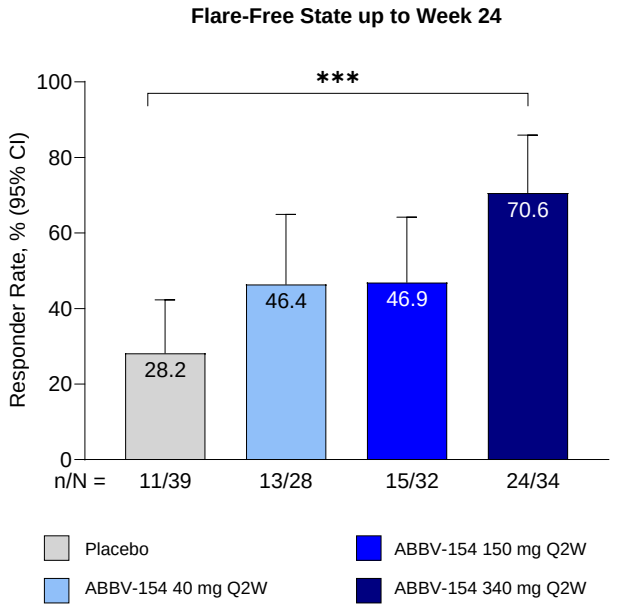

Figure 3. Proportion of patients achieving flare-free state at week 24 (ITT population). The 95% CI for the response rate is based on the normal approximation to the binomial distribution. The *P* value for the difference between each ABBV-154 group and the placebo group is from Cochran-Mantel-Haenszel test adjusting for baseline randomization stratification factors (glucocorticoid use at baseline [≥10 mg/day; <10 mg/day prednisone equivalent]) and length of prior glucocorticoid treatment for PMR (≤1 year; >1 year). Patients with missing assessments who were flare free at the previous visit were imputed as flare free for the missing assessment. Missing assessments for patients who had a flare or had intercurrent events were imputed as flare. *** $P < 0.001$. CI, confidence interval; ITT, intent-to-treat; PMR, polymyalgia rheumatica; Q2W, every two weeks.

CI, 0.2–33.3]; $P = 0.047$; 340 mg, 30.8% [95% CI, 13.6–48.1]; $P < 0.001$) (Supplementary Figure 1B).

Patient-reported outcomes. Patient-reported outcomes are reported at week 24. The weekly average patient assessment of pain severity was reduced compared with placebo from baseline through the majority of study weeks in the ABBV-154 340-mg group (week 24: placebo: 0.3, 95% CI, –0.4 to 0.9; ABBV-154 340 mg: –1.1, 95% CI, –1.7 to –0.6; $P = 0.002$) (Supplementary Figure 2A).

Compared with placebo (1.8; 95% CI, 0.7–2.8), stiffness severity reduced in weekly average rating from baseline in the ABBV-154 150 mg (–0.3, 95% CI, –1.0 to 0.4; $P = 0.001$) and 340 mg groups (–1.3, 95% CI, –2.1 to –0.5; $P < 0.001$) (Supplementary Figure 2B).

The duration of morning stiffness did not change from baseline, except in the ABBV-154 40-mg group, which had an increase in daily morning stiffness duration from baseline (181.3 minutes/day; 95% CI, 102.7–260.0; $P = 0.006$) (Supplementary Figure 2C); however, three patients had outlying data during weeks 20 to 24 possibly due to data entry errors.

There were no differences from baseline in HAQ-DI scores in any treatment group (Supplementary Figure 2D).

Pharmacokinetics and immunogenicity. The geometric mean trough total ABBV-154 concentrations were 1.70, 6.29, and 25.9 μg/mL for the 40-, 150-, and 340-mg doses, respectively, and the geometric mean trough total antibody concentrations were 1.02, 6.15, and 29.9 μg/mL at week 24, respectively. The unconjugated GRM payload reached geometric trough concentrations of 0.028, 0.065, and 0.177 ng/mL at week 24 in the ABBV-154 40, 150, and 340 mg dose groups, respectively.

ABBV-154 showed typical ADC pharmacokinetics in patients with PMR, with antibody-like pharmacokinetic profiles for the ADC and total antibody, and a formation-rate–limited pharmacokinetic profile for the unconjugated GRM payload with plasma concentrations that were several orders of magnitude lower than serum concentrations of total ABBV-154 and total antibody.

At baseline, preexisting ADAs and nAbs were detected in 13.6% (17 of 125) and 0.8% (1 of 125), respectively, of patients who received one or more doses of ABBV-154 during the study. Treatment-emergent ADA incidence was 83.1% (108 of 130), while nAb incidence was 19.2% (25 of 130) among evaluable patients receiving ABBV-154. ADA incidence was associated with lower ADC exposure. However, no clear trends were detected between ADA incidence and efficacy outcomes.

Safety and tolerability. The majority of patients experienced TEAEs with similar rates between groups (Table 2). The most common TEAEs in the ABBV-154 groups were COVID-19, nasopharyngitis, and arthralgia, with relatively low rates of grade ≥3 TEAEs, serious AEs, and treatment discontinuations due to TEAEs. The highest rate of treatment discontinuation due to a TEAE occurred in the ABBV-154 340-mg group. No deaths occurred during the study.

More AESIs occurred in the ABBV-154 340-mg group compared with the other treatment groups (Table 2). The most common AESIs were serious infections and hypersensitivity reactions. Serious infections included pneumonia (5 events), urinary tract infection (1 event), and cellulitis (1 event) in the ABBV-154 340-mg group; respiratory tract infection (1 event), lower respiratory tract infection (1 event), and urosepsis (1 event) in the ABBV-154 150-mg group; and perforated appendicitis (1 event) and peritonitis (1 event) in the same patient in the ABBV-154 40-mg group. Possibly treatment-related serious infections (by investigators' assessments) in the ABBV-154 groups were pneumonia (5 events), respiratory tract infection (1 event), lower respiratory tract infection (1 event), and urosepsis (1 event).

All hypersensitivity reactions were mild or moderate. Hypersensitivity reactions in the ABBV-154 groups considered possibly

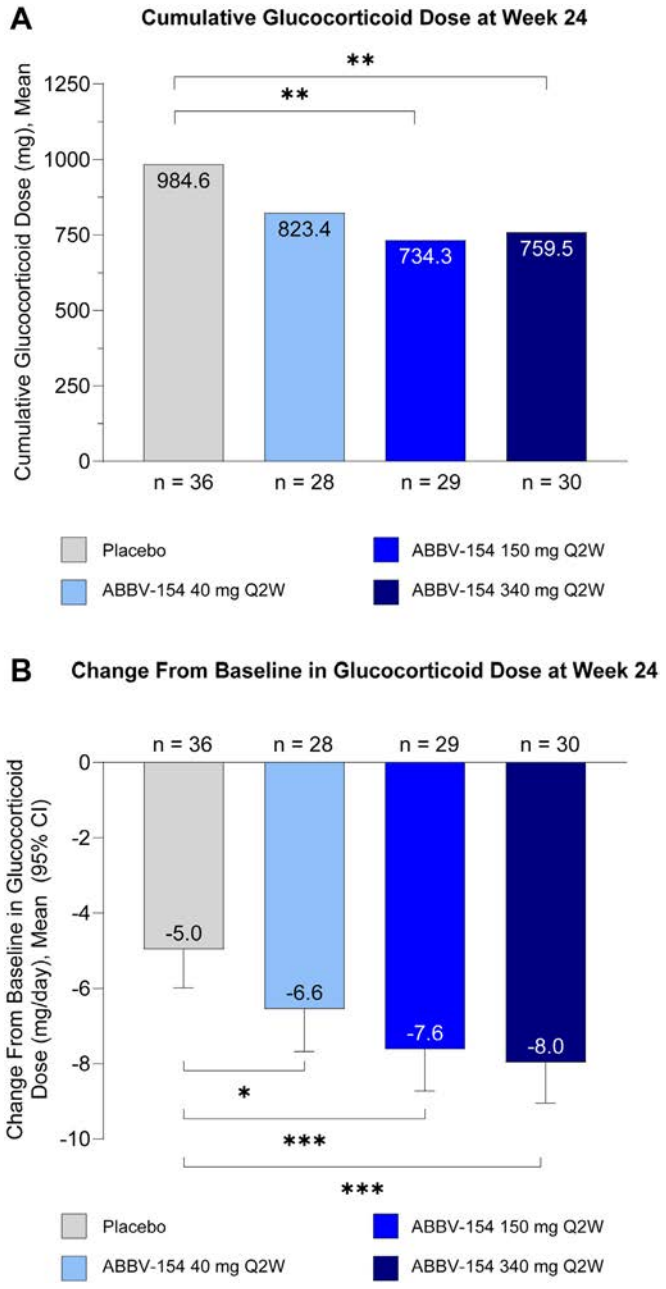

Figure 4. Dose of glucocorticoid (ITT population). (A) Mean cumulative dose (mg) at week 24 and (B) mean (95% CI) change from baseline to week 24 (mg/day). Data shown as observed for number of patients with measurements at baseline and week 24. The *P* values are based on an ANCOVA model adjusting for baseline randomization stratification factors (glucocorticoid use at baseline [≥10 mg/day; <10 mg/day prednisone equivalent]), length of prior glucocorticoid treatment for PMR (≤1 year; >1 year), and baseline glucocorticoid dose to compare ABBV-154 with placebo. For change from baseline, patients with one or more available change from baseline value and no missing data for the factors and covariates in the model. * $P \leq 0.05$; ** $P \leq 0.01$; *** $P \leq 0.001$. ANCOVA, analysis of covariance; CI, confidence interval; ITT, intent-to-treat; PMR, polymyalgia rheumatica; Q2W, every 2 weeks. Color figure can be viewed in the online issue, which is available at http://onlinelibrary.wiley.com/doi/10.1002/art.43129/abstract.

treatment related were injection site rash (10 events), rash (2 events), injection site urticaria (1 event), and toxic skin reaction (1 event). Malignancies observed in the ABBV-154 treatment groups included mild-or-moderate nonmelanoma skin cancer (40 mg, 2 events; 150 mg, 2 events), severe acute myeloid leukemia (340 mg, 1 event), and severe prostate cancer (340 mg, 1 event). Two malignancies were considered possibly treatment related by investigators (ABBV-154 150 mg, 1 event of nonmelanoma skin cancer; ABBV-154 340 mg, 1 event of acute myeloid leukemia). The few observed adjudicated systemic glucocorticoid side effects occurred at a similar rate among placebo and ABBV-154 treatment groups.

Changes were observed in laboratory values, vital signs, or electrocardiogram assessments. However, a higher proportion of patients in the ABBV-154 groups experienced a >7% decrease in body weight (40 mg, 11.9% [n = 5]; 150 mg, 15.9% [n = 7]; 340 mg, 18.2% [n = 8]) compared with the placebo group (6.3% [n = 3]).

DISCUSSION

This study reports the efficacy and safety of ABBV-154, a novel ADC comprising adalimumab conjugated to a proprietary GRM payload[12] versus placebo in patients with glucocorticoid-dependent PMR. A treatment effect was observed in all three ABBV-154 groups, with longer time to flare (primary endpoint) in the ABBV-154 groups compared with placebo.

A higher proportion of patients receiving ABBV-154 than placebo achieved flare-free state up to week 24. By week 24, patients receiving ABBV-154 (vs placebo) had lower cumulative dose of glucocorticoid and greater reduction from baseline in daily glucocorticoid dose. Similarly, a higher proportion of patients receiving ABBV-154 showed improvement in markers of inflammation by week 24 than those receiving placebo. In patient-reported outcomes collected to week 24, results reflecting primary symptoms experienced daily by patients revealed potential improvements among some treatment arms; pain severity was reduced from baseline in the ABBV-154 340-mg group, and stiffness severity was reduced from baseline in the ABBV-154 150- and 340-mg groups. The four-week assessments of morning stiffness duration and physical function (HAQ-DI) did not improve from baseline regardless of treatment group, which may indicate the need for more precise assessment of these concepts in PMR, with greater frequency of measurement and instruments more specific to PMR for physical function. Furthermore, patients in this study had controlled PMR, making observation of improvement difficult.

Although data were limited due to early study termination, ABBV-154 was generally well tolerated in patients with PMR. Rates of hypersensitivity reactions were higher in the ABBV-154

Table 2. TEAEs during the double-blind treatment period (full analysis set)*

TEAE, n (%)	Placebo (n = 50)	ABBV-154 40 mg (n = 42)	ABBV-154 150 mg (n = 45)	ABBV-154 340 mg (n = 44)
Safety overview				
Any TEAE	41 (82.0)	32 (76.2)	39 (86.7)	41 (93.2)
COVID-19–related TEAE	9 (18.0)	9 (21.4)	5 (11.1)	7 (15.9)
TEAE with reasonable possibility of being drug related	17 (34.0)	15 (35.7)	21 (46.7)	29 (65.9)
Grade ≥3 TEAE	9 (18.0)	6 (14.3)	7 (15.6)	8 (18.2)
SAE	8 (16.0)	5 (11.9)	8 (17.8)	9 (20.5)
TEAE leading to study drug discontinuation	3 (6.0)	1 (2.4)	1 (2.2)	7 (15.9)
TEAE leading to death	0	0	0	0
Most common TEAEs[a]				
COVID-19	9 (18.0)	9 (21.4)	5 (11.1)	7 (15.9)
Nasopharyngitis	3 (6.0)	4 (9.5)	4 (8.9)	7 (15.9)
Arthralgia	3 (6.0)	4 (9.5)	6 (13.3)	3 (6.8)
Urinary tract infection	5 (10.0)	3 (7.1)	2 (4.4)	7 (15.9)
Headache	2 (4.0)	3 (7.1)	4 (8.9)	4 (9.1)
Fatigue	2 (4.0)	3 (7.1)	4 (8.9)	2 (4.5)
Hypertension	5 (10.0)	1 (2.4)	4 (8.9)	3 (6.8)
Nausea	2 (4.0)	3 (7.1)	2 (4.4)	3 (6.8)
Pneumonia	0	2 (4.8)	1 (2.2)	5 (11.4)
Contusion	0	2 (4.8)	2 (4.4)	3 (6.8)
Diarrhea	4 (8.0)	2 (4.8)	2 (4.4)	3 (6.8)
Injection site erythema	0	2 (4.8)	3 (6.7)	2 (4.5)
Rash	2 (4.0)	2 (4.8)	2 (4.4)	3 (6.8)
Upper respiratory tract infection	2 (4.0)	2 (4.8)	3 (6.7)	2 (4.5)
AEs of special interest				
Serious infections	1 (2.0)	1 (2.4)	3 (6.7)	6 (13.6)
Serious infections excluding COVID-19–related AEs	1 (2.0)	1 (2.4)	3 (6.7)	6 (13.6)
Opportunistic infections	0	0	0	0
Active TB	0	0	0	0
Hypersensitivity reactions	4 (8.0)	4 (9.5)	8 (17.8)	7 (15.9)
Serious allergic reactions	0	0	0	0
Malignancies	0	2 (4.8)	2 (4.4)	2 (4.5)
Malignancies excluding NMSC	0	0	0	2 (4.5)[b]
NMSC	0	2 (4.8)	2 (4.4)	0
Lymphoma	0	0	0	0
Adjudicated systemic glucocorticoid side effects[c]	1 (2.0)	3 (7.1)	1 (2.2)	1 (2.3)
Adrenal insufficiency	0	0	0	0
Iatrogenic Cushing syndrome	0	0	0	1 (2.3)

* AE, adverse event; NMSC, nonmelanoma skin cancer; SAE, serious adverse event; TB, tuberculosis; TEAE, treatment-emergent adverse event.
[a] Most common defined as >5% incidence of TEAEs in any ABBV-154 dose cohort.
[b] One event of acute myeloid leukemia (considered by the investigator as possibly related to study treatment) and 1 event of prostate cancer (considered by the investigator as having no reasonable possibility of being related to study treatment).
[c] Reviewed by an Independent Adjudication Committee.

150 mg and 340 mg groups than in the ABBV-154 40 mg or placebo groups (Table 2). All hypersensitivity reactions were mild or moderate in severity. Serious infections occurred in few patients and were more frequent in the ABBV-154 340-mg (n = 6) group than in all other groups (placebo n = 1, ABBV-154 40 mg n = 1, 150 mg n = 3).

This study had several limitations. Due to the voluntary early termination of the study, the available data set had a limited sample size, variable duration of exposure to study drug, and a wide range of PMR durations. Moreover, as a phase 2 study exploring initial efficacy and dose response, statistical comparisons for efficacy outcomes used a two-sided α of 0.1 without multiplicity control, which could increase the potential for Type I error. Thus, interpretation of data should be treated with caution. In addition, including an adalimumab comparator arm would have been interesting to elucidate further and confirm the contribution of the GRM payload to efficacy and safety in PMR; however, an adalimumab comparator arm was not included in this study because current EULAR/ACR recommendations for PMR recommend against using anti-TNF agents (primarily based on small randomized controlled trials with etanercept and infliximab).[2] The safety of ABBV-154 cannot be directly compared with adalimumab or glucocorticoids due to the early study termination and lack of adalimumab comparator arm; for example, we could not determine

whether the higher rate of serious infections in the ABBV-154 340-mg group was due to higher antibody exposure, higher systemic exposure to the GRM payload, or chance. The identical 24-week oral glucocorticoid taper in all arms may be viewed as both a strength and a weakness because it allows for a direct comparison of glucocorticoid use between treatment arms, but it may also be faster than the taper that some other clinical trials have utilized in the placebo group.[23] A subgroup analysis suggested that time since most recent flare may be associated with a likelihood of developing a PMR flare while tapering glucocorticoid. Further studies may benefit from including patients with the most recent PMR flare closer to baseline than the 24 weeks required in this trial, facilitating the enrollment of patients with active disease (albeit controlled at baseline). Finally, comparison with other studies may be limited because the PMR-AS was not included as a primary or secondary endpoint (see Supplementary Table 2 for PMR-AS data).

The ADC ABBV-154, comprising the anti-TNF antibody adalimumab conjugated to the anti-inflammatory GRM payload, was developed to reduce the risks of systemic glucocorticoid-related AEs by delivering the GRM to cells that express transmembrane TNF, including activated immune cells.[12,13] However, an interim data review determined that the benefit-risk profile did not sufficiently differentiate ABBV-154 from other currently available therapies for PMR; consequently, the sponsor decided to cease development of ABBV-154 and terminate the study early due to the lack of differentiation and not due to safety reasons.

In conclusion, ABBV-154 was generally well tolerated with benefits observed versus placebo demonstrating longer time to flare, fewer flares, and reduction in cumulative glucocorticoid dose, markers of inflammation, pain severity, and stiffness severity. However, given the limited sample size and duration of exposure to study drug, no definite conclusions can be drawn from this study of ABBV-154 in patients with PMR and caution should be exercised when interpreting the results. Nevertheless, this study supports that a GRM payload targeted to transmembrane TNF-expressing cells, including activated immune cells, could be beneficial in PMR.

ACKNOWLEDGMENTS

AbbVie and the authors thank all study investigators for their contributions and the patients who participated in this study.

AUTHOR CONTRIBUTIONS

All authors contributed to at least one of the following manuscript preparation roles: conceptualization AND/OR methodology, software, investigation, formal analysis, data curation, visualization, and validation AND drafting or reviewing/editing the final draft. As corresponding author, Dr Spiera confirms that all authors have provided the final approval of the version to be published and takes responsibility for the affirmations regarding article submission (eg, not under consideration by another journal), the integrity of the data presented, and the statements regarding compliance with institutional review board/Declaration of Helsinki requirements. No honoraria or payments were made for authorship.

ROLE OF THE STUDY SPONSOR

AbbVie participated in the study design, research, data collection, analysis, interpretation of data, reviewing, and approval of this manuscript. Publication of this article was not contingent upon approval by AbbVie. Medical writing support was provided by Abegale Templar, PhD, and Ray Beck Jr, PhD, of JB Ashtin and funded by AbbVie.

REFERENCES

1. Salvarani C, Cantini F, Boiardi L, et al. Polymyalgia rheumatica and giant-cell arteritis. N Engl J Med 2002;347(4):261–271.
2. Dejaco C, Singh YP, Perel P, et al; European League Against Rheumatism; American College of Rheumatology. 2015 Recommendations for the management of polymyalgia rheumatica: a European League Against Rheumatism/American College of Rheumatology collaborative initiative. Ann Rheum Dis 2015;74(10):1799–1807.
3. Gabriel SE, Sunku J, Salvarani C, et al. Adverse outcomes of antiinflammatory therapy among patients with polymyalgia rheumatica. Arthritis Rheum 1997;40(10):1873–1878.
4. Hutchings A, Hollywood J, Lamping DL, et al. Clinical outcomes, quality of life, and diagnostic uncertainty in the first year of polymyalgia rheumatica. Arthritis Rheum 2007;57(5):803–809.
5. Dejaco C, Duftner C, Dasgupta B, et al. Polymyalgia rheumatica and giant cell arteritis: management of two diseases of the elderly. Aging Health 2011;7(4):633–645.
6. Floris A, Piga M, Chessa E, et al. Long-term glucocorticoid treatment and high relapse rate remain unresolved issues in the real-life management of polymyalgia rheumatica: a systematic literature review and meta-analysis. Clin Rheumatol 2022;41(1):19–31.
7. Sattui SE, Xie F, Wan Z, et al. Treatment of polymyalgia rheumatica by rheumatology providers: analysis from the American College of Rheumatology RISE registry. Arthritis Care Res (Hoboken) 2024;76(2):259–264.
8. Mazzantini M, Torre C, Miccoli M, et al. Adverse events during long-term low-dose glucocorticoid treatment of polymyalgia rheumatica: a retrospective study. J Rheumatol 2012;39(3):552–557.
9. Li JX, Cummins CL. Fresh insights into glucocorticoid-induced diabetes mellitus and new therapeutic directions. Nat Rev Endocrinol 2022;18(9):540–557.
10. Buttgereit F, Dejaco C, Matteson EL, Dasgupta B. Polymyalgia rheumatica and giant cell arteritis: a systematic review. JAMA 2016;315(22):2442–2458.
11. Kaufman MB. FDA approves sarilumab for the treatment of adults with glucocorticoid-resistant PMR. The Rheumatologist website. 2023. Accessed March 18, 2024. https://www.the-rheumatologist.org/article/fda-approves-sarilumab-for-the-treatment-of-adults-with-glucocorticoid-resistant-pmr/?singlepage=1
12. Hobson AD, Xu J, Welch DS, et al. Discovery of ABBV-154, an anti-TNF glucocorticoid receptor modulator immunology antibody-drug conjugate (iADC). J Med Chem 2023;66(17):12544–12558.
13. Hobson AD, McPherson MJ, Waegell W, et al. Design and development of glucocorticoid receptor modulators as immunology antibody-drug conjugate payloads. J Med Chem 2022;65(6):4500–4533.
14. Kreiner F, Langberg H, Galbo H. Increased muscle interstitial levels of inflammatory cytokines in polymyalgia rheumatica. Arthritis Rheum 2010;62(12):3768–3775.

15. Cutolo M, Montecucco CM, Cavagna L, et al. Serum cytokines and steroidal hormones in polymyalgia rheumatica and elderly-onset rheumatoid arthritis. Ann Rheum Dis 2006;65(11):1438–1443.
16. Corrao S, Pistone G, Scaglione R, et al. Fast recovery with etanercept in patients affected by polymyalgia rheumatica and decompensated diabetes: a case-series study. Clin Rheumatol 2009;28(1): 89–92.
17. Catanoso MG, Macchioni P, Boiardi L, et al. Treatment of refractory polymyalgia rheumatica with etanercept: an open pilot study. Arthritis Rheum 2007;57(8):1514–1519.
18. Kreiner F, Galbo H. Effect of etanercept in polymyalgia rheumatica: a randomized controlled trial. Arthritis Res Ther 2010;12(5):R176.
19. Aikawa NE, Pereira RM, Lage L, et al. Anti-TNF therapy for polymyalgia rheumatica: report of 99 cases and review of the literature. Clin Rheumatol 2012;31(3):575–579.
20. Salvarani C, Cantini F, Niccoli L, et al. Treatment of refractory polymyalgia rheumatica with infliximab: a pilot study. J Rheumatol 2003; 30(4):760–763.
21. Salvarani C, Macchioni P, Manzini C, et al. Infliximab plus prednisone or placebo plus prednisone for the initial treatment of polymyalgia rheumatica: a randomized trial. Ann Intern Med 2007;146(9):631–639.
22. Dasgupta B, Cimmino MA, Kremers HM, et al. 2012 Provisional classification criteria for polymyalgia rheumatica: a European League Against Rheumatism/American College of Rheumatology collaborative initiative. Arthritis Rheum 2012;64(4):943–954.
23. Spiera RF, Unizony S, Warrington KJ, et al; SAPHYR Investigators. Sarilumab for relapse of polymyalgia rheumatica during glucocorticoid taper. N Engl J Med 2023;389(14):1263–1272.

Arthritis & Rheumatology
Vol. 77, No. 8, August 2025, pp 1052–1062
DOI 10.1002/art.43146

Long-Term Safety and Efficacy of Mepolizumab in Eosinophilic Granulomatosis With Polyangiitis

Michael E. Wechsler,[1] Jared Silver,[2] Gerhard Wolff,[3] Robert G. Price,[4] Rejina Verghis,[5] Peter F. Weller,[6] Peter A. Merkel,[7] and Paneez Khoury,[8] on behalf of the EGPA Mepolizumab Open-Label Extension Study Group

Objective. Eosinophilic granulomatosis with polyangiitis (EGPA) is a rare, relapsing, inflammatory disease. Management of EGPA predominantly relies on oral corticosteroids (OCS), which are associated with many adverse effects. The phase 3 MIRRA trial demonstrated efficacy and safety of mepolizumab, anti-interleukin-5 biologic, for EGPA. This open-label extension (OLE) of MIRRA assessed long-term safety and OCS-sparing effects of mepolizumab.

Methods. The OLE (NCT03298061) was a multicenter study that enrolled patients from MIRRA who required OCS ≥5 mg/day up to six months after the end of MIRRA. All patients received mepolizumab 300 mg subcutaneously every four weeks plus standard of care until mepolizumab was discontinued or became approved and reimbursed for EGPA in the respective country. Key outcomes included adverse events (AEs) and use of OCS.

Results. One hundred patients were enrolled in the OLE. Mean (SD) and median (min–max) exposure during OLE was 38.5 (27.0) and 27.0 (1.0–89.0) months. On-treatment AEs were experienced by 98% of patients (43% treatment related; most frequent: injection site reaction [10%]) and serious AEs by 38% of patients (6% treatment related) with no new safety signals versus MIRRA identified. Median (Q1–Q3) OCS dose decreased from 10.0 (7.8–15.0) mg/day at OLE baseline to 5.0 (0.0–10.0) mg/day at study exit. Proportion of patients using OCS >7.5 mg/day decreased from 75% at baseline to 32% at study exit; 28% of patients discontinued OCS.

Conclusion. Long-term use of mepolizumab to treat EGPA was well tolerated and resulted in sustained reductions in OCS use.

INTRODUCTION

Eosinophilic granulomatosis with polyangiitis (EGPA) is a rare, progressive, relapsing/remitting inflammatory disease in which elevated eosinophil counts, asthma, sino-nasal disease, pulmonary infiltrates, other organ manifestations, and vasculitis may cause significant morbidity.[1–8] EGPA treatment has historically relied on oral corticosteroids (OCS), other immunosuppressive drugs, and cytotoxic therapies, although more recently biologic treatments have become available to patients.[1,9,10] Achieving remission (controlled symptoms in absence of clinical signs of disease) with low-dose OCS alone is often associated with relapse.[1] As prolonged use of OCS increases the risk of adverse effects over time and is associated with acute infections, there is a pressing need for effective treatment strategies that spare OCS.[11–13]

Mepolizumab is a humanized monoclonal antibody that specifically targets interleukin (IL)-5 to reduce proliferation, activation, and survival of eosinophils, and is approved in multiple regions worldwide for the treatment of severe asthma with an eosinophilic

ClinicalTrials.gov identifier: NCT03298061.

Please refer to the GlaxoSmithKline (GSK) weblink to access GSK's data sharing policies and, as applicable, to seek anonymized patient level data: https://www.gsk-studyregister.com/en/.

Supported by GSK (GSK ID: MEA116841; NCT03298061). Supported in part by the Division of Intramural Research, National Institute of Allergy and Infectious Diseases/NIH.

[1]Michael E. Wechsler, MD, MMSc: National Jewish Health, Denver, Colorado; [2]Jared Silver, MD, PhD: GSK, Durham, North Carolina (current address: Amgen, Thousand Oaks, CA); [3]Gerhard Wolff, MD, PhD: GSK, Collegeville, Pennsylvania; [4]Robert G. Price, MSc: GSK, Stevenage, Hertfordshire, United Kingdom; [5]Rejina Verghis, PhD: GSK, London, United Kingdom; [6]Peter F. Weller, MD: Beth Israel Deaconess Medical Center, Harvard Medical School, Boston, Massachusetts; [7]Peter A. Merkel, MD, MPH: University of Pennsylvania, Philadelphia; [8]Paneez Khoury, MD, MHSc: National Institute of Allergy and Infectious Diseases, NIH, Bethesda, Maryland. Members of the EGPA Mepolizumab Open-Label Extension study group are listed in Appendix A.

Drs Wechsler and Silver are co-first authors and contributed equally to this work.

Additional supplementary information cited in this article can be found online in the Supporting Information section (https://acrjournals.onlinelibrary.wiley.com/doi/10.1002/art.43146).

Author disclosures and graphical abstract are available at https://onlinelibrary.wiley.com/doi/10.1002/art.43146.

Address correspondence via email to Paneez Khoury, MD, MHSc, at khouryp@niaid.nih.gov.

Submitted for publication August 15, 2024; accepted in revised form February 10, 2025.

phenotype, chronic rhinosinusitis with nasal polyps, hypereosinophilic syndrome (HES), and EGPA.[14–16] Mepolizumab is recommended for active nonsevere EGPA as well as for add-on therapy to maintain remission in severe or nonsevere EGPA.[1,9,10] The phase 3 placebo-controlled MIRRA trial (NCT02020889) demonstrated that patients with nonsevere relapsing or refractory EGPA undergoing IL-5 inhibition through treatment with mepolizumab achieved higher rates of remission, including at both weeks 36 and 48 of treatment, and had significantly fewer relapses over 52 weeks of treatment compared with those patients receiving placebo.[17] Additionally, MIRRA demonstrated OCS-sparing benefits patients treated with mepolizumab had less cumulative exposure to OCS over 52 weeks (4.3 mg/day lower for mepolizumab) as compared with patients receiving placebo.[18] The efficacy of both mepolizumab and the anti-IL-5 receptor monoclonal antibody benralizumab were further reinforced in the recent noninferiority phase 3 trial of benralizumab or mepolizumab for relapsing or refractory EGPA.[19]

The safety and clinical benefits of receiving mepolizumab for up to one year have been demonstrated, but systematic reports of long-term use in EGPA are limited.[17–21] A real-world, observational, multicenter European study demonstrated the effectiveness of mepolizumab in reducing disease activity and use of OCS up to 24 months,[22] and results of a real-world observational study in Japan (MARS study) demonstrated the safety, sustained OCS-sparing benefits and long-term disease control after a minimum of 192 weeks of treatment.[23] This open-label extension (OLE) study aimed to provide continued mepolizumab access while monitoring the long-term extended safety profile and OCS-sparing benefits of mepolizumab to patients with EGPA who participated in MIRRA until it received regulatory approval and became available in each respective country.

PATIENTS AND METHODS

Study design and treatments. The OLE of MIRRA (GSK ID: MEA116841, NCT03298061) was a phase 3, multicenter, OLE study conducted at 31 sites in seven countries. Between April 14, 2015, and February 16, 2023 (latest completion date), the OLE enabled eligible patients from MIRRA to receive open-label mepolizumab before local market approval and reimbursement of mepolizumab was granted (or until July 2022 in the United Kingdom, as requested by the UK regulatory authority). For patients who received mepolizumab during MIRRA, this was a reintroduction of mepolizumab after being off treatment for at least eight weeks for the posttreatment follow-up period. All patients received mepolizumab 300 mg subcutaneously every four weeks, in addition to standard of care. Mepolizumab treatment was stopped if there was a lack of benefit as determined by the physician (if a treatment-limiting adverse event [AE] occurred or because of pregnancy) (Figure 1A). There was no guidance on tapering of OCS during the OLE and doses were reduced at investigator discretion.

Patients. Patients who previously participated in MIRRA in Belgium, Canada, France, Germany, Japan, the United Kingdom, and the United States were eligible for the OLE if they required ≥5 mg/day of prednisolone (or equivalent) for the control of their EGPA within six months after completing participation in MIRRA. Eligible patients included those who withdrew prematurely and reached what would have been the end of study timepoint. MIRRA inclusion and exclusion criteria have been published; key MIRRA criteria and full OLE eligibility criteria are shown in Supplementary Table 1.[17] Full details on how patient race and ethnicity were determined are shown in the Supplementary Material. Briefly, MIRRA included patients ≥18 years of age diagnosed with relapsing/refractory EGPA receiving a stable dose of OCS ≥7.5 mg/day for at least four weeks before baseline. Patients were excluded from MIRRA if they had life-threatening or organ-threatening EGPA or were receiving a dose of OCS >50 mg/day.[17] The 1990 American College of Rheumatology (ACR) classification criteria for EGPA were modified for the purposes for MIRRA to ensure recruited patients had a diagnosis of EGPA including key manifestations of the disease (asthma [remission or active] plus eosinophilia and two other common features of EGPA).[24]

Outcomes and assessments. The OLE was designed to provide mepolizumab to eligible patients who had participated in MIRRA while monitoring long-term safety; formal endpoints were not defined. Patients who received at least one dose of open-label mepolizumab defined the safety population for which all outcomes are reported. Outcomes are also described by subgroups according to whether patients previously received mepolizumab or placebo during MIRRA. Outcomes include patient demographic characteristics at OLE baseline, treatment completion rate (defined as continuing mepolizumab treatment until commercial availability), mepolizumab exposure duration, number of treatments administered, and patient years of exposure. Safety-related assessments included AEs, serious AEs (SAEs), and AEs of special interest (AESI) throughout the study, collected through an electronic clinical report form.

On-treatment AEs were defined as any untoward medical occurrence occurring from administration of the first treatment up to 28 days after the last study treatment. SAEs were defined as AEs that resulted in death, were life threatening, required hospitalization or prolongation of existing hospitalization, or resulted in disability or incapacity, a congenital anomaly or birth defect, liver injury and impaired liver function, or other serious events in the investigator's medical or scientific judgment. AEs and SAEs were classified as treatment related or not related to study treatment based on the opinion of the investigator. AESI included systemic reactions, including allergic or hypersensitivity and

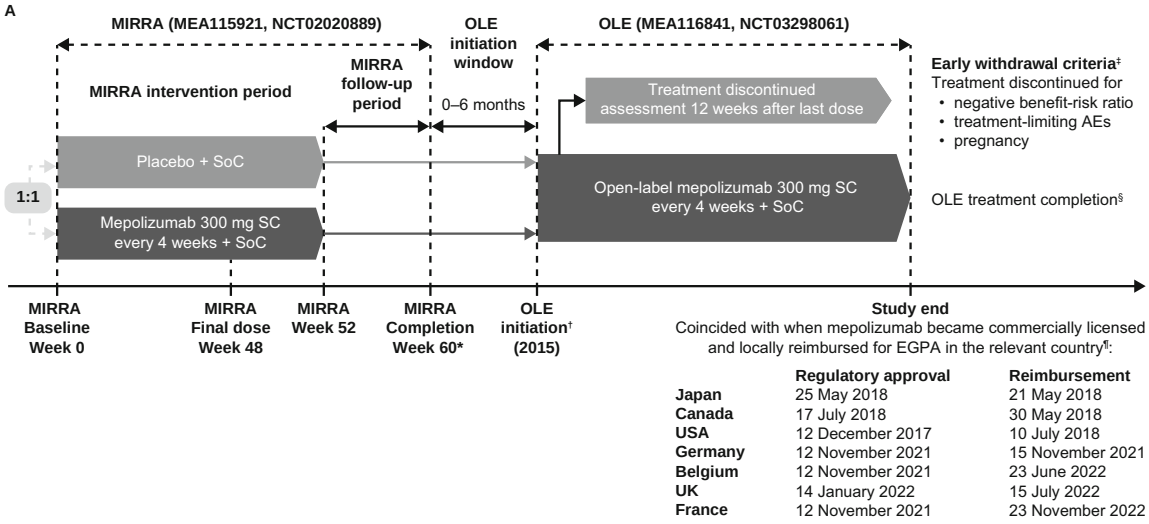

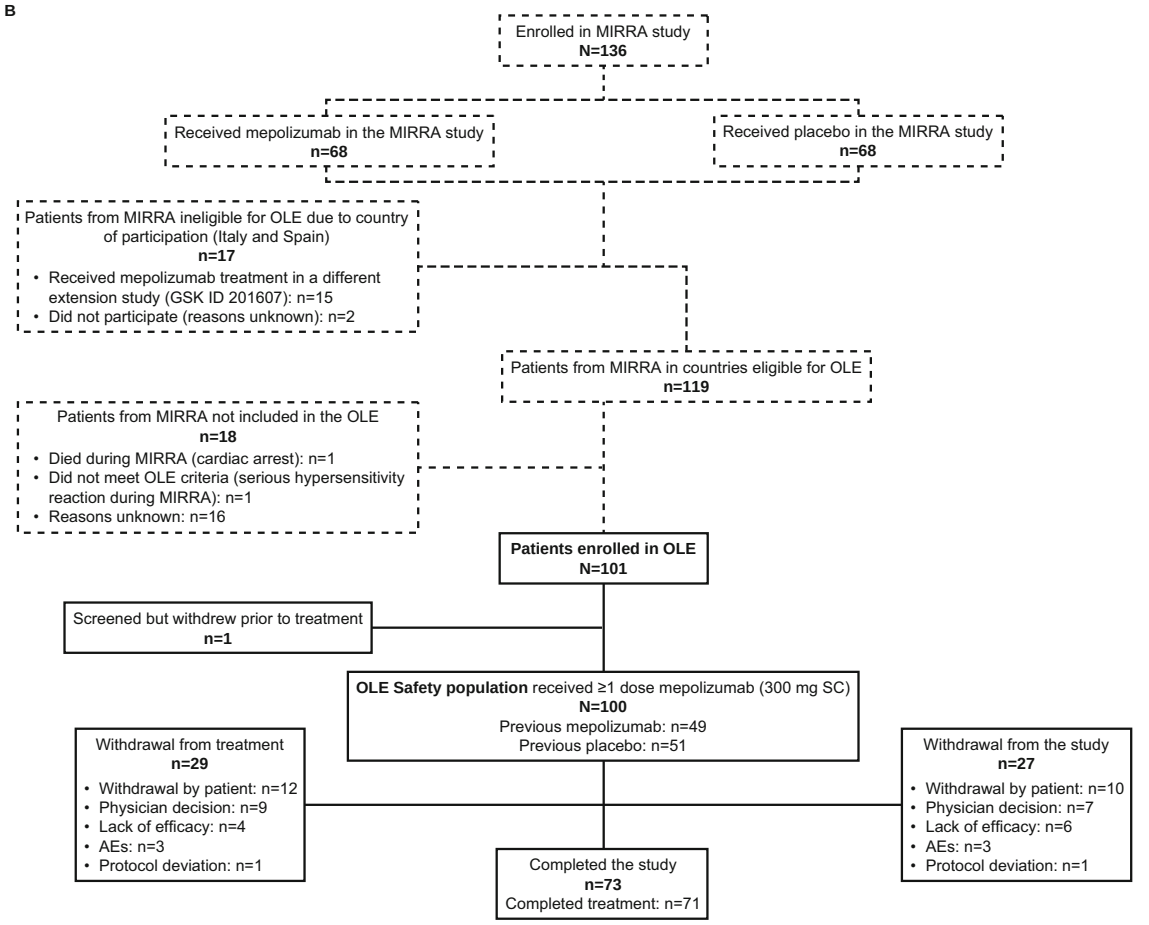

Figure 1. (A) OLE study design. (B) Patient disposition. *Patients had either completed the MIRRA trial and reached the week 60 timepoint or were withdrawn prematurely from MIRRA and had reached the date that would have been week 60 if they had completed the study. †Eligible patients could initiate mepolizumab under the OLE within a six-month period starting from week 60 (or what would have been week 60) of MIRRA. Initiation of mepolizumab treatment under the OLE more than six months after the MIRRA week 60 timepoint was considered on an individual basis by the GSK Medical Monitor. ‡Any patient discontinuing mepolizumab during the OLE was assessed 12 weeks after receiving their last mepolizumab dose at a follow-up or end of program visit. If the patient was lost to follow-up, an Early Withdrawal form was completed. §Patients marked as "completed treatment" remained in the study and received mepolizumab until the study end at their local site. ¶Study end in the United Kingdom was not determined by approval. UK eligible patients could continue to receive mepolizumab under the OLE until July 2022. AE, adverse event; EGPA, eosinophilic granulomatosis with polyangiitis; GSK, GlaxoSmithKline; OLE, open-label extension; SC, subcutaneous; SoC, standard of care.

nonallergic reactions, local injection site reactions, serious and opportunistic infections, neoplasms, malignancies, cardiac disorders, including serious cardiac, vascular or thromboembolic events and ischemic events.

Post hoc outcomes included change in dose of OCS over the course of the study. Data on daily dose of OCS were gathered until a patient discontinued mepolizumab (last dose +28 days), study withdrawal, or completion, whichever occurred earlier. OCS doses are reported at MIRRA baseline, OLE baseline, and at three-month periods while the patient was receiving treatment. The final three-month period of available OCS data up until the patient either reached study end or discontinued treatment early defined the study exit timepoint. All doses of OCS are reported as prednisolone equivalent.

Sample size and statistical analysis. No formal significance testing was conducted, and sample size considerations were not applicable. The population sample consisted of the number of patients who were eligible from MIRRA and desired access to mepolizumab. Exposure time was reported as total patient-years exposure, mean (SD), and median (min–max) months of exposure during the OLE. Safety-related outcomes were summarized as the proportion of patients and exposure-adjusted rate of events per 1,000 patient-years (total number of AEs/[total duration of exposure in days/365.25]×1,000) to account for the length of exposure observed within this study.

Dose of OCS was summarized (post hoc) as mean (SD) and median (lower quartile [Q1], upper quartile [Q3]) dose, and as the number of patients on doses of 0, ≤4, ≤7.5, or >7.5 mg/day by three-monthly periods while on treatment and at study exit, and as the percent change from MIRRA baseline at study timepoints and study exit. The threshold of OCS dose ≤7.5 mg/day was based on the OCS requirement for the EULAR definition of remission, whereas the dose of ≤4 mg formed part of the more stringent remission criteria used in MIRRA.[10,17]

Ethics and approval. The study was conducted in accordance with International Council for Harmonisation (ICH) Good Clinical Practice, applicable patient privacy requirements, the Declaration of Helsinki, and according to the protocol. Written

Table 1. Demographic characteristics at OLE baseline, location of study population, and clinical features at MIRRA baseline*

	Total population, mepolizumab 300 mg SC (n = 100)	Previous placebo in MIRRA (n = 51)	Previous mepolizumab in MIRRA (n = 49)
At OLE baseline			
Female, n (%)	57 (57)	29 (57)	28 (57)
Age (years)			
Mean (SD)	49.6 (13.9)	49.7 (15.0)	49.4 (12.9)
19–64, n (%)	87 (87)	44 (86)	43 (88)
≥65, n (%)	13 (13)	7 (14)	6 (12)
Ethnicity, n (%)			
Hispanic or Latino	1 (1)	0	1 (2)
Not Hispanic or Latino	99 (99)	51 (100)	48 (98)
Race, n (%)			
American Indian or Alaskan Native	1 (1)	0	1 (2)
Asian	8 (8)	5 (10)	3 (6)
White	91 (91)	46 (90)	45 (92)
Country, n (%)			
Belgium	3 (3)	0	3 (6)
Canada	5 (5)	2 (4)	3 (6)
France	11 (11)	6 (12)	5 (10)
Germany	15 (15)	10 (20)	5 (10)
Japan	6 (6)	3 (6)	3 (6)
United Kingdom	11 (11)	6 (12)	5 (10)
United States	49 (49)	24 (47)	25 (51)
At MIRRA baseline			
BVAS total score			
Mean (SD)	3.1 (4.61)	3.2 (4.12)	3.1 (5.12)
Median (Q1–Q3)	1.0 (0.0–4.0)	1.0 (0.0–5.0)	1.0 (0.0–4.0)
Min–max	0–22	0–19	0–22
VDI score			
Mean (SD)	4.3 (2.73)	3.9 (2.59)	4.7 (2.84)
Median (Q1–Q3)	4.0 (2.0–6.0)	4.0 (2.0–6.0)	4.0 (3.0–6.0)
Min–max	0–12	0–10	0–12
History of positive ANCA test, n (%)	15 (15)	8 (16)	7 (14)

* ANCA, antineutrophil cytoplasmic antibody; BVAS, Birmingham Vasculitis Activity Score; OLE, open-label extension; Q1, lower quartile; Q3, upper quartile; SC, subcutaneous; VDI, Vasculitis Damage Index.

informed consent was obtained from each patient before performing any study-specific procedures and the study was monitored according to ICH E6, Section 5.18. The local institutional review board or ethics committee at each site oversaw trial procedures (see Supplementary Material for further details).

RESULTS

Patient population. Of the 136 patients enrolled in MIRRA, 119 were in countries eligible for the OLE; patients from Italy and Spain received mepolizumab in a separate extension study. In the OLE, 101 patients were screened and 100 received treatment (Figure 1B). The mean (SD) age at OLE baseline was 49.6 (13.9) years, 57% of the patients were female, and 91% of patients were White. Patients were treated in seven countries with the largest proportion in the United States (49%), followed by Germany (15%), the United Kingdom, and France (11% each) (Table 1). Patients from the United States, Japan, and Canada were the first to reach the end of the OLE as the first countries to receive regulatory approval and local reimbursement for mepolizumab in EGPA in 2018 (Figure 1A).

Overall, 73 (73%) patients completed the study and 27 (27%) discontinued early (Figure 1B). Treatment was completed by 71 (71%) patients, who received mepolizumab until the end of the study in their location and subsequently could receive commercially available mepolizumab. Of the 27 patients who discontinued the study early, the primary reasons for study withdrawal were patient decision (n = 10), physician decision (n = 7), lack of efficacy (n = 6), AEs (n = 3), and protocol deviation (n = 1) (Figure 1B). Additional details of reasons for discontinuation are shown in Supplementary Table 2; in total across all primary and subreasons, lack of, or partial efficacy or benefit or wanting to try another biologic was identified as a contributing reason for study withdrawal for 10 patients.

Exposure. In the OLE, patients were exposed to mepolizumab for a mean (SD) of 38.5 (27.0) months (3.2 [2.25] years); the median length of exposure was 27.0 months with a minimum of 1 month and a maximum of 89 months (7.4 years) (Table 2). The total mepolizumab exposure in the OLE was 320.5 patient-years. Exposure among patients who completed treatment versus those who discontinued early is shown in Supplementary Table 3. In addition, 49 patients had received previous mepolizumab treatment under MIRRA for a full year, with the exception of two patients who were withdrawn from MIRRA after 3.7 months and 9.1 months, respectively. For these 49 patients who previously

Table 2. Mepolizumab completions, discontinuations, exposure, and missed doses*

	Total population, mepolizumab 300 mg SC (n = 100)	Previous placebo in MIRRA (n = 51)	Previous mepolizumab in MIRRA (n = 49)
Treatments status, n (%)			
Completed	71 (71)	38 (75)	33 (67)
Discontinued early	29 (29)	13 (25)	16 (33)[a]
Primary reason for treatment discontinuation,[b] n (%)			
AE	3 (3)	2 (4)	1 (2)
Lack of efficacy	4 (4)	1 (2)	3 (6)
Protocol deviation	1 (1)	1 (2)	0
Physician decision	9 (9)	2 (4)	7 (14)
Withdrawal by patient	12 (12)	7 (14)	5 (10)
Treatments administered			
Mean (SD)	39.5 (28.4)	39.4 (27.8)	39.6 (29.3)
Median (range)	29.0 (1–97)	30.0 (1–96)	28.0 (3–97)
Range of exposure, months[c]			
Mean (SD)	38.5 (27.0)	38.6 (26.5)	38.3 (27.7)
Median (min–max)	27.0 (1–89)	28.0 (1–88)	26.0 (3–89)
Total patient-years exposure[d]	320.5	164.1	156.4
Missed doses, n (%)			
No missed doses	62 (62)	26 (51)	36 (73)
≥1 missed dose	38 (38)	25 (49)	13 (27)
≥2 missed doses	22 (22)	16 (31)	6 (12)
2 consecutive missed doses	13 (13)	9 (18)	4 (8)
≥3 missed doses	17 (17)	11 (22)	6 (12)
3 consecutive missed doses	8 (8)	5 (10)	3 (6)

* AE, adverse event; SC, subcutaneous.
[a] Two patients in the previous mepolizumab group completed the study but discontinued treatment early (see Supplementary Table 2).
[b] Patients may have only one primary reason for treatment discontinuation, in five cases this differed from the primary reason given for study withdrawal (see Supplementary Table 2).
[c] Exposure (therapeutic coverage) = treatment stop date – treatment start date + 29 days.
[d] Sum across patients of (treatment stop date – treatment start date + 29 days)/365.25.

Table 3. Summary of AEs, SAEs, and AESI*

	Total population, mepolizumab 300 mg SC (n = 100)	Previous placebo in MIRRA (n = 51)	Previous mepolizumab in MIRRA (n = 49)
Number of patients with AEs, n (%)			
On-treatment AEs[a]	98 (98)	50 (98)	48 (98)
Posttreatment AEs[a]	18 (18)	6 (12)	12 (24)
Treatment-related AEs	43 (43)	21 (41)	22 (45)
AEs leading to permanent discontinuation of study treatment or withdrawal from study	3 (3)	2 (4)	1 (2)
Number of patients with SAEs,[a] n (%)			
On-treatment SAEs[a]	38 (38)	16 (31)	22 (45)
Posttreatment SAEs[a]	3 (3)	2 (4)	1 (2)
Treatment-related SAEs (nonfatal)	6 (6)	2 (4)	4 (8)
Fatal SAEs	1 (1)	1 (2)	0
Treatment-related fatal SAEs	0	0	0
Number of patients with on-treatment AESI,[b] n (%)			
Systemic reactions	4 (4)	3 (6)	1 (2)
Hypersensitivity reactions	3 (3)	3 (6)	0
Nonallergic reactions	1 (1)	0	1 (2)
Anaphylaxis	0	0	0
Local injection site reactions	20 (20)	10 (20)	10 (20)
All infections[c]	86 (86)	42 (82)	44 (90)
Serious infections	18 (18)	8 (16)	10 (20)
Potential opportunistic infections[d]	3 (3)	2 (4)	1 (2)
Neoplasms benign, malignant, and unspecified (including cysts and polyps)	10 (10)	4 (8)	6 (12)
Malignancies[e]	4 (4)	1 (2)	3 (6)
Cardiac disorders[f]	12 (12)	5 (10)	7 (14)
Serious cardiac disorders	7 (7)	3 (6)	4 (8)
Serious cardiac, vascular, or thromboembolic events[g]	9 (9)	5 (10)	4 (8)
Serious ischemic events[h]	3 (3)	1 (2)	2 (4)
Number of patients with on-treatment treatment-related AESIs, n (%)			
Systemic reactions	4 (4)	3 (6)	1 (2)
Hypersensitivity reactions	3 (3)	3 (6))	0 (0)
Nonallergic reactions	1 (1)	0 (0)	1 (1)
Anaphylaxis	0	0	0
Local injection site reactions	17 (17)	7 (14)	10 (20)
All infections[c]	15 (15)	9 (18)	6 (12)
Serious infections	4 (4)	2 (4)	2 (4)
Potential opportunistic infections[d]	1 (1)	1 (2)	0 (0)
Neoplasms benign, malignant, and unspecified (including cysts and polyps)	4 (4)	1 (2)	3 (6)
Malignancies[e]	2 (2)	0 (0)	2 (4)
Cardiac disorders[f]	0	0	0
Serious cardiac disorders	0	0	0
Serious cardiac, vascular or thromboembolic events[g]	0	0	0
Serious ischemic events[h]	0	0	0

* AE, adverse event; AESI, adverse event of special interest; MedDRA, Medical Dictionary for Regulatory Activities; SAE, serious adverse event; SC, subcutaneous; SMQ, standardized MedDRA queries.
[a] AEs and SAEs were defined as on treatment if occurring after the date of first treatment within the study and before 28 days after last study treatment. AEs and SAEs occurring more than 28 days after last treatment were defined as post treatment.
[b] AESIs included systemic reactions, including allergic/hypersensitivity and nonallergic reactions, local injection site reactions, serious and opportunistic infections, neoplasms, malignancies, cardiac disorders, including serious, cardiac, vascular, thromboembolic, and ischemic events.
[c] Infections and infestations system organ class.
[d] Identified from SMQs or events with the preferred term of herpes zoster.
[e] Identified from SMQs.
[f] Cardiac disorders system organ class.
[g] Serious cardiac, vascular, thromboembolic events identified from cardiac disorders system organ class, vascular disorders system organ class, and SMQs.
[h] A subset of serious cardiac, vascular, thromboembolic events, identified from MedDRA SMQ.

received mepolizumab the time between the end of treatment with mepolizumab in MIRRA and enrollment in the OLE varied between 8 weeks (MIRRA follow-up period) and 20 months. Treatment adherence was incomplete with 38 patients missing at least one mepolizumab dose (Table 2). Consecutive missed doses were numerically more common among patients who discontinued early with six (21%) patients who discontinued missing three consecutive doses versus two (3%) patients who completed the doses (Supplementary Table 3).

Safety. On-treatment AEs were experienced by 98 patients (98%; exposure-adjusted rate 4,708.0 events/1,000 patient-years exposure), with 43 patients having treatment-related AEs (43%; 508.5 events/1,000 patient-years exposure) (Table 3; Supplementary Table 4). The most frequent AEs were nasopharyngitis (33%; 352.6 events/1,000 patient-years), upper respiratory tract infections (31%; 134.2 events/1,000 patient-years), worsening of asthma (30%; 293.3 events/1,000 patient-years), sinusitis (30%; 162.2 events/1,000 patient-years), and bronchitis (29%; 152.9 events/1,000 patient-years) (Supplementary Table 4).

AEs led to permanent treatment discontinuation in three patients. Of these, one patient previously treated with placebo in MIRRA had fatal AEs of severe cardiac arrest, dyspnea, and hypoxia 258 days after the first dose and 12 days after the last dose of mepolizumab; this was the only death recorded in the study and these events were reported as not treatment related. The second patient had moderate-severity colon cancer reported 628 days after the first dose and 9 days after the last dose of mepolizumab; this AE was reported treatment related by the investigator. The third patient experienced an AE of asthma and AEs of arthralgia, myalgia, and paresthesia 10 days and 12 days, respectively, after their first and only dose of mepolizumab; none of the AEs were reported as serious or treatment related.

On-treatment SAEs were reported in 38% of patients (299.5 events/1,000 patient-years) and were considered treatment related in 6% of patients (Table 3). The most frequent SAEs were worsening of asthma (6%; 21.8 events/1,000 patient-years), worsening of EGPA (3%; 9.4 events/1,000 patient-years), and pneumonia (3%; 21.8 events/1,000 patient-years) (Supplementary Table 4). On-treatment AESIs included systemic reactions (n = 4 of 100; treatment related: n = 4 of 4), local injection site reactions (n = 20 of 100; treatment related: n = 17 of 20), potential opportunistic infections (n = 3 of 100; treatment related: n = 1 of 3), neoplasms (n = 10 of 100; treatment related: 4 of 10), malignancies (n = 4 of 100; treatment related: n = 2 of 4), cardiac disorders (n = 12 of 100; treatment related: 0 of 12), and serious cardiac, vascular, or thromboembolic events (n = 9 of 100; treatment related: n = 0 of 9) (Table 3). No event of anaphylaxis was reported. The four malignancies reported during the OLE included one event each of renal cell carcinoma and colon cancer (both reported as treatment related by the investigator) and two events of basal cell carcinoma (not reported as treatment related). A breakdown of cardiovascular events is shown in Supplementary Table 5; no cardiac events were reported as treatment related.

Long-term OCS-sparing effects. At entry into the OLE, 75% of patients were taking OCS >7.5 mg/day with a median (Q1–Q3) dose of OCS of 10 (7.8–15.0) mg/day versus 12.5 (10.0–20.0) mg/day at MIRRA baseline (Figure 2A and B). At OLE baseline 2% (2 of 100) and 25% (25 of 100) of patients required OCS ≤4 or ≤7.5 mg/day, respectively, and by months 16 to 18, 38% (33 of 88) and 68% (60 of 88) had achieved a dose of ≤4 and ≤7.5 mg/day, respectively, with 20% (18 of 88) being able to stop OCS entirely. At study exit (the latest 3-month period before either study completion or early discontinuation), 43% (43 of 100) and 68% (68 of 100) of patients were receiving an average dose of OCS ≤4 and ≤7.5 mg/day, respectively, with 28% (28 of 100) discontinuing OCS entirely (Figure 2A). Thirteen patients had no reduction or an increase in the dose of OCS at study exit versus MIRRA baseline, whereas 66 (66%) had reduced OCS by ≥50% (Figure 2C; Supplementary Table 6).

The median (Q1–Q3) daily dose of OCS decreased steadily from 10.0 (7.8–15.0) mg/day at OLE baseline over the first 12 months of OLE to 5.3 (3.0–9.9) mg/day at months 10 to 12 (n = 89) and remained reduced from baseline for most patients over the course of the study, with a median 5.0 (0.0–10.0) mg/day at study exit (Figure 2B). Median and mean doses of OCS and discontinuation of OCS during the OLE were similar regardless of prior mepolizumab or placebo treatment (Supplementary Figure 1A and B; Supplementary Table 7).

Patterns of use of OCS at the individual patient level over the course of the OLE are represented as heat maps shown in Supplementary Figure 2 (absolute dose) and Supplementary Figure 3 (percentage change compared with MIRRA baseline). In both plots, the steady and sustained shift in color toward pale blue (Supplementary Figure 2) or yellow (Supplementary Figure 3) for many patients indicates that patients were able to successfully taper OCS. Overall, 31 (31%) patients discontinued OCS completely for one or more three-month period during the study. Darker blue (Supplementary Figure 2) and red colors (Supplementary Figure 3) represent higher doses of OCS demonstrating that some patients were not able to taper or experienced a relapse requiring increased treatment. For most patients, increases in use of OCS did not correspond to discontinuation of mepolizumab.

DISCUSSION

This OLE study of treatment with mepolizumab for patients from MIRRA adds to the body of evidence on the long-term safety and OCS-sparing effects of mepolizumab,[22,23,25–27] and demonstrates a positive long-term benefit:risk profile of mepolizumab for patients with EGPA. More than two-thirds of patients continued to receive mepolizumab treatment under the OLE until mepolizumab

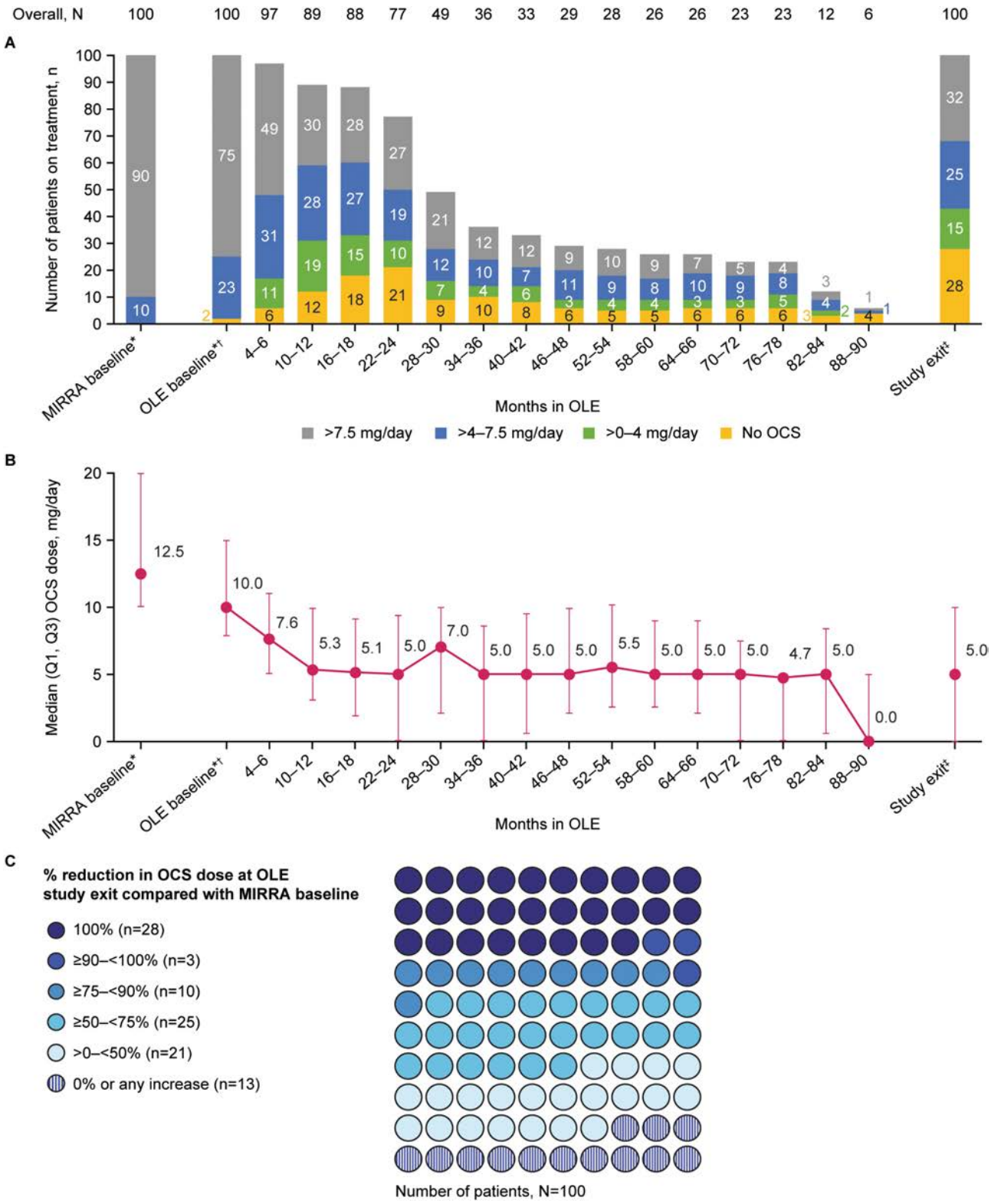

Figure 2. (A) Number of patients receiving dose of OCS (prednisolone equivalent) by category. (B) Median (Q1–Q3) dose of OCS. (C) Percentage reduction in dose of OCS from MIRRA baseline, at exit from the OLE study. *Between the end of the MIRRA treatment period and initiation of OLE, mepolizumab treatment was discontinued for between 8 weeks and 20 months. †At OLE entry, two patients were classified as receiving OCS 0 mg/day because of a gap in the reporting of concomitant medication data. Both patients were receiving OCS of ≥5 mg/day and met all necessary eligibility criteria for the OLE. ‡Study exit is defined as the latest three-month period before patients either reached study end/completed (coinciding with commercial license of mepolizumab for EGPA in the relevant country) or discontinued treatment early. EGPA, eosinophilic granulomatosis with polyangiitis; OLE, open-label extension; OCS, oral corticosteroids; Q1, lower quartile; Q3, upper quartile.

became commercially available, suggesting that long-term IL-5 inhibition by mepolizumab was generally well tolerated and provided OCS-sparing benefits over several years.

In total the OLE captured 320.5 patient-years of mepolizumab exposure, nearly five times the patient-years observed in the parent MIRRA study with an overall safety profile consistent with that seen in MIRRA,[17] and prior studies in HES,[28,29] and EGPA,[23,25] with no new safety concerns identified. Previous long-term international data on the use of mepolizumab beyond one year were available only for the mepolizumab 100 mg dose for severe asthma treatment[30–35] and for a higher dose (mepolizumab 750 mg) with variable dosing intervals in patients with HES.[36]

Of the patients who withdrew from the OLE early, few cases reported a lack of efficacy (6) or AEs (3) as the primary reason for early discontinuation, consistent with MIRRA in which only 3% of 68 patients receiving mepolizumab discontinued because of AEs.[17] The more commonly observed AEs in the OLE were consistent with typical manifestations of EGPA observed in other studies, with worsening asthma being the most common SAE and nasopharyngitis, upper respiratory tract infection, sinusitis, arthralgia, and headache among the most common AEs.[3–5,7,17,19,22] Systemic reactions and local injection site reactions were similar to those observed in MIRRA, with no anaphylaxis reported. Four patients reported malignancies during the OLE (two reported as treatment related by the investigator), which was similar to that reported in the long-term, real-world MARS study in Japan (six AEs of malignant tumors).[23]

As higher cumulative OCS exposure is associated with increased risk of AEs,[13,37] minimizing OCS use is an important treatment goal.[1,38] In the OLE study, the median daily dose of OCS was reduced from 10 mg/day at baseline to 5 mg/day at study exit. In MIRRA, 54% of mepolizumab-treated patients were on a dose of OCS ≤7.5 mg/day at weeks 36 and 48. The OLE permitted even greater OCS reductions, with 68% of patients receiving ≤7.5 mg/day, 43% on OCS ≤4 mg/day, and 28% having discontinued OCS at study exit.

The long-term OCS-sparing effects of mepolizumab for patients with EGPA were demonstrated in real-world studies,[22,23,26,27] including the MARS study in which 36% of patients discontinued OCS after a minimum 192 weeks of mepolizumab treatment.[23] It is likely that benefits of mepolizumab accrue over time, with 31% of patients being OCS free for three months or longer during the OLE, an increase from 25% of patients treated with mepolizumab in MIRRA who accrued any OCS-free weeks.[18] At an individual level, many patients experienced durable reductions in OCS use lasting from months to years, a clinically meaningful outcome from long-term mepolizumab use.

OCS-tapering in the OLE was reflective of real-world clinical practice. Efforts to reduce OCS at expert sites, before approval of mepolizumab by the US Food and Drug Administration, reflects strong motivation by both patients and clinicians. Notably, the OCS reductions occurred even in the context of imperfect adherence (one or more doses of mepolizumab missed) as would be expected in real-world practice.

There are several limitations of the current study, including the fact this was an open-label, nonrandomized, single-arm study with no comparator group, and variable length of follow-up, and there was no defined OCS-tapering protocol. Data on concomitant medications beyond OCS such as immunosuppressive, cytotoxic, or inhaled or topical therapies (such as for asthma or sinus disease) were not collected, nor were data on blood eosinophil counts, sequelae such as relapses of EGPA, remission status, Birmingham vasculitis activity scores, or organ manifestations. AEs were collected via a prespecified strategy on standardized electronic case report forms but were not adjudicated. As an extension from MIRRA, there is the potential that this study reflects a population that is more likely to tolerate and respond well to mepolizumab; however, only two (3%) patients treated with mepolizumab in MIRRA experienced treatment-limiting AEs, and most patients chose to continue in the OLE.[17] Finally, 38% of patients missed at least one dose of mepolizumab and 17% missed up to three doses, which may have led to an underestimation of the OCS-sparing benefit of mepolizumab.

This OLE study, the first long-term prospective, international study for patients with EGPA treated with mepolizumab 300 mg subcutaneously (SC), extends and expands on previous long-term follow-up data with mepolizumab 300 mg SC. Incorporating AEs, exposure data, and OCS reduction, these results support a positive long-term safety profile as well as sustained efficacy of prolonged use of mepolizumab in the treatment of EGPA. Studies are needed to examine the ability of mepolizumab to help achieve reduction of other immunosuppressive drugs, prevent organ damage associated with long-term OCS use, and allow patients to achieve complete remission.

ACKNOWLEDGMENTS

The authors would like to thank the participating patients and their families, clinicians, and study investigators. We would like to thank the EGPA Mepolizumab Open-Label Extension study group investigators for their contributions. Medical writing support (in the form of writing assistance, including preparation of the draft manuscript under the direction and guidance of the authors, collating, and incorporating authors' comments for each draft, assembling tables and figures, grammatical editing, and referencing) was provided by Alice Rees, PhD, at Fishawack Indicia UK, Ltd, part of Avalere Health.

AUTHOR CONTRIBUTIONS

All authors contributed to at least one of the following manuscript preparation roles: conceptualization AND/OR methodology, software, investigation, formal analysis, data curation, visualization, and validation AND drafting or reviewing/editing the final draft. As corresponding author, Dr Khoury confirms that all authors have provided the final approval of the version to be published, and takes responsibility for the affirmations regarding article submission (eg, not under consideration

by another journal), the integrity of the data presented, and the statements regarding compliance with institutional review board/Declaration of Helsinki requirements.

ROLE OF THE STUDY SPONSOR

GSK was involved in study design and implementation, as well as data collection, analysis, interpretation, writing the study report and reviewing this manuscript. Writing support provided by Alice Rees, PhD, was funded by GSK. Publication of this article was not contingent upon approval by GSK.

REFERENCES

1. Emmi G, Bettiol A, Gelain E, et al. Evidence-Based Guideline for the diagnosis and management of eosinophilic granulomatosis with polyangiitis. Nat Rev Rheumatol 2023;19:378–393.
2. Greco A, Rizzo MI, De Virgilio A, et al. Churg-Strauss syndrome. Autoimmun Rev 2015;14:341–348.
3. Comarmond C, Pagnoux C, Khellaf M, et al; French Vasculitis Study Group. Eosinophilic granulomatosis with polyangiitis (Churg-Strauss): clinical characteristics and long-term followup of the 383 patients enrolled in the French Vasculitis Study Group cohort. Arthritis Rheum 2013;65:270–281.
4. Cottin V, Bel E, Bottero P, et al; the Groupe d'Etudes et de Recherche sur les Maladies Orphelines Pulmonaires (GERM"O"P). Respiratory manifestations of eosinophilic granulomatosis with polyangiitis (Churg-Strauss). Eur Respir J 2016;48:1429–1441.
5. Durel CA, Berthiller J, Caboni S, et al. Long-term followup of a multicenter cohort of 101 patients with eosinophilic granulomatosis with polyangiitis (Churg-Strauss). Arthritis Care Res (Hoboken) 2016;68:374–387.
6. Grayson PC, Ponte C, Suppiah R, et al; DCVAS Study Group. 2022 American College of Rheumatology/European Alliance of Associations for Rheumatology Classification Criteria for Eosinophilic Granulomatosis with Polyangiitis. Ann Rheum Dis 2022;81:309–314.
7. Doubelt I, Cuthbertson D, Carette S, et al; Vasculitis Clinical Research Consortium. Clinical manifestations and long-term outcomes of eosinophilic granulomatosis with polyangiitis in North America. ACR Open Rheumatol 2021;3:404–412.
8. Trivioli G, Terrier B, Vaglio A. Eosinophilic granulomatosis with polyangiitis: understanding the disease and its management. Rheumatology (Oxford) 2020;59(suppl 3):iii84–iii94.
9. Chung SA, Langford CA, Maz M, et al. 2021 American College of Rheumatology/Vasculitis Foundation Guideline for the management of antineutrophil cytoplasmic antibody-associated vasculitis. Arthritis Rheumatol 2021;73:1366–1383.
10. Hellmich B, Sanchez-Alamo B, Schirmer JH, et al. EULAR recommendations for the management of ANCA-associated vasculitis: 2022 update. Ann Rheum Dis 2024;83:30–47.
11. Dalal AA, Duh MS, Gozalo L, et al. Dose-response relationship between long-term systemic corticosteroid use and related complications in patients with severe asthma. J Manag Care Spec Pharm 2016;22:833–847.
12. Lefebvre P, Duh MS, Lafeuille MH, et al. Burden of systemic glucocorticoid-related complications in severe asthma. Curr Med Res Opin 2017;33:57–65.
13. Price DB, Trudo F, Voorham J, et al. Adverse outcomes from initiation of systemic corticosteroids for asthma: long-term observational study. J Asthma Allergy 2018;11:193–204.
14. European Medicines Agency (EMA). Mepolizumab (Nucala) summary of product characteristics. Accessed June 18, 2024. https://www.ema.europa.eu/en/documents/product-information/nucala-epar-product-information_en.pdf
15. Mepolizumab (Nucala). Prescribing information. GlaxoSmithKline; 2023. Accessed June 18, 2024. https://www.accessdata.fda.gov/drugsatfda_docs/label/2023/125526Orig1s021,761122Orig1s011Corrected_lbl.pdf
16. Mepolizumab (Nucala). Prescribing information (Japan). GlaxoSmithKline; 2023. Accessed November 7, 2024. https://gskpro.com/content/dam/global/hcpportal/ja_JP/products-info/nucala/nucala-sci.pdf
17. Wechsler ME, Akuthota P, Jayne D, et al. Mepolizumab or placebo for eosinophilic granulomatosis with polyangiitis. N Engl J Med 2017;376:1921–1932.
18. Jayne DRW, Terrier B, Hellmich B, et al. Mepolizumab has clinical benefits including oral corticosteroid sparing irrespective of baseline EGPA characteristics. ERJ Open Res 2024;10:00509–02023.
19. Wechsler ME, Nair P, Terrier B, et al; MANDARA Study Group. Benralizumab versus mepolizumab for eosinophilic granulomatosis with polyangiitis. N Engl J Med 2024;390:911–921.
20. Steinfeld J, Bradford ES, Brown J, et al. Evaluation of clinical benefit from treatment with mepolizumab for patients with eosinophilic granulomatosis with polyangiitis. J Allergy Clin Immunol 2019;143:2170–2177.
21. Terrier B, Jayne DRW, Hellmich B, et al; EGPA mepolizumab study team. Clinical benefit of mepolizumab in eosinophilic granulomatosis with polyangiitis for patients with and without a vasculitic phenotype. ACR Open Rheumatol 2023;5(7):354–363.
22. Bettiol A, Urban ML, Dagna L, et al. Mepolizumab for eosinophilic granulomatosis with polyangiitis: a European multicenter observational study. Arthritis Rheumatol 2022;74(2):295–306.
23. Ishii T, Kunishige H, Kobayashi T, et al. Real-world safety and effectiveness of mepolizumab for patients with eosinophilic granulomatosis with polyangiitis in Japan: long-term observation of the MARS study. Mod Rheumatol 2024;roae100.
24. Masi AT, Hunder GG, Lie JT, et al. The American College of Rheumatology 1990 criteria for the classification of Churg-Strauss syndrome (allergic granulomatosis and angiitis). Arthritis Rheum 1990;33(8):1094–100.
25. Masumoto N, Oshikata C, Nakadegawa R, et al. Long-term mepolizumab treatment reduces relapse rates in super-responders with eosinophilic granulomatosis with polyangiitis. Allergy Asthma Clin Immunol 2023;19:40.
26. Matsuyama T, Matsuyama H, Dotake Y, et al. Long-term efficacy of mepolizumab on eosinophilic granulomatosis with polyangiitis: a retrospective study. Explor Asthma Allergy 2024;2:461–472.
27. Shiomi M, Watanabe R, Matsuda S, et al. Long-term efficacy of mepolizumab in patients with eosinophilic granulomatosis with polyangiitis: a propensity score matching analysis in the multicenter REVEAL cohort study. Front Immunol 2024;15:1457202.
28. Roufosse F, Kahn JE, Rothenberg ME, et al; HES Mepolizumab study group. Efficacy and safety of mepolizumab in hypereosinophilic syndrome: a phase III, randomized, placebo-controlled trial. J Allergy Clin Immunol 2020;146:1397–1405.
29. Gleich GJ, Roufosse F, Chupp G, et al; HES Mepolizumab Study Group. Safety and efficacy of mepolizumab in hypereosinophilic syndrome: an open-label extension study. J Allergy Clin Immunol Pract 2021;9:4431–4440.e1.
30. Bagnasco D, Nicola S, Testino E, et al; On Behalf Of Sani. Long-term efficacy of mepolizumab at 3 years in patients with severe asthma: comparison with clinical trials and super responders. Biomedicines 2023;11:11.

31. Khatri S, Moore W, Gibson PG, et al. Assessment of the long-term safety of mepolizumab and durability of clinical response in patients with severe eosinophilic asthma. J Allergy Clin Immunol 2019;143:1742–1751.e7.
32. Khurana S, Brusselle GG, Bel EH, et al. Long-term safety and clinical benefit of mepolizumab in patients with the most severe eosinophilic asthma: the COSMEX Study. Clin Ther 2019;41:2041–2056.e5.
33. Lugogo N, Domingo C, Chanez P, et al. Long-term efficacy and safety of mepolizumab in patients with severe eosinophilic asthma: a multicenter, open-label, phase IIIb study. Clin Ther 2016;38:2058–2070.e1.
34. Moore WC, Kornmann O, Humbert M, et al. Stopping versus continuing long-term mepolizumab treatment in severe eosinophilic asthma (COMET study). Eur Respir J 2022;59:59.
35. Pavord I, Chan R, Brown N, et al. Long-term safety of mepolizumab for up to ~10 years in patients with severe asthma: open-label extension study. Ann Med 2024;56:2417184.
36. Roufosse FE, Kahn JE, Gleich GJ, et al. Long-term safety of mepolizumab for the treatment of hypereosinophilic syndromes. J Allergy Clin Immunol 2013;131:461–467.e1–5.
37. Broder MS, Sarsour K, Chang E, et al. Corticosteroid-related adverse events in patients with giant cell arteritis: a claims-based analysis. Semin Arthritis Rheum 2016;46:246–252.
38. Del Pozo V, Bobolea I, Rial MJ, et al. Expert consensus on the use of systemic glucocorticoids for managing eosinophil-related diseases. Front Immunol 2024;14:1310211.

APPENDIX A: EGPA MEPOLIZUMAB OPEN-LABEL EXTENSION STUDY GROUP MEMBERS

Members of the EGPA Mepolizumab Open-Label Extension study group are as follows: Arnaud Bourdin, Hôpital Arnaud de Villeneuve, Montpellier, France; Pascal Chanez, Hôpital Nord, Marseille, France; Anoop Chauhan, Queen Alexandra Hospital, Portsmouth, United Kingdom; Vincent Cottin, Hôpital Louis Pradel, Bron, France; Gerald Gleich, University of Utah, Murray, Utah; Berhnard Hellmich, Medius Klinik Kirchheim, Kirchheim-Teck, Germany; Tomonori Ishii, Tohoku University Hospital, Sendai-city, Miyagi, Japan; David Jayne, Addenbrookes Hospital NHS Trust, Cambridge, United Kingdom; Jean-Emmanuel Kahn, Hôpital Foch, Suresnes, France; Peter Kern, Klinikum Fulda-MVZ Osthessen, Hessen, Germany; Nader Khalidi, St. Joseph's Healthcare Hamilton, Hamilton, Ontario, Canada; Ina Koetter, Rheumaklinik Bad Bramstedt and Universitaetsklinikum Schleswig-Holstein, Schleswig-Holstein, Germany; Carol Langford, Cleveland Clinic Foundation, Cleveland, Ohio; Amy Markezich; Overlake Medical Center, Bellevue, Washington; Paul Monach, Boston University School of Medicine, Boston, Massachusetts; Shamsa Naveed, Glenfield Hospital, Leicester, United Kingdom; Peter Oelzner, Universitaetsklinikum Jena, Jena, Thueringen, Germany; Kenneth Pinna, Southwest Allergy and Asthma Clinic, St. George, Utah; Xavier Puechal, Hôpital Cochin, Paris, France; Emory H. Robinette, Pulmonary Research of Abingdon, Abingdon, Virginia; Florence Roufosse, Hôpital Erasme, Bruxelles, Belgium; Reinhard Voll, Universitaetsklinikum Freiburg, Freiburg, Germany; Andrew Schafer, Weill Medical College of Cornell University/New York Presbyterian Hospital, New York City, New York; Kaharu Sumino, Washington University School of Medicine, St. Louis, Missouri; Masami Taniguchi, Sagamihara National Hospital, Kanagawa, Japan; Phillip Lieberman, Baptist Medical Group, Germantown, Tennessee.

Arthritis & Rheumatology
Vol. 77, No. 8, August 2025, pp 1063–1076
DOI 10.1002/art.43151

American College of Rheumatology
Empowering Rheumatology Professionals

Antifibrotic effects of specific targeting of the 5-hydroxytryptamine 2B receptor (5-HT_{2B}R) in murine models and ex vivo models of scleroderma skin

Thuong Trinh-Minh,[1] Cuong Tran-Manh,[1] Andrea-Hermina Györfi,[1] Nicholas Dickel,[2] Christoph Liebel,[1] Xiang Zhou,[1] Jiucun Wang,[3] Meik Kunz,[2] Helena Arozenius,[4] Lars Pettersson,[4] Sam Lindgren,[4] Christina Wenglén,[4] and Jörg H. W. Distler[1]

Objective. Systemic sclerosis (SSc) is a connective tissue disease with fibrotic remodeling of the skin and various internal organs. SSc is associated with the highest case-specific mortality of all rheumatic autoimmune diseases with limited antifibrotic treatment options. Here, we evaluated the therapeutic effects of the highly selective 5-hydroxytryptamine 2B receptor (5-HT_{2B}R) inhibitor AM1476.

Methods. The antifibrotic effects of AM1476 were evaluated in the mouse models of bleomycin-induced pulmonary fibrosis in Tsk-1 mice and in mice with sclerodermatous chronic graft-versus-host disease. For further validation, the antifibrotic effects of AM1476 were analyzed in precision cut skin (PCS) slices from patients with SSc.

Results. AM1476 demonstrated high selectivity for 5-HT_{2B}R over more than 200 other receptors, including other 5-HT receptors in vitro. AM1476 reduced accumulation of hydroxyproline and fibrotic tissue remodeling of skin and/or lungs in all three mouse models at well-tolerated doses with a comparable efficacy to that of nintedanib. In PCS of SSc skin, treatment with AM1476 reduced the expression of SSc-specific signature genes. AM1476 demonstrated more pronounced regulation of terms related to fibroblast activation and fibrotic remodeling than mycophenolate mofetil.

Conclusion. We describe AM1476 as a highly selective inhibitor of 5-HT_{2B}R. Treatment with AM1476 ameliorated fibrosis in three mouse models of SSc and normalized the expression of fibrosis-related genes directly in SSc skin. Because AM1476 also demonstrated good tolerability in a phase 1 trial, further clinical trials with AM1476 are currently in the planning stage.

INTRODUCTION

Fibrosis describes the excessive deposition of extracellular matrix in a tissue.[1] Aberrant fibrotic remodeling commonly induces organ dysfunction or failure. Fibrosis is one of today's major health care challenges. Fibrotic tissue remodeling accounts for up to 40% of the deaths in industrialized countries and results in socioeconomic costs of dozens of billions of euros per year to date.[2] Moreover, the global incidence of fibrosis and the associated health care burden are further increasing.[3] Systemic

Supported by the German Research Foundation (grants DI 1537/14-1, DI 1537/17-1, DI 1537/20-1, DI 1537/22-1, DI 1537/23-1, DI 1537/27-1, and DI 1537/28-1) the German Research Foundation (SFB CRC1181 [project C01] and SFB TR221/project 324392634 [B04]), Wilhelm-Sander-Foundation (grant 2013.056.1), Else-Kröner-Fresenius-Foundation (grants 2014_A47 and 2014_A184), the German Federal Ministry of Education and Research (BMBF), the MASCARA program, TP 2 (01EC1903A), a Career Support Award of Medicine of the Ernst Jung Foundation and an unrestricted research grant from the Hiller-Foundation (to Dr Distler), CompLS (program grant 031L0262C to Drs Dickel and Kunz), the German Research Foundation (SFB TR221/project 324392634 INF to Dr Kunz, GRK 2740 [B02 to Dr Kunz]), the ELAN-Foundation Erlangen (grant 21-07-23-1 to Dr Györfi), the National Science Foundation of China (grant 82030003), and the research committee of the Medical Faculty of Heinrich Heine University Düsseldorf (Forschungskommission [Foko]; ID 2022-18, ID 2023-33, and ID 2023-31). Also supported by project-specific funding of AnaMar.

[1]Thuong Trinh-Minh, PhD, Cuong Tran-Manh, PhD, Andrea-Hermina Györfi, MD, Christoph Liebel, BS, Xiang Zhou, PhD, Jörg H.W. Distler, MD: Department of Rheumatology, University Hospital Düsseldorf, Heinrich Heine University, Düsseldorf, Germany; Hiller Research Center, University Hospital Düsseldorf, Heinrich Heine University, Düsseldorf, Germany; [2]Nicholas Dickel, MSc, Kunz, PhD: Chair of Medical Informatics, Friedrich-Alexander University of Erlangen-Nürnberg; Erlangen, Germany; [3]Jiucun Wang, PhD: State Key Laboratory of Genetic Engineering, School of Life Sciences and Human Phenome Institute, Fudan University, Shanghai, China; [4]Helena Arozenius, MSc, Lars Pettersson, PhD, Sam Lindgren, MD, Christina Wenglén, PhD: AnaMar AB, Stockholm, Sweden.

Drs Trinh-Minh and Tran-Manh contributed equally to this work. Drs Wenglén and Distler contributed equally to this work.

Additional supplementary information cited in this article can be found online in the Supporting Information section (https://acrjournals.onlinelibrary.wiley.com/doi/10.1002/art.43151).

Author disclosures are available at https://onlinelibrary.wiley.com/doi/10.1002/art.43151.

Address correspondence via email to Jörg H. W. Distler, MD, at joerg.distler@med.uni-duesseldorf.de; or to Christina Wenglén, PhD, at christina.wenglen@icloud.com.

Submitted for publication May 6, 2024; accepted in revised form February 10, 2025.

sclerosis (SSc) is an idiopathic systemic fibrotic disease of the skin and multiple internal organs and is associated with the highest case-specific mortality of all autoimmune rheumatic diseases, with half of the patients dying as a direct consequence of the disease.[4] Despite considerable efforts, only a few antifibrotic therapies are approved for clinical use, generating a great need for novel effective antifibrotic therapies.

Myofibroblasts are activated fibroblasts that express contractile proteins and release abundant amounts of collagen and other components of the extracellular matrix. Although these cells are considered as core effector cells of all fibrotic diseases, the mechanisms that lead to their accumulation in fibrotic tissues remain incompletely understood. However, one recently identified mechanism is the activation of the 5-hydroxytryptamine 2B receptor (5-HT_{2B}R) by serotonin released from platelets at sites of vascular damage in SSc.[5] In addition to fibroblast modulation, 5-HT regulates macrophage plasticity, and activation of the 5-HT_{2B}R promotes profibrotic alternatively activated M2 macrophages (AAMs), a rich source of transforming growth factor β (TGFβ).[6] However, clinical translation of these findings has been hindered by the lack of highly selective, peripherally acting inhibitors of 5-HT_{2B}R with sufficient pharmacokinetics for clinical use.

We describe here the development and antifibrotic effects of a novel 5-HT_{2B}R inhibitor intended for oral treatment in humans. AM1476 (AnaMar AB; Pettersson, L. PCT appl. WO2016/207231) is an orally bioavailable small molecule targeting the peripheral 5-HT_{2B}R. AM1476 is a potent and competitive 5-HT_{2B}R antagonist devoid of agonistic activity and highly selective for the 5-HT_{2B}R. AM1476 has a favorable pharmacokinetic profile and has no preference to distribute to the brain. AM1476 demonstrated antifibrotic effects in different murine models and ameliorated the SSc-specific gene signature in an ex vivo model of SSc skin.

MATERIALS AND METHODS

Treatment. AM1476 was dissolved in sterile distilled water for the ex vivo and in vivo experiments. A concentration of 30 μ*M* was applied for the ex vivo experiment. For the in vivo experiments, 1, 3, or 10 mg/kg was administered orally once or twice daily.

Receptor binding and functionality profile of the 5-HT_{2B}R antagonist AM1476. The binding profile of AM1476 was evaluated for binding to human 5-HT_{2A}R, 5-HT_{2B}R, and 5-HT_{2C}R in radioligand binding assays using Chinese hamster ovary (CHO-K1) cells overexpressing human receptors (in vitro assays 271650, 271700, and 271800; Eurofins Panlabs Discovery). AM1476 was evaluated at 0.1, 1, 10, 100, 1,000, and 10,000 n*M* (5-HT_{2B}R) or at 1, 10, 100, 1,000, and 10,000 n*M* (5-HT_{2A}R and 5-HT_{2C}R). Human 5-HT_{2A}R and 5-HT_{2B}R functionality was measured with homogeneous time-resolved fluorescence quantification of IP1 accumulation in CHO-K1 cells (in vitro assays 355250 and 355260). Compounds creating a ≥50% inhibition of 5-HT (5 n*M*) induced fluorescence response specified receptor antagonist activity. 5-HT_{2C}R functionality was assessed with [35S] GTPγS for quantification of bound GTPγS. Compounds creating a ≥50% inhibition of 5-HT (100 n*M*) induced [35S] GTPγS binding response specified receptor antagonist activity (in vitro assay 355200). AM1476 was evaluated at 0.1, 0.3, 1, 3, 10, 30, and 300 n*M* (5-HT_{2B}R) or 1, 10, 100, 1,000, and 10,000 n*M* (5-HT_{2A}R and 5-HT_{2C}R). A nonlinear least squares regression analysis was used to determine half-maximal inhibitory concentration (IC_{50}) values. Mouse 5-HT_{2B}R functionality was measured in a calcium influx assay (Charles River) in CHO-KI cells expressing the mouse 5-HT_{2B}R using a calcium sensitive dye and a fluorescence imaging plate reader (FLIPRTETRA) instrument. AM1476 was evaluated at 0.3, 1, 3, 10, 30, 100, 300, and 1,000 n*M*.

Effects were considered significant if AM1476's mean value was three or more SDs above the vehicle control mean in the agonist assay or three or more SDs below the positive control agonist (5-n*M* α-methylserotonin) mean in the antagonist assay. AM1476 was screened for selectivity against approximately 200 targets using a Eurofins Panlabs Spectrum screen panel including enzymatic and receptor binding assays. Targets with potential peripheral effects to which AM1476 displayed a hit, defined as ≥50% inhibition at 10 μ*M*, were further evaluated at a lower concentration and/or in functionality assays at Eurofins Panlabs.

Patients. Ten patients with a diagnosis of SSc according to the 1980 American College of Rheumatology (ACR) criteria for SSc[7] and the 2013 EULAR/ACR classification criteria[8] provided informed written consent to participate in the study and were included. Only patients over 18 years of age were included in the study. One patient with SSc, who developed symptoms of myositis on clinical follow-up and was diagnosed with an overlap syndrome of SSc and dermatomyositis, was excluded from the analysis. The study was approved by the ethical committee of Friedrich-Alexander University Erlangen-Nürnberg and of the Heinrich Heine University Düsseldorf (applications 30-19B, 98-18B, and 2022-2158). Human studies were performed in compliance with the relevant ethical regulations. Patient demographics and clinical characteristics are provided in Supplementary Table S1.

Mouse models. *Experimental sclerodermatous chronic graft-versus-host disease.* The B10.D2→BALB/c (H-2d) minor histocompatibility antigen–mismatched model was performed as described.[9,10] Briefly, female BALB/c (H-2d) mice were purchased from Janvier. Male B10.D2 (H-2d) mice were initially purchased from Jackson Laboratory. All mice were maintained in specific pathogen-free conditions with sterile pellet food and water and a normal day–night cycle. For isolation of unfractionated bone marrow cells, tibial and femoral bones were

prepared under sterile conditions. Phosphate buffered saline (PBS) was used to flush bone marrow cells from bone marrow cavities. Subsequently, bone marrow cells were filtered through 70-μm nylon meshes (BD Biosciences), followed by erythrocyte hemolysis. The remaining bone marrow cells were kept on ice until transplantation. Transplantation of bone marrow cells and splenocytes was performed as follows: Recipient mice (BALB/c [H-2d]) eight weeks of age received total body irradiation with 750 cGy. Six hours after irradiation, all BALB/c (H-2d) recipients received bone marrow from either BALB/c (H-2d) in a syngeneic transplantation manner or B10.D2 (H-2d) in an allogeneic transplantation manner. For transplantation, 5×10^6 splenocytes and 2×10^6 bone marrow cells from donor mice were resuspended in 0.2 mL of PBS and injected via tail veins.[9,10] To reflect the clinical situation with treatment initiation upon clinical signs of chronic graft-versus-host disease (cGvHD), treatment was started 21 days after bone marrow transplantation (BMT) and thus after the first clinically detectable manifestations of cGvHD in allogeneically transplanted mice. The outcome of treatment was analyzed seven weeks after transplantation. Eight mice per group were analyzed.

Tsk-1 mouse model. In the murine Tsk-1 model of SSc, a dominant mutation in the fibrillin 1 gene leads to an SSc-like disease, with minor inflammatory infiltrates, autoantibody production, and fibrosis of the skin. This model reflects the later stages of SSc characterized by noninflammatory self-sustaining fibrosis. Eight to 12 mice per group were analyzed. Treatment was initiated at an age of five weeks, and the outcome was analyzed at an age of 10 weeks.[11]

Bleomycin-induced pulmonary fibrosis. Pulmonary fibrosis was induced by a single intratracheal instillation of bleomycin (25 μg in 50 μL of 0.9% NaCl).[12] Treatment was initiated at two weeks after the first injection of bleomycin. AM1476 was administered orally at 1, 3, or 10 mg/kg once daily. Solvent (double-distilled water) was used as a control, and nintedanib at 30 mg/kg orally every day (qd) was included as a comparator. The outcome was analyzed at two and four weeks after the first injection of bleomycin. Mice injected with 0.9% NaCl, the vehicle of bleomycin, served as nonfibrotic controls. Eight mice per group were analyzed.

General monitoring of mice. Mice were monitored clinically on a daily basis for behavior, activity, texture of the fur, weight, and consistency of the stool.[13] After the mice were killed, a gross macroscopic evaluation of the lungs and the skin was performed.

Clinical scoring of cutaneous cGvHD. Recipient mice were clinically monitored on a daily basis from the day of transplantation to the indicated days after transplantation to determine the incidence and severity of cutaneous cGvHD as well as mobility, diarrhea, and weight loss.[10,14] The following scoring system for cutaneous cGvHD was used: healthy appearance = 0; skin lesions with alopecia <1 cm^2 in area = 1; skin lesions with alopecia 1 to 2 cm^2 in area = 2; and skin lesions with alopecia >2 cm^2 in area = 3. Incidence was expressed as the percentage of mice that showed clinical manifestations.

Histologic evaluation of dermal and pulmonary fibrosis. Skin samples were fixed in 4% formalin for six hours and embedded in paraffin. Five-micrometer sections were cut and stained with hematoxylin and eosin (H&E). The dermal thickness was quantified on H&E-stained sections using images captured with a light microscope (Nikon eclipse 80i) at 100-fold magnification by manually measuring the distance between the epidermal-dermal junction and the dermal-subcutaneous fat junction at four sites per mouse.[15,16] For lung samples, the whole left lung was fixed in 4% formalin for six hours and embedded in paraffin. Five-micrometer sections were cut and stained with trichrome and sirius red. Histologic readouts were evaluation of the fibrotic area as the percentage of the total lung area in sirius red–stained sections (two sections per mouse) and quantification of pulmonary changes using the Ashcroft score (four sections per mouse).[17,18]

Hydroxyproline assay. The amount of collagen protein in skin and lung samples was determined by hydroxyproline assay.[19,20] After digestion in 6 *M* HCl for three hours at 120°C, the pH of the samples was adjusted to a pH range of 6–7 with 6 *M* NaOH. Afterward, 0.06 *M* chloramine T was added to each sample and incubated for 20 minutes at room temperature. Next, 3.15 *M* perchloric acid and 20% *p*-dimethylaminobenzaldehyde were added, and samples were incubated for an additional 20 minutes at 60°C. The absorbance was determined at 557 nm with a Spectra MAX 190 microplate spectrophotometer. Absolute values were determined using a standard curved generated with type I collagen (Sigma-Aldrich).

Detection of myofibroblasts. Myofibroblasts are characterized by the expression of α-smooth muscle actin (α-SMA). Fibroblasts positive for α-SMA were detected by immunohistochemistry staining with monoclonal anti–α-SMA antibodies (clone 1A4, Sigma-Aldrich). The expression was visualized with horseradish peroxidase–labeled secondary antibodies and 3,3-diaminobenzidine tetra hydrochloride (Sigma-Aldrich). Monoclonal mouse IgG antibodies (Calbiochem) were used as controls. Images of sections stained for α-SMA were captured on a light microscope (Nikon eclipse 80i). The myofibroblast number was manually evaluated at four different areas at 200-fold magnification. Myofibroblasts were defined as α-SMA positive, single, and spindle-shaped cells in the dermis.[5,21]

Immunofluorescence staining. Immunofluorescence staining was performed as described previously.[22] AAMs are defined as cells positively stained for anti-cMAF antibody

(PA5-23179, Thermo Scientific, 1:100 dilution), anti-arginase antibody (ab60176, Abcam, 1:100 dilution), and anti-F4/80 antibody (MCA497G, Bio-rad, 1:100 dilution). Donkey anti-rat Alexa Fluor 488, donkey anti-goat Alexa Fluor 555, and donkey anti-rabbit Alexa Fluor 647 (Life Technologies) were used as secondary antibodies for AAM staining. Counter staining was performed with the DNA dye DAPI (Santa Cruz Biotechnology). The analysis of AAM cells was performed by an experienced reviewer in a blinded manner in three sections per sample.

The staining of skin sections was performed by using the antibodies against CCL2 (LS-C169178-100, LSBio, 1:100 dilution), CCL5 (MAB478-100, Biotechne, 1:100 dilution), CCL18 (22303-1-AP, Proteintech, 1:100 dilution), PAI-1 (66261-1-Ig, Proteintech, 1:100 dilution), P-STAT3 (MA5-15193, Thermo Scientific, 1:100 dilution), MAOB (12602-1-AP, Proteintech, 1:100 dilution), or SLC6A4 (LS-C154958-100, LSBio, 1:100 dilution). Donkey anti-mouse or anti-rabbit Alexa Fluor 488 was used as secondary antibodies. Counter staining was performed with the DNA dye DAPI (Santa Cruz Biotechnology). The analysis of target average intensity was performed by an experienced researcher in a blinded manner in two sections per sample.

RNA sequencing and bioinformatics analysis of murine and human skin. Total RNA from the cGvHD mouse model and from human precision cut skin (PCS) slices was extracted using the Qiagen total RNA kit according to the instructions of the manufacturer. RNA sequencing (RNASeq) was performed by Novogene on an Illumina NovaSeq platform using a paired-end 150-bp sequencing strategy. Raw paired-end reads were mapped to the reference genome of *Homo sapiens* (GRCh38) and *Mus musculus* (GRCm38, mm10) using STAR aligner (version 2.0.2). The sorted bam files were processed by featureCounts to obtain a count matrix. Principal component analysis was performed using the ggplot2 package (version 3.4.0) to determine the potential outliers among samples in each batch. After quality control, a differential gene expression analysis was performed using edgeR (version 3.38.4), in which a normalization method Trimmed Mean of M-values was applied. A threshold of adjusted $P \leq 0.05$ and $|\log_2$ fold change ($\log_2$FC)$| \geq 1$ was used to identify the statistically significantly differentially expressed genes (DEGs). The results were visualized as a volcano plot using the ggplot2 package (version 3.4.0) according to the $\log_2$FC and –log10 adjusted *P* value of DEGs. Hierarchical cluster analyses were performed using the pheatmap package (version 1.0.12). A functional overrepresentation analysis was performed using clusterProfiler (version 4.4.4), and results were depicted in a dot plot. A gene set enrichment analysis (GSEA) on normalized gene counts was performed using the fgsea package (version 1.22.0), in which the collected gene sets of c2-KEGG from the Molecular Signatures Database (MSigDB) were used. Analysis was performed in R (version 4.2.1).

Pharmacokinetic study of AM1476. A pharmacokinetic study of AM1476 was performed using the cGvHD model described previously. After repeated oral administration for 28 days, whole blood was collected from each treatment group 15 minutes, 30 minutes, and 1, 2, 4, 6, 8, and 24 hours after a final morning dose (two animals were used for each time point), and plasma was separated from blood within 30 minutes. The plasma concentration of AM1476 was measured by a Waters TQ-S triple quadrupole Mass Spectrometer system coupled with Acquity UPLC (Admescope).

PCS slices of SSc skin. Freshly taken skin punches (diameter of 3 mm) of 10 patients with SSc were embedded in 3% low melting agarose (#16520100, Thermo Fisher Scientific). Cylindrical cores of solidified agarose containing the skin punch were generated, and consecutive PCS slices with a thickness of 230 μm containing epidermis, dermis, and hypodermis layers were generated using an Alabama R&D Tissue Slicer (Alabama Research and Development). PCS slices were subsequently transferred into 24-well plates filled with prewarmed minimum essential media (Life Technologies) containing 11.34 m*M* glucose (Komtur Pharmaceuticals), 26 m*M* $NaHCO_3$ (Sigma-Aldrich), 25 m*M* HEPES, 1 m*M* sodium pyruvate, 2 m*M* GlutaMax (all Gibco), penicillin/streptomycin, and amphotericin (both Sigma-Aldrich) at 37°C, 5% CO_2, and atmospheric O_2. After 12 hours, PCS slices were incubated with AM1476 (30 μ*M*), mycophenolate mofetil (1 μ*M*), or vehicle (medium) for 48 hours. Afterward, PCS slices were collected in RNAlater (#AM7020, Thermo Fisher) and stored at –80°C until RNA isolation was performed.

Statistics. All non–RNASeq data are presented as mean ± SEM, with individual values displayed as dots. Differences between the groups were tested for their statistical significance by one-way analysis of variance. *P* values less than 0.05 were considered significant.

Data availability. All data generated or analyzed during this study are included in this article (and its supplementary files). Additional supporting information or raw data are available from the corresponding author upon request.

RESULTS

Characterization of AM1476 as a selective inhibitor of 5-HT_{2B}R. The 5-HT_2 receptor binding affinity and functionality for AM1476 AnaMar AB; PCT appl. WO2016/207231) was evaluated in vitro by Eurofins Panlabs using CHO-K1 cells that stably express human recombinant 5-HT_{2A}R, 5-HT_{2B}R, or 5-HT_{2C}R. Receptor studies showed that AM1476 binds to the human 5-HT_{2B}R with an inhibition constant (K_i) of 6.0 n*M*, (Ki of 800 n*M* for 5-HT_{2A}R and 60 n*M* for 5-HT_{2C}R). AM1476 strongly antagonizes the 5-HT_{2B}R with a half-maximal IC_{50} of 5.8 n*M*

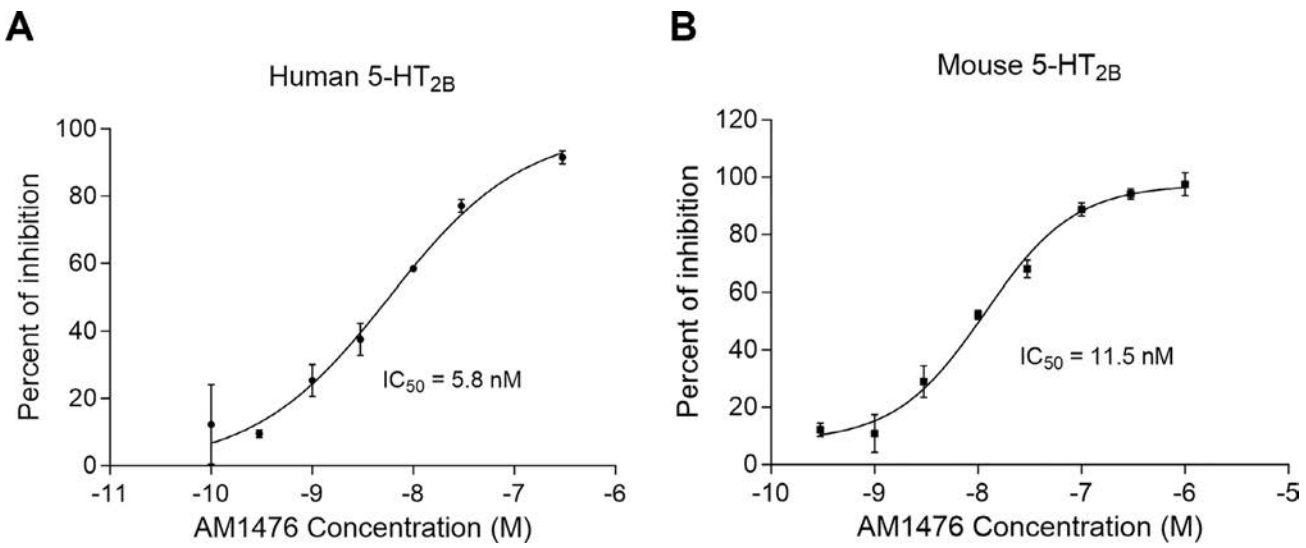

Figure 1. Inhibition curves for AM1476 in (A) human and (B) mouse 5-HT$_{2B}$R functionality assays. 5-HT$_{2B}$R, 5-hydroxytryptamine 2B receptor; IC$_{50}$, inhibitory concentration.

(Figure 1A) but showed only low activity at the 5-HT$_{2A}$R (IC$_{50}$ > 10,000 n*M*) and 5-HT$_{2C}$R (IC$_{50}$ = 3100 n*M*) (Supplementary Table S2). The AM1476 IC$_{50}$ value to mouse 5-HT$_{2B}$R was 11.5 n*M* (Figure 1B). Testing of approximately 200 other targets, including several members of the 5-HT receptor family, demonstrated no binding to the majority of targets (defined as <50% inhibition at 10 μ*M*). Targets with potential peripheral effects to which AM1476 displayed a hit (defined as ≥50% inhibition at 10 μ*M*) were further evaluated at a lower concentration (Supplementary Table S3) or in functionality assays (Supplementary Table S4). No interactions at clinically relevant concentrations were detected, thereby confirming the high selectivity of AM1476 to the 5-HT$_{2B}$R (Supplementary Tables S3 and S4).

Inhibition of 5-HT$_{2B}$R ameliorates dermal fibrosis in murine cGvHD and tight skin models. We next aimed to evaluate the effects of AM1476 in mouse models of SSc (Figure 2A). We chose the cGvHD model because of its rapidly progressive and systemic fibrotic remodeling, which includes the skin and lungs as major tissues evaluated in clinical trials of SSc. Allogeneic BMT induced progressive weight loss, with a significantly lower mean body weight in allogeneically transplanted, vehicle-treated mice compared to syngeneic controls 49 days after BMT (Supplementary Figure 1). The composite score of cutaneous cGvHD progressively increased in vehicle-treated, allogeneically transplanted mice after BMT compared to syngeneic controls (Figure 2B). Moreover, allogeneic transplantation induced prominent skin fibrosis with increased dermal thickness, up-regulated the hydroxyproline content, and induced the accumulation of myofibroblasts (Figure 2C and D). Dermal thickness, hydroxyproline content, and myofibroblasts numbers increased over time, with higher levels at seven weeks after BMT as compared to three weeks after BMT (Figure 2D).

Treatment with all three doses of AM1476 was well tolerated without obvious signs of toxicity on clinical examination, on gross necropsy, or on histology at any dose. Treatment with AM1476 started at day 21 after BMT demonstrated antifibrotic effects on cGvHD-induced skin fibrosis and reduced dermal thickening, accumulation of hydroxyproline, and myofibroblast differentiation as compared to vehicle-treated mice observed for seven weeks after BMT (Figure 2C). The antifibrotic effects of doses of 10 mg/kg twice a day (bid) and 10 mg/kg qd were comparable to each other, and both were more pronounced than with 1 mg/kg bid. Myofibroblast counts of mice treated with all three doses were significantly lower than that of mice killed three weeks after BMT (Figure 2D). A significant reduction compared to mice killed after three weeks was also observed for the hydroxyproline content in mice treated with doses of 10 mg/kg qd (Figure 2D).

In the murine Tsk-1 model of SSc, a dominant mutation in the fibrillin 1 gene leads to skin fibrosis. This model resembles features of later stages of SSc without major inflammatory infiltrates in the skin, where fibrotic remodeling is mainly driven by endogenously active fibroblasts. Tsk-1 mice do not show major changes in the thickness of the dermal layer, but extracellular matrix (ECM) accumulates in the hypodermis. Tsk-1 mice developed prominent skin fibrosis with hypodermal thickening, myofibroblast differentiation, and increased hydroxyproline content that progressed between ages 5 and 10 weeks. All three doses of AM1476 reduced hypodermal thickening, myofibroblast counts, and hydroxyproline content compared to vehicle-treated 10-week-old Tsk-1 mice (Figure 2E–G). The hypodermal thickness and the hydroxyproline content of mice treated with 10 mg/kg qd or treated with 10 mg/kg bid were comparable to that of five-

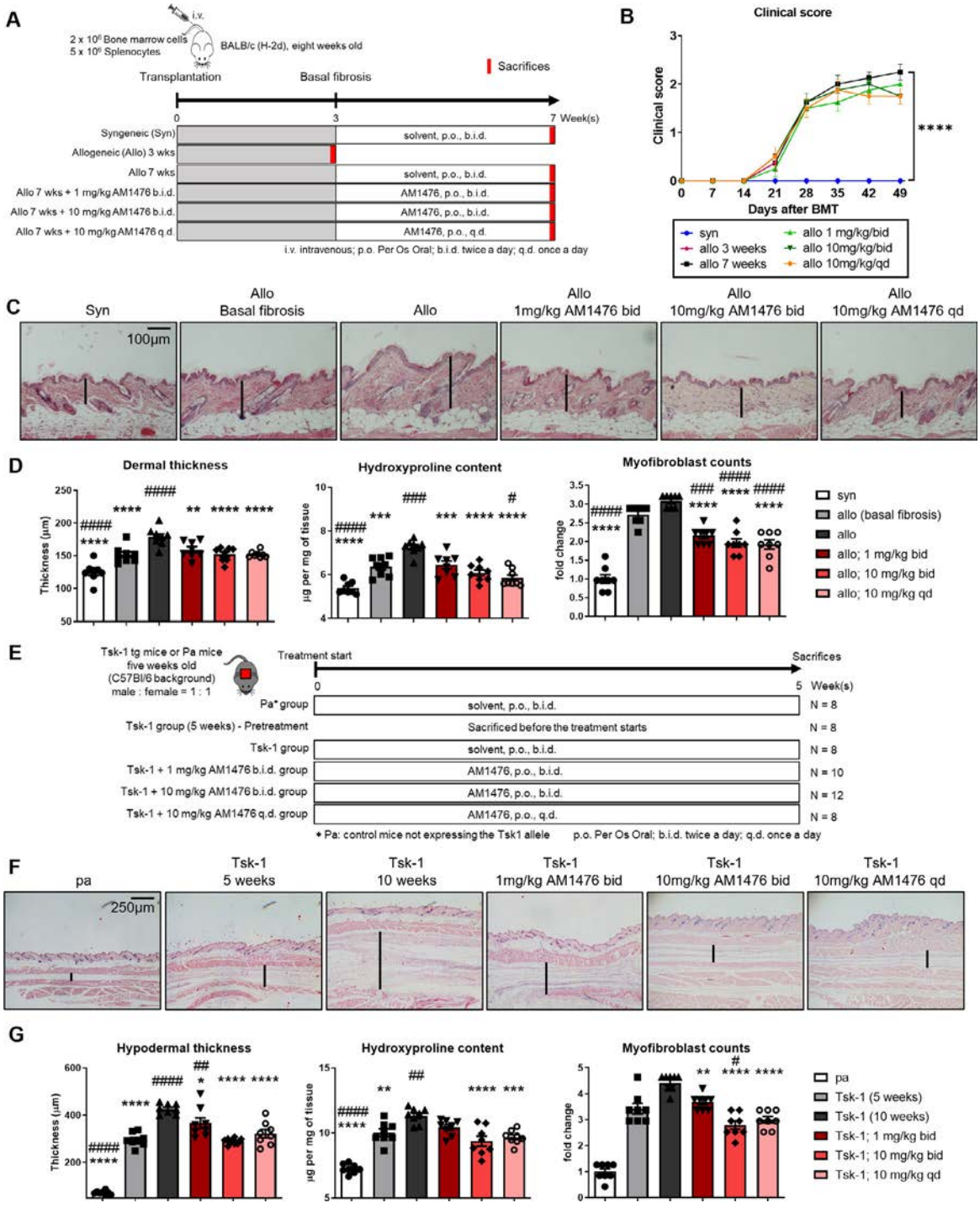

Figure 2. AM1476 ameliorates fibrosis in experimental cGvHD and Tsk-1-mice. (A–D) cGvHD-induced dermal fibrosis. (A) Schematic illustration of the experimental design of cGvHD-induced dermal fibrosis. (B) Effects of AM1476 on clinical cutaneous scores in cutaneous cGvHD. (C) Representative hematoxylin and eosin staining of cGvHD-induced dermal fibrosis. (D) Quantification of dermal thickness, hydroxyproline content, and myofibroblast counts. (E–G) Skin fibrosis in Tsk-1 mice. (E) Schematic illustration of the experimental outline. (F) Representative hematoxylin and eosin staining. (G) Quantification of hypodermal thickness, hydroxyproline content, and myofibroblast counts. All data are presented as mean ± SEM, with individual values displayed as column plus dots. Differences between the groups were tested for their statistical significance by one-way analysis of variance with Dunnett's multiple comparison. Adjusted P values <0.05 were considered significant. Adjusted P values are expressed as follows: *$0.05 > P > 0.01$; **$0.01 > P > 0.001$; ***$0.001 > P > 0.0001$; ****$P < 0.0001$ as compared to fibrotic control mice (allo 7 weeks or Tsk-1 10 weeks). Adjusted P values are expressed as follows: $^{\#}0.05 > P > 0.01$; $^{\#\#}0.01 > P > 0.001$; $^{\#\#\#}0.001 > P > 0.0001$; $^{\#\#\#\#}P < 0.0001$ as compared to baseline fibrotic control mice (allo 3 weeks or Tsk-1 5 weeks). allo, allogeneic; BMT, bone marrow transplantation; cGvHD, chronic graft-versus-host disease; syn, syngeneic.

week-old Tsk-1 mice (pretreatment level) (Figure 2F and G). Plasma concentrations of AM1476 after 28 days of repeated oral once daily administration in the cGvHD mice were measured. The results show that the level of systemic exposure of AM1476 exceeded the IC_{50} of mouse 5-HT$_{2B}$R antagonistic activity (Supplementary Figure 2).

AM1476 alleviates pulmonary fibrosis induced by cGvHD and bleomycin. Allogeneic BMT induced moderate pulmonary fibrosis, with increases in Ashcroft scores, in the collagen-covered lung area and in the hydroxyproline content (Figure 3A and B and Supplementary Figure 3). Treatment with AM1476 at all three doses reduced the Ashcroft scores, the collagen-covered lung area, and the hydroxyproline content as compared to vehicle-treated mice observed for seven weeks after BMT (Figure 3A and B). Treatment with AM1476 in doses of 10 mg/kg qd reduced the hydroxyproline levels to below those of mice killed three weeks after BMT, indicative of reversion of collagen accumulation.

We chose bleomycin-induced pulmonary fibrosis as a well-established model of rapidly progressive and severe pulmonary fibrosis, in contrast to the mild-to-moderate changes in the lungs of cGvHD mice. Bleomycin-challenged mice developed prominent pulmonary fibrosis, with increased Ashcroft scores, increases in the collagen-covered area, and increased hydroxyproline content (Figure 3C–E). All doses of AM1476 demonstrated antifibrotic effects, with decreases in Ashcroft scores, the collagen-covered area, and hydroxyproline content as compared to vehicle-treated, bleomycin-challenged mice (Figure 3D and E). The antifibrotic effects of AM1476 were comparable to those of nintedanib, a tyrosine kinase inhibitor approved for the treatment of progressive pulmonary fibrosis, across the different readouts.

Inhibition of 5-HT$_{2B}$R regulates core pathways of fibrosis in murine cGvHD. To obtain insights into the molecular effects of AM1476, we performed RNASeq. The comparison of samples from AM1476-treated mice undergoing allogeneic transplantation and vehicle-treated mice undergoing allogeneic transplantation yielded 260 DEGs, including 171 up-regulated genes and 89 down-regulated genes (adjusted $P \leq 0.05$, $|\log_2 FC| \geq 1$) (Figure 4A).

Functional enrichment via Gene Ontology based on the Biological Process database demonstrated AM1476-induced changes in several processes related to tissue remodeling, such as connective tissue development, extracellular matrix organization, and smooth muscle tissue development, or processes involved in inflammation, such as negative regulation of immune system process, negative regulation of leukocyte migration, myeloid cell activation involved in immune response, negative regulation of leukocyte chemotaxis, negative regulation of mononuclear cell migration, and negative regulation of the type I interferon–mediated signaling pathway (Figures 4B). We found several well-known fibrotic genes to be down-regulated, including *Shh*, *Col25a1*, and *Col11a1*, as well as many antifibrotic genes to be up-regulated, including *Dkk2*, *Ccn3*, *Fgf18*, *Hpse2*, *Cilp*, and *Prox1* (Figure 4C). Moreover, many genes involved in inflammatory processes are found significantly regulated by AM1476, such as *Nr1d1*, *Mmp28*, *Sox11*, *Ccn3*, *Dcst1*, and *Isg15* (Figure 4D). AM1476 may also inhibit accumulation of AAMs. Quantifications of AAM counts in the skin also demonstrated reduction of AAM accumulation for all three doses, with statistically significant differences for 10 mg/kg qd and 10 mg/kg bid (Figure 4E). This effect was not a mere reflection of reduced inflammation upon AM1476 treatment because none of the concentrations of AM1476 reduced the number of CD45$^+$ leukocytes (Supplementary Figure 4).

Evaluation of the effects of AM1476 in PCS slices of SSc skin. We established precision-cut skin (PCS) slices from SSc skin biopsies as an ex vivo model system that allows the evaluation of treatment responses directly in the pathophysiologically relevant human target tissue of patients with SSc (Figure 5A). These PCS slices maintain all relevant cellular players and pathophysiologic niches of SSc skin, thereby enabling an ex vivo trial approach for drug testing.[23,24] Differential gene expression analysis of SSc-PCS treated with AM1476 (n = 9 patients) compared with donor-matched PCS treated with the vehicle showed 425 DEGs ($P \leq 0.05$, $|\log_2 FC| \geq 1$), 294 of which were up-regulated and 131 of which were down-regulated (Figure 5B).

A functional overrepresentation analysis of AM1476-DEGs demonstrated deregulation of several processes related to tissue remodeling (such as cell adhesion, intermediate filament cytoskeleton organization, intermediate filament-based process, negative regulation of wound healing, integrin activation, mesenchyme morphogenesis, and negative regulation of myoblast differentiation) and inflammatory responses (such as leukocyte chemotaxis, myeloid leukocyte migration, mononuclear cell migration, granulocyte chemotaxis, neutrophil chemotaxis, and lymphocyte chemotaxis) (Figures 5C). GSEA results highlighted that AM1476 negatively regulated GvHD and induced the peroxisome proliferator–activated receptor signaling pathway," which is a well-known antifibrotic signaling pathway (Figure 5D). A direct comparison of AM1476 and mycophenolate mofetil (MMF) revealed that AM1476 regulated more terms related to tissue remodeling than MMF (Figure 5E). MMF is recommended for the treatment of dermal and pulmonary fibrosis in SSc and is the most widely used immunomodulatory treatment used in patients with SSc. Of note, AM1476 and MMF both modulated terms related to various immune cell types, including myeloid leukocytes, granulocytes, and mononuclear cells for AM1476 and T cells, natural killer cells, myeloid leukocytes, and neutrophils for MMF (Figure 5E). These findings suggest that although AM1476 shares some similarities with MMF in regulation of immune responses, it

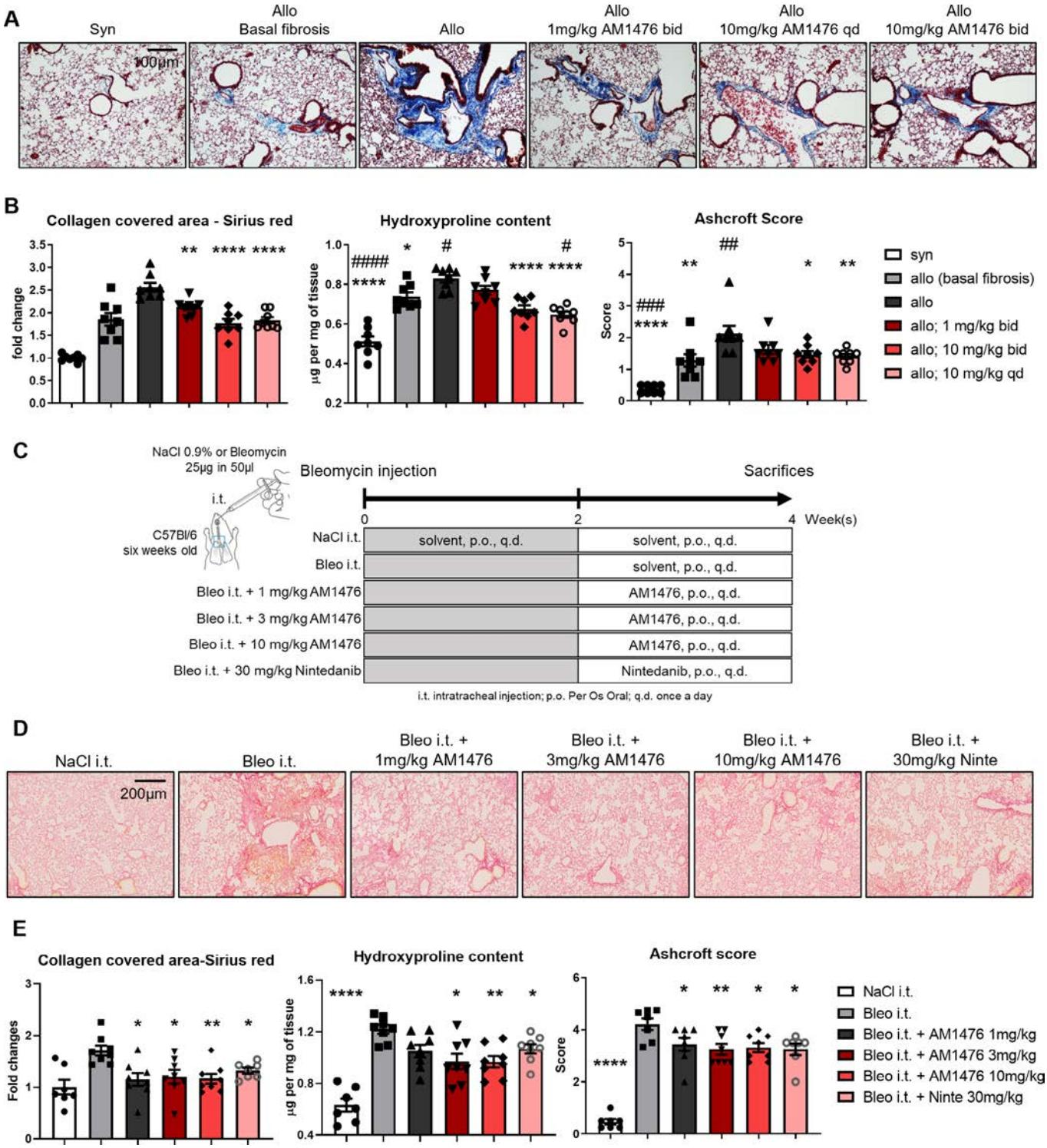

Figure 3. Inhibition of 5-HT$_{2B}$R by AM1476 ameliorates cGvHD- and bleomycin-induced pulmonary fibrosis. (A and B) cGvHD-induced pulmonary fibrosis. (A) Representative trichrome staining in lungs from cGvHD-induced dermal fibrosis experiment and (B) quantifications of collagen-covered area (sirius red staining), hydroxyproline content, and Ashcroft score. (C–E) Bleomycin-induced pulmonary fibrosis: (C) Schematic illustration of the experimental design of bleomycin-induced pulmonary fibrosis. (D) Representative sirius red staining from lung sections. (E) Quantification of collagen-covered area (sirius red staining), hydroxyproline content, and Ashcroft scores. All data are presented as mean ± SEM, with individual values displayed as column plus dots. Differences between the groups were tested for their statistical significance by one-way analysis of variance with Dunnett's multiple comparison. Adjusted P values are expressed as follows: $^{*}0.05 > P > 0.01$; $^{**}0.01 > P > 0.001$; $^{***}0.001 > P > 0.0001$; $^{****}P < 0.0001$ as compared to fibrotic control mice (allo 7 weeks or Bleo i.t.). Adjusted P values are expressed as follows: $^{\#}0.05 > P > 0.01$; $^{\#\#}0.01 > P > 0.001$; $^{\#\#\#}0.001 > P > 0.0001$; $^{\#\#\#\#}P < 0.0001$ as compared to baseline fibrotic control mice (allo 3 weeks). 5-HT$_{2B}$R, 5-hydroxytryptamine 2B receptor; allo, allogeneic; Bleo i.t., bleomycin intratracheal injection; cGvHD, chronic graft-versus-host disease; syn, syngeneic. Color figure can be viewed in the online issue, which is available at http://onlinelibrary.wiley.com/doi/10.1002/art.43151/abstract.

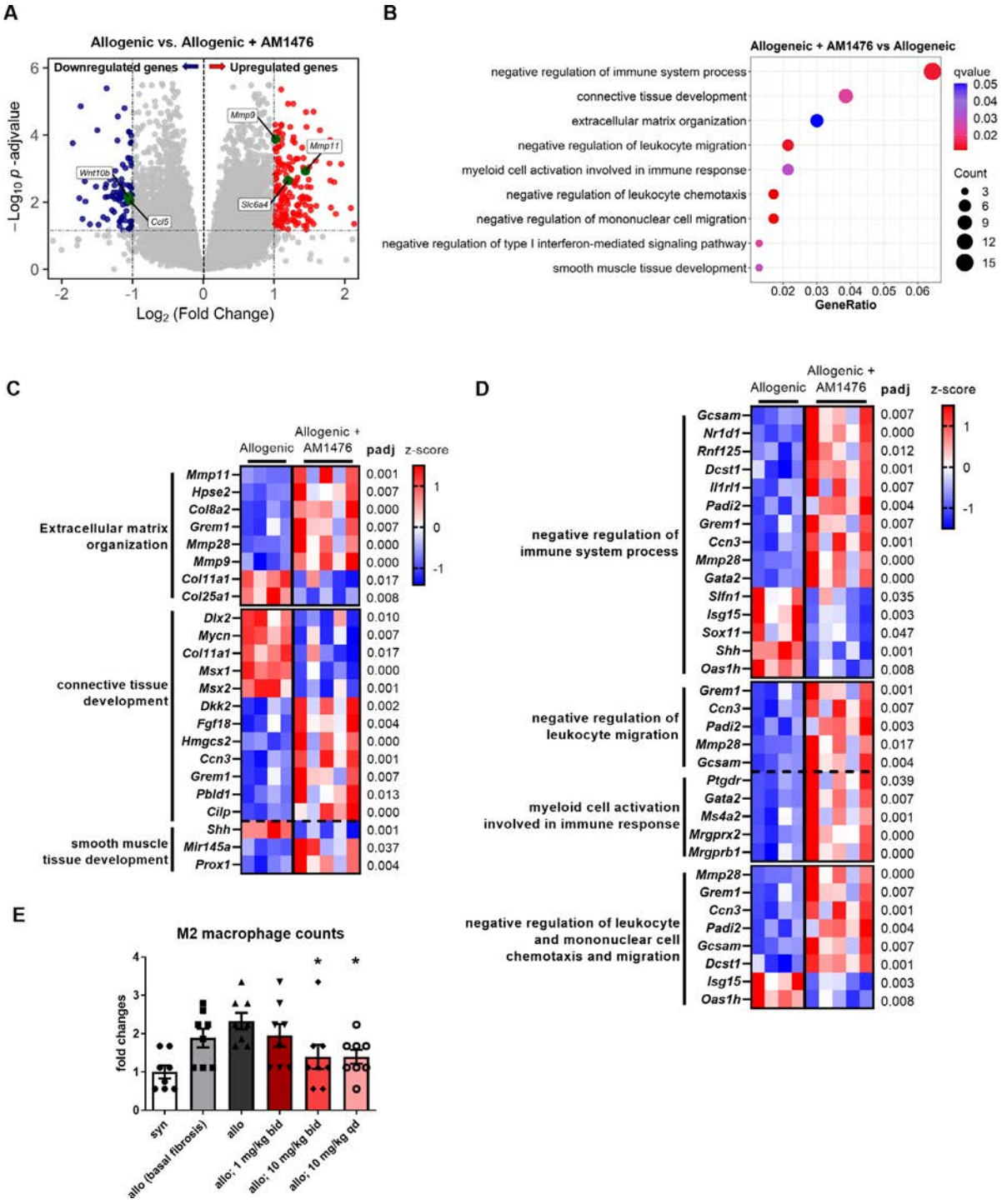

Figure 4. AM1476 ameliorates profibrotic transcriptional programs and alternative macrophage activation in cGvHD skin. (A) Volcano plot of the comparison of vehicle-treated allogeneic mice (n = 4) with allogeneic mice treated with AM1476 at 10 mg/kg once daily (n = 5). (B) Functional over-representation analysis of AM1476-allo-DEGs based on the GO-BP database showing deregulation of several gene sets related to extracellular matrix remodeling and activation of innate immunity upon treatment with AM1476. (C) Heatmap showing significant signature genes of GO-BP enrichment terms related to fibrosis and tissue remodeling. (D) Heatmap showing significant signature genes of GO-BP enrichment terms related to immune response. (E) Bar graphs with dots show quantification of the number of activated M2 macrophages in allo mice treated with different concentrations of AM1476. All data are presented as mean ± SEM, with individual values displayed as column plus dots. Differences between the groups were tested for their statistical significance by one-way analysis of variance with Dunnett's multiple comparison. Adjusted *P* values <0.05 were considered significant. Adjusted *P* values are expressed as follows: *0.05 > *P* > 0.01; **0.01 > *P* > 0.001; ***0.001 > *P* > 0.0001; ****$P <$ 0.0001 as compared to fibrotic control mice. allo, allogeneic; cGvHD, chronic graft-versus-host disease; DEGs, differentially expressed genes; GO-BP, Gene Ontology Biological Process. Color figure can be viewed in the online issue, which is available at http://onlinelibrary.wiley.com/doi/10.1002/art.43151/abstract.

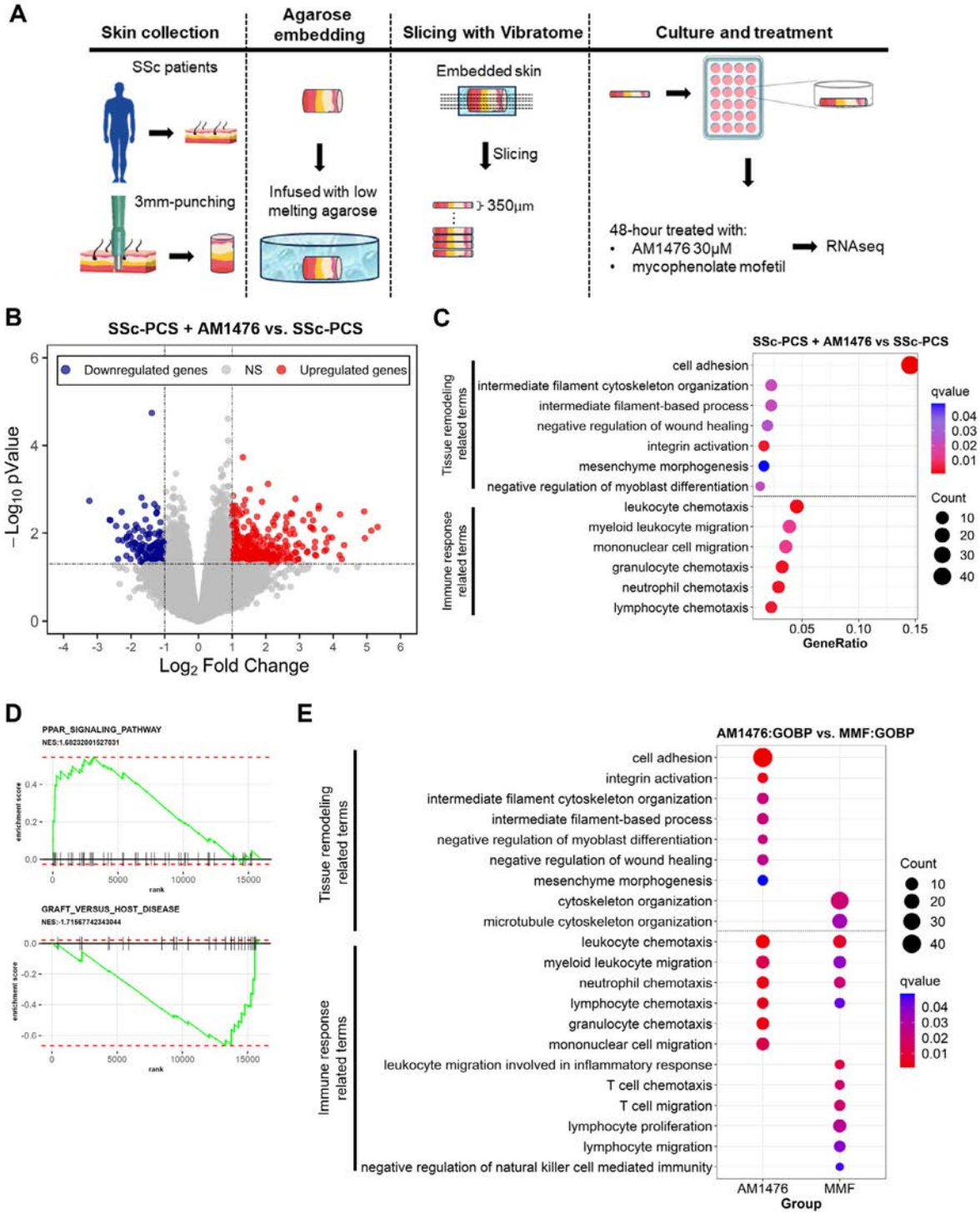

Figure 5. Inhibition of 5-HT_{2B}R by AM1476 modulates inflammation and fibrosis-related transcriptional responses in SSc skin. (A) Schematic visualization of the experiment. (B) Volcano plot illustrating AM1476-DEGs (down-regulated genes in dark blue and up-regulated genes in red) representing 5-HT_{2B}R inhibitor (AM1476, 30 μ*M*)–treated SSc-PCS compared to control SSc-PCS treated with vehicle. (C) Bubble plot of the functional overrepresentation analysis of AM1476-DEGs showing terms related to tissue remodeling and immune response. (D) GSEA of the AM1476-DEGs showing enrichment of the gene set "PPAR_signaling_pathway" and de-enrichment of the gene set "graft_versus_host_disease." (E) Bubble plot presenting the comparison of the functional overrepresentation analysis between AM1476:GOBP and MMF:GOBP showing terms related to tissue remodeling and immune response. 5-HT_{2B}R, 5-hydroxytryptamine 2B receptor; DEGs, differentially expressed genes; GOBP, Gene Ontology Biological Process; GSEA, gene set enrichment analysis; MMF, mycophenolate mofetil; PCS, precision cut skin; PPAR, peroxisome proliferator–activated receptor; RNAseq, RNA sequencing; SSc, systemic sclerosis. Color figure can be viewed in the online issue, which is available at http://onlinelibrary.wiley.com/doi/10.1002/art.43151/abstract.

exerts a more pronounced effect on fibrosis-related terms than MMF in PCS slices of SSc skin.

Integration of RNASeq data from SSc-PCS and murine cGvHD models, both treated with AM1476, identified up-regulation of MAOB and SLC6A4 (Supplementary Figure 5). These findings suggest reduced 5-HT availability in fibrotic tissues treated with AM1476, providing a novel mechanism by which 5-HT$_{2B}$R inhibition using AM1476 exerts antifibrotic effects. RNA-Seq data showed consistent up-regulation of matrix metalloproteinases across both models, suggesting a role in ECM degradation (Supplementary Figure 6A). Additionally, AM1476 down-regulated WNT5A and WNT10B, two crucial pro-fibrotic cytokines known to promote fibroblast activation and ECM production in tissue fibrosis,[14,25–29] while up-regulating WNT antagonists (DKK1, SFRP1/2),[21,29,30] indicating suppression of WNT signaling (Supplementary Figure 6B). AM1476 also reduced proinflammatory chemokines (eg, CCL2, CCL5, and CCL18)[31–35] and interleukin-1 family members[36–39] (Supplementary Figure 6C). Finally, AM1476 reduced the levels of P-STAT3 and PAI-1, both downstream targets of TGFβ in SSc. Immunofluorescence staining validated the RNASeq findings, showing consistent changes in MAOB and SLC6A4 (markers of 5-HT metabolism), CCL2, CCL5, and CCL18 (inflammatory chemokines), as well as PAI-1[40–42] and P-STAT3 (TGFβ signaling targets)[15,20,23,41,43,44] (Figure 6A–D and Supplementary Figure 7). These integrated results demonstrate the robust and multifaceted antifibrotic mechanisms of AM1476.

Safety and tolerability of AM1476 in a phase 1 clinical trial. These findings prompted us to perform a phase 1 clinical trial investigating safety, tolerability, and the pharmacokinetic profile of AM1476 in healthy individuals (ClinicalTrials.gov identifier NCT04691115). AM1476 was well tolerated, most of the adverse events were mild in severity, and no serious adverse events were reported. An excerpt of the summary of adverse events is found in Supplementary Table S5. Following single and multiple oral administration of AM1476 in the fasted state, AM1476 was rapidly absorbed, and steady state was achieved by day two of the multiple-dose period. The anticipated clinical efficacy exposure was well covered by investigated doses.

DISCUSSION

We describe herein the pharmacological development of the novel 5-HT$_{2B}$R inhibitor AM1476 and its effects in preclinical and ex vivo models of SSc. AM1476 overcomes several limitations of previously described 5-HT$_{2B}$R inhibitors by showing high 5-HT$_{2B}$R potency with no agonism and with excellent selectivity as well as favorable pharmacokinetic properties. In addition, the low preference of AM1476 to distribute to the brain makes it suitable for chronic treatment, devoid of central nervous system–related side effects.

AM1476 demonstrated potent antifibrotic effects across different preclinical models of SSc. AM1476 reduced fibrotic tissue remodeling in three complementary mouse models of SSc, bleomycin-induced pulmonary fibrosis, Tsk-1, and cGvHD, which model different aspects of the pathogenesis of SSc and may resemble different subpopulations of patients with SSc. Bleomycin-induced pulmonary fibrosis mimics patients with inflammatory, progressive interstitial lung disease in SSc; Tsk-1 mice resemble patients with noninflammatory, wide-spread skin disease; and cGvHD mice represent early inflammatory SSc with rapid progression of skin and lung disease. AM1476 reduced myofibroblast differentiation, reduced collagen deposition, and ameliorated dermal and pulmonary fibrosis, respectively, across the different models at well-tolerated doses. Of note, AM1476 was dosed in a therapeutic manner in all mouse models, with treatment initiation only after fibrosis had already been established. Moreover, we demonstrate therapeutic effects of AM1476 in PCS slices from patients with SSc. PCS slices offer potential to evaluate therapeutic effects of drug candidates in an ex vivo trial approach, with evaluation of drug candidates directly in patient-derived target tissues with all relevant cellular players and pathogenic tissue niches. AM1476 ameliorated the SSc-specific gene expression profile and regulated numerous genes and functional processes relevant for the pathogenesis of SSc. Of note, AM1476 regulated more terms related to tissue remodeling in PCS slices than MMF used as an active comparator and representative for the current standard of care. These data highlight antifibrotic effects of AM1476 across different tissues and species.

Our study also reveals that the potent antifibrotic effects of AM1476 might be mediated by a combination of different mechanisms. (1) AM1476 inhibits fibroblast activation in SSc: 5-HT is released from platelets upon activation at sites of vascular damage in SSc. 5-HT binds to 5-HT$_{2B}$R to activate fibroblasts and stimulate collagen release to promote progression of fibrosis. Blockade of 5-HT$_{2B}$R by AM1476 thus interrupts the link between vascular injury and platelet and fibroblast activation to inhibit progression of tissue fibrosis. (2) AM1476 interferes with the release of inflammatory mediators such as CCL2, CCL5, CCL18, CCL20, IL-36, and IL-1RAP. (3) AM1476 inhibits the alternative activation of macrophages in experimental fibrosis. Alternative activation of macrophages is a cardinal feature of SSc and other fibrotic diseases, and AAMs are considered as central cellular players in the pathogenesis of fibrotic tissue remodeling. We demonstrate that AM1476 decreases the number of AAMs in murine cGvHD and reduces functional terms related to macrophage activation in PCS slices of SSc skin. These findings are consistent with previously published results in which 5-HT was shown to skew macrophage polarization toward AAM through engagement of the 5-HT$_{2B}$R and 5-HT$_7$ receptor.[45] (4) AM1476 inhibits innate inflammatory cells. Using RNASeq of PCS slices, we highlight for the first time that inhibition of

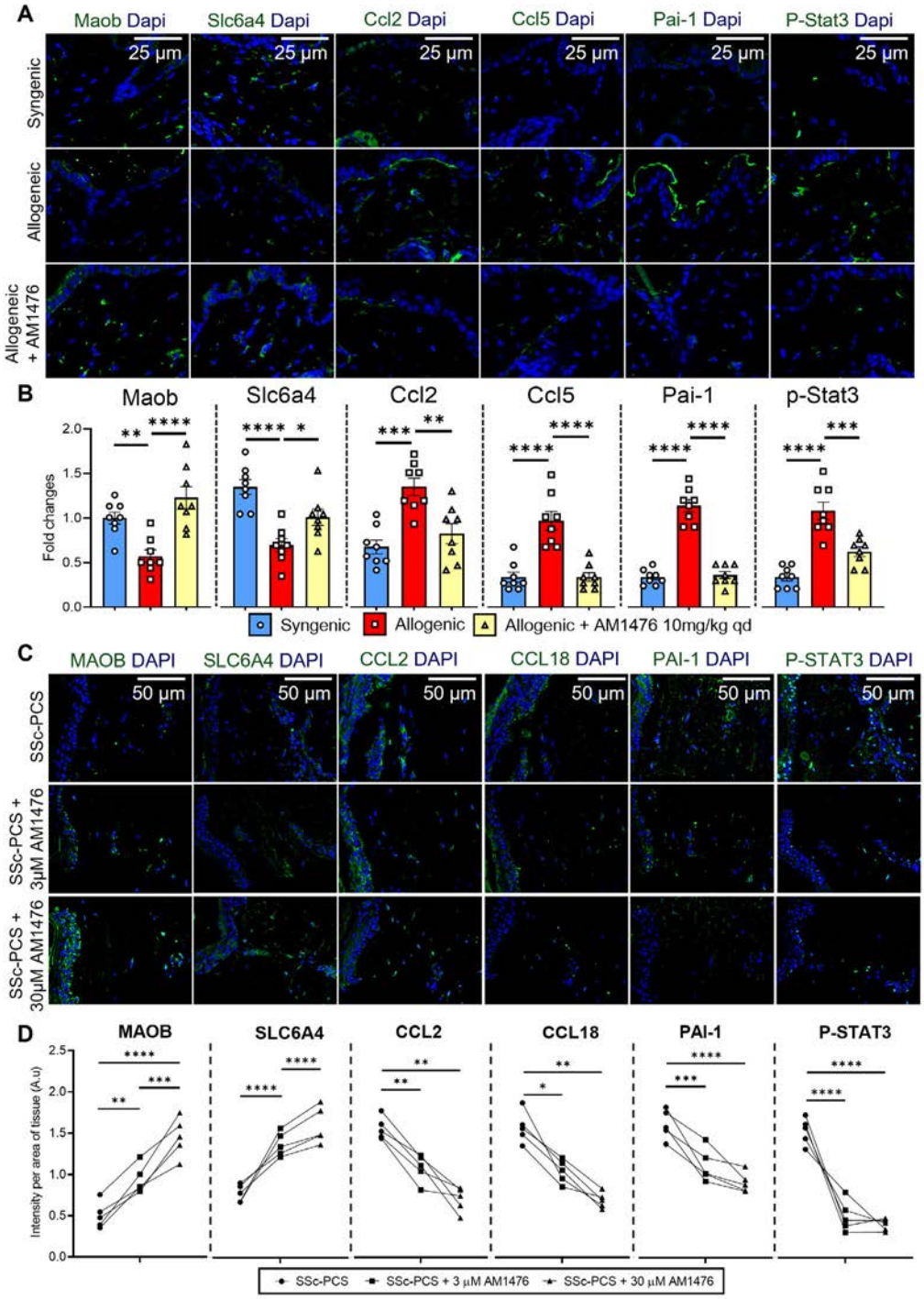

Figure 6. Inhibition of 5-HT_{2B}R by AM1476 modulates the expression of MAOB, SCL6A4, CCL2, CCL5, PAI-1, and P-STAT3 in murine cGvHD and PCS slices of SSc skin. (A and B) Murine cGvHD model. (A) Representative images of immunofluorescence staining and (B) quantification of Maob, Slc6a4, Ccl2, Ccl5, Pai-1, and P-Stat3 in the skin of syngeneically and allogeneically transplanted mice with or without AM1476 treatment. All data are presented as mean ± SEM, with individual values displayed as column plus dots. Differences between the groups were tested for their statistical significance by one-way analysis of variance with Dunnett's multiple comparison. Adjusted *P* values less than 0.05 were considered significant. Adjusted *P* values are expressed as follows: *0.05 > *P* > 0.01; **0.01 > *P* > 0.001; ***0.001 > *P* > 0.0001; ****$P < 0.0001$ as compared to the control allogenic group. (C and D) PCS slices of SSc skin. (C) Representative immunofluorescence staining images and (D) quantification of MAOB, SLC6A4, CCL2, CCL18, PAI-1, and P-STAT3 in SSc-PCS with or without AM1476. All data points are presented as individual values displayed as dots. Differences between the groups were tested for their statistical significance by two-way analysis of variance with Sidak's multiple comparison. Adjusted *P* values less than 0.05 were considered significant. Adjusted *P* values are expressed as follows: *0.05 > *P* > 0.01; **0.01 > *P* > 0.001; ***0.001 > *P* > 0.0001; ****$P < 0.0001$ as compared to the SSc-PCS control group. 5-HT_{2B}R, 5-hydroxytryptamine 2B receptor; cGvHD, chronic graft-versus-host disease; PCS, precision cut skin; SSc, systemic sclerosis. Color figure can be viewed in the online issue, which is available at http://onlinelibrary.wiley.com/doi/10.1002/art.43151/abstract.

5-HT$_{2B}$R modulates several functional terms related to activation of several innate immune cell subsets of the myeloid lineage. The anti-inflammatory terms partially overlap with those of MMF, though with more pronounced regulation of myeloid cells and no major effects on T lymphocytes. Although previous studies suggest a direct effect of 5-HT$_{2B}$R inhibition on macrophages, further studies are required to determine whether the effects of AM1476 on other myeloid cells are mediated via direct effects on these cells or occur indirectly via impaired release of mediators from fibroblasts and AAM activation. (5) We present first evidence that treatment with AM1476 up-regulates the messenger RNA levels of matrix-degrading enzymes, providing evidence that 5-HT$_{2B}$R inhibition may promote ECM degradation. However, these results require confirmation on the protein level and with enzyme activity assays. (6) Consistent with our previous study, we present evidence that AM1476 inhibits TGFβ signaling with down-regulation of two downstream targets relevant to the pathogenesis of fibrotic tissue remodeling: PAI-1 and P-STAT3.[15,20,23,41,43]

Of note, these preclinical findings may have direct translational implications. AM1476 demonstrated good safety and tolerability in a phase 1 clinical trial. Follow-up trials investigating the efficacy and tolerability of AM1476 in patients with diffuse cutaneous SSc are currently considered.

ACKNOWLEDGMENTS

We thank Wolfgang Espach and Regina Kleinlein for excellent technical assistance. Open Access funding enabled and organized by Projekt DEAL.

AUTHOR CONTRIBUTIONS

All authors contributed to at least one of the following manuscript preparation roles: conceptualization AND/OR methodology, software, investigation, formal analysis, data curation, visualization, and validation AND drafting or reviewing/editing the final draft. As corresponding author, Dr Distler confirms that all authors have provided the final approval of the version to be published and takes responsibility for the affirmations regarding article submission (eg, not under consideration by another journal), the integrity of the data presented, and the statements regarding compliance with institutional review board/Declaration of Helsinki requirements.

ROLE OF THE STUDY SPONSOR

AnaMar had no role in collection, analysis, or interpretation of the data.

REFERENCES

1. Distler JHW, Györfi AH, Ramanujam M, et al. Shared and distinct mechanisms of fibrosis. Nat Rev Rheumatol 2019;15(12):705–730.
2. Gurtner GC, Werner S, Barrandon Y, et al. Wound repair and regeneration. Nature 2008;453(7193):314–321.
3. Wynn TA. Cellular and molecular mechanisms of fibrosis. J Pathol 2008;214(2):199–210.
4. Denton CP, Khanna D. Systemic sclerosis. Lancet 2017;390(10103):1685–1699.
5. Dees C, Akhmetshina A, Zerr P, et al. Platelet-derived serotonin links vascular disease and tissue fibrosis. J Exp Med 2011;208(5):961–972.
6. Kishore A, Petrek M. Roles of macrophage polarization and macrophage-derived miRNAs in pulmonary fibrosis. Front Immunol 2021;12:678457.
7. Alfonse T, Gerald P, Thomas A, et al. Preliminary criteria for the classification of systemic sclerosis (scleroderma). Arthritis Rheum 1980;23(5):581–590.
8. van den Hoogen F, Khanna D, Fransen J, et al. 2013 classification criteria for systemic sclerosis: an American College of Rheumatology/European League against Rheumatism collaborative initiative. Arthritis Rheum 2013;65(11):2737-2747.
9. Zerr P, Distler A, Palumbo-Zerr K, et al. Combined inhibition of c-Abl and PDGF receptors for prevention and treatment of murine sclerodermatous chronic graft-versus-host disease. Am J Pathol 2012;181(5):1672–1680.
10. Zerr P, Palumbo-Zerr K, Distler A, et al. Inhibition of hedgehog signaling for the treatment of murine sclerodermatous chronic graft-versus-host disease. Blood 2012;120(14):2909–2917.
11. Dees C, Tomcik M, Palumbo-Zerr K, et al. JAK-2 as a novel mediator of the profibrotic effects of transforming growth factor β in systemic sclerosis. Arthritis Rheum 2012;64(9):3006–3015.
12. Zhou X, Trinh-Minh T, Tran-Manh C, et al. Impaired mitochondrial transcription factor a expression promotes mitochondrial damage to drive fibroblast activation and fibrosis in systemic sclerosis. Arthritis Rheumatol 2022;74(5):871–881.
13. Mähler Convenor M, Berard M, Feinstein R, et al; FELASA working group on revision of guidelines for health monitoring of rodents and rabbits. FELASA recommendations for the health monitoring of mouse, rat, hamster, guinea pig and rabbit colonies in breeding and experimental units. Lab Anim 2014;48(3):178–192.
14. Zhang Y, Shen L, Dreißigacker K, et al. Targeting of canonical WNT signaling ameliorates experimental sclerodermatous chronic graft-versus-host disease. Blood 2021;137(17):2403–2416.
15. Dees C, Pötter S, Zhang Y, et al. TGF-β-induced epigenetic deregulation of SOCS3 facilitates STAT3 signaling to promote fibrosis. J Clin Invest 2020;130(5):2347–2363.
16. Chakraborty D, Zhu H, Jüngel A, et al. Fibroblast growth factor receptor 3 activates a network of profibrotic signaling pathways to promote fibrosis in systemic sclerosis. Sci Transl Med 2020;12(563):eaaz5506.
17. Ashcroft T, Simpson JM, Timbrell V. Simple method of estimating severity of pulmonary fibrosis on a numerical scale. J Clin Pathol 1988;41(4):467–470.
18. Györfi AH, Matei AE, Fuchs M, et al. Engrailed 1 coordinates cytoskeletal reorganization to induce myofibroblast differentiation. J Exp Med 2021;218(9):e20201916.
19. Zehender A, Li YN, Lin NY, et al. TGFβ promotes fibrosis by MYST1-dependent epigenetic regulation of autophagy. Nat Commun 2021;12(1):4404.
20. Zehender A, Huang J, Györfi AH, et al. The tyrosine phosphatase SHP2 controls TGFβ-induced STAT3 signaling to regulate fibroblast activation and fibrosis. Nat Commun 2018;9(1):3259.
21. Akhmetshina A, Palumbo K, Dees C, et al. Activation of canonical Wnt signalling is required for TGF-β-mediated fibrosis. Nat Commun 2012;3(1):735.
22. Li YN, Chen CW, Trinh-Minh T, et al. Dynamic changes in O-GlcNAcylation regulate osteoclast differentiation and bone loss via nucleoporin 153. Bone Res 2022;10(1):51.
23. Trinh-Minh T, Györfi AH, Tomcik M, et al. Effect of anti-S100A4 monoclonal antibody treatment on experimental skin fibrosis and systemic

sclerosis-specific transcriptional signatures in human skin. Arthritis Rheumatol. 2024;76(5):783–795.

24. Liang M, Dickel N, Györfi AH, et al. Attenuation of fibroblast activation and fibrosis by adropin in systemic sclerosis. Sci Transl Med 2024; 16(740):eadd6570.
25. Trinh-Minh T, Chen CW, Tran Manh C, et al. Noncanonical WNT5A controls the activation of latent TGF-β to drive fibroblast activation and tissue fibrosis. J Clin Invest 2024;134(10):e159884.
26. Chen CW, Beyer C, Liu J, et al. Pharmacological inhibition of porcupine induces regression of experimental skin fibrosis by targeting Wnt signalling. Ann Rheum Dis 2017;76(4):773–778.
27. Beyer C, Reichert H, Akan H, et al. Blockade of canonical Wnt signalling ameliorates experimental dermal fibrosis. Ann Rheum Dis 2013; 72(7):1255–1258.
28. Beyer C, Schramm A, Akhmetshina A, et al. β-catenin is a central mediator of pro-fibrotic Wnt signaling in systemic sclerosis. Ann Rheum Dis 2012;71(5):761–767.
29. Wei J, Fang F, Lam AP, et al. Wnt/β-catenin signaling is hyperactivated in systemic sclerosis and induces Smad-dependent fibrotic responses in mesenchymal cells. Arthritis Rheum 2012;64(8):2734–2745.
30. Dees C, Schlottmann I, Funke R, et al. The Wnt antagonists DKK1 and SFRP1 are downregulated by promoter hypermethylation in systemic sclerosis. Ann Rheum Dis 2014;73(6):1232–1239.
31. Bandinelli F, Del Rosso A, Gabrielli A, et al. CCL2, CCL3 and CCL5 chemokines in systemic sclerosis: the correlation with SSc clinical features and the effect of prostaglandin E1 treatment. Clin Exp Rheumatol 2012;30(2 suppl 71):S44–S49.
32. Distler JHW, Akhmetshina A, Schett G, et al. Monocyte chemoattractant proteins in the pathogenesis of systemic sclerosis. Rheumatology (Oxford) 2009;48(2):98–103.
33. Distler O, Pap T, Kowal-Bielecka O, et al. Overexpression of monocyte chemoattractant protein 1 in systemic sclerosis: role of platelet-derived growth factor and effects on monocyte chemotaxis and collagen synthesis. Arthritis Rheum 2001;44(11):2665–2678.
34. Distler JH, Jüngel A, Caretto D, et al. Monocyte chemoattractant protein 1 released from glycosaminoglycans mediates its profibrotic effects in systemic sclerosis via the release of interleukin-4 from T cells. Arthritis Rheum 2006;54(1):214–225.
35. Carulli MT, Ong VH, Ponticos M, et al. Chemokine receptor CCR2 expression by systemic sclerosis fibroblasts: evidence for autocrine regulation of myofibroblast differentiation. Arthritis Rheum 2005; 52(12):3772–3782.
36. Grönberg C, Rattik S, Tran-Manh C, et al. Combined inhibition of IL-1, IL-33 and IL-36 signalling by targeting IL1RAP ameliorates skin and lung fibrosis in preclinical models of systemic sclerosis. Ann Rheum Dis 2024;83(9):1156–1168.
37. O'Reilly S. Interleukin-36α is elevated in diffuse systemic sclerosis and may potentiate fibrosis. Cytokine 2022;156:155921.
38. De Luca G, Cavalli G, Campochiaro C, et al. Interleukin-1 and systemic sclerosis: getting to the heart of cardiac involvement. Front Immunol 2021;12:653950.
39. Xu D, Mu R, Wei X. The roles of IL-1 family cytokines in the pathogenesis of systemic sclerosis. Front Immunol 2019;10:2025.
40. Ma LJ, Fogo AB. PAI-1 and kidney fibrosis. Front Biosci (Landmark Ed) 2009;14(6):2028–2041.
41. Ghosh AK, Vaughan DE. PAI-1 in tissue fibrosis. J Cell Physiol 2012; 227(2):493–507.
42. Flevaris P, Vaughan D. The role of plasminogen activator inhibitor type-1 in fibrosis. Semin Thromb Hemost 2017;43(2):169–177.
43. Chakraborty D, Šumová B, Mallano T, et al. Activation of STAT3 integrates common profibrotic pathways to promote fibroblast activation and tissue fibrosis. Nat Commun 2017;8(1):1130.
44. Park JS, Kim C, Choi J, et al. MicroRNA-21a-5p inhibition alleviates systemic sclerosis by targeting STAT3 signaling. J Transl Med 2024; 22(1):323.
45. de las Casas-Engel M, Domínguez-Soto A, Sierra-Filardi E, et al. Serotonin skews human macrophage polarization through HTR2B and HTR7. J Immunol 2013;190(5):2301–2310.

Arthritis & Rheumatology
Vol. 77, No. 8, August 2025, pp 1077–1086
DOI 10.1002/art.43127

American College of Rheumatology
Empowering Rheumatology Professionals

Proinflammatory Dietary Pattern and the Risk of Female Gout: Sex-Specific Findings From Three Prospective Cohort Studies

Sharan K. Rai,[1] Hyon K. Choi,[1] Na Lu,[2] Chio Yokose,[3] Kehuan Lin,[4] Dong Hoon Lee,[5] Fred K. Tabung,[6] and Natalie McCormick[1]

Objective. We aimed to determine whether a proinflammatory dietary pattern (mechanism-based diet) is associated with incident female gout in two large cohorts of US women.

Methods. We prospectively observed 79,104 women from the Nurses' Health Study (1984–2016) and 94,382 women from the Nurses' Health Study II (1991–2017); 45,445 men from the Health Professionals Follow-up Study (1986–2016) served as a comparison cohort. Validated food frequency questionnaires were used to calculate Empirical Dietary Inflammatory Pattern (EDIP) (food-based index predictive of circulating inflammatory biomarkers) scores every four years. Cox proportional hazards models were used to evaluate multivariable associations between EDIP and incident, physician-diagnosed gout. We further tested whether these associations were independent of key guideline-based healthy eating patterns that previously showed beneficial associations with gout (ie, Dietary Approaches to Stop Hypertension [DASH], Alternative Healthy Eating Index [AHEI]).

Results. We documented 5,425 incident female gout cases over 4,372,243 person-years. EDIP was positively associated with female gout risk; hazard ratio (HR) (95% confidence interval [CI]) for the most versus least proinflammatory quintile was 2.02 (1.83–2.22). Additional adjustment for body mass index attenuated this association (HR 1.71 [95% CI 1.55–1.88]). Reversing the EDIP score, women in the most anti-inflammatory EDIP quintile had the largest magnitude of protective association for gout (HR 0.58 [95% CI 0.53–0.65]) compared with HRs for healthiest DASH (HR 0.80 [95% CI 0.73–0.87]) and AHEI quintiles (HR 0.81 [95% CI 0.74–0.89]). The magnitude of association between EDIP and male gout was substantially smaller (HR 1.24 [95% CI 1.13–1.37]; *P*-heterogeneity <0.0001).

Conclusion. These findings support a pivotal role of inflammation as a potential modulator between diet and gout onset, particularly among women.

INTRODUCTION

Gout is the most common inflammatory arthritis; it affects more than 41 million adults worldwide,[1] and its prevalence is rising disproportionately among women compared with men.[2] Gout is caused by hyperuricemia, which promotes monosodium urate (MSU) crystal deposition within the joints and subsequently triggers joint inflammation and damage.[3] Multiple shared lifestyle factors have been identified, although their impacts may differ between women and men (eg, dietary patterns may play a greater

Supported by the National Institute of Arthritis and Musculoskeletal and Skin Diseases, NIH (grants P50-AR-060772 and R01-AR-065944). Dr Rai's work was supported by a Fellowship Award from the Canadian Institutes of Health Research. Dr Yokose's work was supported by the NIH (grant K23-AR-081425). Dr Lee's work was supported by the Yonsei University Research Fund of 2024-22-0093. Dr McCormick's work was supported by a Career Development Award from the NIH (award K99-AR-080243). The Nurses' Health Study, Nurses' Health Study II, and Health Professionals Follow-Up study were supported by the National Cancer Institute, NIH (grants UM1-CA-186107, U01-CA-176726, and U01-CA-167552).

[1]Sharan K. Rai, PhD, Hyon K. Choi, MD, DrPH, Natalie McCormick, PhD: Massachusetts General Hospital, Harvard Medical School, Channing Division of Network Medicine, and The Mongan Institute, Massachusetts General Hospital, Boston, and Arthritis Research Canada, Vancouver, British Columbia, Canada; [2]Na Lu, MPH: Arthritis Research Canada, Vancouver, British Columbia, Canada; [3]Chio Yokose, MD, MS: Massachusetts General Hospital, Harvard Medical School, and The Mongan Institute, Massachusetts General Hospital, Boston; [4]Kehuan Lin, MS: Harvard T. H. Chan School of Public Health, Boston, Massachusetts; [5]Dong Hoon Lee, ScD: Harvard T. H. Chan School of Public Health, Boston, Massachusetts, and Yonsei University, Seoul, South Korea; [6]Fred K. Tabung, PhD: Harvard T. H. Chan School of Public Health, Boston, Massachusetts, and The Ohio State University Comprehensive Cancer Center, Columbus.

Additional supplementary information cited in this article can be found online in the Supporting Information section (https://acrjournals.onlinelibrary.wiley.com/doi/10.1002/art.43127).

Author disclosures and graphical abstract are available at https://onlinelibrary.wiley.com/doi/10.1002/art.43127.

Address correspondence via email to Natalie McCormick, PhD, at nmccormick@mgh.harvard.edu.

Submitted for publication October 23, 2024; accepted in revised form January 7, 2025.

role among women,[4] whereas alcohol intake may be a greater driver among men[5]). Approximately, only 20% of individuals with hyperuricemia develop clinically evident gout[6]; conversely, in others, MSU crystals may still form without inciting an inflammatory response.[7] This suggests that other factors may modify the inflammatory response to hyperuricemia and MSU crystal deposition.[8]

Certain lifestyle factors may promote (or dampen) inflammation, which may modulate gout pathogenesis. Obesity is associated with low-grade chronic inflammation[9]; adiposity is also a well-established, causal factor for hyperuricemia and gout.[10,11] Diet is another major modifiable determinant of many chronic conditions, including gout. Adherence to established healthy eating patterns such as the Dietary Approaches to Stop Hypertension (DASH) and the Alternative Healthy Eating Index (AHEI), which are each associated with lower plasma concentrations of inflammatory biomarkers,[12–15] is also inversely associated with gout incidence.[16,17] However, neither of these dietary patterns were derived specifically to predict inflammation, and research on a proinflammatory dietary pattern and gout remains limited.

The Empirical Dietary Inflammatory Pattern (EDIP) is a mechanism-based diet developed to reflect the long-term inflammatory potential of an individual's diet[18] and is only modestly correlated with conventional healthy eating patterns, including the DASH diet and AHEI.[19] Lower EDIP scores (indicating a more anti-inflammatory diet) are associated with attenuated weight gain[20] and lower risks of multiple diseases commonly associated with gout, including type 2 diabetes (T2D)[19] and cardiovascular disease (CVD).[21] Such a diet may be particularly relevant to gout risk among women, who experience an elevated prevalence of obesity, T2D, hypertension, and other cardiometabolic comorbidities compared with men,[22] even when accounting for their average older age (female gout onset typically follows menopause[23]). Women with gout also experience greater pain, disability, and physical dysfunction than men with gout.[24,25] Such health disparities for women are not unique to gout,[26,27] and increasing recognition of this persistent health gap has catalyzed national and global efforts to improve health equity for women, including the White House Initiative on Women's Health Research[28] and the World Economic Forum's Global Alliance for Women's Health.[29]

These findings suggest a compelling link between diet, inflammation, and the risk of gout, particularly among women.[30,31] Using two large prospective cohorts of women, as well as a comparable cohort of men, we aimed to investigate the independent association of a proinflammatory dietary pattern with incident gout.

PATIENTS AND METHODS

Study population. The Nurses' Health Study (NHS) enrolled 121,700 female nurses aged 30 to 55 years in 1976,[32] the Nurses' Health Study II (NHSII) enrolled 116,429 female nurses aged 25 to 42 years in 1989,[33] and the Health Professionals Follow-up Study (HPFS) enrolled 51,529 male health professionals aged 40 to 75 years in 1986.[34] We included 79,104 women from the NHS, 94,382 women from the NHSII, and 45,445 men from the HPFS, who had complete dietary information, plausible energy intake, and were free of gout at baseline (ie, 1984 for NHS, 1991 for NHSII, and 1986 for HPFS). The study protocol was approved by the Institutional Review Boards at Mass General Brigham and the Harvard T. H. Chan School of Public Health. Completion and return of study questionnaires implied informed consent.

Dietary assessment. We used a validated semiquantitative food frequency questionnaire (FFQ)[35] to collect dietary data on all the participants' habitual diets over the previous year at baseline and every four years thereafter. The EDIP (our primary exposure) was developed in the NHS and validated in the NHSII and HPFS[18] with further external replication in the Women's Health Initiative.[36] A total of 39 predefined food groups were entered into a reduced rank regression model to derive a dietary pattern predictive of plasma C-reactive protein (CRP), interleukin-6 (IL-6), and tumor necrosis factor α receptor 2 (TNFαR2). As such, higher EDIP scores are indicative of a more proinflammatory dietary pattern.[18] Detailed distributions of nutrients and food groups according to quintiles of baseline EDIP score are shown in Supplementary Table 1. Briefly, the EDIP is composed of 18 food groups (9 proinflammatory and 9 anti-inflammatory). Proinflammatory food groups included red and processed meats, refined grains, tomatoes, and sugar-sweetened beverages, whereas anti-inflammatory food groups included green leafy vegetables, yellow vegetables, fruit juices, coffee, and tea. We additionally calculated DASH and AHEI scores for all participants. Further information on construction of all three diet scores is in the Supplementary Materials.

Covariate assessment. Beginning at baseline, participants provided information about lifestyle factors, diagnoses, and medication use on biennial questionnaires (response rate >90% at each follow-up cycle). We collected data on height and race at baseline and updated data on body weight, smoking status, physical activity, hypertension status, diuretic use, and, among women only, postmenopausal status and hormone use over the study follow-up.

Case ascertainment. Incident gout cases were ascertained using biennial questionnaires. Specifically, these cases were based on the participating health professionals' reporting of new-onset, physician-diagnosed gout as done previously in these cohorts, and date of first occurrence.[23,37]

Statistical analysis. We calculated person-time for each participant from the baseline questionnaire return date until date of gout diagnosis, death, date of the last return of a valid

questionnaire, or end of the follow-up (ie, June 2016 for the NHS, June 2017 for the NHSII, and January 2016 for the HPFS)—whichever occurred first. We divided the EDIP into quintiles (highest quintile reflecting most inflammatory diet) to avoid making assumptions about linearity and reduce the influence of outliers. Second, we cumulatively averaged each participant's EDIP score over the follow-up to better capture habitual long-term dietary intake and reduce within-person variability. Third, because conditions like diabetes, hypertension, and dyslipidemia are potentially associated with gout and these diagnoses may prompt a change in an individual's diet, we stopped updating EDIP scores after participants reported any of these conditions. Finally, we energy-adjusted all EDIP scores using the residual method.[38]

We used Cox proportional hazards regression models to evaluate the association between quintiles of EDIP and incident gout. We stratified all models by age and calendar time in two-year intervals. We tested the proportional hazard assumption by adding an interaction term between each quintile of EDIP and age; no violation was detected ($P > 0.05$). We conducted a trend test by modeling the EDIP score as a continuous variable. In our primary analysis, our multivariable models were first adjusted for smoking status, diuretic use, physical activity, history of hypertension, alcohol consumption, race, and for women, menopausal status and postmenopausal hormone use.[17] As done previously,[31] we included alcohol intake as a covariate because of its established positive association with gout[5]; beer and wine were identified as anti-inflammatory components in EDIP, which may bias the associations under study toward the null without proper adjustment. We further adjusted for body mass index (BMI) (potential causal intermediate between EDIP and gout) in a separate model. We conducted a secondary analysis in which we adjusted for either the DASH or AHEI score to ascertain whether any observed associations between EDIP and gout were independent of these healthy eating patterns. We further compared the association between EDIP and gout with the DASH/AHEI and gout by reversing the EDIP scores so the highest quintiles for all diet scores were regarded as the healthiest, as done previously.[39] Finally, we examined potential joint associations of EDIP with either the DASH or AHEI.

To further minimize the potential for baseline disease diagnoses affecting dietary exposures, we conducted a sensitivity analysis excluding participants who reported baseline diagnoses of T2D, CVD, or cancer, because individuals with these conditions may be more likely to change their diets in response to the diagnosis. Finally, we conducted subgroup analyses according to age, BMI, physical activity level, and alcohol intake. We evaluated potential effect modification using a Wald test by including a product term between EDIP and each of the above stratifying variables.

We conducted all analyses separately by sex and tested for heterogeneity using a likelihood ratio test. All statistical analyses were performed with SAS 9.4 for Unix. All tests were 2-sided with $\alpha = 0.05$.

RESULTS

Baseline characteristics. In all three cohorts, participants consuming a more proinflammatory diet tended to have a higher BMI, exercised less, and were more likely to use diuretics and have prevalent hypertension (Table 1). These individuals also had lower DASH and AHEI scores and ate more protein and fat than those consuming a less inflammatory diet (Table 1 and Supplementary Table 1). The EDIP was moderately inversely associated with DASH and AHEI scores in the cohort (Spearman correlation coefficient = –0.35 to –0.21) (Supplementary Table 2).

EDIP and incident gout. We documented 5,425 incident gout cases among women during 4,372,243 person-years of follow up and 4,453 cases among men during 993,994 person-years of follow up (Table 2). After multivariable adjustment, a higher EDIP score was associated with an increased risk of gout in women and men (both P for trend <0.001) (Table 2). We found statistically significant heterogeneity between sexes (P for heterogeneity < 0.001) but not between the two cohorts of women (P for heterogeneity = 0.22); therefore, we pooled the two cohorts of women and presented all final estimates separately for women and men (estimates according to NHS cohort are available in Supplementary Table 3). Before BMI adjustment, EDIP was positively associated with gout, although the magnitude of this association was stronger among women. Comparing extreme quintiles, hazard ratio (HR) (95% confidence interval [CI]) was 2.02 (1.83–2.22) among women and 1.34 (1.21–1.47) among men (Table 2). These positive associations became slightly attenuated after further adjustment for BMI but remained statistically significant in both sexes (both P for trend <0.001) (Table 2).

Further adjustment for other healthy eating patterns (ie, DASH and AHEI) also slightly attenuated the positive association between EDIP and incident gout, although the results did not change materially (Table 3). Finally, our results remained robust in a sensitivity analysis in which we excluded those with major diseases at baseline (Supplementary Tables 4 and 5).

Comparison with other healthy eating patterns. Figure 1 shows a comparison of EDIP, DASH, and AHEI following reversal of the EDIP scores; the highest level reflects the healthiest (most anti-inflammatory) quintile and the lowest (least anti-inflammatory) level reflects the referent category. Among women, the magnitude of association between the most (referent) and least anti-inflammatory quintiles of EDIP and incident gout was greater than those between the highest (ie, healthiest) and lowest quintiles of the DASH and AHEI scores and gout. Specifically, comparing extreme quintiles of each diet score, women in the most anti-inflammatory EDIP quintile had a 50% lower risk of gout

Table 1. Baseline characteristics of women and men enrolled in the NHS, NHS II, and HPFS according to quintiles of EDIP score*

	NHS, 1984 (n = 79,104)			NHSII, 1991 (n = 94,382)			HPFS, 1986 (n = 45,445)		
Baseline characteristics	Quintile 1 (least inflammatory)	Quintile 3	Quintile 5 (most inflammatory)	Quintile 1 (least inflammatory)	Quintile 3	Quintile 5 (most inflammatory)	Quintile 1 (least inflammatory)	Quintile 3	Quintile 5 (most inflammatory)
EDIP score, mean ± SD	−0.5 ± 0.2	0 ± 0	0.4 ± 0.2	−0.4 ± 0.2	0.1 ± 0	0.5 ± 0.2	−0.5 ± 0.3	0 ± 0	0.5 ± 0.2
Age, mean ± SD, y	50.7 ± 6.9	50.8 ± 7.3	49.5 ± 7.3	36.7 ± 4.5	36.1 ± 4.7	35.8 ± 4.7	52.7 ± 9.1	54.3 ± 9.8	53.7 ± 10.0
White, %	99	98	96	98	97	95	97	95	93
BMI, mean ± SD	23.8 ± 3.7	24.8 ± 4.4	26.6 ± 5.7	23.7 ± 4.6	24.3 ± 5.0	26.2 ± 6.3	24.6 ± 4.8	24.7 ± 4.8	25.4 ± 5.4
Current smoker, %	30	22	22	11	12	16	11	8	8
Postmenopausal, %	49	49	50	3	4	4	-	-	-
Postmenopausal hormone use, %	12	12	10	0	0	0	-	-	-
History of hypertension, %	7	8	11	5	6	9	19	20	24
Diuretic use, %	10	12	16	2	2	3	9	9	12
Physical activity, mean ± SD, MET-hours/week	16.3 ± 24.2	14.2 ± 21.8	12.4 ± 18.4	24.4 ± 31.1	19.7 ± 25.1	19.1 ± 26.6	20.7 ± 26.8	18.7 ± 27.2	17.0 ± 24.5
Alcohol, mean ± SD, g/day	13.8 ± 15.9	5.4 ± 8.8	3.8 ± 8.5	6.1 ± 9.7	2.4 ± 4.5	1.8 ± 4.1	21.4 ± 20.5	9.0 ± 12.0	6.2 ± 11.5
Total calorie intake, mean ± SD, kcal/day	1,815.8 ± 524.7	1,679.6 ± 508.5	1,833.9 ± 566.4	1,894.6 ± 545.8	1,680.7 ± 516.5	1914.6 ±, 588.4	2,090.8 ± 614.7	1,891.4 ± 587.8	2,146.2 ± 664.8
AHEI score, mean ± SD	50.7 ± 11.0	48.8 ± 10.4	44.8 ± 10.7	51.3 ± 11.4	47.8 ± 10.1	44.1 ± 10.2	54.5 ± 11.7	53.8 ± 11.1	48.7 ± 11.3
DASH score, mean ± SD	24.2 ± 4.7	23.0 ± 4.7	20.8 ± 5.0	25.7 ± 5.0	23.4 ± 4.6	21.7 ± 4.7	25.2 ± 5.1	24.4 ± 5.1	22.2 ± 5.3

* All variables are age standardized. AHEI, Alternative Healthy Eating Index; BMI, body mass index; DASH, Dietary Approaches to Stop Hypertension; EDIP, Empirical Dietary Inflammatory Pattern; HPFS, Health Professionals Follow-up Study; MET, metabolic equivalent of task; NHS, Nurses' Health Study; NHSII, Nurses' Health Study II.

Table 2. Analysis results for incident gout cases among women and men according to quintiles of EDIP score*

	Quintile 1 (least inflammatory)	Quintile 2	Quintile 3	Quintile 4	Quintile 5 (most inflammatory)	*P* for trend
Women						
Number of incident gout cases	677	827	1,022	1,253	1,646	
Person-years	874,160	875,089	874,884	874,500	873,610	
Incidence rate ratio, (95% CI)	1.00 (ref)	1.22 (1.10–1.35)	1.51 (1.37–1.67)	1.87 (1.71–2.06)	2.54 (2.32–2.77)	<0.001
MV HR (95% CI)	1.00 (ref)	1.26 (1.13–1.39)	1.48 (1.33–1.63)	1.71 (1.55–1.89)	2.02 (1.83–2.22)	<0.001
MV HR + BMI (95% CI)	1.00 (ref)	1.22 (1.10–1.36)	1.40 (1.26–1.54)	1.55 (1.41–1.72)	1.71 (1.55–1.88)	<0.001
Men						
Number of incident gout cases	867	803	824	949	1,010	
Person-years	199,104	199,159	198,856	198,382	198,493	
Incidence rate ratio (95% CI)	1.00 (ref)	0.91 (0.83–1.00)	0.92 (0.84–1.01)	1.07 (0.97–1.17)	1.15 (1.05–1.26)	<0.001
MV HR (95% CI)	1.00 (ref)	1.00 (0.91–1.10)	1.07 (0.97–1.18)	1.26 (1.14–1.39)	1.34 (1.21–1.47)	<0.001
MV HR + BMI (95% CI)	1.00 (ref)	0.99 (0.90–1.09)	1.05 (0.95–1.16)	1.22 (1.10–1.34)	1.24 (1.13–1.37)	<0.001

* The EDIP score was adjusted for total energy intake using the residual method. Incidence rate ratios are stratified by age group. Multivariable models were adjusted for age (years), race (White or not White), smoking (never, past, or current: 1–14, 15–24, or >24 cigarettes/day), physical activity (<3, 3–8.9, 9–17.9, 18–26.9, or ≥27 MET-hours/week), history of hypertension (yes or no), diuretic use (yes or no), alcohol consumption (0, 0.1–4.9, 5–9.9, 10–14.9, or ≥15 g/day), and among women only, cohort (NHS or NHSII), menopausal status, and postmenopausal hormone use (premenopausal, postmenopausal current user, or postmenopausal never/past user). Our final model was additionally adjusted for BMI (<21, 21–22.9, 23–24.9, 25–26.9, 27–29.9, 30–34.9, 35–39.9, or ≥40). *P* for trend was calculated using the continuous EDIP score. BMI, body mass index; CI, confidence interval; EDIP, Empirical Dietary Inflammatory Pattern; HR, hazard ratio; MET, metabolic equivalent of task; MV, multivariable; NHS, Nurses' Health Study; NHSII, Nurses' Health Study II; ref, reference.

(HR 0.50 [95% CI 0.45–0.55]), compared with a 22% to 25% lower risk for gout in the healthiest DASH (HR 0.75 [95% CI 0.69–0.83]) and AHEI (HR 0.78 [95% CI 0.71–0.85]) quintiles; estimates were slightly attenuated following further adjustment for BMI (HR 0.58 [95% CI 0.53–0.65], 0.80 [0.73–0.87], and 0.81 [0.7–0.89] for EDIP, DASH, and AHEI, respectively) (Figure 1A). Conversely, among men, we observed similar magnitudes of association between EDIP and DASH scores with incident gout (HRs for extreme quintiles 0.76 [95% CI 0.69–0.84] for EDIP and 0.74 [0.67–0.81] for DASH); for the AHEI, we observed an HR of 0.86 (95% CI 0.78–0.95) for extreme quintiles; again, all three estimates were slightly attenuated after BMI adjustment (Figure 1B).

Joint associations. The EDIP, DASH, and AHEI scores were jointly associated with incident gout risk (Figure 2). Among women, those in the highest risk category (ie, the highest [most inflammatory] EDIP quintile combined with the lowest [least adherent] DASH or AHEI quintile) had an approximately two-fold risk of incident gout compared with the lowest-risk category (ie, the lowest [least inflammatory] EDIP quintile combined with the highest [most adherent] DASH or AHEI quintile). Comparing these extreme risk categories among women, the joint HR (95% CI) was 1.83 (1.55–2.16) for EDIP + DASH (Figure 2A) and 2.00 (1.67–2.40) for EDIP + AHEI (Figure 2B). The corresponding joint HRs (95% CI) among men were 1.49 (1.24–1.78) for EDIP + DASH (Figure 2C) and 1.24 (1.04–1.48) for EDIP + AHEI (Figure 2D).

Table 3. Analysis results for incident gout cases among women and men according to quintiles of EDIP score with additional adjustment for other diet scores*

Variable	Quintile 1 (least inflammatory)	Quintile 2	Quintile 3	Quintile 4	Quintile 5 (most inflammatory)	*P* for trend
Women						
MV HR + AHEI (95% CI)	1.00 (ref)	1.25 (1.13–1.39)	1.46 (1.32–1.62)	1.69 (1.53–1.86)	1.98 (1.80–2.19)	<0.001
MV HR + AHEI + BMI (95% CI)	1.00 (ref)	1.22 (1.10–1.35)	1.39 (1.25–1.54)	1.54 (1.39–1.70)	1.68 (1.52–1.86)	<0.001
MV HR + DASH (95% CI)	1.00 (ref)	1.25 (1.12–1.38)	1.45 (1.31–1.61)	1.67 (1.51–1.85)	1.96 (1.77–2.16)	<0.001
MV HR + DASH + BMI (95% CI)	1.00 (ref)	1.21 (1.09–1.35)	1.38 (1.24–1.52)	1.52 (1.37–1.68)	1.66 (1.50–1.83)	<0.001
Men						
MV HR + AHEI (95% CI)	1.00 (ref)	1.00 (0.91–1.10)	1.07 (0.97–1.18)	1.25 (1.14–1.38)	1.32 (1.19–1.46)	<0.001
MV HR + AHEI + BMI (95% CI)	1.00 (ref)	0.99 (0.90–1.09)	1.05 (0.95–1.16)	1.22 (1.10–1.34)	1.24 (1.12–1.37)	<0.001
MV HR + DASH (95% CI)	1.00 (ref)	0.99 (0.90–1.09)	1.04 (0.95–1.15)	1.21 (1.10–1.34)	1.25 (1.13–1.39)	<0.001
MV HR + DASH + BMI (95% CI)	1.00 (ref)	0.98 (0.89–1.08)	1.03 (0.93–1.14)	1.18 (1.07–1.30)	1.18 (1.07–1.31)	0.0026

* The EDIP score was adjusted for total energy intake using the residual method. Multivariable models were adjusted for age (years), race (White or not White), smoking (never, past, or current: 1–14, 15–24, or >24 cigarettes/day), physical activity (<3, 3–8.9, 9–17.9, 18–26.9, or ≥27 MET-hours/week), history of hypertension (yes or no), diuretic use (yes or no), alcohol consumption (0, 0.1–4.9, 5–9.9, 10–14.9, or ≥15 g/day), and among women only, cohorts (NHS or NHSII), menopausal status and postmenopausal hormone use (premenopausal, postmenopausal current user, or postmenopausal never/past user). Our final model was additionally adjusted for BMI (<21, 21–22.9, 23–24.9, 25–26.9, 27–29.9, 30–34.9, 35–39.9, or ≥40). *P* for trend was calculated using the continuous EDIP score. AHEI, Alternative Healthy Eating Index; BMI, body mass index; CI, confidence interval; DASH, Dietary Approaches to Stop Hypertension; EDIP, Empirical Dietary Inflammatory Pattern; HR, hazard ratio; MET, metabolic equivalent of task; MV, multivariable; ref, reference.

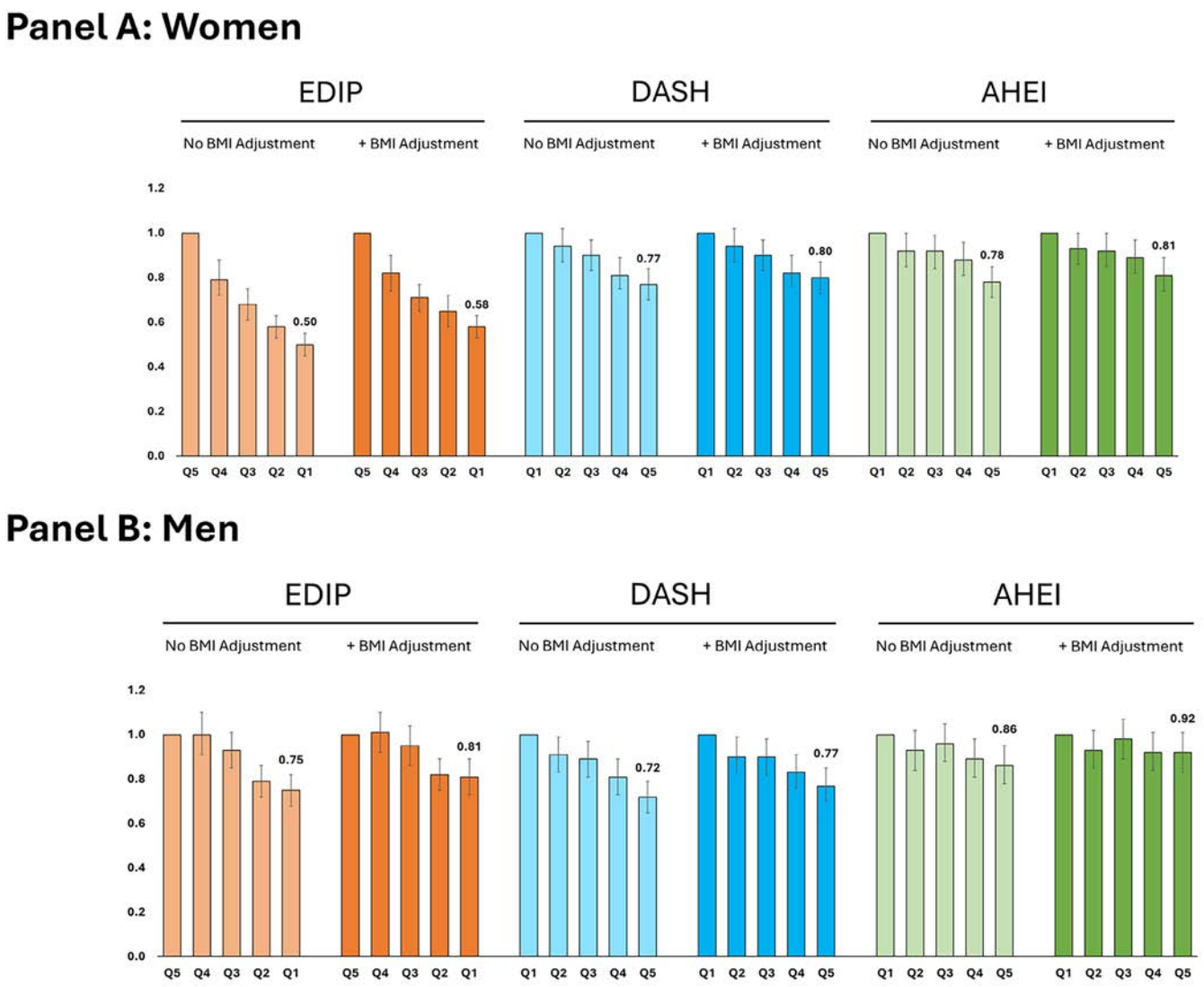

Figure 1. Comparison of associations between diet scores and incident gout in (A) women and (B); men. Values are HRs and corresponding 95% CIs. For EDIP, Q1 represents the least inflammatory quintile ("most healthy"); for DASH and AHEI, Q5 represents the greatest adherence ("most healthy"). Multivariable models were adjusted for the same covariates as in the main analysis. AHEI, Alternative Healthy Eating Index; BMI, body mass index; CI, confidence interval; DASH, Dietary Approaches to Stop Hypertension; EDIP, Empirical Dietary Inflammatory Pattern; HR, hazard ratio; Q1–Q5, quintile 1–5.

Subgroup analyses. In our subgroup analyses, EDIP remained positively associated with incident gout. The associations between EDIP and incident gout were generally consistent across subgroups by age, BMI, physical activity level, and alcohol intake in women and men (all *P* for interaction >0.05) (Supplementary Table 6).

DISCUSSION

In this study of three large prospective cohorts of 218,003 US women and men, we found that a greater adherence to a proinflammatory diet was associated with increased gout risk, especially among women. This association was independent of BMI, and the magnitude of association was greater than that observed for key established healthy eating patterns. The EDIP, a mechanism-based diet, may serve as a more comprehensive dietary index that can better capture the biologically relevant aspects of diet and gout risk. These findings support the deleterious role of diet-related chronic inflammation in relation to gout onset, particularly among women whose gout burden is rising disproportionately to men and highlight the importance of avoiding a proinflammatory diet for gout prevention, in addition to such a diet's risk reduction benefits for related cardiometabolic outcomes.[19–21]

Our findings add to the limited literature that suggest diet may modulate inflammatory pathways in gout pathogenesis.[7] Induction of hyperuricemia may be one mechanism underlying

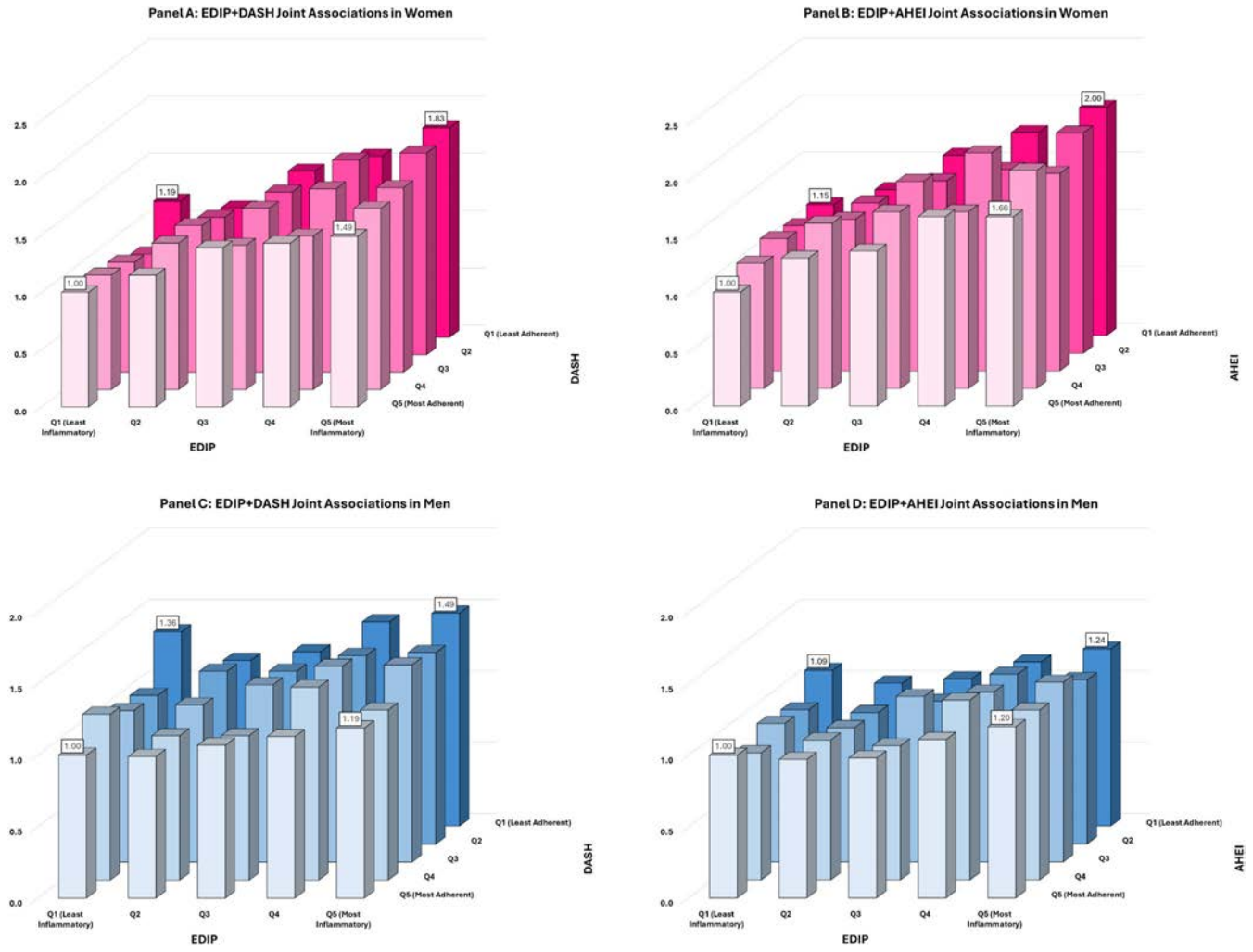

Figure 2. Joint associations between EDIP, DASH, and AHEI and incident gout. Multivariable models were adjusted for the same covariates as in the main analysis. AHEI, Alternative Healthy Eating Index; DASH, Dietary Approaches to Stop Hypertension; EDIP, Empirical Dietary Inflammatory Pattern; Q1–Q5, quintile 1–5.

the observed association between proinflammatory dietary pattern and the clinical endpoint of gout evaluated in the current study.[30,31] However, proinflammatory diets may additionally promote gout onset by modulating the inflammatory response triggered by hyperuricemia and MSU crystals, including activation of the NLRP3 inflammasome, release of IL-1β and other proinflammatory cytokines, and recruitment of monocytes and neutrophils.[7] Indeed, a study in the Women's Health Initiative found that greater adherence to a proinflammatory diet (also measured using EDIP) is associated with higher concentrations of certain inflammatory biomarkers including CRP, IL-6, TNFαR2, and leptin, as well as a lower concentration of adiponectin.[40] The different food and beverage components of the EDIP are likely to modulate this inflammatory response using a variety of mechanisms. The anti-inflammatory effect of coffee has been documented,[41] including in these cohorts in which coffee consumption is prospectively associated with lower concentrations of CRP, IL-6, and TNFαR2.[42] Chlorogenic acids, a family of bioactive compounds abundant in coffee, may decrease production of inflammatory mediators through several mechanisms, including the inhibition of protein tyrosine phosphatase 1B, inhibition of proinflammatory cytokine gene expression, and modulation of nuclear factor κB activation.[43] C18 long-chain saturated fatty acids, found in red meat and fish,[44] have been shown to act synergistically with MSU crystals to induce IL-1β production.[45] Further, diet is an important driver of alternations in the gut microbiota, and gastrointestinal tract-microbiota interactions are capable of influencing immune function, including through the promotion of low-grade inflammation.[46] Moreover, previous work suggests that intestinal microbiota also play a role in regulating the body's inflammatory response to MSU crystal deposition, including through NLRP3 inflammasome activation.[47]

Importantly, our observed associations remained robust after additional adjustment for BMI, indicating they are only partly

mediated through adiposity. Indeed, a previous longitudinal study found that individuals who shifted toward a more inflammatory diet gained more weight.[20] Given the BMI-independent nature of the association observed in our study, it would be valuable for future work to investigate the additional physiologic mechanisms underlying the association between diet, inflammation, and gout. Future mechanistic studies that leverage omics approaches would be particularly valuable.

To our knowledge, this is the first prospective study to examine the association between a proinflammatory pattern and the clinical endpoint of gout. One cross-sectional analysis of the National Health and Nutrition Examination Survey found that greater intake of a proinflammatory diet (measured using the literature-derived Dietary Inflammation Index [DII] composed mainly of nutrients) was associated with higher odds of prevalent gout, although a subgroup analysis revealed that this association was not significant among women.[48] Conversely, our prospective study found the positive association between a hypothesis-driven, empirically derived proinflammatory diet score (which is composed mainly of food groups and has been shown to be more predictive of circulating plasma inflammatory biomarker levels than the DII[49]) and gout was the strongest among women compared with men. Previous cross-sectional studies have also found a positive association between a proinflammatory diet and serum urate levels with reported sex differences; one study among Chinese participants found that a higher DII score was associated with a greater odds of hyperuricemia among women versus men,[30] whereas a Korean study reported a significant positive association between the DII and serum urate levels only among women.[31] The reasons for the observed sex heterogeneity are not immediately clear, but estrogen may play a role. Higher estrogen levels in women may have anti-inflammatory properties under certain conditions, although this effect may be lost after menopause, thereby potentially contributing to gout risk.[50,51] Future prospective studies ought to replicate this observed heterogeneity.

The current association between the EDIP and incident gout is independent of conventional healthy eating patterns that have previously shown inverse associations with gout in the NHS and HPFS.[16,17] The DASH and AHEI diet scores were originally developed to help prevent cardiometabolic diseases and promote longevity,[52–56] whereas EDIP is a mechanism-based pattern that specifically captures dietary inflammatory potential, which is particularly relevant to gout. Indeed, after reversing the EDIP scores, the least inflammatory quintile of EDIP showed the greatest magnitude of inverse association with gout risk compared with the DASH and AHEI diets among women, suggesting EDIP may capture the most biologically relevant aspects of diets that promote gout onset. Moreover, we found a lower EDIP score combined with greater adherence to either of the DASH or AHEI diets was jointly associated with a lower risk of gout. This suggests that there may be an incremental benefit to consuming an anti-inflammatory dietary pattern and also adhering to an overall healthy dietary pattern to optimize gout prevention.

Our study has strengths and limitations. We leveraged three prospective cohort studies of US women and men with decades of follow up and many incident gout cases, although we did not collect corresponding repeated measures of serum urate and other biomarkers. Cohort participants provided dietary data every four years before gout diagnosis using a validated FFQ, which minimizes the potential for recall bias. Using these data, we constructed a validated empirical measure of dietary inflammatory potential that has been shown to be more predictive of circulating plasma inflammatory biomarkers than the literature-derived DII.[18,49] Moreover, the food-based nature of our EDIP makes this pattern more readily translatable into dietary recommendations for gout prevention.[21] Nevertheless, our study has its limitations. As in all observational studies, unmeasured confounding (eg, data on renal failure history were not routinely collected among all three cohorts) and reverse causation are possible. However, we conducted a sensitivity analysis that was restricted to individuals free of major diseases at baseline, and the associations between EDIP and gout remained robust. Moreover, we collected detailed covariate data and adjusted for a broad panel of time-varying confounders, including BMI. Some measurement error remains inevitable; however, this is likely to be nondifferential with respect to our outcome and would most likely bias the observed associations toward the null. Finally, because our study population was primarily composed of White US health professionals, replication in diverse populations is imperative.

In conclusion, we found evidence for a positive and BMI-independent association between greater adherence to a proinflammatory dietary pattern and incident gout, particularly among women. Our findings support a role for diet-related chronic inflammation in the development of gout, similar to that seen in CVD and T2D. Consuming a more anti-inflammatory diet may modulate systemic and metabolic inflammation, potentially reducing gout risk and its life-threatening comorbidities, particularly for women, who are experiencing a disproportionate rise in gout burden.

AUTHOR CONTRIBUTIONS

All authors contributed to at least one of the following manuscript preparation roles: conceptualization AND/OR methodology, software, investigation, formal analysis, data curation, visualization, and validation AND drafting or reviewing/editing the final draft. As corresponding author, Dr McCormick confirms that all authors have provided the final approval of the version to be published, and takes responsibility for the affirmations regarding article submission (eg, not under consideration by another journal), the integrity of the data presented, and the statements regarding compliance with institutional review board/Declaration of Helsinki requirements.

REFERENCES

1. Safiri S, Kolahi AA, Cross M, et al. Prevalence, incidence, and years lived with disability due to gout and its attributable risk factors for

195 countries and territories 1990-2017: a systematic analysis of the Global Burden of Disease Study 2017. Arthritis Rheumatol 2020;72(11):1916–1927.
2. Xia Y, Wu Q, Wang H, et al. Global, regional and national burden of gout, 1990-2017: a systematic analysis of the Global Burden of Disease Study. Rheumatology (Oxford) 2020;59(7):1529–1538.
3. Choi HK, Mount DB, Reginato AM; American College of Physicians; American Physiological Society. Pathogenesis of gout. Ann Intern Med 2005;143(7):499–516.
4. Major TJ, Topless RK, Dalbeth N, et al. Evaluation of the diet wide contribution to serum urate levels: meta-analysis of population based cohorts. BMJ 2018;363:k3951.
5. Lyu JQ, Miao MY, Wang JM, et al. Consumption of total and specific alcoholic beverages and long-term risk of gout among men and women. JAMA Netw Open 2024;7(8):e2430700.
6. Dalbeth N, Phipps-Green A, Frampton C, et al. Relationship between serum urate concentration and clinically evident incident gout: an individual participant data analysis. Ann Rheum Dis 2018;77(7):1048–1052.
7. So AK, Martinon F. Inflammation in gout: mechanisms and therapeutic targets. Nat Rev Rheumatol 2017;13(11):639–647.
8. Zhang WZ. Why does hyperuricemia not necessarily induce gout? Biomolecules 2021;11(2):280.
9. Rohm TV, Meier DT, Olefsky JM, et al. Inflammation in obesity, diabetes, and related disorders. Immunity 2022;55(1):31–55.
10. Aune D, Norat T, Vatten LJ. Body mass index and the risk of gout: a systematic review and dose-response meta-analysis of prospective studies. Eur J Nutr 2014;53(8):1591–1601.
11. Zhang L, Zhang W, Xiao C, et al. Using human genetics to understand the epidemiological association between obesity, serum urate, and gout. Rheumatology (Oxford) 2023;62(10):3280–3290.
12. Aleksandrova K, Koelman L, Rodrigues CE. Dietary patterns and biomarkers of oxidative stress and inflammation: a systematic review of observational and intervention studies. Redox Biol 2021;42:101869.
13. Fung TT, Chiuve SE, McCullough ML, et al. Adherence to a DASH-style diet and risk of coronary heart disease and stroke in women. Arch Intern Med 2008;168(7):713–720.
14. Fung TT, McCullough ML, Newby PK, et al. Diet-quality scores and plasma concentrations of markers of inflammation and endothelial dysfunction. Am J Clin Nutr 2005;82(1):163–173.
15. Fung TT, Rimm EB, Spiegelman D, et al. Association between dietary patterns and plasma biomarkers of obesity and cardiovascular disease risk. Am J Clin Nutr 2001;73(1):61–67.
16. Rai SK, Fung TT, Lu N, et al. The Dietary Approaches to Stop Hypertension (DASH) diet, Western diet, and risk of gout in men: prospective cohort study. BMJ 2017;357:j1794.
17. Yokose C, McCormick N, Lu N, et al. Adherence to 2020 to 2025 dietary guidelines for Americans and the risk of new-onset female gout. JAMA Intern Med 2022;182(3):254–264.
18. Tabung FK, Smith-Warner SA, Chavarro JE, et al. Development and validation of an empirical dietary inflammatory index. J Nutr 2016;146(8):1560–1570.
19. Lee DH, Li J, Li Y, et al. Dietary inflammatory and insulinemic potential and risk of type 2 diabetes: results from three prospective US cohort studies. Diabetes Care 2020;43(11):2675–2683.
20. Tabung FK, Satija A, Fung TT, et al. Long-term change in both dietary insulinemic and inflammatory potential is associated with weight gain in adult women and men. J Nutr 2019;149(5):804–815.
21. Li J, Lee DH, Hu J, et al. Dietary inflammatory potential and risk of cardiovascular disease among men and women in the US. J Am Coll Cardiol 2020;76(19):2181–2193.
22. Patel AV, Gaffo AL. Managing gout in women: current perspectives. J Inflamm Res 2022;15:1591–1598.
23. Hak AE, Curhan GC, Grodstein F, et al. Menopause, postmenopausal hormone use and risk of incident gout. Ann Rheum Dis 2010;69(7):1305–1309.
24. Harrold LR, Etzel CJ, Gibofsky A, et al. Sex differences in gout characteristics: tailoring care for women and men. BMC Musculoskelet Disord 2017;18(1):108.
25. Dehlin M, Muller S, Mallen C, et al. Sex and country differences in gout: cross-country comparison between Sweden and the UK. Scand J Rheumatol 2023;52(6):673–682.
26. Clemens KK, Woodward M, Neal B, et al. Sex disparities in cardiovascular outcome trials of populations with diabetes: a systematic review and meta-analysis. Diabetes Care 2020;43(5):1157–1163.
27. Carrero JJ, Hecking M, Chesnaye NC, et al. Sex and gender disparities in the epidemiology and outcomes of chronic kidney disease. Nat Rev Nephrol 2018;14(3):151–164.
28. The White House. The White House initiative on women's health research. Accessed September 10, 2024. https://www.whitehouse.gov/womenshealthresearch/
29. World Economic Forum. The Global Alliance for Women's Health. Accessed September 10, 2024. https://initiatives.weforum.org/global-alliance-for-womens-health/home
30. Ye C, Huang X, Wang R, et al. Dietary inflammatory index and the risk of hyperuricemia: a cross-sectional study in Chinese adult residents. Nutrients 2021;13(12):4504.
31. Kim HS, Kwon M, Lee HY, et al. Higher pro-inflammatory dietary score is associated with higher hyperuricemia risk: results from the case-controlled Korean Genome and Epidemiology Study Cardiovascular Disease Association Study. Nutrients 2019;11(8):1803.
32. Colditz GA, Manson JE, Hankinson SE. The Nurses' Health Study: 20-year contribution to the understanding of health among women. J Womens Health 1997;6(1):49–62.
33. Ley SH, Ardisson Korat AV, Sun Q, et al. Contribution of the Nurses' Health Studies to uncovering risk factors for type 2 diabetes: diet, lifestyle, biomarkers, and genetics. Am J Public Health 2016;106(9):1624–1630.
34. Rimm EB, Giovannucci EL, Willett WC, et al. Prospective study of alcohol consumption and risk of coronary disease in men. Lancet 1991;338(8765):464–468.
35. Feskanich D, Rimm EB, Giovannucci EL, et al. Reproducibility and validity of food intake measurements from a semiquantitative food frequency questionnaire. J Am Diet Assoc 1993;93(7):790–796.
36. Tabung FK, Giovannucci EL, Giulianini F, et al. An empirical dietary inflammatory pattern score is associated with circulating inflammatory biomarkers in a multi-ethnic population of postmenopausal women in the United States. J Nutr 2018;148(5):771–780.
37. Lin K, McCormick N, Yokose C, et al. Interactions between genetic risk and diet influencing risk of incident female gout: discovery and replication analysis of four prospective cohorts. Arthritis Rheumatol 2023;75(6):1028–1038.
38. Willett WC, Howe GR, Kushi LH. Adjustment for total energy intake in epidemiologic studies. Am J Clin Nutr 1997;65(S4):1220S–1228S.
39. Wang P, Song M, Eliassen AH, et al. Optimal dietary patterns for prevention of chronic disease. Nat Med 2023;29(3):719–728.
40. Shi N, Aroke D, Jin Q, et al. Proinflammatory and hyperinsulinemic dietary patterns are associated with specific profiles of biomarkers predictive of chronic inflammation, glucose-insulin dysregulation, and dyslipidemia in postmenopausal women. Front Nutr 2021;20(8):690428.
41. Paiva C, Beserra B, Reis C, et al. Consumption of coffee or caffeine and serum concentration of inflammatory markers: a systematic review. Crit Rev Food Sci Nutr 2019;59(4):652–663.

42. Hang D, Kværner AS, Ma W, et al. Coffee consumption and plasma biomarkers of metabolic and inflammatory pathways in US health professionals. Am J Clin Nutr 2019;109(3):635–647.
43. Grosso G, Godos J, Galvano F, Giovannucci EL. Coffee, caffeine, and health outcomes: an umbrella review. Annu Rev Nutr 2017;37(1): 131–156.
44. Kris-Etherton PM, Griel AE, Psota TL, et al. Dietary stearic acid and risk of cardiovascular disease: intake, sources, digestion, and absorption. Lipids 2005;40(12):1193–1200.
45. Joosten LA, Netea MG, Mylona E, et al. Engagement of fatty acids with Toll-like receptor 2 drives interleukin-1β production via the ASC/-caspase 1 pathway in monosodium urate monohydrate crystal-induced gouty arthritis. Arthritis Rheum 2010;62(11):3237–3248.
46. Minihane AM, Vinoy S, Russell WR, et al. Low-grade inflammation, diet composition and health: current research evidence and its translation. Br J Nutr 2015;114(7):999–1012.
47. Wang Z, Li Y, Liao W, et al. Gut microbiota remodeling: a promising therapeutic strategy to confront hyperuricemia and gout. Front Cell Infect Microbiol 2022;12:935723.
48. Zhang Y, Song J, Lai Y, et al. Association between the dietary inflammatory index and gout in the National Health and Nutrition Examination Survey 2007–2018. Heliyon 2023;9(12):e22930.
49. Tabung FK, Smith-Warner SA, Chavarro JE, et al. An empirical dietary inflammatory pattern score enhances prediction of circulating inflammatory biomarkers in adults. J Nutr 2017;147(8):1567–1577.
50. Vegeto E, Benedusi V, Maggi A. Estrogen anti-inflammatory activity in brain: a therapeutic opportunity for menopause and neurodegenerative diseases. Front Neuroendocrinol 2008;29(4):507–519.
51. Martín-Millán M, Castaneda S. Estrogens, osteoarthritis and inflammation. Joint Bone Spine 2013;80(4):368–373.
52. Sacks FM, Campos H. Dietary therapy in hypertension. N Engl J Med 2010;362(22):2102–2112.
53. Moore TJ, Vollmer WM, Appel LJ, et al; DASH Collaborative Research Group. Effect of dietary patterns on ambulatory blood pressure: results from the Dietary Approaches to Stop Hypertension (DASH) Trial. Hypertension 1999;34(3):472–477.
54. Willett W, Sacks F, Trichopoulou A, et al. Mediterranean diet pyramid: a cultural model for healthy eating. Am J Clin Nutr 1995;61(S6): 1402S–1406S.
55. Kennedy ET, Ohls J, Carlson S, et al. The healthy eating index: design and applications. J Am Diet Assoc 1995;95(10):1103–1108.
56. Hu FB, Rimm EB, Stampfer MJ, et al. Prospective study of major dietary patterns and risk of coronary heart disease in men. Am J Clin Nutr 2000;72(4):912–921.

Arthritis & Rheumatology
Vol. 77, No. 8, August 2025, pp 1087–1091
DOI 10.1002/art.43145

AMERICAN COLLEGE of RHEUMATOLOGY
Empowering Rheumatology Professionals

BRIEF REPORT

Sustained Interferon Signature Suppression With Anifrolumab in a Patient With STING-Associated Vasculopathy with Onset in Infancy Refractory to JAK Inhibitor and Dazukibart Therapy

Sara Alehashemi,[1] Bjoern Buehring,[2] Adriana A. de Jesus,[1] Sachin Gaurav,[1] Andre Rastegar,[1] Alexi Baumgardner,[1] Kip Friend,[1] Oluwatobi T. Arisa,[3] William D. Figg,[3] Danielle Fink,[4] Douglas B. Kuhns,[4] Ben Colton,[5] Cody J. Peer,[3] and Raphaela Goldbach-Mansky[1]

Objective. The objective was to report the safety and efficacy of an anti-IFNAR1 antibody (anifrolumab) in a patient with STING-associated vasculopathy with onset in infancy (SAVI) who presented with vasculitic ulcers and systemic inflammation refractory to JAK inhibition (JAKi) and to the interferon-β–neutralizing monoclonal antibody dazukibart.

Methods. A patient with SAVI and a de novo *STING1* p.(Asn154Ser) mutation, a known pathogenic variant, and uncontrolled disease received 21 doses of dazukibart under a compassionate use investigational new drug protocol, which was followed by treatment with the anti-IFNAR1 antibody anifrolumab. Clinical and laboratory parameters, including wound healing, whole-blood type I interferon (IFN I) signature, and safety markers were closely monitored throughout both treatment periods.

Results. Despite initial reductions in C-reactive protein levels and IFN I scores following dazukibart administration, the patient experienced rebound inflammation and recurrent vasculitic lesions. Dazukibart dose adjustments failed to sustainably control IFN I signaling. Subsequent combination therapy of baricitinib and tocilizumab proved partially effective. Treatment with anifrolumab, an IFNAR1 blocker, in conjunction with tocilizumab led to sustained suppression of IFN I scores, allowed discontinuation of JAKi, and resulted in significant improvement in vasculitic wounds.

Conclusion. This case underscores the challenges in treating patients with SAVI and highlights the utility of IFN I scores as a theragnostic biomarker. Although high-dose JAKi and dazukibart failed to achieve sustained control of IFN I signaling, treatment with anifrolumab durably suppressed IFN scores and demonstrated promising efficacy, which allows for the investigation of the role of IFN I signaling in the disease pathogenesis of SAVI and other interferonopathies in future clinical trials.

INTRODUCTION

STING-associated vasculopathy with onset in infancy (SAVI) is a rare autoinflammatory interferonopathy that manifests early in life and is characterized by systemic inflammation, progressive interstitial lung disease, and peripheral vascular complications.[1] Patients with SAVI have a prominent type I interferon (IFN I) signature in their blood. Current practice is to use JAK-inhibitors (JAKi) to mitigate IFN I–mediated inflammation (Figure 1A).[2] However, even optimized JAKi regimens often yield only partial responses

Supported by the Intramural Research Program at the National Institute of Allergy Immunology and Infectious Diseases (NIAID) of the NIH and partially supported by federal funds provided by the National Cancer Institute, NIH (contract no. 75N91019D000024).

[1]Sara Alehashemi, MD, MPH, Adriana A. de Jesus, MD, PhD, Sachin Gaurav, PhD, Andre Rastegar, BS, Alexi Baumgardner, BS, Kip Friend, BS, Raphaela Goldbach-Mansky, MD, MHS: Translational Autoinflammatory Diseases Section, National Institute of Allergy and Infectious Diseases, NIH, Bethesda, Maryland; [2]Bjoern Buehring, MD: Bergisches Rheuma-Zentrum, Wuppertal, Germany; [3]Oluwatobi T. Arisa, PhD, William D. Figg, PharmD, Cody J. Peer, PhD: Clinical Pharmacology Program, National Cancer Institute, NIH, Bethesda, Maryland; [4]Danielle Fink, PhD, Douglas B. Kuhns, PhD: Frederick National Laboratory for Cancer Research, Frederick, Maryland; [5]Pharmacy Department, Ben Colton, PharmD: National Institutes of Health Clinical Center, NIH, Bethesda, Maryland.

Additional supplementary information cited in this article can be found online in the Supporting Information section (https://acrjournals.onlinelibrary.wiley.com/doi/10.1002/art.43145).

Author disclosures are available online at https://onlinelibrary.wiley.com/doi/10.1002/art.43145.

Address correspondence via email to Sara Alehashemi, MD, MPH, at sara.alehashemi@nih.gov.

Submitted for publication May 11, 2024; accepted in revised form January 22, 2025.

in patients with SAVI. The JAKi doses required for clinical benefit frequently cause side effects such as cytopenias and BK viruria/viremia, which necessitates close monitoring.[3] Additionally, the US Food and Drug Administration has issued warnings about potential serious side effects linked to JAKi, such as cardiovascular events, cancer, blood clots, and death.[4] The partial treatment responses to JAKi, combined with safety concerns, underscore the need for novel SAVI treatments.

Dazukibart[5] is a humanized immunoglobulin G1 antibody that binds IFNβ and aims at inhibiting signaling through the IFNAR1 (Figure 1A). Dazukibart has been investigated in dermatomyositis, an inflammatory myositis characterized by skin involvement and elevated interferon-β (IFNβ) levels in peripheral blood and affected muscles (NCT05895786).[6,7] Anifrolumab, a monoclonal antibody that binds and blocks IFNAR1, is approved for treating systemic lupus erythematosus.[8] In SAVI, successful treatment with interferon-blocking drugs would lead to suppression of the IFN I response gene signature, a theragnostic biomarker that allows for monitoring the efficacy of IFN I pathway blockade[9] (Figure 1A).

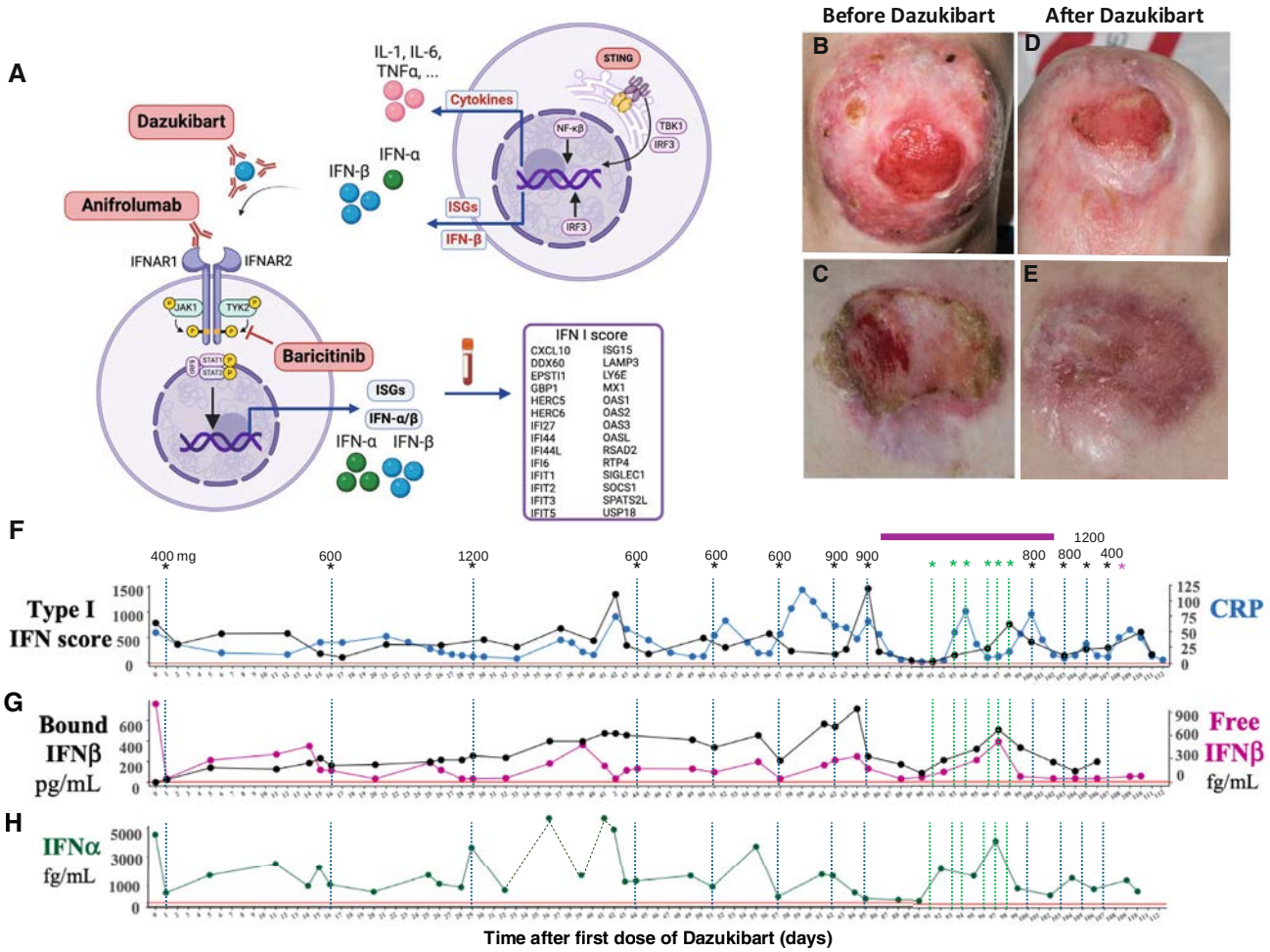

Figure 1. (A) Schematic of SAVI pathogenesis and targeted treatments. In SAVI, constitutive activation of stimulator of interferon genes (a dinucleotide sensor) initiates *IFNB1* transcription, leading to increased production of IFNβ. IFNβ signals through the IFNAR-1, triggering upregulation of IFNα and interferon-stimulated genes, which contribute to the 28-gene IFN I score. The targeted treatments used in this patient are depicted: (1) Baricitinib, a JAKi, blocks JAK/STAT signaling downstream of the IFNAR-1; (2) dazukibart, a neutralizing monoclonal antibody against IFNβ, prevents IFNβ from binding to and signaling through IFNAR-1; (3) anifrolumab, an anti–IFNAR-1 monoclonal antibody, blocks downstream IFN I signaling at the receptor level. (B–E) Clinical images of vasculitic lesions on the right knee (B) and right lateral thigh (C) at baseline, which improved with dazukibart but did not fully close (D and E). (F) Plot showing the associations between CRP levels and IFN I scores. (G) Plot depicting serum levels of bound-to-drug-IFNβ (black) and free IFNβ (purple) during dazukibart treatment. Although bound IFNβ rose, fluctuating levels of free IFNβ were still detectable in the serum. (H) Serum levels of IFNα (green) levels were elevated during dazukibart treatment. Black stars indicate IV infusions of dazukibart; the doses are specified. Green stars indicate subcutaneous injections of dazukibart, which were all administered at a 200 mg dose. The pink star indicates the tocilizumab injection. The purple block denotes the period of systemic steroid administration due to severe flare following the thrombosed port access. CRP, C-reactive protein; IFN I, type I interferon; IL, interleukin; ISG, interferon-stimulated gene; IV, intravenous; JAKi, JAK inhibitor; SAVI, STING-associated vasculopathy with onset in infancy; TNF, tumor necrosis factor.

PATIENTS AND METHODS

To find alternative treatment approaches to JAKi (Figure 1A), we evaluated the impact of an IFNβ neutralizing monoclonal antibody (dazukibart) under a compassionate use investigational new drug (IND) protocol in a 22-year-old patient with SAVI and a de novo *STING1* p.(Asn154Ser) mutation. The patient, whose disease onset occurred in infancy, experienced recurrent vasculitis ulcers, progressive osteolysis, minimal lung disease, persistently elevated systemic markers of inflammation including C-reactive protein (CRP), erythrocyte sedimentation rate, and anemia, despite recommended doses of baricitinib.[9] The patient began baricitinib treatment in 2014 at age 17 as part of a cohort to establish a dosing regimen for IFN-opathies.[2] However, the patient developed JAKi-related side effects, including BK viruria and viremia, Epstein-Barr virus (EBV) viremia, and facial molluscum contagiosum (Figure 1B and 1C).

The patient consented to the IND protocol *(20-I-9955)*, was monitored at the National Institutes of Health (NIH) for over 100 days, and received 15 intravenous (IV) doses of dazukibart (including 2 doses at an outside facility) and 6 subcutaneous doses (21 doses total). The patient was premedicated with acetaminophen and diphenhydramine before IV administration of dazukibart to minimize potential infusion reactions. During this period, baricitinib (7 mg daily) and valacyclovir for zoster prophylaxis were continued. Wound healing was assessed twice weekly, and IFN I score and safety laboratory tests were used to monitor treatment effects and guide dose adjustments.

Because of insufficient suppression of IFN I signaling and poor clinical response to dazukibart, treatment was subsequently switched to anifrolumab combined with tocilizumab, and baricitinib was gradually tapered. Anifrolumab was administered intravenously over 30 minutes every 4 weeks with the same premedication, whereas zoster prophylaxis with valacyclovir was maintained. Throughout this period, the IFN I score, safety markers, and wound healing were monitored on protocol NCT02974595. The patient enrolled under the institutional review board (IRB)-approved natural history protocol (NCT02974595) and single patient emergency IND 146152: NIH IRB: 20-I-9955 and consented to participate in clinical research.

RESULTS

The anti-IFNβ antibody, dazukibart, was initially administered at 400 mg IV infusions every four weeks. At baseline, the patient had significantly elevated markers of inflammation, including a CRP level of 51 (normal <5 mg/L), an IFN I score of 789 (normal <25), a serum-free IFNβ level of 1,083 (normal: 0–573 fg/mL), and an IFNα level of 4,565 (normal 0–42 fg/mL) (Figure 1F–H).

Following the first infusion, there was a transient decrease in both the CRP and IFN I score (Figure 1F). However, by day five after the infusion, all markers, including IFN I score, IFNβ, and IFNα levels, rebounded. This coincided with a flare in vasculitic skin lesions. In response to these flares, dose adjustments were made, escalating to 600 mg and later 1,200 mg IV on day 29. Despite more frequent dosing intervals, as short as five days apart, the patient continued to experience recurrent rebound flares of IFN I signaling that were evidenced by rising IFN I score, IFNβ and IFNα levels, and elevated CRP. Improvement in the healing of the vasculitic ulcers, which was observed with the initial infusions, plateaued, and the patient developed new lesions following rebound flare episodes.

The patient encountered complications related to IV access, including subclavian port thrombosis, which necessitated port removal that further led to escalation of the systemic inflammatory response. Throughout dazukibart treatment, adverse skin reactions, including acneiform pustular eruptions was observed, requiring topical management.

Using a proprietary test, the Pfizer team measured serum IFNβ bound to dazukibart. Serum IFNβ levels were also measured using ultra-sensitive S-PLEX ELISA kits from Meso Scale. Although the assay was not validated, the pattern suggested that the antibody likely detected unbound, free IFNβ (Figure 1G). A rudimentary, single-subject pharmacokinetic/pharmacodynamic model employing target-mediated drug disposition[10] (Supplementary Figure 1A) satisfactorily captured drug exposure of unbound drug and drug-IFNβ complex, providing additional evidence of the ability of dazukibart to bind free INFβ. The model also predicted an elevated production rate of free IFNβ that continued to rise (Figure 1G) despite the increase in drug levels (Supplementary Figure 1B). The absence of antidrug antibodies (ADAs) performed by the Pfizer team ruled out decreased drug exposure from ADAs as an explanation for the rising free IFNβ levels.

Serum IFNα levels were simultaneously measured (Figure 1H) and rose during the treatment course with dazukibart because the drug only binds to IFNβ. These elevated levels of IFNα, along with the presence of free IFNβ, were likely responsible for the rebound rise in IFN I score and inflammatory flares despite higher and more frequent administration of dazukibart.

The patient's clinical and laboratory parameters, including liver and kidney function, complete blood counts, muscle enzymes, and viral titers (BK, JC, EBV, and Herpes Simplex Virus), did not raise safety concerns. Valacyclovir was maintained to prevent varicella-zoster virus infection, and molluscum contagiosum remained limited to focal areas on her face.

Because of the inability of dazukibart to durably suppress the IFN I signature, treatment was transitioned to a combination of baricitinib and the interleukin-6 (IL-6) blocker, tocilizumab, administered subcutaneously every two weeks. Given the persistent elevation in IFN I score and the emergence of new vasculitic ulcers on this regimen, the decision was made to initiate anifrolumab therapy combined with tocilizumab. Anifrolumab was administered as 300 mg IV infusions every four weeks. Anifrolumab treatment marked a turning point in the patient's treatment course. Within the first two months of anifrolumab treatment, the IFN I score dropped substantially and remained suppressed over the

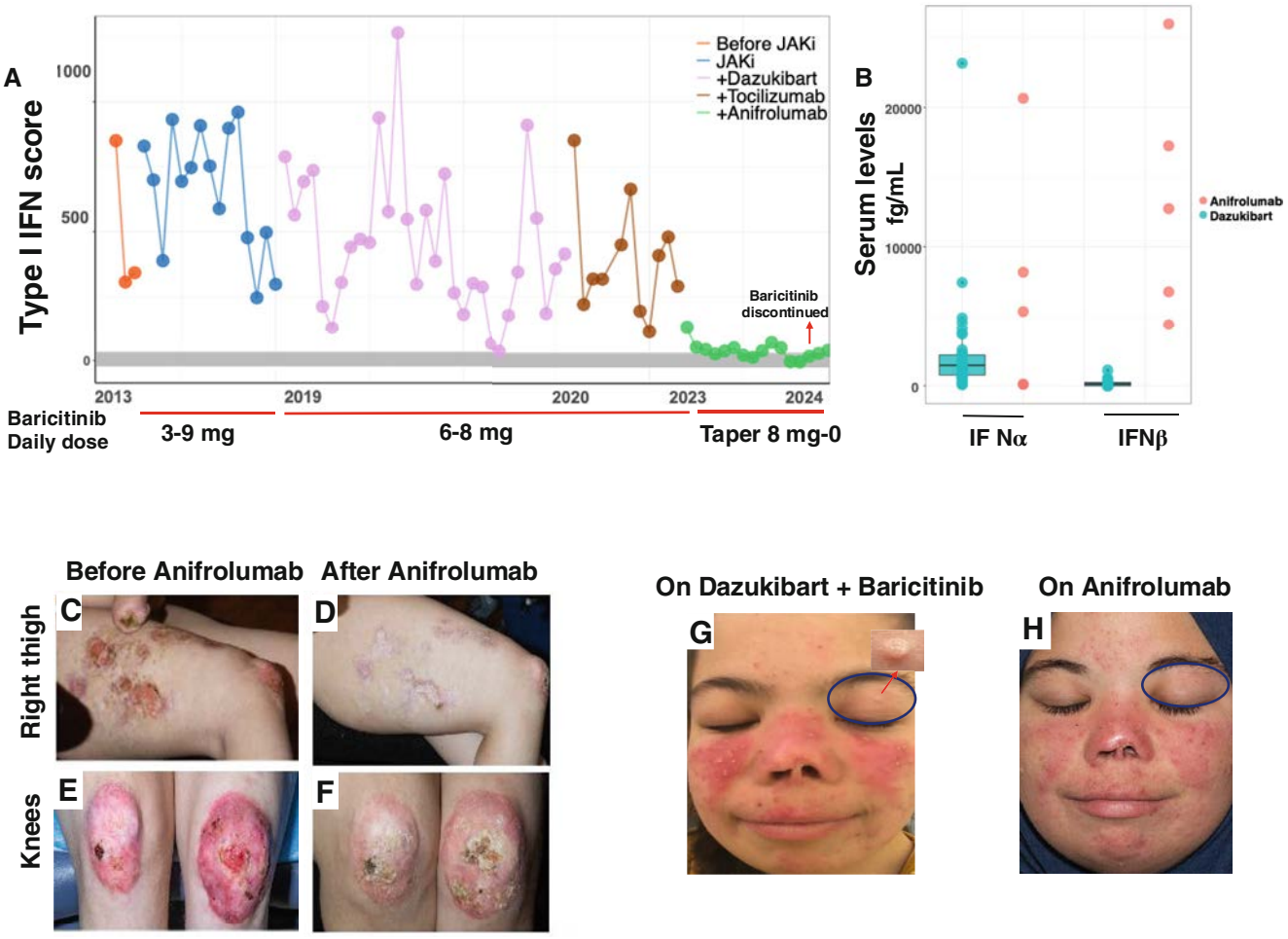

Figure 2. Impact of anifrolumab on IFN I scores, vasculitic lesions, and clinical outcomes: (A) The IFN I score in the blood was persistently elevated at baseline, despite over ten years of treatment with baricitinib. Attempts to suppress IFN I signaling with dazukibart in combination with baricitinib, followed by the addition of tocilizumab to baricitinib, failed to achieve effective suppression, with levels continuing to fluctuate. In contrast, treatment with anifrolumab led to sustained and remarkable normalization of IFN I scores in the context of continued tocilizumab treatment but tapering and discontinuation of baricitinib. (B) Serum levels of free IFNα and IFNβ were measured on anifrolumab and presented alongside the observed ranges of IFNα and IFNβ levels that were measured when the patient was on treatment with dazukibart. (C–F) Anifrolumab treatment resulted in marked improvement in vasculitic skin lesions, leading to complete closure of all wounds. Shown are the lateral right thigh and both knees before and after anifrolumab. (G–H) Anifrolumab treatment allowed for the tapering of baricitinib, which ultimately led to clearance of the facial molluscum lesions. The area marked on the left palpebral region demonstrates significant improvement. IFN I, type I interferon; JAKi, JAK inhibitor.

subsequent months while the baricitinib dose was tapered and discontinued (Figure 2A).

This durable suppression of the IFN I score was accompanied by an increase in IFNα (ranging from 119 fg/mL to 20.6 pg/mL) and IFNβ levels (ranging from 6,775 fg/mL to 26 pg/mL) in the serum (Figure 2B), but vasculitic ulcers that had been refractory to previous treatments healed (Figure 2C–F). During the tapering of baricitinib, systemic viral reactivations, including BK and EBV viremia, as well as facial molluscum contagiosum lesions, gradually improved and ultimately cleared (Figure 2G–H). Over 15 months of anifrolumab therapy, the patient's vasculitic lesions significantly improved with rare and limited flares throughout the course. Notably, liver and kidney functions, complete blood counts, and other safety markers remained stable throughout anifrolumab treatment.

In summary, whereas dazukibart failed to sustainably suppress IFN I signaling and control clinical symptoms, anifrolumab treatment resulted in sustained suppression of the IFN I activity and overall good disease control, including healing of vasculitic lesions and discontinuation of the JAKi with subsequent resolution of viral reactivation (BK, EBV, and molluscum); treatment was well tolerated.

DISCUSSION

This report illustrates the challenges of treating vasculitic ulcers in SAVI. Our data support the use of the IFN I score as a theragnostic biomarker to assess and monitor IFN I signaling in treatments targeting IFN I, such as dazukibart and anifrolumab. Frequent monitoring of the IFN I score provided

an assessment of IFN I signaling in peripheral blood cells that assisted in interpreting elevated free IFNα and IFNβ levels during dazukibart and anifrolumab treatment. High serum cytokine levels on treatment with cytokine-, or cytokine receptor–blocking antibodies, such as tumor necrosis factor blockers like adalimumab administration[11] or IL-6 receptor blockade with sarilumab,[12] which respond to treatment are described and attributed to changes in cytokine clearance on anticytokine or anticytokine receptor treatment. On anifrolumab treatment, higher IFNβ levels in the context of a normal IFN I score indicated an effective blockade of IFN I signaling in contrast to dazukibart for which elevated serum IFNα and IFNβ levels in the context of an elevated IFN I score indicated continued IFN I signaling. These data validate the frequent assessment of the IFN I score in optimizing drug regimens and establishing proof of mechanism.

Several limitations should be considered when interpreting the findings of this study. The single-case nature of the study limits the generalizability of the results to a broader population of patients with SAVI. The compassionate use IND protocol may introduce bias due to the absence of randomization and control groups, and the patient's disease severity and complex medical history could have influenced the response to dazukibart. The inability to establish a sustainable dosing regimen for dazukibart, coupled with a successful response to anifrolumab, make anifrolumab an attractive treatment option for patients with severe interferonopathies, including SAVI.[13–14] However, dazukibart may be beneficial for other patients with SAVI or other IFN-opathies with milder disease.

The promising response to the IFNAR1 blocker, anifrolumab, highlights its potential for SAVI treatment because it achieved durable suppression of the IFN I score and allowed for the discontinuation of JAKi. Despite these encouraging results, current treatment strategies remain limited to blocking interferon signaling. Further research, including controlled trials, is needed to establish more effective treatments for patients with SAVI, who continue to face significant medical challenges.

ACKNOWLEDGMENTS

We thank Pfizer for their generous provision of the compassionate use medication, dazukibart. We would like to thank Myron Chu at Pfizer for his valuable assistance across various aspects of the dazukibart study. Our thanks also go to several individuals for their contributions to patient care, including Gina Montealegre, Richard Chang, Kimberly Johnson, Karen Chandler Axelrod, Hanna Hildenbrand, Lena Bichell, and regulatory support, Gema Souto Adeva at the NIH. Furthermore, we acknowledge Srividya Neelakantan, John Prybylski, and Qiang Qu at Pfizer for their invaluable contributions to the pharmacokinetic analysis.

AUTHOR CONTRIBUTIONS

All authors contributed to at least one of the following manuscript preparation roles: conceptualization AND/OR methodology, software, investigation, formal analysis, data curation, visualization, and validation AND drafting or reviewing/editing the final draft. As corresponding author, Dr Alehashemi confirms that all authors have provided the final approval of the version to be published and takes responsibility for the affirmations regarding article submission (eg, not under consideration by another journal), the integrity of the data presented, and the statements regarding compliance with institutional review board/Declaration of Helsinki requirements.

REFERENCES

1. Liu Y, Jesus AA, Marrero B, et al. Activated STING in a vascular and pulmonary syndrome. N Engl J Med 2014;371(6):507–518.
2. Sanchez GAM, Reinhardt A, Ramsey S, et al. JAK1/2 inhibition with baricitinib in the treatment of autoinflammatory interferonopathies. J Clin Invest 2018;128(7):3041–3052.
3. Cetin Gedik K, Souto Adeva G, Wade J, et al. Monitoring of BK reactivation and long-term safety on JAK1/2 inhibition with baricitinib [abstract]. Arthritis Rheumatol 2020;72(suppl 10).
4. U.S. Food and Drug Administration. "FDA requires warnings about increased risk of serious heart-related events, cancer, blood clots, and death for JAK inhibitors that treat certain chronic inflammatory conditions." U.S. Food and Drug Administration Drug Safety Communication, 1 Sept. 2021. https://www.fda.gov/drugs/drug-safety-and-availability/fda-requires-warnings-about-increased-risk-serious-heart-related-events-cancer-blood-clots-and-death.
5. Neelakantan S, Oemar B, Johnson K, et al. Safety, tolerability, and pharmacokinetics of PF-06823859, an anti-Interferon β monoclonal antibody: a randomized, phase I, single- and multiple-ascending-dose study. Clin Pharmacol Drug Dev 2021;10(3):307–316.
6. Liao AP, Salajegheh M, Nazareno R, et al. Interferon β is associated with type 1 interferon-inducible gene expression in dermatomyositis. Ann Rheum Dis 2011;70(5):831–836.
7. Huard C, Gullà SV, Bennett DV, et al. Correlation of cutaneous disease activity with type 1 interferon gene signature and interferon β in dermatomyositis. Br J Dermatol 2017;176(5):1224–1230.
8. Morand EF, Furie R, Tanaka Y, et al; TULIP-2 Trial Investigators. Trial of anifrolumab in active systemic lupus erythematosus. N Engl J Med 2020;382(3):211–221.
9. Kim H, Brooks KM, Tang CC, et al. Pharmacokinetics, pharmacodynamics, and proposed dosing of the oral JAK1 and JAK2 inhibitor baricitinib in pediatric and young adult CANDLE and SAVI patients. Clin Pharmacol Ther 2018;104(2):364–373.
10. Mager DE. Target-mediated drug disposition and dynamics. Biochem Pharmacol 2006;72(1):1–10.
11. Berkhout LC, L'ami MJ, Ruwaard J, et al. Dynamics of circulating TNF during adalimumab treatment using a drug-tolerant TNF assay. Sci Transl Med 2019;11(477):eaat3356.
12. Mohammadi K, Sleeman MW, Boyapati A, et al. Effect of IL-6R blockade on plasma lipids and clinical outcomes among hospitalized patients with COVID-19 infection. J Lipid Res 2024;65(6):100568.
13. Alehashemi S, Baumgardner A, Shakoory B, et al. Anifrolumab normalizes the type I interferon signature in a cohort of patients with type I interferonopathies [abstract]. Arthritis Rheumatol 2023;75(suppl 9).
14. Kretzschmar G, Piñero Páez L, Tan Z, et al. Normalized interferon signatures and clinical improvements by IFNAR1 blocking antibody (Anifrolumab) in patients with type I interferonopathies. J Clin Immunol 2024;45(1):31.

American College of Rheumatology
Empowering Rheumatology Professionals

Arthritis & Rheumatology
Vol. 77, No. 8, August 2025, pp 1092–1105
DOI 10.1002/art.43157

Sex Differences in B Cells From the Joints of Children With Oligoarticular Juvenile Idiopathic Arthritis

Ki Pui Lam,[1] Claudia Harris,[2] Maria L. Taylor,[3] Daniela Fernandez-Salinas,[4] Jing Cui,[5] Biju Issac,[6] Liang Sun,[6] Indu Raman,[7] Chengsong Zhu,[7] Maryrose Hahn,[2] Maryam Ashoor,[1] Ahmad Bakhsh,[1] Maria C. Bryant,[1] Siobhan Case,[8] Mia Chandler,[1] Joyce C. Chang,[1] Ezra Cohen,[1] Fatma Dedeoglu,[1] Olha Halyabar,[1] Jonathan S. Hausmann,[9] Melissa Hazen,[1] Daniel Ibanez,[1] Liyoung Kim,[1] Jeffrey Lo,[1] Mindy S. Lo,[1] Esra Meidan,[1] Megan Perron,[1] Helene Powers,[1] Mary Beth Son,[1] Holly Wobma,[1] Erin Janssen,[10] Pui Y. Lee,[1] Peter A. Nigrovic,[8] Laurie Ohlms,[11] A. Eliot Shearer,[11] Margaret H. Chang,[1] Maria Gutierrez-Arcelus,[4] and Lauren A. Henderson[1]

Objective. Disordered T peripheral helper (Tph)–B cell interactions have been implicated in several forms of inflammatory arthritis, including oligoarticular (oligo) juvenile idiopathic arthritis (JIA). We sought to evaluate the Tph–B cell axis in oligo JIA through an analysis of intra-articular B cells.

Methods. B cells from the blood and synovial fluid (SF) of 44 children with oligo JIA were compared to those from the blood and tonsils of controls. Flow cytometry, B cell receptor (BCR) repertoire analysis, and autoantibody profiling were used to characterize B cells.

Results. Memory B (Bmem) cells and heterogeneous subsets of CD21^{lo} B cells were enriched in oligo JIA-SF versus blood of patients and controls. Compared to male patients, female patients with oligo JIA had greater proportions of intra-articular Tph cells that expressed B cell help factors as well as Bmem cells, plasmablasts, and age-/autoimmune-associated B cells. The sex differences in B cells were observed only in the joints and were not found in the blood or tonsil, nor were they explained by other disease features such as age at onset, antinuclear antibody status, or severity. Bmem cells in SF from female patients displayed characteristics of autoreactivity, including longer complementarity determining region 3 lengths and increased usage of autoreactive BCR gene segments, which were not found in blood Bmem cells. A diverse array of autoantibodies accumulated in the SF of female patients with oligo JIA compared to the blood of patients with JIA and controls.

Conclusion. These findings demonstrate prominent B cell dysregulation in oligo JIA and implicate sex as an important biologic factor in B cell responses in this disease.

INTRODUCTION

Juvenile idiopathic arthritis (JIA) is an umbrella term that encompasses several distinct diseases.[1] The oligoarticular (oligo) form of JIA is defined by limited joint involvement (fewer than five joints) within the first six months of disease and accounts for more than half of all children with chronic inflammatory arthritis living in North America.[1,2] A subgroup of patients with oligo JIA shares a

Dr J. C. Chang's work was supported by the National Heart, Lung, and Blood Institute, NIH (grant K23-HL-148539). Dr Son's work was supported by the Samara Jan Turkel Clinical Center for Pediatric Autoimmune Disease. Dr Nigrovic's work was supported by the National Institute of Arthritis and Musculoskeletal and Skin Diseases, NIH (awards R01-AR-073201, R01-AR-075906, and P30-AR-070253). Dr Gutierrez-Arcelus's work was supported by the National Institute of Arthritis and Musculoskeletal and Skin Diseases, NIH (grant P30-AR-070253); the Arthritis National Research Foundation; and the Vic Braden Family, the Lupus Research Alliance, and the Cell Discovery Network, a collaborative initiative funded by the Manton Foundation and the Warren Alpert Foundation at Boston Children's Hospital. Dr Henderson's work was supported in part by the National Institute of Arthritis and Musculoskeletal and Skin Diseases, NIH (grants R01-AR-083424 and P30-AR-070253).

[1]Ki Pui Lam, PhD, Maryam Ashoor, MB, BCh, BAO, Ahmad Bakhsh, MD, Maria C. Bryant, MD, Mia Chandler, MD, MPH, Joyce C. Chang, MD, MSCE, Ezra Cohen, MD, Fatma Dedeoglu, MD, Olha Halyabar, MD, Melissa Hazen, MD, Daniel Ibanez, MD, Liyoung Kim, MD, Jeffrey Lo, MD, Mindy S. Lo, MD, PhD, Esra Meidan, MD, Megan Perron, MD, RhMSUS, Helene Powers, RN, MSN, FNP, Mary Beth Son, MD, Holly Wobma, MD, PhD, Pui Y. Lee, MD, PhD, Margaret H. Chang, MD, PhD, Lauren A. Henderson, MD, MSc: Division of Immunology, Boston Children's Hospital and Harvard Medical School, Boston, Massachusetts; [2]Claudia Harris, BS, Maryrose Hahn, BS: Division of Immunology, Boston Children's Hospital, Boston, Massachusetts; [3]Maria L. Taylor, BS: Division of Immunology, Boston Children's Hospital, Boston, Massachusetts, and Wright State University Boonshoft School of Medicine, Dayton, Ohio; [4]Daniela Fernandez-Salinas, BSc, Maria Gutierrez-Arcelus, PhD: Division of Immunology, Boston Children's Hospital, Boston, Massachusetts, and Program in Medical and Population Genetics, Broad Institute of Harvard and Massachusetts Institute of Technology, Cambridge, Massachusetts; [5]Jing Cui, PhD, Division of Rheumatology, Inflammation, and Immunity, Brigham and Women's Hospital and Harvard Medical School, Boston, Massachusetts; [6]Biju Issac, PhD, Liang Sun, PhD: Research Computing, Department of Information Technology Boston Children's Hospital, Boston, Massachusetts; [7]Indu Raman, MS, Chengsong Zhu, PhD: Department of Immunology, Microarray & Immune Phenotyping Core Facility, University of Texas Southwestern Medical Center, Dallas, Texas; [8]Siobhan Case, MD, MHS, Peter A. Nigrovic: Division of Immunology, Boston Children's Hospital and Harvard

unique constellation of features: early age of disease onset (younger than six years old), female sex predominance, high risk for chronic anterior uveitis, and antinuclear antibody (ANA) positivity.[3–5] The underlying biology that drives the clustering of these clinical characteristics in oligo JIA is not fully understood; however, there is evidence that B cell responses may be important in this subset of patients. Patients with early-onset oligo JIA have increased expression of B cell–related genes in whole blood along with increased frequencies of circulating, switched memory B (Bmem) cells that are not found in older patients.[6–9] There is evidence of disordered T–B cell interactions in patients with ANA-positive oligo JIA. In the synovial tissue, the presence of T–B cell aggregates and germinal center (GC) reactions correlates with ANA positivity more so than other factors like disease severity or duration.[10] In adults with rheumatoid arthritis (RA), pathogenic T peripheral helper (Tph) cells in inflamed joints stimulate excessive B cell responses and the generation of antibodies.[11] We, and others, have previously demonstrated that Tph cells are also enriched in the synovial fluid (SF) of children with ANA-positive oligo JIA compared to patients with ANA negativity. These intra-articular Tph cells are clonally expanded, overexpress factors associated with B cell help, and promote the differentiation of antibody-producing plasmablasts.[12–15] Thus, B cell responses, potentially mediated by Tph cells, are likely important in oligo JIA, particularly in the subset of patients characterized by female sex, early-onset disease, and ANA positivity.

To evaluate B cell responses in oligo JIA, we conducted detailed B cell immunophenotyping, B cell receptor (BCR) repertoire analysis, and autoantibody profiling. Our results show that Tph cells that express factors associated with B cell help, Bmem cells, plasmablasts, and B cells with characteristics of age-/autoimmune-associated B cells (ABCs) are all more frequent in the joints of female versus male patients. These intra-articular B cells demonstrate features of autoreactivity, and a diverse spectrum of autoantibodies is present in the SF of female patients. Our results demonstrate that sex is an important variable in B cell responses in oligo JIA.

PATIENTS AND METHODS

Patients and samples. Children with oligo JIA defined by International League of Associations for Rheumatology classification criteria and seen in the Boston Children's Hospital (BCH) Rheumatology Clinic provided peripheral blood (PB) and/or discard SF samples that were obtained during a clinically indicated procedure.[1] Pediatric healthy controls without a rheumatologic diagnosis who were seen in the Rheumatology Clinic for noninflammatory causes of joint pain and healthy adults recruited from the area local to the hospital provided blood samples. Discard tonsils were obtained from otherwise healthy children undergoing tonsillectomy for sleep apnea. A list of samples and the experiments they contributed to are available in Supplementary Table S1. Medical records were reviewed to gather clinical information. New-onset samples from patients with oligo JIA were collected within six months of symptom onset. ANA detected at any titer and at any time in disease course was considered positive. The study was approved by the BCH Institutional Review Board.

Studies conducted with patient samples. Mononuclear cells from PB, SF, and tonsils were studied with flow cytometry and analyzed using standard gating in FlowJo as well as unsupervised clustering conducted with OMIQ (Domatics, www.omiq.ai; Supplementary Table S2). As described previously, genomic DNA was extracted from sorted naive ($CD3^-CD19^+CD27^-IgD^+CD21^+$), $CD21^{lo}$ ($CD3^-CD19^+CD27^-CD21^{lo}$), nonswitched memory ($CD3^-CD19^+CD27^+IgD^+$), and switched memory ($CD3^-CD19^+CD27^+IgD^-$) B cells from paired PB and SF samples from female patients with oligo JIA as well as PB of pediatric controls. The complementarity determining region 3 (CDR) 3 of the Ig heavy (IgH) chain of the BCR was sequenced (Adaptive Biotechnologies; data available at https://clients.adaptivebiotech.com/pub/lam-2025-arj, doi:10.21417/JM2025ARJ).[16,17] The ImmunoSEQ suite of online tools was used to determine productive clonality, the distribution of CDR3 lengths, usage of heavy chain variable (V_H) and heavy chain joining (J_H) genes, V_H–J_H gene pairing, shared clonotypes, and counts of somatic hypermutation (SHM). Plasma from pediatric healthy controls, together with paired plasma and SF supernatant from patients with oligo JIA, were assayed with a 120-plex autoantigen panel to profile IgA and IgG autoantibodies (Supplementary Table S3; Microarray Core Facility, University of Texas Southwestern Medical Center). Heatmaps were generated based on the Z-scores of each autoantigen in reference to healthy control plasma. Each sample was considered individually

Medical School, and Division of Rheumatology, Inflammation, and Immunity, Brigham and Women's Hospital and Harvard Medical School, Boston, Massachusetts; [9]Jonathan S. Hausmann, MD: Division of Immunology, Boston Children's Hospital and Harvard Medical School, and Division of Rheumatology, Allergy, and Immunology, Massachusetts General Hospital, and Harvard Medical School, Boston, Massachusetts; [10]Erin Janssen, MD, PhD: Division of Immunology, Boston Children's Hospital and Harvard Medical School, Boston, Massachusetts, and Department of Pediatrics, Michigan Medicine, Ann Arbor, Michigan; [11]Laurie Ohlms, MD, A. Eliot Shearer, MD, PhD: Department of Otolaryngology & Communication Enhancement, Boston Children's Hospital, and Harvard Medical School, Boston, Massachusetts.

Additional supplementary information cited in this article can be found online in the Supporting Information section (https://acrjournals.onlinelibrary.wiley.com/doi/10.1002/art.43157).

Author disclosures are available at https://onlinelibrary.wiley.com/doi/10.1002/art.43157.

Address correspondence via email to Lauren A. Henderson, MD, MSc, at lauren.henderson@childrens.harvard.edu.

Submitted for publication January 7, 2025; accepted in revised form March 11, 2025.

for clustering analysis, which was performed by running dist() using the default Euclidean distance metric. Detailed methods are in Supplementary File S1.

Statistics. One-way analysis of variance (ANOVA) with Holm–Šidák's correction for multiple comparisons or unpaired *t*-tests were used to compare groups. Pearson correlation coefficient was used to study the relationship between Tph and B cell subsets. Two-way ANOVA with Dunnett's correction for multiple comparisons was performed to compare study groups and the frequency of usage for each V_H and J_H gene in the BCR repertoire analysis. The autoantibody analysis was performed in Statistical Analysis Software (SAS), and a false discovery rate (FDR) of <0.05 was used to adjust the *P* values for multiple testing (Supplementary File S1). All other statistical testing was performed with GraphPad Prism (version 10.0) or R.

RESULTS

A total of 44 children with oligo JIA were studied, most before the start of immunomodulatory treatment (Table 1; Supplementary Table S1). Male and female patients with oligo JIA had similar disease characteristics, including active joint count (Supplementary Table S4). Controls provided PB (n = 19 pediatric; n = 8 adult) and tonsils (n = 13; children undergoing tonsillectomy for nonimmunologic indications).

Memory and antibody-producing plasmablasts are enriched in the joints of female patients with oligo JIA. We evaluated B cell populations in the PB and SF of patients with oligo JIA and the PB and tonsils of controls (Figure 1). The proportion of $CD19^+$ B cells in blood was significantly increased in patients with oligo JIA compared to pediatric controls; however, $CD19^+$ B cells were less prevalent in SF compared to all other study groups and sample types (Figure 1A and B). We evaluated traditional B cell subsets that include naive, nonswitched memory, switched memory, and transitional B cells as well as plasmablasts and $CD27^-IgD^-$ B cells. The proportion of naive B cells was significantly decreased, whereas switched Bmem cells were significantly increased in the SF of patients with oligo JIA compared to circulating and tonsillar B cells (Figure 1C and D). Indeed, the average frequency (mean ± SE) of switched Bmem cells in the SF of patients with oligo JIA was 29.5% ± 2.9% compared to 4.9% ± 0.7% in the PB of patients with oligo JIA and 3.9% ± 0.5% in the PB of pediatric controls ($P < 0.01$). Even when

Table 1. Clinical characteristics of study participants*

Characteristic	Oligo JIA (N = 44)	Adult controls (N = 8)	Pediatric controls (N = 32)
Age at disease onset, median (IQR), y	5.0 (7.3)	–	–
Age at sampling, median (IQR), y	7.4 (7.6)	25.0 (7.3)	4.0 (5.0)
Female, %	68	50	53
Self-reported race, n (%)			
American Indian/Alaska Native	0 (0)	0 (0)	0 (0)
Asian	3 (7)	2 (25)	0 (0)
Black	0 (0)	0 (0)	0 (0)
Native Hawaiian/Pacific Islander	0 (0)	0 (0)	0 (0)
Other	4 (9)	0 (0)	0 (0)
Undisclosed	11 (25)	3 (38)	27 (84)
White	26 (59)	3 (38)	5 (16)
Ethnicity (n, %)			
Hispanic	6 (14)	0 (0)	0 (0)
Non-Hispanic	28 (64)	5 (63)	5 (16)
Undisclosed	10 (23)	3 (38)	27 (84)
Oligo JIA disease course, n (%)[a]			
New onset	34 (77)	–	–
Persistent	10 (23)	–	–
Extended	0 (0)	–	–
Active joints at sampling, median (IQR)	1.0 (1.0)	–	–
ANA status, n (%)			
Positive	23 (52)	–	–
Negative	20 (45)	–	–
Unknown	1 (2)	–	–
Medications at sampling, n (%)			
Methotrexate	6 (14)	–	–
TNF inhibitor	1 (2)	–	–
NSAIDs	19 (43)	–	–
None	18 (41)	–	–

* ANA, antinuclear antibody; IQR, interquartile range; JIA, juvenile idiopathic arthritis; NSAID, nonsteroidal anti-inflammatory drug; oligo, oligoarticular; TNF, tumor necrosis factor.
[a] Oligo JIA disease course was determined at the time of sampling.

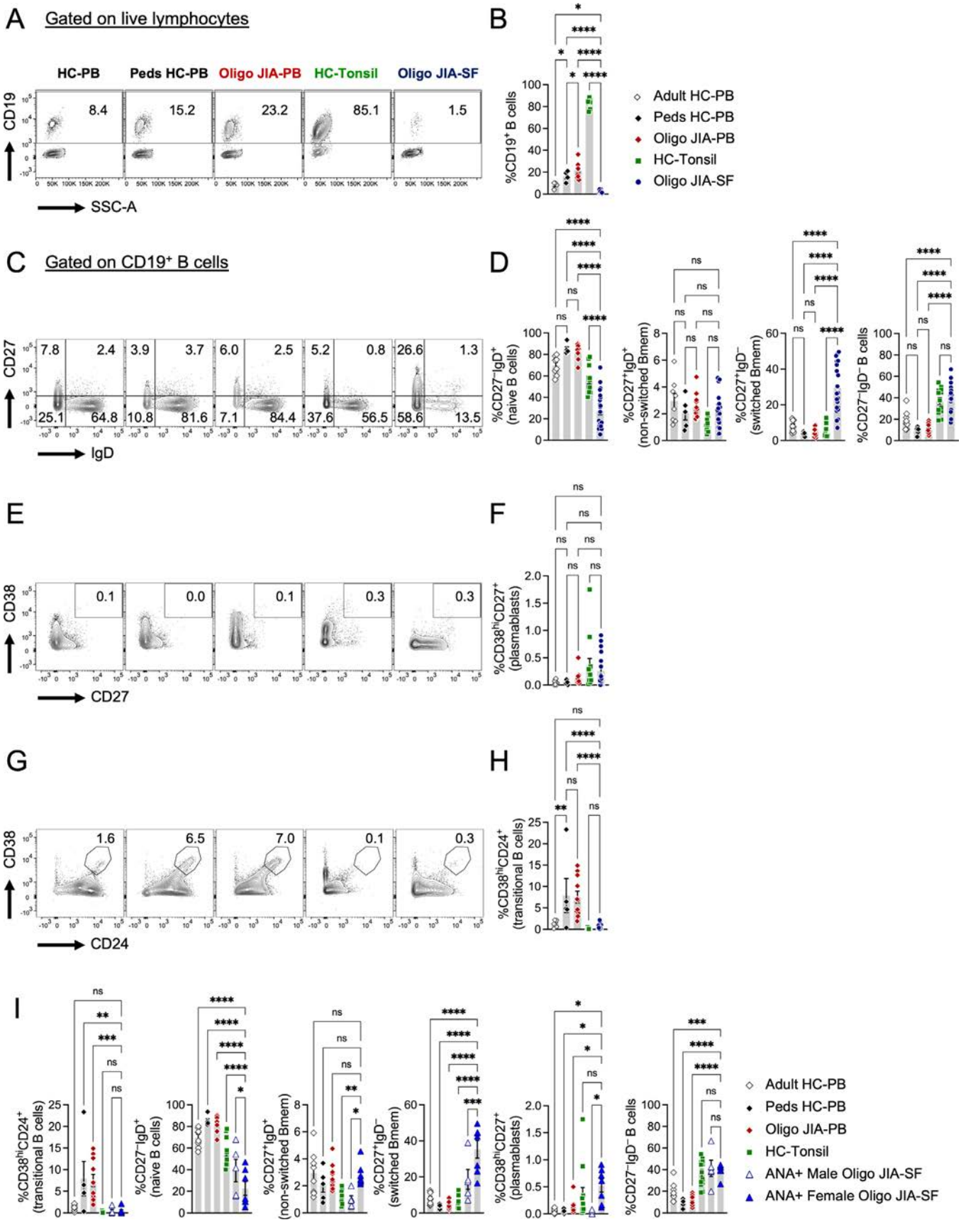

(Figure legend continues on next page.)

evaluating the SF of patients with oligo JIA compared to tonsils where B cell maturation and GC reactions occur, the frequency of plasmablasts was similar, and the proportion of switched Bmem cells remained significantly enriched in the joints of patients with oligo JIA (Figure 1C–F). The $CD27^{-}IgD^{-}$ B cell subset was also enriched in the SF of patients with oligo JIA compared to the PB of controls and patients (Figure 1C and D).

Next, we assessed these B cell subsets in the SF of patients with oligo JIA subdivided by age at disease onset, ANA status, and sex. Frequencies of these B cell populations did not differ based on the age at oligo JIA onset or ANA status (Supplementary Figure S1A and B). Plasmablasts were significantly increased in the SF of female patients with oligo JIA compared to male patients, whereas there was no such sex-specific difference in other compartments (PB, tonsils; Supplementary Figure S1C and D). In order to make an equivalent comparison, we evaluated SF from female versus male patients with ANA positivity; female patients had significantly higher proportions of nonswitched Bmem cells, switched Bmem cells, and plasmablasts (Figure 1I). These results show that Bmem cells and plasmablasts accumulate in the joints of patients with oligo JIA, particularly in female patients.

ABCs accumulate in the joints of female patients with oligo JIA. We next used an unsupervised, clustering algorithm to identify novel B cell populations in oligo JIA. Using an extended B cell flow cytometry panel, we compared B cells in the PB of controls (n = 6 adults, n = 5 children), tonsils of pediatric controls (n = 11), and PB and SF of patients with oligo JIA (n = 11). We identified 14 clusters of $CD19^{+}$ B cells (Figure 2A). Uniform manifold approximation and projection visualization of the clusters showed relatively comparable distributions of B cells in the PB of healthy controls and patients with oligo JIA, aside from increased proportions of B cells in the PB from controls with preswitched/unswitched/switched Bmem cell features found in clusters 3 and 4 (Figure 2A and B; Supplementary Figure S2). Tonsillar B cells had increased proportions of cells in cluster 2, corresponding to $IgD^{-}CD27^{-}CD21^{+}$ B cells (Figure 2A and B; Figure S2).

Compared to B cells from the PB, B cells from the SF of patients with oligo JIA were underrepresented in clusters with features of transitional (cluster 5) and naive (cluster 8) B cells and more frequent in the antibody-secreting B cell cluster (cluster 9; Figure 2A and B; Supplementary Figure S2). Clusters 1 and 10 through 14 were significantly and uniquely expanded in the SF of patients with oligo JIA (Figure 2A–C). Cluster 1 contained cells with features of switched Bmem cells that express CD11c, whereas clusters 10 through 14 all contained populations of $CD21^{lo}$ B cells. This includes $IgD^{-}CD27^{-}$/double-negative 2 cells (cluster 10) that coexpress CD11c and T-box transcription factor 21 (Tbet) and are known to be enriched in patients with systemic lupus erythematosus (SLE).[18] Cluster 11 contained activated naive $CD21^{lo}$ B cells, and cluster 12 encompassed $IgD^{-}CD27^{-}CD24^{+}CD21^{lo}$ B cells. B cells in clusters 13 and 14 displayed features of ABCs, which were originally identified in the spleens of aged female mice and have been linked to autoimmunity in humans.[19–23] In particular, cluster 13 included $CD27^{+}$B cells with high expression of known ABC markers (CD11c, Tbet, CXCR3). When comparing SF B cells from male and female patients with oligo JIA, cluster 9 (antibody-secreting B cells) and cluster 13 (ABCs) were significantly enriched in female patients (Figure 2D and E; Supplementary Figure S2).

Tph cells that express B cell help factors are enriched in the SF of female patients with oligo JIA. Tph cells were previously identified in the joints of patients with oligo JIA and may shape the intra-articular B cell responses. Thus, we sought to evaluate for sex differences in the frequency and phenotype of Tph cells in patients with oligo JIA. Tph cells that expressed factors associated with B cell help, including CXCL13 and interleukin (IL)-21, were significantly increased in the SF of female compared to male children with oligo JIA (Figure 3A, B, D, and E). Further, the frequency of these Tph cells positively correlated with B cell populations enriched in female versus male joints, including nonswitched Bmem cells, plasmablasts, and $CD21^{lo}$ B cells (Figure 3C and F; Figure S3). In particular, $IL\text{-}21^{+}$Tph and $IL\text{-}21^{+}$interferon gamma $(IFN\gamma)^{+}$ Tph cells were both associated with antibody-producing plasmablasts found in the SF of patients with oligo JIA (Figure 3F–H; Supplementary Figure S3). Thus, observed sex differences in the joints of patients with oligo JIA included the B cell compartment as well as Tph cells.

(Figure legend continued from previous page.)

Figure 1. Enrichment of memory B (Bmem) cells and plasmablasts in the synovial fluid (SF) of female patients with oligo JIA. (A, C, E, and G) Representative flow cytometry staining. (B) Percentage of $CD19^{+}$ B cells among viable lymphocytes in adult healthy control (HC) peripheral blood (PB; n = 4), pediatric (peds) HC-PB (n = 4), peds tonsils (n = 8), oligo JIA-PB (n = 11), and oligo JIA-SF (n = 16). $^{*}P < 0.05$; $^{****}P \leq 0.0001$. (D) Percentage of naive, nonswitched Bmem cells, switched Bmem cells, and $CD27^{-}IgD^{-}$ cells among viable $CD19^{+}$ B cells in the study groups. $^{****}P \leq 0.0001$. (F) Percentage of plasmablasts among viable $CD19^{+}$ B cells in study groups. (H) Percentage of transitional B cells among viable $CD19^{+}$ B cells in study groups. $^{**}P \leq 0.01$; $^{****}P \leq 0.0001$. (D, F, and H) Included are adult HC-PB (n = 8), peds HC-PB (n = 5), peds tonsils (n = 13), oligo JIA-PB (n = 11), and oligo JIA-SF (n = 22). (I) Percentage of the given B cell subset among viable $CD19^{+}$ B cells, comparing B cell populations in ANA^{+} female oligo JIA-SF (n= 7) to all groups (adult HC-PB, n = 8; peds HC-PB, n = 5; oligo JIA-PB, n = 11; peds HC-tonsil, n = 13; ANA^{+} male oligo JIA-SF, n = 5). $^{*}P < 0.05$; $^{**}P \leq 0.01$; $^{***}P \leq 0.001$; $^{****}P \leq 0.0001$. Mean ± SE is shown in the bar graphs. Statistical testing performed was one-way analysis of variance corrected for Holm–Šidák's multiple comparisons. ANA, antinuclear antibody; JIA, juvenile idiopathic arthritis; oligo, oligoarticular; ns, not significant.

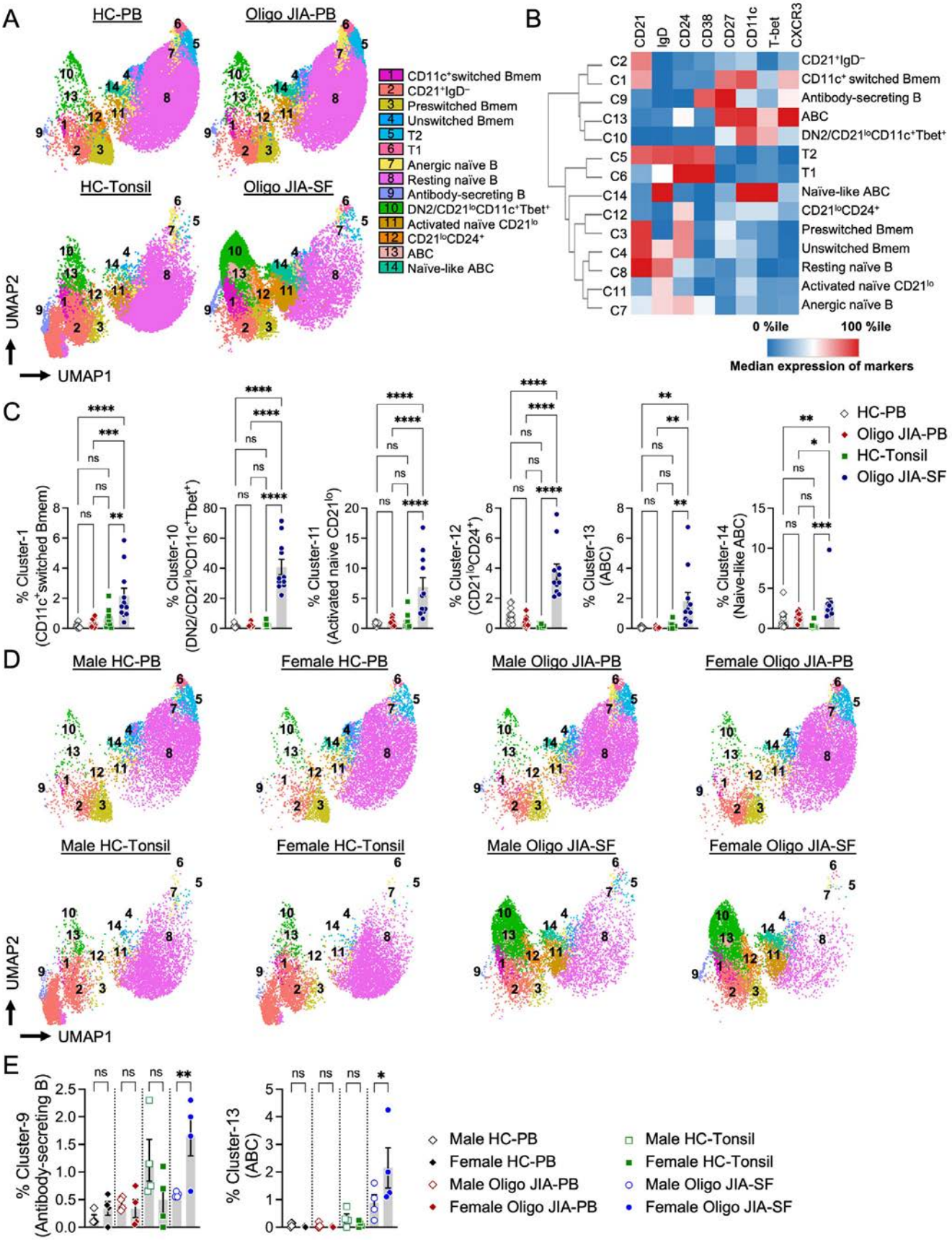

(Figure legend continues on next page.)

B cells in the joints of females with oligo JIA display features of autoreactivity and evidence of T cell–dependent maturation. BCR repertoire analysis was used to further characterize naive, nonswitched memory, switched memory, and CD21^{lo} B cells from paired PB and SF samples of five female patients with oligo JIA as well as PB samples from three pediatric controls (Supplementary Table S5). To measure BCR repertoire diversity, Shannon entropy was estimated at a fixed sample coverage (Supplementary Figure S4A). Circulating B cells in female patients with oligo JIA and healthy children were diverse and without differences in clonality (Figure 4A and B). By contrast, naive, nonswitched, and switched Bmem cells from the SF of female patients with oligo JIA were less diverse than B cells from the PB of these same patients as well as controls (Figure 4A and B). These B cell populations were also more clonally expanded in the SF versus PB of patients with oligo JIA (Figure 4B; Supplementary Table S5). Similar trends of restricted diversity and increased clonality were noted in CD21^{lo} B cells from the joints, although these differences did not reach statistical significance.

BCR repertoire skewing was similarly captured by evaluating the antigen-binding portion of the IgH chain, also called the CDR3. Switched Bmem cells from the SF of female patients with oligo JIA showed non-normal distribution of CDR3 lengths, with skewing toward longer lengths, shown in other studies to be associated with autoreactivity and typically selected against in antigen-experienced B cells (Figure 4C; Supplementary Figure S4B and C).[24] We next examined the distribution of V_H and J_H genes encoding the CDR3. Skewed usage of V_H and J_H genes was observed in B cells from the SF of patients with oligo JIA (Figure 4E; Supplementary Tables S6 and S7). Of note was the usage pattern of VH4-34, which is intrinsically autoreactive and is selected against during B cell maturation.[25,26] VH4-34 usage in naive B cells was similar across samples from all study groups (Figure 4E). By contrast, there was a significant increase in VH4-34 usage in nonswitched and switched Bmem cells from the SF compared to the same Bmem cell populations in the PB of patients with oligo JIA and controls (Figure 4E). B cells in the SF of female patients with oligo JIA that expressed VH4-34 also showed aberrant pairing with J_H genes with increased usage of the JH6-1 gene (Figure 4F and G; Supplementary Figure S4D).

When evaluating the sharing of B cell clonotypes (defined by amino acid sequence and V_H/J_H family usage), we found little overlap for naive and CD21^{lo} B cells across study participants and compartments (Figure 4H). For nonswitched Bmem cells, there was low-level sharing of B cell clonotypes between patients with oligo JIA and pediatric controls that was observed only in the PB (Figure 4H). The pattern of clonotype sharing was markedly different for switched Bmem cells with a large degree of intra-individual, clonal overlap in the PB and SF of a given patient with oligo JIA (Figure 4H). In some patients, more than 12% of the switched Bmem cell repertoire was shared between PB and SF. Interestingly, switched Bmem cell clonotypes were private to the individual, with essentially no sharing across patients with oligo JIA. These results indicate that although switched Bmem cells and CD21^{lo} B cells are found at increased proportions in the SF of patients with oligo JIA, only switched Bmem cells move frequently between the PB and SF.

We then evaluated the rate of SHM as a proxy for measuring T cell–dependent maturation in B cells, either in GC reactions or in extrafollicular responses. As expected, SHM occurred more frequently in Bmem cells compared to naive B cells in all studied groups (Figure 4I). The overall rate of SHM was comparable in Bmem cells found in the SF of patients with oligo JIA compared to Bmem cells in PB of patients with oligo JIA and controls. Expanded B cell clonotypes in PB and SF had high rates of SHM (Figure 4J; Supplementary Figure S4E). Finally, highly mutated B cell clonotypes were found in joints of patients with oligo JIA, particularly in CD21^{lo} B cells and switched Bmem cells (Figure 4K; Supplementary Figure S4F). The patient with oligo JIA with the highest levels of SHM (patient 4 with oligo JIA) had longstanding disease, whereas most of the other evaluated patients were assessed close to disease onset (Supplementary Figure S4F). In summary, B cells found in the joints of female patients with oligo JIA had restricted diversity, increased clonality, features of autoreactivity, and evidence of SHM indicative of T cell help.

A broad array of autoantibodies is present in the SF of female patients with oligo JIA. Plasma from pediatric controls as well as paired plasma and SF from female patients with oligo JIA were inputted into an autoantigen microarray. We stratified the female patients into three groups based on age at disease onset and ANA status: six years old or younger

(Figure legend continued from previous page.)

Figure 2. Heterogeneous populations of CD21^{lo} B cells identified in the synovial fluid (SF) of patients with oligo JIA. (A) UMAPs of B cells generated from flow cytometry data and unsupervised clustering in healthy control (HC) peripheral blood (PB; n = 11), oligo JIA-PB (n = 11), pediatric HC-tonsil (n = 11), and oligo JIA-SF (n = 11). (B) Heatmap showing median expression of a given marker in each cluster. (C) Clusters uniquely enriched in oligo JIA-SF. The bar graphs show the percentage of B cells in the given cluster for each of the study groups. *$P < 0.05$; **$P \leq 0.01$; ***$P \leq 0.001$; ****$P \leq 0.0001$. (D) UMAPs of B cells in female versus male study participants in the following study groups: HC-PB, oligo JIA-PB, pediatric HC-tonsil, and oligo JIA-SF (n = 4 in each group). (E) Clusters enriched in the SF of female versus male patients with oligo JIA. The bar graphs show the percentage of B cells in the given cluster of male versus female study participants in the given study groups (n = 4 in each group). *$P < 0.05$; **$P \leq 0.01$. Mean ± SE is shown on the bar graphs. Statistical testing performed was one-way analysis of variance corrected for Holm–Šidák's multiple comparisons. ABC, age-/autoimmune-associated B cell; Bmem, memory B; DN, double negative; JIA, juvenile idiopathic arthritis; ns, not significant; oligo, oligoarticular; Tbet, T-box transcription factor 21; UMAP, uniform manifold approximation and projection.

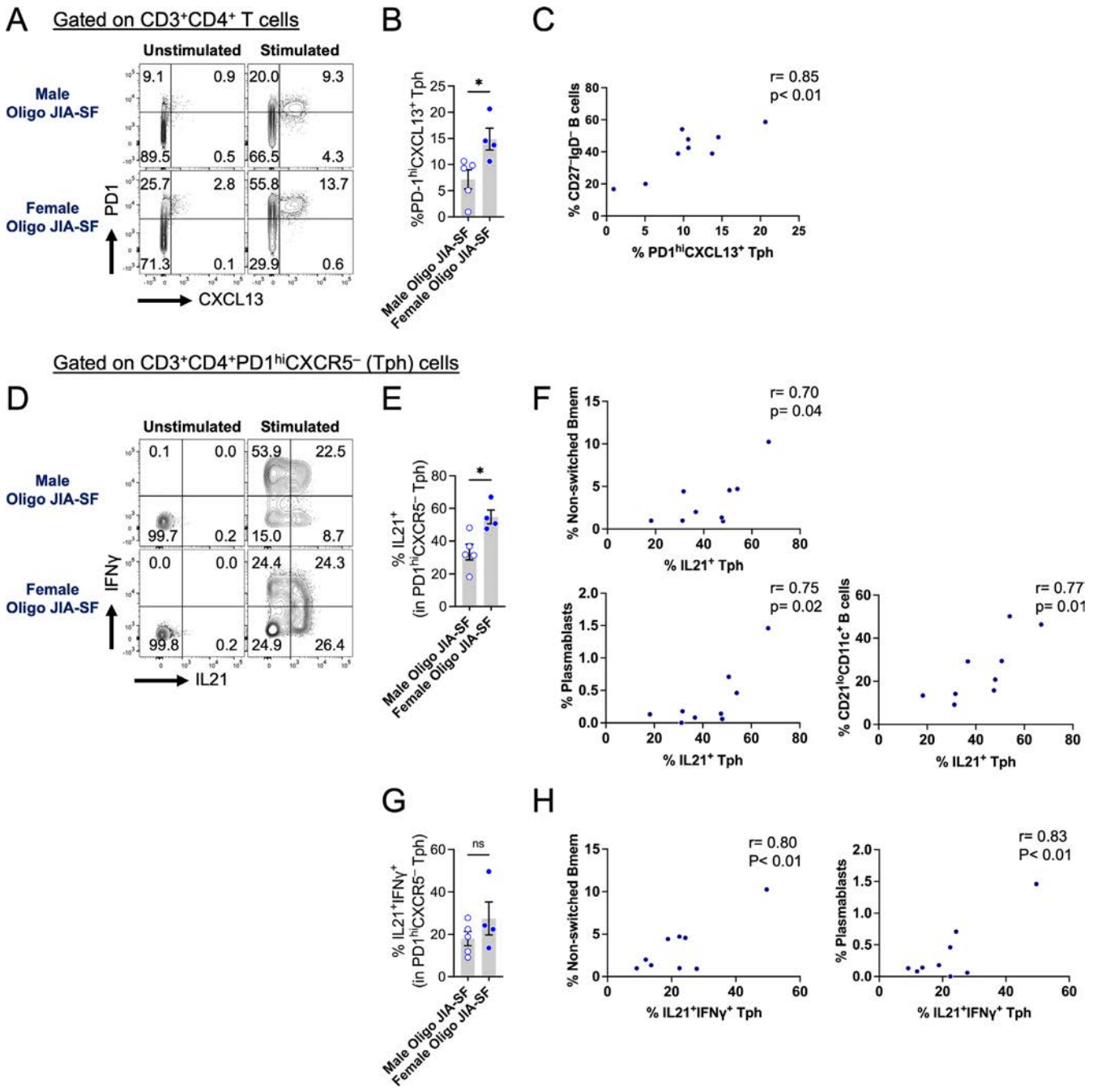

Figure 3. T peripheral helper (Tph) cells that express B cell help factors are enriched in the synovial fluid (SF) of female patients with oligo JIA and are associated with increased frequencies of intra-articular memory B (Bmem) cells, plasmablasts, and age-/autoimmune-associated B cells. (A) Representative staining of PD1^{hi}CXCL13^{+} Tph cells, gated on CD3^{+}CD4^{+} T cells, with and without CD3/CD28 bead stimulation. (B) Percentage of PD1^{hi}CXCL13^{+} Tph cells among CD4^{+} T cells in SF of male versus female patients with oligo JIA. *$P < 0.05$. (C) Correlation between the percentage of PD1^{hi}CXCL13^{+} Tph cells and CD27^{-}IgD^{-} B cells in oligo JIA-SF. (D) Representative staining of cytokine production, gated on PD1^{hi}CXCR5^{-} Tph cells with and without phorbol 12-myristate 13-acetate/ionomycin stimulation. (E) Percentage of IL21^{+} cells among Tph cells in SF comparing male versus female patients with oligo JIA. *$P < 0.05$. (F) Correlation between the percentage of IL21^{+} Tph cells and of the given B cell population in oligo JIA-SF. (G) Percentage of IL21^{+}IFNγ^{+} cells among Tph cells in SF comparing male versus female patients with oligo JIA. (H) Correlation between the percentage of IL21^{+}IFNγ^{+} T cells and of the given B cell population in patients with oligo JIA-SF. Nine patients with oligo JIA were studied, including five male and four female patients. Mean ± SE is shown in the bar graphs. Statistical analyses performed were (B, E, and G) unpaired *t*-tests and (C, F, and H) Pearson correlation. IFN, interferon; IL, interleukin; JIA, juvenile idiopathic arthritis; oligo, oligoarticular.

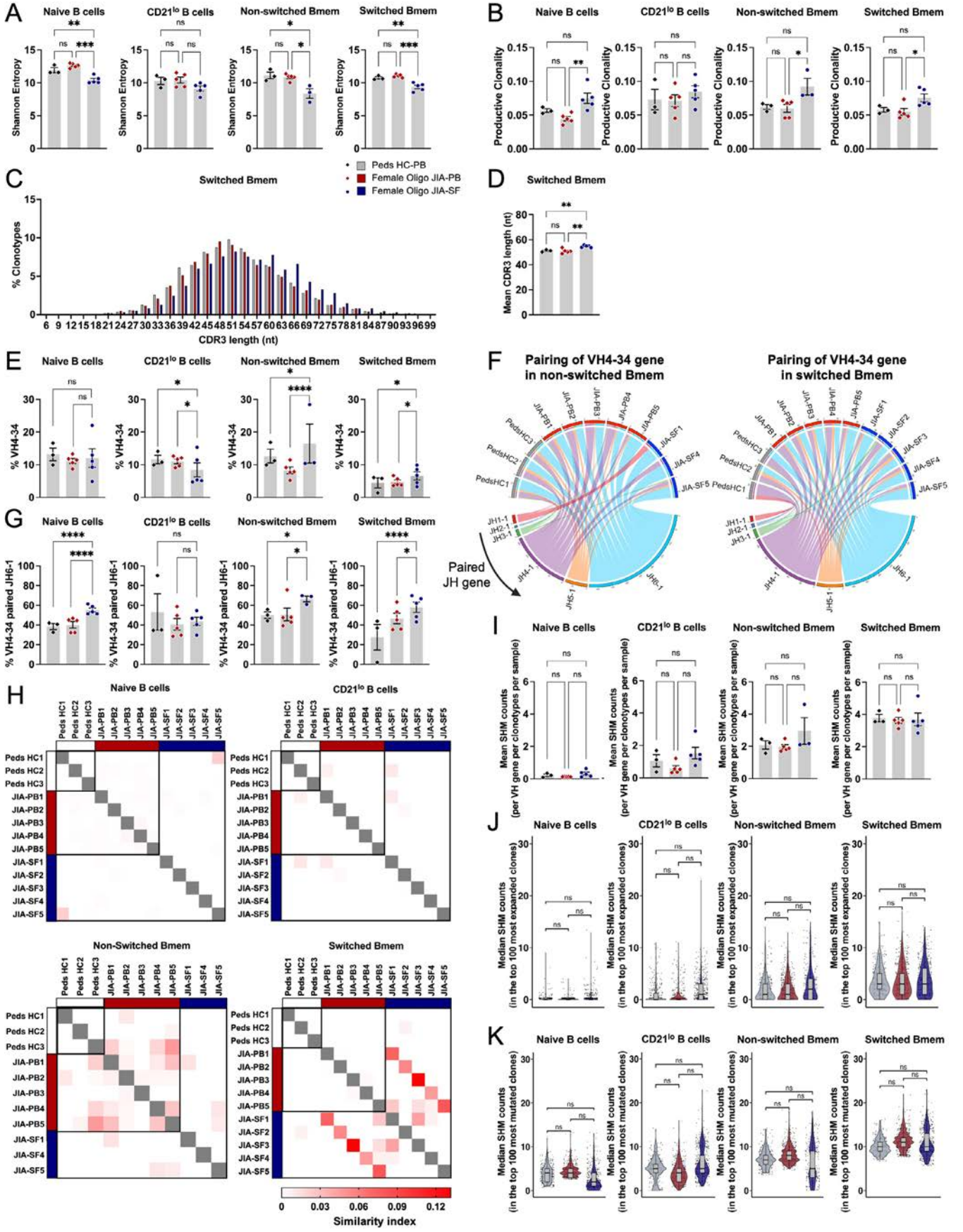

(Figure legend continues on next page.)

with ANA positivity, six years old or younger with ANA negativity, and older than six years old. After quality control, 95 IgG autoantigens and 86 IgA autoantigens were included in the analysis. We first compared autoantibodies of all study groups to the plasma of pediatric controls. A small number of autoantibodies were significantly elevated in the plasma from female patients with oligo JIA versus plasma from pediatric controls (17 IgG and 7 IgA autoantibodies), mostly in the patients with oligo JIA with age at disease onset of six years old or younger (Supplementary Tables S8 and S9). To verify that this finding was not due to hypergammaglobulinemia in the patients with oligo JIA, we confirmed that IgG levels were normal in all of the patients who had clinical testing sent (n = 16). Autoantibodies preferentially accumulated in the SF of patients with oligo JIA compared to the plasma of pediatric controls, with 56 IgG and 48 IgA autoantibodies significantly elevated in the SF of all three strata of patients with oligo JIA (Figure 5; Supplementary Tables S8 and S9). An additional 19 IgG and 32 IgA autoantibodies were significantly increased in the SF of female patients with oligo JIA and disease onset at six years of age or younger, regardless of ANA status (Supplementary Tables S8 and S9). We set an FDR of 5% to account for testing multiple autoantigens, finding that 72 IgG and 80 IgA autoantibodies remained significantly different across the study groups (Supplementary Tables S8 and S9). Next, we directly compared female patients with disease onset at six years of age or younger (regardless of ANA status) to those who were older at initial presentation and confirmed that all differentially expressed autoantibodies were higher in the patients with early-onset disease (35 IgG and 52 IgA autoantibodies in SF; 8 IgG and 34 IgA autoantibodies in plasma; Figure 5; Supplementary Tables S8 and S9). We tested SF from a small number of male patients with oligo JIA; heatmap analysis showed that samples from these patients tended to cluster with plasma samples that had lower levels of autoantibodies (Supplementary Figure S5). These results indicate that autoantibodies are more plentiful in the SF versus PB of female patients with oligo JIA, with the highest levels of autoantibodies detected in patients with early-onset disease.

DISCUSSION

We sought to further evaluate the Tph–B cell axis in oligo JIA through an in-depth characterization of intra-articular B cells. Although Bmem cells and a heterogenous collection of CD21^{lo} B cells accumulated in the SF of patients with oligo JIA of both sexes, female patients had higher proportions of Bmem cells, plasmablasts, and ABCs. These sex differences in B cells from patients with oligo JIA were restricted to the joints and not observed in the PB of patients and controls nor the tonsils of healthy children. Further, the variation in the B cell compartment was not explained by other disease features that differ between male and female patients such as ANA status, age at disease onset, or disease severity. Although not identified in B cells in circulation, B cells from the SF of female patients with oligo JIA demonstrated signs of autoreactivity with increased CDR3 length and preferential usage of gene segments associated with autoimmunity. Finally, an extensive panel of autoantibodies was identified in the joints of female patients with oligo JIA. These findings document evidence of aberrant intra-articular B cell phenotype and responses in patients with oligo JIA that are more prominent in female compared to male patients.

The preferential accumulation of CD21^{lo} B cells in SF of children with oligo JIA that was not observed in PB or secondary lymphoid organs (SLOs) was notable. Although CD21^{lo} B cells have been previously observed in the SF of patients with oligo JIA, our unsupervised clustering approach uncovered significant diversity in CD21^{lo} B cells that has not yet been recognized.[13,15] We found five clusters of CD21^{lo} B cells that were enriched in SF of patients with oligo JIA, including those that expressed naive (IgD^{+}, CD27^{-}) and memory markers (CD27) as well as various combinations of CD11c, Tbet, and CXCR3.

CD21^{lo} B cells with varying phenotypes have been reported previously in patients with immune dysregulation and autoimmunity. As in the B cells we identified in cluster 14, CD21^{lo} B cells with naive features (IgM^{+}, IgD^{+}, CD27$^{-/lo}$) were found in patients with combined variable immunodeficiency (CVID), RA, and SLE.[27,28] These naive-like CD21^{lo} B cells had low levels of SHM, reduced calcium flux after BCR stimulation,

(Figure legend continued from previous page.)

Figure 4. B cell receptor repertoire abnormalities observed in synovial fluid (SF) B cells from female patients with oligo JIA. (A) Shannon entropy and (B) productive clonality in B cell subsets. *$P < 0.05$; **$P \leq 0.01$; ***$P \leq 0.001$. CDR3 (C) distribution and (D) length in switched Bmem cells. **$P \leq 0.01$. (E) Frequency of VH4-34 usage in B cell subsets. *$P < 0.05$; ****$P \leq 0.0001$. (F) Chord diagram showing J_H gene pairing in B cells expressing VH4-34. (G) Frequency of B cells expressing VH4-34 paired with JH6-1. *$P < 0.05$; ****$P \leq 0.0001$. (H) Heatmap showing the sharing of B cell clonotypes in sample pairs. The similarity index is the fraction of shared clonotypes among total clonotypes in a sample. (I) Mean SHM count in the V_H gene of each clonotype per sample. (J) The top 100 most expanded B cell clonotypes from each study participant in the given group were pooled together, and the median SHM count in the V_H gene was determined. (K) The 100 B cell clonotypes with highest V_H gene SHM counts from each study participant in a given group were pooled together, and the median SHM count was determined. Statistical analyses performed were (A, B, and D) one-way ANOVA with Holm–Šidák's correction for multiple comparisons and (E and G) two-way ANOVA with correction for multiple comparisons. (A, B, D, E, G, and I) Mean ± SE and (J–K) median ± SD are shown on the bar graphs. ANOVA, analysis of variance; Bmem, memory B; HC, healthy control; CDR, complementarity determining region; J_H, heavy chain joining region; JIA, juvenile idiopathic arthritis; ns, not significant; nt, nucleotide; oligo, oligoarticular; PB, peripheral blood; peds, pediatric; SHM, somatic hypermutation; V_H, heavy chain variable region.

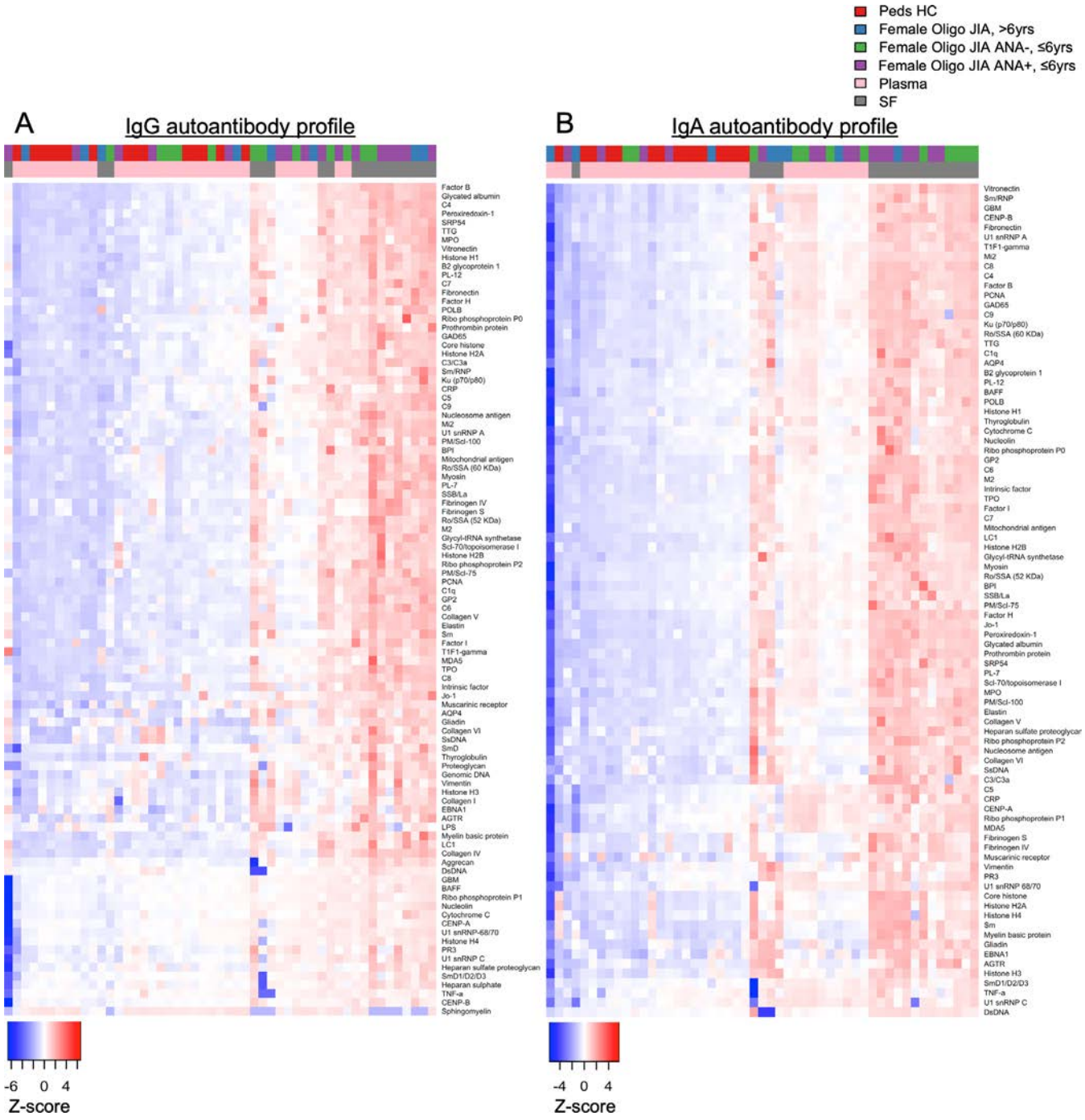

Figure 5. A broad array of autoantibodies is present in the synovial fluid (SF) of female patients with oligo JIA. Plasma and SF samples from pediatric (peds) controls (n = 15) and female patients with oligo JIA (n = 18) were evaluated with (A) IgG and (B) IgA autoantigen microarrays, with the results shown on the heatmaps. The color represented the distance in SDs from the mean of controls (Z-score), with red indicating an increase in reactivity above controls and blue indicating a decrease in reactivity compared to controls. ANA, antinuclear antibody; HC, healthy control; JIA, juvenile idiopathic arthritis; oligo, oligoarticular; yr, year.

and autoreactive BCRs with reduced receptor editing.[27,29] Notably, these B cells lacked markers that typically recruit B cells to SLOs (CXCR5, CCR7), expressed inflammatory chemokine receptors (CXCR3, CXCR6) suggestive of tissue homing, and accumulated in the bronchoalveolar lavage fluid of patients with CVID as well as the SF of patients with RA.[27] Alternately, CD21^{lo} B cells with a memory phenotype, similar to the B cells identified in clusters 13 and 10 (Figure 2), have

also been linked with autoimmunity. Often referred to as ABCs, these B cells were first identified in the spleens of aged, female, wild-type mice. ABCs have also been associated with autoimmunity in mouse models and human diseases such as SLE, RA, Sjögren disease, and systemic sclerosis.[19–22,30–33] As in some of the CD21^{lo} B cells we identified in SF of patients with oligo JIA, markers that define this subset include Tbet, CD11c, and CXCR3.[20,30] ABCs may express memory features (IgD^{-}) and have moderate levels of SHM, indicative of T cell–dependent immune responses.[34] Factors required for ABC differentiation and activation in mice include a combination of BCR and toll-like receptor (TLR) 7/9 stimulation coupled with exposure to IFNγ and IL-21.[19,20] In mice, ABCs have been shown to produce autoantibodies, and in humans with SLE, ABCs correlate with autoantibody titers and disease activity.[20,22] Thus, CD21^{lo} B cells in the SF of patients with oligo JIA were diverse and included subsets described in the literature that have been associated with autoimmunity. Consistent with the literature, ABCs in SF were more prevalent in female versus male patients with oligo JIA. Although ABCs have been linked with older age, we found these cells in the tissues of young children with autoimmunity.

The factors that drive the preferential enrichment of Bmem cells, plasmablasts, and CD21^{lo} B cells in the joints of patients with oligo JIA remain to be defined. It is possible that all or some of these B cell subsets are recruited from the circulation into the joint. Indeed, our BCR repertoire analysis suggests that switched Bmem cells move freely between the PB and SF, although the directionality of this migration cannot be determined with our data. However, there are several findings supporting an intra-articular origin for some of these B cell populations. The scarcity of CD21^{lo} B cells in the PB of patients with oligo JIA coupled with the lack of BCR repertoire overlap between PB and SF CD21^{lo} B cells suggests limited recirculation between these compartments. Tph cells reside in the joints of patients with oligo JIA and promote the differentiation of plasmablasts and CD21^{lo} B cells in vitro.[13,15] In this study, and others, there is a positive correlation between the frequency of Tph cells in the joint and the presence of B cells with ABC features as well as plasmablasts.[15,31] Tph cells in oligo JIA and other diseases are known to produce IL-21 and IFNγ, cytokines that favor the differentiation of ABCs.[35] Further, CD21^{lo} and Bmem cells from SF of patients with oligo JIA demonstrated evidence of SHM, which is indicative of T cell–dependent B cell maturation. It is possible that intra-articular Tph–B cell interactions produce B cells prone to autoimmunity. The Bmem cells from SF of patients with oligo JIA displayed autoreactive features not found in the PB of the same patients. This included longer CDR3 lengths and use of gene segments that recognize self-antigens that are selected against during maturation in typical GC reactions in SLOs. The large burden of autoantibodies detected in SF of patients with oligo JIA was surprising, although these patients are usually not tested clinically for autoantibodies aside from ANA. This accumulation of autoantibodies in SF may be a marker of poorly regulated Tph cells mediated help to B cells, resulting in the production of B cells that generate many low-affinity autoantibodies.

As in RA and SLE, in which Tph–B cell interactions are increasingly considered central to disease pathogenesis, oligo JIA is characterized by a marked female predominance.[11,21,22,35,36] Although B cell abnormalities in the SF were observed in patients with oligo JIA of both sexes, it was female patients who had the most prominent B cell–related findings as well as increased frequencies of Tph cells that expressed B cell help markers. The question remains as to which factors are driving these observed sex differences. Unlike RA and SLE, oligo JIA is a disease of prepubertal female patients with a peak age at onset between one and three years of age.[37] This is a time when differences in sex hormones are minimal between male and female children.[38] Although many mechanisms may contribute to sex differences in this disease, one potential contributor may be the X-linked gene *TLR7*. ABCs have distinct activation requirements compared to other B cell populations, including need for TLR7 stimulation.[19,20] In mice, ABCs do not develop in *TLR7* knockout models, ABCs and autoantibodies accumulate with chronic TLR7 stimulation, and increased proportions of ABCs are found in the spleens of female versus male mice receiving TLR7 agonists.[20,39] Mechanisms such as skewed X inactivation, which has been reported in oligo JIA, or tissue-specific reactivation of the silenced copy of this gene, may result in alterations in the TLR7 pathway.[40]

As in all human-based studies, our work is limited by the complexities of evaluating biosamples from patients. We attempted to address this limitation by studying a clearly defined group of patients with oligo JIA who have similar disease severity and stratifying the analysis by factors such as sex, ANA status, and age at disease onset. We also focused on patients who were treatment naive and limited inclusion of samples from patients exposed to immunomodulatory medications. The significant female predominance in oligo JIA coupled with the difficulty in obtaining SF samples from young children resulted in limited access to samples from male patients. Therefore, we chose to focus our BCR repertoire and autoantibody array studies on female patients. In order to study to naive, nonswitched Bmem cells, switched Bmem cells, and CD21^{lo} B cells, a sorting strategy that defined CD21^{lo} B cells as CD27^{-} was used, which restricted the diversity of CD21^{lo} B cells in the repertoire analysis. Finally, the autoantigen microarray does not provide information about the clinical significance of detected autoantibodies nor their antigen affinity.

Our results show that distinct populations of B cells with autoreactive features along with a broad array of autoantibodies accumulate in the joints of patients with oligo JIA and these abnormalities are more prominent in female patients. Sex differences may be important in forms of inflammatory arthritis characterized by disordered Tph–B cell interactions, even in prepubertal children.

AUTHOR CONTRIBUTIONS

All authors contributed to at least one of the following manuscript preparation roles: conceptualization AND/OR methodology, software, investigation, formal analysis, data curation, visualization, and validation AND drafting or reviewing/editing the final draft. As corresponding author, Dr Henderson confirms that all authors have provided the final approval of the version to be published and takes responsibility for the affirmations regarding article submission (eg, not under consideration by another journal), the integrity of the data presented, and the statements regarding compliance with institutional review board/Declaration of Helsinki requirements.

REFERENCES

1. Petty RE, Southwood TR, Manners P, et al. International League of Associations for Rheumatology classification of juvenile idiopathic arthritis: second revision, Edmonton, 2001. J Rheumatol 2004;31(2):390–392.
2. Oen KG, Cheang M. Epidemiology of chronic arthritis in childhood. Semin Arthritis Rheum 1996;26(3):575–591.
3. Ravelli A, Varnier GC, Oliveira S, et al. Antinuclear antibody-positive patients should be grouped as a separate category in the classification of juvenile idiopathic arthritis. Arthritis Rheum 2011;63(1):267–275.
4. Ravelli A, Felici E, Magni-Manzoni S, et al. Patients with antinuclear antibody-positive juvenile idiopathic arthritis constitute a homogeneous subgroup irrespective of the course of joint disease. Arthritis Rheum 2005;52(3):826–832.
5. Saurenmann RK, Levin AV, Feldman BM, et al. Prevalence, risk factors, and outcome of uveitis in juvenile idiopathic arthritis: a long-term followup study. Arthritis Rheum 2007;56(2):647–657.
6. Marasco E, Aquilani A, Cascioli S, et al. Switched memory B cells are increased in oligoarticular and polyarticular juvenile idiopathic arthritis and their change over time is related to response to tumor necrosis factor inhibitors. Arthritis Rheumatol 2018;70(4):606–615.
7. Barnes MG, Grom AA, Thompson SD, et al. Biologic similarities based on age at onset in oligoarticular and polyarticular subtypes of juvenile idiopathic arthritis. Arthritis Rheum 2010;62(11):3249–3258.
8. Hollenbach JA, Thompson SD, Bugawan TL, et al. Juvenile idiopathic arthritis and HLA class I and class II interactions and age-at-onset effects. Arthritis Rheum 2010;62(6):1781–1791.
9. Murray KJ, Moroldo MB, Donnelly P, et al. Age-specific effects of juvenile rheumatoid arthritis-associated HLA alleles. Arthritis Rheum 1999;42(9):1843–1853.
10. Gregorio A, Gambini C, Gerloni V, et al. Lymphoid neogenesis in juvenile idiopathic arthritis correlates with ANA positivity and plasma cells infiltration. Rheumatology (Oxford) 2007;46(2):308–313.
11. Rao DA, Gurish MF, Marshall JL, et al. Pathologically expanded peripheral T helper cell subset drives B cells in rheumatoid arthritis. Nature 2017;542(7639):110–114.
12. Jule AM, Hoyt KJ, Wei K, et al. Th1 polarization defines the synovial fluid T cell compartment in oligoarticular juvenile idiopathic arthritis. JCI Insight 2021;6(18):e149185.
13. Jule AM, Lam KP, Taylor M, et al. Disordered T cell-B cell interactions in autoantibody-positive inflammatory arthritis. Front Immunol 2022;13:1068399.
14. Fischer J, Dirks J, Haase G, et al. IL-21(+) CD4(+) T helper cells co-expressing IFN-gamma and TNF-alpha accumulate in the joints of antinuclear antibody positive patients with juvenile idiopathic arthritis. Clin Immunol 2020;217:108484.
15. Fischer J, Dirks J, Klaussner J, et al. Effect of clonally expanded PD-1 (high) CXCR5-CD4+ peripheral T helper cells on B cell differentiation in the joints of patients with antinuclear antibody-positive juvenile idiopathic arthritis. Arthritis Rheumatol 2022;74(1):150–162.
16. Robins HS, Campregher PV, Srivastava SK, et al. Comprehensive assessment of T-cell receptor beta-chain diversity in alphabeta T cells. Blood 2009;114(19):4099–4107.
17. Carlson CS, Emerson RO, Sherwood AM, et al. Using synthetic templates to design an unbiased multiplex PCR assay. Nat Commun 2013;4:2680.
18. Wei C, Anolik J, Cappione A, et al. A new population of cells lacking expression of CD27 represents a notable component of the B cell memory compartment in systemic lupus erythematosus. J Immunol 2007;178(10):6624–6633.
19. Hao Y, O'Neill P, Naradikian MS, et al. A B-cell subset uniquely responsive to innate stimuli accumulates in aged mice. Blood 2011;118(5):1294–1304.
20. Rubtsov AV, Rubtsova K, Fischer A, et al. Toll-like receptor 7 (TLR7)-driven accumulation of a novel CD11c(+) B-cell population is important for the development of autoimmunity. Blood 2011;118(5):1305–1315.
21. Jenks SA, Cashman KS, Zumaquero E, et al. Distinct effector B cells induced by unregulated toll-like receptor 7 contribute to pathogenic responses in systemic lupus erythematosus. Immunity 2018;49(4):725–739.e6.
22. Wang S, Wang J, Kumar V, et al. IL-21 drives expansion and plasma cell differentiation of autoreactive CD11c(hi)T-bet(+) B cells in SLE. Nat Commun 2018;9(1):1758.
23. Adlowitz DG, Barnard J, Biear JN, et al. Expansion of activated peripheral blood memory B cells in rheumatoid arthritis, impact of B cell depletion therapy, and biomarkers of response. PLoS One 2015;10(6):e0128269.
24. Wardemann H, Yurasov S, Schaefer A, et al. Predominant autoantibody production by early human B cell precursors. Science 2003;301(5638):1374–1377.
25. Willims RC Jr, Kunkel HG, Capra JD. Antigenic specificities related to the cold agglutinin activity of gamma M globulins. Science 1968;161(3839):379–381.
26. Pugh-Bernard AE, Silverman GJ, Cappione AJ, et al. Regulation of inherently autoreactive VH4-34 B cells in the maintenance of human B cell tolerance. J Clin Invest 2001;108(7):1061–1070.
27. Rakhmanov M, Keller B, Gutenberger S, et al. Circulating CD21low B cells in common variable immunodeficiency resemble tissue homing, innate-like B cells. Proc Natl Acad Sci U S A 2009;106(32):13451–13456.
28. Wehr C, Eibel H, Masilamani M, et al. A new CD21low B cell population in the peripheral blood of patients with SLE. Clin Immunol 2004;113(2):161–171.
29. Isnardi I, Ng YS, Menard L, et al. Complement receptor 2/CD21$^-$ human naive B cells contain mostly autoreactive unresponsive clones. Blood 2010;115(24):5026–5036.
30. Cancro MP. Age-associated B cells. Annu Rev Immunol 2020;38:315–340.
31. Qin Y, Cai ML, Jin HZ, et al. Age-associated B cells contribute to the pathogenesis of rheumatoid arthritis by inducing activation of fibroblast-like synoviocytes via TNF-alpha-mediated ERK1/2 and JAK-STAT1 pathways. Ann Rheum Dis 2022;81(11):1504–1514.
32. Zhang F, Wei K, Slowikowski K, et al. Defining inflammatory cell states in rheumatoid arthritis joint synovial tissues by integrating single-cell transcriptomics and mass cytometry. Nat Immunol 2019;20(7):928–942.
33. Saadoun D, Terrier B, Bannock J, et al. Expansion of autoreactive unresponsive CD21-/low B cells in Sjogren's syndrome-

associated lymphoproliferation. Arthritis Rheum 2013;65(4): 1085–1096.

34. Russell Knode LM, Naradikian MS, Myles A, et al. Age-associated B cells express a diverse repertoire of V_H and V_K genes with somatic hypermutation. J Immunol 2017;198(5):1921–1927.
35. Bocharnikov AV, Keegan J, Wacleche VS, et al. PD-1hiCXCR5- T peripheral helper cells promote B cell responses in lupus via MAF and IL-21. JCI Insight 2019;4(20):e130062.
36. Ravelli A, Martini A. Juvenile idiopathic arthritis. Lancet 2007; 369(9563):767–778.
37. Sullivan DB, Cassidy JT, Petty RE. Pathogenic implications of age of onset in juvenile rheumatoid arthritis. Arthritis Rheum 1975;18(3):251–255.
38. Lucaccioni L, Trevisani V, Boncompagni A, et al. Minipuberty: looking back to understand moving forward. Front Pediatr 2020;8:612235.
39. Berghofer B, Frommer T, Haley G, et al. TLR7 ligands induce higher IFN-alpha production in females. J Immunol 2006;177(4):2088–2096.
40. Uz E, Mustafa C, Topaloglu R, et al. Increased frequency of extremely skewed X chromosome inactivation in juvenile idiopathic arthritis. Arthritis Rheum 2009;60(11):3410–3412.

American College of Rheumatology
Empowering Rheumatology Professionals

Arthritis & Rheumatology
Vol. 77, No. 8, August 2025, pp 1106–1107

DOI 10.1002/art.43119

Clinical Images: Granulomatosis with polyangiitis presenting as strawberry gingivitis: diagnostic challenges with negative antineutrophil cytoplasmic antibody

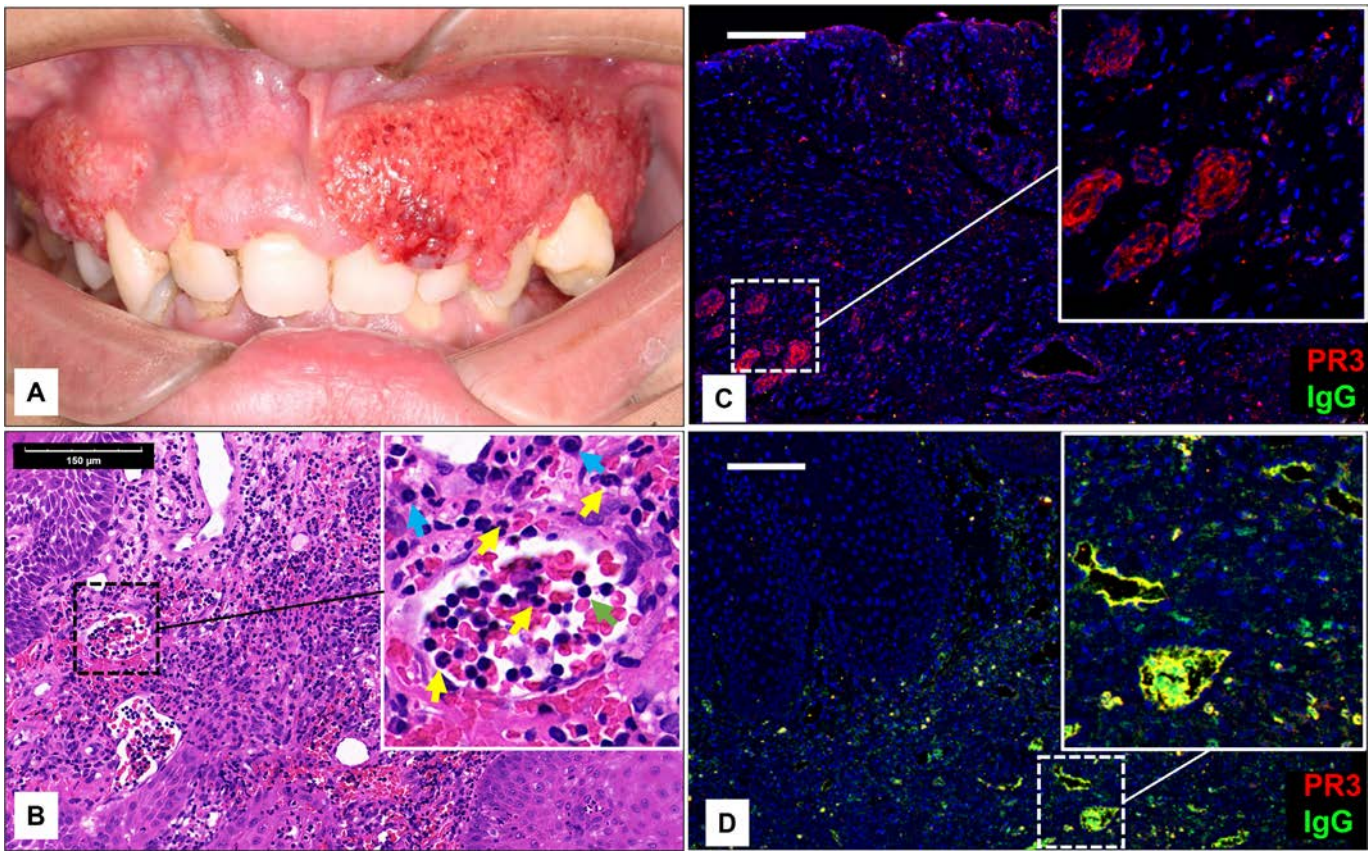

A 28-year-old man presented to the dental clinic with a six-week history of painful gingival hyperplasia, exhibiting "strawberry gingivitis"[1] with swollen, red-purple, friable and granular gingiva (Figure A). Cone-beam computed tomography showed normal bone height with no evidence of alveolar bone resorption. Notably, the patient had a perianal abscess diagnosed eight weeks earlier, which was surgically drained but remained unresolved. Gingival biopsy revealed mucosal hyperplasia, dense inflammatory infiltration, microabscesses, and necrotizing vasculitis, whereas perianal tissue biopsy showed similar inflammation (Figure B).

Immunologic testing was initially a negative result for antineutrophil cytoplasmic antibody (ANCA) by indirect immunofluorescence (IIF), complicating the potential diagnosis of granulomatosis with polyangiitis (GPA). Subsequent enzyme-linked immunosorbent assay testing, however, showed a low positive proteinase 3 (PR3)-ANCA result, and co-localization staining for PR3 and IgG revealed specific PR3-ANCA positivity within gingival microabscesses by gingiva biopsy (Figure C and D). After suspicion, patients were classified as having GPA according to the 2012 Chapel Hill Consensus Conference criteria and the 2022 American College of Rheumatology/EULAR criteria.[2,3] This case underscores the diagnostic challenge of GPA, especially in ANCA-negative presentations by IIF, necessitating reliance on histopathology and targeted immunologic testing to establish diagnosis. The patient was treated with oral steroid therapy over a nine-week period (initially 4 mg twice daily for two weeks and then reduced to 4 mg once daily for seven weeks). Following treatment, both the gingival lesions and perianal abscess showed significant improvement. At the five-year follow-up, the patient remained free of gingival hyperplasia and perianal abscess recurrence, with no abnormalities detected in other organ systems. However, serological testing continued to show persistently elevated cytoplasmic ANCA and PR3-ANCA levels.

Supported by the Health Commission of Sichuan Province Medical Science and Technology Program (24LCYJPT16) and the Research and Development Program, West China Hospital of Stomatology Sichuan University (LCYJ-HL-202303). Hanghang Liu

and Wenting Qi contributed equally to this work. This study was approved by the Ethics Committee of West China Hospital of Stomatology (WCHS-IRB-D-2018-135).

Author disclosures are available at https://onlinelibrary.wiley.com/doi/10.1002/art.43119.

1. Ghiasi M. Strawberry gingivitis in granulomatosis with polyangiitis. N Engl J Med 2017;377(21):2073.
2. Jennette JCFR, Falk RJ, Bacon PA, et al. 2012 revised International Chapel Hill Consensus Conference nomenclature of vasculitides. Arthritis Rheum 2013;65(1):1–11.
3. Robson JC, Grayson PC, Ponte C, et al; DCVAS Study Group. 2022 American College of Rheumatology/European Alliance of Associations for Rheumatology classification criteria for granulomatosis with polyangiitis. Arthritis Rheumatol 2022;74(3):393–399.

Hanghang Liu, DDS
Wenting Qi, MS
Qi Han, DMD
Linyi Liu, DDS
Yongle Shi, MSN
En Luo, DDS
Chongyun Bao, DDS
Xian Liu, DDS
Jssyliuxian@163.com
State Key Laboratory of Oral Diseases & National Center for Stomatology & National Clinical Research Center for Oral Diseases, West China Hospital of Stomatology, Sichuan University
Chengdu, Sichuan, China

American College of Rheumatology
Empowering Rheumatology Professionals

Arthritis & Rheumatology
Vol. 77, No. 8, August 2025, pp 1108–1114

LETTER

DOI 10.1002/art.43122

Unexplored limitations in a randomized trial that examines efficacy and safety of upadacitinib or elsubrutinib alone or in combination for patients with systemic lupus erythematosus: comment on the article by Merrill et al

To the Editor:

We read with interest the recent publication by Merrill et al evaluating the efficacy and safety of upadacitinib and elsubrutinib in patients with systemic lupus erythematosus (SLE) through a phase 2 randomized controlled trial.[1] The study presents significant findings regarding upadacitinib's potential to reduce disease activity and flares in patients with SLE. However, although the authors acknowledged several study limitations, there are additional concerns that deserve further consideration, which were not discussed in the article.

Firstly, the trial reports that the combination of upadacitinib and elsubrutinib did not enhance efficacy beyond upadacitinib monotherapy, despite achieving adequate plasma concentrations. While the authors cited a lack of observed efficacy for BTK inhibitors in SLE as justification, the decision to not investigate this further leaves an important gap. The biologic rationale behind combining JAK and BTK inhibition is sound, with each pathway playing distinct roles in the pathophysiology of SLE.[2] More rigorous exploration of biomarker modulation or patient subgroup responses might have clarified whether specific populations could benefit from dual inhibition.

Another unmentioned limitation is the heterogeneity of background immunosuppressive treatments across the study groups. Although this is common in SLE trials, the variability in concomitant therapies, such as immunosuppressants and antimalarials, could have influenced outcomes, particularly in terms of flare reduction and disease activity. The lack of a more standardized background therapy across treatment arms could confound the assessment of the true efficacy of the investigational drugs.

Moreover, the study would have benefited from a deeper exploration of inflammatory biomarkers, especially considering that a modest reduction in complement levels (C3 and C4) was observed. It remains unclear whether these reductions were linked to disease modulation or merely reflected transient suppression without clinical benefit. The inclusion of complement activation products and a more comprehensive cytokine panel would provide a clearer picture of how upadacitinib and elsubrutinib modulate inflammatory pathways in SLE.

Lastly, placebo response rates remain an ongoing challenge in SLE clinical trials.[3] Although this trial employed a blinded data review to minimize placebo responses, the potential influence of unrecognized low-grade activity in the placebo group may still have inflated response rates. Future studies should consider strategies to further address this, such as a more stringent patient selection process to ensure uniform disease activity at baseline.

In summary, although the SLEek study contributes valuable insights into the treatment of SLE with upadacitinib, these unexplored limitations highlight the need for further refinement in the study design and deeper investigation into the underlying mechanisms of action.

Supported by Shanxi Province Clinical Research Center for Dermatologic and Immunologic Diseases (Rheumatic diseases) (LYZX-202301) and Research and Innovation Team Project for Scientific Breakthroughs at Shanxi Bethune Hospital (2024AOXIANG02).

Author disclosures are available at https://onlinelibrary.wiley.com/doi/10.1002/art.43122.

Qianyu Guo, MD, PhD
Junkang Zhao, MD, PhD
Li-yun Zhang, MD, PhD
zhangly@sxbqeh.com.cn
Shanxi Bethune Hospital, Shanxi Academy of Medical Sciences, Third Hospital of Shanxi Medical University
Tongji Shanxi Hospital
Taiyuan, China
James Cheng-Chung Wei, MD, PhD
Shanxi Bethune Hospital, Shanxi Academy of Medical Sciences, Third Hospital of Shanxi Medical University
Tongji Shanxi Hospital
Taiyuan, China
Chung Shan Medical University Hospital
China Medical University
and Chung Shan Medical University
Taichung, Taiwan

1. Merrill JT, Tanaka Y, D'Cruz D, et al. Efficacy and safety of upadacitinib or elsubrutinib alone or in combination for patients with systemic lupus erythematosus: a phase 2 randomized controlled trial. Arthritis Rheumatol 2024;76(10):1518–1529.
2. Tsokos GC. Systemic lupus erythematosus. N Engl J Med 2011; 365(22):2110–2121.
3. Dörner T, Furie R. Novel paradigms in systemic lupus erythematosus. Lancet 2019;393(10188):2344–2358.

DOI 10.1002/art.43123

Reply

To the Editor:

We appreciate the comments of Guo et al about our article "Efficacy and Safety of Upadacitinib or Elsubrutinib Alone or in

Combination for Patients With Systemic Lupus Erythematosus: A Phase 2 Randomized Controlled Trial." We acknowledge and would like to address the concerns expressed.

Guo et al point out that the ABBV-599 combination of elsubrutinib with upadacitinib was not found to be more efficacious than upadacitinib alone, and further phase 3 development involves only upadacitinib (NCT05843643). Although there was a strong biologic rationale for the combination of a JAK inhibitor and a BTK inhibitor, the BTK inhibitor did not provide any relevant contribution to efficacy, and other studies of BTK inhibitors in lupus have also not shown efficacy despite strong pathway inhibition.[1,2]

Systemic lupus erythematosus (SLE) is a heterogeneous disease, so it is possible that subsets of patients might benefit from BTK inhibition. We have begun to address this possibility with a comprehensive biomarker analysis of upadacitinib and ABBV-599 versus placebo, as presented at recent congresses.[3,4] For most key immunologic pathways relevant to SLE, effects of upadacitinib versus ABBV-599 were similar, including reduction of type 1 interferon gene signature, innate immune proteins, T and B cell–associated cytokines, B cells, and macrophages.[3] Most protein biomarkers were modulated similarly by upadacitinib and ABBV-599, demonstrating that the main effect was attributable to upadacitinib alone.[3] A unique difference was observed with ABBV-599 versus upadacitinib in gene expression patterns related to neutrophil or other myeloid cell activity, but there was no difference in effect on B cell modules.[4]

Another concern expressed by Guo et al is the heterogeneity of background immunosuppressive treatments, which is a potential confounding factor in lupus trials.[5] However, this factor can be offset by a balance of entry variables between treatment arms and placebo, as was achieved in our study. The reason why variable background treatments are used almost ubiquitously in lupus clinical trials is intrinsic to the complex nature of the disease itself. To study patients with lupus with sufficient disease so that a difference can be detected between treatment and placebo requires the use of some stabilizing medication. Requiring all patients to receive only one background treatment would not be logistically or clinically feasible because one background treatment does not have sufficient impact on all patients with lupus. A trial designed with only one possible background treatment would restrict the immunophenotypes of participants and reduce the generalizability of the results.

Lastly, Guo et al raise concern about placebo response rates. This study used expert review of all screened patients to ensure active lupus at entry and blinded review of clinical scoring to reduce placebo response. Placebo response was low compared to many past SLE clinical trials, enabling differences to be observed between the treatment arms and placebo.

We share the correspondents' eagerness for the robust biomarker investigation of this study, which is ongoing and will be submitted for publication once complete. Further efficacy, safety, and biomarker analyses will also be made available after the conclusion of the phase 3 studies (NCT05843643).

Joan T. Merrill, MD
joan-merrill@omrf.org
Oklahoma Medical Research Foundation
Oklahoma City
Marie-Claude Gaudreau, MD, MPH
Kristin M. D'Silva, PhD
AbbVie
North Chicago, IL

1. Isenberg D, Furie R, Jones NS, et al. Efficacy, safety, and pharmacodynamic effects of the Bruton's tyrosine kinase inhibitor fenebrutinib (GDC-0853) in systemic lupus erythematosus: results of a phase II, randomized, double-blind, placebo-controlled trial. Arthritis Rheumatol 2021;73(10):1835–1846.
2. Wallace DJ, Dörner T, Pisetsky DS, et al. Efficacy and safety of the Bruton's tyrosine kinase inhibitor evobrutinib in systemic lupus erythematosus: results of a phase II, randomized, double-blind, placebo-controlled dose-ranging trial. ACR Open Rheumatol 2023;5(1):38–48.
3. Gaudreau MC, Fann J, Contrepois S. Treatment of systemic lupus erythematosus patients with upadacitinib results in the coordinated inhibition of type 1 IFN-related biomarkers: biomarker analysis of the M19-130 (SLEEK) phase 2 study. Ann Rheum Dis 2023;82(1):894–895.
4. Merrill J, Catalina MD, Filip I, et al. Modular gene expression changes in the SLEEK phase 2 study of upadacitinib and ABBV-599 in patients with systemic lupus erythematosus [abstract]. Ann Rheum Dis 2024;83(suppl 1):977.
5. Merrill JT, Manzi S, Aranow C, et al. Lupus community panel proposals for optimising clinical trials: 2018. Lupus Sci Med 2018;5(1):e000258.

DOI 10.1002/art.43126

Study on mupirocin treatment in cutaneous lupus erythematosus: comment on the article by Abernathy-Close et al

To the Editor:

Abernathy-Close et al[1] provide a valuable contribution to the understanding of therapy for cutaneous lupus erythematosus (CLE) through their proof-of-concept study examining the effects of mupirocin, a topical antibiotic, on inflammatory pathways within CLE lesions. Their data indicate a correlation between reduced *Staphylococcus aureus* bacterial load and a subsequent decline in local inflammation, as well as decreased expression of inflammatory genes, particularly those related to type I interferon (IFN) signaling. These findings highlight the pivotal role of the skin microbiome in influencing immune responses and advancing treatment options for lupus-associated skin lesions.

A critical aspect of CLE pathophysiology is the interplay between antibiotics and inflammatory regulation. Elevated IFN levels in individuals with CLE are known to activate inflammatory pathways, suggesting that modulating microbial colonization may offer a novel strategy for addressing these inflammatory responses.

American College of Rheumatology
Empowering Rheumatology Professionals

Arthritis & Rheumatology
Vol. 77, No. 8, August 2025, pp 1108–1114

LETTER

DOI 10.1002/art.43122

Unexplored limitations in a randomized trial that examines efficacy and safety of upadacitinib or elsubrutinib alone or in combination for patients with systemic lupus erythematosus: comment on the article by Merrill et al

To the Editor:

We read with interest the recent publication by Merrill et al evaluating the efficacy and safety of upadacitinib and elsubrutinib in patients with systemic lupus erythematosus (SLE) through a phase 2 randomized controlled trial.[1] The study presents significant findings regarding upadacitinib's potential to reduce disease activity and flares in patients with SLE. However, although the authors acknowledged several study limitations, there are additional concerns that deserve further consideration, which were not discussed in the article.

Firstly, the trial reports that the combination of upadacitinib and elsubrutinib did not enhance efficacy beyond upadacitinib monotherapy, despite achieving adequate plasma concentrations. While the authors cited a lack of observed efficacy for BTK inhibitors in SLE as justification, the decision to not investigate this further leaves an important gap. The biologic rationale behind combining JAK and BTK inhibition is sound, with each pathway playing distinct roles in the pathophysiology of SLE.[2] More rigorous exploration of biomarker modulation or patient subgroup responses might have clarified whether specific populations could benefit from dual inhibition.

Another unmentioned limitation is the heterogeneity of background immunosuppressive treatments across the study groups. Although this is common in SLE trials, the variability in concomitant therapies, such as immunosuppressants and antimalarials, could have influenced outcomes, particularly in terms of flare reduction and disease activity. The lack of a more standardized background therapy across treatment arms could confound the assessment of the true efficacy of the investigational drugs.

Moreover, the study would have benefited from a deeper exploration of inflammatory biomarkers, especially considering that a modest reduction in complement levels (C3 and C4) was observed. It remains unclear whether these reductions were linked to disease modulation or merely reflected transient suppression without clinical benefit. The inclusion of complement activation products and a more comprehensive cytokine panel would provide a clearer picture of how upadacitinib and elsubrutinib modulate inflammatory pathways in SLE.

Lastly, placebo response rates remain an ongoing challenge in SLE clinical trials.[3] Although this trial employed a blinded data review to minimize placebo responses, the potential influence of unrecognized low-grade activity in the placebo group may still have inflated response rates. Future studies should consider strategies to further address this, such as a more stringent patient selection process to ensure uniform disease activity at baseline.

In summary, although the SLEek study contributes valuable insights into the treatment of SLE with upadacitinib, these unexplored limitations highlight the need for further refinement in the study design and deeper investigation into the underlying mechanisms of action.

Supported by Shanxi Province Clinical Research Center for Dermatologic and Immunologic Diseases (Rheumatic diseases) (LYZX-202301) and Research and Innovation Team Project for Scientific Breakthroughs at Shanxi Bethune Hospital (2024AOXIANG02).

Author disclosures are available at https://onlinelibrary.wiley.com/doi/10.1002/art.43122.

Qianyu Guo, MD, PhD
Junkang Zhao, MD, PhD
Li-yun Zhang, MD, PhD
zhangly@sxbqeh.com.cn
Shanxi Bethune Hospital, Shanxi Academy of Medical Sciences, Third Hospital of Shanxi Medical University
Tongji Shanxi Hospital
Taiyuan, China
James Cheng-Chung Wei, MD, PhD
Shanxi Bethune Hospital, Shanxi Academy of Medical Sciences, Third Hospital of Shanxi Medical University
Tongji Shanxi Hospital
Taiyuan, China
Chung Shan Medical University Hospital
China Medical University
and Chung Shan Medical University
Taichung, Taiwan

1. Merrill JT, Tanaka Y, D'Cruz D, et al. Efficacy and safety of upadacitinib or elsubrutinib alone or in combination for patients with systemic lupus erythematosus: a phase 2 randomized controlled trial. Arthritis Rheumatol 2024;76(10):1518–1529.
2. Tsokos GC. Systemic lupus erythematosus. N Engl J Med 2011; 365(22):2110–2121.
3. Dörner T, Furie R. Novel paradigms in systemic lupus erythematosus. Lancet 2019;393(10188):2344–2358.

DOI 10.1002/art.43123

Reply

To the Editor:

We appreciate the comments of Guo et al about our article "Efficacy and Safety of Upadacitinib or Elsubrutinib Alone or in

Combination for Patients With Systemic Lupus Erythematosus: A Phase 2 Randomized Controlled Trial." We acknowledge and would like to address the concerns expressed.

Guo et al point out that the ABBV-599 combination of elsubrutinib with upadacitinib was not found to be more efficacious than upadacitinib alone, and further phase 3 development involves only upadacitinib (NCT05843643). Although there was a strong biologic rationale for the combination of a JAK inhibitor and a BTK inhibitor, the BTK inhibitor did not provide any relevant contribution to efficacy, and other studies of BTK inhibitors in lupus have also not shown efficacy despite strong pathway inhibition.[1,2]

Systemic lupus erythematosus (SLE) is a heterogeneous disease, so it is possible that subsets of patients might benefit from BTK inhibition. We have begun to address this possibility with a comprehensive biomarker analysis of upadacitinib and ABBV-599 versus placebo, as presented at recent congresses.[3,4] For most key immunologic pathways relevant to SLE, effects of upadacitinib versus ABBV-599 were similar, including reduction of type 1 interferon gene signature, innate immune proteins, T and B cell–associated cytokines, B cells, and macrophages.[3] Most protein biomarkers were modulated similarly by upadacitinib and ABBV-599, demonstrating that the main effect was attributable to upadacitinib alone.[3] A unique difference was observed with ABBV-599 versus upadacitinib in gene expression patterns related to neutrophil or other myeloid cell activity, but there was no difference in effect on B cell modules.[4]

Another concern expressed by Guo et al is the heterogeneity of background immunosuppressive treatments, which is a potential confounding factor in lupus trials.[5] However, this factor can be offset by a balance of entry variables between treatment arms and placebo, as was achieved in our study. The reason why variable background treatments are used almost ubiquitously in lupus clinical trials is intrinsic to the complex nature of the disease itself. To study patients with lupus with sufficient disease so that a difference can be detected between treatment and placebo requires the use of some stabilizing medication. Requiring all patients to receive only one background treatment would not be logistically or clinically feasible because one background treatment does not have sufficient impact on all patients with lupus. A trial designed with only one possible background treatment would restrict the immunophenotypes of participants and reduce the generalizability of the results.

Lastly, Guo et al raise concern about placebo response rates. This study used expert review of all screened patients to ensure active lupus at entry and blinded review of clinical scoring to reduce placebo response. Placebo response was low compared to many past SLE clinical trials, enabling differences to be observed between the treatment arms and placebo.

We share the correspondents' eagerness for the robust biomarker investigation of this study, which is ongoing and will be submitted for publication once complete. Further efficacy, safety, and biomarker analyses will also be made available after the conclusion of the phase 3 studies (NCT05843643).

Joan T. Merrill, MD
joan-merrill@omrf.org
Oklahoma Medical Research Foundation
Oklahoma City
Marie-Claude Gaudreau, MD, MPH
Kristin M. D'Silva, PhD
AbbVie
North Chicago, IL

1. Isenberg D, Furie R, Jones NS, et al. Efficacy, safety, and pharmacodynamic effects of the Bruton's tyrosine kinase inhibitor fenebrutinib (GDC-0853) in systemic lupus erythematosus: results of a phase II, randomized, double-blind, placebo-controlled trial. Arthritis Rheumatol 2021;73(10):1835–1846.
2. Wallace DJ, Dörner T, Pisetsky DS, et al. Efficacy and safety of the Bruton's tyrosine kinase inhibitor evobrutinib in systemic lupus erythematosus: results of a phase II, randomized, double-blind, placebo-controlled dose-ranging trial. ACR Open Rheumatol 2023;5(1):38–48.
3. Gaudreau MC, Fann J, Contrepois S. Treatment of systemic lupus erythematosus patients with upadacitinib results in the coordinated inhibition of type 1 IFN-related biomarkers: biomarker analysis of the M19-130 (SLEEK) phase 2 study. Ann Rheum Dis 2023;82(1):894–895.
4. Merrill J, Catalina MD, Filip I, et al. Modular gene expression changes in the SLEEK phase 2 study of upadacitinib and ABBV-599 in patients with systemic lupus erythematosus [abstract]. Ann Rheum Dis 2024;83(suppl 1):977.
5. Merrill JT, Manzi S, Aranow C, et al. Lupus community panel proposals for optimising clinical trials: 2018. Lupus Sci Med 2018;5(1):e000258.

DOI 10.1002/art.43126

Study on mupirocin treatment in cutaneous lupus erythematosus: comment on the article by Abernathy-Close et al

To the Editor:

Abernathy-Close et al[1] provide a valuable contribution to the understanding of therapy for cutaneous lupus erythematosus (CLE) through their proof-of-concept study examining the effects of mupirocin, a topical antibiotic, on inflammatory pathways within CLE lesions. Their data indicate a correlation between reduced *Staphylococcus aureus* bacterial load and a subsequent decline in local inflammation, as well as decreased expression of inflammatory genes, particularly those related to type I interferon (IFN) signaling. These findings highlight the pivotal role of the skin microbiome in influencing immune responses and advancing treatment options for lupus-associated skin lesions.

A critical aspect of CLE pathophysiology is the interplay between antibiotics and inflammatory regulation. Elevated IFN levels in individuals with CLE are known to activate inflammatory pathways, suggesting that modulating microbial colonization may offer a novel strategy for addressing these inflammatory responses.

Recent research conducted by our team provides mechanistic insights that complement the findings of Abernathy-Close et al. We have demonstrated that B cell adapter for phosphoinositide 3-kinase (BCAP) participates in an amplification loop of IFN-mediated inflammation driven by bacterial components, which is particularly relevant to systemic lupus erythematosus (SLE). In fibroblasts from a monogenic model simulating SLE, known as DNase2 interferonopathy, elevated BCAP expression correlates with a skewed immune response favoring IFN production over classic antibacterial cytokines upon Toll-like receptor 4 (TLR4) stimulation. These outcomes were also replicated in cellular models characterized by baseline IFN activation via the cyclic GMP-AMP synthase–stimulator of IFN genes–TANK-binding kinase 1 pathway (cGAS-STING-TBK1). Collectively, our data underscore BCAP's critical involvement in amplifying IFN-mediated inflammation following bacterial stimulation.[2]

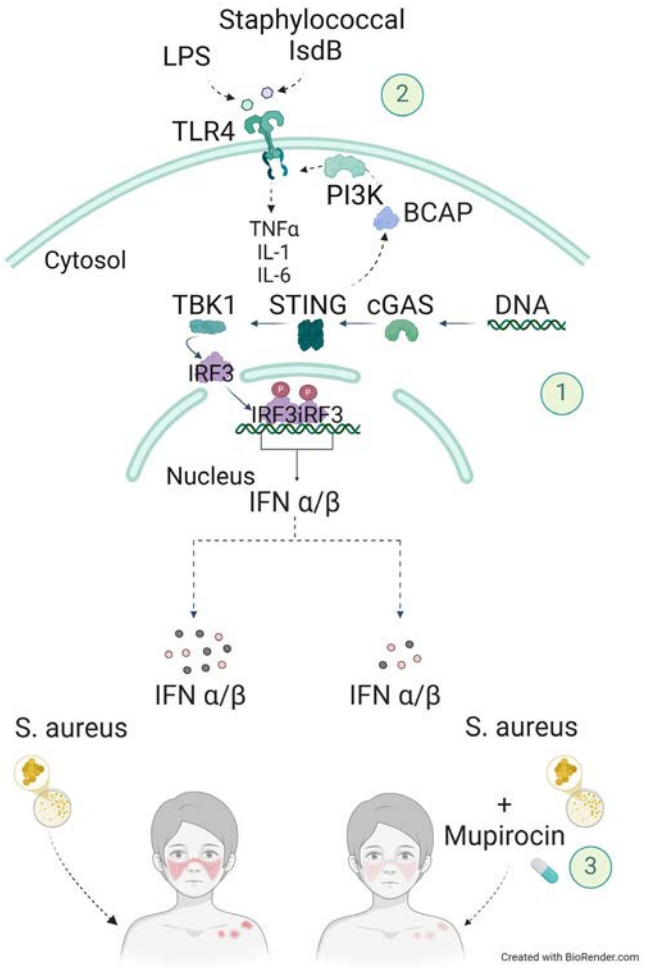

Figure 1. Proposed molecular mechanisms by which antimicrobial treatment may disrupt the IFN amplification loop in which BCAP might be involved. (1) Basal activation of type I IFN signaling. (2) Signaling amplification after bacterial stimulus. (3) Possible interaction between amplification loop and type I IFN after antibiotic treatment. BCAP, B cell adapter for phosphoinositide 3-kinase; cGAS, cyclic GMP-AMP synthase; IFN, interferon; IL, interleukin; IRF, interferon regulatory factor; IsdB, Iron-regulated surface determinant B protein; LPS, lipopolysaccharide; PI3K, phosphatidylinositol 3-kinase; STING, stimulator of interferon genes; TBK1, TANK-binding kinase 1; TLR, Toll-like receptor; TNF, tumor necrosis factor.

It is plausible that the antimicrobial treatment employed in the study by Abernathy-Close et al may disrupt this amplification loop by attenuating TLR activation in IFN-primed cells (staphylococcal Iron-regulated surface determinant B (IsdB) protein is sensed by TLR4) (Figure 1). Importantly, analysis of raw data from their investigation reveals substantial BCAP expression in skin biopsy samples from patients with CLE, suggesting a potential role in exacerbating inflammation associated with bacterial colonization. Unfortunately, we lack the ability to compare BCAP expression levels in skin samples from affected versus healthy individuals because this was beyond the scope of the initial research. We propose that future studies should address this gap, as it may yield valuable insights.

In summary, the compelling findings of Abernathy-Close et al suggest that diminished *S aureus* colonization in CLE lesions may indirectly alter inflammatory signaling pathways that contribute to worsening of the disease. These results endorse further investigation into topical antibiotics, not only as treatments for bacterial infections but also as adjunctive therapies for managing skin inflammation in autoimmune conditions. Future research should aim to elucidate the specific molecular mechanisms through which mupirocin and similar agents might modulate BCAP and IFN signaling pathways.

Ultimately, the work of Abernathy-Close et al enhances existing knowledge regarding the connection between skin microbiota, inflammatory responses, and potential therapeutic interventions for CLE. Integrating our findings on BCAP's role in inflammatory signaling could inform a more comprehensive understanding of the mechanisms linking skin health with immune function, paving the way for innovative treatment strategies that leverage both antibacterial and anti-inflammatory properties to improve the management of lupus-related skin conditions.

This work was supported by the Ministry of Health, Rome, Italy, in collaboration with the Institute for Maternal and Child Health IRCCS Burlo Garofolo, Trieste, Italy (#RC08/2021).

Marianna Di Rosa, BSc
University of Trieste
Trieste, Italy
Alessia Pin, PhD
alessia.pin@burlo.trieste.it
Institute for Maternal and Child Health - IRCCS Burlo Garofolo
Trieste, Italy
Giulia Maria Piperno, PhD
International Centre for Genetic Engineering and Biotechnology
Trieste, Italy
Serena Pastore, MD
Institute for Maternal and Child Health - IRCCS Burlo Garofolo
Trieste, Italy
Alberto Tommasini, MD, PhD
University of Trieste
and the Institute for Maternal and Child Health - IRCCS Burlo Garofolo
Trieste, Italy

Alessandra Tesser, PhD
Institute for Maternal and Child Health - IRCCS Burlo Garofolo
Trieste, Italy

1. Abernathy-Close L, Mears J, Billi AC, et al. Topical mupirocin treatment reduces interferon and myeloid signatures in cutaneous lupus erythematous lesions through targeting of *Staphylococcus* species. Arthritis Rheumatol 2025;77(6):705–715. doi:https://doi.org/10.1002/art.43079.
2. Tesser A, Piperno GM, Pin A, et al. Priming of the cGAS-STING-TBK1 pathway enhances LPS-induced release of type I interferons. Cells 2021;10(4):785.

DOI 10.1002/art.43128

Reply

To the Editor:

We thank Di Rosa et al for their interest and insightful comments on our article. As they note, sustained cutaneous type I interferon (IFN) signaling is a critical trigger of cutaneous lupus erythematosus (CLE) lesions. This IFN milieu is a result of hyperactive epidermal production of type I IFNs that signal in a feed-forward inflammatory loop of IFN and inflammatory cytokine production with myeloid cells in the skin.[1–4] Modifications that promote sustained activation or decreased inhibition of pathways, such as cyclic GMP-AMP synthase/stimulator of IFN genes signaling, are important targets in modulating the chronic IFN overproduction in the skin of patients with lupus. Here, using our data, they identified increased expression of an important regulator of type I IFN production, B cell adapter for phosphoinositide 3-kinase (BCAP) (gene name *PI3KAP1*), in our lesional CLE samples. As they have identified a role for BCAP in skewing toward IFN production in response to Toll-like receptor 4 ligands produced by *Staphylococcus aureus*, it is feasible that BCAP could be playing a role in IFN production in CLE lesions. To examine this further, we pulled data from our previously published single-cell RNA sequencing study[5] to examine the distribution of *PI3KAP1* expression in healthy control and lesional CLE skin biopsy samples. As shown in Figure 1, the dominant expression pattern of this gene is in the myeloid rather than the stromal or keratinocyte population. Thus, if mupirocin is having effects on BCAP-related signaling, it may be more in the myeloid-derived IFN response. This is especially intriguing given that one of the effects of mupirocin we see is decreased myeloid infiltration into the skin. We agree with the authors that further study of the intersection between microbial products and their effects on inflammatory and autoimmune skin disease is an important next step.

Lisa Abernathy-Close, PhD
Allison C. Billi, MD, PhD
J. Michelle Kahlenberg, MD, PhD
mkahlenb@med.umich.edu
University of Michigan
Ann Arbor

1. Berthier CC, Tsoi LC, Reed TJ, et al. Molecular profiling of cutaneous lupus lesions identifies subgroups distinct from clinical phenotypes. J Clin Med 2019;8(8):8.
2. Sarkar MK, Hile GA, Tsoi LC, et al. Photosensitivity and type I IFN responses in cutaneous lupus are driven by epidermal-derived interferon kappa. Ann Rheum Dis 2018;77(11):1653–1664.
3. Stannard JN, Reed TJ, Myers E, et al. Lupus skin is primed for IL-6 inflammatory responses through a keratinocyte-mediated autocrine type I interferon loop. J Invest Dermatol 2017;137(1):115–122.
4. Patel J, Vazquez T, Chin F, et al. Multidimensional immune profiling of cutaneous lupus erythematosus in vivo stratified by patient response to antimalarials. Arthritis Rheumatol 2022;74(10):1687–1698.
5. Billi AC, Ma F, Plazyo O, et al. Nonlesional lupus skin contributes to inflammatory education of myeloid cells and primes for cutaneous inflammation. Sci Transl Med 2022;14(642):eabn2263.

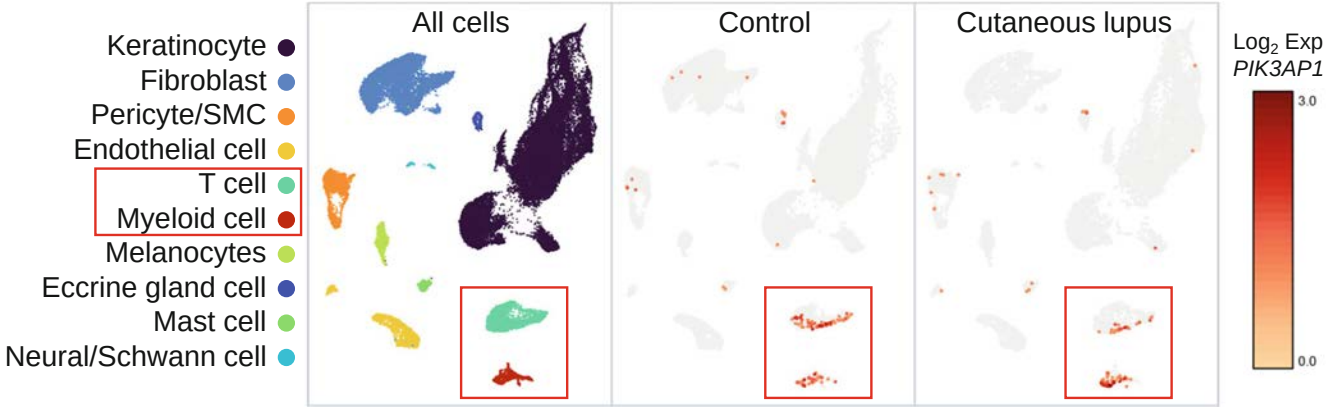

Figure 1. *PI3KAP1* expression is primarily in myeloid and T cell populations in CLE skin. Uniform manifold approximation and projection from single-cell RNA sequencing of healthy control (n = 14) and nonlesional and lesional CLE skin biopsy samples (n = 7 each) from the study by Billi et al[5] highlighting distribution of *PI3KAP1* expression. CLE, cutaneous lupus erythematosus; SMC, smooth muscle cell.

Alessandra Tesser, PhD
Institute for Maternal and Child Health - IRCCS Burlo Garofolo
Trieste, Italy

1. Abernathy-Close L, Mears J, Billi AC, et al. Topical mupirocin treatment reduces interferon and myeloid signatures in cutaneous lupus erythematous lesions through targeting of *Staphylococcus* species. Arthritis Rheumatol 2025;77(6):705–715. doi:https://doi.org/10.1002/art.43079.
2. Tesser A, Piperno GM, Pin A, et al. Priming of the cGAS-STING-TBK1 pathway enhances LPS-induced release of type I interferons. Cells 2021;10(4):785.

DOI 10.1002/art.43128

Reply

To the Editor:

We thank Di Rosa et al for their interest and insightful comments on our article. As they note, sustained cutaneous type I interferon (IFN) signaling is a critical trigger of cutaneous lupus erythematosus (CLE) lesions. This IFN milieu is a result of hyperactive epidermal production of type I IFNs that signal in a feed-forward inflammatory loop of IFN and inflammatory cytokine production with myeloid cells in the skin.[1–4] Modifications that promote sustained activation or decreased inhibition of pathways, such as cyclic GMP-AMP synthase/stimulator of IFN genes signaling, are important targets in modulating the chronic IFN overproduction in the skin of patients with lupus. Here, using our data, they identified increased expression of an important regulator of type I IFN production, B cell adapter for phosphoinositide 3-kinase (BCAP) (gene name *PI3KAP1*), in our lesional CLE samples. As they have identified a role for BCAP in skewing toward IFN production in response to Toll-like receptor 4 ligands produced by *Staphylococcus aureus*, it is feasible that BCAP could be playing a role in IFN production in CLE lesions. To examine this further, we pulled data from our previously published single-cell RNA sequencing study[5] to examine the distribution of *PI3KAP1* expression in healthy control and lesional CLE skin biopsy samples. As shown in Figure 1, the dominant expression pattern of this gene is in the myeloid rather than the stromal or keratinocyte population. Thus, if mupirocin is having effects on BCAP-related signaling, it may be more in the myeloid-derived IFN response. This is especially intriguing given that one of the effects of mupirocin we see is decreased myeloid infiltration into the skin. We agree with the authors that further study of the intersection between microbial products and their effects on inflammatory and autoimmune skin disease is an important next step.

Lisa Abernathy-Close, PhD
Allison C. Billi, MD, PhD
J. Michelle Kahlenberg, MD, PhD
mkahlenb@med.umich.edu
University of Michigan
Ann Arbor

1. Berthier CC, Tsoi LC, Reed TJ, et al. Molecular profiling of cutaneous lupus lesions identifies subgroups distinct from clinical phenotypes. J Clin Med 2019;8(8):8.
2. Sarkar MK, Hile GA, Tsoi LC, et al. Photosensitivity and type I IFN responses in cutaneous lupus are driven by epidermal-derived interferon kappa. Ann Rheum Dis 2018;77(11):1653–1664.
3. Stannard JN, Reed TJ, Myers E, et al. Lupus skin is primed for IL-6 inflammatory responses through a keratinocyte-mediated autocrine type I interferon loop. J Invest Dermatol 2017;137(1):115–122.
4. Patel J, Vazquez T, Chin F, et al. Multidimensional immune profiling of cutaneous lupus erythematosus in vivo stratified by patient response to antimalarials. Arthritis Rheumatol 2022;74(10):1687–1698.
5. Billi AC, Ma F, Plazyo O, et al. Nonlesional lupus skin contributes to inflammatory education of myeloid cells and primes for cutaneous inflammation. Sci Transl Med 2022;14(642):eabn2263.

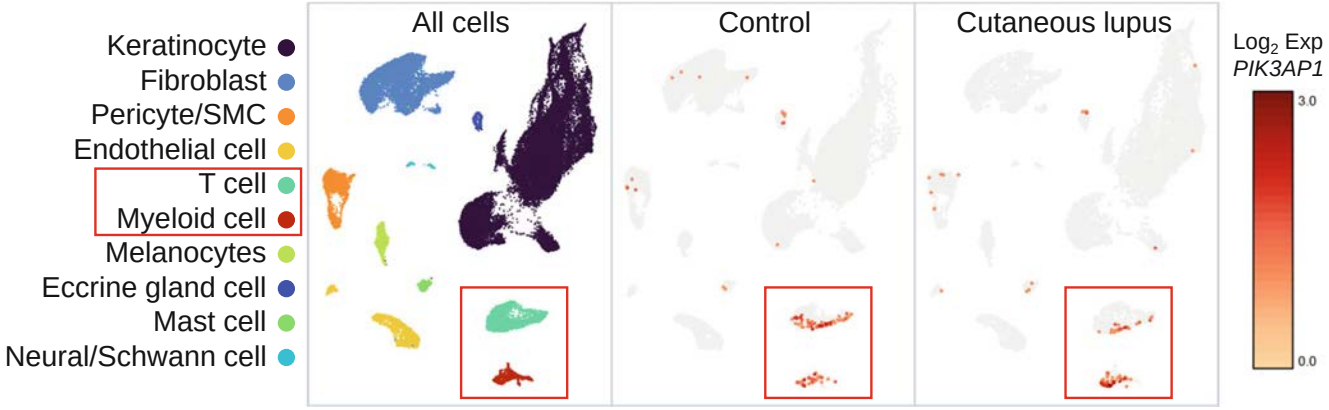

Figure 1. *PI3KAP1* expression is primarily in myeloid and T cell populations in CLE skin. Uniform manifold approximation and projection from single-cell RNA sequencing of healthy control (n = 14) and nonlesional and lesional CLE skin biopsy samples (n = 7 each) from the study by Billi et al[5] highlighting distribution of *PI3KAP1* expression. CLE, cutaneous lupus erythematosus; SMC, smooth muscle cell.

DOI 10.1002/art.43132

Efficacy of BI 655064 in improving renal outcome in patients with lupus nephritis: comment on the article by Uzzo et al

To the Editor:

We read with great interest the article by Uzzo and colleagues.[1] The study investigated the outcome of patients with lupus nephritis (LN) who had kidney biopsies with the presence of glomerular monocytes and were treated with BI 655064 (an anti-CD40 monoclonal antibody).[1] The research revealed that a higher dose (180/240 mg) of BI 655064 corresponded to better spot urine protein/urine creatinine ratio (UP/UC) and complete renal response (CRR) results when glomerular monocytes were present in renal biopsy.[1] Renal biopsy features including karyorrhexis, endocapillary hypercellularity, and interstitial fibrosis were associated with a better kidney outcome evaluated by UP/UC, estimated glomerular filtration rate (eGFR), and CRR.[1] However, we believe that some crucial factors should be considered to explain the study's significance and interpretation of the study results.

First, the study did not include the comparison of kidney outcomes between the presence and absence of monocytes. Quantitative data results could better evaluate the effectiveness and safety of BI 655064 in patients with kidney biopsy present with monocytes. In recent years, two Phase 2 clinical trials of BI 655064 for the treatment of LN have been recruited and conducted. Among them, the clinical trial (ClinicalTrials.Gov identifier NCT03385564) to explore the effectiveness of BI 655064 in the maintenance treatment of LN has not yet seen the official publication of the results. Another clinical trial (ClinicalTrials.Gov identifier NCT02770170) investigating the efficacy of different doses of BI 655064 as an add-on therapy in the treatment of active LN failed to demonstrate a dose-response relationship for the primary CRR end point at week 52.[2] Post hoc analysis showed that BI 655064 at 180 mg has potential benefits for patients with active LN.[2] Overall, none of the above results support the effectiveness of BI 655064 in the treatment of LN.

Second, the absorption, distribution, and metabolism of BI 655064 in patients with LN may not be ignored in future studies, to determine how dosage modifications affect the blood concentration and the relationship with the incidence of side events. BI 655064 exhibited nonlinear and saturable pharmacokinetics (PKs) that 240 mg of BI 655064 results in a disproportionately higher maximum plasma concentration and total exposure in vivo.[3] In addition, nonlinear PK characteristics are also one of the key factors related to adverse events of the medication. This study did not mention any differences in adverse events between kidney biopsies with and without the presence of monocytes. However, in addition to UP/UC and eGFR, adverse events related to treatment are also important indicators for evaluating renal remission in patients with LN. Previous studies published by the research team pointed out that BI 655064 at 240 mg can cause a higher proportion of patients with neutropenia, leukopenia, and lymphopenia.[2]

Third, whether the co-administered medications have a competitive role of enzymes or carrier systems that affect the PK of BI 655064 requires further study. Dendritic cell maturation was affected by mycophenolic acid therapy, which was evident in the reduction of costimulatory molecules such as CD40 expression up-regulation.[4] In summary, the current research results show that the benefits and risks of BI 655064 are not matched, but patients with LN with the presence of monocytes in renal biopsy may become the target population. Individualized treatment might be achieved in patients with LN by selecting a reasonable dosage of BI 655064 and blood concentration monitoring.

Author disclosures are available at https://onlinelibrary.wiley.com/doi/10.1002/art.43132.

Mi Zhou, PhD
Sichuan Provincial People's Hospital Wenjiang Hospital
Chengdu, China
Ru-yang Jing, BPH
Chengdu University of Traditional Chinese Medicine
Chengdu, China
Li-xue Yin, MD
yinlixue_cardiac@163.com
Ultrasound in Cardiac Electrophysiology and Biomechanics Key Laboratory of Sichuan Province, Sichuan Provincial People's Hospital, University of Electronic Science and Technology of China
Chengdu, China

1. Uzzo M, Schumacher H, Steffgen J, et al. Outcome of lupus nephritis patients treated with an anti-CD40 monoclonal antibody according to kidney biopsy features. Arthritis Rheumatol 2025;77(6):696–704. doi: https://doi.org/10.1002/art.43076.
2. Jayne DR, Steffgen J, Romero-Diaz J, et al. Clinical and biomarker responses to BI 655064, an antagonistic anti-CD40 antibody, in patients with active lupus nephritis: a randomized, double-blind, placebo-controlled, phase II trial. Arthritis Rheumatol 2023;75(11):1983–1993.
3. Tsuda Y, Grimaldi C, Huang F, et al. Safety, pharmacokinetics and pharmacodynamics of BI 655064 in phase 1 clinical trials in healthy Chinese and Japanese subjects. Br J Clin Pharmacol 2021;87(4):2000–2013.
4. Lagaraine C, Hoarau C, Chabot V, et al. Mycophenolic acid-treated human dendritic cells have a mature migratory phenotype and inhibit allogeneic responses via direct and indirect pathways. Int Immunol 2005;17(4):351–363.

DOI 10.1002/art.43134

Reply

To the Editor:

We thank Zhou et al for their interest in our study,[1] and we here address their points of consideration. First, Zhou et al state that we did not make a comparison of kidney outcome between biopsies with and without monocytes, but this is a misconception. Our study was an exploratory study from the previously published

main trial report,[2] and we demonstrated that there was a difference in outcome based on biopsies with and without monocytes: in kidney biopsies with glomerular monocytes, high-dose BI 655064 treatment significantly improved proteinuria at 52 weeks and resulted in a higher complete renal response compared to biopsies without glomerular monocytes.[1] The information retrieved from the analysis of the biopsy samples is new. This information, especially whether monocytes were present, was not available in the analysis of the main trial report.[2] Given the interaction between treatment and presence or absence of monocytes, that is, the differential effect of high doses of BI 655064 in the two strata, it is no surprise that no treatment effect was seen in the former analysis.

Second, safety and pharmacokinetics were not the focus of this histologic study, and we fail to understand the rationale behind the question of how differences in adverse events (AEs) could be related to biopsies with and without monocytes. Nevertheless, we have run an analysis to investigate the effect of presence or absence of monocytes on the frequency of AEs. This analysis shows no difference in the frequency of any AE, severe AEs, serious AEs, or serious infections between the presence and absence of monocytes when high doses of BI 655064 are used. A higher frequency of severe AEs and severe infections in the 180/240 mg group compared to the placebo/120 mg group is driven by the higher frequency of severe AEs and severe infections in the 240 mg cohort, as already described by Jayne et al[2]; however, there is no effect of the presence or absence of monocytes. The nonlinear supraproportional pharmacokinetics of BI 655064 is due to target mediated disposition and similar for all anti-CD40 monoclonal antibodies in clinical development.

Third, we have no evidence that comedication of, for example, mycophenolate mofetil, has an effect on pharmacokinetics; however, comedication may affect the frequency and severity of AEs. Stating that the benefits and risks of BI 655064 are not matched goes far beyond the reported results of our study. However, we do agree with Zhou et al that, indeed, individualized treatment may be achieved in patients with lupus nephritis, for instance, on the basis of biopsy findings, as demonstrated in our study.

Martina Uzzo, MD
m.uzzo@campus.unimib.it
University of Milano-Bicocca
Monza, Italy
and University Medical Center Groningen, University of Groningen
Groningen, The Netherlands
Helmut Schumacher, PhD
Ingelheim, Germany
Juergen Steffgen, MD, PhD
Boehringer Ingelheim International, GmbH
Biberach, Germany
Simone Deutschel, MSc
Boehringer Ingelheim Regional Center Vienna, GmbH & Co KG
Vienna, Austria
David Jayne, MD
University of Cambridge
Cambridge, UK
Ingeborg Bajema, MD, PhD
University Medical Center Groningen, University of Groningen
Groningen, The Netherlands

1. Uzzo M, Schumacher H, Steffgen J, et al. Outcome of lupus nephritis patients treated with an anti-CD40 monoclonal antibody according to kidney biopsy features. Arthritis Rheumatol 2025;77(6):696–704. https://doi.org/10.1002/art.43076.
2. Jayne DR, Steffgen J, Romero-Diaz J, et al. Clinical and biomarker responses to BI 655064, an antagonistic anti-CD40 antibody, in patients with active lupus nephritis: a randomized, double-blind, placebo-controlled, phase II trial. Arthritis Rheumatol 2023;75(11):1983–1993.

DOI 10.1002/art.43117

Risk of gastrointestinal perforation in patients with rheumatic diseases exposed to JAK inhibitors versus adalimumab: a nationwide cohort study: comment on the article by Hoisnard et al

To the Editor:

We read with interest the article by Hoisnard et al,[1] who reported on the risk of gastrointestinal perforation (GIP) in patients with rheumatoid arthritis (RA) exposed to JAK inhibitors (JAKis) and adalimumab in a French national cohort study, a through multigroup subgroup analysis in which no significant difference was found. In addition, with GIP being one of the serious gastrointestinal complications, this study provides a basis for our clinical application of JAKis. However, we would like to highlight some of our main concerns with this article.

First, the authors note that there are two definitions of discontinuation, the first type being when a patient stops taking a JAKi or adalimumab for more than 90 days, which may be due to the patient's disease remission discontinuation. The second type is when a patient switches to another biologic disease-modifying antirheumatic drug (DMARD) or targeted synthetic DMARD, which may be due to disease progression, requiring a change in treatment strategy. In addition, in patients with RA, the incidence of gastrointestinal complications in patients with disease progression is six times higher than in patients with disease remission, and the progression of gastrointestinal complications is also related to the progression of RA.[2] Although GIP has been analyzed in multiple subgroups, the effect of disease remission or progression on GIP has not been studied, so we recommend the two definitions of discontinuation of treatment be analyzed separately.

Second, as a cohort study, we noticed the research team had considered incorporating nonsteroidal anti-inflammatory drugs (NSAIDs) as a time-varying variable. However, NSAIDs are available in various types. These include nonselective cyclooxygenase (COX) inhibitors, such as diclofenac, naproxen, and ibuprofen, as well as

DOI 10.1002/art.43132

Efficacy of BI 655064 in improving renal outcome in patients with lupus nephritis: comment on the article by Uzzo et al

To the Editor:

We read with great interest the article by Uzzo and colleagues.[1] The study investigated the outcome of patients with lupus nephritis (LN) who had kidney biopsies with the presence of glomerular monocytes and were treated with BI 655064 (an anti-CD40 monoclonal antibody).[1] The research revealed that a higher dose (180/240 mg) of BI 655064 corresponded to better spot urine protein/urine creatinine ratio (UP/UC) and complete renal response (CRR) results when glomerular monocytes were present in renal biopsy.[1] Renal biopsy features including karyorrhexis, endocapillary hypercellularity, and interstitial fibrosis were associated with a better kidney outcome evaluated by UP/UC, estimated glomerular filtration rate (eGFR), and CRR.[1] However, we believe that some crucial factors should be considered to explain the study's significance and interpretation of the study results.

First, the study did not include the comparison of kidney outcomes between the presence and absence of monocytes. Quantitative data results could better evaluate the effectiveness and safety of BI 655064 in patients with kidney biopsy present with monocytes. In recent years, two Phase 2 clinical trials of BI 655064 for the treatment of LN have been recruited and conducted. Among them, the clinical trial (ClinicalTrials.Gov identifier NCT03385564) to explore the effectiveness of BI 655064 in the maintenance treatment of LN has not yet seen the official publication of the results. Another clinical trial (ClinicalTrials.Gov identifier NCT02770170) investigating the efficacy of different doses of BI 655064 as an add-on therapy in the treatment of active LN failed to demonstrate a dose-response relationship for the primary CRR end point at week 52.[2] Post hoc analysis showed that BI 655064 at 180 mg has potential benefits for patients with active LN.[2] Overall, none of the above results support the effectiveness of BI 655064 in the treatment of LN.

Second, the absorption, distribution, and metabolism of BI 655064 in patients with LN may not be ignored in future studies, to determine how dosage modifications affect the blood concentration and the relationship with the incidence of side events. BI 655064 exhibited nonlinear and saturable pharmacokinetics (PKs) that 240 mg of BI 655064 results in a disproportionately higher maximum plasma concentration and total exposure in vivo.[3] In addition, nonlinear PK characteristics are also one of the key factors related to adverse events of the medication. This study did not mention any differences in adverse events between kidney biopsies with and without the presence of monocytes. However, in addition to UP/UC and eGFR, adverse events related to treatment are also important indicators for evaluating renal remission in patients with LN. Previous studies published by the research team pointed out that BI 655064 at 240 mg can cause a higher proportion of patients with neutropenia, leukopenia, and lymphopenia.[2]

Third, whether the co-administered medications have a competitive role of enzymes or carrier systems that affect the PK of BI 655064 requires further study. Dendritic cell maturation was affected by mycophenolic acid therapy, which was evident in the reduction of costimulatory molecules such as CD40 expression up-regulation.[4] In summary, the current research results show that the benefits and risks of BI 655064 are not matched, but patients with LN with the presence of monocytes in renal biopsy may become the target population. Individualized treatment might be achieved in patients with LN by selecting a reasonable dosage of BI 655064 and blood concentration monitoring.

Author disclosures are available at https://onlinelibrary.wiley.com/doi/10.1002/art.43132.

Mi Zhou, PhD
Sichuan Provincial People's Hospital Wenjiang Hospital
Chengdu, China
Ru-yang Jing, BPH
Chengdu University of Traditional Chinese Medicine
Chengdu, China
Li-xue Yin, MD
yinlixue_cardiac@163.com
Ultrasound in Cardiac Electrophysiology and Biomechanics Key Laboratory of Sichuan Province, Sichuan Provincial People's Hospital, University of Electronic Science and Technology of China
Chengdu, China

1. Uzzo M, Schumacher H, Steffgen J, et al. Outcome of lupus nephritis patients treated with an anti-CD40 monoclonal antibody according to kidney biopsy features. Arthritis Rheumatol 2025;77(6):696–704. doi: https://doi.org/10.1002/art.43076.
2. Jayne DR, Steffgen J, Romero-Diaz J, et al. Clinical and biomarker responses to BI 655064, an antagonistic anti-CD40 antibody, in patients with active lupus nephritis: a randomized, double-blind, placebo-controlled, phase II trial. Arthritis Rheumatol 2023;75(11):1983–1993.
3. Tsuda Y, Grimaldi C, Huang F, et al. Safety, pharmacokinetics and pharmacodynamics of BI 655064 in phase 1 clinical trials in healthy Chinese and Japanese subjects. Br J Clin Pharmacol 2021;87(4):2000–2013.
4. Lagaraine C, Hoarau C, Chabot V, et al. Mycophenolic acid-treated human dendritic cells have a mature migratory phenotype and inhibit allogeneic responses via direct and indirect pathways. Int Immunol 2005;17(4):351–363.

DOI 10.1002/art.43134

Reply

To the Editor:

We thank Zhou et al for their interest in our study,[1] and we here address their points of consideration. First, Zhou et al state that we did not make a comparison of kidney outcome between biopsies with and without monocytes, but this is a misconception. Our study was an exploratory study from the previously published

main trial report,[2] and we demonstrated that there was a difference in outcome based on biopsies with and without monocytes: in kidney biopsies with glomerular monocytes, high-dose BI 655064 treatment significantly improved proteinuria at 52 weeks and resulted in a higher complete renal response compared to biopsies without glomerular monocytes.[1] The information retrieved from the analysis of the biopsy samples is new. This information, especially whether monocytes were present, was not available in the analysis of the main trial report.[2] Given the interaction between treatment and presence or absence of monocytes, that is, the differential effect of high doses of BI 655064 in the two strata, it is no surprise that no treatment effect was seen in the former analysis.

Second, safety and pharmacokinetics were not the focus of this histologic study, and we fail to understand the rationale behind the question of how differences in adverse events (AEs) could be related to biopsies with and without monocytes. Nevertheless, we have run an analysis to investigate the effect of presence or absence of monocytes on the frequency of AEs. This analysis shows no difference in the frequency of any AE, severe AEs, serious AEs, or serious infections between the presence and absence of monocytes when high doses of BI 655064 are used. A higher frequency of severe AEs and severe infections in the 180/240 mg group compared to the placebo/120 mg group is driven by the higher frequency of severe AEs and severe infections in the 240 mg cohort, as already described by Jayne et al[2]; however, there is no effect of the presence or absence of monocytes. The nonlinear supraproportional pharmacokinetics of BI 655064 is due to target mediated disposition and similar for all anti-CD40 monoclonal antibodies in clinical development.

Third, we have no evidence that comedication of, for example, mycophenolate mofetil, has an effect on pharmacokinetics; however, comedication may affect the frequency and severity of AEs. Stating that the benefits and risks of BI 655064 are not matched goes far beyond the reported results of our study. However, we do agree with Zhou et al that, indeed, individualized treatment may be achieved in patients with lupus nephritis, for instance, on the basis of biopsy findings, as demonstrated in our study.

Martina Uzzo, MD
m.uzzo@campus.unimib.it
University of Milano-Bicocca
Monza, Italy
and University Medical Center Groningen, University of Groningen
Groningen, The Netherlands
Helmut Schumacher, PhD
Ingelheim, Germany
Juergen Steffgen, MD, PhD
Boehringer Ingelheim International, GmbH
Biberach, Germany
Simone Deutschel, MSc
Boehringer Ingelheim Regional Center Vienna, GmbH & Co KG
Vienna, Austria
David Jayne, MD
University of Cambridge
Cambridge, UK
Ingeborg Bajema, MD, PhD
University Medical Center Groningen, University of Groningen
Groningen, The Netherlands

1. Uzzo M, Schumacher H, Steffgen J, et al. Outcome of lupus nephritis patients treated with an anti-CD40 monoclonal antibody according to kidney biopsy features. Arthritis Rheumatol 2025;77(6):696–704. https://doi.org/10.1002/art.43076.
2. Jayne DR, Steffgen J, Romero-Diaz J, et al. Clinical and biomarker responses to BI 655064, an antagonistic anti-CD40 antibody, in patients with active lupus nephritis: a randomized, double-blind, placebo-controlled, phase II trial. Arthritis Rheumatol 2023;75(11):1983–1993.

DOI 10.1002/art.43117

Risk of gastrointestinal perforation in patients with rheumatic diseases exposed to JAK inhibitors versus adalimumab: a nationwide cohort study: comment on the article by Hoisnard et al

To the Editor:

We read with interest the article by Hoisnard et al,[1] who reported on the risk of gastrointestinal perforation (GIP) in patients with rheumatoid arthritis (RA) exposed to JAK inhibitors (JAKis) and adalimumab in a French national cohort study, a through multigroup subgroup analysis in which no significant difference was found. In addition, with GIP being one of the serious gastrointestinal complications, this study provides a basis for our clinical application of JAKis. However, we would like to highlight some of our main concerns with this article.

First, the authors note that there are two definitions of discontinuation, the first type being when a patient stops taking a JAKi or adalimumab for more than 90 days, which may be due to the patient's disease remission discontinuation. The second type is when a patient switches to another biologic disease-modifying antirheumatic drug (DMARD) or targeted synthetic DMARD, which may be due to disease progression, requiring a change in treatment strategy. In addition, in patients with RA, the incidence of gastrointestinal complications in patients with disease progression is six times higher than in patients with disease remission, and the progression of gastrointestinal complications is also related to the progression of RA.[2] Although GIP has been analyzed in multiple subgroups, the effect of disease remission or progression on GIP has not been studied, so we recommend the two definitions of discontinuation of treatment be analyzed separately.

Second, as a cohort study, we noticed the research team had considered incorporating nonsteroidal anti-inflammatory drugs (NSAIDs) as a time-varying variable. However, NSAIDs are available in various types. These include nonselective cyclooxygenase (COX) inhibitors, such as diclofenac, naproxen, and ibuprofen, as well as

selective COX-2 inhibitors like celecoxib and etoricoxib. Because the analgesic and anti-inflammatory effects of NSAIDs are primarily mediated by the inhibition of COX-2, and their gastrointestinal side effects are largely due to the inhibition of COX-1, NSAIDs that selectively inhibit COX-2 may reduce the risk of gastrointestinal toxicity compared to nonselective NSAIDs.[3,4] The risk of gastrointestinal tract infection varies among different types of NSAIDs[5]; naproxen was associated with a significantly higher risk of gastrointestinal complications than celecoxib.[6] We recommend specifying the type of NSAIDs used by the patient based on the identified Anatomical Therapeutic Chemical code in order to minimize the influence of this confounding factor on the research outcomes.

Third, although classic propensity score (PS) methods of inverse probability of treatment weighting (IPTW) and matching can adjust for differences in measured characteristics, these methods have potential limitations with respect to target population, balance, and precision.[7] There are many covariables in this article, and some covariables have large differences between the two groups, and they are still not balanced between the two groups even after weighting with the IPTW method. These methods can modify the target population,[8] fail to achieve good balance, or substantially worsen precision.[7] In addition, the article does not mention whether extreme PS values occur with IPTW. In this case, we considered trying to use overlapped weighting to ensure the robustness of the results. Overlap weighting can overcome above limitations by assigning weights to each patient that are proportional to the probability of that patient belonging to the opposite treatment group.[9] If there are no extreme PS values, overlap weighting can be as efficient as randomization if no adjustment was needed. If there are extreme PS values, these weights obtained by overlapping weighting are smaller for extreme PS values so that outliers who are nearly always treated (PS near 1) or never treated (PS near 0) do not dominate results and worsen precision, as occurs with IPTW.

Last, for all PS methods, they cannot adjust for patient characteristics that are not measured and included in the model for the PS. Residual measured or unmeasured confounders can bias results in this observational study, but this is not reflected in the limitations in the discussion. In order to assess the robustness of the observed associations in the presence of potential unmeasured confounders, we suggest that a sensitivity analysis be performed using the methods of VanderWeele and Ding[10] to calculate E-values.

In conclusion, although the authors concluded that there was no difference in the incidence of GIP in patients receiving JAKis and adalimumab through multiple subgroup analyses, further attention is needed in terms of disease remission or progression and the risk of developing GIP with NSAIDs. Attention should also be paid to the use of overlap weighting and the methods of VanderWeele and Ding[10] to reduce bias in results. We eagerly await feedback from the authors and are very interested in learning about their upcoming work, which will further our understanding of this critical topic.

Jing-jin Hu
Yang-yang Lu
Jun-kang Zhao
Dan Ma, MD, PhD
madan@sxbqeh.com.cn
Li-yun Zhang, MD, PhD
zhangly@sxbqeh.com.cn
Third Hospital of Shanxi Medical University
Shanxi Bethune Hospital
Shanxi Academy of Medical Sciences
and Tongji Shanxi Hospital
Taiyuan, China
James Cheng-Chung Wei, MD, PhD
Chung Shan Medical University
Chung Shan Medical University Hospital
and China Medical University
Taichung, Taiwan

1. Hoisnard L, Meyer A, Dray-Spira R, et al. Risk of gastrointestinal perforation in patients with rheumatic diseases exposed to Janus kinase inhibitors versus adalimumab: a nationwide cohort study. Arthritis Rheumatol 2024;76(9):1364–1376.
2. Rustamovich TD, Alisherovna KM, Nizamitdinovich KS, et al. Gastrointestinal conditions in rheumatoid arthritis patients. Tex J Med Sci 2022;15:68–72.
3. Schnitzer TJ, Burmester GR, Mysler E, et al; TARGET Study Group. Comparison of lumiracoxib with naproxen and ibuprofen in the Therapeutic Arthritis Research and Gastrointestinal Event Trial (TARGET), reduction in ulcer complications: randomised controlled trial. Lancet 2004;364(9435):665–674.
4. Chan FKL, Lanas A, Scheiman J, et al. Celecoxib versus omeprazole and diclofenac in patients with osteoarthritis and rheumatoid arthritis (CONDOR): a randomised trial. Lancet 2010;376(9736):173–179.
5. Coxib and Traditional NSAID Trailists' Collaboration; Bhala N, Emberson J, Merhi A, et al. Vascular and upper gastrointestinal effects of non-steroidal anti-inflammatory drugs: meta-analyses of individual participant data from randomised trials. Lancet 2013;382(9894):769–779.
6. Simon LS, Weaver AL, Graham DY, et al. Anti-inflammatory and upper gastrointestinal effects of celecoxib in rheumatoid arthritis: a randomized controlled trial. JAMA 1999;282(20):1921–1928.
7. Li F, Thomas LE, Li F. Addressing extreme propensity scores via the overlap weights. Am J Epidemiol 2019;188(1):250–257.
8. Thomas L, Li F, Pencina M. Using propensity score methods to create target populations in observational clinical research. JAMA 2020;323(5):466–467.
9. Li F, Morgan KL, Zaslavsky AM. Balancing covariates via propensity score weighting. J Am Stat Assoc 2018;113(521):390–400.
10. VanderWeele TJ, Ding P. Sensitivity analysis in observational research: introducing the e-value. Ann Intern Med 2017;167(4):268–274.